

231st AAS
Washington, DC – January, 2018
Meeting Abstracts

Session Table of Contents

- HAD I: The Future of Astronomy's Archived Observations – An Open Discussion
100 – Welcome Address by AAS President Christine Jones (Harvard-Smithsonian, CfA)
101 – Kavli Foundation Lecture: The New Jupiter: Results from the Juno Mission, Scott Bolton (SwRI)
144 – The Solar System Poster Session
157 – Stellar Topics iPoster Session
102 – First Data from the Pan-STARRS Survey and How to Use It
103 – NASA Decadal Preparations I: Large-scale Studies
104 – Detection of Extrasolar Planets I
105 – AGN, QSO, Blazars I
106 – Astrophysics Enabled by HST's UV Initiative
107 – Gamma Ray Bursts
108 – HAD II: From the Earliest Astronomy to Space Missions: Explorations in the History of Astronomy
109 – Pulsators and Binaries
110 – Galaxy Formation and Evolution I
111 – Extrasolar Planets I
112 – Starburst Galaxies
113 – Innovations in Astronomy Teaching and Learning II
114 – Star Formation I
115 – The Solar System
117 – Plenary Talk: A New Measurement of the Expansion Rate of the Universe, Evidence of New Physics?, Adam Riess (Johns Hopkins University)
160 – HEAD I: Astrophysics and Exploration from the International Space Station with NICER
116 – Cosmology I
120 – Understanding Stellar Abundances in the Solar Neighborhood using Large Online Catalogs
121 – NASA Decadal Preparations II: Probes Mission Concept Studies
122 – The Triple Threat to Multi-wavelength Observational Astronomy
123 – AGN, QSO, Blazars II
124 – Gravitational Waves and EM Counterparts I
125 – Science with the Wideband Submillimeter Array
126 – HAD III: History, Eclipses, and Planetaria
127 – Galaxy Formation and Evolution II
128 – Extrasolar Planets II
129 – Circumstellar Disks I
130 – ISM I
131 – Learning with NASA Astrophysics: How to Get Connected
132 – White Dwarfs and Neutron Stars I
133 – Stars and Friends I
134 – Doggett Prize Lecture: Tangible Things of American Astronomy, Sara Schechner (Harvard University)
135 – RAS Medal Prize Lectureship: The Effect of Non-Linear Structure on Cosmological Observables, Nick Kaiser (University of Hawaii)
136 – Star Formation Poster Session
137 – First Data for the Pan-STARRS Survey and How to Use It Poster Session
139 – Innovations in Astronomy Teaching and Learning II Poster Session
140 – NASA Decadal Preparations II: Probes Mission Concept Studies Poster Session
142 – The Triple Threat to Multi-wavelength Observational Astronomy Poster Session
143 – HAD IV: Poster Session
145 – White Dwarfs Poster Session
146 – Variable Stars Poster Session
147 – Circumstellar Disks Poster Session
148 – Extrasolar Planets: Characterization and Theory Poster Session
149 – Galaxy Evolution Poster Session
150 – Computation, Data Handling, Image Analysis Poster Session
151 – Catalogs Poster Session
152 – Instrumentation: Ground Based or Airborne Poster Session
153 – Cosmology Poster Session
154 – Cosmic Microwave Background Poster Session
155 – CosmoQuest and NITARP: Two Examples of Engaging Students, Teachers, and Lifelong Learners in Astronomy Poster Session
156 – Professional Development for Teachers, Grads, Postdocs, and College Instructors Poster Session
158 – The Sun, Extrasolar Planets and Stars iPoster Session
200 – AAS Prize Presentations by AAS President Christine Jones (Harvard-Smithsonian, CfA)
201 – Plenary Talk: Unveiling the Low Surface Brightness Stellar Peripheries of Galaxies, Annette Ferguson (University of Edinburgh)
257 – Stellar Topics, Galaxies iPoster Session
202 – Sustainability at Professional Societies: best Practices in Environmental Stewardship
203 – IGM and QSO Absorption Line Systems I
204 – Detection of Extrasolar Planets II
205 – AGN, QSO, Blazars III
206 – Multimessenger Astronomy in light of LIGO-Virgo Discoveries
207 – Exoplanet Characterization Through Emission Spectroscopy: A Roadmap To Detecting Biosignatures
208 – HAD V: Genealogy, History, and Technology
209 – Supernovae I
210 – Galaxy Formation and Evolution III
211 – Extrasolar Planets III
212 – Milky Way and Galactic Center I
213 – Computation, Data Science, and Image Analysis
214 – Star Formation II
215 – Instrumentation: Ground Based and Airborne I
216 – Preparing Our Next Generation: Education Research and Practice from High School Through the Major
261 – Cosmology II
262 – HEAD II: GW170817/GRB 170817A: Multi-messenger Astrophysics from a Neutron Star Merger
217 – Plenary Talk: The Stormy Life of Galaxy Clusters, Larry Rudnick (Minnesota Institute for Astrophysics)
219 – Dark Energy Survey: Results and Data Release
220 – Results from the August 21, 2017, Total Solar Eclipse
221 – Beyond the Academy: Panel Discussion on Entering Non-Academic Careers
222 – AGN, QSO, Blazars IV
223 – Data Driven Discoveries in Serendipitous X-ray Catalogs
224 – Gravitational Waves and EM Counterparts II
225 – Applied Statistical Methods in Astronomy: Gaussian Processes and Machine Learning
226 – Cosmology III
227 – Galaxy Formation and Evolution IV
228 – Extrasolar Planets IV
229 – Circumstellar Disks II
230 – ISM II
231 – Surveys and Large Programs I
232 – Astronomy Outreach: From Large Observatory to Memorable Music
233 – White Dwarfs and Neutron Stars II
234 – Stars and Friends II
235 – Dannie Heineman Prize for Astrophysics: The Value of Change: Surprises and Insights in Stellar Evolution, Lars Bildsten (University of California, Santa Barbara)
236 – HEAD Bruno Rossi Prize: Gravitational Waves Astrophysics, Gabriela Gonzalez (Louisiana State University for the LIGO Scientific Collaboration and the Virgo Collaboration)
237 – The Milky Way & The Galactic Center Poster Session
238 – Data Driven Discoveries in Serendipitous X-ray Catalogs Poster Session
239 – Applied Statistical Methods in Astronomy: Gaussian Processes and Machine Learning Poster Session
241 – Planetary Nebulae and SNRs Poster Session
242 – Results from the August 21, 2017, Total Solar Eclipse Poster Session
243 – Neutron Stars (Pulsars, Magnetars, Pulsar Wind Nebulae) Poster Session
244 – Binary Stars Poster Session
245 – Supernovae Poster Session
246 – Extrasolar Planets: Detection Poster Session
247 – ISM, HII Regions and Molecular Clouds Poster Session
248 – Spiral Galaxies Poster Session
249 – Elliptical Galaxies Poster Session
250 – AGN, QSO, Blazars Poster Session
251 – Starburst Galaxies Poster Session
252 – Galaxy Clusters Poster Session
253 – Laboratory Astrophysics Poster Session

- 254 – Gamma Ray Bursts Poster Session
 255 – Gravitational Waves, Relativistic Astrophysics and Related Topics Poster Session
 256 – Gen. Ed. Astronomy Education: Research, Resources, and Practice Poster Session
 258 – Galaxies, Cosmology iPoster Session
 300 – Plenary Talk: Venus: Our Misunderstood Sister, Darby Dyar (Planetary Science Institute)
 361 – Dark Matter, Instrumentation and Other Topics iPoster Session
 301 – Water, Water, Everywhere
 302 – IGM and QSO Absorption Line Systems II
 303 – Detection of Extrasolar Planets III
 304 – AGN, QSO, Blazars V
 305 – Multi-messenger Observations of Intermediate Mass Black Holes with LISA
 306 – Galaxy Clusters I
 307 – Astronomy Software Publishing: Community Roles and Services
 308 – Supernovae II
 309 – Galaxy Formation and Evolution V
 310 – Extrasolar Planets V
 311 – Milky Way and Galactic Center II
 312 – Dwarf and Irregular Galaxies I
 313 – Star Formation III
 314 – Instrumentation: Ground Based and Airbourne II
 315 – The Sun
 316 – Gen. Ed. Astronomy Education: Research, Resources, and Practice
 365 – Status of the Astronomy Workforce
 317 – Plenary Talk: Astro Data Science: The Next Generation, Chris Mentzel (Moore Foundation)
 320 – New Results on Nearby AGN with Swift BAT
 321 – The Very Large Array Today and Tomorrow: First Molecules to Life on Exoplanets
 322 – New Views of the Universe from 1 to 115 GHz with the Green Bank Telescope
 323 – AGN, QSO, Blazars VI
 324 – Astronomy Visualization in Research, Outreach, and Entertainment
 325 – Gravitational Waves and EM Counterparts III
 326 – Stars, Stellar Evolution and Stellar Populations I
 327 – Cosmology IV
 328 – Galaxy Formation and Evolution VI
 329 – Extrasolar Planets VI
 330 – Circumstellar Disks III
 331 – ISM III
 332 – Surveys and Large Programs II
 333 – White Dwarfs and Neutron Stars III
 334 – Stars and Friends III
 335 – The AAS Committee on the Status of Women: Then and Now and Where Do We Go from Here?
 336 – Helen B. Warner Prize: The Evolution of Stars & Galaxies, Charlie Conroy (Harvard University)
 337 – Henry Norris Russell Lectureship: Fifty-four Years of Adventures in Infrared Astronomy, Eric Becklin (University of California, Los Angeles)
 338 – The Sun Poster Session
 339 – Young Stellar Objects, Very Young Stars, T-Tauri Stars, H-H Object Poster Session
 340 – Dwarf and Irregular Galaxies Poster Session
 341 – Stellar Atmospheres, Winds, and Wolf-Rayet Phenomena Poster Session
 342 – The Very Large Array Today and Tomorrow: First Molecules to Life on Exoplanets Poster Session
 343 – New Results on Nearby AGN with Swift BAT Poster Session
 344 – Star Clusters and Associations Poster Session
 347 – Black Holes Poster Session
 348 – Stellar Evolution, Stellar Populations Poster Session
 349 – Stars, Cool Dwarfs, Brown Dwarfs Poster Session
 350 – Dust Poster Session
 351 – Large Scale Structure, Cosmic Distance Scale Poster Session
 353 – Observatory Site Protection, Light Pollution, Radio Interference, and Space Debris Poster Session
 354 – Surveys and Large Programs Poster Session
 355 – Instrumentation: Space Missions Poster Session
 356 – CMB, Dark Matter & Dark Energy Poster Session
 357 – IGM, QSO Absorption Lines Poster Session
 358 – Cataclysmic Variables Poster Session
 359 – Preparing Our Next Generation: REUs and Mentorship Programs, Program Evaluation, and Curriculum Poster Session
 360 – Outreach Across the Human Continuum Poster Session
 362 – Surveys, Data, Computation and Lab Astro iPoster Session
 400 – Plenary Talk: Illuminating Gravitational Waves, Mansi Kasliwal (California Institute of Technology)
 401 – Astrobiology
 402 – Instrumentation: Space Missions I
 403 – Detection of Extrasolar Planets IV
 404 – AGN, QSO, Blazars VII
 405 – Black Holes I
 406 – Galaxy Clusters II
 407 – AAS Public Policy Panel: The Ongoing Evolution of the WFIRST Mission and Implications for Future Flagship Missions
 408 – Supernovae III
 409 – Galaxy Formation and Evolution VII
 410 – Extrasolar Planets VII
 411 – Milky Way and Galactic Center III
 412 – Dwarf and Irregular Galaxies II
 413 – Star Clusters
 414 – Various Stellar Topics
 415 – Gravitational Lenses
 417 – Plenary Talk: The Fate of Exploding White Dwarfs, Rob Fisher (University of Massachusetts, Dartmouth)
 434 – Binary Stars (Late) Poster Session
 435 – Black Holes (Late) Poster Session
 436 – Catalogs, Surveys, Computation, Etc. (Late) Poster Session
 437 – Circumstellar Disks (Late) Poster Session
 438 – Cosmology Etc. (Late) Poster Session
 439 – Extrasolar Planets (Late) Poster Session
 440 – Galaxies, AGN & Friends (Late) Poster Session
 441 – Galaxy Clusters & Large Scale Structure (Late) Poster Session
 442 – Instrumentation on the Ground and in the Air (Late) Poster Session
 443 – Laboratory Astrophysics (Late) Poster Session
 444 – Light Pollution & Education (Late) Poster Session
 445 – Molecular Clouds, ISM and Dust (Late) Poster Session
 446 – Novae, Supernovae & Friends (Late) Poster Session
 447 – Space Missions Instrumentation (Late) Poster Session
 448 – Star Associations & Clusters (Late) Poster Session
 449 – Star Formation and YSOs (Late) Poster Session
 450 – Stars and Stellar Evolution (Late) Poster Session
 451 – The Milky Way (Late) Poster Session
 452 – The Sun, the Solar System and Astrobiology (Late) Poster Session
 453 – White Dwarfs, Neutron Stars (Late) Poster Session
 454 – Galaxy Evolution (Late) Poster Session
 419 – Instrumentation: Space Missions II
 420 – Large Scale Structure
 421 – Binary Stars
 422 – AGN, QSO, Blazars VIII
 423 – Black Holes II
 424 – Stars, Stellar Evolution and Stellar Populations II
 425 – Spiral Galaxies
 426 – Galaxy Formation and Evolution VIII
 427 – Extrasolar Planets VIII
 428 – Circumstellar Disks IV
 429 – ISM IV
 430 – Cosmology V
 431 – Detection of Extrasolar Planets V
 432 – Plenary Talk: Science Policy Plenary Talk--The Politics of Science Funding: Is the Fault in Our Stars, David Goldston (MIT)
 433 – Lancelot M. Berkeley Prize: The Instruments that Launched Gravitational-wave Astronomy, Peter Fritschel (MIT Kavli Institute) for LIGO

HAD I: The Future of Astronomy's Archived Observations – An Open Discussion

Description: A give and take discussion concerning the current state of astronomy's photographic plate archives and plans for ensuring the long-term preservation of these irreplaceable observations and historical records. The following topics will be introduced by brief – perhaps provocative – statements from experts followed by round table discussions/debates by those attending. 1. Why preserve astronomy's photographic plates and their related artifacts (e.g., log books, plate markings, envelope annotations)? The present scientific and historical value of plate material, anticipated future uses and the current, in many cases potentially grave, situation regarding this under-utilized resource with examples. 2. What needs to be done to preserve as much of the plates' information content as possible and reasonable? Best practices for the preservation and storage of plates and their associated documentation, cataloguing the holdings of plate archives for public access, cleaning and handling of plates and digitization of plates and documents in accord with scientific, archival and historical standards. Balancing best practices with practical constraints. 3. How might the challenges of preserving this irreplaceable astronomical information be overcome?

Problems of funding, adequate manpower, centralized versus individual archives and the rapidly disappearing knowledge about extant plate archives and the technical details of photographic observations. The organizers want this session both to raise awareness of a critical issue and to help in the formulation of general guidelines for plate archive preservation. Input from the HAD will be particularly valuable, as will add a unique perspective. What is learned from the session will assist in developing a statement expressing the duty of the astronomical community, both collectively and individually, to protect its heritage of artifacts and irreproducible observations. This will be YOUR session. Progress comes through interactive debate, so bring your queries, questions, comments, ideas and suggestions to the meeting and share them whenever the opportunity arises. Individuals wishing to be sure they are called on to make a specific point should contact the session chair. The expert panel: • Sara Schechner (museum curator and historian, Harvard) – moderator • Michael Castelaz (Brevard College and PARI Plate Archive Center) • Elizabeth Griffin (plate user as stellar spectroscopist, DAO) • Josh Grindlay (DASCH digitization project director, Harvard) • Omar Nasim (user of plates for history research, U. Regensburg) • Wayne Osborn (user of plates for astronomy research; astronomical plate curator, Yerkes) • Lee Robbins (astronomy librarian and plate curator, U. Toronto) • Brad Schaefer (user of direct plates for astronomy research, Louisiana State U.) • Kevin Schindler (historian, Lowell Observatory)

– The Future of Astronomy's Archived Observations—An Open Discussion

A discussion concerning the current state of astronomy's photographic plate archives and plans for ensuring the long-term preservation of these irreplaceable observations and historical

100 – Welcome Address by AAS President Christine Jones (Harvard-Smithsonian, CfA)

101 – Kavli Foundation Lecture: The New Jupiter: Results from the Juno Mission, Scott Bolton (SwRI)

101.01 – The New Jupiter: Results from the Juno Mission

NASA's Juno mission to Jupiter launched in 2011 and arrived at Jupiter on July 4, 2016. Juno's scientific objectives include the study of Jupiter's interior, atmosphere and magnetosphere with the goal of understanding Jupiter's origin, formation and evolution. An extensive campaign of Earth based observations of Jupiter and the solar wind were orchestrated to complement Juno measurements during Juno's approach to Jupiter and during its orbital mission around Jupiter. This presentation provides an

144 – The Solar System Poster Session

records. The following topics will be introduced by brief—perhaps provocative—statements from experts followed by round table discussions/debates by those attending.

1. *Why preserve astronomy's photographic plates and their related artifacts (e.g., log books, plate markings, envelope annotations)?* The present scientific and historical value of plate material, anticipated future uses, and the current—in many cases potentially grave—situation regarding this under-utilized resource.

2. *What needs to be done to preserve as much of the plates' information content as possible and reasonable?* Best practices for the preservation and storage of plates and documentation. Cataloguing the holdings of plate archives for public access. Cleaning, handling, and digitization of plates and documents in accord with scientific, archival, and historical standards. Balancing best practices with practical constraints.

3. *How might the challenges of preserving this irreplaceable astronomical information be overcome?* Problems of funding, adequate manpower, centralized versus individual archives, and the rapidly disappearing knowledge about extant plate archives and the technical details of photographic observations.

The organizers want this session both to raise awareness of a critical issue and to help in the formulation of general guidelines for plate archive preservation. Input from the HAD will be particularly valuable, as it will add a unique perspective. What is learned from the session will assist in developing a statement expressing the duty of the astronomical community, both collectively and individually, to protect its heritage of artifacts and irreproducible observations.

This will be YOUR session. Progress comes through interactive debate, so bring your queries, questions, comments, ideas, and suggestions to the meeting and share them whenever the opportunity arises. Individuals wishing to be sure they are called on to make a specific point should contact the session chair.

“This session is endorsed by the AAS Working Group for the Preservation of Astronomical Heritage.”

Author(s): Sara Jane Schechner³, Wayne H. Osborn⁹, Elizabeth Griffin², Michael Castelaz¹, Jonathan Grindlay⁴, Omar Nasim⁷, Lee Robbins⁸, Bradley E. Schaefer⁵, Kevin Schindler⁶
Institution(s): 1. Brevard College, 2. DAO, 3. Harvard, 4. Harvard-Smithsonian, CfA, 5. Louisiana State University, 6. Lowell Observatory, 7. U. Regensburg, 8. U. Toronto, 9. Yerkes Observatory

overview of results from the Juno measurements during the early phases of Juno's prime mission. Scientific results include Jupiter's interior structure, magnetic field, deep atmospheric dynamics and composition, and the first in-situ exploration of Jupiter's polar magnetosphere and aurorae.

Author(s): Scott Bolton¹
Institution(s): 1. SwRI

144.01 – The Saturn Probe Interior and aTmosphere Explorer (SPRITE) Mission

A key question in planetary science is how the planets formed in our Solar System, and, by extension, in exoplanet systems. The abundances of the noble gases (He, Ne, Ar, Kr, Xe), heavy elements (C, N, O, S), and their isotopes provide important forensic clues as to location and time of formation in the early Solar System. Jupiter and Saturn contain most of the planetary mass in our solar system, and their chemical fingerprints will distinguish between competing models of the formation of all the planets. After the end of the Cassini mission, some of these elements have only ambiguous values above the cloud tops, while others (particularly the noble gases) have not been measured at all. Resolving this requires direct *in situ* measurements. The proposed NASA New Frontiers Saturn PRobe Interior and aTmosphere Explorer (SPRITE) mission delivers an instrumented entry probe from a carrier relay spacecraft that also provides context imaging. The powerful probe instrument suite is comprised of a Quadrupole Mass Spectrometer, a Tunable Laser Spectrometer, and an Atmospheric Structure Instrument including a Doppler Wind Experiment and a simple backscatter nephelometer. These instruments measure the elemental and isotopic abundances of helium, the heavier noble gases, and the major elements, as well as constraining cloud properties, 3-D atmospheric dynamics, and disequilibrium chemistry to at least 10 bars in Saturn's troposphere. *In situ* measurements of Saturn's atmosphere by SPRITE will provide a significantly improved context for interpreting the results from the Galileo probe, Juno, and Cassini missions. SPRITE will revolutionize our understanding of the formation and evolution of the gas giant planets, and ultimately the present-day structure of the Solar System.

Author(s): Amy Simon³, Donald Banfield¹, David Atkinson²
Institution(s): 1. Cornell University, 2. Jet Propulsion Lab, 3. NASA Goddard Space Flight Center
Contributing team(s): SPRITE Science Team

144.02 – Characterizing Rapidly Rotating Asteroids with Filtered Photometry

It is challenging to characterize rapidly rotating asteroids, as their aspect changes significantly between exposures using different filters. Indeed, small asteroids may very well be agglomerations of smaller components that may have differing compositions, and thus the shape and composition of the body may be incorrectly inferred. We have observed a number of smaller, rapidly rotating bodies to try to separate compositional and shape elements from light curves in B, V, R, and I. Results from these observations will be presented, as well as identifying the challenges in conducting this research will be discussed. This work has been supported by the Wisconsin Space Grant Consortium.

Author(s): Douglas Arion¹
Institution(s): 1. Carthage College

144.03 – Topographic and Other Influences on Pluto's Volatile Ices

Pluto's surface is known to consist of various volatile ices, mostly N₂, CH₄, and CO, which sublime and condense on varying timescales, generally moving from points of high insolation to those of low insolation. The New Horizons Pluto encounter data provide multiple lenses through which to view Pluto's detailed surface topography and composition and to investigate the distribution of volatiles on its surface, including albedo and elevation maps from the imaging instruments and composition maps from the LEISA spectral imager. The volatile surface ice is expected to be generally isothermal, due to the fact that their vapor pressures are in equilibrium with the atmosphere. Although secular topographic transport mechanisms suggest that points at low elevation should slowly fill with volatile ices (Trafton 2015 DPS abstract, Bertrand and Forget 2017), there are counter-examples of this across the surface, implying that energy discrepancies caused by insolation differences, albedo variations, local slopes, and other effects may take precedence at shorter timescales. Using data from the 2015 New Horizons flyby, we present our results of this investigation into the effects of

variations in insolation, albedo, and topography on the presence of the different volatile ices across the surface of Pluto.

Author(s): Briley Lynn Lewis¹, John Stansberry⁷, William M. Grundy³, Bernard Schmitt⁹, Silvia Protopapa¹⁰, Laurence M. Trafton⁸, Bryan J. Holler⁷, William B. McKinnon¹¹, Paul M. Schenk⁴, S. Alan Stern⁶, Leslie Young⁶, Harold A. Weaver², Catherine Olkin⁶, Kimberly Ennico⁵
Institution(s): 1. Columbia University, 2. Johns Hopkins University Applied Physics Laboratory, 3. Lowell Observatory, 4. Lunar and Planetary Institute, 5. NASA Ames Research Center, 6. Southwest Research Institute, 7. Space Telescope Science Institute, 8. The University of Texas at Austin, 9. Universite Grenoble Alpes, 10. University of Maryland, 11. Washington University
Contributing team(s): The New Horizons Science Team, The New Horizons Composition Team

144.04 – Debiassing the Dark Energy Survey's Search for Trans-Neptunian Objects

The Dark Energy Survey (DES) is rich in transient detections of trans-Neptunian objects (TNOs). This has resulted in many newly detected TNOs. It is important to be mindful that astronomical surveys are intrinsically biased in their detections. Understanding a survey's bias is necessary to understand the significance of any clustering in the orbital parameters of our detections. To quantify this bias, we examine the DES's selection function for the detection of TNOs. To do so, we developed a survey simulator in Python. We generate clones of known TNOs with uniformly varied argument of perihelion, longitude of ascending node, and mean anomaly. We test the detectability of each clone based on the pointing location and limiting magnitude of each exposure in DES. Our preliminary results show that our simulator is functional. However, we do not yet have any conclusions about the DES's bias, as we have not yet run the simulator on the entirety of DES for all of our TNOs.

Author(s): Kevin Napier¹, David Gerdes¹
Institution(s): 1. University of Michigan

144.05 – Developing an Asteroid Rotational Theory

The goal of this project is to develop a theoretical asteroid rotational theory from first principles. Starting at first principles provides a firm foundation for computer simulations which can be used to analyze multiple variables at once such as size, rotation period, tensile strength, and density. The initial theory will be presented along with early models of applying the theory to the asteroid population.

Early results confirm previous work by Pravec et al. (2002) that show the majority of the asteroids larger than 200m have negligible tensile strength and have spin rates close to their critical breakup point. Additionally, results show that an object with zero tensile strength has a maximum rotational rate determined by the object's density, not size. Therefore, an iron asteroid with a density of 8000 kg/m³ would have a minimum spin period of 1.16h if the only forces were gravitational and centrifugal.

The short-term goal is to include material forces in the simulations to determine what tensile strength will allow the high spin rates of asteroids smaller than 150m.

Author(s): Gena Geis¹, Miguel Williams¹, Tyler Linder¹, Donald Pakey¹
Institution(s): 1. Eastern Illinois University

144.06 – Turbulent Cloud Structure and Power Spectrum from 23 years of HST Observations

Images of Jupiter's clouds show that turbulence is a ubiquitous phenomenon over many orders of scale size. According to Kolmogorov's theory for turbulence, the frequency/distribution of clouds at various scales can be used to produce an energy power

spectrum of a passive tracer. Kolmogorov theory predicts the spectral slopes for “shallow” and “deep” fluids in motion by following how energy is injected and dissipated in the fluid. We are quantifying the turbulent nature of Jupiter’s clouds over 23 years of Hubble Space Telescope (HST) observations using an algorithm first presented in Choi and Showman (2011, Icarus 216). We applied the power spectrum fitting algorithm to a variety of filters from available HST data and tested its sensitivity to free parameters and compare our results to Choi and Showman (2011). We will comment on the evidence for a 2D turbulent regime in Jupiter’s clouds and will report on empirical values found in the spectra and their physical interpretations, such as the Rhines scale. We also will report on the behavior of the passive tracer power spectrum and trends that exist over time for different latitudinal regions, primarily the belts and zones and the north and south equatorial belts.

Author(s): Richard Cosentino¹, Amy Simon¹, Raul Morales-Juberias²

Institution(s): 1. *Goddard Space Flight Center*, 2. *New Mexico Institute of Mining and Technology*

144.07 – Improving the Determination of Eastern Elongations of Planetary Satellites in the *Astronomical Almanac*

The Astronomical Almanac is an annual publication of the US Naval Observatory (USNO) and contains a wide variety of astronomical data used by astronomers worldwide as a general reference or for planning observations. Included in this almanac are the times of greatest eastern and northern elongations of the natural satellites of the planets, accurate to 0.1 hour UT. The production code currently used to determine elongation times generates X and Y coordinates for each satellite (16 total) in 5 second intervals. This consequentially caused very large data files, and resulted in the program devoted to determining the elongation times to be computationally intensive. To make this program more efficient, we wrote a Python program to fit a cubic spline to data generated with a 6-minute time step. This resulted in elongation times that were found to agree with those determined from the 5 second data currently used in a large number of cases and was tested for 16 satellites between 2017 and 2019. The accuracy of this program is being tested for the years past 2019 and, if no problems are found, the code will be considered for production of this section of *The Astronomical Almanac*.

Author(s): Christopher Rura², Mark Stollberg¹

Institution(s): 1. *United States Naval Observatory*, 2. *Villanova University*

144.08 – Finding Kuiper Belt Objects Below the Detection Limit

We demonstrate a novel approach for uncovering the signatures of moving objects (e.g. Kuiper Belt Objects) below the detection thresholds of single astronomical images. To do so, we will employ a matched filter moving at specific rates of proposed orbits through a time-domain dataset. This is analogous to the better-known “shift-and-stack” method; however it uses neither direct shifting nor stacking of the image pixels. Instead of resampling the raw pixels to create an image stack, we will instead integrate the object detection probabilities across multiple single-epoch images to accrue support for a proposed orbit. The filtering kernel provides a measure of the probability that an object is present along a given orbit, and enables the user to make principled decisions about when the search has been successful, and when it may be terminated. The results we present here utilize GPU to speed up the search by two orders of magnitudes over CPU implementations.

Author(s): Peter Whidden¹, Bryce Kalmbach¹, Dino Bektsevich¹, Andrew Connolly¹, Lynne Jones¹, Hayden Smotherman¹, Andrew Becker¹

Institution(s): 1. *University of Washington*

144.09 – Searching for Planet Nine and Other Nearby Worlds with WISE and NEOWISE

Launched nearly eight years ago, NASA’s WISE satellite continues to collect millions of infrared images at 3-5 microns as part of its asteroid-hunting NEOWISE mission. We have repurposed these NEOWISE exposures for science beyond the main belt by generating a novel full-sky set of time-resolved coadded images. This reprocessing allows for moving object searches reaching ~1.3 magnitudes fainter than previous studies while also providing a factor of ten increase in time baseline. This creates an exciting opportunity for motion-based discovery of very cold and faint objects which may have thus far eluded detection despite residing close to the Sun. We present the results of our latest WISE/NEOWISE search for ‘Planet Nine’, a giant planet hypothesized to orbit the Sun at hundreds of astronomical units. Our search incorporates over four years of WISE W1 observations spanning a seven year time period, and covers more than 75% of the sky. Variants of the WISE/NEOWISE Planet Nine search methodology we have developed should enable motion-based discoveries of large numbers of cold, faint brown dwarfs, especially those which are not detectable with Gaia.

Author(s): Aaron Michael Meisner³, Benjamin Bromley⁴, Peter Nugent¹, David Schlegel¹, Scott Kenyon², Eddie Schlafly¹, Kyle Dawson⁴, Teddy Anderson⁴

Institution(s): 1. *Lawrence Berkeley National Laboratory*, 2. *Smithsonian Astrophysical Observatory*, 3. *University of California Berkeley*, 4. *University of Utah*

144.10 – Synchronization behind the formation of Orbital Systems

This paper aims to gain a greater understanding of why planetary and galactic orbital systems form as either synchronous or asynchronous systems. We simulate the orbiting particles and their movements. We believe that it is possible Kuramoto’s model for synchronization can be used to explain the behavior of the particles orbiting about the larger mass object. We believe that the difference between synchrony and asynchrony will be a function of parameters for the system. We examine the effect the parameters have on the order parameter, defined by the Kuramoto model. We additionally examine the simplest system, one with two orbiting particles. We see that there are equilibrium points, indicating the possibility of both synchrony and asynchrony, depending on the system parameters. Our results merit further investigation into the equilibrium of the system with a large number of particles.

Author(s): Jennifer Ruda², Daniel Abrams¹

Institution(s): 1. *Northwestern University*, 2. *Wheaton College*

144.11 – The Reappearance of Venus Observed 8 October 2015

The reappearance of Venus on October 8, 2015 offered a unique opportunity to attempt observation of the ashen light of Venus as the unlit side of Venus emerged from behind the dark side of the Moon. The dark side of Venus would be offered to observers without interference from the bright side of Venus or of the Moon. Observations were made from Alice Springs, Australia visually with a 20-cm Schmidt-Cassegrain and with a low-light level surveillance camera on a 25-cm reflector. No evidence of the dark side was noted by the visual observer, the video shows little indication of Venus prior to the bright side reappearance. The conclusion reached is that the ashen light, as it was classically defined, is not observable visually or with small telescopes in the visual regime.

The presentation describes the prediction, observation technique, and various analyses by the authors and others to draw conclusions from the data.

To date, the authors have been unable to locate any reports of others attempting to observe this unique event. That is a pity since, not only was it interesting for an attempt to verify past

observations of the ashen light, it was also a visually stunning event.

Author(s): David W Dunham¹, Joan B Dunham¹

Institution(s): 1. *International Occultation Timing Association*

144.12 – The evolution of a dead zone in a circumplanetary disk

Studying the evolution of a circumplanetary disk can help us to understand the formation of Jupiter and the four Galilean satellites. With the grid-based hydrodynamic code, FARGO3D, we simulate the evolution of a circumplanetary disk with a dead zone, a region of low turbulence. Tidal torques from the sun constrain the size of the circumplanetary disk to about $0.4 R_H$. The dead zone provides a cold environment for icy satellite formation. However, as material builds up there, the temperature of the dead zone may reach the critical temperature required for the magnetorotational instability to drive turbulence. Part of the dead zone accretes on to the planet in an accretion outburst. We explore possible disk parameters that provide a suitable environment for satellite formation.

Author(s): Cheng Chen¹, Rebecca Martin¹, Zhaohuan Zhu¹

Institution(s): 1. *University of Nevada, Las Vegas*

144.13 – Constraining the Volatile Composition and Coma Photochemistry in Jupiter Family Comet 41P/Tuttle-Giacobini-Kresak with High Resolution IR and Optical Spectroscopy

Over the past 20 years optical and IR spectroscopy of cometary comae has expanded our understanding both of cometary volatile composition and coma photochemistry. However, these observations tend to be biased towards Nearly Isotropic Comets (NIC'S) from the Oort Cloud, rather than the generally fainter and less active Jupiter Family Comets (JFC's) that are thought to originate from the Scattered Disk. However, early 2017 provided a rare opportunity to study several JFC's. We present preliminary results from IR and optical spectroscopy of JFC 41P/Tuttle-Giacobini-Kresak obtained during its 2017 apparition. IR spectra were obtained with the NIRSPEC instrument on Keck II and the new iSHELL spectrograph on NASA IRTF. High spectral resolution optical spectra were obtained with the Tull Coude spectrograph on the 2.7-meter Harlan J. Smith Telescope at McDonald Observatory. We will discuss mixing ratios of HCN, NH₃, C₂H₆, C₂H₂, H₂CO, and CH₃OH compared to H₂O and compare these to previous observations of comets. Preliminary results from the NIRSPEC observations indicate that 41P has typical C₂H₂ and HCN abundances compared to other JFC's, while the C₂H₆ abundance is similar to that of NIC's, but is enriched compared to other JFC's. H₂CO appears to be heavily depleted in 41P. Analysis of the iSHELL spectra is underway and we will include results from these observations, which complement those from NIRSPEC and extend the scope of our compositional study by measuring additional molecules. We will also present abundances for CN, C₂, NH₂, C₃, and CH obtained from the optical spectra and discuss the implications for the coma photochemistry.

This work is supported by the NASA Postdoctoral Program, administered by the Universities Space Research Association, with additional funding from the NSF and NASA PAST.

Author(s): Adam McKay⁵, Michael DiSanti⁴, Anita Cochran⁷, Neil Dello Russo², Boncho Bonev¹, Ronald Vervack², Erika Gibb⁶, Nathan Roth⁶, Hideyo Kawakita³

Institution(s): 1. *American University*, 2. *Johns Hopkins Applied Physics Laboratory*, 3. *Kyoto Sangyo University*, 4. *NASA GSFC*, 5. *NASA GSFC/USRA*, 6. *University of Missouri-St. Louis*, 7. *University of Texas at Austin/McDonald Observatory*

144.14 – Bi-directional Reflectance of Icy Surface Analogs: A Dual Approach

Bi-directional reflectance measurements of analogs for planetary

regolith have provided insight into the surface properties of planetary satellites and small bodies. Because Aluminum Oxide (Al₂O₃) and water ice share a similar hexagonal crystalline structure, the former has been used in laboratory experiments to simulate the regolith of both icy and dusty planetary bodies. By measuring various sizes of well sorted size fractions of Al₂O₃, the reflectance phase curve and porosity of a planetary regolith can be determined. We have designed an experiment to test the laboratory measurements produced by Nelson et al. (2000). Additionally, we made reflectance measurements for other alkali-halide compounds that could be used for applications beyond astronomy and planetary science.

In order to provide an independent check on the Nelson et al. data, we designed an instrument with a different configuration. While both instruments take bidirectional reflectance measurements, our instrument, the Rigid Photometric Goniometer (RPG), is fixed at a phase angle of 5° and detects the scattered light with a photomultiplier tube (PMT). The PMT current is then measured with an electrometer. Following the example of Nelson et al., we measured the bidirectional reflectance of Al₂O₃ particulate size fractions between $0.1 < d < 30.09$ microns. Additionally, we made reflectance measurements for NaCl and KCl of sizes from $20 < d < 63$ microns; these compounds have been suggested for reflectance applications beyond astronomy and planetary science. The objective of the experiment was to determine the particle size that provided optimal, or maximum, reflectance for each compound. Our conclusions bring confirmation and clarity to photometric sciences.

Author(s): Juan Manuel Quinones¹, Christina Vides¹, Robert M Nelson¹, Mark Boryta¹, Ken s Mannat¹

Institution(s): 1. *Mount San Antonio College*

144.15 – WFIRST: Science in the Solar System

Future space telescopes offer unprecedented sensitivity and spatial resolution at wavelengths that are inaccessible from the ground due to the Earth's atmosphere, and will work in concert with future *in situ* robotic crafts and large ground-based facilities to address key questions for planetary science. Additionally, they provide broader perspectives in both targets and timelines for planetary missions that orbit, land, or fly by a given target. Space observatories are not constrained to a specific target, and provide global context as well as source-to-source comparisons that are not always achieved from directed missions.

WFIRST will provide imaging and spectroscopic capabilities from 0.6-2.0 μm and will be a potential contemporary and eventual successor to JWST. Observations of asteroids, the giant planets and their satellites, Kuiper Belt Objects (KBOs), and comets will be possible through both the Guest Investigator (GI) and Guest Observer (GO) programs. Surveys of minor bodies and time domain studies of variable surfaces and atmospheres are uniquely well-suited for WFIRST with its 0.28 deg² field of view (at ~0.11"/pixel). We will present our recent study of the capabilities for solar system science and highlight unique cases presented in the WFIRST white paper (arXiv: <http://arxiv.org/abs/1709.02763>).

Author(s): Stefanie N Milam², Bryan J. Holler³, James M Bauer⁴, Robert West¹

Institution(s): 1. *JPL*, 2. *NASA/GSFC*, 3. *STScI*, 4. *University of Maryland*

Contributing team(s): WFIRST Solar System Working Group

144.16 – Formation of Ice Giant Satellites During Thommes Model Migration

Inconsistencies between ice giant planet characteristics and classic planet formation theories have led to a re-evaluation of the formation of the outer Solar system. Thommes model migration delivers proto-Uranus and Neptune from orbits interior to Saturn to their current locations. The Thommes model has also been able to reproduce the large Galilean and Saturnian moons via interactions between the proto-ice giants and the gas giant moon disks.

As part of a series of investigations examining the effects of Thommes model migration on the formation of moons, N-body simulations of the formation of the Uranian and Neptunian satellite systems were performed. Previous research has yielded conflicting results as to whether satellite systems are stable during planetary migration. Some studies, such as Beaugé (2002) concluded that the system was not stable over the proposed duration of migration. Conversely, Fuse and Neville (2011) and Yokoyama et al. (2011) found that moons were retained, though the nature of the resulting system was heavily influenced by interactions with planetesimals and other large objects. The results of the current study indicate that in situ simulations of the Uranus and Neptune systems can produce stable moons. Whether with current orbital parameters or located at pre-migration, inner Solar system semi-major axes, the simulations end with 5.8 ± 0.15 or 5.9 ± 0.7 regular satellites around Uranus and Neptune, respectively. Preliminary simulations of a proto-moon disk around a single planet migrating via the Thommes model have failed to retain moons. Furthermore, simulations of ejection of the current Uranian satellite system retained at most one moon. Thus, for the Thommes model to be valid, it is likely that moon formation did not begin until after migration ended. Future work will examine the formation of gas and ice giant moons through other migration theories, such as the Nice model (Tsiganis et al. 2006).

Author(s): Christopher Fuse¹, Josephine Spiegelberg¹
Institution(s): 1. Rollins College

144.17 – Modeling a Large Heterogeneous Set of CIRS Spectra of Titan: The ν_4 band of $^{12}\text{C}_2\text{HD}$

157 – Stellar Topics iPoster Session

157.01 – The Fundamentals: Angular Diameter Measurements of 90 Stars from the NPOI

We used the Navy Precision Optical Interferometer (NPOI) to measure the fundamental properties of 90 stars. The sample consists of 6 dwarfs, 3 subgiants, 71 giants, and 7 supergiants, and span a wide range of spectral classes from B to M. We combined our angular diameters with photometric and distance information from the literature to determine each star's physical radius, effective temperature, bolometric flux, luminosity, mass, and age. We present the results here.

Author(s): Ellyn Baines², J. Thomas Armstrong², Henrique Schmitt², R. T. Zavala³, James A. Benson³, Gerard van Belle¹
Institution(s): 1. Lowell Observatory, 2. Naval Research Laboratory, 3. U. S. Naval Observatory

157.02 – Evolving R Coronae Borealis Stars with MESA

R Coronae Borealis (RCB) stars form a small class of cool, carbon-rich supergiants that have almost no hydrogen. They undergo extreme, irregular declines in brightness of up to 8 magnitudes due to the formation of thick clouds of carbon dust. Two scenarios have been proposed for the origin of an RCB star: the merger of a CO/He white dwarf (WD) binary and a final helium-shell flash. We are using a combination of 3D hydrodynamics codes and the 1D MESA (Modules for Experiments in Stellar Astrophysics) stellar evolution code including nucleosynthesis to construct post-merger spherical models based on realistic merger progenitor models and on our hydrodynamical simulations, and then following the evolution into the region of the HR diagram where RCB stars are located. We are investigating nucleosynthesis in the dynamically accreting material of CO/He WD mergers which may provide a suitable environment for significant production of ^{18}O and the very low $^{16}\text{O}/^{18}\text{O}$ values observed.

Our MESA modeling consists of two steps: first mimicking the WD merger event using two different techniques, (a) by choosing a very high mass accretion rate with appropriate abundances and (b) by applying "stellar engineering" to an initial CO WD model to account for the newly merged material by applying an entropy

A technique has been developed which allows global average abundances of trace species to be derived from large heterogeneous data sets using the Spectral Synthesis Program [SSP] originally developed by Kunde & McGuire (1974). The method was applied to a large average of 24,000 individual spectra of Titan from the Composite Infrared Spectrometer (CIRS) on *Cassini*. The spectra were centered on the 581.6 cm^{-1} ν_4 band of $^{12}\text{C}_2\text{HD}$ and were taken in order to obtain a global average abundance for this species. The spectra covered a wide range of planetary latitudes and emission angles. The results obtained are generally in agreement with those derived by Coustenis et al. (2008) derived from their analysis of the ν_5 band of this species at 678 cm^{-1} .

References

Coustenis, A., Jennings, D. E., Jolly, A., Nilan, Y., Nixon, C. A., Vinatier, S., Gautier, D., Bjoraker, G. L., Romani, P. N., Carlson, R. C., & Flasar, F. 2008, *Icarus*, 197, 539-548.

Kunde, V. G. & McGuire, W. C. 1974, *JQSRT*, 14, 803-817

Author(s): Robert J. Boyle¹, Dr. Donald Jennings², Dr. Gordon Bjoraker²
Institution(s): 1. Dickinson College, 2. NASA/Goddard Space Flight Center

adjusting procedure. Second, we follow the post-merger evolution using a large nuclear reaction network including the effects of convective and rotational instabilities to the mixing of material in order to match the observed RCB abundances. MESA follows the evolution of the merger product as it expands and cools to become an RCB star. We then examine the surface abundances and compare them to the observed RCB abundances. We also investigate how long fusion continues in the He shell near the core and how this processed material is mixed up to the surface of the star. We then model the later evolution of RCB stars to determine their likely lifetimes and endpoints when they have returned to being a WD. Solving the mystery of how the RCB stars evolve will lead to a better understanding of other important types of stellar merger events such as Type Ia SNe.

Author(s): Geoffrey C Clayton¹, Amber Lauer¹, Emmanouil Chatzopoulos¹, Juhan Frank¹
Institution(s): 1. Louisiana State University

157.03 – Branching Fractions and $\log(\text{gf})$ s for Weak Lines of Co II connected to the Ground and Low Metastable Levels

New branching fraction (BF) measurements and $\log(\text{gf})$ s of Highly Reliable Lines (HRLs) of Co II are reported. Our measurements test and confirm earlier work by Salih et al. [1985] and Mullman et al. [1998] and expand the earlier BF measurements to include more weak and very weak HRLs. HRLs are UV lines that connect to the population reservoir levels including the ground and low metastable levels of Co^+ . Such levels contain most of the cobalt in the photospheres of typical F, G, and K stars used in abundance studies. HRLs are essentially immune to departures from Local Thermodynamic Equilibrium (LTE) because they connect to the primary reservoir levels. Lightly-populated high-lying levels of the ion and essentially all levels of the neutral atom have some possibility of being pulled out of LTE through various reactions. Weak and very weak HRLs are needed to determine Co abundances in higher metallicity stars while dominant branches are useful in low metallicity stars of abundance surveys. A large set of HRLs with reliable $\log(\text{gf})$ s is desired to avoid blending and saturation problems in photospheric studies. The relative abundance of Fe-peak

elements changes as a function of metallicity [e.g. Henry et al. 2010, Sneden et al. 2016] but contributions to the trends from nuclear physics effects in early stars need to be cleanly separated from effect due to limitations of classic photospheric models based on One Dimensional (1D) and LTE approximations. The 1D/LTE approximations of classic photospheric models, which work in well in metal rich dwarf stars such as the Sun, are a source of some concern in Metal Poor (MP) giant stars due to much lower electron and atom pressures. Our new measurements on HRLS of Co II are applied to determine stellar abundances in MP stars.

Henry, R. B. C., Cowan, J. J., & Sobeck, J. 2010, ApJ 709, 715
Mullman, K. L., Cooper, J. C., & Lawler, J. E. 1998, ApJ, 495, 503
Salih, S., Lawler, J. E., & Whaling, W. 1985, PhRvA, 31, 744
Sneden et al. 2016, ApJ 817:53
Supported by the Univ. of Wisconsin – Hilldale Foundation, NASA grant NNX16AE96G, and NSF grants AST-1516182 & AST1616040.

Author(s): James Edward Lawler³, Thomas Feigenson³, Chris Sneden², John J Cowan¹

Institution(s): 1. Univ. of Oklahoma - Norman, 2. Univ. of Texas - Austin, 3. Univ. of Wisconsin - Madison

157.04 – Rejuvenation of the Innocent Bystander: Results from a Pilot X-ray Study of Dwarf Carbon Stars

We present the results of a pilot study by the Chandra X-ray Observatory of X-ray emission from dwarf Carbon (dC) stars. Carbon stars were thought to be exclusively AGB stars but main sequence dwarfs showing carbon molecular bands appear to be the dominant variety. The existence of dC stars is surprising since dwarf stars cannot intrinsically produce carbon as an AGB star can. It is hypothesized that dC stars are polluted by an evolved companion star. Evidence of past pollution can appear in X-ray emission where increased coronal activity (“spin-up”) or mass accretion via a disk can be detected. Using the Chandra X-ray Observatory we detected X-ray photons in the vicinity of all the dC stars in our a pilot sample. For each detection we characterized the X-ray emission and compared to the emission expected from potential emission scenarios. Although the process that produces the X-ray emission from dC stars is presently unclear and our pilot sample is small, our results suggest that X-ray emission might be a universal characteristic of dC stars. Further examination of the X-ray emission plus future X-ray and multiwavelength observations will help us better understand the nature of these intriguing stars.

Author(s): Fernando Mazzoni², Rodolfo Montez¹, Paul Green¹

Institution(s): 1. Smithsonian Astrophysical Observatory, 2. University of Massachusetts Lowell

157.05 – STELLAR CONTRIBUTION FUNCTIONS IN THE AGE OF CHEMICAL STRATIFICATION

Contribution functions (CF's) were important tools to probe formation depths of features in the early numerical calculations of analytical stellar spectroscopy. In more recent work, CF's have played a minor role. Gray's (2005) text briefly discusses CF's, but CF's are not in Hubeny and Mihalas (2015). Gurtovenko and Sheminova (2015) give an extensive review of contribution functions in a recent preprint (arXiv:1505.00975). The realization that the atmospheres of certain stars are chemically stratified (Ryabchikova, Wade & LeBlanc, 2003, in IAU Symp. 210), and much subsequent work makes CF's of current interest. We employ new as well as older methods to compute CF's to find important layers, either for specific intensity or line depth for various points on the line profile. The most important layer is the one that causes the biggest change in the magnitude of the feature when the line absorption coefficient is set equal to zero for successive layers. This is readily done for a stratified or unstratified model. For an equivalent width, W , we calculate $\$(W-W_i/W)\$, where W_i is the equivalent width without absorption from the i^{th} layer. We concentrate on cases where$

stratification is most obvious, for example, the Ca II K-line profile in the roAp stars and HR 6000 (Castelli, et al. 2017, A&A, 601, A119).

Author(s): Charles Cowley⁴, Valya Sheminova¹, Fiorella Castelli³, Richard Monier²

Institution(s): 1. Astron. Obs. NAS, Ukraine, 2. LEISA, Observatoire de Paris, 3. Osservatorio Astronomico di Trieste, 4. University of Michigan

157.06 – Be Stars in M31

We identify Be candidate stars in M31 using two-epoch F625W + F658N photometry from HST/ACS+WFC3 combined with the Panchromatic Hubble Andromeda Treasury (PHAT) Catalog. Using the PHAT catalog allows us to extract stellar parameters such as surface temperature and gravity, thereby allowing us to identify the main sequence B type stars in the field of view. Be candidate stars are identified by comparing their HST narrow-band H α excess magnitudes with that predicted by Kurucz spectra. We find 314 Be candidate stars out of 5699 B + Be candidate stars (5.51%) in our first epoch and 301 Be candidate stars out of 5769 B + Be candidate stars (5.22%) in our second epoch. Our Be fraction, while lower than that of the SMC, LMC, and MW, is possibly consistent with the fact the M31 has a higher metallicity than the other galaxies because Be fraction varies inversely with metallicity. We note that earlier spectral types have the largest Be fraction, and that the Be fraction strictly declines as the spectral type increases to later types. We then match our Be candidate stars with clusters, establishing that 39 of 314 are cluster stars in epoch one and 36 of 301 stars are cluster stars in epoch two. We assign ages, using the cluster age to characterize cluster Be candidate stars and star formation histories to characterize field Be candidate stars. Finally, we determine which Be candidate stars exhibited disk loss or disk growth between epochs, finding that, of the Be stars that did not show source confusion or low SNR in one of the epochs, 65 / 265 (24.5%) showed disk loss or renewal, while 200 / 265 (75.5%) showed only small changes in H α excess. Our research provides context for the parameters of candidate Be stars in M31, which will be useful in further determining the nature of Be stars. This paper was supported by a grant from STScI via GO-13857.

Author(s): Matthew L Peters², John Wisniewski², Yumi Choi³, Ben Williams⁶, Jamie Lomax⁶, Karen Bjorkman⁵, Meredith Durbin⁶, Lent Cliff Johnson⁴, Alexia Lewis¹, Julie Lutz⁶, Aaron Sigut⁷, Aislynn Wallach⁶, Julianne Dalcanton⁶

Institution(s): 1. Ohio State University, 2. University of Oklahoma, 3. University of Arizona, 4. University of California, 5. University of Toledo, 6. University of Washington, 7. University of Western Ontario

157.07 – Modeling Protoplanetary Disks to Characterize the Evolution of their Structure

Stars form from gravitationally collapsing clouds of gas and dust. Most young stars retain a protoplanetary disk for a few million years. This disk's dust reemits stellar flux in the infrared, producing a spectral energy distribution (SED) observable by Spitzer and other telescopes. To understand the inner clearing of dust cavities and evolution in the SED, we used the Chiang & Goldreich two-layer approximation. We first wrote a python script based on refinements by Dullemond that includes a hot, puffed inner rim, shadowed mid region, flaring outer disk, and a variable inner cavity. This was then coupled with a Markov Chain Monte Carlo procedure to fit the observed SEDs of disks in the star forming Lupus region. The fitting procedure recovers physical characteristics of the disk including temperature, size, mass, and surface density. We compare the characteristics of circumstellar disks without holes and more evolved transition disks with cleared inner regions.

Author(s): Magdalena Allen², Nienke van der Marel¹, Jonathan Williams¹

Institution(s): 1. Institute for Astronomy, 2. University of California, Berkeley

157.08 – Accurate Masses, Radii, and Temperatures for the Eclipsing Binary V2154 Cyg, and Tests of Stellar Evolution Models

We report new spectroscopic observations of the F-type triple system V2154 Cyg, in which two of the stars form an eclipsing binary with a period of 2.6306303 ± 0.0000038 days. We combine the results from our spectroscopic analysis with published light curves in the uvby Strömgren passbands to derive the first reported absolute dimensions of the stars in the eclipsing binary. The masses and radii are measured with high accuracy to better than 1.5% precision. For the primary and secondary respectively, we find that the masses are $1.269 \pm 0.017 M_{\odot}$ and $0.7542 \pm 0.0059 M_{\odot}$, the radii are $1.477 \pm 0.012 R_{\odot}$ and $0.7232 \pm 0.0091 R_{\odot}$, and the temperatures are 6770 ± 150 K and 5020 ± 150 K. Current models of stellar evolution agree with the measured properties of the primary, but the secondary is larger than predicted. This may be due to activity in the secondary, as has been shown for other systems with a star of similar mass with this same discrepancy.

The SAO REU program is funded by the National Science Foundation REU and Department of Defense ASSURE programs under NSF Grant AST-1659473, and by the Smithsonian Institution. GT acknowledges partial support for this work from NSF grant AST-1509375.

Author(s): Jane Bright¹, Guillermo Torres²
Institution(s): 1. Denison University, 2. Harvard-Smithsonian, CfA

157.09 – K-KIDS: K Dwarfs and Their Companions. First Results from Radial Velocity Survey with CHIRON Spectrograph

We present the K-KIDS project, an effort to survey a large sample of K dwarfs and their companions, the KIDS. We are observing a carefully vetted equatorial sample (DEC = -30 to +30) of more than 1000 K dwarfs within 50 pc to make a comprehensive assessment of stellar, substellar and planetary companions with separations of 0.1 to 10,000 AU.

The initial sample of 1048 stars has been compiled using astrometric data from Hipparcos and photometric data from Tycho-2 and 2MASS. Four different imaging and spectroscopic surveys are underway. Here we present the strategy and initial results for our high-precision radial velocity survey for the closest companions using the CHIRON spectrograph on the CTIO/SMARTS 1.5m telescope. Individual measurements with CHIRON at $R = 80,000$ using ThAr wavelength calibration, indicate that for K dwarf radial velocity standards with $V = 5.8, 7.0$ and 8.0 yield precisions over 6 weeks of observing of 7.4 m/s, 9.8 m/s and 5.7 m/s. In the first two months, a core sample of 42 K dwarfs, including carefully selected calibration systems as well as previously unobserved stars, was observed every few nights to detect the radial velocity signals of close companions. In our calibration stellar systems, we have confirmed the suitability of CHIRON for our studies, by having found periodic radial velocity perturbations consistent with hot Jupiter and stellar companions previously detected. This set forms the foundation of our one-year survey of 100 K dwarfs with magnitudes as faint as $V = 11.5$, for which we should detect companions with masses as low as Jupiter.

In light of the promising performance and efficiency of the CHIRON spectrograph for a long-term radial velocity survey, we have expanded our initial sample using Gaia Data Release 1 to 1824 K dwarfs within 50 pc. Ultimately, the combination of all four surveys will provide an unprecedented portrait of K dwarfs and their kids.

This effort has been supported by the NSF through grant AST-1517413, and via observations made possible by the SMARTS Consortium.

Author(s): Leonardo Paredes¹, Todd Henry³, Daniel Nusdeo¹, J. Winters², Tolga Dincer⁴
Institution(s): 1. Georgia State University, 2. Harvard-Smithsonian Center for Astrophysics, 3. RECONS Institute, 4. Yale University

157.10 – Improved Masses and Radii for DA White Dwarfs

The mass-radius relation for white dwarf stars is a critical tool of modern stellar astrophysics. Nevertheless, it has proved difficult to precisely define this relationship with independent observations of the masses and radii of actual white dwarfs. Radii can be determined from observed stellar fluxes and parallaxes and masses estimated from determinations of spectroscopic surface gravities and measurements of gravitational redshifts. However, to estimate white dwarf masses and radii at the few percent level, precise fluxes, temperatures, gravities, and above all, parallax distances must be available. Using newly determined ground-based parallaxes; we determined new mass and radii estimates for half the stars discussed in Holberg et al. (2012, AJ 143, 68). This work was in part supported by NSF grant AST-1413537 to the UofA and AST-1358787 award to ERAU.

Author(s): Jay Holberg³, John P. Subasavage⁴, E. M. Sion¹, T. D. Oswalt², Hugh C. Harris⁴, Conard C. Dahn⁴
Institution(s): 1. Department of Astronomy and Astrophysics, Villanova University, 2. Embry-Riddle Aeronautical University, Daytona Beach, 3. University of Arizona Lunar and Planetary Lab, 4. US Naval Observatory, 10391 West Naval Observatory Road

157.11 – Millisecond Pulsar Timing Precision with NICER

The Neutron Star Interior Composition Explorer (NICER) is an array of 56 X-ray detectors mounted on the outside of the International Space Station. It allows high-precision timing of millisecond pulsars (MSPs) without the pulse broadening effects due to dispersion and scattering by the interstellar medium that plague radio timing. We present initial timing results from four months of NICER data on the MSPs B1937+21, B1821-24, and J0218+4232, and compare them to simulations and theoretical models for X-ray times-of-arrival, and radio observations.

Author(s): Julia Deneva¹, Paul S Ray⁶, Scott Ransom⁵, Kent S. Wood⁷, Matthew T Kerr⁶, Andrea Lommen³, Zaven Arzoumanian⁴, Kevin Black⁴, Keith C Gendreau⁴, Natalia Lewandowska², Craig B. Markwardt⁴, Samuel Price⁴, Luke Winternitz⁴
Institution(s): 1. George Mason University, 2. Green Bank Observatory, 3. Haverford College, 4. NASA GSFC, 5. National Radio Astronomy Observatory, 6. Naval Research Laboratory, 7. Praxis

157.12 – Localizing New Pulsars with Intensity Mapping

Although low-frequency, single dish pulsar surveys provide an efficient means of searching large regions of sky quickly, the localization of new discoveries is poor. For example, discoveries from 350 MHz surveys using the Green Bank Telescope (GBT) have position uncertainties up to the FWHM of the telescope's "beam" on the sky, over half a degree! Before finding a coherent timing solution (requires 8-12 months of dedicated timing observations) a "gridding" method is usually employed to improve localization of new pulsars, whereby a grid of higher frequency beam positions is used to tile the initial error region. This method often requires over an hour of observing time to achieve arcminute-precision localization (provided the pulsar is detectable at higher frequencies).

Here, we describe another method that uses the same observing frequency as the discovery observation and scans over Right Ascension and Declination directions around the nominal position. A Gaussian beam model is fit to folded pulse profile intensities as a function of time/position to provide improved

localization. Using five test cases, we show that intensity mapping localization at 350 MHz with the GBT yields pulsar positions to 1 arcminute precision, facilitating high-frequency follow-up and higher significance detections for future pulsar timing. This method is also well suited to be directly implemented in future low-frequency drift scan pulsar surveys (e.g. with the Five hundred meter Aperture Spherical Telescope; FAST).

Author(s): Joe Swiggum¹, Peter Gentile²
Institution(s): 1. UW-Milwaukee, 2. West Virginia University

157.13 – Early Results from NICER Observations of Accreting Neutron Stars

The Neutron Star Interior Composition Explorer (NICER) offers significant new capabilities for the study of accreting neutron stars relative to previous X-ray missions including large effective area, low background, and greatly improved low-energy response. The NICER Burst and Accretion Working Group has designed a 2 Ms observation program to study a number of phenomena in accreting neutron stars including type-I X-ray bursts, superbursts, accretion-powered pulsations, quasi-periodic oscillations, and accretion disk reflection spectra. We present some early results from the first six months of the NICER mission.

Author(s): Deepto Chakrabarty⁴, Feryal Özel¹⁰, Zaven Arzoumanian⁵, Keith C Gendreau⁵, Peter Bult⁵, Ed Cackett¹³, Jerome Chenevez¹, Andy Fabian¹¹, Sebastien Guillot⁸, Tolga Guver³, Jeroen Homan², Laurens Keek⁵, Frederick Lamb⁹, Renee Ludlam¹², Simin Mahmoodifar⁵, Craig B. Markwardt⁵, Jon M Miller¹², Dimitrios Psaltis¹⁰, Tod E Strohmayer⁵, Colleen A. Wilson-Hodge⁶, Michael T. Wolff⁷

Institution(s): 1. DTU Space, 2. Eureka Scientific, 3. Istanbul University, 4. MIT, 5. NASA/GSFC, 6. NASA/MSFC, 7. NRL, 8. PUC, 9. UIUC, 10. University of Arizona, 11. University of Cambridge, 12. University of Michigan, 13. Wayne State University

157.14 – Joint Meteorological Statistics of Observing Sites for the Event Horizon Telescope

The Event Horizon Telescope (EHT) aims to resolve the general relativistic shadow of Sgr A*, the supermassive black hole at the center of our galaxy, via Very Long Baseline Interferometry (VLBI) measurements with a multinational array of radio observatories. In order to optimize the scheduling of future observations, we have developed tools to model the atmospheric opacity at each EHT site using the past 10 years of Global Forecast System (GFS) data describing the atmospheric state. These tools allow us to determine the ideal observing windows for EHT observations and to assess the suitability and impact of new EHT sites. We describe our modeling framework, compare our models to in-situ measurements at EHT sites, and discuss the implications of weather limitations for planned extensions of the EHT to higher frequencies, as well as additional sites and observation windows.

Author(s): Rodrigo Eduardo Lope Córdoba Rosado¹, Sheperd Doeleman², Scott Paine², Michael Johnson²

Institution(s): 1. Harvard-Smithsonian Center for Astrophysics, 2. Smithsonian Astrophysical Observatory
Contributing team(s): Event Horizon Telescope (EHT)

102 – First Data from the Pan-STARRS Survey and How to Use It

The Pan-STARRS survey offers an invaluable resource to astronomy, providing very high photometric and astrometric quality and significant depth over the three-fourths of the sky that are above -30 degrees. Pan-STARRS Data Release 1 is now available from the MAST archive and provides a static view of average magnitudes. DR2 is expected to become available in December and will provide measurements from the many individual images that were taken, thereby enabling time-series studies. This Special Session will describe Pan-STARRS and will show some of the first science being done.

102.01 – The Pan-STARRS1 Surveys

157.15 – Accretion Geometry of Ultra-Luminous X-ray Source Population Study

Eddington luminosities can be used to determine the maximum theoretical luminosity of an accreting system. Ultra-Luminous X-ray sources (ULX's) are a class of high energy X-Ray emitters that seem to break with typical Eddington limited accretion luminosities. However, when using them to describe intermediate mass black holes (IMBH), ULXs obtain a luminosity greater than what the stellar mass black holes could achieve. Luminosities this high cannot be explained by normal accretion physics, therefore, another aspect of the IMBH must be considered. In this presentation, multiple ULX luminosities are analyzed and compared directly to multiple black hole accretion geometries. From this analysis, we hope to find a model that best fits the luminosity of these IMBHs. This, in turn, will allow us to better understand the accretion physics that is occurring within these unique systems.

Author(s): William Baker¹, Sean Spencer¹, Parviz Ghavamian¹

Institution(s): 1. Towson University

157.16 – Case Study of Data Mining in Observational Astronomy: The Search for New OB Stars in the Small Magellanic Cloud

OB stars are the most luminous and massive stars, living short lives and exerting a disproportionate influence on their environments. They are key to understanding progenitors of gravitational wave sources and reionization of the early Universe. To detect new OB stars, we combine photometric catalog data with TLUSTY and ATLAS9 stellar atmospheres. This method is also believed to be sensitive to elusive “stripped” stars, thought to lose their hydrogen envelope through binary interaction.

OB stars are intrinsically luminous, so complete populations are assumed for local group galaxies such as the Small Magellanic Cloud. Our findings challenge this, as we find 26 new OB candidates. Spectroscopy of 7 candidates shows a 100% detection rate. Most interestingly, 5 of our candidates are consistent with “stripped” stars.

To date only 5 “stripped” candidates have been found serendipitously (e.g. HD 45166) as current methods are not sensitive to them. Our work doubles the sample of detected candidates, highlighting that our approach is the first to identify them in a targeted, systematic way. The finding of “stripped” stars could rewrite our understanding of the early Universe, offering an alternative hypothesis to Wolf-Rayet driven cosmic reionization.

Author(s): Cormac Larkin², Jorick Vink¹, Venu Kalari³, Jose Groh²

Institution(s): 1. Armagh Observatory, 2. Trinity College Dublin & Armagh Observatory, 3. Universidad de Chile

The Pan-STARRS1 Surveys are complete and the first data release, DR1, is available from the Mikulski Archive for Space Telescopes (MAST) at the Space Telescope Science Institute. The data include a database of measured attributes of 3 billion objects, stacked images, and metadata of the 3pi Steradian Survey. The DR1 contains all stationary objects with mean and stack photometry registered on the GAIA astrometric frame. DR2 is in preparation and will be released this winter with all the individual epoch images and time domain photometry and forced photometry on the individual epoch images. The characteristics of the Pan-STARRS1 Surveys will be presented, including image quality, depth, cadence, and coverage. Measured attributes

include PSF model magnitudes, aperture magnitudes, Kron Magnitudes, radial moments, Petrosian magnitudes, DeVaucoulers, Exponential, and Sersic magnitudes for extended objects. Images include total intensity, variance, and masks.

An overview of the Pan-STARRS1 Surveys and data releases will be presented together with a brief description of the data collected since the end of the PS1 Science Consortium surveys, and the plans for the upcoming survey with PS1 and PS2 beginning in February 2018.

Author(s): Kenneth Chambers¹
Institution(s): 1. *University of Hawaii*
Contributing team(s): The Pan-STARRS Team

102.02 – The Pan-STARRS pipeline and data products

I will give a brief overview of the pipeline, database, and data products for Pan-STARRS1 data release 1 (DR1) and data release 2 (DR2). DR1 and DR2 provides access to data from the Pan-STARRS1 3pi survey, a survey which covers $\frac{3}{4}$ of the sky over 4 years (2010-2014), everything with a declination greater than -30 , in 5 filters (g,r,i,z,y), with at least 12 epochs per filter per area of sky. DR1, released in December 2016, and available to the public at <http://stsci.panstarrs.edu>, consists of two parts: the stacked images with a 5 sigma depth of (23.3,23.2,23.1,22.3,21.3) for (g,r,i,z,y), and the catalog database, which consists of 10 billion distinct objects, their mean properties from single exposures, and stack photometry. DR2, to be released early 2108, will contain the individual exposure images, with a 5 sigma depth of (22.0,21.8,21.5,20.9,19.7) for (g,r,i,z,y), and the time domain catalogs, from the 374k individual exposures taken for the 3pi survey. I will primarily focus on the catalog database, describing a subset of the tables and different use cases for them. Specifically, I will describe the major tables and metadata of DR1 - objects, their mean properties, and stack photometry, when different tables should be used, and basics on how to filter the data.

Author(s): Heather Flewelling¹
Institution(s): 1. *University of Hawaii*

102.03 – Precision Photometry and Astrometry from Pan-STARRS

The Pan-STARRS 3pi Survey has been calibrated with excellent precision for both astrometry and photometry. The Pan-STARRS Data Release 1, opened to the public on 2016 Dec 16, provides photometry in 5 well-calibrated, well-defined bandpasses (grizy) astrometrically registered to the Gaia frame. Comparisons with other surveys illustrate the high quality of the calibration and provide tests of remaining systematic errors in both Pan-STARRS and those external surveys. With photometry and astrometry of roughly 3 billion astronomical objects, the Pan-STARRS DR1 has substantial overlap with Gaia, SDSS, 2MASS and other surveys. I will discuss the astrometric tie between Pan-STARRS DR1 and Gaia and show comparisons between Pan-STARRS and other large-scale surveys.

Author(s): Eugene A Magnier¹
Institution(s): 1. *University of Hawaii*
Contributing team(s): Pan-STARRS Team

102.04 – The Milky Way's Dust in Three Dimensions with PS1

The Milky Way's dust is of basic importance in astronomy. It is both crucial to the formation of stars and is a pervasive observational nuisance. Despite the dust's importance, existing dust maps are largely limited to two dimensions, with the distance to the dust unknown. Data from the Pan-STARRS1 survey has allowed us to map dust in three dimensions in unprecedented detail. In this talk, I will describe how we use observations of stars in the Milky Way to map dust and its properties in three dimensions. Our map covers three quarters of the sky and has 20 mmag E(B-V) accuracy, reaching roughly 4

kpc into the Galactic plane. The map allows stars to be dereddened in three dimensions, enabling a wide variety of science in the Milky Way.

Author(s): Edward Schlafly¹, Gregory M Green²
Institution(s): 1. *LBL*, 2. *Stanford*

102.05 – Using PS1 and Type Ia Supernovae To Make Most Precise Measurement of Dark Energy To Date

I will review recent results that present optical light curves, redshifts, and classifications for 361 spectroscopically confirmed Type Ia supernovae (SNIa) discovered by the Pan-STARRS1 (PS1) Medium Deep Survey. I will go over improvements to the PS1 SN photometry, astrometry and calibration that reduce the systematic uncertainties in the PS1 SN Ia distances. We combined distances of PS1 SNe with distance estimates of SNIa from SDSS, SNLS, various low-z and HST samples to form the largest combined sample of SN Ia consisting of a total of ~ 1050 SN Ia ranging from $0.01 < z < 2.3$, which we call the 'Pantheon Sample'. Photometric calibration uncertainties have long dominated the systematic error budget of every major analysis of cosmological parameters with SNIa. Using the PS1 relative calibration, we have reduced these calibration systematics to the point where they are similar in magnitude to the other major sources of known systematic uncertainties: the nature of the intrinsic scatter of SNIa and modeling of selection effects. I will present measurements of dark energy which are now the most precise measurements of dark energy to date.

Author(s): Daniel Scolnic¹
Institution(s): 1. *KICP at University of Chicago*
Contributing team(s): Pan-STARRS

102.06 – Tidal Disruption Events in Pan-STARRS1

The Pan-STARRS1 (PS1) Medium Deep Survey made an important contribution to the study of tidal disruption events (TDEs) by discovering TDEs on the rise to peak and enabling prompt spectroscopic follow-up observations. The two PS1 TDEs, PS1-10jh and PS1-11af, were the first TDEs to have detailed light curves and transient broad line features in their spectra, both of which could be used to constrain the physical parameters of the events. I will describe how cotemporal NUV observations from the GALEX Time Domain Survey were critical in the identification of these relatively rare events as bonifide TDEs among the PS1 transient alert stream. I will also show how we can use the PS1+GALEX data set as a training set to prepare for culling TDEs from the deluge of transients to be produced by the next generation of optical time domain surveys, in order that they may be used as effective probes of supermassive black hole demographics and accretion physics.

Author(s): Suvi Gezari¹
Institution(s): 1. *University of Maryland*

102.07 – Transient Science from PanSTARRS1

Operating between 2009 and 2014, the PanSTARRS1 survey has made significant contributions to our understanding of the full landscape of astronomical transients. I will highlight key scientific results from the study of super-luminous supernova, core-collapse supernovae, rapidly-evolving transients, and low-luminosity transients. I will also discuss factors in the survey design of PS1 that made these discoveries possible, and implications for the next generation of surveys such as LSST.

Author(s): Maria Drout¹
Institution(s): 1. *Carnegie Observatories*
Contributing team(s): PanSTARRS1

102.08 – Transformative Small Body Science Enabled with Pan-STARSS Survey Data

In the first 5 Myr of Solar System formation, gas imprinted a local chemical signature on the planetesimals which were subsequently

redistributed during planet formation. Decades-long ground- and space-based studies have tried to map our solar system's protoplanetary disk chemistry using volatiles in comets. We now know that comet volatiles (H₂O, CO, CO₂ and organics) have distinct chemical classes. This data contradicts traditional ideas that all volatile-rich bodies formed in the outer disk. In-situ space comet missions have suggested, however, that comets preserve their pristine volatile inventory, and perhaps even their heritage of ices prior to the protoplanetary disk. Recently, a profusion of dynamical models has been developed that can reproduce some of the key characteristics of today's solar system. Some models require significant giant planet migration, while others do not. The UH-led Pan-STARRS1 survey (PS1) can offer transformative insight into small bodies and the early solar system, providing a preview of LSST.

In 2013 PS1 discovered an asteroidal object on a long-period comet orbit, the first of a class of tailless objects informally called Manxes. The second Manx discovered had a surface composition similar to inner solar system rocky S-type material, suggesting the intriguing possibility that we are looking at fresh inner solar system Earth-forming material, preserved for billions of years in

103 – NASA Decadal Preparations I: Large-scale Studies

103.01 – Origins Space Telescope

The Origins Space Telescope (OST) is the mission concept for the Far-Infrared Surveyor, a study in development by NASA in preparation for the 2020 Astronomy and Astrophysics Decadal Survey. Origins is planned to be a large aperture, actively-cooled telescope covering a wide span of the mid- to far-infrared spectrum. Its spectrographs will enable 3D surveys of the sky that will discover and characterize the most distant galaxies, Milky-Way, exoplanets, and the outer reaches of our Solar system. Origins will enable flagship-quality general observing programs led by the astronomical community in the 2030s. The Science and Technology Definition Team (STDT) would like to hear your science needs and ideas for this mission. The team can be contacted at firsurveyor_info@lists.ipac.caltech.edu. This presentation will provide a summary of the OST STDT, our completed first mission concept and an introduction to the second concept that will be studied at the study center in 2018. This presentation will also summarize key science drivers and the key study milestones between 2018 and 2020.

Author(s): Asantha Cooray¹

Institution(s): 1. University of California Irvine

Contributing team(s): Origins Space Telescope Study Team

103.02 – The LUVOIR Large Mission Concept

LUVOIR is one of four large mission concepts for which the NASA Astrophysics Division has commissioned studies by Science and Technology Definition Teams (STDTs) drawn from the astronomical community. We are currently developing two architectures: Architecture A with a 15.1 meter segmented primary mirror, and Architecture B with a 9.2 meter segmented primary mirror. Our focus in this presentation is the Architecture A LUVOIR. LUVOIR will operate at the Sun-Earth L₂ point. It will be designed to support a broad range of astrophysics and exoplanet studies. The initial instruments developed for LUVOIR Architecture A include 1) a high-performance optical/NIR coronagraph with imaging and spectroscopic capability, 2) a UV imager and spectrograph with high spectral resolution and multi-object capability, 3) a high-definition wide-field optical/NIR camera, and 4) a high resolution UV/optical spectropolarimeter. LUVOIR will be designed for extreme stability to support unprecedented spatial resolution and coronagraphy. It is intended to be a long-lifetime facility that is both serviceable, upgradable, and primarily driven by guest observer science programs. In this presentation, we will describe the observatory, its instruments, and survey the transformative science LUVOIR can accomplish.

the Oort cloud. Currently 10-15 of these objects are discovered each year, with PS1 dominating the discoveries. The number of rocky inner solar system Manx objects can be used to constrain solar system formation models. PS1 is also very good at discovering faint active objects at large distances, including the remarkable discovery of a comet active beyond 16 au from the sun. By searching the PS1 database once these discoveries are made, it is possible to extend the orbit arc backwards in time, allowing us to model the activity, and understand the chemistry and physics of ices and activity in the outer solar system. These discoveries will help us tie together chemistry and dynamics in our solar system with new resolved ALMA observations of protoplanetary disks.

Support from NSF grants AST-1617015, 1413736.

Author(s): Karen J Meech³, Jan T Kleyna³, Jacqueline V Keane³, Olivier R Hainaut², Marco Micheli¹

Institution(s): 1. ESA SSA-NEO Coordination Centre, 2. European Southern Observatory, 3. Institute for Astronomy

Author(s): John O'Meara¹

Institution(s): 1. Saint Michael's College

Contributing team(s): LUVOIR Science and Technology Definition Team

103.03 – The Habitable Exoplanet Imaging Mission (HabEx)

The Habitable Exoplanet Imaging Mission (HabEx) is a candidate flagship mission being studied by NASA and the astrophysics community in preparation of the 2020 Decadal Survey. The HabEx mission concept is a large (~4 to 6.5m) diffraction-limited optical space telescope, providing unprecedented resolution and contrast in the optical, with likely extensions into the near UV and near infrared domains. We discuss the primary science goals of HabEx. First, HabEx will survey a large sample of stars to search for planets potentially habitable planets: roughly Earth-sized planets with separations consistent with being in the habitable zones of their parent stars. Promising candidates will be followed up in detail, in order to characterize their orbits and atmospheres, and so confirm that they are indeed terrestrial-sized planets in the habitable zones of their parent stars, and search for signatures of habitability and potentially biosignatures. Second, HabEx will perform a 'deep dive' survey of roughly a dozen of the nearest and most promising stellar systems, providing the first complete "family portraits" of planets around our nearest Sun-like neighbors, and placing the solar system in the context of a diverse set of these planetary systems. Additionally, HabEx will enable a wide range of other astrophysical investigations, including detailed characterization of the properties of nearby stars and galaxies.

Author(s): B. Scott Gaudi¹

Institution(s): 1. The Ohio State University

Contributing team(s): The Habitable Exoplanet Imaging Mission Science and Technology Definition Team

103.04 – Lynx mission concept study

Lynx is an observatory-class mission, featuring high throughput, exquisite angular resolution over a substantial field of view, and high spectral resolution for point and extended X-ray sources. The design requirements provide a tremendous leap in capabilities relative to missions such as Chandra and Athena. Lynx will observe the dawn of supermassive black holes through detection of very faint X-ray sources in the early universe and will reveal the "invisible drivers" of galaxy and structure formation through observations of hot, diffuse baryons in and around the galaxies. Lynx will enable breakthroughs across all of astrophysics, ranging from detailed understanding of stellar activity including effects on habitability of associated planets to population statistics of neutron stars and black holes in the Local

Group galaxies, to earliest groups and clusters of galaxies, and to cosmology

Author(s): Alexey Vikhlinin¹

Institution(s): 1. *Smithsonian Astrophysical Observatory*

104 – Detection of Extrasolar Planets I

104.01 – Novel Optical SETI Observations of Three Exoplanets

We report on observations of three nearby stars (Trappist-1, GJ 422 and Wolf 1061) that possess exoplanets located in their respective habitable zones to search for optical signals generated by an advanced alien civilization. Using the photon data collected with the Berkeley Visible Image Tube attached to the 10m Southern African Large Telescope, we searched for very high amplitude events in the pulse height distributions that statistically could only be produced by non-astrophysical means such as an optical laser used for communications purposes.

Assuming that a purported ET civilization has access to an orbiting 10m mirror and an optical laser to send signals over the three sight-lines to Earth, we derive upper limits to the output power of their lasers which might be used for inter-stellar communication.

Author(s): Barry Welsh¹, John Valleraga³, Marissa Kotze², Jonathan Wheatley³

Institution(s): 1. *Eureka Scientific*, 2. *South African Astronomical Observatory*, 3. *UC Berkeley*

104.02 – Direct imaging search for the "missing link" in giant planet formation

While transit and radial velocity detection techniques have probed giant planet populations at close separations (within a few au), current direct imaging surveys are finding giant planets at separations of 10s-100s au. Furthermore, these directly imaged planets are very massive, including some with masses above the deuterium burning limit. It is not certain whether these objects represent the high mass end of planet formation scenarios or the low mass end of star formation. We present a direct imaging survey to search for the "missing link" population between the close-in RV and transiting giant planets and the extremely distant directly imaged giant planets (i.e. giant planets between 5-10 au). Finding and characterizing this population allows for comparisons with the formation models of closer-in planets and connects directly imaged planets with closer-in planets in semi-major axis phase space. In addition, microlensing surveys have suggested a large reservoir of giant planets exist in this region. To find these "missing link" giant planets, our survey searches for giant planets around M-stars. The ubiquity of M-stars provide a large number of nearby targets and their L-band contrast with planets allow for sensitivities to smaller planet masses than surveys conducted at shorter wavelengths. Along with careful target selection, we use Keck's L-band vector vortex coronagraph to enable sensitivities of a few Jupiter masses as close as 4 au to their host stars. We present our completed 2-year survey targeting 200 young (10-150 Myr), nearby M-stars and our ongoing work to follow-up over 40 candidate objects.

Author(s): Henry Ngo², Dimitri Mawet¹, Garreth Ruane¹, Wenhao Xuan⁴, Brendan Bowler⁶, Therese Cook⁵, Zoe Zawol³
Institution(s): 1. *California Institute of Technology*, 2. *NRC Herzberg Astronomy & Astrophysics*, 3. *Pasadena High School*, 4. *Pomona College*, 5. *University of California, Los Angeles*, 6. *University of Texas at Austin*

104.03 – A Possible Technology Development Path to Direct Imaging of Exo-Earths from Space

We describe a possible roadmap to achieving the technological capability to search for biosignatures on an Earth-like exoplanet from a future space telescope. The detection of Earth-like exoplanets in the habitable zone of their stars, and their spectroscopic characterization in a search for biosignatures, requires starlight suppression that exceeds the current best

ground-based performance by orders of magnitude. The required planet/star brightness ratio of order $1e-10$ at visible wavelengths can be obtained by blocking stellar photons with an occulter, either externally (a starshade) or internally (a coronagraph) to the telescope system, and managing diffracted starlight, so as to directly image the exoplanet in reflected starlight. Coronagraph instruments require advancement in telescope aperture (either monolithic or segmented), aperture obscurations (obscured by secondary mirror and its support struts), and wavefront error sensitivity (e.g. line-of-sight jitter, telescope vibration, polarization). The starshade, which has never been used in a science application, benefits a mission by being decoupled from the telescope, allowing a loosening of telescope stability requirements. In doing so, it transfers the difficult technology from the telescope system to a large deployable structure (tens of meters to greater than ~ 100 m in diameter) that must be positioned precisely at a distance of tens of thousands of kilometers from the telescope. Two ongoing mission concept studies, HabEx and LUVOIR, include the direct imaging of Earth-sized habitable exoplanets as a central science theme.

Author(s): Nicholas Siegler¹

Institution(s): 1. *Jet Propulsion Laboratory*

104.04 – Looking for transiting warm Jupiters - win some, lose some

We have initiated a project to discover transiting warm Jupiters - gas giant planets receiving stellar irradiation below 10^8 erg s⁻¹ cm⁻², corresponding to orbital periods beyond about 10 days around Sun-like stars, through follow-up of transiting candidates identified by K2 and other transit surveys. Our goals are to (1) investigate the inflated gas giants conundrum, (2) study the mystery of hot Jupiters orbital evolution, and (3) identify targets for extending exoplanet atmosphere and stellar obliquity studies beyond the hot Jupiters class. This project has so far resulted in the discovery of two new transiting warm Jupiters (K2-114b and K2-115b), and the identification of three statistically validated planets as low-mass stars.

Author(s): Avi Shporer⁵, George Zhou², Andrew Vanderburg², Benjamin Fulton¹, Allyson Bieryla², David Ciardi⁸, Karen Collins¹⁹, Néstor Espinoza¹¹, Howard Isaacson¹⁴, Timothy Morton¹², Guillermo Torres², James Armstrong¹⁵, Daniel Bayliss¹⁰, Joao Bento⁶, Perry Berlind², Francois Bouchy¹⁰, Mike Calkins², Andrew Cameron¹⁷, William Cochran¹⁸, Knicole Colon⁹, Ian Crossfield⁵, Diana Dragomir⁵, Gil Esquerdo², Andrew Howard¹, Steve Howell⁷, John Kielkopf¹⁶, David Latham², Felipe Murgas³, Ramotholo Sefako¹³, Evan Sinukoff¹, Robert Siverd⁴, Stephane Udry¹⁰

Institution(s): 1. *Caltech*, 2. *Harvard CfA*, 3. *Instituto de Astrofísica de Canarias*, 4. *Las Cumbres Observaory*, 5. *MIT*, 6. *Mount Stromlo Observatory*, *Australian National University*, 7. *NASA Ames Research Center*, 8. *NASA Exoplanet Science Institute/Caltech*, 9. *NASA Goddard Space Flight Center*, 10. *Observatoire Astronomique de l'Université de Geneve*, 11. *Pontificia Universidad Católica de Chile*, 12. *Princeton University*, 13. *South African Astronomical Observatory*, 14. *University of California, Berkeley*, 15. *University of Hawaii*, 16. *University of Louisville*, 17. *University of St Andrews*, 18. *University of Texas, Austin*, 19. *Vanderbilt University*
Contributing team(s): TECH

104.05 – Three Super-Earths Transiting the nearby star GJ 9827

We report on the discovery of three transiting planets around GJ-9827. The planets have radii of $1.75 R_{\oplus}$, $1.36 R_{\oplus}$, and $2.11 R_{\oplus}$.

and periods of 1.20896, 3.6480, and 6.2014 days, respectively. The detection was made in Campaign 12 observations as part of our $\{K_2\}$ survey of nearby stars. GJ-9827 is a $V = 10.39$ mag K6V star at distance of 30.3 ± 1.6 parsecs and the nearest star to be found hosting planets by $\{K_2\}$ and $\{K_2\}$. The radial velocity follow-up, high resolution imaging, and detection of multiple transiting objects near commensurability drastically reduce the false positive probability. The orbital periods of GJ-9827-b, c and d planets are very close to the 1:3:5 mean motion resonance. Our preliminary analysis shows that GJ-9827 planets are excellent candidates for atmospheric observations. Besides, the planetary radii span both sides of the rocky and gaseous divide, hence the system will be an asset in expanding our understanding of the threshold.

Author(s): Prajwal Niraula¹

Institution(s): 1. Wesleyan University

Contributing team(s): Seth Redfield, Fei Dai, Oscar Barragán, Davide Gandolfi, P. Wilson Cauley, Teruyuki Hirano, Judith Korth, Alexis M., S. Smith, Jorge Prieto-Arranz, Sascha Grziwa, Malcolm Fridlund, Carina M. Persson, Anders Bo Justesen, Joshua N. Winn, Simon Albrecht, William D. Cochran, Szilard Csizmadia, Girish M. Duvvuri, Michael Endl, Artie P. Hatzes, John H. Livingston, Norio Narita, David Nespral, Grzegorz Nowak, Martin Pätzold, Enric Palle, and Vincent Van Eylen.

104.06D – System Architectures Near the 2:1 Resonance

Uncovering the architectures of planetary systems give insight into their formation and evolution. For example, the protoplanetary disk in multi-planet systems can drive adjacent planets into mean-motion resonances (such as the 2:1), while simultaneously damping their eccentricities. On the other hand, planet-planet scattering will produce single planets with eccentric orbits.

In the RV signal, there is a degeneracy between models with two planets on circular orbits near the 2:1 period ratio and single planets on eccentric orbits. Historically, single planet models have been favored on simplicity grounds. However, the prominence of the 2:1 period ratio for systems observed by Kepler motivates additional scrutiny for single eccentric systems.

We analyzed 95 planetary systems from the NASA Exoplanet Archive that are reported as single planet systems. We fit models of single eccentrics, circular doubles with a period ratio of 2:1, and circular doubles with a period ratio near 2.17:1 to the data. We computed the Bayes factors between each model in order to determine which is more likely given the current data. We find a significant fraction of these systems prefer double planet models. New observations are being planned to further break the degeneracy for these systems. This fraction suggests that disk-migration may be more important than the currently reported parameters propose.

Author(s): John Boisvert², Jason H. Steffen², Benjamin E. Nelson¹

Institution(s): 1. Northwestern University, 2. University of Nevada, Las Vegas

104.07 – A Binary System in the Hyades Cluster Hosting a Neptune-Sized Planet

105 – AGN, QSO, Blazars I

105.01 – Uncovering Heavily Obscured AGN with WISE and NuSTAR

Supermassive black holes gain their mass through accretion as active galactic nuclei (AGN), but it is now clear that a large fraction of this growth is "hidden" behind large columns of gas and dust. Of particular interest are Compton-thick (CT) AGN, with columns $N_H > 10^{24} \text{ cm}^{-2}$, that have been difficult to identify using optical or soft X-ray surveys. We will present two studies of heavily obscured AGN that aim to uncover more of the full

We report the discovery of a Neptune-size planet ($R_p = 3.0 R_{\text{Earth}}$) in the Hyades Cluster. The host star is in a binary system, comprising a K5V star and M7/8V star with a projected separation of 40 AU. The planet orbits the primary star with an orbital period of 17.3 days and a transit duration of 3 hours. The host star is bright ($V = 11.2$, $J = 9.1$) and so may be a good target for precise radial velocity measurements. The planet is the first Neptune-sized planet to be found orbiting in a binary system within an open cluster. The Hyades is the nearest star cluster to the Sun, has an age of 625-750 Myr, and forms one of the fundamental rungs in the distance ladder; understanding the planet population in such a well-studied cluster can help us understand and set constraints on the formation and evolution of planetary systems.

Author(s): Adina Feinstein⁴, David Ciardi², Ian Crossfield⁶, Joshua Schlieder⁹, Erik Petigura⁸, Trevor J David¹, Makennah Bristow⁷, Rahul Patel², Lauren Arnold³, Björn Benneke¹⁰, Jessie Christiansen², Courtney Dressing¹¹, Benjamin Fulton¹, Andrew Howard¹, Howard Isaacson¹¹, Evan Sinukoff¹, Beverly Thackeray⁵

Institution(s): 1. Cahill Center for Astrophysics, Caltech, 2. Caltech/IPAC-NASA Exoplanet Science Institute, 3. Center for Marine and Environmental Studies, University of the Virgin Islands, Saint Thomas, 4. Department of Physics and Astronomy, Tufts University, 5. Department of Physics, California State University San Bernardino, 6. Department of Physics, MIT, 7. Department of Physics, UNC at Asheville, 8. Division of Geological and Planetary Sciences, Caltech, 9. Exoplanets and Stellar Astrophysics Laboratory, Code 667, NASA Goddard Space Flight Center, 10. Université of Montréal, 11. University of California at Berkeley

104.08 – RVxK2: Simultaneous PRV Program with Kepler/K2 Campaign 16

Introducing the RVxK2 program: simultaneous precise radial velocity (PRV) observations with Kepler/K2 Campaign 16, from Dec 7 2017 through Feb 26 2018 (website: rvxk2.com). K2 will provide short cadence photometric data on five carefully selected stars, including the brightest M dwarf in C16 field, a solar analog, and three bright G/K subgiants. K2 will also provide long cadence data on the next three brightest K or M dwarfs in the C16 field. Our campaign includes several precise RV instruments around the globe, including Keck/HIRES, APF, IRTF/iSHELL, SONG, MINERVA, PARAS, representing the first organized, extensive, simultaneous RV campaign with space photometry. Our primary science goal is to characterize and understand stellar jitter and stellar activity. This RV+K2 campaign will provide the community with an unprecedented dataset of RV spectra and precise photometry to study stellar jitter on a broad range of time scales, from minutes to 80 days. We will gather the first ever RV+photometry dataset aiming at characterizing stellar granulation, the most poorly understood term among all astrophysical sources of stellar jitter. This project will also enable the first asteroseismic studies with simultaneous precise RVs and photometry, while searching for planets in the brightest nearby G to M dwarfs in the field.

Author(s): Sharon Xuesong Wang¹

Institution(s): 1. Carnegie DTM

Contributing team(s): The RVxK2 team

population of "hidden" growing black holes: (1) Analysis of the spectral energy distributions of millions of galaxies with photometry from WISE (mid-IR), UKIDSS (near-IR), and SDSS (optical), that uncovers large populations of weak or heavily buried AGN, and (2) NuSTAR observations of a sample of candidate highly obscured AGN, selected from WISE and SDSS photometry, and confirmed using SALT and Keck spectroscopy. The NuSTAR data reveal the existence of powerful CT quasars with extremely large columns $N_H > 10^{25} \text{ cm}^{-2}$, which may represent a significant fraction of previously hidden black hole

growth. This work is supported by NASA grant numbers NNX16AN48G and NNX15AP24G, and the NSF through grant numbers 1515364 and 1554584.

Author(s): Ryan C. Hickox¹, Christopher M. Carroll¹, Wei Yan¹, Michael A DiPompeo¹, Kevin N Hainline²
Institution(s): 1. Dartmouth College, 2. Steward Observatory, University of Arizona
Contributing team(s): NuSTAR Obscured AGN Team

105.02D – Supermassive Black Hole Binary Candidates from the Pan-STARRS1 Medium Deep Survey

Supermassive black hole binaries (SMBHBs) should be a common product of the hierarchical growth of galaxies and gravitational wave sources at nano-Hz frequencies. We have performed a systematic search in the Pan-STARRS1 Medium Deep Survey for periodically varying quasars, which are predicted manifestations of SMBHBs, and identified 26 candidates that are periodically varying on the timescale of ~300-1000 days over the 4-year baseline of MDS. We continue to monitor them with the Discovery Channel Telescope and the LCO network telescopes and thus are able to extend the baseline to 3-8 cycles and break false positive signals due to stochastic, normal quasar variability. From our imaging campaign, five candidates show persistent periodic variability and remain strong SMBHB candidates for follow-up observations. We calculate the cumulative number rate of SMBHBs and compare with previous work. We also compare the gravitational wave strain amplitudes of the candidates with the capability of pulsar timing arrays and discuss the future capabilities to detect periodic quasar and SMBHB candidates with the Large Synoptic Survey Telescope.

Author(s): Tingting Liu¹, Suvi Gezari¹
Institution(s): 1. University of Maryland

105.03 – The Search for AGN in Dusty Star Forming Hosts with JWST

The bulk of the stellar growth over cosmic time is dominated by IR luminous galaxies at cosmic noon ($z=1-2$), many of which harbor a hidden active galactic nucleus (AGN). I use state of the art infrared color diagnostics, combining Spitzer and Herschel observations, to separate dust-obscured AGN from dusty star forming galaxies (SFGs) in the CANDELS and COSMOS surveys. I calculate 24 micron counts of SFGs, AGN/star forming "Composites", and AGN. AGN and Composites dominate the counts above 0.8 mJy at 24 micron, and Composites form at least 25% of an IR sample even to faint detection limits. I develop methods to use the Mid-Infrared Instrument (MIRI) on JWST to identify dust-obscured AGN and Composite galaxies from $z=1-2$. I demonstrate that MIRI color techniques can select AGN with lower Eddington ratios and higher specific SFRs than X-ray techniques alone. JWST/MIRI will enable critical steps forward in identifying and understanding dust-obscured AGN and the link to their host galaxies.

Author(s): Allison Kirkpatrick⁴, Stacey Alberts², Alexandra Pope³, George Rieke², Anna Sajina¹
Institution(s): 1. Tufts University, 2. University of Arizona, 3. University of Massachusetts, 4. Yale University

105.04D – Is Black Hole Growth a Universal Process? Exploring Selection Effects in Measurements of AGN Accretion Rates and Host Galaxies.

At the center of essentially every massive galaxy is a monstrous black hole producing luminous radiation driven by the accretion of gas. By observing these active galactic nuclei (AGN) we may trace the growth of black holes across cosmic time. However, our knowledge of the full underlying AGN population is hindered by complex observational biases. My research aims to untangle these biases by using a novel approach to simulate the impact of selection effects on multiwavelength observations.

The most statistically powerful studies of AGN to date come from optical spectroscopic surveys, with some reporting a complex relationship between AGN accretion rates and host galaxy characteristics. However, the optical waveband can be strongly influenced by selection effects and dilution from host galaxy star formation. I have shown that accounting for selection effects, the Eddington ratio distribution for optically-selected AGN is consistent with a broad power-law, as seen in the X-rays (Jones et al. 2016). This suggests that a universal Eddington ratio distribution may be enough to describe the full multiwavelength AGN population.

Building on these results, I have expanded a semi-numerical galaxy formation simulation to include this straightforward prescription for AGN accretion and explicitly model selection effects. I have found that a simple model for AGN accretion can broadly reproduce the host galaxies and halos of X-ray AGN, and that different AGN selection techniques yield samples with very different host galaxy properties (Jones et al. 2017). Finally, I will discuss the capabilities of this simulation to build synthetic multiwavelength SEDs in order to explore what AGN populations would be detected with the next generation of observatories. This research is supported by a NASA Jenkins Graduate Fellowship under grant no. NNX15AU32H.

Author(s): Mackenzie Jones¹
Institution(s): 1. Dartmouth College

105.05 – What molecular gas teaches us about AGN feedback

In galaxy evolution, "AGN feedback" (the action of an accreting supermassive black hole to heat and expel star-forming fuel) has been invoked in order to stunt the growth of the most massive red elliptical galaxies and rapidly cease star formation in a transitioning galaxy by blowing out the remaining star-forming fuel. Observations in the last 5 years have shown that outflows of gas around AGNs are ubiquitous. Although on the surface, these observed outflows appear to provide the necessary power to remove gas rapidly, their ubiquity also directly challenges their effectiveness. I will discuss my analysis of these observations of AGN outflow host galaxies at $z=0$, and what implications they have on how AGN outflows function in black hole growth, our interpretation of AGN feedback, and on the evolution of gas in AGN host galaxies.

Author(s): Katherine Alatalo¹
Institution(s): 1. Space Telescope Science Institute

105.06 – Properties of AGNs in Dwarf Galaxies

It is well known that in massive galaxies, there are tight scaling relations between BH mass and host galaxy properties like bulge mass and stellar velocity dispersion. The existence of these scaling relations suggests co-evolution of the galaxy and central BH. The low-mass ends of these scaling relations (i.e., $M_{\text{BH}} < 10^6 M_{\text{sun}}$; galaxy $M_{\text{star}} < 10^{9.5} M_{\text{sun}}$) remain largely unconstrained, but are essential for informing our understanding of black hole formation and growth over cosmic time.

Searching for signs of black hole accretion is the best way of identifying massive black holes (BHs) in dwarf galaxies. In the last several years, the number of dwarf galaxies with known active galactic nuclei (AGNs) has increased by over an order of magnitude, thanks to large scale surveys such as the Sloan Digital Sky Survey. I will discuss the current state of the low-mass end of host galaxy-black hole scaling relations, particularly focusing on new results using Hubble Space Telescope WFC3 imaging of RGG 118, a dwarf galaxy hosting an actively accreting 50,000 solar mass black hole in its core.

Author(s): Vivienne Baldassare⁴, Amy Reines¹, Elena Gallo³, Jenny Greene²
Institution(s): 1. Montana State University, 2. Princeton University, 3. University of Michigan, 4. Yale University

106 – Astrophysics Enabled by HST's UV Initiative

Observations with the Hubble Space Telescope open up a window on ultraviolet (UV) wavelengths which enables astrophysics that would not be possible otherwise. UV observations complete the census of star formation at its peak epoch; probe star-formation-driven winds in galaxies; reveal the spatial and temporal structuring of star formation in galaxies on scales from individual stars to star clusters; constrain the nature of energetic events and outflows from supermassive black holes; describe the scattering in exoplanet atmospheres; and unveil evidence for water plumes in the solar system. The Ultraviolet Astrophysics Legacy Initiative, in place since Cycle 21, recognizes the unique resource that Hubble has in its access to the UV portion of the electromagnetic spectrum and encourages proposals for this finite limited resource. A total of 391 accepted observing programs in Cycles 21 through 24 have made use of the UV Initiative, totaling more than 7100 orbits. This special session will highlight the science outcomes of programs undertaken as part of the UV initiative, set the landscape for future science at these wavelengths, and present the key role UV observations will have in interpreting results from future missions like the James Webb Space Telescope. The invited speaker list consists of astronomers who are involved in projects on a selection of topics spanning the astronomical scales of the cosmos, from solar system science to the early universe, in observing programs making use of the UV Initiative. We propose to have an associated poster session as well, to showcase further the breadth of science being done under the UV initiative.

106.01 – Deciphering AGN outflows with joint UV and X-ray observations

In this presentation I will show some recent highlights of large, joint monitoring campaigns on Active Galactic Nuclei outflows. The combination of UV grating observations with HST for the best velocity decomposition and the broad-range sensitivity on ionisation state offered by X-ray grating detectors on Chandra and XMM-Newton is a powerful tool to decipher AGN outflows. I will discuss the diagnostic power of density sensitive lines in the UV and delayed recombination measurement in X-rays to estimate densities and distances of the outflow. A good example is the large X-ray/UV campaign on Markarian 509.

A breakthrough has been made by the observation of the prototype Seyfert galaxy NGC 5548 in an obscured state. Here the X-ray obscuration gives the column density and ionisation state of lowly ionized material close to the broad-line region that blocks most of the soft X-rays from the central regions in our line of sight, while UV spectroscopy provides all details on the outflow velocity, which cannot be obtained from the X-ray spectra. Also the obscured state allows to measure accurately the density and distance of the regular outflow at pc distances, which is de-ionized by the obscuring material.

A second example of an obscuration event is provided by NGC 3783, where a trigger from Swift alerted us of the obscured state. I will compare these obscuration events and briefly discuss their impact on other AGN physics like the BLR analysis. Finally I present some future prospects of AGN studies with upcoming X-ray missions like XARM, Arcus and Athena.

Author(s): Jelle Kaastra¹

Institution(s): 1. SRON

Contributing team(s): Mrk 509 team

106.02 – Linking the Scales of Star Formation

Understanding galaxy evolution requires understanding star formation and its dependence on the local environment, spanning the scales from individual stars to kpc-size structures. The physical conditions within galaxies determine the formation of stars, star clusters, and larger structures, and their subsequent evolution. Observations of external galaxies with the HST that include the UV have enabled the characterization of the young stellar populations with unprecedented accuracy and detail, thus aiding the census and description of those populations. We are now in a position to quantify the spatial distribution and

clustering of young stars, and investigate the impact and imprint of the physical conditions of both the local and global environment on the formation and evolution of the multi-scale structures. This talk describes the Legacy ExtraGalactic UV Survey (LEGUS), an HST Treasury programs aimed at investigating these issues using multi-color imaging, from the near-UV to the I, of a sample of fifty nearby galaxies.

Author(s): Daniela Calzetti¹

Institution(s): 1. University of Massachusetts

Contributing team(s): and the LEGUS Team

106.03 – Evidence of Plumes on Europa from far-ultraviolet observations with HST

Evidence for plumes of water emerging from the icy surface of Europa has been found by the Hubble Space Telescope (HST) using two different UV observing techniques. Roth et al. (2014) found line emission from the dissociation products of water. Sparks et al. (2016, 2017) found evidence for off-limb continuum absorption as Europa transited Jupiter. We describe the transit method which obtains far ultraviolet images of Europa as it passes in front of the smooth face of Jupiter, seeking off-limb absorption patches that may be due to plumes on Europa. This approach exploits the time resolution, sensitivity and spatial resolution of HST, coupled to the high cross-sections for molecules of interest at these wavelengths. We show that a well-localized plume candidate appears more than once, and that it is at the same position as a nighttime thermal anomaly seen by the Galileo spacecraft, the warmest point on the observed Europa nightside. The favored interpretation of the thermal anomaly is a modification to the local thermal inertia, which could be causally related to plume activity. Future plans for additional work in this area are described.

Author(s): William B. Sparks⁵, Melissa McGrath³, Britney Schmidt¹, Eddie Bergeron⁵, Kevin Hand², John Spencer⁴, Misty Cracraft⁵, Susana Deustua⁵

Institution(s): 1. Georgia Institute of Technology, 2. Jet Propulsion Laboratory, 3. SETI, 4. Southwest Research Institute, 5. Space Telescope Science Institute

106.04 – The Ultraviolet Hubble Ultra Deep Field

The Ultraviolet Hubble Ultra Deep Field (UVUDF) consists of WFC3/UVIS imaging of the HUDF in the F225W, F275W, and F336W filters (30 orbits per filter, half of which included post-flash). The UVUDF complements the optical through near-infrared imaging, adding UV diagnostics to the most well studied extragalactic field in the sky. I will present the science results enabled by this UV imaging, including improved photometric redshift estimates, the UV galaxy luminosity function, the UV morphology of star-forming galaxies, limits on the escape fraction of ionizing radiation, bursty star-formation in low-mass galaxies, and the star-formation efficiency of HI rich galaxies. I will conclude with a reflection about the future of UV imaging in the final years of the Hubble Space Telescope (HST).

Author(s): Marc Rafelski¹

Institution(s): 1. Space Telescope Science Institute

Contributing team(s): UVUDF

106.05 – Circumgalactic Matter Matters in Galaxy Evolution

The circumgalactic medium (CGM; non-ISM gas within a galaxy virial radius) regulates the gas flows that shape the assembly and evolution of galaxies. Owing to the vastly improved capabilities in space-based UV spectroscopy with the installation of HST/COS, observations and simulations of the CGM have emerged as the new frontier of galaxy evolution studies. In the last decade, we have learned that the CGM of Milky Way mass galaxies likely contains enough material to harbor most of the metals lost in galaxy winds and to sustain star-formation for billions of years. Remarkably, this implies that most of the heavy elements on

earth cycled back and forth multiple times through the Milky Way's own CGM before the formation of the solar system. In this talk, I will describe constraints we have placed on the origin and fate of this material by studying the gas kinematics, metallicity and ionization state. I will conclude by posing several unanswered questions about the CGM that will be addressed with future

107 – Gamma Ray Bursts

107.01 – A Constant LGRB Metallicity Distribution Across Redshifts < 2.5

Recent improvements in the population of Long-duration Gamma Ray Burst (LGRB) host galaxies with measured metallicities and host masses allows us to investigate how the distributions of both these properties change with redshift. First we examine possible biases in the populations caused by the efficiency of obtaining mass and metallicity measurements at different redshifts. In comparing the redshift distributions of a variety of LGRB populations we find little bias out to a redshift of 2.5 with the exception of a reduced metallicity sampling at redshifts high enough to require a separate IR spectrum ($z < 0.5$). However observations using X-shooter (which allow for obtaining metallicities across a wide range of redshifts) do not show this bias. We also compare the observed LGRB redshift distribution with the recent predictions of Graham & Schady (2015) and find good agreement.

Having established that the mass and metallicity samples are unbiased we then find a curious consistency in the metallicity distribution across different redshifts. This is at odds with the general evolution in the mass metallicity relation, which becomes progressively more metal poor with increasing redshift. By converting the measured LGRB host masses and redshifts to their expected metallicities, we further find that the LGRB host galaxy mass distribution increase with redshift seen in the Perley et al. (2016) SHOALS sample is consistent with that needed to preserve the LGRB metallicity distribution as the mass metallicity relation decreases with redshift. Furthermore we find that such estimated LGRB host metallicities consistently overestimate the actual measured host metallicities by approximately a quarter dex. This corresponds to about a factor of two in raw metallicity and resolves much of the difference between the LGRB formation metallicity cutoff of about a third solar in Graham & Fruchter (2015) with the cutoff value of solar claimed in Perley et al. (2016) in favor of the former. As LGRB hosts do not follow the general mass metallicity relation, there is no substitute for actually measuring their metallicities!

Author(s): John Graham¹

Institution(s): 1. *Kavli Institute for Astronomy and Astrophysics*

107.02 – A Unified Model for GRB Prompt Emission from Optical to Gamma-Rays: Exploring GRBs as Standard Candles

The Band function traditionally used for Gamma Ray Bursts (GRB) often fails to fit their prompt emission spectra. Our new model composed of three separate components provides an excellent description of the time-resolved prompt emission: a thermal-like and two non-thermal components. For the first time, analysis of GRBs with correlated optical and gamma-ray prompt emission show that our new model describes very accurately the whole broadband spectrum from the optical regime to higher energy gamma rays. In addition, this new model enables a new luminosity/hardness relation intrinsic to one of the non-thermal components showing that GRBs may be standard candles. If statistically confirmed, this relation will be used to (i) constrain the mechanisms powering GRB jets, (ii) estimate GRB distances, (iii) probe the early Universe, and (iv) constrain the cosmological parameters. I will present this new unified model using analysis of GRBs detected with various observatories and instruments such as Fermi, CGRO/BATSE and the combination of the three instruments on board Swift and Suzaku/WAM. I will discuss here the striking similarities of GRB spectral shapes,

survey data and hydrodynamic simulations in a cosmological context.

Author(s): Jessica Werk¹

Institution(s): 1. *University of Washington*

whose components inform on the nature of the prompt emission, as well as the possible universality of the proposed luminosity/hardness relation in the context of our new model.

Author(s): Sylvain Guiriec¹

Institution(s): 1. *George Washington University*

107.03 – Time Domain Astronomy with Fermi GBM in the Multi-messenger Era

As the Multi-Messenger era begins with detections of gravitational waves with LIGO/Virgo and neutrinos with IceCube, the Fermi Gamma-ray Burst Monitor (GBM) provides context observations of gamma-ray transients between 8 keV and 40 MeV. Fermi GBM has a wide field of view, high uptime, and both in-orbit triggering and high time resolution continuous data enabling offline searches for weaker transients. GBM detects numerous gamma-ray bursts (GRBs), soft gamma-ray repeaters, X-ray bursters, solar flares and terrestrial gamma-ray flashes. Longer timescale transients, predominantly in our galaxy so far, are detected using the Earth occultation technique and epoch-folding for periodic sources. The GBM team has developed two ground-based searches to enhance detections of faint transients, especially short GRBs. The targeted search uses the time and location of an event detected with another instrument to coherently search the GBM data, increasing the sensitivity to a transient. The untargeted search agnostically searches the GBM data for all directions and times to find weaker transients. This search finds about 80 short GRBs per year, adding to the 40 per year triggered on-orbit. With its large field of view, high duty cycle and increasingly sophisticated detection methods, Fermi GBM is expected to have a major role in the Multi-Messenger era.

Author(s): Colleen A. Wilson-Hodge¹

Institution(s): 1. *NASA MSFC*

Contributing team(s): Fermi GBM team, GBM-LIGO team

107.04D – Cosmic Extremes: Probing Energetic Transients with Radio Observations

With the advent of sensitive facilities like the Karl G. Jansky Very Large Array (VLA) and planning well underway for vastly more powerful wide-field interferometers like the Square Kilometer Array, the study of radio astrophysical transients is poised for dramatic growth. Radio observations provide a unique window into a wide variety of transient events, from gamma-ray bursts (GRBs) to supernovae to tidal disruption events (TDEs) in which a star is torn apart by a supermassive black hole. In particular, GRBs and TDEs have emerged as valuable probes of some of the most extreme physics in the Universe. In these high-energy laboratories, the longer timescale of radio emission allows for extensive followup and characterization of the event energies and the densities of surrounding material. I will present high-cadence broadband radio studies of GRB afterglows and TDEs undertaken with the goal of learning more about their physical properties, the physics underlying the formation and growth of relativistic jets and outflows, and the environments in which these events occur. Our observations confirm that only a small fraction of TDEs produce relativistic jets but reveal low-luminosity, non-relativistic outflows in two nearby TDEs, allowing us to begin constraining the bulk of the TDE population. Our GRB radio observations reveal both intrinsic variability (reverse shocks) and extrinsic variability (interstellar scintillation). The insights derived from these studies will be invaluable for designing and interpreting the results from future radio transient surveys.

Author(s): Kate Denham Alexander¹

Institution(s): 1. *Harvard University*

107.05 – Finding Sub-threshold Short Gamma-ray Bursts in Fermi GBM Data

The all-sky monitoring capability of Fermi GBM makes it ideal for finding transients, and the most prolific detector of short gamma-ray bursts with about 40 on-board triggers per year. Because the observed brightness of short gamma-ray bursts has no correlation with redshift, weak short gamma-ray bursts are important during the gravitational wave era. With this in mind, we discuss two searches of GBM data to find short gamma-ray which were below the on-board trigger threshold. The untargeted search looks for significant background-subtracted signals in two or more detectors at various timescales in the continuous data, detecting ~80 additional short GRB candidates per year. The targeted search is the most sensitive search for weak gamma-ray signals in GBM data and is run over limited time intervals around sources of interest like gravitational waves.

Author(s): Eric Burns¹

Institution(s): 1. NASA/GSFC

Contributing team(s): Fermi Gamma-ray Burst Monitor Team

107.06 – A subpopulation of nearby, low luminosity, short gamma-ray bursts as triggers for subthreshold transient gravitational wave searches

Two years ago, LIGO opened the new area of gravitational wave astrophysics with the detection of the coalescence of two black holes. Neutron star mergers (either double neutron star or neutron star - black hole systems) will be the next key target for gravitational wave observatories such as Advanced-Virgo (AdV), Advanced-LIGO (aLIGO) and the future Einstein Telescope (ET). Those binary compact objects are also thought to be the progenitor of short Gamma-Ray Bursts (GRB). A coincident detection of Gravitational Waves (GW) and the electromagnetic emission would extend the new window in astrophysics: the multimessenger era.

Using the most reliable sample of short GRB with known redshift, we have identified a new population of low luminous short GRBs at low redshift. This population was reproduced using realistic Monte Carlo simulations accounting for both GW and GRB selection effects. In this talk, we will discuss the properties of the progenitors that are supposed to produce this class of short GRBs. We will also present an estimation of the detection rate of such events, that could be seen both by a GRB satellite and AdV/aLIGO/ET. We will then present the offline refined analysis of LIGO, introducing the different method used to achieve this goal. We will discuss future aLIGO/AdV running.

108 – HAD II: From the Earliest Astronomy to Space Missions: Explorations in the History of Astronomy

108.01 – The Early Astronomy Toolkit was Universal

From historical, anthropological, and archaeological records, we can reconstruct the general properties of the earliest astronomy for many cultures worldwide, and they all share many similar characteristics. The 'Early Astronomy Toolkit' (EAT) has the Earth being flat, and the heavens as a dome overhead populated by gods/heroes that rule Nature. The skies provided omens in a wide variety of manners, with eclipses, comets, and meteors always being evil and bad. Constellations were ubiquitous pictures of gods, heroes, animals, and everyday items; all for story telling. The calendars were all luni-solar, with no year counts and months only named by seasonal cues (including solstice observations and heliacal risings) with vague intercalation. Time of day came only from the sun's altitude/azimuth, while time at night came from star risings. Graves are oriented astronomically, and each culture has deep traditions of quartering the horizon. The most complicated astronomical tools were just a few sticks and stones. This is a higher level description and summary of the astronomy of all ancient cultures.

This basic EAT was universal up until the Greeks, Mesopotamians, and Chinese broke out around 500 BC and afterwards. Outside the Eurasian milieu, with few exceptions (for

Author(s): Karelle Siellez¹

Institution(s): 1. Georgia Institute of Technology

Contributing team(s): LIGO

107.07 – Fermi GBM Observations During the Second Observing Run of LIGO/Virgo

The Fermi Gamma-ray Burst Monitor (GBM) is a prolific detector of gamma-ray bursts (GRBs) and detects more short duration GRBs than any other instrument currently in operation. Short GRBs are thought to be associated with the mergers of binary neutron star systems (or neutron star-black hole systems), and are therefore considered likely counterparts to gravitational-wave detections from LIGO/Virgo. We report on the GBM observations during the second observing run of LIGO/Virgo and detail the physical and astrophysical insights that might be gleaned from a joint detection of a short GRB and a gravitational-wave source.

Author(s): Adam Goldstein¹

Institution(s): 1. Universities Space Research Association

Contributing team(s): Fermi-GBM

107.08 – What is the difference between an ultra-long GRB and a long GRB?

The new class of ultra-long gamma-ray bursts is a fascinating class of events, where the very long duration of these events theoretically allows for pointing sensitive instruments during the prompt phase. However, this is complicated by the initially uncertain nature of the event. How to predict that an event will be an ultralong GRB, i.e. duration more than 3 hours, while high-energy detectors are recording only the first tens of seconds? We present here our study about potential discriminators that can distinguish ultra-long GRBs from normal long ones during the first minute of the prompt event. This would allow for the observation of the source with a large set of detectors at various energies.

Author(s): Quianah T. Joyce⁵, Bruce Gendre⁵, N. Brice Orange³, Michel Boër¹, Jean-Luc Atteia², Giulia Stratta⁴, David Morris⁵

Institution(s): 1. ARTEMIS/CNRS/OCA, 2. IRAP, 3. OrangeWave Innovative Science, LLC, 4. Università di Urbino, 5. University of the Virgin Islands

example, planetary position measures in Mexico), this EAT represents astronomy for the rest of the world up until around 1600 AD. The EAT is present in these many cultures with virtually no variations or extensions. This universality must arise either from multiple independent inventions or by migration/diffusion. The probability of any culture independently inventing all 19 items in the EAT is low, but any such calculation has all the usual problems. Still, we realize that it is virtually impossible for many cultures to independently develop all 19 items in the EAT, so there must be a substantial fraction of migration of the early astronomical concepts. Further, the utter lack, as far as I know, of any culture that has one or more items different from the EAT argues strongly that the EAT was transmitted as a whole. Australian Aborigines have the entire EAT, so I think it is substantially older than ~50,000 years.

Author(s): Bradley E. Schaefer¹

Institution(s): 1. Louisiana State University

108.02 – William Herschel and Comets

I examine the observational and theoretical researches of William Herschel on 21 comets that he observed over the period 1781 to 1812. Herschel's focus, unlike most contemporaries, was on their physical structure, not their orbits. He forged a strong connection between comets and his nebulae with a scheme of cometary

"maturation" (1812) involved a comet traveling from star to star after its central "planetary body"; was born from gravitational collapse of a nebula. During close passages of a star, the comet brightened and lost mass from its atmosphere; at other times, when between stars, it encountered nebulae and was rejuvenated by picking up more mass. Laplace soon adopted these ideas to improve his nebula hypothesis for solar system formation.

Author(s): Woodruff Sullivan¹

Institution(s): 1. *University of Washington, Seattle*

108.03 – Benjamin Banneker's 18th Century Astronomy

Benjamin Banneker is considered to be the first African-American man of science (1731-1806), a contemporary of George Washington and Thomas Jefferson. He was a self taught clock maker, mathematician, and astronomer. He owned land in Baltimore County near Ellicott City, Maryland where he farmed tobacco. He is especially known for his work on the Boundary Survey of our new Capital. Surveyors place boundary stones along the boundary of the nascent Capital. Banneker was part of the team who measured the latitude and longitude for each stone. Using 18th century surveying techniques Banneker became part of the early history of Washington DC. He also published popular almanacs.

Author(s): Sethanne Howard¹

Institution(s): 1. *USNO/retired*

108.04 – The Evolution of Spacelab Ultraviolet Astronomy Missions from OSS-3 through -7 to Astro-1

In the 1960s and 1970s, NASA was building towards a robust program in space astronomy. An evolutionary step from ground-based astronomy to space astronomy was human operation of space telescopes as astronomy in general evolved from astronomers directly at the telescope to application of computers and long distance communications to control to operate remote telescopes. Today ground-based telescopes and space observatories from cubesats to the Hubble Space Telescope and

109 – Pulsators and Binaries

109.01 – Close Binaries in the Orion Nebula Cluster: On the Universality of Stellar Multiplicity and the Origin of Field Stars

While stellar multiplicity is an ubiquitous outcome of star formation, there is a clear dichotomy between the multiplicity properties of young (~1 Myr-old) stellar clusters, like the ONC, which host a mostly field-like population of visual binaries, and those of equally young sparse populations, like the Taurus-Auriga region, which host twice as many stellar companions. Two distinct scenarios can account for this observation: one in which different star-forming regions form different number of stars, and one in which multiplicity properties are universal at birth but where internal cluster dynamics destroy many wide binaries. To solve this ambiguity, one must probe binaries that are sufficiently close so as not to be destroyed through interactions with other cluster members. To this end, we have conducted a survey for 10-100 au binaries in the ONC using the aperture masking technique with the VLT adaptive optics system. Among our sample of the 42 ONC members, we discovered 13 companions in this range of projected separations. This is consistent with the companion frequency observed in the Taurus population and twice as high as that observed among field stars. This survey thus strongly supports the idea that stellar multiplicity is characterized by near-universal initial properties that can later be dynamically altered. On the other hand, this exacerbates the question of the origin of field stars, since only clusters much denser than the ONC can effectively destroyed binaries closer than 100 au.

Author(s): Gaspard Duchene³, Sylvestre Lacour², Estelle Moraux¹, Jerome Bouvier¹, Simon Goodwin⁴

Institution(s): 1. *Institut de Planetologie et d'Astrophysique de Grenoble*, 2. *Observatoire de Paris*, 3. *University of California Berkeley*, 4. *University of Sheffield*

soon the James Webb Space Telescope are routinely operated remotely.

In response to the Spacelab Announcement of Opportunity in the early 1980s, three ultraviolet experiments – the Hopkins Ultraviolet Telescope, the Ultraviolet Imaging Telescope and the Wisconsin Ultraviolet PhotoPolarimetry Experiment -- all instruments derived from multiple sounding rocket flights--were selected to fly as an integrated payload attached to a space shuttle. The justification for professional astronomers, both as Mission Specialists from the astronaut cadre and Payload Specialists from the instrument teams, was built to ensure key technical skills both of the science and the instruments. Bundled together as OSS-3 through -7 flights focused on Comet Halley, the experiments went through many changes and delays as a pathfinder for an anticipated series of attached astronomy payloads.

By 1986, the five-flight mission had evolved into two missions, Astro-1 dedicated primarily to observe Halley's Comet in early March 1986 and Astro-2 to fly about one year later. Due to the Challenger disaster 35 days before scheduled launch of Astro-1, the mission went through an initial cancellation and then re-scheduling once the instrument complement of Astro-1 was expanded to include Broad Band X-ray Telescope with emphasis on studying SN1987A. Ultimately Astro-1 flew in December 1990 partnered with an X-ray experiment focused on SN1987A.

The nine-day mission was mostly successful despite multiple technical issues overcome by the NASA and instrument teams. Dozens of refereed papers results and five years later, Astro-2, with the three ultraviolet instruments accomplished a seventeen-day mission.

Author(s): Theodore Gull¹

Institution(s): 1. *NASA/GSFC*

109.02 – Stellar Companions of Exoplanet Host Stars in K2

Stellar multiplicity has significant implications for the detection and characterization of exoplanets. A stellar companion can mimic the signal of a transiting planet or distort the true planetary radii, leading to improper density estimates and over-predicting the occurrence rates of Earth-sized planets. Determining the fraction of exoplanet host stars that are also binaries allows us to better determine planetary characteristics as well as establish the relationship between binarity and planet formation. Using high-resolution speckle imaging to obtain diffraction limited images of K2 planet candidate host stars we detect stellar companions within one arcsec and up to six magnitudes fainter than the host star. By comparing our observed companion fraction to TRILEGAL star count simulations, and using the known detection limits of speckle imaging, we find the binary fraction of K2 planet host stars to be similar to that of Kepler host stars and solar-type field stars. Accounting for stellar companions in exoplanet studies is therefore essential for deriving true stellar and planetary properties as well as maximizing the returns for TESS and future exoplanet missions.

Author(s): Rachel Matson¹, Steve Howell¹, Elliott Horch³, Mark Everett²

Institution(s): 1. *NASA Ames*, 2. *NOAO*, 3. *Southern Connecticut State University*

109.03D – Beyond Blue Stragglers: Products of Non-Standard Stellar Evolution Across the Color Magnitude Diagram

Optical color-magnitude diagrams (CMDs) of open clusters reveal large populations of stars that do not fall along standard isochrones, and thus are not evolving according to standard

theory. The most numerous of these stars are the blue stragglers, stars brighter and bluer than the cluster turnoff that are likely formed from mass transfer in a binary, stellar mergers, or collisions during dynamical encounters. The origins of other non-standard stars are not well understood, including the “yellow stragglers” found between the blue straggler region and the red giant branch, and “sub-subgiants” found fainter and redder than the giant branch. Understanding the formation and evolution of these non-standard stars is critical to properly modeling galactic stellar populations and revealing the binary evolution channels that form exotic end products like X-ray binaries, double degenerates, and Type 1a supernovae. In this talk I will present results of the first asteroseismic study of a yellow straggler in the old open cluster M67. This study shows the yellow straggler to be a red clump giant with a mass of at least twice the turnoff mass of M67, suggesting it is an evolved blue straggler formed from a merger or collision. I will also discuss the observed properties of the growing population of sub-subgiants discovered in open and globular clusters, and present models describing three possible formation pathways for these stars: mass-transfer in a binary, rapid envelope mass loss, and inhibition of convection due to the presence of strong magnetic fields. These studies represent some of the first efforts to understand cluster CMD outliers beyond the blue stragglers, and are a critical step forward in understanding binary evolution pathways.

Author(s): Emily Leiner¹

Institution(s): 1. *University of Wisconsin-- Madison*

109.04 – All-Sky Census of Variable Stars from the ATLAS Survey

The Asteroid Terrestrial-Impact Last Alert Survey uses two custom-built 0.5 meter telescopes to scan the whole accessible sky down to magnitude 19.5 every two nights, with a cadence optimized to detect small asteroids on their 'final plunge' toward impact with Earth. This cadence is also well suited to the detection of variable stars with a huge range of periods and properties, while ATLAS' use of two filters provides additional scientific depth. From the first two years of ATLAS data we have constructed a catalog of several hundred thousand variable objects with periods from one hour to hundreds of days. These include RR Lyrae stars, Cepheids, eclipsing binaries, spotted stars, ellipsoidal variables, Miras; and other objects both regular and irregular. We describe the construction of this catalog, including our multi-step confirmation process for genuine variables; some big-picture scientific conclusions; and prospects for more detailed results.

Author(s): Aren Nathaniel Heinze², John Tonry², Larry Denneau², Brian Stalder¹

Institution(s): 1. *LSST*, 2. *University of Hawaii*

109.05 – Exploring the η Aquila System: Another Cepheid Parallax and Further Evidence for a Tertiary

We report progress towards a re-analysis of Hubble Space Telescope Fine Guidance Sensor astrometric data, originally acquired to determine a parallax for and absolute magnitudes of the classical Cepheid, η Aquila. This object was not included in past Cepheid Period-Luminosity Relation (PLR) work (Benedict et al. 2007, *AJ*, 133, 1810), because we had an insufficient number of epochs with which to establish a suspected and complicating companion orbit. Our new investigation is considerably aided by including a significant number of radial velocity measures (RV) from six sources, including new, high-quality Hobby-Eberly Telescope spectra. We first derive a 12 Fourier coefficient description of the Cepheid pulsation, solving for velocity offsets required to bring the six RV data sets into coincidence. We next model the RV residuals to that fit with an orbit. The resulting orbit has very high eccentricity. The astrometric residuals show only a very small perturbation, consistent with a prediction from

the spectroscopic orbit. We finally include that orbit in a combined astrometry and radial velocity model. This modeling, similar to that presented in Benedict and Harrison (2017, *AJ*, 153, 258) yields a parallax, allowing inclusion of η Aquila in a PLR. It also establishes a Cepheid/companion mass ratio for the early-type star companion identified in IUE spectra (Evans 1991, *ApJ*, 372, 597).

Author(s): George Frederick Benedict³, Thomas G. Barnes³, Nancy Evans¹, William Cochran³, Barbara E. McArthur³, Thomas E. Harrison²

Institution(s): 1. *Center for Astrophysics*, 2. *New Mexico State University*, 3. *The University of Texas*

109.06D – Using High-Mass X-ray Binaries to Probe Massive Binary Evolution

High-mass X-ray binaries (HMXBs) provide an exciting window into the underlying processes of both binary as well as massive star evolution. Because HMXBs are systems containing a compact object accreting from a high-mass star at close orbital separations they are also likely progenitors of gamma-ray bursts and gravitational wave sources. I will present work on the classification and age measurements of HMXBs in M33 using a combination of deep Chandra X-ray imaging, and archival Hubble Space Telescope data. I am able to constrain the ages of the HMXB candidates by fitting the color-magnitude diagrams of the surrounding stars, which yield the star formation histories of the surrounding region. Unlike the age distributions measured for HMXB populations in the Magellanic Clouds, the age distribution for the HMXB population in M33 contains a number of extremely young (<5 Myr) sources, including M33 X-7, an eclipsing binary composed of a ~15 Msun black hole accreting from a 70 Msun O star companion. I will discuss these results for M33 in the context of the effect of host galaxy properties on the observed HMXB population.

Author(s): Kristen Garofali¹, Ben Williams¹

Institution(s): 1. *University of Washington*

109.07 – Infrared Studies of the Variability and Mass Loss of Dusty Asymptotic Giant Branch Stars in the Magellanic Clouds

The asymptotic giant branch (AGB) phase is one of the last phases of a star's life. AGB stars lose mass in an outflow in which dust condenses and is pushed away from the star. Extreme AGB stars are so named because their very red colors suggest very large amounts of dust, which in turn suggests extremely high mass loss rates. AGB stars also vary in brightness, and studies show that extreme AGB stars tend to have longer periods than other AGB stars and are more likely to be fundamental mode pulsators than other AGB stars. Extreme AGB stars are difficult to study, as their colors are so red due to their copious amounts of circumstellar dust that they are often not detected at optical wavelengths. Therefore, they must be observed at infrared wavelengths to explore their variability. Using the Spitzer Space Telescope, my team and I have observed a sample of extreme AGB stars in the Large Magellanic Cloud (LMC) and Small Magellanic Cloud (SMC) over Cycles 9 through 12 during the Warm Spitzer mission. For each cycle, we typically observed a set of extreme AGB stars at both 3.6 and 4.5 microns wavelength approximately monthly for most of a year. These observations reveal a wide range of variability properties. I present results from our analysis of the data obtained from these Spitzer variability programs, including light curve analyses and comparison to period-luminosity diagrams. Funding is acknowledged from JPL RSA # 1561703.

Author(s): Benjamin Sargent², M. A. T. Groenewegen¹

Institution(s): 1. *Koninklijke Sterrenwacht van België*, 2. *Space Telescope Science Institute*

110 – Galaxy Formation and Evolution I

110.01 – Resolving the Circumgalactic Medium in the NEPHTHYS Simulations

NEPHTHYS is a RAMSES Cosmological-zoom galaxy simulation suite investigating the impact of stellar feedback (winds, radiation, and type Ia and II SNe) on $z > 1$ $\sim L^*$ galaxies and their environments. NEPHTHYS has ~ 10 pc resolution in the galaxy, where the scales driving star formation and the interaction of stellar feedback with the ISM can begin to be resolved. As outflows, winds, and radiation permeate through the circumgalactic medium (CGM) they can heat or cool gas, and deposit metals throughout the CGM. Such material in the CGM is seen by spectroscopic studies of distant quasars, where CGM gas of foreground galaxies is observed in absorption. It is still unclear what the origin and evolution of this gas is. To help answer this, NEPHTHYS includes additional refinement in the CGM, refining it to an unrivaled 80 pc resolution. I will discuss how this extra resolution is crucial for resolving the complex structure of outflows and accretion in the CGM. Specifically, the metal mass and covering fraction of metals and high energy ions is increased, while the better resolved outflows leads to a decrease in the overall baryon content of galaxy halos, and individual outflow events can have larger velocities. Our results suggest that absorption observations of CGM are tracing a clumpy column of gas with multiple kinematic components.

Author(s): Mark Lawrence Albert Richardson¹, Julien Devriendt⁴, Adrienne Slyz⁴, Karl Joakim Rosdahl³, Taysun Kimm²

Institution(s): 1. American Museum of Natural History, 2. University of Cambridge, 3. University of Lyon, 4. University of Oxford

110.02D – Multi-Wavelength Photometric Identification of Quenching Galaxies in ZFOURGE

In the new millennium, multi-wavelength photometric surveys of thousands of galaxies, such as SDSS, CANDELS, NMBS, and ZFOURGE have become the standard for analyzing large populations.

With ongoing surveys such as DES, and upcoming programs with LSST and JWST, finding ways to leverage large amounts of data will continue to be an area of important research.

Many diagnostics have been used to classify these galaxies, most notably the rest-frame UVJ color-color diagram, which splits galaxies into star-forming and quiescent populations.

With the plethora of data probing wavelengths outside of the optical however, we can do better.

In this talk I present a scheme for classifying galaxies with using composite SEDs that clearly reveals rare populations such as extreme emission line galaxies and post-starburst galaxies.

We use a sample of ~ 8000 galaxies from ZFOURGE which have $\text{SNR}_{Ks} > 20$, observations from 0.3-8 microns, and are at $1 < z < 4$.

Using this method we are additionally able to find galaxies which have SFRs below the main sequence and morphologies between those of typical star-forming and quiescent galaxies, indicating they are not the quenched spirals and star-forming disks that occupy much of the so-called 'green valley.'

This is suggestive of a quenching pathway that more closely traces the evolution of the quiescent population than the post-starburst (E+A) pathway.

Author(s): Ben Forrest¹, Kim-Vy Tran¹

Institution(s): 1. Texas A&M University

Contributing team(s): ZFOURGE Collaboration

110.03 – CANDELS Sheds Light on the Environmental Quenching of Low-mass Galaxies

We investigate the environmental quenching of galaxies, especially those with stellar masses (M^*) smaller than $10^{9.5} M_{\odot}$, beyond the local universe. Essentially all local low-mass quenched galaxies (QGs) are believed to live close to massive central galaxies, which is a demonstration of environmental quenching. We use CANDELS data to test whether or not such a dwarf QG--massive central galaxy connection exists beyond the local universe. For this purpose, we only need a statistically

representative, rather than a complete, sample of low-mass galaxies, which enables our study out to $z > 1.5$. For each low-mass galaxy, we measure the projected distance (d_{proj}) to its nearest massive ($M^* > 10^{10.5} M_{\odot}$) neighbor within a redshift range. At a given z and M^* , the environmental quenching effect is considered to be observed if the d_{proj} distribution of QGs is significantly skewed toward lower values than that of star-forming galaxies (SFGs). For galaxies with $10^8 M_{\odot} < M^* < 10^{10} M_{\odot}$, such a difference between the d_{proj} distributions of quenched and star-forming populations is detected up to $z \sim 1$. Also, about 10% of the quenched galaxies in our sample are located between two and four virial radii (R_{Vir}) of the massive halos. The median projected distance from low-mass QGs to their massive neighbors (d_{proj}/R_{Vir}) decreases with satellite M^* at $M^* < 10^{9.5} M_{\odot}$, but increases with satellite M^* at $M^* > 10^{9.5} M_{\odot}$. This trend suggests a smooth, if any, transition of the quenching timescale around M^* of $10^{9.5} M_{\odot}$ at $0.5 < z < 1.0$.

Author(s): Yicheng Guo⁴, Eric F. Bell³, Yu Lu¹, David C. Koo², Sandra M. Faber²

Institution(s): 1. Carnegie Observatories, 2. UCO/Lick Observatory, UCSC, 3. University of Michigan, 4. University of Missouri

Contributing team(s): CANDELS

110.04D – Star Formation in low mass galaxies

Our current hierarchical view of the universe asserts that the large galaxies we see today grew via mergers of numerous smaller galaxies. As evidenced by recent literature, the collective impact of these low mass galaxies on the universe is more substantial than previously thought. Studying the growth and evolution of these low mass galaxies is critical to our understanding of the universe as a whole. Star formation is one of the most important ongoing processes in galaxies. Forming stars is fundamental to the growth of a galaxy. One of the main goals of my thesis is to analyze the star formation in these low mass galaxies at different redshifts.

Using the Hubble UltraViolet Ultra Deep Field (UVUDF), I investigate the star formation in galaxies at the peak of the cosmic star formation history using the ultraviolet (UV) light as a star formation indicator. Particularly, I measure the UV luminosity function (LF) to probe the volume-averaged star formation properties of galaxies at these redshifts. The depth of the UVUDF is ideal for a direct measurement of the faint end slope of the UV LF. This redshift range also provides a unique opportunity to directly compare UV to the "gold standard" of star formation indicators, namely the H α nebular emission line. A joint analysis of the UV and H α LFs suggests that, on average, the star formation histories in low mass galaxies ($\sim 10^9 M_{\odot}$) are more bursty compared to their higher mass counterparts at these redshifts.

Complementary to the analysis of the average star formation properties of the bulk galaxy population, I investigate the details of star formation in some very bursty galaxies at lower redshifts selected from Spitzer Large Area Survey with Hyper-Suprime Cam (SPLASH). Using a broadband color-excess selection technique, I identify a sample of low redshift galaxies with bright nebular emission lines in the Subaru-XMM Deep Field (SXDF) from the SPLASH-SXDF catalog. These galaxies are highly star forming and have extremely low masses (10^5 - $10^7 M_{\odot}$). They are much fainter equivalents of the "green pea" galaxies found in SDSS. These objects are followed up with HectoSpec on the MMT to confirm their redshift as well as study their star formation properties in detail.

Author(s): Vihang Mehta¹

Institution(s): 1. University of Minnesota

110.05 – Star Formation Histories of Extreme Emission Line Galaxies at $z \sim 3.5$ in the ZFOURGE Survey

We analyze the properties of Extreme Emission Line Galaxies (EELGs) identified in the ZFOURGE survey at redshifts $2.5 \leq z \leq 4$. In this redshift range, ZFOURGE contains photometric data covering rest-frame wavelengths from the UV to the near-IR in the CDFS, COSMOS, and UDS fields. We use the PROSPECTOR- α model to determine properties of our EELGs and compare them to properties of Lyman-break galaxies (LBGs) at similar redshifts. Specifically, we compare stacks of nonparametric star formation histories for EELGs and LBGs. We find that EELGs show little to no star formation until the most recent time bin before observation, when they undergo a strong burst of star formation activity.

Author(s): Jonathan Cohn², Joel Leja¹, Kim-Vy Tran², Ben Forrest², Benjamin Johnson¹

Institution(s): 1. *Harvard-Smithsonian Center for Astrophysics*, 2. *Texas A&M University*

110.06 – Environments of $z \sim 0.2$ Star Forming Galaxies: Building on the Citizen Science Discovery of the Green Peas

'Green Pea' galaxies, discovered in the Galaxy Zoo citizen science project, are rare low-mass ($M < 1 \times 10^{10} M_{\odot}$) galaxies, experiencing an episode of compact, relatively low-metallicity ($z \approx 1/5 z_{\odot}$), intense starformation (3–60 M_{\odot}/yr). While their spectra have been investigated in a wide-array of follow-up studies, a detailed study of their environments is missing. Two-point correlation functions have been used to show the environmental dependence of an array of galaxy properties (eg., mass, luminosity, color, star formation, and morphology). In this study, we present a cross-correlation analysis between the Green Peas and the Luminous Red Galaxies throughout the SDSS footprint, and we find that the population of Green Peas at $0.11 < z < 0.35$ is anti-biased (bias < 1). This suggests that this population typically reside in under-dense environments.

Author(s): Carolin Cardamone¹, Nico Cappelluti², Meredith Powell², Meg Urry²

Institution(s): 1. *Wheelock College*, 2. *Yale University*

Contributing team(s): Galaxy Zoo Science Team

111 – Extrasolar Planets I

111.01 – First year of MINERVA operations

MINERVA is a robotic observatory with four 0.7 meter telescopes at Mt. Hopkins, Arizona, dedicated to precise photometry and radial velocity observations of bright, nearby stars for the discovery and characterization of small exoplanets. Here we give a status report on MINERVA from the first year of operation and a summary of our results and lessons learned. Our results demonstrate that MINERVA is capable of achieving its primary science goal of finding super-Earths around the nearest, brightest stars.

Author(s): Jason Eastman¹, John Asher Johnson¹, Nate McCrady³, Jason T Wright², Robert Wittenmyer⁴, Maurice Wilson¹

Institution(s): 1. *Harvard-Smithsonian Center for Astrophysics*, 2. *Pennsylvania State University*, 3. *University of Montana*, 4. *University of Southern Queensland*

111.02 – Dynamical Studies of N-Body Gravity and Tidal Dissipation in the TRAPPIST-1 Star System

To date, we have discovered a total of 2,729 planetary systems that contain more than 3,639 known exoplanets [1]. A majority of these are defined as compact systems, containing multiple exoplanets within 0.25 AU of the central star. It has been shown that tightly packed exoplanets avoid colliding due to long-term resonance-induced orbit stability [2]. However, due to extreme proximity, these planets experience intense gravitational forces from each other that are unprecedented within our own solar system, which makes the existence of exomoons doubtful. We present the results of an initial study evaluating dynamical stability of potential exomoons within such highly compact systems.

110.07 – Galaxy Zoo: Comparing the visual morphology of synthetic galaxies from the Illustris simulation with those in the real Universe.

We present a comparison between the Illustris simulations and classifications from Galaxy Zoo, aiming to test the ability of modern large-scale cosmological simulations to accurately reproduce the local galaxy population. This comparison is enabled by the increasingly high spatial and temporal resolution obtained by such surveys.

Using classifications that were accumulated via the Galaxy Zoo citizen science interface, we compare the visual morphologies for simulated images of Illustris galaxies with a compatible sample of images drawn from the Sloan Digital Sky Survey (SDSS) Legacy Survey.

For simulated galaxies with stellar masses less than $10^{11} M_{\odot}$, significant differences are identified, which are most likely due to the limited resolution of the simulation, but could be revealing real differences in the dynamical evolution of populations of galaxies in the real and model universes. Above $10^{11} M_{\odot}$, Illustris galaxy morphologies correspond better with those of their SDSS counterparts, although even in this mass range the simulation appears to underproduce obviously disk-like galaxies. Morphologies of Illustris galaxies less massive than $10^{11} M_{\odot}$ should be treated with care.

Author(s): Hugh Dickinson⁶, Chris Lintott⁸, Claudia Scarlata⁶, Lucy Fortson⁶, Steven Bamford⁷, Carolin Cardamone⁹, William C Keel⁴, Sandor Kruk⁸, Karen Masters¹, Brooke D Simmons⁵, Mark Vogelsberger², Paul Torrey², Gregory Snyder³

Institution(s): 1. *Haverford College*, 2. *Massachusetts Institute of Technology*, 3. *Space Telescope Science Institute*, 4. *University of Alabama*, 5. *University of California, San Diego*, 6. *University of Minnesota*, 7. *University of Nottingham*, 8. *University of Oxford*, 9. *Wheelock College*

Contributing team(s): Galaxy Zoo Science Team

This work is baselined around TRAPPIST-1, an ultra-cool dwarf star that hosts seven temperate terrestrial planets, three of which are in the habitable zone, orbiting within 0.06 AU [3]. N-body simulations place a grid of test particles varying semi-major axis, eccentricity, and inclination around the three habitable zone planets. We find that most exomoons with semi-major axes less than half the Hill sphere of their respective planet are stable over 10 kyrs, with several stable over 300 kyrs.

However, in compact systems, tidal influences from other planets can compete with tidal effects from the primary planet, resulting in possible instabilities and massive amounts of tidal dissipation. We investigate these effects with a large grid search that incorporates exomoon radius, tidal quality factor and a range of planet rigidities. Results of simulations that combine n-body gravity effects with both planetary and satellite tides are presented and contrasted with n-body results. Finally, we examine long-term stability (> 1Myrs) of the stable subset of test particles from the n-body simulation with the addition of tidal dissipation, to determine if exomoons can survive around planets e, f, and g in the TRAPPIST-1 system.

[1] Schneider (2017). The Extrasolar Planets Encyclopedia. <http://exoplanet.eu/catalog/>.

[2] Tamayo et al (2017). Convergent Migration Renders TRAPPIST-1 Long-lived. *ApJL*, 840(2), L19.

[3] Gillon et al (2016). Temperate Earth-sized planets transiting a nearby ultracool dwarf star. *Nature*, 533 (7602), 221-224.

Author(s): Michael Nayak¹, Donald H Kuetzel³, Shane T Stebler², Bogdan Udrea²

Institution(s): 1. Air Force Research Laboratory, 2. Embry-Riddle Aeronautical University, 3. University of Colorado Boulder

111.03 – Phase Curve Analysis of Super-Earth 55 Cancri e

One of the primary questions when characterizing Earth-sized and super-Earth-sized exoplanets is whether they have a substantial atmosphere like Earth and Venus, or a bare-rock surface that may come with a tenuous atmosphere like Mercury. Phase curves of the planets in thermal emission provide clues to this question, because a substantial atmosphere would transport heat more efficiently than a bare-rock surface. Analyzing phase curve photometric data around secondary eclipse has previously been used to study energy transport in the atmospheres of hot Jupiters. Here we use phase curve, *Spitzer* time-series photometry to study the thermal emission properties of the super-Earth exoplanet 55 Cancri e. We utilize a previously developed semi-analytical framework to fit a physical model to infrared photometric data of host star 55 Cancri from the *Spitzer* telescope IRAC 2 band at 4.5 μm . The model uses various parameters of planetary properties including Bond albedo, heat redistribution efficiency (i.e., the ratio between the radiative timescale and advective timescale of the photosphere), and atmospheric greenhouse factor. The phase curve of 55 Cancri e is dominated by thermal emission with an eastward-shifted hot spot located on the planet surface. We determine the heat redistribution efficiency to be ≈ 1.47 , which implies that the advective timescale is on the same order as the radiative timescale. This requirement from the phase curve cannot be met by the bare-rock planet scenario, because heat transport by currents of molten lava would be too slow. The phase curve thus favors the scenario with a substantial atmosphere. Our constraints on the heat redistribution efficiency translate to a photosphere pressure of ~ 1.4 bar. The *Spitzer* IRAC 2 band is thus a window into the deep atmosphere of the planet 55 Cancri e.

Author(s): Isabel Angelo², Renyu Hu¹

Institution(s): 1. NASA Jet Propulsion Laboratory, 2. UC Berkeley

111.04 – Statistical Analysis of Hubble/WFC3 Transit Spectroscopy of Extrasolar Planets

Transmission spectroscopy provides a window to study exoplanetary atmospheres, but that window is fogged by clouds and hazes. Clouds and haze introduce a degeneracy between the strength of gaseous absorption features and planetary physical parameters such as abundances. One way to break that degeneracy is via statistical studies. We collect all published HST/WFC3 transit spectra for 1.1-1.65 micron water vapor absorption, and perform a statistical study on potential correlations between the water absorption feature and planetary parameters. We fit the observed spectra with a template calculated for each planet using the Exo-Transmit code. We express the magnitude of the water absorption in scale heights, thereby removing the known dependence on temperature, surface gravity, and mean molecular weight. We find that the absorption in scale heights has a positive baseline correlation with planetary equilibrium temperature; our hypothesis is that decreasing cloud condensation with increasing temperature is responsible for this baseline slope. However, the observed sample is also intrinsically degenerate in the sense that equilibrium temperature correlates with planetary mass. We compile the distribution of absorption in scale heights, and we find that this distribution is closer to log-normal than Gaussian. However, we also find that the distribution of equilibrium temperatures for the observed planets is similarly log-normal. This indicates that the absorption values are affected by observational bias, whereby observers have not yet targeted a sufficient sample of the hottest planets.

Author(s): Guangwei Fu⁵, Drake Deming⁵, Heather Knutson¹, Nikku Madhusudhan⁴, Avi Mandell², Jonathan Fraine³

Institution(s): 1. California Institute of Technology, 2. NASA's Goddard Space Flight Center, 3. Space Telescope Science Institute, 4. University of Cambridge, 5. University of Maryland - College Park

111.05 – The Mega-MUSCLES HST Treasury Survey

JWST will be able to observe the atmospheres of rocky planets transiting nearby M dwarfs. A few such planets are already known (around GJ1132, Proxima Cen, and Trappist-1) and TESS is predicted to find many more, including ~ 14 habitable zone planets. To interpret observations of these exoplanets' atmospheres, we must understand the high-energy SED of their host stars: X-ray/EUV irradiation can erode a planet's gaseous envelope and FUV/NUV-driven photochemistry shapes an atmosphere's molecular abundances, including potential biomarkers like O₂, O₃, and CH₄. Our MUSCLES Treasury Survey (Cycles 19+22) used Hubble/COS+STIS UV observations with contemporaneous X-ray and ground-based data to construct complete SEDs for 11 low-mass exoplanet hosts. MUSCLES is the most widely used database for early-M and K dwarf ($>0.3 M_{\text{sun}}$) irradiance spectra and has supported a wide range of atmospheric stability and biomarker modeling work. However, TESS will find most of its habitable planets transiting stars less massive than this, and these will be the planets to characterize with JWST. Here, we introduce the Mega-MUSCLES project, an approved HST Cycle 25 Treasury program. Following on the successful MUSCLES survey, Mega-MUSCLES will expand our target list to focus on: (a) new M dwarf exoplanet hosts with varying properties; (b) reference M dwarfs below 0.3 solar masses that may be used as proxies for M dwarf planet hosts discovered after HST's lifetime; and (c) more rapidly rotating stars of GJ1132's mass to probe XUV evolution over gigayear timescales. We will also gather the first panchromatic SEDs of rocky planet hosts GJ1132 and Trappist-1. Here, we present an overview of the Mega-MUSCLES motivation, targets list, and status of the survey and show how it extends proven methods to a key new sample of stars, upon which critically depends the long-term goal of studying habitable planet atmospheres with JWST and beyond.

Author(s): Cynthia S. Froning³, Kevin France⁴, R.O. Parke Loyd¹, Allison Youngblood², Alexander Brown⁴, Christian Schneider³, Zachory Berta-Thompson⁴, Adam Kowalski⁴

Institution(s): 1. Arizona State University, 2. GSFC, 3. Hamburger Sternwarte, 4. University of Colorado at Boulder

111.06D – New Clues to the Mysterious Origin of Wide-Separation Planetary-Mass Companions

Over the past decade, direct imaging searches for young gas giant planets have revealed a new population of young planetary-mass companions with extremely wide orbital separations (>50 AU) and masses near or at the deuterium-burning limit. These companions pose significant challenges to standard formation models, including core accretion, disk instability, and turbulent fragmentation. In my talk I will discuss new results from high-contrast imaging and high-resolution infrared spectroscopy of a sample of directly imaged wide-separation companions that can be used to directly test these three competing formation mechanisms. First, I use high-contrast imaging to strongly discount scattering as a hypothesis for the origin of wide-separation companions. Second, I measure rotation rates of a subset of these companions using their near-IR spectra, and place the first constraints on the angular momentum evolution of young planetary-mass objects. Finally, I explore the ability of high-resolution spectroscopy to constrain the atmospheric C/O ratios of these companions, providing a complementary test of competing formation scenarios.

Author(s): Marta Bryan¹

Institution(s): 1. Caltech

111.07 – Characterizing Giant Exoplanets through Multiwavelength Transit Observations

Observing the characteristics of giant exoplanets is possible with ground-based telescopes and modern observational methods. We are performing characterizations of multiple giant exoplanets based on 85 allotted nights of transit observations with the 2.3 m Wyoming Infrared Observatory using Sloan filters. In particular, constraints can be made on the atmospheres of our targets from the wavelength (in)dependence in the depth of the transit observations. We present early multiwavelength photometric results on the exoplanet HD 189733 b with comparison to literature sources to exemplify the methodology employed. In total, 15 exoplanets were observed across multiple wavelengths. The majority of the observing allotted to the project was completed as part of the 2017 Summer REU at the University of Wyoming. This work will significantly contribute to the growing number of observed atmospheres and influence interpretation of future WFIRST, JWST, and TESS targets. This work is supported by the National Science Foundation under REU grant AST 1560461.

Author(s): David Kasper⁷, Jackson L. Cole⁴, Cristilyn N. Gardner¹, Bethany R. Garver⁶, Kyla L. Jarka², Aman Kar⁷, Aylin M. McGough⁷, David J. PeQueen³, Daniel Ivan Rivera⁵, Hannah Jang-Condell⁷, Henry A. Kobulnicky⁷, Daniel A. Dale⁷
Institution(s): 1. Cal State San Bernadino, 2. Colorado College, 3. Embry-Riddle Aeronautical University, 4. Middle Tennessee State, 5. San Diego State University, 6. Seattle Pacific University, 7. University of Wyoming

111.08 – Theory and Simulation of Exoplanetary Atmospheric Haze: Giant Spectral Line Broadening

112 – Starburst Galaxies

112.01 – Multiwavelength Properties of Faint Submillimeter Galaxies with Archival ALMA Data

Detection of Faint submillimeter galaxies was made possible by large improvements in the spatial resolution and sensitivity by interferometric observations. These galaxies are a dominant contributor to the extragalactic background light at millimeter wavelengths and are likely to play a significant role in galaxy evolution. We present a catalog of 28 such galaxies with $S(1.1 \text{ mm}) < 1.0 \text{ mJy}$ that have 13-band optical/near IR photometry (Spitzer DeepDrill, VIDEO, CFHTLS, and HSC) and serendipitous detections in ALMA band 6. ALMA 1.1 mm continuum observations were cross-matched with the K-band VIDEO catalog in the XMM-LSS field to identify multiwavelength counterparts. A forced Photometry approach based on the Tractor image modeling code is used to construct the catalog. The median photometric redshift of the sample is $z \sim 1.96$ along with two high redshift candidates at $z \sim 5$. We have provided population statistics using multiband photometry and estimated galaxy properties such as dust and gas masses. We aim to provide a detailed characterization of this population to ultimately devise better selection techniques for future wide-area sky surveys.

Author(s): Pallavi Patil², Mark Lacy¹, Kristina Nyland¹
Institution(s): 1. National Radio Astronomy Observatory (NRAO), 2. University of Virginia
Contributing team(s): Pallavi Patil

112.02D – Ground based THz Spectroscopy of Obscured Starbursts in the Early Universe enabled by the 2nd generation Redshift (z) & Early Universe Spectrometer (ZEUS-2)

Galaxies were surprisingly dusty in the early Universe, with more than half of the light emitted from stars being absorbed by dust within the system and re-radiated into far infrared (FIR, $\sim 50\text{-}150\mu\text{m}$) wavelengths. Dusty star forming galaxies (DSFGs) dominate the co-moving star formation rate density of the Universe that peaks around redshift, $z \sim 2$, making it compelling to study them in rest frame FIR bands. From galaxies at $z > 1$, the FIR line emission from abundant ions like [O III], [C II] and [N

II], are redshifted into the short sub-mm telluric windows. My thesis work is based on building and deploying the 2nd Generation Redshift (z) and Early Universe Spectrometer (ZEUS-2), a long-slit, echelle grating spectrometer optimized to study broad ($\Delta v = 300\text{km/s}$) spectral lines from galaxies in the 200-650 μm telluric windows using TES bolometers. These far-IR lines being extinction free and major coolants of the gas heated by (young) massive stars, are powerful probes of the physical conditions of the gas and the stellar radiation field. I present results from our survey of the [O III] 88 μm line in galaxies at redshift, $z \sim 2.8$ to 4.6, with ZEUS-2 at the Atacama Pathfinder Experiment (APEX) Telescope. To interpret our observations along with ancillary data from optical to radio facilities, we apply photoionization models for HII regions and Photo Dissociation Region (PDR) models and confirm that the galaxies host substantial ongoing obscured star formation. The presence of doubly ionized oxygen suggests hard radiation fields and hence, elevated ionization parameters that can only be accounted for by a large population of massive stars formed during the ongoing starburst, that contribute a large fraction of the infrared luminosity. This study highlights the use of FIR line emission to trace the assembly of current day massive galaxies, conditions of star formation and details of their stellar populations. The construction and operation of ZEUS-2 were funded by NSF ATI and AAG grants including AAG 1109476 and has served as a training ground for students interested in astronomical instrumentation.

Author(s): Hossein Sadeghpour², Zineb Felfeli¹, Vasili Kharchenko², James Babb², Daniel Vranceanu³
Institution(s): 1. Clark Atlanta University, 2. Harvard-Smithsonian CfA, 3. Texas Southern Univ.

Author(s): Amit Vishwas², Gordon Stacey², Thomas Nikola¹, Carl Ferkinhoff¹², Stephen Parshley¹, Justin Schoenwald¹, Cody James Lamarche², James Higdon³, Sarah Higdon³, Drew Brisbin⁹, Rolf Güesten⁴, Axel Weiss⁴, Karl Menten⁴, Kent Irwin⁸, Hsiao-Mei Cho⁷, Michael Niemack², Gene Hilton⁵, Johannes Hubmayr⁵, Mandana Amiri¹⁰, Mark Halpern¹⁰, Donald Wiebe¹⁰, Matthew Hasselfield⁶, Peter Ade¹¹, Carole Tucker¹¹

Institution(s): 1. Cornell Center for Astrophysics and Planetary Science, 2. Cornell University, 3. Georgia Southern University, 4. Max-Planck-Institut für Radioastronomie, 5. National Institute of Standards and Technology, 6. Penn State University, 7. SLAC National Accelerator Laboratory, 8. Stanford University, 9. Universidad Diego Portales, 10. University of British Columbia, 11. University of Cardiff, 12. Winona State University

112.03 – Exploring the Dust Content, Metallicity, Star Formation and AGN Activity in Distant Dusty, Star-Forming Galaxies Using Cosmic Telescope

We present our recent ALMA observations of Herschel-detected gravitationally lensed dusty, star-forming galaxies (DSFGs) and how they complement our near-infrared spectroscopic observations of their rest-frame optical nebular emission. This provides the complete picture of star formation; from the molecular gas that fuels star formation, to the dust emission which are the sites of star formation, and the nebular emission which is the gas excited by the young stars. DSFGs undergo the largest starbursts in the Universe, contributing to the bulk of the cosmic star formation rate density between redshifts $z = 1 - 4$. Internal processes within high-redshift DSFGs remains largely unexplored; such as feedback from star formation, the role of turbulence, gas surface density of molecular gas, AGN activity, and the rates of metal production. Much that is known about DSFGs star formation properties comes from their CO and dust emission. In order to fully understand the star formation history of DSFGs, it is necessary to observe their optical nebular emission. Unfortunately, UV/optical emission is severely attenuated by dust, making it challenging to detect. With the Herschel Lensing Survey, a survey of the cores of almost 600 massive galaxy clusters, we are able to probe faint dust-attenuated nebular emission. We are currently conducting a new survey using Keck/OSIRIS to resolve a sample of gravitationally lensed DSFGs from the Herschel Lensing Survey (>100 mJy, with SFRs >100 Msun/yr) at redshifts $z=1-4$ with magnifications $>10\times$ all with previously detected nebular emission lines. We present the physical and resolved properties of gravitationally lensed DSFGs at unprecedented spatial scales; such as ionization, metallicity, AGN activity, and dust attenuation.

Author(s): Gregory Walth¹, Eiichi Egami⁷, Benjamin Clément³, Wiphu Rujopakarn², Tim Rawle⁴, Johan Richard³, Miroslava Dessauges⁶, Pablo Perez-Gonzalez⁸, Harald Ebeling⁵, Andrew Vayner¹, Shelley Wright¹, Maren Cosens¹

Institution(s): 1. Center for Astrophysics and Space Sciences, UC San Diego, 2. Chulalongkorn University, 3. CRAL, Observatoire de Lyon, 4. ESA/STScI, 5. IfA, University of Hawaii, 6. Observatoire de Genève, 7. Steward Observatory, University of Arizona, 8. Universidad Complutense de Madrid

Contributing team(s): Herschel Lensing Survey

112.04D – Measurements of Lyman-Alpha Escape From HST Far-UV Spectral SNAP Survey of 33 Starforming Galaxies: Initial Results

This thesis will describe and analyze far-UV spectra from nearby starforming galaxies to investigate how line features like the hydrogen Lyman-alpha (Ly α) line at 1216 Å are related to the local properties of the host galaxy. It has been suggested that Ly α can be used as a proxy for the escape of Lyman continuum (LyC)

radiation, the escape of which from bright regions of galaxies is of particular interest. Most notably, the reionization epoch of neutral atomic hydrogen in the universe over a redshift range from $z\sim 6$ to $z\sim 12$, was highly dependent on the flux of ionizing LyC photons in the interstellar and intergalactic media. Expanding our understanding of the dynamics of the Ly α escape fraction ($f_{\text{Ly}\alpha}$) from the local environment of its emission could be key to determining a total LyC escape fraction (f_{LyC}) across all morphologies of galaxies. The wide range of Ly α emitters and absorbers (occasionally both) of this Cycle 22 SNAP survey observed by the *Cosmic Origins Spectrograph* (COS) onboard *Hubble Space Telescope* (HST) provides a unique look at far-UV spectra in candidate LyC emitters. Ly α profiles are easily observable in short exposures, and line features discernable in the low-resolution G140L mode can inform and guide future observations by COS or other FUV spectroscopy.

Author(s): Keith Redwine¹

Institution(s): 1. Johns Hopkins University

112.05 – The Evolution of Luminous Compact Blue Galaxies in the COSMOS Field

Luminous Compact Blue Galaxies (LCBGs) are a class of compact star forming galaxies that are common at $z=1$ and rare in the local universe. The rapid increase in LCBG number density between $z=0.0-1.0$ roughly follows the increase in the star formation rate density of the universe over the same redshift range. We present the first study of the evolution of the number density LCBGs using a single data set covering redshifts from $z=0.0-1.0$. We do this by generating the luminosity function of LCBGs using a reanalysis of COSMOS photometry and spectroscopic redshift information generated by the Galaxy and Mass Assembly team. We find that M^* increases by ~ 0.7 mag, ϕ^* increases by a factor of 6, and the number density of LCBGs increases by a factor of ~ 10 between $z=0.0-1.0$ roughly matching previous studies using small samples over narrow redshift ranges. We find that LCBGs make up $\sim 62\%$ of galaxies brighter than $MB=-18.5$ at $z=0.9$ and only $\sim 10\%$ at $z=0.1$.

Author(s): Lucas Hunt¹, D.J. Pisano⁴, Matthew Bershady³, Steve Crawford²

Institution(s): 1. George Mason University, 2. South African Astronomical Observatory, 3. U. Wisconsin-Madison, 4. West Virginia University

112.06 – Clues to LyC Escape from the Most Highly Ionized Green Peas

The Green Pea galaxies include the strongest known Lyman continuum emitters at low redshift. As such, they offer important clues to the properties of the galaxies that reionized the universe. We present new HST COS spectra of 13 of the most highly ionized GPs at low redshift and identify LyC-leaker candidates based on strong, narrow Ly α line profiles and weak low-ionization absorption lines. On average, galaxies with more highly ionized gas tend to have narrower Ly α profiles, a sign of low HI column densities. Candidate LyC-emitting GPs also show strong LyC production and features indicative of young (< 3 Myr) ages. In contrast, outflows may not be important for LyC and Ly α escape in the GPs; the UV absorption lines of several LyC-leaker candidates reveal slow-moving gas. We suggest that in the GPs, radiative feedback, not supernova feedback, is likely the dominant mechanism that facilitates LyC escape.

Author(s): Anne Jaskot¹, Sally Oey², Claudia Scarlata³, Tara Dowd¹

Institution(s): 1. University of Massachusetts, 2. University of Michigan, 3. University of Minnesota

113 – Innovations in Astronomy Teaching and Learning II

Astronomy education research gives us insight into the teaching and learning of astronomy, one of the most dynamic science topics for students to engage in. Presenters in this special session

will discuss the results of recent research related to innovations in assessment and instruction for high school, college, and life-long learners in astronomy related courses and interactive

experiences, including informal learning environments. Topics will include curriculum, pedagogy, assessment, online citizen science tools, and adaptive course ware to effectively engage these audiences.

113.01 – Leveraging New and Social Media to Educate the Masses

In today's connected world, scientists as individuals and as projects and institutions are turning to blogs, videos, and social media outlets like Twitter to share achievements, request aid, and discuss the issues of our science. Beyond sharing the thing-of-the-moment, these platforms also provide an environment where education is possible, and where creativity allows educators to engage broad audiences in active learning. In this presentation, we discuss how polling, ask-me-anything sessions, emoji, and animated gifs can be leveraged to test knowledge and facilitate engagement.

Beyond looking at these techniques, we also examine audience engagement. Previously, it has been unclear if our day-to-day social media efforts have been merely preaching to one homogeneous choir from which we have all drawn our audiences, or if our individual efforts have been able to reach into different communities to multiply our impact. In this preliminary study, we examine the social media audiences of several space science Twitter feeds that relate to: podcasting; professional societies; individual programs; and individuals. This study directly measures the overlap in audiences and the diversity of interests held by these audiences. Through statistical analysis, we can discern if these audiences are all drawn from one single population, or if we are sampling different base populations with different feeds. The data generated in this project allow us to look beyond how our audiences interact with space science, with the added benefit of revealing their other interests. These interests are reflected by the non-space science accounts they follow on Twitter. This information will allow us to effectively recruit new people from space science adjacent interests.

Author(s): Pamela Gay¹

Institution(s): 1. *Astronomical Society of the Pacific*

Contributing team(s): CosmoQuest Team

113.02 – Science Literacy and Prior Knowledge of Astronomy MOOC Students

Many of science classes offered on Coursera fall into fall into the category of general education or general interest classes for lifelong learners, including our own, Astronomy: Exploring Time and Space. Very little is known about the backgrounds and prior knowledge of these students. In this talk we present the results of a survey of our Astronomy MOOC students. We also compare these results to our previous work on undergraduate students in introductory astronomy courses. Survey questions examined student demographics and motivations as well as their science and information literacy (including basic science knowledge, interest, attitudes and beliefs, and where they get their information about science). We found that our MOOC students are different than the undergraduate students in more ways than demographics. Many MOOC students demonstrated high levels of science and information literacy. With a more comprehensive understanding of our students' motivations and prior knowledge about science and how they get their information about science, we will be able to develop more tailored learning experiences for these lifelong learners.

Author(s): Chris David Impey¹, Sanlyn Buxner¹, Matthew Wenger¹, Martin Formanek¹

Institution(s): 1. *University of Arizona*

113.03 – Motivations and Participation in an Astronomy MOOC

Student motivation, engagement, and completion are important topics in the study of Massive Open Online Courses (MOOCs). Many science-focused Massive Open Online Courses (MOOCs) appeal to lifelong learners interested in general education as

opposed to career development, yet little motivation-related research has been conducted with students in these courses. We present the results of a study that examined the motivations of MOOC students in our class, Astronomy: Exploring Time and Space. We examined trends in motivation and participation for these non-career-focused students. Although we have been able to show that the students in our class are similar, demographically, to other MOOC classes, our research has shown that they have very different motivations from undergraduate students, or MOOC students who are intere "average" MOOC user. Astronomy: Exploring Time and Space students are much more likely to be astronomy hobbyists, or taking the class to satisfy their curiosity and not attempting to change careers or achieve a credential. We were also able to correlate the results of the motivation survey instruments with student engagement with course materials and rates of course completion. We examined the motivations of students using both the validated Science Motivation Questionnaire II by Glynn et. al (2011) and a motivation instrument developed by John Falk for learners in free-choice settings. These allowed us to compare our results with other researchers who have used these instrument in other educational settings, including MOOCs. Students who reported high levels of self-determination were the most likely to complete the course, while high social motivation was a poor predictor of completion and performance.

Author(s): Matthew Wenger¹, Sanlyn Buxner¹, Martin Formanek¹, Chris David Impey¹

Institution(s): 1. *University of Arizona*

113.04 – Whiteboard Confessionals: Investigating a New Model Using Student Representations in Teaching Astro 101

Astronomy education researchers in the Department of Astronomy at the University of Arizona have been investigating a new framework for getting students to engage in discussions about fundamental astronomy topics. This framework is intended to also provide students with explicit feedback on the correctness and coherency of their mental models on these topics. This framework builds upon our prior efforts to create productive Pedagogical Discipline Representations (PDR). Students are asked to work collaboratively to generate their own representations (drawings, graphs, data tables, etc.) that reflect important characteristics of astrophysical scenarios presented in class. We have found these representation tasks offer tremendous insight into the broad range of ideas and knowledge students possess after instruction that includes both traditional lecture and actively learning strategies. In particular, we find that some of our students are able to correctly answer challenging multiple-choice questions on topics, however, they struggle to accurately create representations of these same topics themselves. Our work illustrates that some of our students are not developing a robust level of discipline fluency with many core ideas in astronomy, even after engaging with active learning strategies.

Author(s): Edward Prather¹

Institution(s): 1. *University of Arizona - CAE*

113.05 – The Development of the Planet Formation Concept Inventory: A Preliminary Analysis of Version 1

The topic of planet formation is poorly represented in the educational literature, especially at the college level. As recently as 2014, when developing the Test of Astronomy Standards (TOAST), Slater (2014) noted that for two topics (formation of the Solar System and cosmology), "high quality test items that reflect our current understanding of students' conceptions were not available [in the literature]" (Slater, 2014, p. 8). Furthermore, nearly half of ASTR 101 enrollments are at 2 year/community colleges where both instructors and students have little access to current research and models of planet formation. In response, we administered six student replied response (SSR) short answer questions on the topic of planet formation to n = 1,050 students enrolled in introductory

astronomy and planetary science courses at The University of Arizona in the Fall 2016 and Spring 2017 semesters. After analyzing and coding the data from the SSR questions, we developed a preliminary version of the Planet Formation Concept Inventory (PFCI). The PFCI is a multiple-choice instrument with 20 planet formation-related questions, and 4 demographic-related questions. We administered version 1 of the PFCI to six introductory astronomy and planetary science courses (n ~ 700 students) during the Fall 2017 semester. We provided students with 7-8 multiple-choice with explanation of reasoning (MCER) questions from the PFCI. Students selected an answer (similar to a traditional multiple-choice test), and then briefly explained why they chose the answer they did. We also conducted interviews with ~15 students to receive feedback on the quality of the questions and clarity of the instrument. We will present an analysis of the MCER responses and student interviews, and discuss any modifications that will be made to the instrument as a result.

Author(s): Molly Simon¹, Chris David Impey², Sanlyn Buxner¹

Institution(s): 1. University of Arizona, 2. University of Arizona, Steward Observatory

113.06 – Comparisons Between Science Knowledge, Interest, and Information Literacy of Learners in Introductory Astronomy Courses

Introductory astronomy courses are exciting opportunities to engage non-major students in scientific issues, new discoveries, and scientific thinking. Many undergraduate students take these courses to complete their general education requirements. Many free-choice learners also take these courses, but for their own interest. We report on a study comparing the basic science knowledge, interest in science, and information literacy of undergraduate students and free choice learners enrolled in introductory astronomy courses run by the University of Arizona. Undergraduate students take both in-person and online courses for college credit. Free choice learners enroll in massive open online courses (MOOCs), through commercial platforms, that can earn them a certificate (although most do not take advantage of that opportunity). In general, we find that undergraduate students outperform the general public on basic science knowledge and that learners in our astronomy MOOCs outperform the undergraduate students in the study. Learners in the MOOC have higher interest in science in general. Overall, learners in both groups report getting information about science from online sources. Additionally, learners' judgement of the reliability of different sources of information is weakly related to their basic science knowledge and more strongly related to how they describe what it means to study something scientifically. We discuss the implications of our findings for both undergraduate students and free-choice learners as well as instructors of these types of courses.

Author(s): Sanlyn Buxner¹, Chris David Impey¹, Martin Formanek¹, Matthew Wenger¹

Institution(s): 1. University of Arizona

113.07 – Educating Through Exploration: Emerging Evidence for Improved Learning Outcomes Using a New Theory of Digital Learning Design

Advances in scientific visualization and public access to data have transformed science outreach and communication, but have yet to realize their potential impacts in the realm of education. Computer-based learning is a clear bridge between visualization and education that benefits students through adaptive personalization and enhanced access. Building this bridge requires close partnerships among scientists, technologists, and educators.

The Infiniscope project fosters such partnerships to produce exploration-driven online learning experiences that teach basic science concepts using a combination of authentic space science narratives, data, and images, and a personalized guided inquiry

approach. Infiniscope includes a web portal to host these digital learning experiences, as well as a teaching network of educators using and modifying these experiences. Infiniscope experiences are built around a new theory of digital learning design that we call "education through exploration" (ETX) developed during the creation of successful online, interactive science courses offered at ASU and other institutions. ETX builds on the research-based practices of active learning and guided inquiry to provide a set of design principles that aim to develop higher order thinking skills in addition to understanding of content. It is employed in these experiences by asking students to solve problems and actively discover relationships, supported by an intelligent tutoring system which provides immediate, personalized feedback and scaffolds scientific thinking and methods. The project is led by ASU's School of Earth and Space Exploration working with learning designers in the Center for Education Through eXploration, with support from NASA's Science Mission Directorate as part of the NASA Exploration Connection program.

We will present an overview of ETX design, the Infiniscope project, and emerging evidence of effectiveness.

Author(s): Ariel Anbar¹

Institution(s): 1. Arizona State University

Contributing team(s): Center for Education Through eXploration

113.08 – Teaching the Thrill of Discovery: Student Exploration of Ultra-Faint Dwarf Galaxies with the NAO Data Lab

We describe an activity aimed at teaching students how ultra-faint Milky Way dwarf galaxies are typically discovered: through filtering of optical photometric catalogs and cross-examination with deep images. The activity, which was developed as part of the Teen Astronomy Café program (<https://teensciencecafe.org/cafes/az-teen-astronomy-cafe-tucson/>), uses the NAO Data Lab (<http://datalab.nao.edu>) and other professional-grade tools to lead high school students through exploration of the object catalog and images from the Survey of the Magellanic Stellar History (SMASH). The students are taught how to use images and color-magnitude diagrams to analyze and interpret stellar populations of increasing complexity, including those of star clusters and the Magellanic Clouds, and culminating with the discovery of the Hydra II ultra-faint dwarf galaxy. The tools and datasets presented allow the students to explore and discover other known stellar systems, as well as unknown candidate star clusters and dwarf galaxies. The ultimate goal of the activity is to give students insight into the methods of modern astronomical research and to allow them to participate in the thrill of discovery.

Author(s): Knut Olsen¹, Constance E. Walker¹, Blake Smith¹

Institution(s): 1. NAO

Contributing team(s): NAO Data Lab Team

113.09 – Original Research By Young Twinkle Students

(ORBYTS): When can students start performing original research?

Involving students in state-of-the-art research from an early age eliminates the idea that science is only for the scientists and empowers young people to explore STEM (Science, Technology, Engineering and Maths) subjects. It is also a great opportunity to dispel harmful stereotypes about who is suitable for STEM careers, while leaving students feeling engaged in modern science and the scientific method. As part of the Twinkle Space Mission's educational programme, EduTwinkle, students between the ages of 15 and 18 have been performing original research associated with the exploration of space since January 2016. The student groups have each been led by junior researchers - PhD student and post-doctoral scientists - who themselves benefit

substantially from the opportunity to supervise and manage a research project. This research aims to meet a standard for publication in peer-reviewed journals. At present the research of one ORBYTS team has been published in the *Astrophysical Journal Supplement Series* and another submitted to *JQSRT*; we expect more papers to follow. Here we outline the necessary steps for a productive scientific collaboration with school children, generalising from the successes and downfalls of the pilot ORBYTS projects.

114 – Star Formation I

114.01 – A GLIMPSE of Star Formation in the Outer Galaxy

The wealth of infrared data provided by recent infrared missions such as Spitzer, Herschel, and WISE has yet to be fully mined in the study of star formation in the outer galaxy. The nearby galaxy and massive star forming regions towards the galactic center have been extensively studied. However the outer regions of the Milky Way, where the metallicity is intermediate in value between the inner galactic disk and the Magellanic Clouds, has not been systematically studied.

We are using Spitzer/IRAC's GLIMPSE (Galactic Legacy Infrared Mid-plane Survey Extraordinaire) observations of the galactic plane at 3.6, 4.5, 5.8, and 8.0 microns to identify young stellar objects (YSOs) via their disk emission in the mid-infrared. A tiered clustering analysis is then performed: preliminary large scale clustering is identified across the field using a Density-Based Spatial Clustering of Applications with Noise (DBSCAN) technique. Smaller scale sub clustering within these regions is performed using an implementation of the Minimum Spanning Tree (MST) technique. The YSOs are then compared to known objects in the SIMBAD catalogue and their photometry and cluster membership is augmented using available Herschel and WISE photometry. We compare our results to those in the inner galaxy to determine how dynamical processes and environmental factors affect the star formation efficiency. These results will have applications to the study of star formation in other galaxies, where only global properties can be determined.

We will present here the results of our initial investigation into star formation in the outer galaxy using the Spitzer/GLIMPSE observations of the SMOG field.

Author(s): Elaine Winston¹, Joseph L. Hora¹, Volker Toll¹
Institution(s): 1. *Harvard-Smithsonian CfA*

114.02D – Hierarchical Star Formation with Young Stellar Clusters with LEGUS

We present findings on using young star clusters to trace the unbound hierarchical star-forming structures in nearby galaxies drawn from the Legacy ExtraGalactic UV Survey (LEGUS) program. LEGUS is a cycle 21 Hubble Space Telescope Treasury program designed to characterize the link between star formation of individual stars, stellar clusters and associations on parsec scales, and that of galaxy disks on kiloparsec scales. We find that star clusters are strongly clustered with respect to each other and that the spatial clustering disappears rapidly across all galaxies for ages as young as a few tens of Myr. This indicates that most, if not all, recent star formation occurs within rapidly dispersing hierarchical complexes. The observed correlations are consistent with arising in a turbulent-driven interstellar medium. We also present recent investigations of correlating CO gas to the star clusters to better understand the environmental connection between gas and recent star formation. We find a clear excess of young star clusters being spatially located near their natal molecular gas, disassociating in as little as 4-6 Myr. Lastly, we find that the spatial clustering of GMCs is significantly suppressed compared to that of star clusters. This suggests that GMCs must produce more than one star cluster, improving our

Author(s): Clara Sousa-Silva¹

Institution(s): 1. *MIT*

Contributing team(s): ORBYTS, Twinkle Space Mission, ExoMol

ability to link the products of star formation to the properties of natal gas from which they originate.

Author(s): Kathryn Grasha¹, Daniela Calzetti¹

Institution(s): 1. *University of Massachusetts, Amherst*

114.03D – The Origin of Scales and Scaling Laws in Star Formation

Star formation is one of the key processes of cosmic evolution as it influences phenomena from the formation of galaxies to the formation of planets, and the development of life. Unfortunately, there is no comprehensive theory of star formation, despite intense effort on both the theoretical and observational sides, due to the large amount of complicated, non-linear physics involved (e.g. MHD, gravity, radiation). A possible approach is to formulate simple, easily testable models that allow us to draw a clear connection between phenomena and physical processes. In the first part of the talk I will focus on the origin of the IMF peak, the characteristic scale of stars. There is debate in the literature about whether the initial conditions of isothermal turbulence could set the IMF peak. Using detailed numerical simulations, I will demonstrate that not to be the case, the initial conditions are "forgotten" through the fragmentation cascade. Additional physics (e.g. feedback) is required to set the IMF peak. In the second part I will use simulated galaxies from the Feedback in Realistic Environments (FIRE) project to show that most star formation theories are unable to reproduce the near universal IMF peak of the Milky Way.

Finally, I will present analytic arguments (supported by simulations) that a large number of observables (e.g. IMF slope) are the consequences of scale-free structure formation and are (to first order) unsuitable for differentiating between star formation theories.

Author(s): David Guszejnov¹, Philip Hopkins¹, Michael Grudich¹

Institution(s): 1. *California Institute of Technology*

114.04 – ATLASGAL -- A molecular view of an unbiased sample of massive star forming clumps

Massive stars play an important role in many areas of astrophysics, from regulating star formation to driving the evolution of their host galaxy. Study of these stars is made difficult by their short evolutionary timescales, small populations and greater distances, and further complicated because they reach the main sequence while still shrouded in their natal clumps. As a result, many aspects of their formation are still poorly understood.

We have assembled a large and statistically representative collection of massive star-forming environments that span all evolutionary stages of development by correlating mid-infrared and dust continuum surveys. We have conducted follow-up single-pointing observations toward a sample of approximately 600 of these clumps with the Mopra telescope using an 8 GHz bandwidth that spans some 27 molecular and mm-radio recombination line transitions. These lines trace a wide range of interstellar conditions with varying thermal, chemical, and kinematic properties. Many of these lines exhibit hyperfine

structure allowing more detailed measurements of the clump environment (e.g. rotation temperatures and column densities).

From these twenty-seven lines, we have identified thirteen line intensity ratios that strongly trace the evolutionary state of these clumps. We have investigated individual molecular and mm-radio recombination lines, contrasting these with radio and sub-mm continuum observations. We present a summary of the results of the statistical analysis of the sample, and compare them with previous similar studies to test their utility as chemical clocks of the evolutionary processes.

Author(s): Charles Figura⁴, James Urquhart³, Friedrich Wyrowski², Andrea Giannetti¹, Wonju Kim²

Institution(s): 1. *Istituto di Radioastronomia*, 2. *Max-Planck-Institut für Radioastronomie*, 3. *University of Kent*, 4. *Wartburg College*

114.05 – Distances, Kinematics, And Structure Of The Orion Complex

I present an analysis of the structure and kinematics of the Orion Molecular Cloud Complex in an effort to better characterize the dynamical state of the closest region of ongoing massive star formation. I measured stellar parallax and proper motions with <5% uncertainty using radio VLBI observations of non-thermally-emitting sources located in various star forming regions within the Orion Complex. This includes the first direct distance measurements for sources that are located outside of the Orion Nebula. I identified a number of binary systems in the VLBI dataset and fitted their orbital motion, which allows for the direct measurement of the masses of the individual components. Additionally, I have identified several stars that have been ejected from the Orion Nebula due to strong gravitational interactions with the most massive members. I complemented the parallax and proper motion measurements with the observations of optical radial velocities of the stars toward the Orion Complex, probing the histories of both dynamic evolution and star formation in the region, providing a 6-dimensional model of the Complex. These observations can serve as a baseline for

115 – The Solar System

115.01 – The End of Cassini: Final VLBA Astrometry Epochs to Improve the Saturn Ephemeris

During the past dozen years we have used the Very Long Baseline Array (VLBA) to measure the position of the Cassini spacecraft in orbit around Saturn. These data, combined with fits of Cassini's orbit with respect to Saturn from Deep Space Network tracking, have provided a time series of positions for the Saturn system barycenter in the inertial International Celestial Reference Frame (ICRF). We report results from the final observing epochs of this program obtained prior to Cassini's intentional destruction in the atmosphere of Saturn in September 2017. We now know Saturn's orbit to approximately 0.2 mas (1 nrad), nearly two orders of magnitude better than it was known before the Cassini mission. Our VLBA positions provide the best constraints on the orientation of Saturn's orbit (inclination and longitude of ascending node), while ranging data provide the best constraints on the orbit semi-major axis and eccentricity.

This work has been partially supported by a grant from the NASA Planetary Astronomy program to the Space Science Institute, Boulder, CO. Part of this work has been carried out at the Jet Propulsion Laboratory, California Institute of Technology, under contract with NASA. The Long Baseline Observatory is a facility of the National Science Foundation operated under cooperative agreement by Associated Universities, Inc.

Author(s): Dayton Jones⁴, William M. Folkner¹, Jonathan D. Romney², Vivek Dhawan³

Institution(s): 1. *Jet Propulsion Laboratory, California Institute of Technology*, 2. *Long Baseline Observatory*, 3. *National Radio Astronomy Observatory*, 4. *Space Science Institute*

comparison of the upcoming results from the *Gaia* space telescope

Author(s): Marina Kounkel², Lee Hartmann¹

Institution(s): 1. *University of Michigan*, 2. *Western Washington University*

114.06 – On the Appearance of Thresholds in the Dynamical Model of Star Formation

A dynamical model of the interstellar medium involving gravitational collapse and feedback from star formation has been used to explain the Kennicutt-Schmidt (KS) relationship between star formation surface density and gas surface density. In a simple version of this model, the relationship has a power law index of ~ 1.5 when plotted versus the total gas surface density and an index of ~ 1 for molecules. The first presumably reflects an underlying three-dimensional collapse at the local gravity rate, which has a $\rho^{1.5}$ dependence for density ρ , applied to the main part of a galaxy where the disk thickness is about constant. The second may be the result of a selection effect for molecular gas at a characteristic density for observation. A third relationship has a slope of ~ 2 for total gas in gas-dominated regions where the gas surface density exceeds the stellar surface density, such as the outer parts of spiral galaxies and in dwarf irregular galaxies. Individual molecular clouds have about this squared-law too, perhaps for the same reason. Other star formation relationships seem to violate the model, however. One is the appearance of a threshold surface density for star formation with a constant rate per unit gas mass above the threshold regardless of density. Another is the increasing inefficiency of star formation in dense molecular gas at high density. Here we use probability distribution functions for density and collapse timing to explain these relationships in a new way and to illuminate possible origins for the threshold effects.

Author(s): Bruce G. Elmegreen¹

Institution(s): 1. *IBM T.J. Watson Research Center*

115.02 – Using collisions and resonances to tilting Uranus

Uranus' large obliquity (98°) is widely thought to have occurred from a polar strike with an Earth sized object. Morbidelli et al. (2012) argue that two or more collisions are required in order to explain the prograde motion of Uranus' satellites. These impactors could have been less massive by about a factor of ten, but multiple polar strikes are still improbable as even larger mass impactors would be needed for more equatorial collisions. Here we explore an alternative non-collisional model inspired by the explanation to Saturn's significant tilt (27°). Ward and Hamilton (2004) & Hamilton and Ward (2004) argue that a secular resonance currently between Saturn's spin axis and Neptune's orbital pole is responsible for Saturn's large obliquity. Unfortunately, Uranus' axial precession frequency today is too long to match any of the current planets' fundamental frequencies. Boué and Laskar (2010) explain that Uranus may have harbored an improbably large moon in the past which could have sped up the planet's axial precession frequency enough to resonate with the regression of its own orbital pole. We explore another scenario which requires only the interactions between the giant planets.

Thommes et al. (1999, 2002, 2003) argue that at least the cores of Uranus and Neptune were formed in between Jupiter and Saturn, as the density of the protoplanetary disk was greater there. If Neptune was scattered outward before Uranus, then a secular spin-orbit resonance between the two planets is possible. However, driving Uranus' obliquity to near 90° with a resonance capture requires a timescale on the order of 100 Myr. If Neptune migrated out quicker or its orbital inclination was initially larger, then we find that the resulting resonance kick can tilt Uranus more than 40° in a reasonable timespan. This could replace one of the impactors required in the collisional scenario described by

Morbidelli et al. (2012), but in most situations the effect of such a kick is only about 10° . Since collisions are therefore necessary to explain at least part of the tilting, we are now considering hybrid models that involve combinations of resonance captures and kicks, and collisions.

Author(s): Zeev Rogozinski¹, Douglas Hamilton¹
Institution(s): 1. *University of Maryland*

115.03 – Colours of the Outer Solar System Origins Survey: An Update

The vast majority of the known dwarf-planet sized bodies are bright enough to be studied through optical and infrared spectroscopy. As a result, we have an understanding of the surface properties for the largest Kuiper belt objects (KBOs) which retain their primordial inventory of volatile ices. For the typically smaller > 22 mag KBO, we must rely instead on what colors reveal by proxy; yet this picture remains incomplete. Most KBO physical property studies examine the hodgepodge set of objects discovered by various surveys with different and varying detection biases that make it difficult if not impossible to reliably estimate the sizes of the different surface color groupings (compositional classes) residing in the modern-day Kuiper belt.

The Colours of the Outer Solar System Origins Survey (Col-OSSOS) probes the surface properties within the Kuiper belt primarily through near simultaneous g,r and J colors with the Gemini North Telescope and u-band with Canada-France-Hawaii Telescope. The project aims to target ~ 100 KBOs brighter than 23.6 r' mag found by the Outer Solar System Origins Survey (OSSOS), a survey with a well-measured detection efficiency. Thus, Col-OSSOS provides the first brightness-complete, compositional-dynamical map of the Outer Solar System, probing in a new light the radial color distribution in the primordial planetesimal disk from which KBOs originated. We will provide an update on the current status of the program highlighting results from the first two years of the survey; including size estimates of the two color KBO subgroups (the red and neutral surfaces) within the dynamically excited Kuiper belt and implications for the early planetesimal disk composition based on neutral-colored binaries found in the cold classical Kuiper belt.

Author(s): Megan E. Schwamb³, Wesley C. Fraser⁷, Rosemary E. Pike², Michele T. Bannister⁷, Michaël Marsset⁷, J.J. Kavelaars⁵, Susan Benecchi⁶, Audrey C. Delsanti¹, Matthew J. Lehner², Shiang-Yu Wang², Audrey Thirouin⁴, David Nesvorný⁸
Institution(s): 1. *Aix Marseille Universit, CNRS, LAM (Laboratoire d'Astrophysique de Marseille)*, 2. *ASIAA*, 3. *Gemini Observatory*, 4. *Lowell Observatory*, 5. *NRC-Herzberg Astronomy and Astrophysics*, 6. *PSI*, 7. *Queen's University Belfast*, 8. *SwRI*

115.04 – Jovian Hotspots in the NEB in the Visible and Near-IR from Hubble and Ground-Based IR Observations

In order to better understand the composition and behavior of Jupiter's atmosphere, radiating regions in the infrared known as 'hotspots' are compared with darker spots in the visible at the same locations within the Northern Equatorial Band (NEB). Hubble images taken in across the visible and into the near-infrared (between 275 nm and 889 nm) are compared with 5.1 μ m images taken using the Subaru telescope and other ground-based observations. The connection between these regions has been known for some time, and comparison between them at these wavelengths showed a general correlation between dimness in the visible and brightness in the infrared, but this was not the case in all observed locations. The origins and cause of these hotspots remains unclear, but because of their quasi-stable nature and reoccurrence at roughly 30-degree longitudes suggests a relationship with Rossby Waves. Continuous spectra from Multi-Unit Spectroscopic Explorer (MUSE) also shows that measured values from the near-infrared fit well with observations, and hints at the composition of the discolored region through the use of NEMESIS software cross-correlation.

Author(s): Matthew Michael Wittal¹, Glenn Orton¹, James Sinclair¹, Michael Wong³, Amy Simon², Patrick Irwin⁴, Ashwin Braude⁴

Institution(s): 1. *Jet Propulsion Laboratory*, 2. *NASA Goddard Space Flight Center*, 3. *University of California Berkeley*, 4. *University of Oxford*

115.05 – The Pan-STARRS search for Near-Earth Objects

The Pan-STARRS¹ telescope on Haleakala, Hawaii has become the leading discovery telescope for Near-Earth Objects (NEOs), and is now responsible for discovering almost half of all new NEOs, more than half of all larger NEOs, and more than half of all new comets. The survey routinely reaches depths of $V=22$ or fainter (in dark sky conditions) over an area of approximately 1,000 square degrees per night. The survey strategy will be described. The survey will soon be augmented by the addition of the Pan-STARRS² telescope, which has similar optics and an improved camera, and which will roughly double the survey power. A sample of the important recent solar system discoveries made by the Pan-STARRS survey will be summarized.

Author(s): Richard J Wainscoat¹, Robert Weryk¹, Kenneth Chambers¹

Institution(s): 1. *University of Hawaii*

115.06 – The Deflector Selector: A Machine Learning Framework for Prioritizing Hazardous Object Deflection Technology Development

Several technologies have been proposed for deflecting a hazardous Solar System object on a trajectory that would otherwise impact the Earth. The effectiveness of each technology depends on several characteristics of the given object, including its orbit and size. The distribution of these parameters in the likely population of Earth-impacting objects can thus determine which of the technologies are most likely to be useful in preventing a collision with the Earth. None of the proposed deflection technologies has been developed and fully tested in space. Developing every proposed technology is currently prohibitively expensive, so determining now which technologies are most likely to be effective would allow us to prioritize a subset of proposed deflection technologies for funding and development. We will present a new model, the Deflector Selector, that takes as its input the characteristics of a hazardous object or population of such objects and predicts which technology would be able to perform a successful deflection. The model consists of a machine-learning algorithm trained on data produced by N-body integrations simulating the deflections. We will describe the model and present the results of tests of the effectiveness of nuclear explosives, kinetic impactors, and gravity tractors on three simulated populations of hazardous objects.

Author(s): Erika Nesvold², Adam Greenberg⁷, Nicolas Erasmus⁶, Elmarie Van Heerden⁴, J. L. Galache¹, Eric Dahlstrom³, Franck Marchis⁵

Institution(s): 1. *Aten Engineering*, 2. *Carnegie Institution of Washington*, 3. *International Space Consultants*, 4. *Oxford University*, 5. *SETI Institute*, 6. *South African Astronomical Observatory*, 7. *UCLA*

115.07 – The Implications of the Excited Rotation of Comet 252P/2000 G1 (LINEAR)

Jupiter Family comet (JFC) 252P/LINEAR had a close encounter to Earth on 2016 March 21. We imaged the comet with the Hubble Space Telescope Wide Field Camera 3 UVIS channel through the V- and r'-band filters spanning ~ 8 hours on 2016 April 4. The pixel scale of 2.7 km/pixel allowed us to study the structure of the cometary coma at scales of a few kilometers to a few hundred kilometers from the nucleus, a characteristic that is unique to our data. The dust coma of 252P showed a strong, well defined, narrow and nearly linear feature in the sunward direction, and its projected position angle moved about the nucleus for ~ 60 deg in 8 hours, consistent with an apparent periodicity of ~ 7.24 hours. On the other hand, the lightcurve

measured in both V- and r'-band images from a 13 km radius aperture, after corrected for color term, showed a variability of >0.14 mag that is consistent with an apparent periodicity of ~ 5.4 hours or its multiples. We suggest that the two different periodicities derived from coma morphology and the lightcurve is a strong indication that the nucleus of 252P is in a non-principal axis (NPA) rotation, joining two other confirmed NPA rotators (1P/Halley and 103P/Hartley 2) and comets that are potentially in NPA rotational states (e.g., 2P/Encke). However, this apparition has been unusual for 252P. In the past three perihelion passages since discovery, the comet was very weakly active compared to other JFCs. Meteor evidence also exists that it probably has been very weakly active for a few hundred years. But in our data, we saw a very active comet in this 2016 apparition with an active fraction of 40% to $>100\%$, representing an increase of 100x with respect to its recent past. Based on our observations, 252P has a small nucleus with a radius of ~ 0.3 km, which suggests that its rotational state could be relatively easily changed by torques caused by outgassing. Since the very weak outgassing in the past is not likely to change the rotational state of 252P, the origin of its excited rotational state is interesting. Exploring the possible scenarios to excite the rotation of 252P may place constraints on its activity history. We will discuss results from our investigations.

Author(s): Jian-Yang Li⁶, Nalin H Samarasinha⁶, Michael S.P. Kelley⁸, Davide Farnocchia³, Max J. Mutchler⁷, Yanqiong Ren⁵, Xiaoping Lu⁵, David J. Tholen², Tim Lister⁴, Marco Micheli¹

Institution(s): 1. ESA SSA-NEO Coordination Centre, 2. Institute for Astronomy, University of Hawaii, 3. Jet Propulsion Laboratory, California Institute of Technology, 4. Las Cumbres Observatory Global Telescope Network, 5. Macau University of Science and Technology, 6. Planetary Science Institute, 7. Space Telescope Science Institute, 8. University of Maryland

115.08 – The Lord of the Rings - Deep Learning Craters on the Moon and Other Bodies

Crater detection has traditionally been done via manual inspection of images, leading to statistically significant disagreements between scientists for the Moon's crater distribution. In addition, there are millions of uncategorized craters on the Moon and other Solar System bodies that will never be classified by humans due to the time required to manually detect craters. I will show that a deep learning model trained on

the near-side of the Moon can successfully reproduce the crater distribution on the far-side, as well as detect thousands of small, new craters that were previously uncharacterized. In addition, this Moon-trained model can be transferred to accurately classify craters on Mercury. It is therefore likely that this model can be extended to classify craters on all Solar System bodies with Digital Elevation Maps. This will facilitate, for the first time ever, a systematic, accurate, and reproducible study of the crater records throughout the Solar System.

Author(s): Ari Silburt¹, Mohamad Ali-Dib², Chenchong Zhu², Alan Jackson², Diana Valencia², Yevgeni Kissin², Daniel Tamayo², Kristen Menou²

Institution(s): 1. Penn State University, 2. University of Toronto

115.09 – Hydrodynamic Modeling of the Deep Impact Mission into Comet Tempel 1

Kinetic impact is one of the primary strategies to deflect hazardous objects off of an Earth-impacting trajectory. The only test of a small-body impact is the 2005 Deep Impact mission into comet Tempel 1, where a 366-kg mass impactor collided at ~ 10 km/s into the comet, liberating an enormous amount of vapor and ejecta. Code comparisons with observations of the event represent an important source of new information about the initial conditions of small bodies and an extraordinary opportunity to test our simulation capabilities on a rare, full-scale experiment. Using the Adaptive Smoothed Particle Hydrodynamics (ASPH) code, Spheral, we explore how variations in target material properties such as strength, composition, porosity, and layering affect impact results, in order to best match the observed crater size and ejecta evolution. Benchmarking against this unique small-body experiment provides an enhanced understanding of our ability to simulate asteroid or comet response to future deflection missions.

This work was performed under the auspices of the U.S. Department of Energy by Lawrence Livermore National Laboratory under Contract DE-AC52-07NA27344. LLNL-ABS-739336-DRAFT.

Author(s): Kya Sorli¹, Tané Remington², Megan Bruck Syal²

Institution(s): 1. Duke University, 2. Lawrence Livermore National Laboratory

117 – Plenary Talk: A New Measurement of the Expansion Rate of the Universe, Evidence of New Physics?, Adam Riess (Johns Hopkins University)

117.01 – A New Measurement of the Expansion Rate of the Universe, Evidence of New Physics?

The Hubble constant remains one of the most important parameters in the cosmological model, setting the size and age scales of the Universe. Present uncertainties in the cosmological model including the nature of dark energy, the properties of neutrinos and the scale of departures from flat geometry can be constrained by measurements of the Hubble constant made to higher precision than was possible with the first generations of Hubble Telescope instruments. A streamlined distance ladder constructed from infrared observations of Cepheids and type Ia supernovae with ruthless attention paid to systematics now provide 2.4% precision and offer the means to do even better. By

steadily improving the precision and accuracy of the Hubble constant, we now see evidence for significant deviations from the standard model, referred to as LambdaCDM, and thus the exciting chance, if true, of discovering new fundamental physics such as exotic dark energy, a new relativistic particle, or a small curvature to name a few possibilities. I will review recent and expected progress in the near term.

Author(s): Adam Riess¹

Institution(s): 1. Space Telescope Science Institute

160 – HEAD I: Astrophysics and Exploration from the International Space Station with NICER

160.01 – NICER Mission Overview, Status, and GO opportunities

The Neutron Interior Composition Explorer (NICER) was launched in June 2017 to the International Space Station (ISS) where it is studying the time-domain X-ray sky. NICER consists of a collection of X-ray concentrators, silicon drift detectors, an optical bench, and pointing system that together provide a large collection area in the soft (0.2-12 keV) X-ray bandpass. NICER

time-stamps individual X-ray photons to an absolute precision of better than 100 nanoseconds while providing moderate CCD-like energy resolution. Since installation, NICER has observed over 100 celestial targets including neutron stars and other objects. The NICER team accepts target of opportunity (TOO) requests for consideration. In addition, NICER will be demonstrating the use of some millisecond pulsars as navigational beacons. NICER will complete its baseline mission in January 2019 with data beginning to be made public in January 2018. Conditional on the

status of its baseline science objectives, NICER will be open to a guest observer program with first round proposals due in mid 2018 for observations beginning in 2019.

Author(s): Keith C Gendreau¹
Institution(s): 1. NASA

160.02 – Taking the measure of neutron stars with NICER

The Neutron Star Interior Composition Explorer (NICER) is NASA's new X-ray timing instrument onboard the ISS that was launched in June 2017. With a large effective area, low background, very precise absolute timing and great low energy response, NICER has been doing a fantastic job in observing many interesting phenomena related to neutron stars and black holes. One of the main goals of the NICER mission is to constrain the equation of state of ultra-dense matter by measuring the masses and radii of several rotation-powered millisecond pulsars. This is being done by fitting pulse waveform models that incorporate all relevant relativistic effects and atmospheric radiation transfer processes to the periodic soft X-ray modulations produced by the rotation of hot spots located near the magnetic polar caps of these pulsars. Some of the other interesting topics that are being studied with NICER includes phenomena related to Type I X-ray bursts, which are thermonuclear flashes observed from the surfaces of accreting neutron stars in Low Mass X-ray Binaries, such as photospheric radius expansion and burst oscillations. NICER's large effective area and excellent low energy response enable new, detailed studies of these bursts in the soft X-ray band. In this talk I will present some of the early results from the first seven months of the NICER mission and will report on the progress being made by the NICER team in measuring the masses and radii of pulsars.

Author(s): Simin Mahmoodifar¹
Institution(s): 1. Universities Space Research Association

160.03 – Early NICER Observations of Magnetars and Young Pulsars

116 – Cosmology I

116.01 – SVD/MCMC Data Analysis Pipeline for Global Redshifted 21-cm Spectrum Observations of the Cosmic Dawn and Dark Ages

We have designed a complete data analysis pipeline for constraining Cosmic Dawn physics using sky-averaged spectra in the VHF range (40-200 MHz) obtained either from the ground (e.g., the Experiment to Detect Global Epoch of Reionization Signal, EDGES; and the Cosmic Twilight Polarimeter, CTP) or from orbit above the lunar farside (e.g., the Dark Ages Radio Explorer, DARE). In the case of DARE, we avoid Earth-based RFI, ionospheric effects, and radio solar emissions (when observing at night). To extract the 21-cm spectrum, we parametrize the cosmological signal and systematics with two separate sets of modes defined through Singular Value Decomposition (SVD) of training set curves. The training set for the 21-cm spin-flip brightness temperatures is composed of theoretical models of the first stars, galaxies and black holes created by varying physical parameters within the *ares* code. The systematics training set is created using sky and beam data to model the beam-weighted foregrounds (which are about four orders of magnitude larger than the signal) as well as expected lab data to model receiver systematics. To constrain physical parameters determining the 21-cm spectrum, we apply to the extracted signal a series of consecutive fitting techniques including two usages of a Markov Chain Monte Carlo (MCMC) algorithm. Importantly, our pipeline efficiently utilizes the significant differences between the foreground and the 21-cm signal in spatial and spectral variations. In addition, it incorporates for the first time polarization data, dramatically improving the constraining power. We are currently validating this end-to-end pipeline using detailed simulations of the signal, foregrounds and instruments. This work was directly supported

Neutron star Interior Composition Explorer (NICER) is an X-ray telescope attached to the International Space Station (ISS). Launched in June 2017, it is designed to precisely measure the masses and radii of neutron stars (NS) and probe NS equations of state. But its precision timing capabilities and large effective area uniquely position NICER for the study of magnetars. The NICER Magnetar & Magnetosphere (M&M) science working group focuses on studying highly-magnetized neutron stars, a diverse program that includes magnetars, high-B pulsars, rotation powered pulsars, and isolated neutron stars. Our ongoing campaign has already observed targets such as 4U 0142+61, a magnetar in outburst with coincident NuSTAR and Swift observations, the radio rotation powered Vela pulsar PSR B0833-45, and a transient magnetar XTE J1810-197. I will discuss the goals of the M&M program, spectral and temporal results from the observed targets, and an overview of upcoming observations.

Author(s): Melania Nynka¹
Institution(s): 1. McGill University

160.04 – Accreting Neutron Star and Black Hole Binaries with NICER

The NICER mission on the International Space Station has significant new capabilities for the study of accreting neutron stars and black holes, including large effective area, low background, and excellent low-energy X-ray response. Both the NICER Burst and Accretion Working Group and the Observatory Science Working Group have designed observing programs that probe various aspects of accretion physics. I will present some early results from the first six months of the NICER mission, including observations of the black hole transients MAXI J1535-571 and GX 339-4, the high-mass X-ray binary pulsars GRO J1008-57 and Swift J02436+6124, and the X-ray burster 4U 1820-30.

Author(s): Deepto Chakrabarty¹
Institution(s): 1. MIT

by the NASA Solar System Exploration Research Virtual Institute cooperative agreement number 80ARCO17M0006 and funding from the NASA Ames Research Center cooperative agreement NNX16AF59G.

Author(s): Professor O. Burns³, Keith Tauscher³, David Rapetti³, Jordan Mirocha², Eric Switzer¹
Institution(s): 1. NASA Goddard Space Flight Center, 2. University of California at Los Angeles, 3. University of Colorado Boulder

116.02D – Antenna Design and Foreground Characterization for Improved Detection of the Redshifted 21 cm Global Signature During the Epoch of Reionization

The Experiment to Detect the Global Epoch of Reionization (EoR) Signature (EDGES) is an effort to measure the sky-averaged redshifted 21 cm difference temperature, T_b , with a single wide field-of-view well-calibrated antenna placed in Western Australia. T_b is due to interactions of the hyperfine ground state of HI with the CMB and is four to five orders of magnitude dimmer than the foreground synchrotron radiation whose removal requires very low systematic errors in data collection. I analyzed two different antenna designs, a rectangular blade-shaped antenna and a fourpoint-shaped antenna, by comparing and quantifying the impact of the chromatic nature of the antenna beam directivity. Foreground removal of simulated antenna temperatures, formed by convolving a frequency scaled Haslam 408 MHz sky map with each of the antenna's chromatic beams, resulted in a factor of 10 lower rms error for the blade antenna when using a five term polynomial for the sky foreground. The signal to noise ratio was at a maximum when five terms were used to represent the sky

foreground and was superior for the blade antenna by factors between 1.35 and 1.95. These results led to the conversion of all EDGES antenna designs to the blade design. The spectral index, β , of the sky was measured, using 211 nights of data, to be $-2.60 > \beta > -2.62$ in lower LST regions, increasing to -2.50 near the Galactic plane. I compared our measurements with spectral index simulations derived from two published sky maps and found good agreement at the transit of the Galactic Center, but at other LST values tended to overpredict by at most by $\Delta\beta < 0.05$ for one map and by $\Delta\beta < 0.12$ for the other. The EDGES instrument is shown to be very stable throughout the observations as the data scatter is very low, $\sigma\beta < 0.003$, and the total systematic uncertainty in β is 0.02. The improved systematic error enhances our ability to detect EoR signatures. I present preliminary results that show an EoR model by Kaurov & Gnedin (2016) is inconsistent with measured EDGES data at a significance of 1.9 σ .

Author(s): Thomas J. Mozdzen¹, Judd D Bowman¹, Raul A Monsalve³, Alan E. E. Rogers²

Institution(s): 1. Arizona State University, 2. Massachusetts Institute of Technology, Haystack Observatory, 3. University of Colorado Boulder

116.03D – Constraining Cosmic Dawn and Cosmological Reionization via the global redshifted 21-cm signal

The formation of first stars and consequent thermal evolution in baryons during Cosmic Dawn and the Epoch of Reionization (EoR) is poorly constrained. The 21-cm line transition of neutral hydrogen is one of the richest probes of the astrophysics during this era. The signal has the potential to reveal the nature and timing of the emergence of first stars, first light, and the consequent evolution in thermal and ionization state of the baryons.

The detection of the global redshifted 21-cm signal, which represents the mean thermal history of the gas, is challenging since it is extremely faint and seen through orders of magnitude stronger contributions from Galactic and extragalactic foregrounds. Man-made terrestrial Radio Frequency Interference (RFI) and the exacting tolerances required on instrument systematics make the detection even more daunting.

The design considerations for a precision spectral radiometer are first listed, and a comparison is made of different radiometer configurations, including short and zero baseline interferometers along with methods to enhance the response. We discuss the relative merits of different methods.

We then describe SARAS 2, a spectral radiometer custom-designed for precision measurement of the global 21-cm signal. SARAS 2 has been designed to have a system transfer function and internal systematics – both multiplicative and additive – to be spectrally smooth so as to allow a separation of foregrounds and systematics from plausible and predicted global cosmological 21-cm signals. The algorithms for calibration and RFI mitigation are carefully developed so that they do not introduce spectral features that may confuse the detection of the 21-cm signal.

We present the outcomes for cosmology from analysis of 60 hr observing with the radiometer deployed at the Timbaktu Collective in Southern India. The detailed analysis of the data reveals an RMS noise level of 11 mK, without being limited by systematic structures. The likelihood ratios are computed from the data for plausible 21-cm signals predicted by theoretical models. First light with SARAS 2 disfavors the scenario of rapid reionization and also the models in which the first X-ray sources have poor heating efficiency.

120 – Understanding Stellar Abundances in the Solar Neighborhood using Large Online Catalogs

120.01 – A Review of Stellar Abundance Databases and the Hypatia Catalog Database

Author(s): Saurabh Singh¹

Institution(s): 1. Raman Research Institute

116.04 – Characterizing the 21-cm Signal from Neutral Hydrogen in the IGM at Redshifts $27 > z > 6$ with EDGES

Understanding the period when the first stars formed and ionized the InterGalactic Medium (IGM) during the Epoch of Reionization (EoR) represents one of the main objectives of modern cosmology. The Experiment to Detect the Global EoR Signature (EDGES) strives to characterize this period by measuring, for the first time, the all-sky spectrum of the 21-cm signal produced by neutral hydrogen in the IGM at redshifts $27 > z > 6$. In this talk I will describe recent EDGES constraints for the 21-cm signal. Specifically, with measurements from the EDGES High-Band instrument in the range 90-190 MHz, we rule out traditional Tanh models for the epoch of reionization with durations of up to $dz=1$ over the redshift range $14 > z > 7$. We also rule out a wide range of phenomenological and physically-motivated 21-cm models that contain a large absorption feature in this redshift range, produced by the complex interaction between UV and X-ray radiation from the first sources and the neutral hydrogen in the IGM. Finally, I will describe our efforts to detect the 21-cm signal in the range $27 > z > 13$ with two Low-Band instruments that have observed over 50-100 MHz since 2015. These instruments implement refined calibration techniques and lessons learned from previous generations of EDGES, and have achieved a level of systematic uncertainty low enough to enable detection. I will present Low-Band analysis results, including a variety of cross-checks performed to discriminate between residual instrumental effects and spectral structure that is intrinsic to the sky. I will conclude by describing the preparation of the next observational campaign with upgraded instrumentation.

Author(s): Raul A. Monsalve³, Alan E. E. Rogers², Judd D Bowman¹, Thomas J. Mozdzen¹, Nivedita Mahesh¹

Institution(s): 1. Arizona State University, 2. Haystack Observatory, 3. University of Colorado

116.06 – The Implications of Interstellar Dust for the Cosmic Microwave Background

A detailed comparison of the full range of PLANCK and WMAP data for small (2 deg by 2 deg) areas of sky and the Cosmic Microwave Background (CMB) ILC maps reveals that the structure of foreground dust may be more complex than previously thought. If 857 and 353 GHz emission is dominated by galactic dust at a distance $<$ few hundred light years, then it should not resemble the cosmological ILC structure originating at a distance ~ 13 billion light years. In some areas of sky, however, we find strong morphological correlations, forcing us to consider the possibility that the foreground subtraction is not complete. Our data also show that there is no single answer for the question, “To what extent does dust contaminate the cosmologically important 143 GHz data?” In some directions, the contamination appears to be quite strong, but in others, it is less of an issue. This complexity needs to be taken in account in order to derive an accurate foreground mask in the quest to understand the CMB small-scale structure. We hope that a continued investigation of these data will lead to a definitive answer to the question above and, possibly, to new scientific insights on interstellar matter, the CMB, or both.

Author(s): Joan T. Schmelz¹, Gerrit Verschuur¹

Institution(s): 1. Arecibo Observatory

The astronomical community is interested in elements from lithium to thorium, from solar twins to peculiarities of stellar evolution, because they give insight into different regimes of star

formation and evolution. However, while some trends between elements and other stellar or planetary properties are well known, many other trends are not as obvious and are a point of conflict. For example, stars that host giant planets are found to be consistently enriched in iron, but the same cannot be definitively said for any other element. Therefore, it is time to take advantage of large stellar abundance databases in order to better understand not only the large-scale patterns, but also the more subtle, small-scale trends within the data.

In this overview to the special session, I will present a review of large stellar abundance databases that are both currently available (i.e. RAVE, APOGEE) and those that will soon be online (i.e. Gaia-ESO, GALAH). Additionally, I will discuss the Hypatia Catalog Database (www.hypatiacatalog.com) -- which includes abundances from individual literature sources that observed stars within 150pc. The Hypatia Catalog currently contains 72 elements as measured within ~6000 stars, with a total of ~240,000 unique abundance determinations. The online database offers a variety of solar normalizations, stellar properties, and planetary properties (where applicable) that can all be viewed through multiple interactive plotting interfaces as well as in a tabular format. By analyzing stellar abundances for large populations of stars and from a variety of different perspectives, a wealth of information can be revealed on both large and small scales.

Author(s): Natalie Rose Hinkel¹
Institution(s): 1. Vanderbilt University

120.02 – The Diversity of Chemical Composition: The Impact of Stellar Abundances on the Evolution of Stars and Habitable Zones

I have investigated how stars of different mass and composition evolve, and how stellar evolution impacts the location of the habitable zone around a star. Current research into habitability of exoplanets focuses mostly on the concept of a “classical” HZ, the range of distances from a star over which liquid water could exist on a planet's surface. This is determined by the host star's luminosity and spectral characteristics; in order to gauge the habitability potential of a given system, both the evolutionary history and the detailed chemical characterization of the host star must be considered. With the ever-accelerating discovery of new exoplanets, it is imperative to develop a better understanding of what factors play a role in creating “habitable” conditions of a planet. I will discuss how stellar evolution is integral to how we define the HZ, and how this work will apply to the search for Earth-like planets in the future.

I have developed a catalog of stellar evolution models for Sun-like stars with variable compositions; masses range from 0.1-1.2 Msol (spectral types M4-F4) at scaled metallicities (Z) of 0.1-1.5 Zsol, and O/Fe, C/Fe, and Mg/Fe values of 0.44-2.28, 0.58-1.72, and 0.54-1.84, respectively. I use a spread in abundance values based on observations of variability in nearby stars. It is important to understand how specific elements, not just total Z, impacts stellar lifetime. Time-dependent HZ boundaries are calculated for each track. I have also created a grid of M-dwarfs, and I am currently working to estimate stellar activity vs. age for each model. This catalog is meant to characterize potential host stars of interest. I have explored how to use existing observational data (i.e. Hypatia Catalog) for a more robust comparison to my grid of theoretical models, and I will discuss a new statistical analysis of the catalog to further refine our definition of “continuous” habitability. This work is an important step to assess whether a planet discovered in the HZ of its star has had sufficient time to develop a biosphere capable of producing detectable biosignatures. The catalog is designed for use by the astrobiology and exoplanet communities to characterize any real planetary systems of interest.

Author(s): Amanda R. Truitt², Patrick A. Young¹
Institution(s): 1. Arizona State University, 2. Los Alamos National Laboratory

120.03 – Calibrating Detailed Chemical Analysis of M dwarfs

The ability to perform detailed chemical analysis of Sun-like F-, G-, and K-type stars is a powerful tool with many applications including studying the chemical evolution of the Galaxy, assessing membership in stellar kinematic groups, and constraining planet formation theories. Unfortunately, complications in modeling cooler stellar atmospheres has hindered similar analysis of M-dwarf stars. Large surveys of FGK abundances play an important role in developing methods to measure the compositions of M dwarfs by providing benchmark FGK stars that have widely-separated M dwarf companions. These systems allow us to empirically calibrate metallicity-sensitive features in M dwarf spectra. However, current methods to measure metallicity in M dwarfs from moderate-resolution spectra are limited to measuring overall metallicity and largely rely on astrophysical abundance correlations in stellar populations. In this talk, I will discuss how large, homogeneous catalogs of precise FGK abundances are crucial to advancing chemical analysis of M dwarfs beyond overall metallicity to direct measurements of individual elemental abundances. I will present a new method to analyze high-resolution, NIR spectra of M dwarfs that employs an empirical calibration of synthetic M dwarf spectra to infer effective temperature, Fe abundance, and Ti abundance. This work is a step toward detailed chemical analysis of M dwarfs at a similar precision achieved for FGK stars.

Author(s): Mark Veyette², Philip Steven Muirhead², Andrew Mann³, John Brewer⁵, France Allard¹, Derek Homeier⁴
Institution(s): 1. Université de Lyon, 2. Boston University, 3. Columbia University, 4. Universität Heidelberg, 5. Yale University

120.04 – Ages of M Dwarf Stars from their Alpha Enhancement

M dwarf stars dominate stellar populations, and recent results from NASA's Kepler Mission suggest rocky planets are abundant around M dwarf stars. With so many planets orbiting M dwarfs, exoplanet scientists can now turn to questions about their history and evolution. Unfortunately, measuring fundamental properties of M dwarfs is challenging for a variety of reasons. I will discuss the importance of near-infrared spectroscopy in this effort. With high-resolution near-infrared spectroscopy covering Y to K band, we can measure detailed fundamental properties of low-mass stars. With new techniques to measure stellar alpha and iron abundances, we can begin to measure the most challenging fundamental property of M dwarfs: their age. These efforts are even more exciting in the coming years, when the TESS spacecraft is expected to discover five times as many planets orbiting low-mass stars as Kepler.

Author(s): Philip Steven Muirhead¹, Mark Veyette¹
Institution(s): 1. Boston University

120.05 – Exo-geneology: Stellar Abundances in Solar-like Stars with Planets

Through the process of star and planet formation, we think that the chemical abundances, or “genes”, of host stars are passed on to their orbiting planets. One prominent example of this is the giant planet-metallicity (iron abundance) correlation, but could other stellar “genes” help explain the growing menagerie of exoplanets? Particularly interesting is the relative importance of C, O, Mg, and Si – for instance, are giant planet cores dominated by ice-forming or rock-forming elements? The ratios of these elements in terrestrial planets also control their interior structure and mineralogy, and can thus affect their similarity (or not) to Earth. In this talk I will discuss how high resolution spectroscopic studies of host stars have been and are being used to investigate how/to what extent planet properties are dependent on host star properties, focusing on solar-like (FGK) stars. I will also highlight the role that upcoming facilities can play in understanding the diversity of planets in the Galaxy.

Author(s): Johanna Teske¹
Institution(s): 1. Carnegie Institution for Science, Department of Terrestrial Magnetism
Contributing team(s): SDSS-IV APOGEE-2

120.06 – Density is not Destiny: Characterizing Terrestrial Exoplanet Geology from Stellar Compositional Abundances

A planet's mass-radius relationship alone is not a good indicator for its potential to be "Earth-like." While useful in coarse characterizations for distinguishing whether an exoplanet is water/atmosphere- or rock/iron-dominated, there is considerable degeneracy in using the mass-radius relation to determine the mineralogy and structure of a purely terrestrial planet like the Earth. The chemical link between host-stars and rocky planets and the utility of this connection in breaking the degeneracy in the mass-radius relationship is well documented. Given the breadth of observed stellar compositions, modeling the complex effects of these compositional variations on a terrestrial planet's mineralogy, structure and temperature profile, and the potential pitfalls therein, falls within the purview of the geosciences.

I will demonstrate here, the utility in adopting the composition of a terrestrial planet's host star for contextualizing individual systems (e.g. TRAPPIST-1), as well as for the more general case of

121 – NASA Decadal Preparations II: Probes Mission Concept Studies

121.01 – The Probe of Inflation and Cosmic Origins

The Probe of Inflation and Cosmic Origins will map the polarization of the cosmic microwave background over the entire sky with unprecedented sensitivity. It will search for gravity wave signals from the inflationary epoch, thus probing quantum gravity and constraining the energy scale of inflation; it will test the standard model of particle physics by measuring the number of light particles in the Universe and the mass of the neutrino; it will elucidate the nature of dark matter and search for new forms of matter in the early Universe; it will constrain star formation history over cosmic time; and it will determine the mechanisms of structure formation from galaxy cluster to stellar scales. I will review the status of design of this probe-scale mission.

Author(s): Shaul Hanany¹

Institution(s): 1. University of Minnesota/Twin Cities

Contributing team(s): Inflation Probe Mission Study Team

121.02 – The Galaxy Evolution Probe

The Galaxy Evolution Probe (GEP) is a concept for a far-infrared observatory to survey large regions of sky for star-forming galaxies from $z = 0$ to beyond $z = 3$. Our knowledge of galaxy formation is incomplete and requires uniform surveys over a large range of redshifts and environments to accurately describe mass assembly, star formation, supermassive black hole growth, interactions between these processes, and what led to their decline from $z \sim 2$ to the present day. Infrared observations are sensitive to dusty, star-forming galaxies, which have bright polycyclic aromatic hydrocarbon (PAH) emission features and warm dust continuum in the rest-frame mid infrared and cooler thermal dust emission in the far infrared. Unlike previous far-infrared continuum surveys, the GEP will measure photometric redshifts commensurate with galaxy detections from PAH emission and Si absorption features, without the need for obtaining spectroscopic redshifts of faint counterparts at other wavelengths.

The GEP design includes a 2 m diameter telescope actively cooled to 4 K and two instruments: (1) An imager covering 10 to 300 μm with 25 spectral resolution $R \sim 8$ bands (with lower R at the longest wavelengths) to detect star-forming galaxies and measure their redshifts photometrically. (2) A 23 – 190 μm , $R \sim 250$ dispersive spectrometer for redshift confirmation and identification of obscured AGN using atomic fine-structure lines. Lines including [Ne V], [O IV], [O III], [O I], and [C II] will probe gas physical conditions, radiation field hardness, and metallicity. Notionally, the GEP will have a two-year mission: galaxy surveys with photometric redshifts in the first year and a second year devoted to follow-up spectroscopy. A comprehensive picture of star formation in galaxies over the last 10 billion years will be assembled from cosmologically relevant volumes, spanning environments from field galaxies and groups, to protoclusters, to

quantifying the geophysical consequences of stellar compositional diversity. This includes the potential for a host-star to produce planets able to undergo mantle convection, surface-to-interior degassing and long-term plate tectonics. As we search for truly "Earth-like" planets, we must move away from the simple density-driven definition of "Earth-like" and towards a more holistic view that includes both geochemistry and geophysics. Combining geophysical models and those of planetary formation with host-star abundance data, then, is of paramount importance. This will aid not only in our understanding of the mass-radius relationship but also provide foundational results necessary interpreting future atmospheric observations through the lens of surface-interior interactions (e.g. volcanism) and planetary evolution as a whole.

Author(s): Cayman T Unterborn¹

Institution(s): 1. Arizona State University

dense galaxy clusters.

Commissioned by NASA, the GEP concept is being developed to demonstrate the ambitious science that could be enabled by a Probe-class mission (defined to be in the cost range \$400M to \$1B). GEP concept study partners are the University of Colorado Boulder, JPL, and Ball Aerospace.

Author(s): Jason Glenn¹

Institution(s): 1. University of Colorado Boulder

Contributing team(s): Galaxy Evolution Probe Team

121.03 – STROBE-X: X-ray Timing & Spectroscopy on Dynamical Timescales from Microseconds to Years

We describe a probe-class mission concept that provides an unprecedented view of the X-ray sky, performing timing and 0.2-30 keV spectroscopy over timescales from microseconds to years. The Spectroscopic Time-Resolving Observatory for Broadband Energy X-rays (STROBE-X) comprises three primary instruments. The first uses an array of lightweight optics (3-m focal length) that concentrate incident photons onto solid state detectors with CCD-level (85-130 eV) energy resolution, 100 ns time resolution, and low background rates to cover the 0.2-12 keV band. This technology is scaled up from NICER, with enhanced optics to take advantage of the longer focal length of STROBE-X. The second uses large-area collimated silicon drift detectors, developed for ESA's LOFT, to cover the 2-30 keV band. These two instruments each provide an order of magnitude improvement in effective area compared with its predecessor (NICER and RXTE, respectively). Finally, a sensitive sky monitor triggers pointed observations, provides high duty cycle, high time resolution, high spectral resolution monitoring of the X-ray sky with ~ 20 times the sensitivity of the RXTE ASM, and enables multi-wavelength and multi-messenger studies on a continuous, rather than scanning basis. We include updated instrument designs resulting from the GSFC IDL run in November 2017.

For the first time, the broad coverage provides simultaneous study of thermal components, non-thermal components, iron lines, and reflection features from a single platform for accreting black holes at all scales. The enormous collecting area allows detailed studies of the dense matter equation of state using both thermal emission from rotation-powered pulsars and harder emission from X-ray burst oscillations. The combination of the wide-field monitor and the sensitive pointed instruments enables observations of potential electromagnetic counterparts to LIGO/Virgo and neutrino events. Extragalactic science, such as constraining bulk metallicity of medium to high redshift clusters and nearby compact groups and unprecedented timing investigations of active galactic nuclei, is also obtained.

Author(s): Paul S Ray¹

Institution(s): 1. *U.S. Naval Research Laboratory*

Contributing team(s): STROBE-X Steering Committee, STROBE-X Science Working Group

121.04 – Synergy of CETUS with Survey Telescopes of the 2020's

There has been an explosion in wide-field telescopes conducting astrophysical surveys that will come to fruition in the 2020's. These wide and deep telescopes will survey the sky at wavelengths ranging from gamma rays to radio waves. E-ROSITA will perform an all-sky X-ray survey with unprecedented sensitivity and resolution. Numerous telescopes on the ground and in space will observe electromagnetic counterparts to gravitational-wave sources. The Large Synoptic Survey Telescope, LSST, will map the southern sky discovering billions of new galaxies and stars and detecting transient objects. Subaru's Hyper Suprime Cam and Prime Focus Spectrograph will work to understand dark energy, and galaxy evolution at redshifts, $z \sim 1-2$ using optical-IR spectra, and to carry out studies of stellar archeology. The Wide-Field Infrared Survey Telescope, WFIRST, will conduct imaging and slitless spectroscopic surveys of the sky at near-IR wavelengths including nebular emission of H-alpha at redshifts up to $z=2$. The Square Kilometer Array (SKA) and other radio telescopes will map a billion galaxies using the 21-cm line of neutral hydrogen. We will show how CETUS's near-UV and far-UV cameras and its near-UV multi-object spectrograph will work in synergy with these other survey telescopes.

Author(s): Sara Heap¹

Institution(s): 1. *Nasa's Goddard emerita*

Contributing team(s): and the CETUS Science Team

121.05 – Transient Astrophysics Probe

The Transient Astrophysics Probe (TAP) is a wide-field multi-wavelength transient mission proposed for flight starting in the late 2020s. The mission instruments include unique "Lobster-eye" imaging soft X-ray optics that allow a ~ 1600 deg² FoV; a high sensitivity, 1 deg² FoV soft X-ray telescope; a 1 deg² FoV Infrared telescope with bandpass 0.6-3 micron; and a set of 8 NaI gamma-ray detectors. TAP's most exciting capability will be the observation of tens per year of X-ray and IR counterparts of GWs involving stellar mass black holes and neutron stars detected by LIGO/Virgo/KAGRA/LIGO-India, and possibly several per year X-ray counterparts of GWs from supermassive black holes, detected by LISA and Pulsar Timing Arrays. TAP will also discover hundreds of X-ray transients related to compact objects, including tidal disruption events, supernova shock breakouts, and Gamma-Ray Bursts from the epoch of reionization.

Author(s): Jordan Camp¹

Institution(s): 1. *Goddard Space Flight Center*

Contributing team(s): Transient Astrophysics Probe Team

121.06 – AXIS - A High Angular Resoluition X-ray Probe Concept Study

AXIS is a probe-class concept under study to the 2020 Decadal survey. AXIS will extend and enhance the science of high angular resolution x-ray imaging and spectroscopy in the next decade with $\sim 0.3''$ angular resolution over a 7' radius field of view and an order of magnitude more collecting area than Chandra in the 0.3-12 keV band with a cost consistent with a probe. These capabilities enable major advances in a wide range of science such as: (i) measuring the event horizon scale structure in AGN accretion disks and the spins of supermassive black holes through observations of gravitationally-microlensed quasars; (ii) determining AGN and starburst feedback in galaxies and galaxy clusters through direct imaging of winds and interaction of jets and via spatially resolved imaging of galaxies at high- z ; (iii) fueling of AGN by probing the Bondi radius of over 20 nearby galaxies; (iv) hierarchical structure formation and the SMBH merger rate through measurement of the occurrence rate of dual AGN and occupation fraction of SMBHs; (v) advancing SNR physics and galaxy ecology through large detailed samples of SNR

in nearby galaxies; (vi) measuring the Cosmic Web through its connection to cluster outskirts.

With a nominal 2028 launch, AXIS benefits from natural synergies with the ELTs, LSST, ALMA, WFIRST and ATHENA. AXIS utilizes breakthroughs in the construction of lightweight X-ray optics from mono-crystalline silicon blocks, and developments in the fabrication of large format, small pixel, high readout rate detectors allowing a robust and cost effective design. The AXIS team welcomes input and feedback from the community in preparation for the 2020 Decadal review.

Author(s): Richard Mushotzky¹

Institution(s): 1. *University of Maryland*

Contributing team(s): AXIS Study Team

121.07 – POEMMA (Probe Of Extreme Multi-Messenger Astrophysics) Science and Design

In this poster we describe the preliminary design of POEMMA (Probe Of Extreme Multi-Messenger Astrophysics). The two satellites flying in formation consists of an innovative Schmidt telescope design optimized for low energy threshold and large geometry factor for observations. The 4 meter mirror was designed to fit in a dual manifest launch vehicle. A novel corrector lens and fast optics are design to optimized the full field of view to 45 degrees. The large focal surface will be populated by two systems: a multi-anode PMT (MAPMT) array for fluorescence detection and a Silicon PM (SiPM) array for Cherenkov detection around the limb of the Earth. At an altitude of 525 km, the LEO orbit will have a 28.5° inclination the mission can be launched from KSC and have a mission life of 3 years with a 5 year goal. The mission will improve by orders of magnitude the observations of ultra-high energy cosmic rays above tens of EeV and search for neutrinos above tens of PeVs.

Author(s): Angela V Olinto², Jeremy S Perkins¹

Institution(s): 1. *GSFC*, 2. *The University of Chicago*

Contributing team(s): POEMMA collaboration

121.08 – EarthFinder: A Precise Radial Velocity Survey Probe Mission of our Nearest Stellar Neighbors for Earth-Mass Habitable Zone Analogs Using High-Resolution UV-Vis-NIR Echelle Spectroscopy on a Space Platform

We are investigating the science case for a 1.0-1.4 meter space telescope to survey the closest, brightest FGKM main sequence stars to search for Habitable Zone (HZ) Earth analogs using the precise radial velocity (PRV) technique at a precision of 1-10 cm/s. Our baseline instrument concept uses two diffraction-limited spectrographs operating in the 0.4-1.0 microns and 1.0-2.4 microns spectral regions each with a spectral resolution of $R=150,000 \sim 200,000$, with the possibility of a third UV arm. Because the instrument utilizes a diffraction-limited input beam, the spectrograph would be extremely compact, less than 50 cm on a side, and illumination can be stabilized with the coupling of starlight into single mode fibers. With two octaves of wavelength coverage and a cadence unimpeded by any diurnal, seasonal, and atmospheric effects, EarthFinder will offer a unique platform for recovering stellar activity signals from starspots, plages, granulation, etc. to detect exoplanets at velocity semi-amplitudes currently not obtainable from the ground. Variable telluric absorption and emission lines may potentially preclude achieving PRV measurements at or below 10 cm/s in the visible and <50 cm/s in the near-infrared from the ground. Placed in an Earth-trailing (e.g. Spitzer, Kepler) or Lagrange orbit, the space-based cadence of observations of a star can be year-round at the ecliptic poles, with two ~ 100 -day "seasons" every 6 months in the ecliptic plane. This will provide a distinct advantage compared to an annual ~ 3 -6 month observing season from the ground for mitigating stellar activity and detecting the orbital periods of HZ Earth-mass analogs (e.g. ~ 6 -months to ~ 2 years). Finally, we are compiling a list of ancillary science cases for the observatory, ranging from asteroseismology to the direct measurement of the expansion of the Universe.

Author(s): Peter Plavchan¹
Institution(s): 1. *George Mason University*
Contributing team(s): EarthFinder Team

121.09 – Starshade Rendezvous Mission Probe Concept

The Starshade Rendezvous Mission Concept Probe is a Starshade that works with the WFIRST Mission, but is built and launched separately, with a rendezvous on orbit. A 2015 Exo-S report first detailed the mission concept. In the current study we develop a new scientific vision for WFIRST exoplanet discovery and characterization, using the complementary coronagraph and starshade to execute the most sensitive and thorough direct imaging campaign ever attempted. The overarching goal of our proposal is to carry out the first “deep dive” direct imaging exploration of planetary systems orbiting the nearest sun-like stars in a search for Earth-like planets using only a fraction of the WFIRST telescope time. The study aims to improve on the Exo-S 2015 report with updated study of the key spacecraft and starshade technology development issues, as related to WFIRST design changes since 2015 that make the timely implementation of such a mission possible.

Author(s): Sara Seager¹, Jeremy Kasdin²
Institution(s): 1. *MIT*, 2. *Princeton University*
Contributing team(s): Starshade Rendezvous Probe Team

121.10 – Cosmic Dawn Intensity Mapper

Cosmic Dawn Intensity Mapper (CDIM) is a 1.0m-class infrared telescope capable of three-dimensional spectro-imaging

122 – The Triple Threat to Multi-wavelength Observational Astronomy

– Introductory Remarks, Jeff C. Hall

122.01 – The Spectrum Landscape: Prospects for Terrestrial Radio Astronomy

Radio astronomers work within broad constraints imposed by commercial and other non-astronomical uses of the radio spectrum, somewhat modified to accommodate astronomy’s particular needs through the provision of radio quiet zones, radio frequency allocations, coordination agreements and other devices of spectrum management. As radio astronomers increase the instantaneous bandwidth, frequency coverage and sensitivity of their instruments, these external constraints, and not the limitations of their own instruments, will increasingly be the greatest obstacles to radio astronomy’s ability to observe the cosmos from the surface of the Earth.

Therefore, prospects for future radio astronomy operations are contingent on situational awareness and planning for the impact of non-astronomical uses of the radio frequency spectrum. New radio astronomy instruments will have to incorporate adaptive reactions to external developments, and radio astronomers should be encouraged to think in untraditional ways. Increased attention to spectrum management is one of these.

In this talk I’ll recap some recent developments such as the proliferation of 76 – 81 GHz car radar and orbiting earth-mapping radars, either of which can burn out a radio astronomy receiver. I’ll summarize present trends for non-astronomical radio spectrum use that will be coming to fruition in the next decade or so, categorized into terrestrial fixed and mobile, airborne and space-borne uses, sub-divided by waveband from the cm to the sub-mm. I’ll discuss how they will impact terrestrial radio astronomy and the various ways in which radio astronomy should be prepared to react. Protective developments must occur both within radio astronomy’s own domain – designing, siting and constructing its instruments and mitigating unavoidable RFI – and facing outward toward the community of other spectrum users. Engagement with spectrum management is no panacea but it is an important means, and perhaps the only means, by which radio astronomy can take an active role in shaping its terrestrial environment.

observations over the wavelength range of 0.75 to 7.5 microns, at a spectral resolving power at or better than 300. This will be achieved with linear variable filters (LVFs) and a large field-of-view (FoV). The survey strategy using spacecraft operations following a shift and stare mode will result in more than 1300 independent narrow-band spectral images of the sky at a given location. Currently prioritized science programs, taking over three-years of a five-year mission, will be accomplished with a two-tiered wedding-cake survey with the shallowest spanning close to 300 sq. degrees and the deepest tier of about 25 sq. degrees. The remaining two-years could be used for additional survey programs (the wide tier can be expanded to 1000 sq. degrees) or for use by the astronomical community through a General Observing (GO) campaign. CDIM survey data will allow us to (i) establish the initial mass function of stars in galaxies present during reionization, (ii) definitively address AGN/quasar contribution to the reionization photon budget; (iii) establish the environmental dependence of star-formation during reionization through clustering and other environmental measurements; (iv) establish the metal abundance of first-light galaxies during reionization over two decades of stellar mass; (v) measure 3D intensity fluctuations during reionization in both Ly-alpha and H-alpha; and (vi) combine intensity fluctuations with 21-cm data to establish the topology of reionization bubbles.

Author(s): Asantha Cooray¹
Institution(s): 1. *University of California Irvine*

Author(s): Harvey Steven Liszt¹
Institution(s): 1. *National Radio Astronomy Observatory*

122.02 – Space Debris and Observational Astronomy

Since the launch of Sputnik 1 in 1957, astronomers have faced an increasing number of artificial objects contaminating their images of the night sky. Currently almost 17000 objects larger than 10 cm are tracked and have current orbits in the public catalog. Active missions are only a small fraction of these objects. Most are inactive satellites, rocket bodies, and fragments of larger objects: all space debris. Several mega-constellations are planned which will increase this number by 20% or more in low Earth orbit (LEO). In terms of observational astronomy, this population of Earth orbiting objects has three implications: 1) the number of streaks and glints from spacecraft will only increase. There are some practical steps that can be taken to minimize the number of such streaks and glints in astronomical imaging data. 2) The risk to damage to orbiting astronomical telescopes will only increase, particularly those in LEO. 3) If you are working on a plan for an orbiting telescope project, then there are specific steps that must be taken to minimize space debris generation during the mission lifetime, and actions to safely dispose of the spacecraft at end of mission to prevent it from becoming space debris and a risk to other missions. These steps may involve sacrifices to mission performance and lifetime, but are essential in today’s orbital environment.

Author(s): Patrick Seitzer¹
Institution(s): 1. *University of Michigan*

122.03 – The Growing Threat of Light Pollution to Ground-Based Observatories

With few exceptions, growing sky glow from artificial sources negatively impacts the sky background recorded at major observatories around the world. We report techniques for measuring night sky brightness and extracting the contribution of artificial sky glow at observatories and other protected sites. The increase in artificial ambient light and its changing spectrum with LED replacements is likely to be significant. A compendium of worldwide regulatory approaches to astronomical site protection gives insight on multiple effective strategies.

Author(s): Richard F. Green², Christian Luginbuhl¹, Richard J Wainscoat³, Dan Duriscoe¹
Institution(s): 1. *Dark Sky Partners, LLC*, 2. *University of Arizona*, 3. *University of Hawaii*

122.04 – Light Pollution - An international perspective

The CIE (Commission Internationale de l'Eclairage, or International Commission on Illumination) is the international organization devoted to worldwide cooperation and the exchange of information on all matters relating to the science and art of light and lighting, colour and vision, photobiology and image technology. Its actions and recommendations affect lighting worldwide, and artificial lighting has a profound impact on ground-based astronomy. The CIE establishes Technical Committees to research specific aspects of lighting. The CIE will hold its biannual meeting in October 2017 in South Korea. I will report on astronomy and light pollution related information from that meeting.

Author(s): Richard J Wainscoat¹
Institution(s): 1. *University of Hawaii*

122.05 – Protecting Dark Skies in Chile

Current projections indicate that Chile will host approximately 70% of the astronomical collecting area on Earth by 2030, augmenting the enormous area of ALMA with that of three next-generation optical telescopes: LSST, GMT, and E-ELT. These cutting-edge facilities represent billions of dollars of investment in the astronomical facilities hosted in Chile. The Chilean government, Chilean astronomical community, and the international observatories in Chile have recognized that these investments are threatened by light pollution, and have formed a strong collaboration to work at managing the threats. We will provide an update on the work being done in Chile, ranging from training municipalities about new lighting regulations to exploring international recognition of the dark sky sites of Northern Chile.

123 – AGN, QSO, Blazars II

123.01 – X-ray Properties and the Environment of Compact Radio Sources.

Compact extragalactic radio sources provide important insights into the initial stages of radio source evolution and probe states of a black hole activity at the time of the formation of the relativistic outflow. Such outflows propagate out to hundreds kpc distances from the origin and impact environment on many scales, and thus influence evolution of structures in the universe. These compact sources show radio features typically observed in large-scale radio galaxies (jets, lobes, hot spots), but contained within the central 1 kpc region of the host galaxy. Compact Symmetric Objects (CSOs), a subclass of GigaHertz Peaked spectrum radio sources) are symmetric and not affected by beaming. Their linear radio size can be translated into a source age if one measures the expansion velocity of the radio structures. Such ages has been measured for a small sample of CSOs. Using the Chandra X-ray Observatory and XMM-Newton we observed a pilot samples of 16 CSOs in X-rays (6 for the first time). Our results show heterogeneous nature of the CSOs X-ray emission indicating a range of AGN luminosities and a complex environment. In particular, we identified four Compton Thick sources with a dense medium (equivalent column $> 1e24 \text{ cm}^{-2}$) capable of disturbing/slowing down the jet and confining the jet to a small region. Thus for the first time we gain the observational evidence in X-ray domain in favor of the hypothesis that in a sub-population of CSOs the radio jets may be confined by the dense X-ray obscuring medium. As a consequence, the kinematic ages of these CSOs may be underestimated.. We discuss the implications of our results on the emission models of CSOs, the earliest stages of the radio source evolution, jet interactions with the ISM, diversity of the environments in which the jets expand, and jet-galaxy co-evolution.

Author(s): R. Chris Smith¹, Pedro Sanhueza³, Mark Phillips²
Institution(s): 1. *AURA*, 2. *Las Campanas Observatory*, 3. *OPCC*

122.07 – LED Street Lighting Solutions: Flagstaff, Arizona as a Case Study

Dark-sky protection in Flagstaff, Arizona extends back to 1958, with the first ordinance in the City banning advertising floodlights. The current ordinance, adopted in 1989, is comprehensive and has played a critical role in maintaining the quality of the night sky for astronomy, tourism, public enjoyment, and other purposes. Flagstaff, like many communities around the world, is now working on a transition from legacy bulb-based technology to LED for its outdoor lighting. The City, Lowell Observatory, the U. S. Naval Observatory, and the Flagstaff Dark Skies Coalition have been working intensively for two years to identify an LED-based street lighting solution that will preserve the City's dark skies while meeting municipal needs. We will soon be installing test fixtures for an innovative solution incorporating narrow-band amber LED and modest amounts of low-CCT white LED. In this talk, I will review the types of LEDs available for outdoor lighting and discuss the plans for Flagstaff's street lighting in the LED era, which we hope will be a model for communities worldwide.

Author(s): Jeffrey C. Hall¹
Institution(s): 1. *Lowell Observatory*

– Panel Discussion, Constance E. Walker, Moderator

– Closing Remarks, Jeff C. Hall

Partial support for this work was provided by the NASA grants GO1-12145X, GO4-15099X, NNX10AO60G, NNX17AC23G and XMM AO15 project 78461. This work supported in part by NASA under contract NAS 8-03060 to the Smithsonian Astrophysical Observatory for operation of the Chandra X-ray Center.

Author(s): Aneta Siemiginowska², Malgorzata Sobolewska², Matteo Guainazzi¹, Martin Hardcastle⁵, Giulia Migliori⁴, Luisa Ostorero⁶, Lukasz Stawarz³

Institution(s): 1. *ESA*, 2. *Harvard-Smithsonian Center for Astrophysics*, 3. *Jagiellonian University*, 4. *Lab. AIM/Univ. Paris Diderot Paris 7/CNRS/CEA-Saclay*, 5. *University of Hertfordshire*, 6. *University of Torino*

– 123.02

123.03D – A geometric distance to CGCG 074-064

As part of the Megamaser Cosmology Project (MCP), we have made a direct measurement of the angular-diameter distance to the megamaser galaxy CGCG 074-064. We have conducted a series of high-sensitivity very long baseline interferometric observations, which reveal that the masers reside in a thin, edge-on accretion disk exhibiting Keplerian rotation at orbital radii $< 0.5 \text{ pc}$ from the central supermassive black hole. Over two years of single-dish spectral monitoring, we have determined that the maser features near the systemic velocity of the galaxy display nearly uniform velocity drifts of $\sim 4.3 \text{ km/s/yr}$, implying that they originate from a thin annulus in the disk. Combining these datasets, we have fit a 3D warped-disk model to the data and derived a distance and corresponding Hubble constant measurement for this galaxy. With an uncertainty of $< 9\%$, our distance measurement to CGCG 074-064 is the most precise yet obtained by the MCP.

Author(s): Dominic Pesce⁷, James Braatz⁵, Mark Reid², James Condon⁵, Feng Gao³, Jenny Greene⁶, Christian Henkel⁴, Cheng-Yu Kuo¹, K. Y. Lo⁵, Wei Zhao³

Institution(s): 1. *Academia Sinica Institute of Astronomy and Astrophysics*, 2. *Harvard-Smithsonian Center for Astrophysics*, 3. *Key Laboratory for Research in Galaxies and Cosmology*, 4. *Max Planck Institute for Radioastronomy*, 5. *National Radio Astronomy Observatory*, 6. *Princeton University*, 7. *University of Virginia*

Contributing team(s): Megamaser Cosmology Project

123.04 – The Extragalactic Background Light in the Fermi Era

The extragalactic background light (EBL), from ultra-violet to infrared, that encodes the emission from all stars, galaxies and actively accreting black holes in the observable Universe is critically important to probe models of star formation and galaxy evolution, but remains at present poorly constrained. The Large Area Telescope (LAT), on board Fermi, produced an unprecedented measurement (relying on 750 blazars and the first 9 years of Pass 8 data) of the EBL optical depth at 12 different epochs from redshift 0 up to a redshift of 3. In this talk, we will present the measurement and how it constrains the EBL energy density and its evolution with cosmic time. We will also discuss how this paves the road to the first point-source-independent determinations of the star-formation history of the Universe.

Author(s): Abhishek A Desai¹, Marco Ajello¹, Vaidehi Paliya¹, Alberto Dominguez³, Justin Finke⁴, Kari Helgason², Dieter Hartmann¹

Institution(s): 1. *Clemson University*, 2. *Max Planck Institute for Astrophysik*, 3. *universidad complutense*, 4. *US Naval Research Observatory*

Contributing team(s): Fermi LAT collaboration

123.05 – Buried Black Hole Growth in Advanced Mergers: The Discovery of a Large Population of Dual AGN Candidates by Chandra

Interactions between galaxies are predicted to cause gas inflows that can potentially trigger nuclear activity. Since the inflowing material can obscure the central regions of interacting galaxies, a potential limitation of previous optical studies is that obscured active galactic nuclei (AGNs) can be missed at various stages along the merger sequence. In a recent large mid-infrared study of AGNs in mergers, we demonstrated that the fraction of obscured AGNs increases with merger stage, with the most energetically dominant optically obscured AGNs becoming more prevalent in the most advanced mergers, consistent with theoretical predictions. In a recent Chandra program, we discovered 8 out of 15 infrared-selected advanced mergers that display two nuclear X-ray sources with separations of a few kiloparsecs consistent with highly absorbed dual AGNs, demonstrating that WISE pre-selection may be effective in identifying a new population of optically invisible dual AGNs. These observations reveal that infrared and X-ray observations are critical in uncovering the most efficient environments for supermassive black hole accretion and a key stage in galaxy evolution. In this talk, I will discuss Chandra, NuSTAR, and near-infrared spectroscopic observations of these dual AGN candidates and recent hydrodynamic simulations that predict that this key stage in galaxy evolution is expected to be highly obscured.

Author(s): Shobita Satyapal¹, Nathan Secrest⁷, Sara L. Ellison⁶, Claudio Ricci², Ryan William Pfeifle¹, Laura Blecha⁵, Barry Rothberg⁴, Mario Gliozzi¹, Anca Constantin³, Jason Ferguson¹

Institution(s): 1. *George Mason University*, 2. *Instituto de Astrofísica, Facultad de Física, Pontificia Universidad Católica de Chile*, 3. *James Madison University*, 4. *LBT*, 5. *University of Florida*, 6. *University of Victoria*, 7. *US Naval Observatory*

124 – Gravitational Waves and EM Counterparts I

124.01 – Multi-messenger studies of compact binary mergers in the ngVLA era

123.06 – The Enhanced X-ray Emission From Highly Radio-Loud Quasars at $z > 4$

Radio-loud quasars usually show jet-linked X-ray emission, making them brighter than their radio-quiet counterparts in X-rays. The enhancement appears to be stronger for $z > 4$ HRLQs than for matched HRLQs at lower redshifts with similar optical/UV and radio luminosities, which may reveal the radiation mechanism of relativistic jets in the early universe by linking the X-ray enhancement of HRLQs with the $(1 + \dots)$ evolution of CMB energy densities. We analyzed X-ray data of 10 HRLQs at $z > 4$, including Chandra observations of 8 objects and archival Swift observations of the remaining two. We also constructed the spectral energy distribution of these objects using multiwavelength data. Through a variety of robust statistical tests, we show that the HRLQs at $z > 4$ have stronger X-ray enhancement than low redshift counterpart.

Author(s): Shifu Zhu¹

Institution(s): 1. *The Department of Astronomy & Astrophysics at Penn State*

123.07 – A far-infrared polarized view of active galactic nuclei with SOFIA/HAWC+

Near- to mid-infrared (NIR, MIR; 1-13 μm) total and polarized flux observations from the ground have been key to advance our understanding about the dust distribution and emission in the central few parsecs of the active galactic nucleus (AGN), i.e. jets and dusty torus, as well as in their central few hundred parsecs, i.e. narrow line regions. Our previous studies provided insights about 1) a potential cut-off wavelength at $> 40 \mu\text{m}$ of the synchrotron emission from the pc-scale jet close to the core of Cygnus A, 2) the peak emission of the dusty torus occurs at wavelengths $> 32 \mu\text{m}$ in a sample of nearby and bright AGN, and 3) thermal emission from magnetic galactic winds in M82. However, the atmosphere is opaque to the far-IR (FIR) range and observations are impossible from ground-based telescopes and also polarimetric capabilities have been very limited in this wavelength range, which it makes difficult to observationally constraint our previous findings. HAWC+ has open a new window to explore AGN and starburst galaxies, providing the best angular resolution and the solely polarimetric capability within the 50-220 μm range of the current suite of instruments.

We here present preliminary results of AGN and starburst galaxies observed with the FIR polarimeter HAWC+ onboard the Stratospheric Observatory for Infrared Astronomy (SOFIA). Specifically, our total flux observations of NGC 1068 at 53 μm have shown for the first time the turn-over emission of the dusty torus in the range of 30-40 μm , which it allows us to put tight constraints on the clumpy torus model parameters such as the torus size, $\sim 6 \text{ pc}$, number and distribution of clouds. Our polarized flux observations of M82, in combination with previously published NIR polarimetric observations, have shown evidences of a galactic magnetic wind at scales of few hundred parsecs.

Author(s): Enrique Lopez Rodriguez¹

Institution(s): 1. *SOFIA Science Center*

Contributing team(s): HAWC+ Science Team

We explore some of the scientific opportunities that the next generation Very Large Array (ngVLA) will open in the field of multi-messenger time-domain astronomy. We focus on compact

binary mergers, golden astrophysical targets of ground-based gravitational wave (GW) detectors such as advanced LIGO. A decade from now, a large number of these mergers is likely to be discovered by a world-wide network of GW detectors. We discuss how a radio array with 10 times the sensitivity of the current Karl G. Jansky VLA and 10 times the resolution, would enable resolved radio continuum studies of binary merger hosts, probing regions of the galaxy undergoing star formation (which can be heavily obscured by dust and gas), AGN components, and mapping the offset distribution of the mergers with respect to the host galaxy light. For compact binary mergers containing at least one neutron star (NS), from which electromagnetic counterparts are expected to exist, we show how the ngVLA would enable direct size measurements of the relativistic merger ejecta and probe, for the first time directly, their dynamics.

Author(s): Alessandra Corsi¹

Institution(s): 1. Texas Tech University

124.02 – Jansky Array mapping of Gravitational Bursts as Afterglows in Radio (JAGWAR): The VLA Large Program and Initial Results

The era of gravitational waves and multi-messenger astronomy has begun. Telescopes around the globe are now in hot pursuit of electromagnetic counterparts (EM) to aLIGO/VIRGO sources, especially double-neutron star (NS-NS) and neutron star-black hole mergers (NS-BH). The EM counterparts are crucial for 1) providing arcsecond localization and identifying the precise host galaxy and merger redshift, 2) understanding the energetics and physics of the merger, 3) mapping their environments and pre-merger mass ejection processes, and 4) confirming the validity of the GW signals at low signal-to-noise ratios. Radio wavelengths provide one of the best diagnostics of both the dynamical sub-relativistic ejecta and any ultra-relativistic jet launched, as well as the possible interaction of these two components. In this talk I will introduce the Jansky Array mapping of Gravitational Bursts as Afterglows in Radio (JAGWAR) program, running on the VLA, aimed at maximizing the discoveries of the radio afterglows of NS-NS and NS-BH mergers. I will also present the JAGWAR results from the aLIGO/VIRGO observing run O2, which concluded in August 2017.

Author(s): Kunal Mooley⁸, Gregg Hallinan¹, Kenta Hotokezaka², Dale Frail⁶, Steven T. Myers⁶, Assaf Horesh⁴, Mansi Kasliwal¹, Shri Kulkarni¹, Leo Pound Singer³, Samaya nissanke⁷, Javed Rana⁵

Institution(s): 1. Caltech, 2. Flatiron Institute, 3. GSFC, 4. HUII, 5. IUCAA, 6. NRAO, 7. Radboud University, 8. University of Oxford

124.03 – Misc. results from LIGO O2

Will provide details at a later time.

Author(s): Daniel Holz¹, Zoheyr Doctor¹

Institution(s): 1. University of Chicago

Contributing team(s): LIGO Scientific Collaboration, Virgo collaboration

124.04D – COSMIC probes into compact binary formation and evolution

The population of compact binaries in the galaxy represents the final state of all binaries that have lived up to the present epoch. Compact binaries present a unique opportunity to probe binary evolution since many of the interactions binaries experience can be imprinted on the compact binary population. By combining binary evolution simulations with catalogs of observable compact binary systems, we can distill the dominant physical processes that govern binary star evolution, as well as predict the abundance and variety of their end products.

The next decades herald a previously unseen opportunity to study compact binaries. Multi-messenger observations from telescopes across all wavelengths and gravitational-wave observatories spanning several decades of frequency will give an unprecedented

view into the structure of these systems and the composition of their components. Observations will not always be coincident and in some cases may be separated by several years, providing an avenue for simulations to better constrain binary evolution models in preparation for future observations.

I will present the results of three population synthesis studies of compact binary populations carried out with the Compact Object Synthesis and Monte Carlo Investigation Code (COSMIC). I will first show how binary-black-hole formation channels can be understood with LISA observations. I will then show how the population of double white dwarfs observed with LISA and Gaia could provide a detailed view of mass transfer and accretion. Finally, I will show that Gaia could discover thousands black holes in the Milky Way through astrometric observations, yielding view into black-hole astrophysics that is complementary to and independent from both X-ray and gravitational-wave astronomy.

Author(s): Katelyn Breivik¹

Institution(s): 1. Northwestern University

124.05 – On the sensitivity of ATLAS and PS1 followup of O2 LIGO events

The potential for the joint detection of electromagnetic and gravitational-wave emissions is one of the most challenging tasks in multi-messenger astronomy. In this analysis, we report on the sensitivity of the Pan-STARRS and ATLAS followup of gravitational-wave triggers reported by LIGO during its most recent science run. We show the sensitivity of the followup campaigns to a variety of potential lightcurve models, including those from kilonovae. We discuss lessons learned with an outlook on improvements as we enter the open alert era.

Author(s): Michael William Coughlin¹

Institution(s): 1. California Institute of Technology

Contributing team(s): Pan-STARRS and ATLAS surveys for EM counterparts of GWs

124.06 – Infrared observations of gravitational-wave sources in Advanced LIGO's second observing run

Advanced LIGO observed gravitational waves (GWs) from a binary black hole merger in its first observing run (O1) in September 2015. It is anticipated that LIGO and Virgo will soon detect the first binary neutron star mergers. The most promising electromagnetic counterparts to such events are kilonovae: fast, faint transients powered by the radioactive decay of the r-process ejecta. Joint gravitational-wave and electromagnetic observations of such transients hold the key to many longstanding problems, from the nature of short GRBs to the cosmic production sites of the r-process elements to "standard siren" cosmology. Due to the large LIGO/Virgo error regions of 100 deg², synoptic survey telescopes have dominated the search for LIGO counterparts. Due to the paucity of infrared instruments with multi-deg² fields of view, infrared observations have been lacking. Near-infrared emission should not only be a more robust signature of kilonovae than optical emission (independent of viewing angle), but should also be several magnitudes brighter and be detectable for much longer, weeks after merger rather than days. In Advanced LIGO's second observing run, we used the FLAMINGOS-2 instrument on Gemini-South to hunt for the near-infrared emission from GW sources by targeted imaging of the most massive galaxies in the LIGO/Virgo localization volumes. We present the results of this campaign, rates, and interpretation of our near-infrared imaging and spectroscopy. We show that leveraging large-scale structure and targeted imaging of the most massive ~10 galaxies in a LIGO/Virgo localization volume may be a surprisingly effective strategy to find the electromagnetic counterpart.

Author(s): Leo Pound Singer², Mansi Kasliwal¹, Ryan Lau¹, Bradley Cenko²

Institution(s): 1. California Institute of Technology, 2. NASA Goddard Space Flight Center

Contributing team(s): Global Relay of Observatories Watching Transients Happen (GROWTH)

124.07 – Magnetized Mini-Disk Simulations about Binary Black Holes

Accretion disks around supermassive binary black holes offer a rare opportunity to probe the strong-field limit of dynamical gravity by using the ambient matter as a lighthouse. Accurate simulations of these systems using a variety of configurations will be critical to interpreting future observations of them. We have performed the first 3-d general relativistic magnetohydrodynamic simulations of mini-disks about a pair of equal mass black holes in the inspiral regime of their orbit. In this talk, we will present our latest results of 3-d general relativistic magnetohydrodynamic

125 – Science with the Wideband Submillimeter Array

125.01 – The Submillimeter Array – current status and future plans

The current SMA receiver systems were designed in the mid-1990s and have been operating for more than fifteen years. With regular upgrades to receivers, deployment of the SWARM correlator, expansion of the IF signal transport bandwidth via improvements to the analog IF signal processing hardware, and many other enhancements, the SMA currently greatly outperforms its original specifications in terms of sensitivity, instantaneous bandwidth, and availability of observing modes such as full-Stokes polarization and dual frequency operation.

We have recently started to implement a three-year instrument upgrade plan, which we are calling the wSMA. The wSMA will offer even wider bandwidth operation than the current SMA and improved sensitivity. The major subsystems that will form the wSMA include significantly improved, dual polarization receiver cartridges housed in a new cryostat; local oscillator units incorporating modern mm-wave technology; an upgraded signal transmission system; and a further expansion of the SWARM correlator. The cryostat will be cooled by a low-maintenance pulse-tube cryocooler. Two dual-polarization receiver cartridges will cover approximately the same sky frequencies as the current receiver sets; the low-band receiver will be fed by an LO unit covering 210-270 GHz, and the high-band receiver will be fed by an LO covering 280-360 GHz. With a receiver IF band of 4-20 GHz, this will enable continuous sky frequency coverage from 190 GHz to 380 GHz.

Details of the upgrade plans will be presented together with a discussion of scientific opportunities afforded by this upgrade, which, once implemented, will enable the SMA to continue to produce the highest quality science throughout the next decade.

Author(s): Raymond Blundell¹

Institution(s): 1. Smithsonian Astrophysical Observatory

125.02 – The wSMA Probes of Sgr A* and Nearby Low Luminosity AGN

I will review past contributions and discuss future opportunities for the study of nearby, low luminosity active galactic nuclei, including Sgr A* with the SMA. The SMA has made important contributions in the areas of polarimetry, time domain, and broadband spectra. The enhanced sensitivity proposed for the SMA will expand the sample of objects that can be studied and increase the density of time domain sampling. Frequent observation of bright sources and rapid response to external triggers are important niches for the SMA in the ALMA era. These studies provide important context for understanding accretion and outflow on scales from a few Schwarzschild radii to the Bondi radius and set boundary conditions for interpretation of images from the Event Horizon Telescope.

supercomputer simulations of accreting binary black holes during the post-Newtonian inspiral phase of their evolution. The goal of our work is to explore whether these systems provide a unique means to identify and characterize them with electromagnetic observations. We will provide a brief summary of the known electromagnetic signatures, in particular spectra and images obtained from post-process ray-tracing calculations of our simulation data. We will also provide a context for our results and describe our future avenues of exploration.

Author(s): Scott Noble², Dennis B. Bowen³, Stephane d'Ascoli³, Vassilios Mewes³, Manuela Campanelli³, Julian Krolik¹

Institution(s): 1. Johns Hopkins University, 2. NASA - GSFC, 3. Rochester Institute of Technology

Author(s): Geoffrey C. Bower¹

Institution(s): 1. ASIAA

125.03 – Submillimeter Array reveals molecular complexity of dying stars

The unique capabilities of the Submillimeter Array (SMA) have allowed unprecedented studies of cool evolved stars at submillimeter wavelengths. In particular, the SMA now offers the possibility to image multiple molecular transitions at once, owing to the 32-GHz wide instantaneous bandwidth of SWARM, the SMA's new correlator. Molecular gas located far and very close to the photosphere of an asymptotic-giant branch (AGB) star, a red supergiant, or a pre-planetary nebula can now be examined in transitions observed simultaneously from a wide range of energy levels. This allows a very detailed quantitative investigation of physical and chemical conditions around these variable objects. Several imaging line surveys have been obtained with the SMA to reveal the beautiful complexity of these evolved systems. The surveys resulted in first submillimeter-wave identifications of molecules of prime astrophysical interest, e.g. of TiO, TiO₂, and of rotational transitions at excited vibrational states of CO. An overview of recent SMA observations of cool evolved stars will be given with an emphasis on the interferometric line surveys. We will demonstrate their importance in unraveling the mass-loss phenomena, propagation of shocks in the circumstellar medium, and production of dust at elevated temperatures. The SMA studies of these molecular factories have a direct impact on our understanding of the chemical evolution of the Galaxy and stellar evolution at low and high masses.

Author(s): Tomasz (Tomek) Kaminski¹

Institution(s): 1. CfA

125.04 – Deciphering Debris Disk Structure with the Submillimeter Array

More than 20% of nearby main sequence stars are surrounded by dusty disks continually replenished via the collisional erosion of planetesimals, larger bodies similar to asteroids and comets in our own Solar System. The material in these 'debris disks' is directly linked to the larger bodies such as planets in the system. As a result, the locations, morphologies, and physical properties of dust in these disks provide important probes of the processes of planet formation and subsequent dynamical evolution. Observations at millimeter wavelengths are especially critical to our understanding of these systems, since they are dominated by larger grains that do not travel far from their origin and therefore reliably trace the underlying planetesimal distribution. The Submillimeter Array (SMA) plays a key role in advancing our understanding of debris disks by providing sensitivity at the short baselines required to determine the structure of wide-field disks, such as the HR 8799 debris disk. Many of these wide-field disks are among the closest systems to us, and will serve as cornerstone templates for the interpretation of more distant, less accessible systems.

Author(s): Meredith Ann MacGregor¹
Institution(s): 1. *Carnegie Institution for Science*

125.05 – Surveying Low-Mass Star Formation with the Submillimeter Array

Large astronomical surveys yield important statistical information that can't be derived from single-object and small-number surveys. In this talk I will review two recent surveys in low-mass star formation undertaken by the Submillimeter Array (SMA): a millimeter continuum survey of disks surrounding variably accreting young stars, and a complete continuum and molecular line survey of all protostars in the nearby Perseus Molecular Cloud. I will highlight several new insights into the processes by which low-mass stars gain their mass that have resulted from the statistical power of these surveys.

Author(s): Michael Dunham¹
Institution(s): 1. *SUNY Fredonia*

125.06 – CMZoom: The Submillimeter Array Survey of our Galaxy's Central Molecular Zone

The inner few hundred parsecs of the Milky Way, the Central Molecular Zone (CMZ), is our closest laboratory for understanding star formation in the extreme environments (hot, dense, turbulent gas) that once dominated the universe. We present an update on the first large-area survey to expose the sites of star formation across the CMZ at high-resolution in submillimeter wavelengths: the CMZoom survey with the Submillimeter Array (SMA). We identify the locations of dense cores and search for signatures of embedded star formation. CMZoom is a three-year survey, completed this year, and has mapped out the highest column density regions of the CMZ in dust continuum and a variety of spectral lines around 1.3 mm. CMZoom combines SMA compact and subcompact configurations with single-dish data from BGPS and the APEX telescope, achieving an angular resolution of about 4" (0.2 pc) and good image fidelity up to large spatial scales.

Author(s): Cara Battersby¹
Institution(s): 1. *University of Connecticut*
Contributing team(s): CMZoom Team

125.07 – Understanding CO Lines in the Whirlpool Galaxy: an SMA Survey

We present new CO 2-1 data for the nearby star forming galaxy M51 taken with the Submillimeter Array (SMA). We have mapped the entire disk of M51 in 12CO J=2-1 and its rarer isotopologues at ~5" resolution. We have also mapped the inner 10 x 6 kpc at a resolution of ~3", as well as imaging a single field in the northern spiral arm at 1" resolution (40 pc) as part of a pilot study for a large scale project. Combining our maps with the existing PdBI map of CO J=1-0, we present a map of the CO J=2-1/J=1-0 (R21) line ratio across M51 at up to cloud-scale resolution. With routine CO J=2-1 high resolution (GMC scale) observations under way

126 – HAD III: History, Eclipses, and Planetaria

126.01 – Television as an Aid to Astronomy

In the late nineteenth-century, readily available dry, gelatin-based photographic emulsions revolutionized astronomy. Photography not only provided a permanent record, but also allowed for integration over extended exposures, helping astronomers observe fainter objects than possible with the eye alone. In 1942, television pioneer Vladimir Zworykin, patented the Telectroscope, an electronic telescope which removed the observer from the eyepiece and replaced photographic emulsion with a television camera. By the mid-1950s, the astronomical community had developed a growing interest in the possible uses of television technology and at the 1955 Dublin meeting of the IAU, a special session was devoted to the application of television in astronomy.

Here, I will examine the use of commercially-available television camera tubes by professional and amateur astronomers and explain how results from these early observations encouraged the

with ALMA, understanding how R21 varies at high resolution across galaxies is paramount to interpret these maps. M51 offers the best opportunity to quantify systematic variation in R21 across the different regions such as spiral arms, spurs, inter-arm and nucleus and as a function of dynamical environment and star formation activity.

Author(s): Glen Petitpas³, Adam Leroy⁹, Kazimierz Sliwa⁷, Eva Shinnerer⁷, David Wilner³, Alyssa Goodman³, Charlie Lada³, Satoki Matsushita², Kazushi Sakamoto², Nanase Harada², Catherine Zucker³, Matthew Ashby³, Mark Gurwell³, Junko Ueda³, Cara Battersby¹⁰, Jan Forbrich¹³, Frank Bigiel¹², Brent Groves¹, Annie Hughes⁴, Erik Rosolowsky¹¹, Andreas Schruba⁶, Antonio Usero⁸, Miguel Querejeta⁷, Christine Wilson⁵
Institution(s): 1. *ANU*, 2. *ASIAA*, 3. *CfA*, 4. *IRAP*, 5. *McMaster University*, 6. *MPE*, 7. *MPLA*, 8. *Observatorio Astronomico Nacional*, 9. *OSU*, 10. *UConn*, 11. *University of Alberta*, 12. *University of Heidelberg*, 13. *University of Vienna*

125.08 – Probing individual star-forming regions in maximal starburst galaxies at redshifts z=2-4 with the SMA (and other major facilities): Planck's Dusty GEMS.

Strongly gravitationally lensed galaxies are veritable gems for our understanding of high-redshift galaxy evolution, allowing us to study dust, gas, and star formation even in the most intense starbursts on scales of individual star-forming regions. On these scales, below one to few 100 pc in the source plane, kpc-scale rotational support no longer dominates, and star formation is regulated by the local gas and stellar mass surface densities and energy injection from turbulence and winds driven by star formation and AGN. I will report on our on-going follow-up of Planck's Dusty GEMS, a small sample of 11 of the brightest, gravitationally lensed high-redshift galaxies on the extragalactic sub-mm sky. SMA 850-micron imaging is playing a critical role in identifying and characterizing the dusty starburst regions, their star-formation properties, and the gravitational lens modeling, and has been paving the way towards a rich multi-wavelength program, which would not have been possible without. This includes VLT, HST and ALMA high-resolution studies of the gas and stellar populations, amongst others. These observations enabled us, e.g., to study the interplay between gravity and turbulence in an Eddington-limited starburst for the first time, and to detect the first absorption line of [CII] from diffuse gas outside the Milky Way. I will also discuss the first direct lensing estimate of a (bottom-heavy) initial mass function in the early Universe and outline how these and similar observations would benefit from increased bandwidth.

Author(s): Nicole Nesvadba¹
Institution(s): 1. *Institut d'Astrophysique Spatiale*

astronomical community to further test, design, and build electronic imaging devices specifically for astronomical use.

Author(s): Samantha Thompson¹
Institution(s): 1. *Arizona State University*

126.02 – The Legacy of the Georgetown College Observatory (D.C.)

Founded in 1841 as part of a nascent worldwide network of Jesuit-run astronomical observatories, the Georgetown College Observatory of Georgetown University in Washington, D.C. has been home to more than 125 years of astronomical research, from Father Curley's calculations of the latitude and longitude of D.C. to Father McNally's award-winning solar eclipse photography. But the impact of the Georgetown astronomy program was not limited to the observatory itself: it reached much further, into the local community and schools, and into the lives of everyone involved. This was never more apparent than under the

directorship of Father Francis J Heyden, S.J., who arrived at Georgetown after World War II and stayed for almost three decades. He started a graduate program with over 90 graduates, hosting student researchers from local high schools and colleges, teaching graduate and undergraduate astronomy courses, and speaking at schools in the area, all while simultaneously managing Georgetown's student radio station and hosting astronomical conferences on campus. Father Heyden's research focused mainly on solar eclipses for geodetic purposes and planetary spectroscopy. But perhaps even more than research, Father Heyden dedicated his time and energy to the astronomy students, the notable of which include Vera Rubin, John P. Hagen of Project Vanguard, and a generation of Jesuit astronomers including Martin McCarthy, George Coyne, and Richard Boyle. Following the closure of the astronomy department in 1972, Father Heyden returned to Manila, where he had begun his astronomical career, to become Chief of the Solar Division at the Manila Observatory. His dedication to his work and to students serves as an inspiration for academic researchers across fields, and for the Georgetown University Astronomical Society, which, even in the absence of a formal astronomy program at Georgetown, continues his work in education and outreach today. In 1987, almost 150 years after its founding, Georgetown College Observatory was rededicated in Father Heyden's name.

Author(s): Laura Caron¹, Grace Maglieri¹, Patrick Seitzer²
Institution(s): 1. *Georgetown University*, 2. *University of Michigan*

126.03 – The Planetarium and the Carl Zeiss Corporation, 1923-1933

The Carl Zeiss Company of Jena, Germany, introduced the first prototype planetarium in the fall of 1923. By 1933, there were a dozen planetaria in Germany alone, and nearly a dozen more abroad. This talk argues that on one hand, Zeiss saw the planetarium as an opportunity to reintroduce German engineering to a skeptical international market. On the other, Zeiss recognized that a large part of the planetarium's domestic appeal lay in the romance of its German origins. Through an examination of Zeiss' corporate correspondence, propaganda, and contemporary international and domestic press, this talk argues that in advertising the planetarium in Germany and abroad, the Zeiss company relied on competing constructions of a post-war German identity rooted in conflicting understandings of space.

Author(s): Katherine Boyce-Jacino¹
Institution(s): 1. *Johns Hopkins University*

126.04 – Whither a "National Planetarium"?

In Spring 1927 Zeiss contacted the Smithsonian Institution about its new wonderful planetarium projector, sending along brochures and testimonials from astronomers. By the end of the year after much back and forth, Zeiss even found backers to underwrite the planetarium for the Smithsonian, feeling that the first planetarium should be built in Washington. Over the following decades, the push for a "national planetarium" revived several times, as a possible option for Jefferson's Memorial or as a commercial enterprise to revitalize the southwest quadrant of the city. It was even the topic for a student essay contest. Nothing caught on, though planetariums soon proved to be wildly popular in the cities that nurtured them. Here I'll outline the efforts for Washington, D.C. and ask what the campaigns reveal about the perception of astronomy on the National Mall.

Author(s): David DeVorkin¹
Institution(s): 1. *Smithsonian*

126.05 – Griffith Observatory: Hollywood's Celestial Theater

The Griffith Observatory, perched atop the Hollywood Hills, is perhaps the most recognizable observatory in the world. Since opening in 1935, this Los Angeles icon has brought millions of visitors closer to the heavens. Through an analysis of planning documentation, internal newsletters, media coverage,

programming and exhibition design, I demonstrate how the Observatory's Southern California location shaped its form and function. The astronomical community at nearby Mt. Wilson Observatory and Caltech informed the selection of instrumentation and programming, especially for presentations with the Observatory's Zeiss Planetarium, the second installed in the United States. Meanwhile the Observatory staff called upon some of Hollywood's best artists, model makers, and scriptwriters to translate the latest astronomical discoveries into spectacular audiovisual experiences, which were enhanced with Space Age technological displays on loan from Southern California's aerospace companies. The influences of these three communities—professional astronomy, entertainment, and aerospace—persist today and continue to make Griffith Observatory one of the premiere sites of public astronomy in the country.

Author(s): Emily A. Margolis¹
Institution(s): 1. *Johns Hopkins University*
Contributing team(s): Dr. Stuart W. Leslie

126.06 – "Spacearium" and the Educational Mission of the National Air and Space Museum

After a campaign that lasted over a decade, in 1971 the Washington Planetarium and Space Center decided to transfer all of its assets to the Smithsonian to be part of its proposed new National Air and Space Museum (NASM), itself recently redefined from being known as the National Air Museum. Here I will argue that the addition of a planetarium, which they called a "Spacearium," reflected a new goal of the Smithsonian to emphasize the educational mission of the new museum and thereby secure positive attention from Congress and the aerospace industry, hastening the appropriations process.

Author(s): Jieun Shin¹
Institution(s): 1. *University of Minnesota*

126.07 – Two Commemorative Expeditions to Celebrate the Return to Totality

Throughout history, total solar eclipses have generated excitement across the scientific community, as they provide a unique opportunity to study the Sun's corona. Occurrences of such events have prompted many American astronomy programs to organize expeditions aimed at studying and photographing the eclipse. Only two observing stations from any of the major 19th and early 20th century eclipse expeditions were once again found in the path of totality of the 21 August 2017 Great American Eclipse. These stations, one in Newberry, SC and the other in Winnsboro, SC, were located in the shadow of the 28 May 1900 eclipse that passed through the southeastern United States from New Orleans to Norfolk. To celebrate this unique opportunity, we organized two expeditions that travelled to these towns to commemorate their return to totality. In this talk, I will describe the circumstances of the 1900 solar eclipse, our modern expeditions, and our effort to bring this eclipse history to life for the community.

Author(s): Kristen Thompson¹, Tom English²
Institution(s): 1. *Davidson College*, 2. *Guilford Technical Community College*

126.08 – Determining the Edges of the Path of Totality on August 21, 2017

The International Occultation Timing Association (IOTA) attempted a citizen-science project to determine the locations of the edges of the path of totality, similar to what was done visually in New York City during the 1925 eclipse. With ubiquitous smart phones, we asked observers to record the eclipse, preferably with clip-on 8x telephoto lenses. The limits are not sharp since the solar intensity drops off gradually at the path edges. We hoped to determine how accurately the path edges could be determined, and the width of their "fuzziness". But it was not possible to find any astronomers who weren't also going to the center, who might otherwise help organize some path edge observations. In 1925, people were less concerned about the possibility of suffering eye

damage from quick glimpses at the eclipse. In 2017, several were concerned about damage to their cell phones, although our tests showed this was not a problem for the two minutes desired. The only successes were at Minden, Nebraska where high school students set up 15 stations across the southern limit and recorded the eclipse with iPads, and near Wheatland, Wyoming, where Jan Kok set up 21 pre-pointed smart phones with 8x lenses that he was able to program, to record the eclipse during the critical two minutes. We found that the dynamic range of the smart phone recordings could not distinguish between the corona, and the Baily's beads around the contacts, so useful times of the duration of "totality" could not be determined. A few IOTA observers recorded Baily's beads telescopically at a few locations near the eclipse limits. An especially good color recording of Baily's beads

127 – Galaxy Formation and Evolution II

127.01 – An Inclination-Dependent IRX-beta Relation for Galaxies at $z \sim 1.5$

Star-forming galaxies near cosmic noon are substantially obscured by dust. Therefore, to measure galaxy star-formation rates (SFRs), it is crucial to accurately account for dust obscuration. This is usually done by measuring the slopes of spectra in the rest-frame ultraviolet (i.e., β). Another independent method is to measure the infrared excess IRX, defined as the ratio between infrared and ultraviolet luminosity. In this work, we present the discovery that the relation between IRX and β varies systematically with galaxy inclination at $z \sim 1.5$. Edge-on galaxies are on average ~ 0.5 dex higher in IRX than face-on galaxies at fixed β . Furthermore, we find that the difference between SFR(UV+IR) and β -corrected SFR(UV) is correlated with inclination. Our finding is consistent with the study of local galaxies (Wild et al. 2011), where the dust attenuation curve is found to flatten with increasing inclination. We interpret our results using a picture where dust and young stars are spatially mixed. In this case, β is more sensitive to the optically-thin regions near the surface of galaxy disks. Therefore, compared to the case of face-on galaxies, β measures a smaller fraction of the total dust optical depth for the edge-on galaxies, whereas IRX always probes the total optical depth. We conclude that inclination must be taken into account when evaluating dust attenuation with β at high redshift.

Author(s): Weichen Wang¹, Susan A. Kassin³, Camilla Pacifici², Alexander de la Vega¹, Raymond C. Simons¹, Guillermo Barro⁴, Karl D. Gordon³, Gregory Snyder³

Institution(s): 1. Johns Hopkins University, 2. NASA Goddard Space Flight Center, 3. Space Telescope Science Institute, 4. University of California, Berkeley

127.02 – Mining CANDELS for Tidal Features to Constrain Major Merging During Cosmic Noon

The role of major merging in the rapid buildup and development of massive galaxies at $z > 1$ remains an open question. New theories and observations suggest that non-merging processes like violent disk instabilities may be more vital than previously thought at assembling bulges, producing clumps, and inducing morphological disturbances that may be misinterpreted as the product of major merging. We will present initial results on a systematic search for hallmark tidal indicators of major merging in a complete sample of nearly 6000 massive $z > 1$ galaxies from CANDELS (Cosmic Assembly Near-infrared Deep Extragalactic Legacy Survey), the premiere HST/WFC3 Treasury program. We have visually inspected published GALFIT F160W residual (image-model) maps and produced a comprehensive new catalog of Sersic residual characteristics based on a variety of natural features and poor-fit artifacts. Using this catalog, we find the frequency of galaxies with tidal signatures is very small in CANDELS data. Accounting for the brief time scale associated with faint transient tidal features, our preliminary finding indicates that merger fractions derived from the CANDELS morphological classification efforts are substantially overestimated. We are using the database of residual classifications as a baseline to (1) produce improved multi-component residual maps using GALFIT_M, (2) automatically

was made by Fred Bruenjes from only 1.3 km inside the southern limit. We hope that similar recordings with accurate time stamping can be obtained at a few locations near both limits of future eclipses. Even better might be recordings of the flash spectrum near both limits, to measure the transition from absorption lines in the photosphere to emission lines of the chromosphere.

Author(s): David W Dunham¹, Paul D Maley¹, Jan Kok¹, Fred Bruenjes¹

Institution(s): 1. International Occultation Timing Association

extract and quantify plausible tidal indicators and substructures (clumps vs. multiple nuclei), (3) develop a new deep-learning classification pipeline to robustly identify merger indicators in imaging data, and (4) inform the systematic analyses of synthetic mock (CANDELized) images from zoom-in hydrodynamic simulations to thoroughly quantify the impacts of cosmological dimming, and calibrate the observability timescale of tidal feature detections. Our study will ultimately yield novel constraints on merger rates at $z > 1$ and a definitive census of massive high-noon galaxies with tidal and double-nuclei merging signatures in rest-frame optical HST imaging.

Author(s): Daniel H. McIntosh⁷, Kameswara Mantha⁷, Cody Ciaschi⁷, Rubyet A. Evan⁷, Logan B. Fries⁷, Luther Landry⁷, Scott E. Thompson⁷, Gregory Snyder⁴, Yicheng Guo⁶, Daniel Ceverino², Boris Häußler⁸, Joel Primack⁵, Raymond C. Simons¹, Xianzhong Zheng³

Institution(s): 1. Johns Hopkins University, 2. Max Planck Institute for Astronomy, 3. Purple Mountain Observatory, 4. Space Telescope Science Institute, 5. U. California, Santa Cruz, 6. U. Missouri, 7. U. Missouri-Kansas City, 8. U. Nottingham

Contributing team(s): The Cosmic Assembly Near-Infrared Deep Extragalactic Legacy Survey (CANDELS) Team

127.03D – Searching for Lyman-alpha Emitters as a Probe of Cosmic Reionization and Peering Inside Galaxies in the First Two Billion Years

In the reionization era an immediately accessible method for studying the intergalactic medium is to measure the equivalent width distribution of Lyman-alpha emission from galaxies with follow-up spectroscopy. To search for Lyman-alpha emission from galaxies at $z \sim 5-8$, we perform spectroscopic observations of candidate galaxies from the Cosmic Assembly Near-infrared Deep Extragalactic Legacy Survey (CANDELS). We utilize data from the Keck DEIMOS (optical) and MOSFIRE (near-infrared) spectrographs, ensuring a comprehensive wavelength coverage of Lyman-alpha emission at $z \sim 5-8$. We have a total of 1170 object-hours of spectroscopic integration of galaxies at $z > 5$: 118 galaxies with DEIMOS and 69 galaxies with MOSFIRE. The equivalent width distribution of Lyman-alpha emission is constrained with the number of detected objects from our dataset by constructing detailed simulations of mock emission lines, which consider observational conditions and the photometric redshift probability distribution function. We present our robust measure of the evolution of the Lyman-alpha emission equivalent width distribution at $z \sim 5-8$.

Understanding what drives star-formation quenching in the early universe is a long-standing puzzle. To reveal the hidden relation of quenching with galaxy structural properties, particularly central stellar mass density, we perform the first spatially resolved stellar population study of galaxies at $z \sim 4$, utilizing the CANDELS imaging data set over the GOODS-S field. We examine 166 photometric-redshift-selected galaxies at $3.5 < z < 4.0$ with additional deep K-band survey data from the HAWK-I UDS and GOODS Survey which covers the 4000Å break at these redshifts. We estimate the stellar mass, star formation rate, and dust extinction for galaxy inner and outer regions via spatially resolved spectral energy distribution fitting based on a Markov Chain Monte Carlo algorithm. By comparing specific star formation

rates (sSFRs) between inner and outer parts of the galaxies we find that the majority of galaxies with high central mass densities show evidence for a preferentially lower sSFR in their centers than in their outer regions, indicative of reduced sSFRs in their central regions.

Author(s): Intae Jung¹, Steven Finkelstein¹
Institution(s): 1. The University of Texas at Austin
Contributing team(s): CANDELS team

127.04 – Evolution of the Interstellar Gas Fraction Over Cosmic Time

Galaxies evolve by transforming gas into stars. The gas is acquired through accretion and mergers and is a highly intricate process where feed-back processes play an important role. Directly measuring the gas content in distant galaxies is, however, both complicated and time consuming. A direct observations involves either observing neutral hydrogen using the 21cm line or observing the molecular gas component using tracer molecules such as CO. The former method is impeded by man-made radio interference, and the latter is time consuming even with sensitive instruments such as ALMA. An indirect method is to observe the Raleigh-Jeans part of the dust SED and from this infer the gas mass. Here we present the results from a project using ALMA to measure the RJ part of the dust SED in a carefully selected sample of 70 galaxies at redshifts $z=2-5$. The galaxies are selected solely based on their redshift and stellar mass and therefore represents an unbiased sample. The stellar masses are selected using the MEAM method and thus the sample corresponds to progenitors of a $z=0$ galaxy of a particular stellar mass. Preliminary results show that the average gas fraction increases with redshift over the range $z=2-3$ in accordance with theoretical models, but at $z \geq 4$ the observed gas fraction is lower.

Author(s): Tommy Wiklind¹
Institution(s): 1. Catholic University of America
Contributing team(s): CANDELS

127.05D – The Masses and Stellar Content of Nuclei in Early-Type Galaxies from Multi-Band Photometry and Spectroscopy

It is now established that most, if not all, massive galaxies host central supermassive black holes (SMBHs), and that these SMBHs are linked to the growth their host galaxies as shown by several scaling relations. Within the last couple of decades, it has become apparent that most lower-mass galaxies without obvious SMBHs nevertheless contain some sort of central massive object in the form of compact stellar nuclei that also follow identical (or similar) scaling relations. These nuclei are challenging to study given their small sizes and relatively faint magnitudes, but understanding their origins and relationship to their hosts is critical to gaining a more complete picture of galaxy evolution. To that end, we highlight selected results from an analysis of 39 nuclei and their early-type hosts in the Virgo Cluster using ten broadband filters: F300W, F475W, F850LP, F160W, u^*griz , and K_s . We estimate masses, metallicities and ages using simple stellar population (SSP) models. For 19 nuclei, we compare to SSP parameters derived from Keck and Gemini spectra and find reasonable agreement between the photometric and spectroscopic metallicity: the RMS scatter is 0.3 dex. We reproduce the nucleus-galaxy mass fraction of $0.33 \pm 0.08\%$ for galaxy stellar masses $10^{8.4}-10^{10.3} M_{\odot}$ with a typical precision of $\sim 35\%$ for the nuclei masses. Based on available model predictions, there is no single preferred formation scenario for nuclei, suggesting that nuclei are formed stochastically through a mix of processes. Nuclei metallicities are statistically identical to those of their hosts, appearing 0.07 ± 0.3 dex more metal-rich on average — although, omitting galaxies with unusual origins (i.e., compact ellipticals), nuclei are 0.20 ± 0.28 dex more metal-rich. We find no clear age difference between nuclei and their galaxies, with nuclei displaying a broad range of ages. Interestingly, we find that the most massive nuclei may be flatter and more closely aligned with the semi-major axes of their hosts, suggesting that they formed through predominantly dissipative processes.

Author(s): Chelsea Spengler¹¹, Patrick Côté³, Joel Roediger³, Laura Ferrarese³, Rubén Sánchez-Janssen³, Elisa Toloba¹⁰, Yiqing Liu⁹, Puragra Guhathakurta⁷, Jean-Charles Cuillandre¹, Stephen Gwyn³, Andrew Zirm², Roberto Muñoz⁶, Thomas Puzia⁶, Ariane Lançon⁸, Eric Peng⁵, Simona Mei⁴, Mathieu Powalka⁸
Institution(s): 1. CEA/IRFU, Observatoire de Paris, 2. Greenhouse Software, 3. Herzberg Institute of Astrophysics, 4. LERMA, Observatoire de Paris, 5. Peking University, 6. Pontificia Universidad Católica de Chile, 7. UCO/Lick Observatory, 8. Université de Strasbourg, 9. University of Oxford, 10. University of the Pacific, 11. University of Victoria

127.06 – Clumpy Star Formation in Local Luminous Infrared Galaxies

We present HST narrow-band imaging of Pa β and Pa α emission in 50 local Luminous Infrared Galaxies from the Great Observatory All-Sky LIRG Survey (GOALS). These data allow us to study spatially resolved star forming regions and directly compare to star forming clumps found in both local and high-redshift galaxies. We find that the ionized gas is concentrated in star-forming clumps with sizes ranging from 70-700pc and star formation rates (SFRs) of .001 to $5 M_{\text{sun}} \text{ yr}^{-1}$. The SFRs of the clumps in GOALS spans the range from normal local galaxies to clump SFRs found in $z=1-3$ galaxies. The clumps have stellar ages of 5×10^6 to 4.5×10^7 yr with a median age of 8.6×10^6 yr and stellar masses of 10^6 to $10^9 M_{\text{sun}}$. The LIRGs in our sample cover the entire merger sequence from isolated galaxies to advanced staged mergers and allow us to study how the size, number, luminosity, and distribution of the clumpy star formation varies with the galaxy's merger stage, mass, and global star formation rates. Finally, we compare our results to clumpy star formation in high resolution hydrodynamical FIRE simulations and find that observed star forming clumps match the same size and star formation rate properties of those found in simulations.

Author(s): Kirsten Larson¹, Lee Armus¹, Tanio Diaz-Santos²
Institution(s): 1. IPAC/ Caltech, 2. Universidad Diego Portales
Contributing team(s): GOALS Team

127.07 – The Merger-Free Growth of Galaxies and Supermassive Black Holes

There is now clear evidence that the merger-driven pathway to black hole and galaxy growth is only half the story. Merger-free evolution contributes roughly equally to the overall growth of black holes in the Universe and is also responsible for a significant amount of galaxy growth over cosmic time. A recent study examining the growth of black holes in unambiguously disk-dominated galaxies shows these black holes reach quasar-like luminosities and black hole masses typical of those hosted in bulge-dominated and elliptical galaxies with major mergers in their evolutionary histories. However, while there appears to be no correlation between the size of the black hole and upper limits on the host galaxy bulges, the fitted correlation between black hole mass and total galaxy stellar mass in these merger-free systems is fully consistent with the canonical relationship based on merger-driven systems. There is further evidence via comparison between observed populations and cosmological simulations confirming that bulgeless systems are generally consistent with having merger-free histories. If bulgeless and disk-dominated galaxies are indeed signatures of systems with no violent mergers in their formation histories, the same correlation between black hole and galaxy in these systems versus that seen in elliptical galaxy samples indicates the black hole-galaxy connection must originate with a process more fundamental than the dynamical configuration of a galaxy's stars.

Author(s): Brooke Simmons¹, Rebecca Smethurst³, Chris Lintott⁴, Garreth Martin², Sugata Kaviraj², Julien Devriendt⁴
Institution(s): 1. UC San Diego, 2. University of Hertfordshire, 3. University of Nottingham, 4. University of Oxford
Contributing team(s): Galaxy Zoo Team

128 – Extrasolar Planets II

128.01 – Understanding Super-Earths with MINERVA-Australis at USQ's Mount Kent Observatory

Super Earths, planets between 5-10 Earth masses, are the most common types of planets known, yet are completely absent from our Solar system. As a result, their detailed properties, compositions, and formation mechanisms are poorly understood. NASA's Transiting Exoplanet Survey Satellite (TESS) will identify hundreds of Super-Earths orbiting bright stars, for the first time allowing in-depth characterisation of these planets. At the University of Southern Queensland, we are host to the MINERVA-Australis project, dedicated wholly to the follow-up characterisation and mass measurement of TESS planets. We give an update on the status of MINERVA-Australis and our expected performance. We also present results from the fully operational Northern MINERVA array, with the primary mission of discovering rocky planets orbiting 80 nearby bright stars.

Author(s): Robert Wittenmyer⁷, Jonathan Horner⁷, Stephen Kane⁵, Peter Plavchan², David Ciardi¹, Jason Eastman³, John Asher Johnson³, Jason Wright⁴, Nate McCrady⁶

Institution(s): 1. California Institute of Technology, 2. George Mason University, 3. Harvard-Smithsonian Center for Astrophysics, 4. Penn State University, 5. University of California, 6. University of Montana, 7. University of Southern Queensland

Contributing team(s): The MINERVA Collaboration

128.02 – Refraction in Exoplanet Transit Observations

Before an exoplanet transit, atmospheric refraction bends light into the line of sight of an observer. The refracted light forms a stellar mirage---a distorted secondary image of the host star---that causes flux increases before transit ingress and after transit egress. The extent of this flux increase provides clues as to the composition and structure of the exoplanetary atmosphere. Here, I model the stellar mirages produced by a comprehensive set of stellar, orbital, planetary, and atmospheric parameters. Refracted light offers unprecedented atmospheric characterization opportunities for cold, long-period gas giant exoplanets. At visible wavelengths, opacity from Rayleigh scattering presents a substantial challenge to detecting stellar mirages for most exoplanets with orbital distances less than 6 AU. Based on physical parameters, I derive a criterion that determines if refracted light will significantly influence observations of a specific exoplanetary system with application to the high-precision *Kepler* data set. I also investigate the potential for refracted light to identify non-transiting exoplanets and serve as a novel means of out-of-transit atmospheric characterization. The atmospheric lensing events produced by non-transiting exoplanets are more detectable than the corresponding flux increases for transiting exoplanets. Compared to visible light observations, those at red to near-infrared wavelengths are more likely to detect refracted light in an exoplanet atmosphere. With upcoming exoplanet discovery and characterization missions in mind, I consider science cases that are uniquely enabled by photometric and spectroscopic observations of refracted light in exoplanetary systems.

Author(s): Paul Dalba¹

Institution(s): 1. Boston University

128.03D – Characterising exoplanet atmospheres as part of the LRG-BEASTS survey

I will present the latest results from the Low Resolution Ground-Based Exoplanet Atmosphere Survey using Transmission Spectroscopy (LRG-BEASTS, 'large beasts'). This programme has demonstrated the capabilities of 4-metre class telescopes to produce transmission spectra with precision comparable to HST and 8- and 10-metre class telescopes. LRG-BEASTS has so far revealed a Rayleigh scattering haze in the atmosphere of HAT-P-18b, clouds in the atmosphere of WASP-52b, and ruled out a previously claimed detection of potassium in the atmosphere of

WASP-80b. Studies of hot Jupiter atmospheres have revealed a startling diversity between systems, with many showing thick clouds and hazes which mask pressure-broadened absorption features. In the small sample of studied planets to date, no strong correlation has emerged between key planetary parameters and the presence, or absence, of clouds and hazes, although there has been a suggestion that temperature might play a role. In order to characterise this diversity and unravel the underlying physical processes, it is essential that we expand the current sample of studied planets. This is the focus of LRG-BEASTS and my dissertation. Clouds and hazes are not just prominent in giant planet atmospheres but also in the handful of smaller planets characterised in transmission. The knowledge and expertise we will gain from the study of giant planets with surveys such as LRG-BEASTS will inform our understanding of analogous processes in the exciting new generation of planets that will be discovered with TESS.

Author(s): James Kirk¹, Peter Wheatley¹

Institution(s): 1. University of Warwick

Contributing team(s): LRG-BEASTS collaboration

128.04 – Dynamics as a 'Red Flag' in Exoplanetary Science

The great majority of exoplanets are discovered indirectly - by observing a star doing something unusual, and inferring the presence of planets from that behaviour. The nature of those planets - their mass and their orbital parameters - is typically somewhat unclear, with a variety of different scenarios offering equally good fits to the observational data.

Typically, authors publish the solution that offers the best fit to the data, without considering the degree to which the planets proposed would interact with one another. This has led to the 'discovery' of planetary systems that are clearly unfeasible - and it is likely that a number of such systems are buried in the catalogue of 'confirmed' exoplanets.

Fortunately, there is a solution to this problem. By carrying out suites of n-body integrations of proposed planetary systems, we can find solutions that both offer a good fit to the observational data and the long-term dynamical stability required to give confidence that the planets proposed are truly all they seem.

Here, we present the results from a number of such dynamical studies, showing the importance of such simulations to the process of exoplanet discovery and characterisation.

Author(s): Jonathan Horner¹, Robert Wittenmyer¹

Institution(s): 1. University of Southern Queensland

128.05 – Robo-AO KOI Survey: LGS-AO imaging of every Kepler planetary candidate host star

Robo-AO is observing every Kepler planetary candidate host star (KOI) in high resolution, made possible using the unprecedented efficiency provided by automation of LGS adaptive optics. Nearby contaminating stars may be the source of false positive transit signals or, if a bona fide planet is in the system, dilute the observed transit signal, resulting in underestimated planet radii. In 3857 observations, we find 632 stars within 4" (approximately the Kepler pixel scale) of KOIs. In particular, we find 26 rocky, habitable zone planets with contaminating nearby stars, 8 of which are now more likely to have large gaseous envelopes. We present evidence that the majority of these nearby stars are unbound, and use the likely bound stars to test theories of planetary formation and evolution within multiple star systems. Finally, we discuss future all-sky, kilo-target surveys made possible by the construction of a Southern Robo-AO analog.

Author(s): Carl Ziegler³, Nicholas Law³, Christoph Baranec², Reed Riddle¹

Institution(s): 1. California Institute of Technology, 2. University of Hawaii, Manoa, 3. University of North Carolina at Chapel Hill

128.06 – Simulated JWST/NIRISS Transit Spectroscopy of Anticipated TESS Planets Compared to Select Discoveries from Space-Based and Ground-Based Surveys

The Transiting Exoplanet Survey Satellite (TESS) will embark in 2018 on a 2-year wide-field survey mission of most of the celestial sky, discovering over a thousand super-Earth and sub-Neptune-sized exoplanets potentially suitable for follow-up observations using the James Webb Space Telescope (JWST). Bouma et al. (2017) and Sullivan et al. (2015) used Monte Carlo simulations to predict the properties of the planetary systems that TESS is likely to detect, basing their simulations upon Kepler-derived planet occurrence rates and photometric performance models for the TESS cameras. We employed a JWST Near InfraRed Imager and Slitless Spectrograph (NIRISS) simulation tool to estimate the signal-to-noise (S/N) that JWST/NIRISS will attain in transmission spectroscopy of these anticipated TESS discoveries, and we then compared the S/N for anticipated TESS discoveries to our estimates of S/N for 18 known exoplanets. We analyzed the sensitivity of our results to planetary composition, cloud cover, and presence of an observational noise floor. We find that only a few anticipated TESS discoveries in the terrestrial planet regime will result in better JWST/NIRISS S/N than currently known exoplanets, such as the TRAPPIST-1 planets, GJ1132b, or LHS1140b. However, we emphasize that this outcome is based upon Kepler-derived occurrence rates, and that co-planar compact systems (e.g. TRAPPIST-1) were not included in predicting the anticipated TESS planet yield. Furthermore, our results show that several hundred anticipated TESS discoveries in the super-Earth and sub-Neptune regime will produce S/N higher than currently known exoplanets such as K2-3b or K2-3c. We apply our results to estimate the scope of a JWST follow-up observation program devoted to mapping the transition region between high molecular weight and primordial planetary atmospheres.

Author(s): Dana Louie², Drake Deming², Loic Albert⁵, Luke Bouma³, Jacob Bean¹, Mercedes Lopez-Morales⁴

Institution(s): 1. Department of Astronomy and Astrophysics, University of Chicago, 2. Department of Astronomy, University of Maryland, 3. Department of Astrophysical Sciences, Princeton University, 4. Harvard-Smithsonian Center for Astrophysics, 5. Institut de recherche sur les exoplanètes (iREx), Université de Montréal

128.07 – Tidal Dissipation in WASP-12

129 – Circumstellar Disks I

129.01 – Weak Turbulence in Protoplanetary Disks as Revealed by ALMA

Gas kinematics are an important part of planet formation, influencing processes ranging from the growth of sub-micron grains to the migration of gas giant planets. Dynamical behavior can be traced with both synoptic observations of the mid-infrared excess, sensitive to the inner disk, and spatially resolved radio observations of gas emission, sensitive to the outer disk. I report on our ongoing efforts to constrain turbulence using ALMA observations of CO emission from protoplanetary disks. Building on our upper limit around HD 163296 ($<0.05c_s$), we find evidence for weak turbulence around TW Hya ($<0.08c_s$) indicating that weak non-thermal motion is not unique to HD 163296. I will also discuss observations of CO/¹³CO/¹⁸O from around V4046 Sgr, DM Tau, and MWC 480 that will help to further expand the turbulence sample, as well as inform our understanding of CO photo-chemistry in the outer edges of these disks.

WASP-12 is a hot Jupiter system with an orbital period of $P = 1.1$ day, making it one of the shortest-period giant planets known. Recent transit timing observations by Maciejewski et al. (2016) and Patra et al. (2017) find a decreasing period with $|P/(dP/dt)| = 3.2$ Myr. This has been interpreted as evidence of either orbital decay due to tidal dissipation or a long term oscillation of the apparent period due to apsidal precession. Here we consider the possibility that it is orbital decay. We show that the parameters of the host star are consistent with either a $M \approx 1.3 M_\odot$ main sequence star or a $M \approx 1.2 M_\odot$ subgiant. We find that if the star is on the main sequence, the tidal dissipation is too inefficient to explain the observed dP/dt . However, if it is a subgiant, the tidal dissipation is significantly enhanced due to nonlinear wave breaking of the dynamical tide near the star's center. The subgiant models have a stellar tidal quality factor $Q \approx 2 \times 10^5$ and an orbital decay rate that agrees well with the observed dP/dt . It would also explain why the planet survived for 3 Gyr while the star was on the main sequence and yet is now inspiraling on a 3 Myr timescale. Although this suggests that we are witnessing the last $\sim 0.1\%$ of the planet's life, the probability of such a detection is a few percent given the observed sample of ≈ 30 hot Jupiters in $P < 3$ day orbits around $M > 1.2 M_\odot$ hosts.

Author(s): Nevin N Weinberg¹, Meng Sun², Phil Arras², Reed Essick¹

Institution(s): 1. Massachusetts Institute of Technology, 2. University of Virginia

128.08 – Evaluating Climate Variability of HD 209458b and HD 189733b Through Multi-Epoch Eclipse Observations Using the Spitzer Space Telescope.

We expect hot Jupiter atmospheres to be dynamic environments exhibiting time varying weather. However, it is uncertain to what extent temporal variability will be observable when considering disc integrated observations. There are very few planets with multi epoch observations at the required precision to probe variability in dayside emission. We present the analysis of multiple eclipse observations, at both 3.6 and 4.5 μm , of HD 209458b and HD 189733b as a probe of variability at long time scales. These observations also provide the precision necessary to resolve the two dimensional dayside thermal structure of the planetary atmosphere through eclipse mapping.

Author(s): Brian Kilpatrick¹, Nikole K. Lewis⁵, Tiffany Kataria³, Julien de Wit⁴, Laura Kreidberg², Kevin Stevenson⁵, Gregory Tucker¹

Institution(s): 1. Brown University, 2. Harvard University, 3. Jet Propulsion Laboratory, 4. MIT, 5. Space Telescope Science Institute

Author(s): Kevin Flaherty⁴, A. Meredith Hughes⁴, Jacob Simon², Sean Andrews¹, Xue-Ning Bai³, David Wilner¹

Institution(s): 1. Harvard-Smithsonian Center for Astrophysics, 2. JILA, University of Colorado, 3. Tsinghua University, 4. Wesleyan University

129.02D – Microphysics Confronted Photoevaporation: Full (Magneto-)Hydrodynamic Simulations Coupled with Consistent Thermochemistry and Radiative Transfer in Protoplanetary Disks and Planet Atmospheres

Mechanisms related to microphysics, including thermochemistry and radiative transfer, are important in astrophysical processes but difficult to calculate. Equipped with the computation power of GPUs, we explore protoplanetary disks (PPDs) and planet atmospheres (PAs) by coupling consistent microphysics with (magneto-)hydrodynamics in photoevaporation driven by ultraviolet and X-ray radiation from the host star, which is an important dispersal mechanism for PPDs and PAs. We develop updated understandings towards the underlying processes that

determine the local thermo-/hydrodynamic evolution, as well as the global structures, of photoevaporating systems. Observable molecules including CO, OH and H₂O may re-form and survive at relatively high wind temperatures due to reactions being out of equilibrium. Mass-loss rates are sensitive to the intensity of radiation in energy bands that interact directly with hydrogen. Comparison with previous works shows that mass loss rates are also sensitive to the treatment of both the hydrodynamics and the thermochemistry. Divergent results concerning the efficiency of X-ray photoevaporation are traced in part to differing assumptions about dust and other coolants.

Author(s): Lile Wang¹

Institution(s): 1. Princeton University

129.03 – Mutual Inclinations of Circumbinary Protoplanetary Disks

Measuring the relative inclinations between binary stars and their circumbinary disks is vital for interpreting the census of known *Kepler* circumbinary planets and understanding their formation environment. Through a series of ALMA programs, we have targeted protoplanetary disks around known spectroscopic binaries to infer the disk structure, dynamically measure the total stellar mass, and determine the mutual inclinations between the stellar orbits and the circumbinary disk. Thus far, we know of 4 systems with 10-20 day orbital periods that all show alignment to within 3 degrees, which is in remarkable agreement with the mutual inclinations of the *Kepler* circumbinary planets and would seem to suggest that coplanarity is a feature of the short-period binary star and planet formation process. However, we caution that selection effects which make aligned systems easier to detect are potentially at work in both the disk and planet samples. In fact, our recent ALMA and RV program revealed a triple system that has its large circumtriple disk misaligned with at least one and possibly both stellar orbits by as much as 45 degrees. Mapping out and understanding the distribution of mutual inclinations has ramifications for the circumbinary planet occurrence rate---if a significant population of misaligned systems exist, then the circumbinary planets might form even more frequently than their single star counterparts.

Author(s): Ian Czekala¹

Institution(s): 1. Stanford University

129.05 – How does a planet excite multiple spiral arms?

Protoplanetary disk simulations show that a single planet excites multiple spiral arms in the background disk, potentially supported by the multi-armed spirals revealed with recent high-resolution observations in some disks. The existence of multiple spiral arms is of importance in many aspects. It is empirically found that the arm-to-arm separation increases as a function of the planetary mass, so one can use the morphology of observed

130 – ISM I

130.01 – The EDGE-CALIFA Survey: Molecular and Ionized Gas Kinematics in Nearby Galaxies

We present a systematic comparative study of molecular and ionized gas kinematics in galaxies, the first time such a comparison has been done for a large sample. These results are based on observations obtained by the EDGE survey, which measured spatially resolved ¹²CO(J=1-0) in 126 nearby galaxies at a typical spatial resolution of ~1.5 kpc. Every galaxy in EDGE has corresponding resolved ionized gas measurements from CALIFA, with a typical spatial resolution of ~1 kpc. Using a subsample of 17 galaxies where precise molecular gas rotation curves could be extracted, we derive CO and H α rotation curves using the same geometric parameters out to $\geq 1 R_e$ and compare their kinematics. We find that ~80% of our sample have smaller ionized rotation velocities than the molecular gas rotation velocities in the outer part of the rotation curve. In no case is the molecular gas rotation velocity measurably lower than that of the ionized gas. We suggest that this is due to extraplanar diffuse ionized gas in a thick, pressure supported disk which rotates more

slowly with increasing height off the plane. Using the high spectral resolution observations available from CALIFA for the same galaxies, we measure H γ velocity dispersions. We find that the galaxies in our subsample have sufficiently large ionized gas velocity dispersions to support a thick ionized gas disk. We perform kinematic simulations of thick disks and show that a thick disk with a vertical velocity gradient can reproduce the observed differences between the CO and H α rotation velocities. There are no trends in the difference between the CO and H α rotation velocities with global parameters, such as inclination, star formation rate, or morphology. We note, however, that nearly all of our galaxies exceed the star formation rate per unit area needed to have an extended diffuse ionized phase.

spiral arms to infer the mass of unseen planets. In addition, a spiral arm opens a radial gap as it steepens into a shock, so when a planet excites multiple spiral arms it can open multiple gaps in the disk. Despite the important implications, however, the formation mechanism of multiple spiral arms has not been fully understood by far.

In this talk, we explain how a planet excites multiple spiral arms. The gravitational potential of a planet can be decomposed into a Fourier series, a sum of individual azimuthal modes having different azimuthal wavenumbers. Using a linear wave theory, we first demonstrate that appropriate sets of Fourier decomposed waves can be in phase, raising a possibility that constructive interference among the waves can produce coherent structures - spiral arms. More than one spiral arm can form since such constructive interference can occur at different positions in the disk for different sets of waves. We then verify this hypothesis using a suite of two-dimensional hydrodynamic simulations. Finally, we present non-linear behavior in the formation of multiple spiral arms.

Author(s): Jaehan Bae¹, Zhaohuan Zhu²

Institution(s): 1. Carnegie Institution of Washington, 2. University of Nevada, Las Vegas

129.06 – A Subarcsecond ALMA Molecular Line Imaging Survey of the Circumbinary, Protoplanetary Disk Orbiting V4046 Sgr

We present a suite of ALMA interferometric molecular line and continuum images of the gas-rich circumbinary disk orbiting the nearby, young, short-period, solar-mass binary system V4046 Sgr (D ~ 73 pc; age ~20 Myr). These Cycle 2 and 3 ALMA observations of V4046 Sgr were undertaken in the 1.1 to 1.4 mm wavelength range (ALMA Band 6) with antenna configurations involving maximum baselines of several hundred meters, yielding subarcsecond-resolution images in more than a dozen molecular species and isotopologues. Collectively, these ALMA images serve to elucidate, on linear size scales of ~30-40 AU, the chemical structure of an evolved, circumbinary, protoplanetary disk.

This research is supported by NASA Exoplanets program grant NNX16AB43G to RIT.

Author(s): Joel H Kastner⁶, C. Qi⁸, Annie Dickson-Vandervelde⁶, Thierry Forveille⁴, Pierre Hily-Blant⁴, Karin Oberg³, David Wilner⁸, Sean Andrews⁸, Uma Gorti⁷, Germano Sacco¹, Valerie Rapson², David Principe⁵

Institution(s): 1. Arcetri Observatory, 2. Dudley Observatory, 3. Harvard University, 4. IPAG, 5. MIT, 6. Rochester Institute of Technology, 7. SETI Institute, 8. Smithsonian Institution

Author(s): Rebecca Chyba⁷, Alberto D. Bolatto⁷, Peter Teuben⁷, Sebastián F. Sánchez⁴, Leo Blitz⁵, Rubén García-Benito¹, Bernd Husemann², Damián Mast³, Dyas Utomo⁵, Stuart N. Vogel⁷, Tony Wong⁶

Institution(s): 1. *Instituto de Astrofísica de Andalucía*, 2. *Max-Planck-Institut für Astronomie*, 3. *Observatorio Astronómico de Córdoba*, 4. *Universidad Nacional Autónoma de México*, 5. *University of California, Berkeley*, 6. *University of Illinois*, 7. *University of Maryland*

Contributing team(s): The EDGE-CALIFA Collaboration

130.02D – Characterizing the Interstellar and Circumgalactic Medium in Star-forming Galaxies

Rest-frame UV and optical spectroscopy provide valuable information on the physical properties of the neutral and ionized interstellar medium (ISM) in star-forming galaxies, including both the systemic interstellar component originating from HII regions, and the multi-phase outflowing component associated with star-formation feedback. My thesis focuses on both the systemic and outflowing ISM in star-forming galaxies at redshift $z \sim 1-4$. With an unprecedented sample at $z \sim 1$ with the rest-frame near-UV coverage, we examined how the kinematics of the warm and cool phases of gas, probed by the interstellar CIV and low-ionization features, respectively, relate to each other. The spectral properties of CIV strongly correlate with the current star-formation rate, indicating a distinct nature of highly-ionized outflowing gas being driven by massive star formation. Additionally, we used the same set of $z \sim 1$ galaxies to study the properties of the systemic ISM in HII regions by analyzing the nebular CIII] emission. CIII] emission tends to be stronger in lower-mass, bluer, and fainter galaxies with lower metallicity, suggesting that the strong CIII] emitters at lower redshifts can be ideal analogs of young, bursty galaxies at $z > 6$, which are possibly responsible for reionizing the universe. We are currently investigating the redshift evolution of the neutral, circumgalactic gas in a sample of ~ 1100 Lyman Break Galaxies at $z \sim 2-4$. The negative correlation between Ly α emission and low-ionization interstellar absorption line strengths appears to be universal across different redshifts, but the fine-structure line emitting regions are found to be more compact for higher-redshift galaxies. With the detailed observational constraints provided by the rest-UV and rest-optical spectroscopy, our study sheds light on how the interstellar and circumgalactic gas components and different phases of gas connect to each other, and therefore provides a comprehensive picture of the overall physical environment in typical star-forming galaxies.

Author(s): Xinnan Du¹, Alice Shapley¹

Institution(s): 1. *University of California, Los Angeles*

Contributing team(s): Crystal Martin, Alison Coil, Charles Steidel, Tucker Jones, Daniel Stark, Allison Strom

130.03 – X-Ray Dust Tomography: Mapping the Galaxy one X-ray Transient at a Time

Tomography using X-ray light echoes from dust scattering by interstellar clouds is an accurate tool to study the line-of-sight distribution of dust. It can be used to measure distances to molecular clouds and X-ray sources, it can map Galactic structure in dust, and it can be used for precision measurements of dust composition and grain size distribution. Necessary conditions for observing echoes include a suitable X-ray lightcurve and sufficient dust column density to the source. I will discuss a tool set for studying dust echoes and show results obtained for some of the brightest echoes detected to date.

Author(s): Sebastian Heinz¹, Lia Corrales¹

Institution(s): 1. *UW Madison*

130.04 – HAWC+/SOFIA observations of Rho Oph A: far-infrared polarization spectrum

In this work, we present preliminary results from the HAWC+ far-infrared polarimeter that operates on the SOFIA airborne observatory. The densest portions of the Rho Ophiuchi molecular complex, known as Rho Oph A, have been mapped using HAWC+

bands C (89 microns) and D (155 microns). Rho Oph A is a well known nearby star forming region. At the target's distance of approximately 130 pc, our observations provide excellent spatial resolution (~ 5 mpc in band C).

The magnetic field map suggests a compressed and distorted field morphology around Oph S1, a massive B3 star that is the main heat source of Rho Oph A. We compute the ratio $p(D)/p(C)$, where $p(C)$ and $p(D)$ are the polarization degree maps at bands C and D, respectively. This ratio estimates the slope of the polarization spectrum in the far-infrared. Although the slope is predicted to be positive by dust grain models, previous observations of other molecular clouds have revealed that negative slopes are common. In Rho Oph A, we find that there is a smooth gradient of $p(D)/p(C)$ across the mapped field. The change in $p(D)/p(C)$ is well correlated with the integrated NH₃ (1,1) emission. A positive slope dominates the lower density and well illuminated portions of the cloud, whereas a transition to a negative slope is observed at the denser and less evenly illuminated cloud core.

We interpret the positive to negative slope transition as being consistent with the radiative torques (RATs) grain alignment theory. For the sight lines of higher column density, polarized emission from the warmer outer cloud layers is added to emission from the colder inner well-shielded layers lying along the same line-of-sight. Given that the outer layers receive more radiation from Oph S1, their grain alignment efficiency is expected to be higher according to RATs. The combination of warmer, well aligned grains with cooler, poorly aligned grains is what causes the negative slope. This effect is not present in the sight lines of lower column density, due to the much lower extinction.

Author(s): Fabio Santos², Charles D. Dowell¹, Martin Houde⁶, Leslie Looney⁴, Enrique Lopez-Rodriguez⁵, Giles Novak², Derek Ward-Thompson³

Institution(s): 1. *Jet Propulsion Laboratory - NASA*, 2. *Northwestern University*, 3. *University of Central Lancashire*, 4. *University of Illinois*, 5. *USRA/SOFIA*, 6. *Western University*

Contributing team(s): HAWC+ Science Team

130.05D – Probing the Plasma Structure of HII Regions with Faraday Rotation

We are involved in study concerning the modification of magnetic fields in the shells of HII regions. We report Faraday Rotation results of lines on sight through or near HII regions associated with OB associations. In our studies of the Rosette Nebula ($l = 206^\circ$, $b = -1.2^\circ$), we measure positive rotation measure (RM) values in excess of $+40$ to $+1200$ rad m^{-2} due to the shell of the nebula and a background RM of $+147$ rad m^{-2} due to the general interstellar medium (Savage et al. 2013, ApJ, 765, 42; Costa et al. 2016, ApJ, 821, 92). We are currently completing an analysis of observations probing an additional HII region, IC 1805 ($l = 135^\circ$, $b = +0.9^\circ$), associated with the W4 Superbubble. We measure negative RM values across the region between -68 and -961 rad m^{-2} . We find the highest RM values for lines of sight which intersect the ionized shell of the HII region for the Rosette Nebula, but in the case of IC 1805, the highest RM values are outside the bright shell of the HII region. However, we find that the magnitude of the RM between the two regions is similar. The sign of the RM across each HII region is consistent with the expected polarity of a Galactic magnetic field that follows the Perseus spiral arm in the clockwise direction, as suggested by Han et al. (2006, ApJ, 642, 868) and Van Eck et al. (2011, ApJ, 728, 14).

Author(s): Allison Costa¹, Steven R Spangler¹

Institution(s): 1. *University of Iowa*

130.06 – Electron Excitation of High Dipole Moment Molecules

Emission from high-dipole moment molecules such as HCN allows determination of the density in molecular clouds, and is often considered to trace the “dense” gas available for star

formation. We assess the importance of electron excitation in various environments. The ratio of the rate coefficients for electrons and H₂ molecules, $\sim 10^5$ for HCN, yields the requirements for electron excitation to be of practical importance if $n(\text{H}_2) < 10^{5.5} / \text{cm}^3$ and $X(e^-) > 10^{-5}$, where the numerical factors reflect critical values $n_c(\text{H}_2)$ and $X^*(e^-)$. This indicates that in regions where a large fraction of carbon is ionized, $X(e^-)$ will be large enough to make electron excitation significant. The situation is in general similar for other “high density tracers”, including HCO⁺, CN, and CS. But there are significant differences in the critical electron fractional abundance, $X^*(e^-)$, defined by the value required for equal effect from collisions with H₂ and e⁻. Electron excitation is, for example, unimportant for CO and C⁺. Electron excitation may be responsible for the surprisingly large spatial extent of the emission from dense gas tracers in some molecular clouds (Pety et al. 2017, Kauffmann, Goldsmith et al. 2017, A&A, submitted). The enhanced estimates for HCN abundances and HCN/CO and HCN/HCO⁺ ratios observed in the nuclear regions of luminous galaxies may be in part a result of electron excitation of high dipole moment tracers. The importance of electron excitation will depend on detailed models of the chemistry, which may well be non-steady state and non-static.

Author(s): Paul Goldsmith¹, Jens Kauffmann²
Institution(s): 1. JPL, 2. Max Planck Institute for Radio Astronomy

130.07 – Characterizing the Multi-Phase Origin of the [CII] Emission in M101 and NGC 6946

131 – Learning with NASA Astrophysics: How to Get Connected

In 2015, NASA selected multiple organizations from across the county to receive cooperative agreement awards. These awards aim to enable organizations to interconnect and collaboratively engage learners with NASA science content and experts for greater impact. For this special session, representatives from multiple NASA Science Mission Directorate cooperative agreement awardees will discuss how they connect scientists and engineers (subject matter experts) with their STEM products and programs - and ultimately with learners of all ages. Included in this session will be short presentations, a panel discussion, and networking time to connect directly with practitioners of NASA STEM engagement. Come join us to find out more about NASA's efforts to connect astrophysics subject matter experts with learners of all ages and how you can be involved.

131.01 – NASA SMD STEM Activation: Enabling NASA Science Experts and Content into the Learning Environment

The NASA Science Mission Directorate (SMD) restructured its efforts to enhance learning in science, technology, engineering, and mathematics (STEM) content areas through a cooperative agreement notice issued in 2015. This effort resulted in the competitive selection of 27 organizations to implement a strategic approach that leverages SMD's unique assets. Three of these are exclusively directed towards Astrophysics. These unique assets include SMD's science and engineering content and Science Discipline Subject Matter Experts. Awardees began their work during 2016 and span all areas of Earth and space science and the audiences NASA SMD intends to reach. The goal of the restructured STEM Activation program is to further enable NASA science experts and content into the learning environment more effectively and efficiently with learners of all ages. The objectives are to enable STEM education, improve US scientific literacy, advance national educational goals, and leverage efforts through partnerships. This presentation will provide an overview of the NASA SMD STEM Activation landscape and its commitment to meeting user needs.

Author(s): Hashima Hasan¹, Kristen Erickson¹
Institution(s): 1. NASA Headquarters

The bright far-infrared line [CII] is a dominant cooling channel of the neutral interstellar medium (ISM) and is a tracer of star formation. However, [CII] can be excited in different environments of the ISM, such as in dense photodissociation regions (PDRs), the cold/warm neutral medium (CNM/WNM), and the warm ionized medium (WIM). Separating the [CII] emission into its multiple components is vital for understanding star formation and for using [CII] as a star formation tracer. We present spectrally resolved SOFIA/GREAT data of the 158 μm [CII] emission, as well as ancillary HI and CO 2-1 data, to disentangle the multiple phases of the ISM. We use 18 pointings that sample the range of different environments present in these galaxies, including star formation activity, metallicity, radiation field strength, and gas content. We find that on average the [CII] is more associated with the dense CO gas coming from PDRs than the neutral medium, consistent with other results in the literature. Additionally, the [CII] observations allow us to access the “CO-faint” molecular gas in regions that have too low of a metallicity to produce CO. This adds to the small number of studies that have explored this “CO-faint” regime.

Author(s): Elizabeth Tarantino², Alberto Bolatto², Rodrigo Herrera-Camus¹
Institution(s): 1. Max-Planck-Institut für Extraterrestrische Physik (MPE), 2. University of Maryland

131.02 – What Do Subject Matter Experts Have to Say about Participating in Education and Outreach?

NASA's Universe of Learning partners wish to actively engage with Subject Matter Experts (scientists and engineers) throughout the design, development, and delivery of products, programs, and professional development. In order to ensure these engagement efforts aligned with the needs of Subject Matter Experts, the external evaluators conducted an online survey. The subject pool included the scientists and engineers employed at the partner organizations as well as other scientists and engineers affiliated with NASA's Astrophysics missions and research programs. This presentation will describe scientists'/engineers' interest in various types of education/outreach, their availability to participate in education/outreach, factors that would encourage their participation in education/outreach, and the preparation and support they have for participation in education/outreach.

Author(s): Colleen Manning¹
Institution(s): 1. Goodman Research Group, Inc.
Contributing team(s): NASA's Universe of Learning Team

131.03 – Overview of NASA's Universe of Learning: An Integrated Astrophysics STEM Learning and Literacy Program

NASA's Universe of Learning creates and delivers science-driven, audience-driven resources and experiences designed to engage and immerse learners of all ages and backgrounds in exploring the universe for themselves. The project is the result of a unique partnership between the Space Telescope Science Institute, Caltech/IPAC, Jet Propulsion Laboratory, Smithsonian Astrophysical Observatory, and Sonoma State University, and is one of 27 competitively-selected cooperative agreements within the NASA Science Mission Directorate STEM Activation program. The NASA's Universe of Learning team draws upon cutting-edge science and works closely with Subject Matter Experts (scientists and engineers) from across the NASA Astrophysics Physics of the Cosmos, Cosmic Origins, and Exoplanet Exploration themes. Together we develop and disseminate data tools and participatory experiences, multimedia and immersive experiences, exhibits and

community programs, and professional learning experiences that meet the needs of our audiences, with attention to underserved and underrepresented populations. In doing so, scientists and educators from the partner institutions work together as a collaborative, integrated Astrophysics team to support NASA objectives to enable STEM education, increase scientific literacy, advance national education goals, and leverage efforts through partnerships. Robust program evaluation is central to our efforts, and utilizes portfolio analysis, process studies, and studies of reach and impact. This presentation will provide an overview of NASA's Universe of Learning, our direct connection to NASA Astrophysics, and our collaborative work with the NASA Astrophysics science community.

Author(s): Denise Smith⁶, Kathleen Lestition⁴, Gordon Squires¹, Anya A. Biferno³, Lynn Cominsky⁵, Colleen Manning²
Institution(s): 1. Caltech / IPAC, 2. Goodman Research Group, 3. Jet Propulsion Laboratory, 4. Smithsonian Astrophysical Observatory, 5. Sonoma State University, 6. Space Telescope Science Institute

Contributing team(s): NASA's Universe of Learning Team

131.04 – NASA's Universe of Learning: The Integral Role of Research Astronomers and Other Subject Matter Experts

Astronomy seeks to understand the workings of the Universe on its largest scales, and to answer fundamental questions about the story of our origins. The science of astronomy thus naturally lends itself to informal education and public outreach activities, as it broadly captures the human imagination.

There are at least three overall goals for investment of resources in Astronomy E/PO: to interest students in pursuing STEM education and careers; to develop Astronomy as context for teaching more basic physical and computer science in service of US National Education Goals; to help motivate continued public support of federally funded Astronomy research and technology development.

Providing a full spectrum of opportunities for the public to learn about recent Astronomy discoveries is key to achieving these societal goals. Thus, the E/PO professional community must have an understanding of recent scientific/technological results, and engage with the researchers who are creating new knowledge to explicate that knowledge to the public. It stands to reason that researchers (or "subject matter experts, SMEs") must be involved in and remain connected to the E/PO endeavor.

In this talk, I will describe how research astronomers and other SMEs play an integral role in a full range of informal education programming developed by the NASA Universe of Learning collaboration, and opportunities to get involved.

Author(s): Janice Lee¹
Institution(s): 1. Caltech/IPAC
Contributing team(s): Universe of Learning Team

131.05 – The Airborne Astronomy Ambassadors (AAA) Program and NASA Astrophysics Connections

The NASA Airborne Astronomy Ambassadors (AAA) program is a three-part professional development (PD) experience for high school physics, astronomy, and earth science teachers. AAA PD consists of: (1) blended learning via webinars, asynchronous content delivery, and in-person workshops, (2) a STEM immersion experience at NASA Armstrong's B703 science research aircraft facility in Palmdale, California, including interactions with NASA astrophysics & planetary science Subject Matter Experts (SMEs) during science flights on SOFIA, and (3) continuing post-flight opportunities for teacher & student connections with SMEs.

Author(s): Dana Edward Backman¹, Coral Clark¹, Pamela Harman¹

Institution(s): 1. SETI Institute

131.06 – Girl Scouts and Subject Matter Experts: What's the Connection?

Reaching for the Stars: NASA Science for Girl Scouts (Girl Scout Stars) fosters interaction between Girl Scouts and NASA Subject Matter Experts (SMEs), disseminates NASA STEM education-related resources, and engages Girl Scouts in NASA science and programs through space science badges and summer camps.

A space science badge is in development for each of the six levels of Girl Scouts: Daisies, Grades K – 1; Brownies, Grades 2 -3; Juniors, Grades 4 -5; Cadettes, Grades 6 -8; Seniors, Grades 9 -10; and Ambassadors, Grades 11 -12. Indirectly, SMEs will reach tens of thousands of girls through the badges. SETI Institute SMEs Institute and SME Co-Is located at ARIES Scientific, Astronomical Society of the Pacific, University of Arizona, and Girl Scouts of Northern California developed and modified astronomy activities for the Girl Scouts USA badge writers to finesse into the Girl Scout formats. Revisions are reviewed by SMEs for accuracy. Each badge includes a step option that encourages girls to connect with SMEs, and recommendations for volunteers.

A total of 127 girls from 31 states and the District of Columbia attended Total Eclipse Destination Camps at three locations. SMEs led activities and tours, inspiring girls to consider STEM careers. University of Arizona (U of A) SMEs lead Astronomy Camp for Volunteers, enabling volunteers to lead and inspire Girl Scouts in their respective Girl Scout Councils. A Destination Camp for Girl Scouts was also held at U of A. Girls experience authentic astronomy, learning how to collect and analyze data.

Eleven teams comprised of two Girl Scouts, a volunteer or Council Staff, and an amateur astronomer attended Astronomy Club Camp, held at NASA GSFC. SMEs delivered science content. The girls will lead the formation of astronomy clubs in their councils, and will train their successors. SMEs will present and coach the clubs during monthly webinars.

This presentation will highlight success and discuss lessons learned that are applicable to working with Girl Scouts.

Author(s): Pamela Harman¹
Institution(s): 1. SETI Institute
Contributing team(s): Girls Scouts of Northern California, Girl Scouts USA, Astronomical Society of the Pacific, University of Arizona, and ARIES Scientific.

131.07 – Sitting with the scientists: a collaborative approach to STEM content development

For over two decades, the Goddard Astrophysics Education Team has been an integrated part of NASA Goddard's Astrophysics Science Division. As part of NASA's largest astrophysics organization, our team is in a unique position to collaborate with the division's scientists, engineers, and technical personnel - our subject matter experts (SMEs) - in a variety of capacities. We often seek input from our SMEs to help implement our education programs - to ensure our programs' scientific accuracy, to help us employ cutting-edge topics, and to promote authentic science processes. At the same time, we act as education experts for our SMEs to help them implement their ideas. We see this as a true partnership, with many opportunities for SME participation. Our current STEM Activation programs, Afterschool Universe and NASA Family Science Night, were created with strong involvement from division scientists, and our latest sessions on galaxies were developed in collaboration with an active researcher. In addition to our own programming, we have been tasked with providing NASA astrophysics content and expertise to the Goddard Office of Education, the Heliophysics Education Consortium (and their cross-division efforts), and the NASA

Science Mission Directorate STEM Activation Community. This talk will provide an overview of our team's current efforts and the ways in which we partner with our division's SMEs.

132 – White Dwarfs and Neutron Stars I

132.01 – Rolling in their Graves: White Dwarf Rotation as a Function of Mass

We have more than doubled the number of rotation rates measured for isolated pulsating white dwarfs thanks to extensive space-based photometry from *Kepler* and *K2*. Using follow-up optical spectroscopy to measure masses, we have put the first constraints on white dwarf rotation as a function of mass, constraining the endpoints of angular momentum evolution in stars. We find that 0.51-to-0.73-solar-mass white dwarfs, which evolved from 0.9-to-3.0-solar-mass ZAMS progenitors, have a mean rotation period of 35 hr with a standard deviation of 28 hr, with notable exceptions for higher-mass white dwarfs. Our raw and reduced data, still growing every *K2* Campaign field, are available for the community to (re-)analyze at <http://www.k2wd.org>.

Author(s): JJ Hermes¹

Institution(s): 1. University of North Carolina at Chapel Hill

132.02 – FRB121102: First detection across 5 - 8 GHz and spectral properties from the Breakthrough Listen instrument

Fast Radio Bursts (FRBs) are some of the most energetic and enigmatic events in the Universe. The origin of these sources is among the most challenging questions of modern-day astrophysics. Thus, it is imperative to understand the properties of these bursts across a range of radio frequencies. Among the known FRBs, FRB121102 is the only source known to show repeated bursts [Spitler et al., *Nature*, 531, 7593 202-205, 2016], which can allow a detailed investigation of various origin models.

In August 2017, we initiated a campaign observing FRB 121102 using the Breakthrough Listen Digital Backend with the C-band receiver at the Robert C. Byrd Green Bank Telescope (GBT). We recorded baseband voltage data across 5.4 GHz of bandwidth, completely covering the C-band receiver's nominal 4-8 GHz band [MacMahon et al. arXiv:1707.06024v2]. The recorded data were searched for dispersed pulses consistent with the known dispersion measure of FRB 121102 (557 pc cm⁻³) using high-speed GPU software tools. We detected 21 bursts above our detection threshold of 6 sigmas in the first 60-minutes, out of which 18 occurred in the first 30-minutes only. To our knowledge, this is the highest event rate seen for FRB121102 at any observing frequency. These observations are the highest frequency and widest bandwidth detection of bursts from FRB 121102 (or any other FRB) obtained to-date. We note that individual bursts show marked changes in spectral extent ranging from hundreds of MHz to several GHz. We have used high frequency dynamic spectra of these bursts to estimate the characteristic scintillation bandwidth and correlation time-scale. We also found distinctive temporal structures, separated by a few milliseconds, in three of the strongest bursts, with each sub-structure exhibiting varied spectral features. We will discuss our findings and how these detections of FRB 121102 around 8 GHz opens up a new regime in scrutinizing various origin models. We will also highlight the unique capabilities of the Breakthrough Listen instrument at the GBT which allowed such sensitive and detailed observations.

Author(s): Barbara Mattson¹

Institution(s): 1. UMCP-CRESST/NASA Goddard

Author(s): Vishal Gajjar⁸, Andrew Siemion⁸, David MacMohan⁸, Steve Croft⁸, Greg Hellbourg⁸, Howard Isaacson⁸, J. Emilio Enriquez⁸, Daniel Price⁸, Matt Lebofsky⁸, David De Boer⁸, Dan Werthimer⁸, Jack Hickish⁸, Casey Brinkman¹⁰, Shami Chatterjee⁹, Scott M. Ransom¹¹, Casey Law⁸, Jason W. T. Hessels², Jim Cordes⁹, Laura Spitler⁶, Ryan Lynch³, Maura McLaughlin¹², Paul Scholz⁷, Benito Marcote⁴, Geoffrey C. Bower¹, Shriharsh Tendulkar⁵

Institution(s): 1. Academia Sinica Institute of Astronomy and Astrophysics, 2. ASTRON, 3. Green Bank Observatory, 4. Joint Institute for VLBI ERIC, 5. McGill University, 6. MPIfR, 7. National Research Council of Canada, 8. University of California, 9. University of Cornell, 10. University of Vermont, 11. University of Virginia, 12. West Virginia University

132.03D – Natal kicks of neutron stars

Knowledge of the velocity distribution of neutron stars is essential for our understanding of the rate of the double neutron stars mergers and the supernova explosion physics. Binaries with a neutron star which receive low natal kick stay bound more frequently after a supernova explosion. We have investigated the most precise parallaxes and proper motions of isolated pulsars (only interferometric measurements) and recycled radio pulsars (timing measurements) through the maximum likelihood technique. We have found that both these groups show a very broad velocity distribution, which we describe with a sum of two Maxwellians. 42% of young neutron stars are drawn from a Maxwellian with $\sigma=77$ km/s, and the remainder from a Maxwellian with $\sigma=320$ km/s. 66% of the recycled neutron stars have $\sigma=38$ km/s and remaining part has $\sigma=150$ km/s. We argue that the low and high velocities in the natal kick distribution are caused by different supernova explosion mechanisms. Neutron stars in millisecond binaries with higher velocities tend to be more massive than those in slower binaries.

Author(s): Andrei Igoshev², Frank Verbunt¹

Institution(s): 1. Radboud University Nijmegen, 2. Technion - Israel Institute of Technology

132.04 – The 2017 Periastron Passage of PSR J2032+4127 in GeV Gamma rays

Pulsations from the 143 ms PSR J2032+4127 were discovered in 2008 using the *Fermi* Large Area Telescope (LAT) and subsequently detected in radio. Continued timing revealed it is in a wide and eccentric binary with the Be star MT91 213. With an orbital period of ~50 years, the periastron on 2017 November 13 is the only one we will observe in our lifetimes. By analogy with PSR B1259-63, a similar system, a GeV gamma-ray flare, from interactions of the Be star and pulsar winds, is expected near periastron. As part of a multi-wavelength campaign, we are continually monitoring the GeV emission from this system with the LAT. We will describe analysis and present preliminary results. Portions of this research performed at the US Naval Research Laboratory are sponsored by NASA DPR S-15633-Y and *Fermi* Guest Investigator Grant #16-Fermi10-0006.

Author(s): Tyrel Johnson¹, Paul S Ray³, Matthew T Kerr³, Kent S Wood²

Institution(s): 1. George Mason University, 2. Praxis Inc., 3. US Naval Research Lab

Contributing team(s): Fermi Large Area Telescope Collaboration

132.05D – X-ray pulsars in nearby irregular galaxies

The Small Magellanic Cloud (SMC), Large Magellanic Cloud (LMC) and Irregular Galaxy IC 10 are valuable laboratories to

study the physical, temporal and statistical properties of the X-ray pulsar population with multi-satellite observations, in order to probe fundamental physics. The known distance of these galaxies can help us easily categorize the luminosity of the pulsars and their age difference can be helpful for studying the origin and evolution of compact objects.

Therefore, a complete archive of 116 XMM-Newton PN, 151 Chandra (Advanced CCD Imaging Spectrometer) ACIS, and 952 RXTE PCA observations for the pulsars in the Small Magellanic Cloud (SMC) were collected and analyzed, along with 42 XMM-Newton and 30 Chandra observations for the Large Magellanic Cloud, spanning 1997-2014. From a sample of 67 SMC pulsars we generate a suite of products for each pulsar detection: spin period, flux, event list, high time-resolution light-curve, pulse-profile, periodogram, and X-ray spectrum. Combining all three satellites, I generated complete histories of the spin periods, pulse amplitudes, pulsed fractions and X-ray luminosities. Many of the pulsars show variations in pulse period due to the combination of orbital motion and accretion torques. Long-term spin-up/down trends are seen in 28/25 pulsars respectively, pointing to sustained transfer of mass and angular momentum to the neutron star on decadal timescales. The distributions of pulse detection and flux as functions of spin period provide interesting findings: mapping boundaries of accretion-driven X-ray luminosity, and showing that fast pulsars ($P < 10$ s) are rarely detected, which yet are more prone to giant outbursts. In parallel we compare the observed pulse profiles to our general relativity (GR) model of X-ray emission in order to constrain the physical parameters of the pulsars.

In addition, we conduct a search for optical counterparts to X-ray sources in the local dwarf galaxy IC 10 to form a comparison sample for Magellanic Cloud X-ray pulsars.

Author(s): Jun Yang¹

Institution(s): 1. *The university of Utah*

132.06 – Optimal Frequency Ranges for Sub-Microsecond Precision Pulsar Timing

Precision pulsar timing requires optimization against measurement errors and astrophysical variance from the neutron stars themselves and the interstellar medium. We investigate optimization of arrival time precision as a function of radio frequency and bandwidth. We find that increases in bandwidth that reduce the contribution from receiver noise are countered by the strong chromatic dependence of interstellar effects and intrinsic pulse-profile evolution. The resulting optimal frequency range is therefore telescope and pulsar dependent. We

133 – Stars and Friends I

133.01 – M Stars in the TW Hydra Association: A Chandra Large Program Survey

We have conducted a Cycle 18 Chandra Large Program survey of very cool members of the ~ 8 Myr-old TW Hydra Association (TWA) to extend our previous study of the potential connections between M star disks and X-rays (Kastner et al. 2016, AJ, 152, 3) to the extreme low-mass end of the stellar initial mass function. The spectral types of our targets extend down to the M/L borderline. Thus we can further investigate the potential connection between the intense X-ray emission from young, low-mass stars and the lifetimes of their circumstellar planet-forming discs, as well as better constrain the age at which coronal activity declines for stellar masses approaching the H-burning limit of $\sim 0.08 M_{\odot}$. We present preliminary results from the Cycle 18 survey, including X-ray detection statistics and measurements of relative X-ray luminosities and coronal (X-ray) temperatures for those TWA stars detected by Chandra. This research is supported by SAO/CXC grant GO7-18002A and NASA Astrophysics Data Analysis program grants NNX12AH37G and NNX16AG13G to RIT.

demonstrate the results for five pulsars included in current pulsar timing arrays and determine that they are not optimally observed at current center frequencies. We also find that arrival-time precision can be improved by increases in total bandwidth. Wideband receivers centered at high frequencies can reduce required overall integration times and provide significant improvements in arrival time uncertainty by a factor of $\sim \sqrt{2}$ in most cases, assuming a fixed integration time. We also discuss how timing programs can be extended to pulsars with larger dispersion measures through the use of higher-frequency observations.

Author(s): Michael Timothy Lam³, Maura McLaughlin³, James Cordes¹, Shami Chatterjee¹, Joseph Lazio²

Institution(s): 1. *Cornell University*, 2. *Jet Propulsion Laboratory/California Institute of Technology*, 3. *West Virginia University*

132.07 – Time-Dependent Electron Acceleration in Pulsar Wind Termination Shocks: Application the 2011 April Crab Nebula Gamma-ray Flare

The strongest gamma-ray flare from the Crab nebula observed by Fermi-LAT took place in 2011 April. Emission (up to a few GeV) exceeded the quiescent flux level by more than an order of magnitude. The Crab nebula gamma-ray flares challenge classical particle acceleration models in pulsar wind nebulae, because the radiating electrons have energies exceeding the classical radiation-reaction limit for synchrotron. However, numerical simulations have suggested that the classical synchrotron limit can be exceeded if electrons experience shock-driven electrostatic acceleration due to magnetic reconnection. In this talk, I present and summarize a new time-dependent model based on a transport equation that accounts for electrostatic acceleration, synchrotron losses, and particle escape. We implement a “blob” paradigm in which magnetically confined electrons from the upstream pulsar wind encounter and cross through the termination shock, producing a flare. We show that our model can reproduce the gamma-ray spectra and the integrated light curve for the 2011 April event, and we find that electrostatic acceleration occurs on both sides of the termination shock, driven by magnetic reconnection. We conclude that the dominant mode of particle escape changes from diffusive escape to advective escape as the blob passes through the shock.

Author(s): John Kroon², Peter A. Becker¹, Justin Finke²

Institution(s): 1. *George Mason University*, 2. *NRL*

Author(s): Kristina Punzi⁵, Joel Kastner⁵, David Principe⁴, Beate Stelzer¹, Uma Gorti⁶, Illaria Pascucci³, Costanza Argiroffi²

Institution(s): 1. *Eberhard Charles University*, 2. *INAF-Osservatorio Astronomico di Palermo*, 3. *Lunar and Planetary Laboratory, The University of Arizona*, 4. *MIT Kavli Institute*, 5. *Rochester Institute of Technology*, 6. *SETI Institute*

133.02 – Low-mass Stars with Extreme Mid-Infrared Excesses: Potential Signatures of Planetary Collisions

I investigate the occurrence of extreme mid-infrared (MIR) excesses, a tracer of large amounts of dust orbiting stars, in low-mass stellar systems. Extreme MIR excesses, defined as an excess IR luminosity greater than 1% of the stellar luminosity ($L_{\text{IR}}/L_{\star} \geq 0.01$), have previously only been observed around a small number of solar-mass (M_{\odot}) stars. The origin of this excess has been hypothesized to be massive amounts of orbiting dust, created by collisions between terrestrial planets or large planetesimals. Until recently, there was a dearth of low-mass ($M_{\star} \leq 0.6 M_{\odot}$) stars exhibiting extreme MIR excesses, even though low-mass stars are ubiquitous ($\sim 70\%$ of all stars), and known to host multiple terrestrial planets (≥ 3 planets per star).

I combine the spectroscopic sample of low-mass stars from the

Sloan Digital Sky Survey (SDSS) Data Release 7 (70,841 stars) with MIR photometry from the Wide-field Infrared Survey Explorer (WISE), to locate stars exhibiting extreme MIR excesses. I find the occurrence frequency of low-mass field stars (stars with ages ≥ 1 Gyr) exhibiting extreme MIR excesses is much larger than that for higher-mass field stars ($0.41 \pm 0.03\%$ versus $0.00067 \pm 0.00033\%$, respectively).

In addition, I build a larger sample of low-mass stars based on stellar colors and proper motions using SDSS, WISE, and the Two-Micron All-Sky Survey (8,735,004 stars). I also build a galactic model to simulate stellar counts and kinematics to estimate the number of stars missing from my sample. I perform a larger, more complete study of low-mass stars exhibiting extreme MIR excesses, and find a lower occurrence frequency ($0.020 \pm 0.001\%$) than found in the spectroscopic sample but that is still orders of magnitude larger than that for higher-mass stars. I find a slight trend for redder stars (lower-mass stars) to exhibit a higher occurrence frequency of extreme MIR excesses, as well as a lower frequency with increased stellar age. These samples probe important questions into the habitability of worlds discovered around low-mass stars.

Author(s): Christopher Theissen¹, Andrew West¹
Institution(s): 1. Boston University

133.03 – Anelastic Models of Fully-Convective Stars: Differential Rotation, Meridional Circulation and Residual Entropy

Low-Mass stars are typically fully convective, and as such their dynamics may differ significantly from sun-like stars. Here we present a series of 3D anelastic HD and MHD simulations of fully convective stars, designed to investigate how the meridional circulation, the differential rotation, and residual entropy are affected by both varying stellar parameters, such as the luminosity or the rotation rate, and by the presence of a magnetic field. We also investigate, more specifically, a theoretical model in which isorotation contours and residual entropy ($\sigma' = \sigma - \sigma(r)$) are intrinsically linked via the thermal wind equation (as proposed in the Solar context by Balbus in 2009). We have selected our simulation parameters in such a way as to span the transition between Solar-like differential rotation (fast equator + slow poles) and 'anti-Solar' differential rotation (slow equator + fast poles), as characterised by the convective Rossby number and $\Delta\Omega$. We illustrate the transition from single-celled to multi-celled MC profiles, and from positive to negative latitudinal entropy gradients. We show that an extrapolation involving both TWB and the σ'/Ω link provides a reasonable estimate for the interior profile of our fully convective stars. Finally, we also present a selection of MHD simulations which exhibit an almost unsuppressed differential rotation profile, with energy balances remaining dominated by kinetic components.

Author(s): Felix Sainsbury-Martinez³, Matthew Browning³, Mark Miesch¹, Nicholas A. Featherstone²
Institution(s): 1. High Altitude Observatory, National Center for Atmospheric Research, 2. University of Colorado, 3. University of Exeter

133.04 – The mass dependence of chromospheric activity evolution & implications for gyrochronology

We know chromospheric emission decays over time, and yet this empirical relation is still fundamentally an interpolation over 3.5 Gyr from the Hyades to the Sun despite 45 years of progress. Furthermore, its very existence was called into question by Pace et al. (2004, 2009, 2013), who argued that activity plummets and flatlines around 1-2 Gyr. I will present new Ca II H & K data for NGC 752 (1.5 Gyr) and Ruprecht 147 (3 Gyr), and ISM-corrected data for M67 (4 Gyr, Curtis 2017), and pair this with the Sun's re-calibrated history (Egeland et al. 2017) and data on field stars from the Keck exoplanet program. I calculated ages for the field star sample using the [Y/Mg] "chemical clock," which was discovered from studies of solar twins and is due to galactic

chemical enrichment. I find a mass dependence that matches the prediction from the activity-rotation-age relation of Mamajek & Hillenbrand (2008), where F stars rapidly plummet at 1-2 Gyr in line with the observations of F stars in clusters of similar age by Pace et al., whereas activity continuously declines for G and K dwarfs to approximately 5 and 7 Gyr, respectively. I will show that comparing ages estimated from [Y/Mg] to activity-rotation ages reveals known hot Jupiter hosts and other potentially anomalous stars. Combining the empirical relation between activity and Rossby number with estimates of stellar mass from spectroscopy and age from [Y/Mg] yields a gyrochronology relationship for FG and early K dwarfs that is independent of the cluster age scale and appears consistent with models from Mamajek & Hillenbrand (2008) and Barnes (2010). However, I have separately measured rotation periods for mid to late K dwarfs in 3 Gyr Ruprecht 147 with K2 and I find that they are rotating too rapidly relative to these empirical models and the semi-physical model of Matt et al. (2015). Apparently, K dwarfs spin down more slowly than the Skumanich square-root Law. Determining the K dwarf spin-down law is critical for developing a precise method for age-dating exoplanets hosted by such stars.

Author(s): Jason Curtis¹
Institution(s): 1. Columbia University

133.05 – Uniform Atmospheric Retrievals of Ultracool Late-T and Early-Y dwarfs

A significant number of ultracool (<600K) extrasolar objects have been unearthed in the past decade thanks to wide-field surveys such as WISE. These objects present a perfect testbed for examining the evolution of atmospheric structure as we transition from typically hot extrasolar temperatures to the temperatures found within our Solar System.

By examining these types of objects with a uniform retrieval method, we hope to elucidate any trends and (dis)similarities found in atmospheric parameters, such as chemical abundances, temperature-pressure profile, and cloud structure, for a sample of 7 ultracool brown dwarfs as we transition from hotter (~700K) to colder objects (~450K).

We perform atmospheric retrievals on two late-T and five early-Y dwarfs. We use the NEMESIS atmospheric retrieval code coupled to a Nested Sampling algorithm, along with a standard uniform model for all of our retrievals. The uniform model assumes the atmosphere is described by a gray radiative-convective temperature profile, (optionally) a self-consistent Mie scattering cloud, and a number of relevant gases. We first verify our methods by comparing it to a benchmark retrieval for Gliese 570D, which is found to be consistent. Furthermore, we present the retrieved gaseous composition, temperature structure, spectroscopic mass and radius, cloud structure and the trends associated with decreasing temperature found in this small sample of objects.

Author(s): Ryan Garland¹, Patrick Irwin¹
Institution(s): 1. University of Oxford

133.06 – The Mass-Luminosity-Metallicity Relation for M Dwarfs

One of the most powerful tools for stellar characterization is the mass-luminosity relation (MLR). In addition to its use for characterizing exoplanet hosts, the MLR for late-type stars is critical to measuring the stellar IMF, testing isochrones, and studies of Galactic archeology. However, existing MLRs do not fully account for metallicity effects, do not extend down to the substellar boundary, and are not precise enough to take full advantage of the impending arrival of Gaia parallaxes for millions of late-type stars. For two years we monitored 72 nearby M-dwarf astrometric binaries using adaptive optics and non-redundant aperture masking, with the goal of better constraining the MLR. We combined our astrometry with measurements from the literature and Keck archive to measure orbits, masses, and flux ratios of all binaries in JHK bands. In parallel, we obtained moderate-resolution NIR spectra of all binaries, from which we determine empirical metallicities for each system. We derived an

updated MLR-metallicity relation that spans most of the M dwarf sequence (K5 to M7) and the metallicity range expected in the solar neighborhood ($-0.5 < [M/H] < +0.4$). With this we explored the role metallicity plays in the MLR. With our revised relation and Gaia-precision parallaxes, it will soon be possible to calculate empirical masses of nearby M dwarfs to better than 2%, and future studies will enable us to extend our relation to more metal-poor stars and explore the role of youth and evolution of the MLR for M dwarfs.

Author(s): Andrew Mann¹, Trent Dupuy³, Aaron Rizzuto³, Adam Kraus³, Eric Gaidos², Megan Ansdell²

Institution(s): 1. Columbia University, 2. University of Hawaii at Manoa, 3. University of Texas at Austin

133.07 – Tests of Substellar Astrophysics Enabled by Dynamical Masses

Mass is the single most important property separating stars from brown dwarfs from gas-giant planets. But this is oftentimes only a qualitative distinction, given that the substellar mass–

134 – Doggett Prize Lecture: Tangible Things of American Astronomy, Sara Schechner (Harvard University)

134.01 – Tangible Things of American Astronomy

As a science that studies celestial objects situated at vast distances from us, astronomy deals with few things that can be touched directly. And yet, astronomy has many tangible things—scientific instruments, observatories, and log books, for example—which link the past to the present. There is little question about maintaining things still valuable for scientific research purposes, but why should we care about documenting and preserving the old and obsolete? One answer is that material things, when closely examined, enhance our knowledge of astronomy’s history in ways that written texts alone cannot do. A second answer is

135 – RAS Medal Prize Lectureship: The Effect of Non-Linear Structure on Cosmological Observables, Nick Kaiser (University of Hawaii)

135.01 – The Effect of Non-Linear Structure on Cosmological Observables

I shall review the various ways in which the emergence of non-linear structure in the universe may affect cosmological observables. I consider the distance-redshift relation, which has implications for the CMB and for cosmic flows, and attempt to clarify the meaning of some of the effects that have been found in

136 – Star Formation Poster Session

136.01 – The Relationship Between Infrared Dark Cloud and Stellar Properties

Massive stars are known to form within infrared dark clouds (IRDCs), but many details about how molecular clouds collapse and form stars remain poorly understood. We determine the relationship between the dark cloud mass and the population of young stellar objects (YSOs) associated with the cloud to shed light on the physical processes occurring within these star forming regions. We chose to use a sample of IRDCs and YSOs within the Cygnus-X region, a close-by giant star formation complex that has every stage of star formation represented. Using observations from IRAC, MIPS, PACS, and SPIRE on *Spitzer* and *Herschel* we identified a sample of 30,903 YSOs and 167 IRDCs. We derived the class of each YSO as well as the mass of YSO and IRDCs from the flux information. Using these parameters, as well as their locations in the cloud, we were sorted IRDC fragments into larger filaments and associate a set of YSOs with each IRDC. By measuring and comparing parameters such as YSO total mass, number of YSOs, Class 0, Class I, and Class II populations, distance from host filament, and filament mass we tested for correlations between the YSO and IRDC parameters. Using this treasure trove of information, we find that Class 0 and I objects are located more closely to their host IRDC than their Class II counterparts. We also find that high-density IRDCs are better environments for star formation than low-density IRDCs. However, we find no correlation between the total

luminosity–age degeneracy prevents us from knowing the masses of single field objects. I will present recent results from our decade-long astrometry programs using the Keck Observatory, Hubble Space Telescope, and Canada-France-Hawaii Telescope to measure the orbits of ultracool binaries with component spectral types M7–T5. Our precise individual masses spanning 30–100 M_{JUP} constitute the first large sample of its kind straddling the hydrogen-fusion boundary, enabling many new empirical tests of substellar theory. I will show that our measurements support a luminosity boost due to cloud clearing in the L/T transition and describe our empirical determination of the substellar boundary ($\approx 70 M_{\text{JUP}}$ in mass and $\approx L4$ in spectral type). Finally, I will discuss the possibility of extending such measurements to planetary masses ($\approx 5\text{--}15 M_{\text{JUP}}$) in the coming years.

Author(s): Trent Dupuy¹, Michael C. Liu², Adolfo A Cancino³
Institution(s): 1. Gemini Observatory, 2. IfA/Hawaii, 3. Missouri State University

that learning about the past helps us live critically in the present. In brief case studies, this talk will find meaning in objects that are extraordinary or commonplace. These will include a sundial, an almanac, telescopes, clocks, a rotating desk, photographic plates, and fly spankers.

Author(s): Sara Jane Schechner¹
Institution(s): 1. Harvard

non-linear perturbation theory. I will also critically examine some recent proposals for dynamical backreaction from structure affecting the expansion rate.

Author(s): Nick Kaiser¹
Institution(s): 1. Ecole Normale Supérieure

mass of the IRDC and the largest YSO mass in the IRDC, suggesting that IRDCs of any mass can have massive YSOs associated with them.

The SAO REU program is funded by the National Science Foundation REU and Department of Defense ASSURE programs under NSF Grant AST-1659473, and by the Smithsonian Institution.

Author(s): Jenny Calahan², Joseph L. Hora¹
Institution(s): 1. Harvard-Smithsonian, 2. University of Arizona

136.02 – Simulations of star-forming molecular clouds: observational predictions

Observations of protostellar molecular cloud cores can be used to test theories of star formation. However, observational results can be biased because of limited information: (a) only two spatial dimensions and one velocity dimension can be measured, (b) and cores generally are not spherically symmetric. We use numerical simulations of the formation and collapse of molecular gas with sink particles to make observational predictions. We use the radiative transfer code LIME to predict CO and NH₃ channel maps. We find reasonable agreement with observed velocity structures and gradients but occasional large differences depending on viewing angle.

Author(s): Shangjia Zhang¹, Lee Hartmann¹, Aleksandra Kuznetsova¹, Manuel Abelardo Zamora¹
Institution(s): 1. University of Michigan

136.03 – Implementing Dust Shielding as a Criteria for Star Formation

Star formation is observed to occur in dense regions of molecular gas. Although the exact nature of the link between star formation and molecular hydrogen is still unclear, it has been suggested that dust shielding of dense gas is the key factor enabling the presence of both. We present a model in which star formation is linked explicitly to local dust shielding, rather than molecular hydrogen abundance, in smoothed particle hydrodynamics galaxy formation simulations. We used simulations of isolated Milky-Way-mass disk galaxies to develop a dust shielding model in which the radiative shielding length was based off of the Jeans length with a $T=40$ K temperature cap. Using this shielding model, we compare the effects of different star formation recipes, including recipes in which star formation is based on the amount of dust shielding or the local molecular hydrogen abundance. We test our star formation models on two sets of isolated disk galaxies with solar and sub-solar metallicities and on a cosmological dwarf galaxy simulation. We find that the shielding-based model can reproduce the observed transition from atomic to molecular hydrogen at realistic surface densities, exhibits periodic bursts of star formation, and allows for star formation at higher temperatures and lower densities than a model in which star formation is tied directly to H₂ abundance.

Author(s): Lindsey Byrne¹, Charlotte Christensen¹
Institution(s): 1. Grinnell College

136.04 – Star Formation Rate Indicators in the FIRE Galaxy Formation Simulations

Understanding the rate at which stars form is vital to understanding galaxy formation. Observationally, the star formation rates (SFRs) of galaxies are typically measured using light in different bands under the assumption of a time-steady SFR. We use galaxy formation simulations from the Feedback In Realistic Environments (FIRE) project, which in some regimes predict (time variable) bursty SFRs, to analyze the timescales probed by H-alpha and far ultraviolet (FUV) SFR indicators. We also quantify the possible dependence of SFR indicators on SFR variability. Our preliminary results based on a Milky Way-mass galaxy simulation indicate that the best-fit timescales probed by these indicators do not depend significantly on whether the SFR is bursty, with best-fitting timescales of about 4 Myr for H-alpha and about 10 Myr for FUV in both the time-steady and bursty regimes.

Author(s): Jose Antonio Flores³, Alex Gurvich², Claude-André Faucher-Giguère², Martin Sparre⁴, Christopher Hayward¹
Institution(s): 1. Center for Computational Astronomy, Flatiron Institute, 2. Department of Physics and Astronomy and CIERA, Northwestern University, 3. Department of Physics and Astronomy, California State Polytechnic University, Pomona, 4. Institute of Physics and Astronomy, Potsdam University
Contributing team(s): Feedback In Realistic Environments (FIRE) Collaboration

136.05 – STAR FORMATION IN THE SPIRAL GALAXY NGC 4736

We estimate star formation properties of the center and circumnuclear ring of spiral galaxy NGC 4736 using its population of observed young star clusters. Compact star clusters in the center and ring are identified and selected from *Hubble Space Telescope's* (HST) Wide Field Planetary Camera 2 (WFPC2) images in F814W, F568N, F555W, F450W, and F336W filters. We fit Bruzual & Charlot's (2003) stellar evolutionary models to the observed photometry of each cluster to determine the masses (M), ages, and extinctions of each. The cluster mass function in the ring and center are both well-approximated by a power law function, $dN/d \log M \propto M^\beta$ with $\beta \sim -1.8$ (though some evidence of truncation at high-mass end is found for the ring). Using total

cluster masses extrapolated from these mass functions along with estimated cluster formation efficiencies, we determine the star formation rates (SFR) in both regions. The surface density of star formation, Σ_{SFR} , is about 7 times as high in the ring as in the center, despite very similar surface gas densities, Σ_{gas} . In both regions, the SFR is below that predicted by the Kennicutt-Schmidt (1998) law, however only the central region has a lower SFR than expected given the intrinsic scatter in the relation.

Author(s): Farhanul Hasan¹, Alison Crocker¹
Institution(s): 1. Reed College

136.06 – Pre-Merger History of Illustris-Simulated Galaxy Pairs

In this work, we analyze the history of 24 simulated major-merger galaxies including star formation and mass growth with emphasis on morphological type dependencies. Pairs were identified as major-merger galaxy candidates (mass ratio < 2.5) within the Illustris simulation; with the goal of comparing them to observations of SDSS-2MASS selected galaxy pairs and visually classifying their morphology. Approximately 7000 total galaxies fit within our mass range with 356 candidate pairs reduced by separation, mass, and relative velocity criteria to a final sample of 24 simulated physical pairs at various stages of pre-merger galaxy interaction. Illustris masses and star formation are presented across the simulation snapshots in an effort to understand the pre-paired history of observationally selected analogs.

Author(s): Alice Jacques¹, Spencer Shortt¹, Kiernan Reising¹, Donovan Domingue¹
Institution(s): 1. Georgia College

136.07 – Radio Interferometry with the SMA: Uncovering Hidden Star Formation in Our Extreme Galactic Center

Radio interferometry provides the best tool to identify embedded star-forming cores in cold, dense, molecular clouds of gas and dust. Observations at long, submillimeter wavelengths can be used to investigate the physical properties in the youngest stages of star formation. Interferometers provide the resolution necessary to resolve small scale structures like dense cores where star formation is expected to occur. CMZoom is the first large area survey of the Central Molecular Zone (CMZ) at high resolution in the submillimeter, allowing us to identify early sites of star formation. The survey uses both the subcompact and compact configurations of the Submillimeter Array (SMA) interferometric radio telescope. The CMZ, or the inner 500 pc of the Milky Way Galaxy, is a high extinction region comprised of hot, dense, and turbulent molecular gas. This region is forming about an order of magnitude fewer stars than predicted based on simple star formation prescriptions. Here, we present new high resolution images of Go.068-0.075, a region from the CMZoom survey, obtained using CASA. We highlight the importance of interferometric observations of different baseline lengths by comparing the spatial information obtained through different configurations. We will use these new images, in conjunction with the rest of the CMZoom survey, to reveal the mechanisms driving star formation at the center of the galaxy.

Author(s): Elizabeth Gutierrez³, Cara Battersby², Meredith Ann MacGregor¹
Institution(s): 1. Carnegie Institution for Science, 2. The University of Connecticut, 3. The University of Texas

136.08 – The Formation and Fate of the Young Star Cluster NGC 6231

The star-formation conditions that produce bound clusters is an important open question. We address this problem through a comparison of NGC 6231, a young star cluster where star-formation has recently ended, to subclusters of stars in star-forming regions from the Massive Young Star-Forming Complex Study in Infrared and X-ray (MYStIX; Feigelson et al. 2013). Our study of NGC 6231 is based on a new census of cluster members, which we use to model the cluster's physical structure. The cluster

is well described by an isothermal ellipsoid density profile, with a moderate ellipticity, a cluster core radius of 1.2 ± 0.2 pc, and a central density of 200 stars pc^{-3} . We find mild mass segregation of stars $> 8 M_{\text{sun}}$ and no radial-age gradient. Substructure includes a small subcluster superimposed on the main cluster. Although NGC 6231 is more dynamically evolved, it follows the same mass, size, and age relations that were previously seen for the MYStIX subclusters. We argue that the NGC 6231 likely formed through the coalescence of subclusters of stars, but has expanded significantly since formation. Cluster properties are consistent with NGC 6231 surviving to become a gravitationally bound open cluster.

Author(s): Michael A. Kuhn³, Konstantin V. Getman², Eric D. Feigelson², Alison Sills¹, Mariusz Gromadzki⁴, Medina Nicolás³, Jordanka Borissova³, Radostin Kurtev³
Institution(s): 1. McMaster University, 2. Pennsylvania State University, 3. Universidad de Valparaíso, 4. Warsaw University Astronomical Observatory
Contributing team(s): MYStIX

136.09 – Effects of Combined Stellar Feedback on Star Formation in Stellar Clusters

We present results of hybrid MHD+N-body simulations of star cluster formation and evolution including self consistent feedback from the stars in the form of radiation, winds, and supernovae from all stars more massive than 7 solar masses. The MHD is modeled with the adaptive mesh refinement code FLASH, while the N-body computations are done with a direct algorithm. Radiation is modeled using ray tracing along long characteristics in directions distributed using the HEALPIX algorithm, and causes ionization and momentum deposition, while winds and supernova conserve momentum and energy during injection. Stellar evolution is followed using power-law fits to evolution models in SeBa. We use a gravity bridge within the AMUSE framework to couple the N-body dynamics of the stars to the gas dynamics in FLASH. Feedback from the massive stars alters the structure of young clusters as gas ejection occurs. We diagnose this behavior by distinguishing between fractal distribution and central clustering using a Q parameter computed from the minimum spanning tree of each model cluster. Global effects of feedback in our simulations will also be discussed.

Author(s): Joshua Edward Wall², Stephen McMillan², Andrew Pellegrino², Mordecai Mac Low¹, Ralf Klessen³, Simon Portegies Zwart⁴
Institution(s): 1. American Museum of Natural History, 2. Drexel University, 3. Heidelberg University, 4. Leiden Observatory

136.10 – Two-Decade Monitoring of MWC349 in Optical and Radio: New Results

Maria Mitchell Observatory (MMO) has completed the two-decade long monitoring of MWC 349 in the optical and radio domains. This poster presentation will be primarily devoted to the new results obtained by optical photometry with broad and narrow band filters and observations of the variability in the masing H30 radio line during the observational season of 2017. The H30 emission arises in the circumstellar disk of the MWC 349A component of the visual double star (with 2.4 arcsec separation between the A and B components). Variable optical emission is also believed to be due to star A. By combining our optical observations with earlier MMO observations, we not only confirmed the previously known quasi-period of ~ 230 days, but confirmed a second period of ~ 700 days. One of the most interesting results of radio monitoring is the long-term variability of the systemic radial velocity of star A, as determined through averaging the radial velocities of the two masing peaks arising in the circumstellar disk. This may be the first case where a possible hidden close companion of a star (a lower mass star or a massive protoplanet) is detected by monitoring the radial velocity of the star via the spectral line radiation from its disk. E.T. completed this project as a 2017 MMO NSF REU intern and would like to

thank the other interns for their help in conducting the optical observations. This project was supported in part by the NSF REU grant AST-1358980 and by the Nantucket Maria Mitchell Association.

Author(s): Eydon Thomashow¹, Regina A. Jorgenson¹, Vladimir Strel'nitski¹, Gary Walker¹
Institution(s): 1. Maria Mitchell Observatory
Contributing team(s): Maria Mitchell Observatory (MMO) Research Experiences for Undergraduate (REU) Interns, 2017

136.11 – The Detection of Hot Cores and Complex Organic Molecules in the Large Magellanic Cloud

We report the detection of the complex organic molecules (COMs) dimethyl ether (CH_3OCH_3) and methyl formate (CH_3OCHO), and their parent species methanol (CH_3OH), toward the N113 star-formation region in the Large Magellanic Cloud (LMC) with the Atacama Large Millimeter/submillimeter Array (ALMA). This constitutes the first detection of CH_3OCH_3 and CH_3OCHO outside the Milky Way. We calculated the rotational temperatures ($T_{\text{rot}} \sim 130$ K) and total column densities ($N_{\text{rot}} \sim 10^{16} \text{ cm}^{-2}$) for two sources in N113 with the COMs detection based on multiple transitions of CH_3OH , and measured abundances for all detected species. The physical and chemical properties of these sources, and the association with H_2O and OH maser emission indicate that they are hot molecular cores. The fractional abundances of COMs scaled by a factor of 2.5 to account for the lower metallicity in the LMC are comparable to those found at the lower end of the range in Galactic hot cores. Our results have important implications for studies of organic chemistry at higher redshift.

Author(s): Marta Sewilo⁶, Remy Indebetouw¹, Steven Charnley⁶, Sarolta Zahorecz⁸, Joana M. Oliveira³, Jacco Th. van Loon³, Jacob L. Ward¹⁰, C.-H. Rosie Chen⁴, Jennifer Wiseman⁶, Yasuo Fukui⁵, Akiko Kawamura⁷, Margaret Meixner⁹, Toshikazu Onishi⁸, Peter Schilke²
Institution(s): 1. Department of Astronomy, University of Virginia, 2. I. Physikalisches Institut der Universität zu Köln, 3. Lennard-Jones Laboratories, Keele University, 4. Max-Planck-Institut für Radioastronomie, 5. Nagoya University, 6. NASA Goddard Space Flight Center, 7. National Astronomical Observatory of Japan, 8. Osaka Prefecture University, 9. Space Telescope Science Institute, 10. Zentrum für Astronomie der Universität Heidelberg

136.12 – The Role of Binarity in the Angular Momentum Evolution of M Dwarfs

We have analysed K2 light curves for of order a thousand low mass stars in each of the 8 Myr old Upper Sco association, the 125 Myr age Pleiades open cluster and the ~ 700 Myr old Praesepe cluster. A very large fraction of these stars show well-determined rotation periods with K2, and where the star is a binary, we usually are able to determine periods for both stars. In Upper Sco, where there are ~ 150 M dwarf binaries with K2 light curves, the binary stars have periods that are much shorter on average and much closer to each other than would be true if drawn at random from the Upper Sco M dwarf single stars. The same is true in the Pleiades, though the size of the differences from the single M dwarf population is smaller. By Praesepe age, the M dwarf binaries are still somewhat rapidly rotating but their period differences are not significantly different from what would be true if drawn by chance from the singles.

Author(s): John Stauffer¹, Luisa Rebull¹
Institution(s): 1. California Institute of Technology
Contributing team(s): K2 clusters team

136.13 – Star Formation in Low Metallicity Environments

How is star formation affected by its environment? How big is the effect of having differing metallicities during the star forming process? The goal of this research is to study star formation in low metallicity environments, which are well represented by dwarf

galaxies. For this project, we used the Atacama Large Millimeter Array (ALMA) telescope to observe the ^{12}CO (115 GHz) distribution in the galaxy Henize 2-10 (He 2-10) (PI: Nia Imara). He 2-10 is an irregular dwarf galaxy about 10 million parsecs away, about 1 kiloparsecs across, and has a mass of about 10 billion solar masses. It has a high gas to dust ratio, is star forming, and has a low metallicity of about $12+\log(\text{O}/\text{H})\sim 8.3$. Additionally it contains a supermassive black hole candidate of about 1 billion solar masses, which could have significant dynamical interactions with the molecular gas. We created a zeroth moment map which we used to estimate several properties of the galaxy: including a molecular gas mass of about 38 million solar masses, an observable area of about 205 square kiloparsecs, and a molecular gas density of about $3.7\times 10^{(-20)}$ grams per cubic centimeter. We also created multiple channel maps which provide preliminary results that indicate the presence of about 10 giant molecular clouds within He 2-10.

Author(s): Daven Cocroft¹

Institution(s): 1. *University of Washington*

136.14 – A Chandra X-ray Mosaic of the Onsala 2 Star-Forming Region

Multiple lines of evidence for active high-mass star-formation in the Onsala 2 (ON2) complex in Cygnus include masers, compact HII (cHII) regions, and massive outflows. ON2 is thought to be physically associated with the young stellar cluster Berkeley 87 which contains several optically-identified OB stars and the rare oxygen-type (WO) Wolf-Rayet star WR 142. WO stars are undergoing advanced nuclear core burning as they approach the end of their lives as supernovae, and only a few are known in the Galaxy. We present results of a sensitive 70 ks Chandra ACIS-I observation of the northern half of ON2 obtained in 2016. This new observation, when combined with our previous 70 ks ACIS-I observation of the southern half in 2009, provides a complete X-ray mosaic of ON2 at arcsecond spatial resolution and reveals several hundred X-ray sources. We will summarize key results emerging from our ongoing analysis including the detection of an embedded population of young stars revealed as a tight grouping of X-ray sources surrounding the cHII region G75.77+0.34, possible diffuse X-ray emission (or unresolved faint point sources) near the cHII region G75.84+0.40, and confirmation of hard heavily-absorbed X-ray emission from WR 142 that was seen in the previous 2009 Chandra observation.

Author(s): Steve L. Skinner¹, Kimberly Sokal², Manuel Guedel³

Institution(s): 1. *Univ. of Colorado*, 2. *Univ. of Texas*, 3. *Univ. of Vienna*

136.15 – Measuring the CO/H Ratio Using a Symmetric Outflow with an Ionized Component in W51

137 – First Data for the Pan-STARRS Survey and How to Use It Poster Session

137.01 – Photometry, Astrometry, and Discoveries of Ultracool Dwarfs in the Pan-STARRS 3 π Survey

The Pan-STARRS1 3 π Survey (PS1)'s far-red optical sensitivity makes it an exceptional new resource for discovering and characterizing ultracool dwarfs. We present a PS1-based catalog of photometry and proper motions of nearly 10,000 M, L, and T dwarfs, along with our analysis of the kinematics of nearby M6-T9 dwarfs, building a comprehensive picture of the local ultracool population. We highlight some especially interesting ultracool discoveries made with PS1, including brown dwarfs with spectral types in the enigmatic L/T transition, wide companions to main sequence stars that serve as age and metallicity benchmarks for substellar models, and free-floating members of the nearby young moving groups and star-forming regions with masses down to $\approx 5 M_{\text{Jup}}$. With its public release, PS1 will continue to be a vital tool for studying the ultracool population.

CO is a trusted tracer of H₂ mass due to its abundance in the ISM and easy excitement in cold molecular clouds. Although H₂ is the most abundant molecule in the Universe and essential to star formation, it is not directly observable. This project provides estimates for the mass of H₂ in W51, which contains the closest pair of high-mass protoclusters in the Galaxy. In the W51 IRS2 area, there is a symmetric outflow, known as the "Lacy Jet", which is molecular on one side and ionized on the other. The outflow's blueshifted component intersects with an HII region, where it has a continuous structure in position-velocity space but becomes externally ionized. We observed the molecular gas with ALMA in the CO 2-1 line and the ionized gas with the VLA in the H77 α recombination line. We measured the CO-to-H₂ ratio by comparing the observed CO emission to the H77 α and assuming that they trace the same material in different states. We present the initial measurements of the CO abundance, or the CO-to-H₂ factor, and the CO "X-factor", or the mass-to-light ratio, at different positions along the jet. We have demonstrated that this jet provides a unique laboratory for measuring the ratios between molecular and ionized species.

Author(s): Theresa Melo¹, Adam Ginsburg²

Institution(s): 1. *Agnes Scott College*, 2. *National Radio Astronomy Observatory*

136.16 – Spatially resolved properties of $z \sim 0.4$ galaxies from the MUSE-Wide Survey

Studying internal processes of individual galaxies at kilo-parsec scales is essential to understand their integrated properties and enhance our understanding of galaxy evolution. This is specially the case for intermediate and high-redshift galaxies. In this work, we investigate the distribution of dust attenuation across individual galaxies for a sample of nearly 40 galaxies from MUSE-Wide survey at $z \sim 0.4$, using Balmer decrement measurements. High spatial resolution of the MUSE integral-field spectrograph has allowed us to derive reliable spatially resolved H α and H β emission line maps ($S/N > 3$) and measure Balmer decrement across individual galaxies. Then they were used to produce resolved dust-corrected star formation maps. At the same time, resolved SFR, dust and SED-predicted emission line maps are derived from pixel-by-pixel SED fitting on high resolution multi-band photometric data from the CANDELS survey. By combining these, we also investigate the feasibility of our pixel-by-pixel SED fitting technique to better constrain measurements of resolved physical properties of galaxies.

Author(s): Marziye Jafariyazani², Bahram Mobasher², Shoubaneh Hemmati¹

Institution(s): 1. *Caltech/IPAC*, 2. *University of California, Riverside*

Author(s): William M J Best², Eugene A Magnier², Michael C. Liu², Niall Deacon¹, Kimberly Aller², Zhoujian Zhang²

Institution(s): 1. *Max Planck Institute for Astronomy*, 2. *University of Hawaii*

Contributing team(s): Pan-STARRS1 Builders

137.02 – First data from the Pan-STARRS survey and how to use it

Program for this Special Session:

Ken Chambers

Introduction to the Pan-STARRS survey

Heather Flewelling

The PS-1 pipeline and data products

Eugene Magnier

A 3-D view of dust in the Galaxy

Eddie Schafly

The PS-1 "ubercal"

Dan Scolnic

Supernovae in PS-1

Suvi Gezari
Tidal disruption events in PS-1
Maria Drout
Transient events in PS-1
Karen Meech
Moving targets in PS-1

Author(s): David Soderblom¹
Institution(s): 1. Space Telescope Science Institute
Contributing team(s): Pan-STARRS team

139 – Innovations in Astronomy Teaching and Learning II Poster Session

139.01 – Teaching the Thrill of Discovery: Student Exploration of the Large-Scale Structures of the Universe

In collaboration with the Teen Astronomy Cafes program, the NOAO Data Lab is developing online Jupyter Notebooks as a free and publicly accessible tool for students and teachers. Each interactive activity teaches students simultaneously about coding and astronomy with a focus on large datasets. Therefore, students learn state-of-the-art techniques at the cross-section between astronomy and data science. During the activity entitled “Our Vast Universe”, students use real spectroscopic data to measure the distance to galaxies before moving on to a catalog with distances to over 100,000 galaxies. Exploring this dataset gives students an appreciation of the large number of galaxies in the universe (2 trillion!), and leads them to discover how galaxies are located in large and impressive filamentary structures. During the Teen Astronomy Cafes program, the notebook is supplemented with visual material conducive to discussion, and hands-on activities involving cubes representing model universes. These steps contribute to build the students’ physical intuition and give them a better grasp of the concepts before using software and coding. At the end of the activity, students have made their own measurements, and have experienced scientific research directly. More information is available online for the Teen Astronomy Cafes (teensciencecafe.org/cafes) and the NOAO Data Lab (datalab.noao.edu).

Author(s): Stephanie Juneau¹, Arjun Dey¹, Constance E. Walker¹

Institution(s): 1. NOAO

Contributing team(s): NOAO Data Lab

140 – NASA Decadal Preparations II: Probes Mission Concept Studies Poster Session

140.01 – Cosmic Dawn Intensity Mapper (CDIM): a New Probe of Cosmic Dawn and Reionization

The Cosmic Dawn Intensity Mapper, CDIM, is a NASA Probe-class Mission Study currently under study. CDIM is designed to be a near-IR survey instrument optimized for Cosmic Dawn and reionization sciences, answering critical questions on how and when galaxies and quasars first formed, the history of metal build-up, and the history and topology of reionization, among other questions. CDIM will provide $R=300$ spectroscopic imaging over ~ 10 sq. degree instantaneous field of view at 1 arcsecond resolution, over the wavelength range of 0.75 to 7.5 μm . A two-tiered wedding-cake survey will consist of a shallow tier spanning close to 300 deg^2 and a deep tier of about 25 deg^2 . CDIM survey data will allow us to (i) determine spectroscopic redshifts of WFIRST-detected Lyman-break galaxies (LBGs) out to a redshift of 10; (ii) establish the environmental dependence of star formation during reionization through clustering and other environmental measurements; (iii) establish the metal abundance of first-light galaxies during reionization over two decades of stellar mass by spectrally separating NII from H α , and detecting both H β and [OIII]; (iv) measure 3D tomographic intensity fluctuations during reionization in both Ly α at $z > 6$ and H α at $0 < z < 10$; and (v) cross-correlating intensity fluctuations with 21-cm data to establish the topology of reionization bubbles.

Author(s): Tzu-Ching Chang¹

Institution(s): 1. Jet Propulsion Laboratory, California Institute of Technology

Contributing team(s): CDIM Team

139.02 – Motivational Differences between MOOC and Undergraduate Astronomy Students

It is vital for the instructors and designers of the Massive Open Online Courses (MOOCs) to understand the motivation of its users for enrolling in the class and their reasons to engage with the material. This is particularly important for MOOCs focusing on scientific topics such as our MOOC on Astronomy (Astronomy: Exploring time and space) whose audience is less motivated by a desire to advance their careers compared to other MOOCs. In order to learn more about the motivation of our learners we deployed in our Astronomy MOOC a survey based on the Science Motivation Questionnaire II developed by Glynn et. al (2011). We specifically asked for reasons to sign up for the course and the overall motivation and attitude towards astronomy and science courses. We compare results of 3360 participants of this survey with a similar instrument administered to 638 students in undergraduate Astronomy classes for non Astronomy majors at the University of Arizona. Our comparison not only looks at the demographic differences, but also at reasons for signing up for the course and scores in motivational categories such as self-determination, self-efficacy, grade motivation, career motivation, hobby motivation, social motivation, and intrinsic motivation showing, that these populations of learners are fundamentally different.

Author(s): Martin Formanek¹, Matthew Wenger¹, Sanlyn Buxner¹, Chris David Impey¹

Institution(s): 1. University of Arizona

140.02 – Cosmic Dawn Intensity Mapper (CDIM): Instrument and Mission Design

CDIM is the Cosmic Dawn Intensity Mapper, one of the probe-class missions currently under study for NASA. A detailed Report from the study will be submitted to NASA and for consideration by the Decadal Survey. The flight system will comprise a wide-field cryogenic telescope with a large focal plane array providing complete coverage from optical through mid-IR. The system will be deployed to L2 or Earth-trailing orbit, to provide a stable thermal environment and allow extended observations of fields selected to be cross-correlated with deep surveys in other wavebands. Spectra will be measured for every point in each target field, using linear variable filters (LVFs). These filters eliminate the need for a spectrometer in the focal plane. Spectra are built up through simple imaging of a series of telescope pointings separated by small angular offsets. This poster presents the initial concept for the instrument and mission design.

Author(s): Stephen C Unwin¹

Institution(s): 1. JPL/Caltech

Contributing team(s): CDIM Team

140.03 – AXIS - Advanced X-ray Imaging Satellite

We present an overview of the Advanced X-ray Imaging Satellite (AXIS), a probe mission concept under study to the 2020 Decadal survey. AXIS follows in the footsteps of the spectacularly successful Chandra X-ray Observatory with similar or higher angular resolution and an order of magnitude more collecting area in the 0.3-10 keV band over a 15' field of view. These capabilities are designed to attain a wide range of science goals such as (i) measuring the event horizon scale structure in AGN accretion disks and the spin of supermassive black holes through

monitoring of gravitationally microlensed quasars; (ii) understanding AGN and starburst feedback in galaxies and galaxy clusters through direct imaging of winds and interaction of jets and via spatially resolved imaging of galaxies at high- z ; (iii) probing the fueling of AGN by resolving the SMBH sphere of influence in nearby galaxies; (iv) investigating hierarchical structure formation and the SMBH merger rate through measurement of the occurrence rate of dual AGN and occupation fraction of SMBHs; (v) advancing SNR physics and galaxy ecology through large detailed samples of SNR in nearby galaxies; (vi) measuring the Cosmic Web through its connection to cluster outskirts. With a nominal 2028 launch, AXIS benefits from natural synergies with LSST, ELTs, ALMA, WFIRST and ATHENA, and will be a valuable precursor to Lynx. AXIS utilizes breakthroughs in the construction of light-weight X-ray optics from mono-crystalline silicon blocks, and developments in the fabrication of large format, small pixel, high readout detectors.

Author(s): Michael Loewenstein¹

Institution(s): 1. University of Maryland, College Park

Contributing team(s): The AXIS Team

140.04 – Supernova Remnant Science with AXIS

We present an overview of the supernova remnant (SNR) science that will be achieved with the Advanced X-ray Imaging Satellite (AXIS). AXIS follows in the footsteps of the spectacularly successful Chandra X-ray Observatory with similar or higher angular resolution and an order of magnitude more collecting area in the 0.3-10 keV band. These capabilities enable major advances in several areas of SNR science. These include, but are not limited to: 1) a more thorough spatial mapping of the ejecta products of both intermediate-mass and iron-group elements in core-collapse and Type Ia SNRs, particularly in remnants with a small diameter. The iron-group elements, specifically Cr, Mn, and Ni, are extremely important for constraining the explosion mechanism for SNe, but are generally weak and difficult to detect with Chandra, XMM-Newton, and Suzaku. 2) Studying the interface of a shock wave with the ambient ISM/CSM to constrain the degree of particle heating and acceleration at shock fronts. Chandra has only provided upper limits on shock precursor emission, and a detailed study of the thermal and nonthermal emission at the shock with greatly increased photon count rates will constrain the properties of the immediate post-shock plasma. 3) A high spatial resolution X-ray observatory will continue to build on the legacy begun by Chandra of studying the proper motion of young remnants. Directly measuring the dynamics of an SNR's evolution is crucial for understanding the explosion mechanism, and with the order of magnitude increase collecting area, we can measure the expansion of individual elemental species in the ejecta. 4) We will greatly increase the statistics of SNRs in nearby galaxies, going much faster and deeper than Chandra's observations. The increased depth of coverage would allow us to do spectroscopy in places where it was previously possible only to do rudimentary statistics. We can compare the local SNR population with the local star-formation rates for galaxies, important for supernova progenitor models. Finally, there is significant ancillary science that can be achieved by surveying nearby galaxies.

Author(s): Brian J Williams², Hiroya Yamaguchi¹

Institution(s): 1. NASA GSFC, 2. Space Telescope Science Institute

Contributing team(s): AXIS Science Team

140.05 – Time-domain Astronomy with the Advanced X-ray Imaging Satellite

The Advanced X-ray Imaging Satellite (AXIS) is a concept NASA Probe class mission that will enable time-domain X-ray observations after the conclusion of the successful Swift Gamma-ray burst mission. AXIS will achieve rapid response, like Swift, with an improved X-ray monitoring capability through high angular resolution (similar to the 0.5 arc sec resolution of the Chandra X-ray Observatory) and high sensitivity (ten times the Chandra count rate) observations in the 0.3-10 keV band. In the up-coming decades, AXIS's fast slew rate will provide the only

rapid X-ray capability to study explosive transient events. Increased ground-based monitoring with next-generation survey telescopes like the Large Synoptic Survey Telescope will provide a revolution in transient science through the discovery of many new known and unknown phenomena – requiring AXIS follow-ups to establish the highest energy emission from these events. This synergy between AXIS and ground-based detections will constrain the rapid rise through decline in energetic emission from numerous transients including: supernova shock breakout winds, gamma-ray burst X-ray afterglows, ionized gas resulting from the activation of a hidden massive black hole in tidal disruption events, and intense flares from magnetic reconnection processes in stellar coronae. Additionally, the combination of high sensitivity and angular resolution will allow deeper and more precise monitoring for prompt X-ray signatures associated with gravitational wave detections. We present a summary of time-domain science with AXIS, highlighting its capabilities and expected scientific gains from rapid high quality X-ray imaging of transient phenomena.

Author(s): Lisa M Winter¹, Tom Vestrand¹, Karl Smith¹, Marc Kippen¹, Richard Schirato¹

Institution(s): 1. Los Alamos National Laboratory

140.06 – STROBE-X: X-ray Timing & Spectroscopy on Dynamical Timescales from Microseconds to Years

We describe a probe-class mission concept that provides an unprecedented view of the X-ray sky, performing timing and 0.2-30 keV spectroscopy over timescales from microseconds to years. The Spectroscopic Time-Resolving Observatory for Broadband Energy X-rays (STROBE-X) comprises three primary instruments. The first uses an array of lightweight optics (3-m focal length) that concentrate incident photons onto solid state detectors with CCD-level (85-130 eV) energy resolution, 100 ns time resolution, and low background rates to cover the 0.2-12 keV band. This technology is scaled up from NICER, with enhanced optics to take advantage of the longer focal length of STROBE-X. The second uses large-area collimated silicon drift detectors, developed for ESA's LOFT, to cover the 2-30 keV band. These two instruments each provide an order of magnitude improvement in effective area compared with its predecessor (NICER and RXTE, respectively). Finally, a sensitive sky monitor triggers pointed observations, provides high duty cycle, high time resolution, high spectral resolution monitoring of the X-ray sky with ~20 times the sensitivity of the RXTE ASM, and enables multi-wavelength and multi-messenger studies on a continuous, rather than scanning basis. We include updated instrument designs resulting from the GSFC IDL run in November 2017.

For the first time, the broad coverage provides simultaneous study of thermal components, non-thermal components, iron lines, and reflection features from a single platform for accreting black holes at all scales. The enormous collecting area allows detailed studies of the dense matter equation of state using both thermal emission from rotation-powered pulsars and harder emission from X-ray burst oscillations. The combination of the wide-field monitor and the sensitive pointed instruments enables observations of potential electromagnetic counterparts to LIGO/Virgo and neutrino events. Extragalactic science, such as constraining bulk metallicity of medium to high redshift clusters and nearby compact groups and unprecedented timing investigations of active galactic nuclei, is also obtained.

Author(s): Colleen A. Wilson-Hodge⁹, Paul S Ray¹⁰, Thomas J. Maccarone¹³, Deepto Chakrabarty⁶, Keith C Gendreau⁸, Zaven Arzoumanian⁸, Peter Jenke¹⁴, David Ballantyne³, Enrico Bozzo¹⁷, Soren Brandt², Laura Brenneman¹², Marc Christophersen¹⁰, Alessandra DeRosa⁴, Marco Feroci⁴, Adam Goldstein¹⁸, Dieter Hartmann¹, Margarita Hernanz⁵, Michael McDonald⁶, Bernard Philips¹⁰, Ronald Remillard⁶, Abigail Stevens¹⁵, John Tomsick¹⁶, Anna Watts¹⁵, Kent S. Wood¹¹, Silvia Zane⁷

Institution(s): 1. *Clemson University*, 2. *DTU Space*, 3. *GaTech*, 4. *IAPS/INAF*, 5. *Institute of Space Sciences, CSIC-IEEC*, 6. *MIT*, 7. *MSSL/UCL*, 8. *NASA GSFC*, 9. *NASA MSFC*, 10. *NRL*, 11. *Praxis, Inc. (Resident at NRL)*, 12. *SAO*, 13. *TTU*, 14. *UAH*, 15. *University of Amsterdam*, 16. *University of California, Berkeley*, 17. *University of Geneva*, 18. *USRA*

Contributing team(s): STROBE-X Collaboration

140.07 – The STROBE-X Science Case: An Overview

STROBE-X is a proposed NASA Probe class mission aimed at the extremes of high throughput X-ray astronomy, making use of an 8 m² total collecting area, CCD-quality spectral resolution, and a state-of-the-art wide field monitor with both very large instantaneous sky coverage (ideal for follow-up of LIGO events) and good intrinsic spectral and time resolution. The core goals are time domain astrophysics and high count spectroscopy. Its capabilities span a broad range of topics, including those traditional to X-ray timing missions, like understanding the equation of states of neutron stars, and the spin distributions and masses of neutron stars and stellar mass and supermassive black holes, and the rates, and detailed properties, of a variety of classes of X-ray transients; and also topics not traditionally studied by such missions such as the spectra of supernova remnants, comets and of clusters and groups of galaxies.

Author(s): Thomas J. Maccarone¹

Institution(s): 1. *Texas Tech University*

Contributing team(s): STROBE-X consortium

140.08 – AGN Science with STROBE-X

The probe concept STROBE-X, with its combination of large collecting area, wide-field monitor, broad bandpass, and rapid timing capability, is a powerful tool for studying many aspects of AGN astrophysics. This unique combination of features opens up the possibility for studying AGNs in ways current and other future missions are unable to accomplish. Here, we show a few of the novel new investigations made possible by STROBE-X: probing the structure of the BLR and torus with reverberation of the narrow Fe K α line and line-of-sight column density, tracking changes in coronal parameters, investigating the origin of the soft excess, Fe K α emission line surveys, and efficient Compton-thick characterization. Additional ideas and suggestions are always welcome and can be communicated to any member of the STROBE-X team.

Author(s): David Ballantyne³, Mislav Balokovic⁴, Javier Garcia¹, Michael Koss²

Institution(s): 1. *California Institute of Technology*, 2. *Eureka Scientific*, 3. *Georgia Institute of Technology*, 4. *Harvard Smithsonian Center for Astrophysics*

Contributing team(s): STROBE-X

140.09 – UV spectroscopy with the CETUS multi-object spectrometer

The ultraviolet multi-object spectrograph (MOS) for the Cosmic Evolution Through UV Spectroscopy (CETUS) concept is a slit-based instrument allowing multiple simultaneous observations over a wide field of view. The UV MOS will be able to target up to 100 objects at a time without the issues of confusion with nearby sources or unwanted background like zodiacal stray light. The multiplexing will allow over 100,000 galaxies to be observed over a typical mission lifetime which greatly enhances the scientific yield.

The MOS utilizes a next-generation micro-shutter array, an

efficient aspheric Offner-like spectrometer design with a convex grating, and nanotube light traps for suppressing unwanted wavelengths. The optical coatings are also designed for optimizing the UV throughput while minimizing out-of-band signal at the detector.

Author(s): Stephen E Kendrick¹, Robert Woodruff⁵, Anthony Hull¹, Sara Heap³, Alexander Kuttyrev⁴, Lloyd Purves², William Danchi²

Institution(s): 1. *Kendrick Aerospace Consulting LLC*, 2. *NASA Goddard Space Flight Center*, 3. *NASA GSFC emerita*, 4. *University of Maryland*, 5. *Woodruff Consulting*

140.10 –

AMEGO: A First Look at the MeV Emission from Local Seyfert Active Galaxies

The NASA concept probe mission the All-sky Medium Energy Gamma-ray Observatory (AMEGO) will observe a previously poorly studied energy band from 200 keV to greater than 10 GeV. AMEGO will reveal new details about Seyfert Galaxies and potentially detect hundreds of new MeV AGN. Previous efforts to view the MeV range with the Imaging Compton Telescope (COMPTEL) did not have high enough sensitivity to study the non-thermal tail of electron distribution for black hole systems. AMEGO can reveal the non-thermal tail, which may be caused by gamma-gamma pair production or reconnection. The non-thermal tail is important to understand the processes relating to temperature regulation of the hot corona surrounding the black hole accretion disk. With AMEGO's increased sensitivity and broad MeV energy range, the MeV emission spectra of a large sample of Seyfert Galaxies can be observed for the first time.

Author(s): Elinor Mullin¹, Lisa M Winter¹, Pat Harding¹, Katherine Mesick¹, Justin Finke²

Institution(s): 1. *Los Alamos National Labs*, 2. *Naval Research Lab*

140.11 – Habitable Exoplanet Imaging Mission (HabEx): Architecture of the 4m Mission Concept

The Habitable Exoplanet Imaging Mission (HabEx) study is tasked by NASA to develop a scientifically compelling and technologically feasible exoplanet direct imaging mission concept, with extensive general astrophysics capabilities, for the 2020 Decadal Survey in Astrophysics. The baseline architecture of this space-based observatory concept encompasses an unobscured 4m diameter aperture telescope flying in formation with a 72-meter diameter starshade occulter. This large aperture, ultra-stable observatory concept extends and enhances upon the legacy of the Hubble Space Telescope by allowing us to probe even fainter objects and peer deeper into the Universe in the same ultraviolet, visible, and near infrared wavelengths, and gives us the capability, for the first time, to image and characterize potentially habitable, Earth-sized exoplanets orbiting nearby stars. Revolutionary direct imaging of exoplanets will be undertaken using a high-contrast coronagraph and a starshade imager. General astrophysics science will be undertaken with two world-class instruments – a wide-field workhorse camera for imaging and multi-object grism spectroscopy, and a multi-object, multi-resolution ultraviolet spectrograph. This poster outlines the baseline architecture of the HabEx flagship mission concept.

Author(s): Gary M Kuan¹, Keith R Warfield¹, Bertrand Mennesson¹, Alina Kiessling¹, H. Philip Stahl², Stefan Martin¹, Stuart B. Shaklan¹, rashied amini¹

Institution(s): 1. *Jet Propulsion Laboratory*, 2. *Marshall Space Flight Center*

140.12 – From the Milky Way to differing galaxy environments: filling critical gaps in our knowledge of star formation and its interplay with dust, and in stellar and galaxy evolution.

Rest-frame UV, uniquely sensitive to luminous, short-lived hot massive stars, trace and age-date star formation across galaxies,

and is very sensitive to dust, whose properties and presence are closely connected to star formation.

With wide f-o-v and deep sensitivity in two broad filters, FUV and NUV, GALEX delivered the first comprehensive UV view of large nearby galaxies, and of the universe to $z \sim 2$ (e.g., Bianchi 2014 ApSS 354,103), detected star formation at the lowest rates, in environments where it was not seen before and not expected (e.g. Bianchi 2011 ApSS 335,51; Thilker+2009 Nature 457,990; 2007 ApJS 173,538), triggering a new era of investigations with HST and large ground-based telescopes. New instrument technology and modeling capabilities make it now possible and compelling to solve standing issues. The scant UV filters available (esp. FUV) and the wide gap in resolution and f-o-v between GALEX and HST leaves old and new questions open. A chief limitation is degeneracies between physical parameters of stellar populations (age/SFR) and hot stars, and dust (e.g. Bianchi+ 2014 JASR 53,928).

We show sample model simulations for filter optimization to provide critical measurements for the science objectives. We also demonstrate how adequate FUV+NUV filters, and resolution, allow us to move from speculative interpretation of UV data to unbiased physical characterization of young stellar populations and dust, using new data from UVIT, which, though smaller than CETUS, has better resolution and filter coverage than GALEX. Also, our understanding of galaxy chemical enrichment is limited by critical gaps in stellar evolution; GALEX surveys enabled the first unbiased census of the Milky Way hot-WD population (Bianchi+2011 MNRAS, 411,2770), which we complement with SDSS, Pan-STARRS, and Gaia data to fill such gaps (Bianchi et al.2018, ApSS). Such objects in CETUS fields (deeper exposures, more filters, and the first UV MOS) will be much better characterized, enabling "Galactic archeology" investigations not possible otherwise.

Author(s): Luciana Bianchi¹

Institution(s): 1. Johns Hopkins University

140.13 – The CETUS Probe Mission Concept 1.5m Optical Telescope Assembly: A high A-Omega approach for ultraviolet astrophysics

We describe the 1.5-m Cosmic Evolution Through Ultraviolet Spectroscopy (CETUS) Optical Telescope Assembly (OTA), a Three Mirror Anastigmat (TMA), providing a large usable focus, which permits non-shared locations for several Ultraviolet (UV) instruments. NASA has selected CETUS as a Probe Mission Concept for consideration by The Decadal Survey ASTRO2020.

CETUS will fly in a L2 halo orbit and typically be pointing between 85 degrees and 135 degrees from the sun, and looking at galaxies at redshifts between $z=1$ and $z=2$. However, the CETUS payload also will be able to rapidly slew to sun angles between 85 degrees and 180 degrees to reach objects of opportunity, an example of which is a neutron star merger event. CETUS thermal stability starts with lightweighted ZERODUR® mirrors, that are an excellent thermal match to a metering structure of carbon fiber reinforced polymer (CFRP) M55J. This basic passive athermalization approach will be supplemented with controlled heaters, especially at metallic mounts, composite terminations and mechanisms. After launch, solid body metering errors will be optimized by an actuated hexapod in the secondary mirror assembly (SMA). Thus the CETUS telescope can respond to any pointing induced change in solar view factors. Contamination is managed by commissioning heaters radiating to each mirror surface, and a capping shutter over the telescope aperture.

The instruments include a wide-field-of-view (WFoV) multi-object spectrometer (MOS), and a complimentary WFoV camera, as well as high-resolution point source Echelle spectrometers ($R \sim 40,000$). They do not require that the OTA deliver diffraction limited performance over the extent of the instrument wavelength range (115nm to 400nm). The camera and spectrometer each cover a field of view of ~ 1000 arcsec by ~ 1000 arcsec compared to ~ 150 arcsec by ~ 150 arcsec for WFC3 on the Hubble Space Telescope (HST). Thus, the AW (etendue) factor for CETUS is $\sim 700 \text{ m}^2\text{-arcmin}^2$, compared to the AW factor for WFC3 on

HST which is $\sim 25 \text{ meter}^2\text{-arcmin}^2$. Thus, CETUS provides a factor of ~ 30 higher etendue than HST.

Author(s): Anthony Hull⁶, Sara Heap⁴, Robert Woodruff⁷, Greg Mehle⁵, Matt Tomic⁵, Kelly Dodson⁵, Jim Burge¹, Ben Lewis¹, Martin Valente¹, Stephen E Kendrick³, Lloyd Purves², William Danchi²

Institution(s): 1. Arizona Optical Systems, 2. GSFC, 3. Kendrick Aerospace Consulting, 4. NASA GSFC Emeritus, 5. Orbital ATK, 6. University of New Mexico, 7. Woodruff Consulting

140.14 – Using CETUS to study the first stars and first metals

The nucleosynthetic signatures of the first stars and supernovae are imprinted in the compositions of the most metal-poor stars found today. Only a few tens of absorption lines are commonly found in the optical spectra of the second-generation stars, so only 5-10 elements are regularly detected. Many others (Be, B, Si, P, S, Sc, V, Cr, Mn, Co, Ni, Cu, and Zn) are expected to be present but are rarely detected, and the upper limits derived from their optical non-detections are often uninteresting. The UV part of the spectrum accessible to the high-resolution UV spectrograph on CETUS would enable all of these elements to be detected if present in the most metal-poor stars known. We illustrate some of the ground-breaking observations of these stars that could be made with this mission.

Author(s): Ian Roederer¹

Institution(s): 1. University of Michigan

Contributing team(s): CETUS Team

140.15 – Optical design for CETUS: a wide-field 1.5m aperture UV payload being studied for a NASA probe class mission study

We are developing a NASA Headquarters selected Probe-class mission concept called the Cosmic Evolution Through UV Spectroscopy (CETUS) mission, which includes a 1.5-m aperture diameter large field-of-view (FOV) telescope optimized for UV imaging, multi-object spectroscopy, and point-source spectroscopy. The optical system includes a Three Mirror Anastigmatic (TMA) telescope that simultaneously feeds three separate scientific instruments: the near-UV (NUV) Multi-Object Spectrograph (MOS) with a next-generation Micro-Shutter Array (MSA); the two-channel camera covering the far-UV (FUV) and NUV spectrum; and the point-source spectrograph covering the FUV and NUV region with selectable $R \sim 40,000$ echelle modes and $R \sim 2,000$ first order modes. The optical system includes fine guidance sensors, wavefront sensing, and spectral and flat-field in-flight calibration sources. This paper will describe the current optical design of CETUS.

Author(s): Robert Woodruff¹

Institution(s): 1. Woodruff Optical Consulting

Contributing team(s): Robert Woodruff, Goddard Space Flight Center, Kendrick Optical Consulting

140.16 – The Cosmic Evolution Through UV Spectroscopy (CETUS) Probe Mission Concept

CETUS is a mission concept for an all-UV telescope with 3 scientific instruments: a wide-field camera, a wide-field multi-object spectrograph, and a point-source high-resolution and medium resolution spectrograph. It is primarily intended to work with other survey telescopes in the 2020's (e.g. E-ROSITA (X-ray), LSST, Subaru, WFIRST (optical-near-IR), SKA (radio) to solve major, outstanding problems in astrophysics. In this poster presentation, we give an overview of CETUS key science goals and a progress report on the CETUS mission and instrument design.

Author(s): William Danchi³, Sara Heap³, Robert Woodruff⁴, Anthony Hull², Stephen E Kendrick², Lloyd Purves³, Stephan McCandliss¹

Institution(s): 1. Johns Hopkins University, 2. Kendrick Aerospace, 3. NASA Goddard Space Flight Center, 4. Woodruff Consulting

Contributing team(s): Kelly Dodson, Greg Mehle, James Burge, Martin Valente, Michael Rhee, Walter Smith, Michael Choi, Eric Stoneking

140.17 – Scientific Goals and Objectives of the Probe of Inflation and Cosmic Origins

The Probe of Inflation and Cosmic Origins (PICO) is a space mission concept that is being studied in preparation for the 2020 Astronomy and Astrophysics Decadal Survey. PICO will conduct a polarimetric full sky survey in 21 frequency bands between 20 and 800 GHz with 70 times the sensitivity of the Planck satellite. Using the data from 8 redundant full sky surveys PICO will detect or place new limits on the energy scale of inflation and the physics of quantum gravity; it will determine the effective number of light degrees of freedom in the early universe and the sum of neutrino masses; it will measure the optical depth to reionization up to cosmic variance limits; it will provide a full sky catalog of thousands of strongly lensed high-z infrared sources, of proto clusters, and of low-z low-mass galaxies extending our understanding of structure formation to populations not yet observed; it will find tens of thousands of new clusters across cosmic time, information that will further constrain cosmological parameters; and it will make sensitive maps of the galactic magnetic field, which will clarify its role in the process of star formation.

We present an overview of the mission's scientific goals, its design, and the current status of the study.

142 – The Triple Threat to Multi-Wavelength

142.01 – The Consortium for Dark Sky Studies: A Transdisciplinary Institute for Understanding the Loss of the Night

Research into the effects of artificial light at night (ALAN) has grown from a niche speciality into a broad field touching on aspects of life science, physics, astronomy, social science, and more, reflecting the highly interconnected subjects whose common characteristic is the alteration of the natural nighttime environment by anthropogenic light pollution. Until recently, there was no focal point for these diverse efforts to foster connections between researchers and initiate new topics of study in ALAN research. In 2016, the Consortium for Dark Sky Studies (CDSS), the world's first organization dedicated to the study of the night and the influence of human nighttime activities on the integrity of natural darkness, was founded at the University of Utah. We describe the motivations for establishing the Consortium, its early activities, and initial outcomes of the effort.

Author(s): John Barentine², David Kieda³, Stephen Goldsmith³, Bettymaya Foott³, Janet Muir¹

Institution(s): 1. Consortium for Dark Sky Studies, 2. International Dark-Sky Association, 3. University of Utah

142.02 – Protection of Hawaii's Observatories from Light Pollution

Maunakea Observatory, located on the island of Hawaii, is among the world darkest sites for astronomy. Strong efforts to preserve the dark night sky over the last forty years have proven successful. Artificial light presently adds only approximately 2% to the natural night sky brightness. The techniques being used to protect Maunakea from light pollution will be described, along with the challenges that are now being faced.

Haleakala Observatory, located on the island of Maui, is also an excellent observing site, and is among the best sites in the United States. Lighting restrictions in Maui County are much weaker, and consequently, the night sky above Haleakala is less well protected. Haleakala is closer to Honolulu and the island of Oahu

Author(s): Qi Wen¹, Shaul Hanany¹, Karl S. Young¹

Institution(s): 1. University of Minnesota

Contributing team(s): PICO Team

140.18 – Optical Design and Sensitivity of the Probe of Inflation and Cosmic Origins

The Probe of Inflation and Cosmic Origins (PICO) is a NASA probe-class mission concept being studied in preparation for the 2020 Astronomy and Astrophysics Decadal Survey. PICO will detect, or place new limits on, the energy scale of inflation and the physics of quantum gravity, determine the effective number of neutrino species and constrain the sum of neutrino masses, measure the optical depth to reionization to the cosmic variance limit, and shed new light on the role of magnetic fields in galactic evolution and star formation by making polarimetric maps of the full mm-wave sky with sensitivity 70 times higher than the Planck space mission. The maps made by PICO will provide a catalog of thousands of new proto clusters and infrared galaxies as well as tens of thousands of galaxy clusters which will further constrain cosmological parameters.

PICO will have a 1.4 meter aperture telescope with 21 bands from 20 to 800 GHz. We show the current PICO optics and discuss trade-offs between types of optical systems, limits imposed by scan strategies, and maximizing the number of detectors on sky. We present the instrument's focal plane and the expected mission sensitivity.

Author(s): Karl S. Young¹, Shaul Hanany¹, Qi Wen¹

Institution(s): 1. University of Minnesota, Twin Cities

Observational Astronomy Poster Session

(population approximately 1 million), and the glow from Oahu makes the northwestern sky brighter.

Much of the lighting across most of the United States, including Hawaii, is presently being converted to LED lighting. This provides an opportunity to replace existing poorly shielded lights with properly shielded LED fixtures, but careful spectral management is essential. It is critically important to only use LED lighting that is deficient in blue and green light. LED lighting also is easy to dim. Dimming of lights later at night, when there is no need for brighter lighting, is an important tool for reducing light pollution.

Techniques used to protect astronomical observatories from light pollution are similar to the techniques that must be used to protect animals that are affected by light at night, such as endangered birds and turtles. These same techniques are compatible with recent human health related lighting recommendations from the American Medical Association.

Author(s): Richard J Wainscoat¹

Institution(s): 1. University of Hawaii

142.03 – Promoting Dark Sky Protection in Chile: the Gabriel Mistral IDA Dark Sky Sanctuary and Other AURA Initiatives

For over 20 years, AURA has been leading efforts promoting the protection of dark skies in northern Chile. Efforts began in the early 1990s at AURA's Cerro Tololo Inter-American Observatory (CTIO), working in collaboration with other international observatories in Chile including Las Campanas Observatory (LCO) and the European Southern Observatory (ESO). CTIO also partnered with local communities, for example supporting Vicuña's effort to establish the first municipal observatory in Chile. Today we have developed a multifaceted effort of dark sky protection, including proactive government relations at national and local levels, a strong educational and public outreach program, and a program of highlighting international recognition of the dark skies through the IDA Dark Sky Places program. Work

on international recognition has included the declaration of the Gabriel Mistral IDA Dark Sky Sanctuary, the first such IDA sanctuary in the world.

Author(s): R. Chris Smith¹, Malcolm Smith¹, Stephen Pompea¹, Pedro Sanhueza¹

Institution(s): 1. *AURA Observatory in Chile*

Contributing team(s): AURA-Chile EPO Team

142.04 – A Regional, Multi-Stakeholder Collaboration for Dark-Sky Protection in Flagstaff, Arizona

Flagstaff, Arizona is home to almost \$200M in astronomical assets, including Lowell Observatory's 4.3-meter Discovery Channel Telescope and the Navy Precision Optical Interferometer, a partnership of Lowell, the U. S. Naval Observatory, and the Naval Research Laboratory. The City of Flagstaff and surrounding Coconino County have comprehensive and effective dark-sky ordinances, but continued regional growth has the potential to degrade the area's dark skies to a level at which observatory missions could be compromised. As a result, a wide array of stakeholders (the observatories, the City, the County, local dark-sky advocates, the business and tourism communities, the national parks and monuments, the Navajo Nation, the U. S. Navy, and others) have engaged in three complementary efforts to ensure that Flagstaff and Coconino County protect the area's dark skies while meeting the needs of the various communities and providing for continued growth and development. In this poster, I will present the status of Flagstaff's conversion to LED outdoor lighting, the Mission Compatibility Study carried out by the Navy to evaluate the dark-sky effects of buildout in Flagstaff, and the Joint Land Use Study (JLUS) presently underway among all the aforementioned stakeholders. Taken in sum, the efforts represent a comprehensive and constructive approach to dark-sky preservation region-wide, and they show what can be achieved when a culture of dark-sky protection is present and deliberate efforts are undertaken to maintain it for decades to come.

Author(s): Jeffrey C. Hall¹

Institution(s): 1. *Lowell Observatory*

142.05 – Light Pollution: A Primer for Astronomers to Engage in Teaching and Outreach

Most astronomers are familiar with the basic problem of light pollution but may not have explored how to teach their students about the problem or to inform officials in their community in order to help mitigate the problem. Indeed, many professional and amateur astronomers leave their light-polluted community to observe the sky from dark research observatories and rural star parties, and then return to take no action to alleviate and reduce the light pollution in their own community. This is not a sustainable approach, and eventually this will lead to fewer sites to do their observations.

In this presentation we give the basics of the problem and provide information on effective solutions. A link will be provided to download a sample PowerPoint, with Notes providing guidance to edit it to include images of both good and bad lighting in their own community. This can be shown to students as part of introductory astronomy and observational techniques courses, so the students might be able to help their with the problem in their own communities. Indeed this may satisfy curriculum requirements as a component of sustainable development. It may also be presented to local planning and permitting officials to develop at least a simple outdoor lighting ordinance.

Author(s): Daniel Bruce Caton¹

Institution(s): 1. *Appalachian State University*

142.06 – Minimizing the Threat of Light Pollution on Observatories through Education: Globe at Night Citizen-Science

Citizen-science is a rewardingly inclusive way to bring awareness to the public on the disappearance of the starry night sky, its cause and solutions. Globe at Night (GaN) encourages citizen-scientists worldwide to record the brightness of the night sky. During ten-days per month of moonless evenings, children and adults match the appearance of a specified constellation with 7 star maps of progressively fainter stars found at www.globeatnight.org. They then submit their choice of star map in-situ with the "webapp" by smart device to add to a light pollution map worldwide. In the eleven years of the program, over 170,000 observations from 180 countries have been contributed to the campaign.

The Globe at Night (open) database is a source of research projects, even with other disciplines. For example, students conducted research to understand the lesser long-nosed bats' avoidance of city center at night. On-the-fly mapping enables citizen-scientists to see contributed observations immediately. The 12 campaigns per year offer 4 ways of taking measurements. The online app for data submission is in 28 languages. STEM activities for young children and problem-based learning activities for older students were created to experience real-life scenarios: role-playing sea turtles hatching (misdirected by lights on shore) or analyzing an ISS image of Houston to estimate the wasted energy, cost and carbon footprint. In-situ and on-line workshops have been given on using GaN in all its capacities, as well as for the activities. Our Facebook page exists to encourage dialogue and bring cutting edge news. To entice interest, we had monthly newsletters and serial podcasts starring the Dark Skies Crusader. GaN has been part of special campaigns like with the National Park Service, the National Geographic BioBlitz and Tucson in 2011. Partnerships also include SciStarter (working with participants), Fieldscope (working with data analysis), and STARS4ALL (working with other light pollution initiatives). We have built a community of practitioners in various ways worldwide and plan to continue to help reduce the effects of one of the threats to observational astronomy through awareness and action.

Author(s): Constance E. Walker¹, Stephen M, Pompea¹

Institution(s): 1. *National Optical Astronomy Observatory*

142.07 – Minimizing the Threat of Light Pollution on Observatories through Education: the Quality Lighting Teaching Kit

Poor quality lighting impedes astronomy research and our right to see a starry night sky. It creates safety issues, affects human circadian sensitivities, disrupts ecosystems, and wastes billions of dollars/year in energy consumption. It also leads to excess carbon emissions. How do you change the mindset of society that is used to turning night into day? You educate the next generation on quality lighting.

As an outcome of the International Year of Light 2015, the National Optical Astronomy Observatory's Education and Public Outreach group has produced a Quality Lighting Teaching (QLT) Kit. The kits are designed around problem-based learning scenarios. The kit's six activities allow students to address real lighting problems that relate to wildlife, sky glow, aging eyes, energy consumption, safety, and light trespass. The activities are optimized for 11-14 year olds but can be expanded to younger and older. All materials are in both English and Spanish. Most of the activities can be done within in a few minutes during class or afterschool and as stations or as stand-alones. Everything you need for the six activities is included in the kit. Tutorial videos on how to do the activities can be found at www.noao.edu/education/qltkit.php. Ninety-two out of one hundred kits have been distributed in thirty-two countries through SPIE (the International Society for Optical Engineering), CIE (the International Commission on Illuminations), OSA (the Optical Society), IDA (the International Dark Sky Association), and the IAU OAD—Office of Astronomy Development. Successful feedback is promoting a choice between commercializing the kit or gaining further grants to build more kits. A plan is being considered to distribute kits to observatories around the world,

hence helping to reduce the effects of one of the three threats to observational astronomy through awareness and action.

Author(s): Constance E. Walker¹, Stephen M. Pompea¹
Institution(s): 1. *National Optical Astronomy Observatory*

142.08 – Protecting Dark Skies as a State-Wide Resource

The state of Arizona contains the highest concentration of research telescopes in the continental United States, contributing more than a quarter of a billion dollars annually to the state's economy. Protecting the dark skies above these observatories is both good for astronomy and good for the state's economy. In this contribution we describe how a coalition of Arizona observatories is working together to protect our dark skies. Efforts date back to the creation of one of the first Outdoor Lighting Codes in the

143 – HAD IV: Poster Session

143.01 – The Future of Past Skies: Historical Celestial Cartography at the Adler Planetarium

The Adler Planetarium is home to a world-class collection of scientific instruments, rare books and works on paper. Since 2014, Adler staff has been digitizing a wide selection of items relating to celestial cartography, including: more than 236 rare books and atlases; 97 works on paper; globes and other artifacts, amounting to 58 objects; and approximately 3,750 Carte du Ciel prints. This work has been carried out under the auspices of the Celestial Cartography Digitization Project (CCDP), which is sponsored by the National Endowment for the Humanities. This poster presentation will include: 1) an update on the project; 2) a description of related resources and tools available to the research community; 3) examples of how the Adler Planetarium is integrating the history of celestial cartography with its public programs; 4) an overview of a prospective citizen science project involving the identification of constellations in historical atlases and charts.

Author(s): Pedro M. P. Raposo¹
Institution(s): 1. *Adler Planetarium*

143.02 – The Discovery of Gravitational Repulsion by Johannes Droste

In 1687 Newton published his universal law of gravitation, which states that the gravitational force is always attractive. This law is based on our terrestrial experience with slowly moving bodies ($v \ll c$). In 1915 Einstein completed his theory of general relativity (also referred to as Einstein's Theory of Gravitation), which is valid not just for slowly moving bodies but also for those with relativistic velocities. In 1916 Johannes Droste submitted a PhD thesis on general relativity to his advisor, H.A. Lorentz. In it he calculated the motion of a particle in what he called a "single center" and today we call the Schwarzschild field and found that highly relativistic particles experience gravitational repulsion. Thus, his thesis written in Dutch and never before translated contains the discovery of gravitational repulsion. Because of its historical importance we translate the entire section of his thesis containing the discovery of gravitational repulsion. We also translate his thesis in the hope of clearing up a major historical misconception. Namely, that David Hilbert in 1917 discovered gravitational repulsion. In fact, Hilbert rediscovered it, apparently completely independent of Droste's work. Finally we note that one of the biggest mysteries of astrophysics is the question of how highly energetic particles in relativistic jets and cosmic rays are accelerated. It has been suggested that gravitational repulsion is the mechanism responsible for these phenomena. An historical understanding of gravitational repulsion is therefore pertinent.

Author(s): Charles Hosewell McGruder¹, Wieb Van der Meer¹
Institution(s): 1. *Western Kentucky University*

143.03 – Project PHaEDRA: Preserving Harvard's Early Data and Research in Astronomy

United States and continue today, including educational outreach, public policy engagement, and consensus building. We review some proven strategies, highlight recent successes and look at current threats.

Author(s): Lori E Allen⁷, Constance E. Walker⁷, Jeffrey C. Hall³, Steve Larson⁴, Grant Williams⁵, Emilio Falco¹, Joannah Hinz⁵, Pascal Fortin¹, Dan Brocius⁶, Christopher Corbally¹¹, Paul Gabor¹¹, Christian Veillet², Paul Shankland¹⁰, Buell Jannuzi⁹, Angela Cotera⁸, Christian Luginbuhl¹⁰
Institution(s): 1. *CfA*, 2. *LBTO*, 3. *Lowell Observatory*, 4. *Lunar and Planetary Lab*, 5. *MMTO*, 6. *NASW*, 7. *NOAO*, 8. *SETI Institute*, 9. *Steward Observatory*, 10. *USNO*, 11. *Vatican Observatory*

Material originally produced during 19th and early 20th century by researchers at the Harvard College Observatory (HCO) was recently re-discovered in the HCO Astronomical Plate Stacks collection. This material helps represent the history of the HCO and acts as an irreplaceable primary source on the evolution of observation methods and astronomy as a science. The material is also relevant to the history of women in science as the collection contains logbooks and notebooks produced by the Harvard Computers, women who have come back into the spotlight due to the recent release of books like "The Glass Universe," "Rise of the Rocket Girls," and movies like "Hidden Figures". To ensure that this remarkable set of items is as accessible and useful as possible Wolbach Library, in collaboration with the SAO/NASA Astrophysics Data System (ADS) and others, is working to catalog, digitize, and preserve the entire collection. The material is also being transcribed by volunteers through the Smithsonian Transcription Center in DC. The transcription will allow the collection to be full-text searchable in ADS and for the notebooks to eventually be linked to their original source material: 500,000 glass plate photographs representing the first ever picture of the visible universe. The novel workflow of this distributed repository and the significance of the PHaEDRA collection both stand to support the research of future generations.

Author(s): Daina Bouquin², Katie Frey², Edwin Henneken³, Maria McEachern², Alex McGrath², Daniel Guarracino², Jennifer Koch², James Damon², Eric Brownell², Lindsay Smith-Zrull¹
Institution(s): 1. *Harvard College Observatory*, *Astronomical Photographic Plate Collection*, 2. *Harvard-Smithsonian Center for Astrophysics*, 3. *SAO/NASA Astrophysics Data System*
Contributing team(s): Daina Bouquin

143.04 – This Month in Astronomical History: Providing Context for the Advancement of Astronomy

This Month in Astronomical History is a short (~500 word) illustrated column hosted on the AAS website (<https://had.aas.org/resources/astro-history>). Its mission is to highlight people and events that have shaped the development of astronomy to convey a historical context to current researchers, to provide a resource for education and public outreach programs seeking to incorporate a historical perspective, and to share the excitement of astronomy with the public. Knowing how the astronomical journey has proceeded thus far allows current professionals to map where to go next and how to get there. The column charts the first part of this journey by celebrating anniversaries of births, discoveries, and deaths, and the technological advances that made discoveries possible. A new "Further Reading" section encourages readers to pursue subjects in greater depth and strengthens the articles as classroom resources.

In the months preceding the 21 August 2017 solar eclipse, the column featured astronomical bodies that come between Earth and the Sun: 2004 Venus transit, the 1878 solar eclipse, and the search for the hypothetical planet Vulcan. Venusian transits were an early but technically challenging way to measure the

astronomical unit, now easily done with radar-ranging. Like this year's event, eclipse chasing and citizen science were part of the 1878 experience. Newton's Laws seemed to require a planet inside Mercury's orbit, but General Relativity explained the behavior of Mercury without it. Studying each of these transiting bodies has expanded our knowledge and understanding of the universe differently. Transiting extrasolar planets remain to be explored in a future column. In September, an article on the discovery of Neptune followed the discussion of the non-existent Vulcan quite naturally and expanded on the brief mention of this event in relation to the discovery of Pluto. Suggestions for additional topics are always welcome.

The Dudley Observatory supported *This Month in Astronomical History* through its 2017 Herbert C. Pollock Award. The author thanks the HAD Executive Committee for their careful review of each edition.

Author(s): Teresa Wilson¹

Institution(s): 1. *Michigan Technological University*

143.05 – The History of the CONCAM Project: All Sky Monitors in the Digital Age

The CONTinuous CAMera (CONCAM) project, which ran from 2000 to (about) 2008, consisted of real-time, Internet-connected, fisheye cameras located at major astronomical observatories. At its peak, eleven CONCAMs around the globe monitored most of the night sky, most of the time. Initially designed to search for transients and stellar variability, CONCAMs gained initial notoriety as cloud monitors. As such, CONCAMs made -- and its successors continue to make -- ground-based astronomy more efficient. The original, compact, fisheye-observatory-in-a-suitcase design underwent several iterations, starting with CONCAM0 and with the last version dubbed CONCAM3. Although the CONCAM project itself concluded after centralized funding diminished, today more locally-operated, commercially-designed, CONCAM-like devices operate than ever before. It has even been shown that modern smartphones can operate in a CONCAM-like mode. It is speculated that the re-instatement of better global coordination of current wide-angle sky monitors could lead to better variability monitoring of the brightest stars and transients.

145 – White Dwarfs Poster Session

145.01 – A Search for Variability in Warm and Cool C-rich DQ White Dwarfs

Hot DQ white dwarfs are a rare class of white dwarfs that have atmospheres dominated by carbon with little to no hydrogen or helium. Recently it has been found that the majority of these stars are photometrically variable likely due to rapid rotation with star spots. The cool progeny of the hot DQs are expected to also be rapidly rotating as no strong braking mechanisms should be present. We present the time-series photometry of multiple warm and cool C-rich DQ white dwarfs as part of an ongoing search for variability in hot DQ white dwarfs and their progeny. This program will permit us to confirm rotation as the source of variability, compare the distribution of rotation rates to those of more common white dwarf spectral types, and constrain the evolutionary rates of hot DQ rotation. These data are one way to better understand the formation scenarios of these stars.

Author(s): Christopher Michael Dupuis¹, Kurtis A Williams¹

Institution(s): 1. *Texas A&M University Commerce*

145.02 – The White-Dwarf Mass-Radius Relation from 40 Eridani B and Other Nearby Visual Binaries

The bright, nearby DA-type white dwarf (WD) 40 Eridani B is orbited by the M dwarf 40 Eri C, allowing determination of the WD's mass. Until recently, however, the mass depended on orbital elements determined four decades ago, and that mass was so low that it created several astrophysical puzzles. Using new astrometric measurements, the binary-star group at the U.S. Naval Observatory has revised the dynamical mass upward, to

Author(s): Robert Nemiroff³, Lior Shamir², Wellesley Pereira¹

Institution(s): 1. *Air Force Research Laboratory*, 2. *Lawrence Technological University*, 3. *Michigan Technological University*

143.06 – Urania in the Marketplace: Using Telescopes to Sell Consumer Goods

For well over a century the iconic image of the astronomical telescope has been widely used to promote distinctly non-astronomical consumer goods. One of the most famous of early examples is the 1893 Chicago newspaper advertisement for Kirk's Soap, which was inspired by the opening of the Yerkes Observatory. But such usage was not limited to periodicals. Advertising trade cards had become popular at the end of the 17th century in Europe, notably in Paris and London. In a time prior to the introduction of formal systems of street address numbering, they served as both advertisement and map, directing consumers to the merchants' stores. In many cases, attention was drawn to the product by picturing it as a heavenly body to be observed telescopically!

In the 20th century trade cards gave way to the modern business card, and manufacturers began to increasingly rely on magazine and newspaper (and radio and television) advertising. But the telescope remains an evocative image! In modern advertising we see it used to sell an incredible variety of consumer goods: candy, coffee, cigarettes, whiskey, foodstuffs, clothing; the list is endless! Examples of these, along with earlier Victorian-era usages, are presented.

This work was supported by a faculty development grant from Valdosta State University.

Author(s): Kenneth S. Rumstay¹

Institution(s): 1. *Valdosta State University and SARA*

$0.573 \pm 0.018 M_{\odot}$. We have used model-atmosphere analysis to update other parameters of the WD, including effective temperature, surface gravity, radius, and luminosity. We then compare these results with WD interior models.

Within the observational uncertainties, theoretical cooling tracks for CO-core WDs of its measured mass are consistent with the position of 40 Eri B in the H-R diagram; equivalently, the theoretical mass-radius relation (MRR) is consistent with the star's location in the mass-radius plane. This consistency is, however, achieved only if we assume a "thin" outer hydrogen layer, with $q_H = M_H/M_{WD} \sim 10^{-10}$.

We discuss other evidence that a significant fraction of DA WDs have such thin H layers, in spite of expectation from canonical stellar-evolution theory of "thick" H layers with $q_H \sim 10^{-4}$. The cooling age of 40 Eri B is ~ 122 Myr, and its total age is ~ 1.8 Gyr. We present the MRRs for 40 Eri B and three other nearby WDs in visual binaries with precise mass determinations, and show that the agreement of current theory with observation is excellent in all cases.

However, astrophysical puzzles remain. The eccentricity of the BC orbit has remained high (0.43), even though the progenitor of B ought to have interacted tidally with C when it was an AGB star. This puzzle exists also for the Sirius and Procyon systems. If thin hydrogen layers are common among WDs, the mass scale will need to be shifted downwards by a few hundredths of a solar mass.

Author(s): Howard E Bond¹, P. Bergeron², A. Bedard²
Institution(s): 1. Pennsylvania State University, 2. University of Montreal

145.03 – Testing Claims of a New Hot White Dwarf Instability Strip with Kepler and K2

We empirically test claims of a possible new instability strip of hydrogen-dominated pulsating white dwarfs between 30,000K and 45,000K. We search for pulsations of 12 DA white dwarfs with effective temperatures in this range using minute-cadence photometry collected by the Kepler Space Telescope. Our study impacts possible structural effects that can explain the scarcity of helium-dominated white dwarfs within this so called DB gap.

Author(s): Brandon Castillo¹, JJ Hermes¹
Institution(s): 1. UNC Chapel Hill

145.04 – RCB stars from double degenerate white dwarf mergers

We have conducted grid based and SPH based hydrodynamic simulations of white dwarf mergers, to investigate the role of dredge-up and mixing during the merger. The goal is to test if sufficiently little ¹⁶O can be brought up to the surface to explain the observed ¹⁶O to ¹⁸O ratio of order unity found in RCB stars. In all simulations, the total mass is $\sim < 1 M_{\odot}$. By initializing both the grid based and the SPH simulations with the same setup, we can compare the results from these different methods. In most of the simulations, more than 0.01 M_{\odot} of ¹⁶O is brought up to the surface. Hence a similar mass of ¹⁸O must be produced in order to explain the observed oxygen ratio. However, in SPH simulations where the accretor is a hybrid He/CO white dwarf, much less ¹⁶O is brought to the surface, making this an excellent candidate for the progenitor of RCB stars.

146 – Variable Stars Poster Session

146.01 – Binary Model for the Heartbeat Star System KIC 4142768

Heartbeat stars are a class of eccentric ($e > 0.2$) binary systems that undergo strong tidal forces. These tidal forces cause the shape of each star and the temperature across the stellar surfaces to change. This effect also generates variations in the light curve in the form of tidally-induced pulsations, which are theorized to have a significant effect on the circularization of eccentric orbits (Zahn, 1975). Using the binary modeling software PHOEBE (Prša & Zwitter 2005) on the Kepler photometric data and Keck radial velocity data for the eclipsing, heartbeat star KIC 4142768, we have determined the fundamental parameters including masses and radii. The frequency analysis of the residual data has surprisingly revealed approximately 29 pulsations with 8 being Delta Scuti pulsations, 10 being Gamma Doradus pulsations, and 11 being tidally-induced pulsations. After subtracting an initial binary model from the original, detrended photometric data, we analyzed the pulsation frequencies in the residual data. We then were able to disentangle the identified pulsations from the original data in order to conduct subsequent binary modeling. We plan to continue this study by applying asteroseismology to KIC 4142768. Through our continued investigation, we hope to extract information about the star's internal structure and expect this will yield additional, interesting results.

Author(s): Joseph Manuel¹, Kelly Hambleton¹
Institution(s): 1. Villanova University

146.02 – Visual photometry: accuracy and precision

Visual photometry, estimation by eye of the brightness of stars, remains an important source of data even in the age of widespread precision instruments. However, the eye-brain system differs from electronic detectors and its results may be expected to differ in several respects. I examine a selection of well-observed variables from the AAVSO database to determine several internal characteristics of this data set. Visual estimates scatter around the fitted curves with a standard deviation of 0.14

Author(s): Jan Staff⁴, Brandon K Wiggins³, Dominic Marcello², Patrick Motl¹, Geoffrey C Clayton²
Institution(s): 1. Indiana University Kokomo, 2. Louisiana State University, 3. Southern Utah University, 4. University of the Virgin Islands

145.05 – Modeling and Analysis of CTIO 1.5m White Dwarf Spectra

We present results to date on spectroscopic reductions of white dwarf stars from the CTIO 1.5m telescope in support of calibrations for the Dark Energy Survey, which is based in the Southern hemisphere to map galaxies and gather information on dark energy.

Science requirements for the survey require a 0.5% uncertainty in color, driven by supernova science. The Dark Energy Survey relies on a calibration technique that uses white dwarf stars to set zero points. These white dwarf spectra are fit to model spectra at the same temperatures and surface gravities. Fits are done both by a WD modeling expert, Pier Emmanuel Tremblay, and by WD model fitting software created by Gautham Narayan. Fits from both are comparable and give similar results, which are then used to generate synthetic photometry. These synthetic photometry values are compared to the measured values from the survey to verify that the zero points are correct.

Author(s): Deborah Jean Gullede¹, Douglas Tucker², John Allyn Smith¹, William Wester², Jacob Robertson¹, Jack H. Mueller³, Mees Fix⁴, Gautham Narayan⁴, P.-E. Tremblay⁵
Institution(s): 1. Austin Peay State University, 2. Fermi National Accelerator Laboratory, 3. Michigan State University, 4. Space Telescope Science Institute, 5. University of Warwick

to 0.34 magnitudes, most clustered in the 0.21-0.25 range. The variation of the scatter does not seem to correlate with color, type of variable, or depth or speed of variation of the star's brightness. The scatter of an individual observer's observations changes from star to star, in step with the overall scatter. The shape of the deviations from the fitted curve is non-Gaussian, with positive excess kurtosis (more outlying observations). These results have implications for use of visual data, as well as other citizen science efforts.

Author(s): Alan Whiting¹
Institution(s): 1. University of Birmingham

146.03 – Pulse Timing Measurements of the Hot Subdwarf B Star CS 1246

CS 1246 is a hot subdwarf B star which was discovered in 2009 to have a single large-amplitude oscillation in its light curve. An O-C diagram constructed from this pulsation mode revealed the presence of a low-mass stellar companion in a 14.1-day orbit, which was later confirmed with radial velocity measurements. We have continued to monitor CS 1246 over the past eight years with the Skynet Robotic Telescope Network, over which time the pulsation amplitude has decreased nonlinearly. Here we present our most recent photometry on the star, along with an updated O-C diagram and pulsation amplitude analysis.

Author(s): Zackary Hutchens¹, Brad Barlow¹, Alan Vasquez Soto¹
Institution(s): 1. High Point University

146.04 – Kepler observes the pulsating subdwarf B star KIC 11558725 (Mungo): Divergent frequency splittings and mode trapping

We analyze the full *Kepler* short cadence data set (Quarters 6 – 17) for the pulsating subdwarf B star KIC 11558725 (Mungo). Mungo is in an sdB+WD binary system with a period of ~ 10 days and is known to be subsynchronously rotating (Telting, J. H., et al. 2012, A&A, 544, A1). From the full data set, we detected 244 pulsation frequencies, mostly in the gravity (g-) mode region, but

some in the pressure (p-) mode region as well.

Results of our preliminary analysis include the identification of 141 $\ell \leq 2$ and 27 $\ell = 6$ modes. Abundant frequency splittings in the g-mode region and minimal frequency splittings in the p-mode region indicate solid body rotation with a period of ~ 44 days. The $\ell = 6$ multiplets do not show a constant splitting, with the splitting increasing over the course of the observations. Mungo also displays mode trapping in two regions of its asymptotic sequence. The $\ell = 1$ g-mode multiplets transition from exclusively $\Delta m = 1$ at low radial orders (short periods) to predominantly $\Delta m = 2$ for higher orders (longer periods), with two full triplets in the transition region. The $\ell > 1$ multiplets, with the exception of only three frequencies, exhibit strictly $|m| = \text{even}$ components. These multiplet features indicate an inclination of the pulsation axis very close to 90° .

Author(s): Joshua W. Kern¹, Michael D. Reed¹, Andrzej Baran³, John H. Telting², Roy H. Østensen¹
Institution(s): 1. Missouri State University, 2. Nordic Optical Telescope, 3. Pedagogical University Cracow

146.05 – An Examination of the High Amplitude delta Scuti V2455 Cygni

We have monitored the pulsating High Amplitude delta Scuti star, V2455 Cyg, for 8 years using spectroscopic and photometric observations. During that time we have noted a number of interesting changes in the light curve that could be associated with a companion or might be intrinsic to the star. We will present radial velocity measurements, photometric light curves, and H-alpha/H-beta observations for this system. We will also explore the potential interpretations of that data.

Author(s): Eric G Hintz¹, Maureen L Hintz¹, Michael D. Joner¹
Institution(s): 1. Brigham Young University

146.06 – Variable Stars in M53

We present early results for a search to find variable stars in the globular cluster M53. Data was collected over a four day span in April 2017. The list of detected variable stars is compared to the Clement catalogue of variable stars.

Author(s): Lucas Gabriel Napolitano¹, Nathaniel E Q Paust¹
Institution(s): 1. Whitman College

146.07 – Calibrating STEREO's Stellar Photometric Capabilities using Contemporaneous Observations from Kepler.

The photometric capabilities of the Helioseismic Imager aboard STEREO's Ahead spacecraft (HI1A) have allowed the yearly observation of a large number of stars situated near the ecliptic over the past decade. While many reliable stellar variability analyses have been performed, unwanted artifacts may still exist in the data that sometimes manifest as false signals.

Between May 22 and July 1, 2016, Kepler's K2 mission executed the second part of Guest Observer Campaign 9 to study gravitational microlensing events in the direction of the Galactic bulge. Coincidentally, during approximately two weeks of this campaign, HI1A was directed toward the same field of view, presenting a rare opportunity to compare the contemporaneous observations from both instruments looking at the same set of stars.

Utilizing the high sensitivity of Kepler, undesirable artifacts within the observed HI1A photometric signals may be identified and removed. Additionally, intrinsic variations of these field stars, such as those with long periodicities, may be confirmed by calibrating the signals from HI1A with those from Kepler. These stars may subsequently undergo retrospective analyses using the available data from STEREO, which will provide further insights into their variability characteristics.

Author(s): Peter Williams¹
Institution(s): 1. Northern Virginia Community College

146.08 – Using the Kepler Full Frame Images to Find Long-Period Variables in the Milky Way

We are using the monthly Full Frame Images (FFIs) images from the 4+ year Kepler mission to conduct a uniform census of long-period variables (LPVs, primarily Miras and semiregular variables) in the Milky Way disk. Our goal is to help understand how stellar pulsation and dust production interact as these dying stars eject their envelopes and enrich the interstellar medium with new fusion products and dust. To that end, we are processing the monthly FFIs for the entire 116 square-degree Kepler field to identify the LPVs and determine their period, pulsation mode, and amplitude measured with the same instrument for the 4+ year mission. Since the FFIs are not fully calibrated, we must first remove the instrumental systematics from the data and determine the flux calibration factors that can then be applied to all the stars in the field. To find these corrections, we use aperture photometry and PRF-fitting from well-characterized stars known to be stable – those with exoplanet candidates. We remove effects of the quarterly spacecraft rolls as well as longterm trends in the responsivity, which reduces the scatter in each star from 5-10% to $<1-3\%$. We examine the effects of the optical distortions that are present in the outer parts of the array, as well as source crowding throughout the field. The fluxes from the PRF fits are typically $\sim 1\%$ higher than those from the aperture photometry. We present preliminary results on previously known and new, candidate, variable stars in a test field near the center of the FFIs.

This work is supported by NASA ADAP grant NNX16AF45G.

Author(s): Melissa A Mullen¹, Kathleen Kraemer¹, T A Kuchar¹, G. C. Sloan²
Institution(s): 1. Boston College, 2. Space Telescope Science Institute

146.09 – X-rays from Cepheid Upper Atmospheres

The Cepheid pulsation cycle is driven by a wave generated in the envelope. As the wave passes through the photosphere and chromosphere at minimum radius there are many signatures of the disturbance, such as ultraviolet lines in emission and an increase in microturbulence. At this phase, however, X-rays have a low level of flux which lasts through most of the cycle. However a burst of X-ray flux occurs just after maximum radius, with a rapid rise, short duration and rapid fall similar to a stellar flare. So far observations have provided 4 examples of this, including two cycles of for Delta Cep itself. This appears to be driven by the pulsation process since it is linked to a specific phase. This is estimated to be about 0.13 stellar radii above the photosphere and may be related to the circumstellar envelopes found via interferometry, at higher levels particularly in the infrared. These new upper atmosphere diagnostics may ultimately answer questions about possible pulsation driven mass-loss.

Author(s): Nancy Evans³, Scott Engle⁵, Edward Guinan⁵, Hilding Neilson⁴, Massimo Marengo¹, Lynn Matthews², H. Moritz Guenther²
Institution(s): 1. Iowa State University, 2. MIT, 3. SAO, 4. University of Toronto, 5. Villanova University

146.10 – Spectroscopic Classification of IR-Excess IRAS Sources

We have carried out classification spectroscopy ($R \sim 2000$) of a sample of about 100 IRAS sources with excess flux at 20 microns. These were obtained with the KPNO 2.1 m and the Steward Observatory 2.3 m telescopes. Our main interest is the identification or confirmation of post-AGB objects. A number of them are indeed post-AGB, including proto-planetary nebulae. These range from K to B types, with the later showing hydrogen emission and in some cases other emission lines. Others appear to be M giants or main sequence stars, plus a couple of pre-main

sequence stars. Some of the sample have previous classifications, which we list for comparison. The post-AGB stars are being monitored for light variability. This research has been supported by the NSF (most recently AST-1413660).

Author(s): Kathryn A Willenbrink³, Bruce Hrivnak³, Kevin Volk¹, Kate Y.L. Su²

Institution(s): 1. *Space Telescope Science Institute*, 2. *University of Arizona*, 3. *Valparaiso University*

146.11 – Pulsational Light Curve Variability in Proto-Planetary Nebulae

We have monitored the light variability in post-AGB, proto-planetary nebula objects to determine their pulsation periods and amplitudes. Observations were carried out with the 0.4 m telescope at Valparaiso University, the 1.0 m SARA telescope at KPNO, and the 0.6 m SARA telescope at CTIO. Periods or quasi-periods have been found for about two dozen objects. They range from about 30 to 160 days, with the longer periods associated with the cooler stars (late-G) and the shorter periods with the hotter ones (early-F). V-band amplitudes range from 0.7 to 0.2 mag, with cooler objects having the larger amplitudes. The pulsations are complex, with multiple periods, changing periods, and/or changing amplitudes. In this study, we have included some fainter, previously unstudied proto-planetary nebulae. This research has been supported by the NSF (most recently AST-1413660).

Author(s): Bruce Hrivnak², Gary Henson¹, Wenxian Lu², Todd Hillwig²

Institution(s): 1. *East Tennessee State University*, 2. *Valparaiso University*

146.12 – Monitoring Cepheid variables using the new BYU Observation Deck Robotic Telescopes

In January 2017 work was completed on the new observation deck of the Eyring Science Center on the Brigham Young University campus. This deck was designed with pedestals to currently hold up to 5 robotic telescope systems. One of the first test projects was to monitor a sample of Classical Cepheid variables to watch for changes in the light curves. Starting with a sample of stars which had previously been monitored spectroscopically using the Dominion Astrophysical Observatory 1.2-m telescope, we collected photometric data in the H-alpha/H-beta system detailed in Joner & Hintz (2015). We will present a preliminary analysis of this data and the abilities of the new deck to monitor these type of objects.

Author(s): Adam Garth Bugg¹, Eric G Hintz¹, Michael D. Joner¹

Institution(s): 1. *Brigham Young University*

146.13 – RR Lyrae in the UMi dSph Galaxy

Over the past two years we have obtained observations of the Ursa Minor dwarf spheroidal galaxy with the goal of completing an updated catalog of the variable stars in the dwarf galaxy. In addition to finding new variable stars, this updated catalog will allow us to look at period changes in the variables and to determine stellar characteristic for the RR Lyrae stars in the dSph. We will compare the RR Lyrae stellar characteristics to other RR Lyrae stars found in the Local Group dSph galaxies; these comparisons can give us insights to the near-field cosmology of the Local Group. In this poster we present our updated catalog of RR Lyrae stars in the UMi dSph; the updated catalog includes Fourier decomposition parameters, metallicities, and other physical properties for the RR Lyrae stars.

Author(s): Charles Kuehn⁴, Karen Kinemuchi¹, Elizabeth Jeffery², Kathleen Grabowski¹, James Neme³, Daniel Herrera⁴
Institution(s): 1. *Apache Point Observatory*, 2. *Brigham Young University*, 3. *Camosun College*, 4. *University of Northern Colorado*

146.14 – Time Resolved Spectroscopy of Cepheid Variable Stars

Galactic Cepheid variable stars have been used for over a century as standard candles and as the first rung of the cosmic distance ladder, integral to the calculation of the Hubble constant. However, it is challenging to observe Cepheids within the Milky Way Galaxy because of extinction, and there are still uncertainties in the Cepheid period-luminosity relation (or Leavitt Law) that affect these important distance calculations. The Apache Point Observatory Galactic Evolution Experiment (APOGEE) survey has provided spectra for a large sample of Galactic Cepheids, but the standard chemical abundance pipeline (ASPCAP) processing is not well-suited to pulsational variables, preventing us from using them to study metallicity effect in the Leavitt Law with standard processing. Using a standalone version of the ASPCAP pipeline, we present an analysis of individual visit spectra from a test sample of nine APOGEE Cepheids, and we compare its output to the stars' literature abundance values. Based on the results of this comparison, we will be able to improve the standard analysis and process the entirety of APOGEE's Cepheid catalogue to improve its abundance measurements. The resulting abundance data will allow us to constrain the effect of metallicity on the Leavitt Law and thus allow for more accurate Cepheid distance measurements for the determination of the Hubble constant.

Author(s): Katherine Hartman¹, Rachael L. Beaton²

Institution(s): 1. *Pomona College*, 2. *Princeton University*
Contributing team(s): SDSS-IV APOGEE-2 Team

146.15 – Monitoring Period and Amplitude Changes in Classical Cepheids

Classical Cepheids are a specific class of radially pulsating variable stars and are fundamentally important to Astronomy and Cosmology. Their pulsations can be used to determine accurate distances, both inside the Milky Way and to other galaxies throughout the Universe, via the well-studied Period-Luminosity Relationship (the Leavitt Law). This makes Cepheids "standard candles," and they are helping Astronomers refine the expansion rate and age of the Universe.

Though Cepheid pulsations were long-theorized to be completely stable, we now know that they undergo small but observable changes in their pulsation periods. The rates of the period change give us invaluable information on the Cepheids themselves, and the advent of reliable all-sky photometry surveys has allowed Cepheid pulsations to be monitored more easily than ever before. Five Cepheids were analyzed for this study – AA Gem, BB Gem, RZ Gem, AD Gem, and DX Gem. Photometric data were obtained from two sources: ASAS (the All-Sky Automated Survey) and the RCT (Robotically Controlled Telescope) at Kitt Peak National Observatory in Arizona, whose consortium Villanova is a member of. This photometry is combined with available data from the literature. The two instruments combined give a longer time span, and increased precision, from which period variations can be monitored. This gives us an excellent look at how the pulsations of these 5 Cepheids are evolving over time. The pulsation behavior of the 5 Cepheids studies will be presented, along with their calculated stellar parameters.

Author(s): Mary Erickson², Scott Engle², Edward Guinan², Mark Wells¹

Institution(s): 1. *Pennsylvania State University*, 2. *Villanova University*

146.16 – Seismic Analysis of Pulsating Subdwarf B Star EPIC 212508753 Using the K2 Mission

EPIC 212508753 is a subdwarf B (hot horizontal branch, sdB) star which has been observed by the Kepler Space Telescope during its extended mission, K2, in short cadence mode where a new image is obtained roughly every minute for about 75 days. Using time series analysis of the data we have found the star to be a rare hybrid pulsator with both g- and p-mode pulsations where most of the pulsations are p modes. These pulsators are extremely important as p modes sample near the surface and g modes can

sample deeper, near to the core. This means that hybrid pulsators allow us to characterize the entire star. The hotter, predominantly p-mode pulsators are rarer so that makes EPIC 212508753 particularly interesting for seismic study. In this poster we will present preliminary results of our analysis of K2 data. We have discovered frequency multiplets in both the p- and g-mode regions which we use to identify pulsation modes and determine that EPIC 212508753 rotates like a solid body, in contrast to some other sdB stars.

Author(s): John Crooke¹, Michael D. Reed¹, Andrzej Baran³, John H. Telting², Roy H. Østensen¹

Institution(s): 1. Missouri State University, 2. Nordic Optical Telescope, 3. Pedagogical University of Kraków

146.17 – Multiband Fourier Analysis and Interstellar Reddening of the Variable Stars in the Globular Cluster NGC 6402 (M14)

We present a detailed study of the variable stars in the globular cluster NGC 6402 (M14). Approximately 1500 *B* and *V* band images were collected from July 2016 to August 2017 using the

147 – Circumstellar Disks Poster Session

147.01 – A Search for Circumstellar Gas-Disk Variability in F-type Stars

Over the past six years, short-term (night-to-night) variability in the CaII K-line (3933Å) absorption has been detected towards 22 rapidly-rotating A-type stars, all but four of them discovered by us. Most of these stars are young (age < 100 million years) and possess dusty debris disks as evidenced by their infrared excesses. The variability is thought to be due to kilometer-sized planetesimals (i.e., exocomets) that release gas during their catastrophic in-falls towards their central star. To expand the relatively small number of systems showing this type of variability, we conducted a search amongst nearby, rapidly-rotating, F-type stars. Here, we present high signal-to-noise, medium-resolution spectral observations of the CaII K-line absorption ($R \approx 60,000$) recorded towards seven F-type stars. Six of these stars were observed multiple times over the course of our seven-night run on the 2.1-meter Otto Struve Telescope (McDonald Observatory) during June 2017. The appearance or absence of similar short-lived, Doppler-shifted absorption in F-type stars serves as a test of our understanding of the underlying phenomena.

Author(s): Ally Adkins¹, Sharon Lynn Montgomery¹, Barry Welsh²

Institution(s): 1. Clarion University, 2. Space Sciences Laboratory, UC Berkeley

147.02 – Effect of Different Angular Momentum Transport Mechanisms on the Radial Volatile Distribution in Protoplanetary Disks

How circumstellar disks evolve and transport angular momentum is a mystery even until today. Magnetorotational instability (MRI; [1]) earlier thought to be a primary driver of disk evolution, has been found to be not as strong a candidate in cold insufficiently ionized protoplanetary disks where non-ideal MHD effects take over to efficiently suppress the instability [2][3]. In the past few years, recent studies have proposed different mechanisms such as magnetically-driven disk winds [4][5], convective overstability [6], and the vertical shear instability (VSI)[7] to be likely drivers of disk evolution. In this work, we consider numerically [8] and/or parametrically derived radial α profiles of three different mechanisms of angular momentum transport (hydrodynamic instabilities such as VSI, disk winds, and MRI) to understand how the underlying disk structure changes and evolves with each mechanism. We overlay our snowline model that incorporates the advection and diffusion of volatiles as well as radial drift of solids [9] to understand how different α profiles can affect the distribution of water in the disk.

References: [1] Balbus, S.A., & Hawley, J.F., 1998, Rev. of Mod.

SARA Consortium Jacobus Kapteyn 1-meter telescope located in the Canary Islands. Using difference image analysis, we were able to identify 145 probable variable stars, confirming the 133 previously known variables and adding 12 new variables. The variables consisted of 117 RR Lyrae stars, 18 long period variables, 2 eclipsing variables, 6 Cepheid variables, and 2 SX Phoenix variables. Of the RR Lyrae variables 55 were of fundamental mode RR0 stars, of which 18 exhibited the Blazhko effect, 57 were of 1st overtone RR1, of which 7 appear to exhibit the Blazhko effect, 1 2nd overtone RR2, and 2 double mode variables. We found an average period of 0.59016 days for RR0 stars and 0.30294 days for RR1 stars. Using the multiband light curves of both the RR0 and RR1 variables we found an average $E(B-V)$ of 0.604 with a scatter of 0.15 magnitudes. Using Fourier decomposition of the RR Lyrae light curves we also determined the metallicity and distance of the NGC 6402.

Author(s): Sedrick Weinschenk¹, Brian Murphy¹, Nathan J Villiger¹

Institution(s): 1. Butler University

Phys., 70, 1 [2] Bai, X.-N., & Stone, J.M. 2011, ApJ, 736, 144 [3] Bai, X.-N., & Stone, J.M., 2013, ApJ, 769, 76 [4] Bai, X.-N., 2016, ApJ, 821, 80 [5] Suzuki, T.K., Ogihara, M., Morbidelli, A., Crida, A., & Guillot, T., 2016, A&A, 596, A74 [6] Klahr, H., & Hubbard, A. 2014, ApJ, 788, 21 [7] Stoll, M.H.R., & Kley, W. 2014, A&A, 572, A77 [8] Kalyaan, A., Desch, S.J., & Monga, N., 2015, ApJ, 815, 112 [9] Desch, S.J., Estrada, P.R., Kalyaan, A., & Cuzzi, J.N., 2017, ApJ, 840, 86

Author(s): Anusha Kalyaan¹, Steven Desch¹

Institution(s): 1. Arizona State University

147.03 – Impact of Fractal Grains on Protoplanetary Disk Evolution

Protoplanetary disk lifetimes are well constrained by observations: around 10 Myr. However, as particle growth proceeds in the disk, solids are expected to radially drift inwards toward the star much earlier in the disks lifetime and can lead to depletion of both the inner and outer disk regions, posing a problem for planet formation. Disk evolution models usually assume disks are composed of gas and purely spherical, solid dust grains. Dust grains are assumed to be spheres for simplicity, but this is incorrect as dust grains likely initially form as fractal, porous aggregates at least up to mm-cm sizes slowing their inward drift. Thus, by incorporating fractal grains and consequent opacities into our protoplanetary disk evolution models, we are able to increase the retention of dust. Here we present a parameter space exploration that shows that invoking fractal grains can solve the discrepancy between theory and observations of dust disk evolution.

Author(s): Sean Haas¹, Uma Gorti², Paul Estrada²

Institution(s): 1. Humboldt State University, 2. SETI Institute

147.04 – A sample of potential disk hosting first ascent red giants

Observations of (sub)giants with planets and disks provide the first set of proof that disks can survive the first stages of post-main-sequence evolution, even though the disks are expected to dissipate by this time. The infrared (IR) excesses present around a number of post-main-sequence (PMS) stars could be due to a traditional debris disk with planets (e.g. kappa CrB), some remnant of enhanced mass loss (e.g. the shell-like structure of R Sculptoris), and/or background contamination. We present a sample of potential disk hosting first ascent red giants. These stars all have infrared excesses at 22 microns, and possibly host circumstellar debris. We summarize the characteristics of the sample to better inform the incidence rates of thermally emitting material around giant stars. A thorough follow-up study of these candidates would serve as the first step in probing the

composition of the dust in these systems that have left the main sequence, providing clues to the degree of disk processing that occurs beyond the main-sequence.

Author(s): Amy Steele², John Debes¹
Institution(s): 1. *Space Telescope Science Institute*, 2. *University of Maryland*

147.05 – Determining Disk Parameters for the Classical Be Star 59 Cyg

The density structure of the gaseous disks around classical Be stars offers strong clues to their formation mechanism, whether it is through viscous accretion, binary interactions, or magnetized flows. Infrared observations are useful in constraining the density structure because the inner disks of Be stars can be optically thick at these wavelengths. By combining SED analysis with infrared interferometric imaging using the MIRC instrument on the CHARA Array, we can determine the radial density structure of the disk along with other important geometric parameters. We used a radiative transfer model, careful to properly include the effects of oblateness and gravity-darkening of the stellar surface while also accounting for absorption of the photosphere due to the inner disk. We present first results for the Be star 59 Cyg, finding evidence in favor of the accretion disk model.

Author(s): Andrea Lin², John D Monnier², Aaron Sigut³, Gail Schaefer¹
Institution(s): 1. *CHARA Array*, 2. *University of Michigan*, 3. *University of Western Ontario*

147.06 – Modeling Protoplanetary Disks

Using spectra models with known parameters and comparing them to spectra gathered from real systems is often the only way to find out what is going on in those real systems. This project uses the modeling programs of RADMC-3D to generate model spectra for systems containing protoplanetary disks. The parameters can be changed to simulate protoplanetary disks in different stages of planet formation, with different sized gaps in different areas of the disks, as well as protoplanetary disks that contain different types of dust. We are working on producing a grid of models that all have different variations in the parameters in order to generate a miniature database to use for comparisons to gathered spectra. The spectra produced from these simulations will be compared to spectra that have been gathered from systems in the Small Magellanic cloud in order to find out the contents and stage of development of that system. This allows us to see if and how planets are forming in the Small Magellanic cloud, a region which has much less metallicity than our own galaxy. The data we gather from comparisons between the model spectra and the spectra of systems in the Small Magellanic Cloud can then be applied to how planets may have formed in the early universe.

Author(s): Megan Holman¹, Drake Tubbs¹, L. D. Keller¹
Institution(s): 1. *Ithaca College*

147.07 – Veiling and Accretion Around the Young Binary Stars S and VV Corona Australis

S CrA and VV CrA are two young binary star systems with separations of 170 AU and 250 AU, respectively, in the southern star-forming region Corona Australis. The spectral types of the four stars in these two systems are similar, approximately K7 to M1, hence the stellar masses are also similar. The study of young stars just emerging from their natal cloud cores at the very limits of observability allows us to probe the extreme environments in which planet formation begins to occur. Stars in this early evolutionary stage can have circumstellar or circumbinary disks, and sometimes remnants of the envelopes which surrounded them during the protostellar stage. Envelopes accrete onto disks and disks in turn accrete onto the central stars, triggering elevated continuum emission, line emission, outflows, and stellar winds. This violent stage marks the onset of the epoch of planet formation. Using high-resolution near-infrared, H-band spectroscopy from the Keck II telescope using the NIRSPEC instrument over 4-6 epochs, we are probing the chaotic

environment surrounding the four stars in these systems. We determine the spectral types for VV CrA and B for the first time, and examine the variable veiling and emission occurring around each of these stars. This research was supported in part by NSF grants AST-1461200 and AST-1313399.

Author(s): Kendall Sullivan², Lisa Prato¹, Ian Avilez³
Institution(s): 1. *Lowell Observatory*, 2. *University of Massachusetts, Amherst*, 3. *University of Virginia*

147.08 – ALMA 1.3 Millimeter Map of the HD 95086 System -- A Young Analog of the HR 8799 System

Planets and minor bodies such as asteroids, Kuiper-belt objects and comets are integral components of a planetary system. Interactions among them leave clues about the formation process of a planetary system. The signature of such interactions is best illustrated through resolved observations of its debris disk. Here we present ALMA 1.3 mm observations of HD 95086, a young analog of the HR 8799 system, that hosts a directly imaged giant planet b and a massive debris disk with both asteroid- and Kuiper-belt analogs. The location of the Kuiper-belt analog is resolved for the first time. Our deep ALMA map also reveals a bright source located near the edge of the ring. The properties of the source, based on limited data, are consistent with it being a luminous star-forming galaxy at high redshift. We will discuss future, resolved observations of debris disks, highlighting the potential of the Origins Space Telescope (OST), one of the four science and technology definition studies commissioned by NASA Headquarters for the 2020 Astronomy and Astrophysics Decadal survey.

Author(s): Kate Su⁵, Meredith Ann MacGregor³, Mark Booth¹, David Wilner³, Renu Malhotra⁴, Sarah Morrison²
Institution(s): 1. *Astrophysikalisches Institut und Universitätssternwarte*, 2. *Center for Exoplanets & Habitable Worlds, Pennsylvania State University*, 3. *CfA*, 4. *Lunar and Planetary Laboratory, University of Arizona*, 5. *Steward Observatory, University of Arizona*
Contributing team(s): OST STDT

147.09 – Characterizing Protoplanetary Disks in a Young Binary in Orion

Planetary systems form in circumstellar disks of gas and dust surrounding young stars. One open question in the study of planet formation involves understanding how different environments affect the properties of the disks and planets they generate. Understanding the properties of disks in high-mass star forming regions (SFRs) is critical since most stars - probably including our Sun - form in those regions. By comparing the disks in high-mass SFRs to those in better-studied low-mass SFRs we can learn about the role environment plays in planet formation. Here we present 0.5" resolution observations of the young two-disk binary system V2434 Ori in the Orion Nebula from the Atacama Large Millimeter/submillimeter Array (ALMA) in molecular line tracers of CO(3-2), HCN(4-3), HCO+(4-3) and CS(7-6). We model each disk's mass, radius, temperature structure, and molecular abundances, by creating synthetic images using an LTE ray-tracing code and comparing simulated observations with the ALMA data in the visibility domain. We then compare our results to a previous study of molecular line emission from a single Orion protoplanetary disk, modeled using similar methods, and to previously characterized disks in low-mass SFRs to investigate the role of environment in disk chemistry and planetary system formation.

Author(s): Jonas Powell³, A. Meredith Hughes³, Rita Mann¹, Kevin Flaherty³, James Di Francesco¹, Jonathan Williams²
Institution(s): 1. *NRC Herzberg*, 2. *University of Hawai'i at Manoa*, 3. *Wesleyan University*

147.10 – The Mass Evolution of Protostellar Disks and Envelopes in the Perseus Molecular Cloud

<!--StartFragment-->In the standard picture for low-mass star formation, a dense molecular cloud undergoes gravitational collapse to form a protostellar system consisting of a new central star, a circumstellar disk, and a surrounding envelope of remaining material. The mass distribution of the system evolves as matter accretes from the large-scale envelope through the disk and onto the protostar. While this general picture is supported by simulations and indirect observational measurements, the specific timescales related to disk growth and envelope dissipation remain poorly constrained. We present a rigorous test of a method introduced by Jørgensen et al. (2009) to obtain observational mass measurements of disks and envelopes around embedded protostars from unresolved (resolution of ~ 1000 AU) observations. Using data from the recent Mass Assembly of Stellar Systems and their Evolution with the SMA (MASSES) survey, we derive disk and envelope mass estimates for 59 protostellar systems in the Perseus molecular cloud. We compare our results to independent disk mass measurements from the VLA Nascent Disk and Multiplicity (VANDAM) survey and find a strong linear correlation. Then, leveraging the size and uniformity of our sample, we find no significant trend in protostellar mass distribution as a function of age, as approximated from bolometric temperatures. These results may indicate that the disk mass of a protostar is set near the onset of the Class 0 protostellar stage and remains roughly constant throughout the Class I protostellar stage.<!--EndFragment-->

Author(s): Bridget Andersen⁴, Ian Stephens¹, Michael Dunham³, Riway Pokhrel¹, Jes Jørgensen², Søren Frimann²
Institution(s): 1. *Harvard-Smithsonian Center for Astrophysics*, 2. *Niels Bohr Institute and Natural History Museum of Denmark*, 3. *State University of New York at Fredonia*, 4. *University of Virginia*

147.11 – A Panchromatic Study of Molecular Gas in the Protoplanetary System RY Lupi

To understand how planet formation occurs in protoplanetary disks, we must first characterize the behavior of material within 10 AU of the central star. We present a study of molecular gas at these radii in the disk around the young star RY Lupi, through spectra from *HST*-COS, *HST*-STIS, and VLT-CRIFES. We model the radial distribution of flux from hot ($T \sim 2000$ K) molecular gas in a surface layer between $r = 0.1$ -10 AU, as traced by LyA-pumped H₂. The result indicates that the H₂ emission originates in a narrow ring centered at 1 AU, with a sharp decline in flux at $r < 0.1$ AU that is consistent with what is expected for transitional disks. When we adopt a more basic approach to evaluate the shapes of the emission lines, we find that a two-component Gaussian profile assuming two rings of gas in the inner disk provides a statistically better fit to the H₂ emission lines than the single-component model of a smooth disk. This two-component profile includes broad (FWHM_{broad}, H₂ = 105 +/- 15 km/s) and narrow (FWHM_{narrow}, H₂ = 43 +/- 13 km/s) lines, corresponding to average gas radii of $\langle r_{\text{broad, H}_2} \rangle \sim 0.4$ AU and $\langle r_{\text{narrow, H}_2} \rangle \sim 3$ AU. An analysis of the spatial origin of 4.7 micron ¹²CO emission shows that this population of warm ($T \sim 1500$ K) gas also produces two-component emission line profiles ($\langle r_{\text{broad, CO}} \rangle \sim 0.4$ AU, $\langle r_{\text{narrow, CO}} \rangle \sim 15$ AU), indicating again that the inner disk is radially stratified. Despite the evidence that this is a transitional disk system, we detect UV CO absorption that is not typically seen in more evolved systems. We model these features along with IR CO absorptions to constrain the properties of the cooler ($T \sim 100$ -300 K) disk atmosphere.

Author(s): Nicole Arulanantham², Kevin France², Keri Hoadley¹
Institution(s): 1. *California Institute of Technology*, 2. *Laboratory for Atmospheric and Space Physics*

147.12 – Using modern imaging techniques to old HST data: a summary of the ALICE program.

Direct imaging of extrasolar systems is a powerful technique to study the physical properties of exoplanetary systems and understand their formation and evolution mechanisms. The

detection and characterization of these objects are challenged by their high contrast with their host star. Several observing strategies and post-processing algorithms have been developed for ground-based high-contrast imaging instruments, enabling the discovery of directly-imaged and spectrally-characterized exoplanets. The Hubble Space Telescope (HST), pioneer in directly imaging extrasolar systems, has yet been often limited to the detection of bright debris disks systems, with sensitivity limited by the difficulty to implement an optimal PSF subtraction strategy, which is readily offered on ground-based telescopes in pupil tracking mode.

The Archival Legacy Investigations of Circumstellar Environments (ALICE) program is a consistent re-analysis of the 10 year old coronagraphic archive of HST's NICMOS infrared imager. Using post-processing methods developed for ground-based observations, we used the whole archive to calibrate PSF temporal variations and improve NICMOS's detection limits. We have now delivered ALICE-reprocessed science products for the whole NICMOS archival data back to the community. These science products, as well as the ALICE pipeline, were used to prototype the JWST coronagraphic data and reduction pipeline. The ALICE program has enabled the detection of 10 faint debris disk systems never imaged before in the near-infrared and several substellar companion candidates, which we are all in the process of characterizing through follow-up observations with both ground-based facilities and HST-STIS coronagraphy. In this publication, we provide a summary of the results of the ALICE program, advertise its science products and discuss the prospects of the program.

Author(s): Elodie Choquet⁵, Remi Soummer⁸, Marshall Perrin⁸, Laurent Pueyo⁸, James Brendan Hagan⁸, Neil Zimmerman⁷, John Henry Debes⁸, Glenn Schneider¹, Bin Ren⁴, Julien Milli³, Schuyler Wolff⁶, Chris Stark⁸, Dimitri Mawet², David A Golimowski⁸, Dean C Hines⁸, Aki Roberge⁷, Eugene Serabyn⁵
Institution(s): 1. *ASU*, 2. *Caltech*, 3. *ESO*, 4. *JHU*, 5. *JPL - Caltech*, 6. *Leiden University*, 7. *NASA GSFC*, 8. *STScI*

147.13 – Rings of Molecular Line Emission in the Disk Orbiting the Young, Close Binary V4046 Sgr

We present analysis of a suite of subarcsecond ALMA Band 6 (1.1 - 1.4 mm) molecular line images of the circumbinary, protoplanetary disk orbiting V4046 Sgr. The ~ 20 Myr-old V4046 Sgr system, which lies a mere ~ 73 pc from Earth, consists of a close (separation ~ 10 R_{sun}) pair of roughly solar-mass stars that are orbited by a gas-rich circumbinary disk extending to ~ 350 AU in radius. The ALMA images reveal that the molecules CO and HCN and their isotopologues display centrally peaked surface brightness morphologies, whereas the cyanide group molecules (HC₃N, CH₃CN), deuterated molecules (DCN, DCO⁺), hydrocarbons (as traced by C₂H), and potential CO ice line tracers (N₂H⁺, and H₂CO) appear as a sequence of sharp and diffuse rings of increasing radii. The characteristic sizes of these molecular emission rings, which range from ~ 25 to >100 AU in radius, are evident in radial emission-line surface brightness profiles extracted from the deprojected disk images. We find that emission from ¹³CO emission transitions from optically thin to thick within ~ 50 AU, whereas C₁₈O emission remains optically thin within this radius. We summarize the insight into the physical and chemical processes within this evolved protoplanetary disk that can be obtained from comparisons of the various emission-line morphologies with each other and with that of the continuum (large-grain) emission on size scales of tens of AU.

This research is supported by NASA Exoplanets program grant NNX16AB43G to RIT

Author(s): Dorothy Dickson-Vandervelde⁶, Joel H Kastner⁶, C. Qi⁸, Thierry Forveille⁴, Pierre Hily-Blant⁴, Karin Oberg³, David Wilner⁸, Sean Andrews⁸, Uma Gorti⁷, Valerie Rapson², Germano Sacco¹, David Principe⁵

Institution(s): 1. *Arecibo Observatory*, 2. *Dudley Observatory*, 3. *Harvard University*, 4. *IPAG*, 5. *MIT*, 6. *Rochester Institute of Technology*, 7. *SETI Institute*, 8. *Smithsonian Institution*

147.14 – Hydrodynamic Simulations of Protoplanetary Disks with GIZMO

Over the past several decades, the field of computational fluid dynamics has rapidly advanced as the range of available numerical algorithms and computationally feasible physical problems has expanded. The development of modern numerical solvers has provided a compelling opportunity to reconsider previously obtained results in search for yet undiscovered effects that may be revealed through longer integration times and more precise numerical approaches. In this study, we compare the results of past hydrodynamic disk simulations with those obtained from modern analytical resources. We focus our study on the GIZMO code (Hopkins 2015), which uses meshless methods to solve the homogeneous Euler equations of hydrodynamics while eliminating problems arising as a result of advection between grid cells. By comparing modern simulations with prior results, we hope to provide an improved understanding of the impact of fluid mechanics upon the evolution of protoplanetary disks.

Author(s): Malena Rice¹, Greg Laughlin¹
Institution(s): 1. *Yale University*

147.15 – Resolved Dual-Frequency Observations of the Debris Disk Around AU Mic: Strengths of Bodies in the Collisional Cascade

Debris disks are hallmarks of mature planetary systems, with second-generation dust produced via collisions between pluto-like planetesimals. The vertical structure of a debris disk encodes unique information about the dynamical state of the system, particularly at millimeter wavelengths where gravitational effects dominate over the effects of stellar radiation. We present 450 μm Atacama Large Millimeter/sub-millimeter Array (ALMA) observations of the edge-on debris disk around AU Mic, a nearby ($d = 9.91 \pm 0.10$ pc) M1-type star. The 0.3" angular resolution of the data allows us to spatially resolve the scale height of the disk, complementing previous observations at a wavelength of 1.3 mm. By resolving the vertical structure of the disk at these two widely-separated frequencies, we are able to spatially resolve the spectral index and study variations in the grain size distribution as a function of disk radius. The comparison of scale heights for two different wavelengths and therefore particle sizes also constrains the velocity dispersion as a function of grain size, which allows us to probe the strengths of bodies in the collisional cascade for the first time outside the Solar System.

Author(s): Evan Carter⁸, A. Meredith Hughes⁸, Cail Daley⁸, Kevin Flaherty⁸, Margaret Pan⁵, Hilke Schlichting⁷, Eugene Chiang⁶, Meredith Ann MacGregor², David Wilner³, Bill Dent¹, John Carpenter¹, Sean Andrews³, Attila Moor⁴, Agnes Kospal⁴
Institution(s): 1. *ALMA/JAO*, 2. *Carnegie DTM*, 3. *Harvard-Smithsonian Center for Astrophysics*, 4. *Konkoly Observatory*, 5. *Massachusetts Institute of Technology*, 6. *University of California, Berkeley*, 7. *University of California, Los Angeles*, 8. *Wesleyan University*

147.16 – Searching for Faint Traces of CO(2-1) and HCN(4-3) Gas In Debris Disks

The surprising presence of molecular gas in the debris disks around main sequence stars provides an opportunity to study the dissipation of primordial gas and, potentially, the composition of gas in other solar systems. Molecular gas is not expected to survive beyond the pre-main sequence phase, and it is not yet clear whether the gas is a remnant of the primordial protoplanetary material or whether the gas, like the dust, is second-generation material produced by collisional or

photodesorption from planetesimals, exocomets, or the icy mantles of dust grains. Here we present two related efforts to characterize the prevalence and properties of gas in debris disks. First, we place the lowest limits to date on the CO emission from an M star debris disk, using 0.3" resolution observations of CO(2-1) emission from the AU Mic system with the Atacama Large Millimeter/submillimeter Array (ALMA). We place a 3-sigma upper limit on the integrated flux of 0.39 Jy km/s, corresponding to a maximum CO mass of 5×10^{-6} (Earth Masses) if the gas is in LTE. We also present the results of an ALMA search for HCN(4-3) emission from the prototypical gas-rich debris disk around 49 Ceti at a spatial resolution of 0.3". Despite hosting one of the brightest CO-rich debris disks yet discovered, our observations of 49 Ceti also yield a low upper limit of 0.057 Jy km/s in the HCN line, leaving CO as the only molecule clearly detected in emission from a debris disk. We employ several methods of detecting faint line emission from debris disks, including a model based on Keplerian kinematics as well as a spectral shifting method previously used to detect faint CO emission from the Fomalhaut debris disk, and compare our results.

Author(s): Zachary Stafford Lambros¹, A. Meredith Hughes¹

Institution(s): 1. *Wesleyan University*

147.17 – Molecular Gas in Disks around Young Stars with ALMA

Molecular gas is a critical component of the planet formation process. In this poster, we present two analyses of the molecular gas component of circumstellar disks at extremes (young, old) of the pre-main sequence phase.

(1) We characterize the molecular gas content of the disk around d216-0939, a pre-main sequence star in the Orion Nebula Cluster, using ALMA observations of CO(3-2), HCO+(4-3), and HCN(4-3) observed at 0.5" resolution. We model the density and temperature structure of the disk, returning abundances generally consistent with chemical modeling of protoplanetary disks, and obtain a dynamical mass measurement of the central star of $2.2 \pm 0.4 M_{\text{sun}}$, which is inconsistent with the previously determined spectral type of K5. We also report the detection of a spatially unresolved high-velocity blue-shifted excess emission feature with a measurable position offset from the central star, consistent with an object in Keplerian orbit at 60 ± 20 au. The feature is due to a local temperature and/or density enhancement consistent with either a hydrodynamic vortex or the expected signature of the envelope of a forming protoplanet within the disk, providing evidence that planet formation is ongoing within this massive and relatively isolated Orion proplyd. This work is published in Factor et al. (2017). (2) We present $\sim 0.4''$ resolution images of CO(3-2) and associated continuum emission from the gas-bearing debris disk around the nearby A star 49 Ceti, observed with ALMA. We analyze the ALMA visibilities in tandem with the broadband spectral energy distribution to measure the radial surface density profiles of dust and gas emission from the system. The radial extent of the gas disk (~ 220 au) is smaller than that of the dust disk (~ 300 au), consistent with recent observations of other gas-bearing debris disks. While there are so far only three broad debris disks with well characterized radial dust profiles at millimeter wavelengths, 49 Ceti's disk shows a markedly different structure from two radially resolved gas-poor debris disks, implying that the physical processes generating and sculpting the gas and dust are fundamentally different. This work is published in Hughes et al. (2017).

Author(s): A. Meredith Hughes¹¹, Samuel Factor¹⁰, Jesse Lieman-Sifry¹¹, Kevin Flaherty¹¹, Cail Daley¹¹, Rita Mann⁶, Aki Roberge⁵, James Di Francesco⁶, Jonathan Williams⁹, Luca Ricci⁷, Brenda Matthews⁶, John Bally¹, Doug Johnstone⁶, Agnes Kospal⁴, Attila Moor⁴, Inga Kamp³, David Wilner², Sean Andrews², Joel H Kastner⁸, Peter Abraham⁴

Institution(s): 1. *CU Boulder*, 2. *Harvard-Smithsonian CfA*, 3. *Kapteyn Astronomical Institute*, 4. *Konkoly Observatory*, 5. *NASA GSFC*, 6. *NRC Herzberg*, 7. *Rice University*, 8. *Rochester Institute of Technology*, 9. *U Hawaii - Manoa*, 10. *UT Austin*, 11. *Wesleyan University*

147.18 – Using Vertical Structure to Infer the Total Mass Hidden in a Debris Disk

Disks of optically thin debris dust surround $\geq 20\%$ of main sequence stars and mark the final stage of planetary system evolution. The features of debris disks encode dynamical interactions between the dust and any unseen planets embedded in the disk. The vertical distribution of the dust is particularly sensitive to the total mass of planetesimal bodies in the disk, and is therefore well suited for constraining the prevalence of otherwise unobservable Uranus and Neptune analogs. Inferences of mass from debris disk vertical structure have previously been applied to infrared and optical observations of several systems, but the smaller particles traced by short-wavelength observations are ‘puffed up’ by radiation pressure, yielding only upper limits on the total embedded mass. The large grains that dominate the emission at millimeter wavelengths are essentially impervious to the effects of stellar radiation, and therefore trace the underlying mass distribution more directly. Here we present 1.3mm dust continuum observations of the debris disk around the nearby M star AU Mic with the Atacama Large Millimeter/submillimeter Array (ALMA). The 3 au spatial resolution of the observations, combined with the favorable edge-on geometry of the system, allows us to measure the vertical structure of a debris disk at millimeter wavelengths for the first time. We analyze the data using a ray-tracing code that translates a 2-D density and temperature structure into a model sky image of the disk. This model image is then compared directly to the interferometric data in the visibility domain, and the model parameters are explored using a Markov Chain Monte Carlo routine. We measure a scale height-to-radius ratio of 0.03, which we then compare to a theoretical model of steady-state, size-dependent velocity distributions in the collisional cascade to infer a total mass within the disk of ~ 1.7 Earth masses. These measurements rule out the presence of a gas giant or Neptune analog in the outer disk, but are suggestive of the presence of large planetesimals required to stir the dust distribution.

Author(s): Cail Daley⁸, A. Meredith Hughes⁸, Evan Carter⁸, Kevin Flaherty⁸, Zachary Stafford Lambros⁸, Margaret Pan⁵, Hilke Schlichting⁷, Eugene Chiang⁶, David Wilner³, Bill Dent¹, John Carpenter¹, Sean Andrews³, Meredith Ann MacGregor², Attila Moor⁴, Agnes Kospal⁴

Institution(s): 1. ALMA/JAO, 2. Carnegie Institution for Science, 3. Harvard-Smithsonian CfA, 4. Konkoly Observatory, 5. MIT, 6. UC Berkeley, 7. UCLA, 8. Wesleyan University

147.19 – WFIRST: CGI Detection and Characterization of Circumstellar Disks

The WFIRST Coronagraphic Instrument (CGI) will be capable of obtaining up to 5×10^{-9} contrast to an inner working angle of ~ 150 mas for a selection of medium band visible light filters using shaped pupil coronagraph and hybrid Lyot coronagraph designs. We present initial work at defining the scientific capabilities of the CGI with respect to different types of circumstellar disks, including warm exo-zodiacal disks, cold debris disks, and protoplanetary disks. With the above designs, CGI will be able to detect bright protoplanetary and debris disks with sizes of >100 AU beyond 500 pc. Additionally, it will be able to discover warm exozodiacal dust disks ten times more massive than that of the Solar System for over 100 nearby solar-type stars. Finally, it will be able to characterize resolved circumstellar dust disks in multiple filters of visible light, providing constraints on the size, shape, and composition of the dust.

Author(s): John Debes⁶, Christine Chen⁶, Bekki Dawson⁸, Ewan S Douglas⁴, Gaspard Duchene¹⁰, Hannah Jang-Condell¹¹, Dean C Hines⁶, Nikole K. Lewis⁶, Bruce Macintosh⁵, Johan Mazoyer⁷, Tiffany Meshkat³, Bijan Nemati⁹, Rahul Patel³, Marshall Perrin⁶, Charles Poteet⁶, Laurent Pueyo⁶, Bin Ren⁷, Maxime Rizzo², Aki Roberge², Chris Stark⁶, Margaret Turnbull¹¹

Institution(s): 1. Global Science Institute, 2. Goddard Space Flight Center, 3. IPAC, 4. Massachusetts Institute of Technology, 5. Stanford University, 6. STScI, 7. The Johns Hopkins University, 8. The Pennsylvania State University, 9. The University of Alabama Huntsville, 10. University of California, Berkeley, 11. University of Wyoming

148 – Extrasolar Planets: Characterization and Theory Poster Session

148.01 – Origins and Destinations: Tracking Planet Composition through Planet Formation Simulations

There are now several thousand confirmed exoplanets, a number which far exceeds our resources to study them all in detail. In particular, planets around M dwarfs provide the best opportunity for in-depth study of their atmospheres by telescopes in the near future. The question of which M dwarf planets most merit follow-up resources is a pressing one, given that NASA’s TESS mission will soon find hundreds of such planets orbiting stars bright enough for both ground and spaced-based follow-up. Our work aims to predict the approximate composition of planets around these stars through n-body simulations of the last stage of planet formation. With a variety of initial disk conditions, we investigate how the relative abundances of both refractory and volatile compounds in the primordial planetesimals are mapped to the final planet outcomes. These predictions can serve to provide a basis for making an educated guess about (a) which planets to observe with precious resources like JWST and (b) how to identify them based on dynamical clues.

Author(s): Quadry Chance², Sarah Ballard¹

Institution(s): 1. Massachusetts Institute of Technology, 2. University of Arizona

148.02 – Atmospheric Retrievals of HAT-P-16b and WASP-11b/HAT-P-10b

We report Bayesian atmospheric retrievals performed on the exoplanets HAT-P-16b and WASP-11b/HAT-P-10b. HAT-P-16b is a hot (equilibrium temperature 1626 ± 40 K, assuming zero Bond albedo and efficient energy redistribution), 4.19 ± 0.09 Jupiter-

mass exoplanet orbiting an F8 star every 2.775960 ± 0.000003 days (Buchhave et al 2010). WASP-11b/HAT-P-10b is a cooler (1020 ± 17 K), 0.487 ± 0.018 Jupiter-mass exoplanet orbiting a K3 star every 3.7224747 ± 0.0000065 days (Bakos et al. 2009, co-discovered by West et al. 2008). We observed secondary eclipses of both planets using the 3.6 μm and 4.5 μm channels of the Spitzer Space Telescope’s Infrared Array Camera (program ID 60003). We applied our Photometry for Orbits, Eclipses, and Transits (POET) code to produce normalized eclipse light curves, and our Bayesian Atmospheric Radiative Transfer (BART) code to constrain the temperature-pressure profiles and atmospheric molecular abundances of the two planets. Spitzer is operated by the Jet Propulsion Laboratory, California Institute of Technology, under a contract with NASA. This work was supported by NASA Planetary Atmospheres grant NNX12AI69G and NASA Astrophysics Data Analysis Program grant NNX13AF38G.

Author(s): Kathleen McIntyre³, Joseph Harrington³, Ryan Challener³, Maria Lenius¹, Joel D Hartman², Gaspar A Bakos², Jasmina Blečić³, Patricio E Cubillos³, Andrew Cameron⁴

Institution(s): 1. Max Planck Institute for Astronomy, 2. Princeton University, 3. University of Central Florida, 4. University of St. Andrews

148.03 – Exoplanet detection synergies between Gaia and the WFIRST Coronagraph

WFIRST (Wide-Field Infrared Survey Telescope) is a NASA mission designed to study dark energy, exoplanets, and infrared astrophysics over a six-year period. One of WFIRST’s instruments, the Coronagraph Instrument (CGI), will use advanced technology to image exoplanets and characterize their

atmospheres in reflected starlight. We used a Monte Carlo approach to model the population of planets around nearby stars (distance < 20 pc), and then applied the detection limitations of Gaia and WFIRST CGI. The distribution model predicts that Gaia observations of bright, single stars ($3 < G \text{ mag} < 6$) will yield around 9 planets, 3 of which will be accessible to the spectroscopic characterization mode of WFIRST CGI.

Author(s): William Charles Fanning¹, Neil Zimmerman³, Michael McElwain³, Gabriel Grell²

Institution(s): 1. *Embry-Riddle Aeronautical University*, 2. *Harvard University*, 3. *NASA Goddard Space Flight Center*

148.04 – 3D hydrodynamic simulations of tidal disruption of terrestrial planets around white dwarfs

Recent K2 mission spotted striking variability due to a group of minor bodies transiting white dwarf WD 1145+017 with periods ranging from 4.5 hours to 4.9 hours. One of the formation scenarios is that those transiting objects are the debris of a tidally disrupted minor planet. This scenario is consistent with fact that the white dwarf also hosts a dusty disk and displays strong metal atmospheric pollution. In this work, we perform state-of-the-art three-dimensional hydrodynamic simulations to study the consequences of tidal disruption of planets with various differentiated compositions by a white dwarf. We study the general outcomes of tidal disruption including partially disruption and total disruption. We also apply our results to the WD 1145+017 system to infer the physical and orbital properties of the progenitor.

Author(s): Shangfei Liu², Jinsu Zhang³, Douglas N. C. Lin¹

Institution(s): 1. *Department of Astronomy and Astrophysics, University of California, Santa Cruz*, 2. *Department of Physics and Astronomy, Rice University*, 3. *Department of Physics, Tsinghua University*

148.05 – The Death Spiral of the Hot Jupiter Exoplanet HD 189733b

HD 189733 is a quintessential example of hot Jupiter-type exoplanet systems in which a gas giant planet with a mass similar to Jupiter is orbiting extremely close to its host star. HD 189733 is the nearest and brightest hot Jupiter system discovered so far and undergoes transit eclipses. Because of this, HD 189733 is well studied across the electromagnetic spectrum. It consists of a 7.7 mag K1.5 V host star and a Jupiter-size planet orbiting with a period of $P = 2.22$ days, only located only 0.030 AU from its host star.

About ten years ago HD 189733 system was discovered to be accompanied by gravitationally-bound red dwarf M4 V star companion (HD 189733 B). It was found previously by Guinan et al. (2017) that the age measurement (~ 0.7 Gyr) of the K-type star indicated by its 11.95 day rotation period and corresponding moderately high levels of coronal X-ray and chromospheric emissions do not agree with the much older age of $\sim 6 - 9$ Gyr indicated from the low X-ray activity of the dM companion star. This age discrepancy is can be resolved by assuming an increase in angular momentum or “spin-up” of the HD 189733A by its hosted planet. It is probable is that this extra angular momentum was acquired from the orbiting exoplanet from the tidal and magnetic interactions of the planet and host star.

Photometric observations of the planetary transit eclipses of HD 189733b have been carried out for over 11 years. Using new transit timings that we have obtained with the 1.3-m Robotically Controlled Telescope (RCT) when combined with numerous timings available in the literature, we have discovered a very small decrease in the orbital period of the HD 189733b. The change in period is $dP/dt = 0.87 \text{ sec}/100 \text{ yrs}$. This finding support the transfer of orbital angular momentum of the planet to the host star - thus spinning-up the host star and shrinking the orbit of the planet. At this rate of period decrease, the planet will be tidally disrupted in less than 40 million years. However, this

planetary disruption will likely occur much sooner because the decrease in the planet’s orbital period is expected to speed-up as the planet gets closer to the star.

Author(s): Liam Dowling Jones¹, Lucas Marchioni¹, Edward Guinan¹, Scott Engle¹

Institution(s): 1. *Villanova*

148.06 – Zodiacal Exoplanets in Time: Searching for Young Stars in K2

Observations of planetary systems around young stars provide insight into the early stages of planetary system formation. Nearby young open clusters such as the Hyades, Pleiades, and Praesepe provide important benchmarks for the properties of stellar systems in general. These clusters are all known to be less than 1 Gyr old, making them ideal targets for a survey of young planetary systems. Few transiting planets have been detected around clusters stars, however, so this alone is too small of a sample. K2, the revived *Kepler* mission, has provided a vast number of light curves for young stars in clusters and elsewhere in the K2 field. This provides us with the opportunity to extend the sample of young systems to field stars while calibrating with cluster stars. We compute rotational periods from starspot patterns for $\sim 36,000$ K2 targets and use gyrochronological relationships derived from cluster stars to determine their ages. From there, we have begun searching for planets around young stars outside the clusters with the ultimate goal of shedding light on how planets and planetary systems evolve in their early, most formative years.

Author(s): Nathan Ryan Morris², Andrew Mann¹, Aaron Rizzuto²

Institution(s): 1. *Columbia University*, 2. *University of Texas at Austin*

148.07 – Characterizing Giant Exoplanets through Multiwavelength Transit Observations: KELT-9b

Multiwavelength observations of host stellar light scattered through an exoplanet’s atmosphere during a transit characterizes exoplanetary parameters. Using the Wyoming Infrared Observatory 2.3-meter telescope, we observed primary transits of KELT-9b in the ugriz Sloan filters. We present an analysis of the phase-folded transit observations of KELT-9b using a Bayesian statistical approach. By plotting the transit depth as a function of wavelength, our preliminary results are indicative of scattering in the atmosphere surrounding KELT-9b. This work is supported by the National Science Foundation under REU grant AST 1560461 and PAARE grant AST 1559559.

Author(s): Cristilyn N. Gardner¹, Jackson L. Cole⁴, Bethany R. Garver⁶, Kyla L Jarka², Aman Kar⁷, Aylin M. McGough⁷, David J. PeQueen³, Daniel I. Rivera⁵, David Kasper⁷, Hannah Jang-Condell⁷, Henry A. Kobulnicky⁷, Daniel A. Dale⁷

Institution(s): 1. *California State University San Bernardino*, 2. *Colorado College*, 3. *Embry-Riddle Aeronautical University*, 4. *Middle Tennessee State University*, 5. *San Diego State University*, 6. *Seattle Pacific University*, 7. *University of Wyoming*

148.08 – BARTTest: Community-Standard Atmospheric Radiative-Transfer and Retrieval Tests

Atmospheric radiative transfer (RT) codes are used both to predict planetary and brown-dwarf spectra and in retrieval algorithms to infer atmospheric chemistry, clouds, and thermal structure from observations. Observational plans, theoretical models, and scientific results depend on the correctness of these calculations. Yet, the calculations are complex and the codes implementing them are often written without modern software-verification techniques. The community needs a suite of test calculations with analytically, numerically, or at least community-verified results. We therefore present the Bayesian Atmospheric Radiative Transfer Test Suite, or BARTTest. BARTTest has four categories of tests: analytically verified RT tests of simple

atmospheres (single line in single layer, line blends, saturation, isothermal, multiple line-list combination, etc.), community-verified RT tests of complex atmospheres, synthetic retrieval tests on simulated data with known answers, and community-verified real-data retrieval tests.

BARTTest is open-source software intended for community use and further development. It is available at <https://github.com/ExOSPORTS/BARTTest>. We propose this test suite as a standard for verifying atmospheric RT and retrieval codes, analogous to the Held-Suarez test for general circulation models. This work was supported by NASA Planetary Atmospheres grant NX12AI69G, NASA Astrophysics Data Analysis Program grant NNX13AF38G, and NASA Exoplanets Research Program grant NNX17AB62G.

Author(s): Joseph Harrington³, Michael D Himes³, Patricio E Cubillos¹, Jasmina Blečić², Ryan C Challener³

Institution(s): 1. Austrian Academy of Science, 2. New York University, Abu Dhabi, 3. University of Central Florida

148.09 – Characterization of Exoplanet Atmospheres with the Optical Coronagraph on WFIRST

WFIRST-CGI will obtain images and low resolution spectra of a handful to a dozen extrasolar planets and proto-planetary disks. It's unprecedented contrast levels in the optical will provide astronomers' first direct look at mature, super-earth to Jupiter sized planets, at moderate separations. This work addresses the question: what science can be done with such data? A parameterized noise model, informed by the latest engineering developments, is used to compute maximum achievable signal-to-noise ratios and scientifically-viable integration times for various star-planet scenarios and to simulate observations using two models for planetary geometric albedos. The first planet model is a hybrid Jupiter-Neptune model, which separately treats the short and long wavelengths where chromophores and methane dominate absorption respectively. The second planet model fixes cloud and haze properties in CoolTlusty to match Jupiter's albedo spectrum at roughly three times solar metallicity, then perturbs the metallicity between 1 and 30 times solar. MCMC retrievals performed on simulated observations are then used to assess the precision with which planet model parameters can be measured subject to different signal-to-noise ratios or exposure times.

Author(s): Brianna Lacy¹, Adam Burrows¹

Institution(s): 1. Princeton University

148.10 – WFIRST Microlensing Exoplanet Characterization with HST Follow up

More than 50 planets are discovered with the different ground based telescopes available for microlensing. But the analysis of ground based data fails to provide a complete solution. To fulfill that gap, space based telescopes, like Hubble space telescope and Spitzer are used. My research work focuses on extracting the planet mass, host star mass, their separation and their distance in physical units from HST Follow-up observations. I will present the challenges faced in developing this method. This is the primary method to be used for NASA's top priority project (according to 2010 decadal survey) Wide Field InfraRed Survey Telescope (WFIRST) Exoplanet microlensing space observatory, to be launched in 2025. The unique ability of microlensing is that with WFIRST it can detect sub-earth- mass planets beyond the reach of Kepler at separation 1 AU to infinity. This will provide us the necessary statistics to study the formation and evolution of planetary systems. This will also provide us with necessary initial conditions to model the formation of planets and the habitable zones around M dwarf stars.

Author(s): Aparna Bhattacharya¹

Institution(s): 1. NASA Goddard Space Flight Centre

Contributing team(s): David Bennett, Jay Anderson, J.P. Beaulieu.

148.11 – Characterizing Giant Exoplanets through Multiwavelength Transit Observations: HD 189733b

Observing the transits of exoplanets in multiple wavelengths enables the characterization of their atmospheres. We used the Wyoming Infrared Observatory to obtain high precision photometry on HD 189733b, one of the most studied exoplanets. We employed the photometry package AIJ and Bayesian statistics in our analysis. Preliminary results suggest a wavelength dependence in the size of the exoplanet, indicative of scattering in the atmosphere. This work is supported by the National Science Foundation under REU grant AST 1560461.

Author(s): Aman Kar⁷, Jackson Lane Cole⁴, Cristilyn N. Gardner¹, Bethany Ray Garver⁶, Kyla L Jarka², Aylin Marie McGough⁷, David Jeffrey PeQueen³, Daniel Ivan Rivera⁵, David Kasper⁷, Hannah Jang-Condell⁷, Henry Kobulnicky⁷, Daniel Dale⁷

Institution(s): 1. California State University, 2. Colorado College, 3. Embry-Riddle Aeronautical University, 4. Middle Tennessee State University, 5. San Diego State University, 6. Seattle Pacific University, 7. University of Wyoming

148.12 – The Impact of Binary Companions on Planetary Systems

The majority of solar-type stars are found in binary systems, and the dynamical influence of binary companions is expected to profoundly influence planetary systems. However, the difficulty of identifying planets in binary systems has left the magnitude of this effect uncertain; despite numerous theoretical hurdles to their formation and survival, at least some binary systems clearly host planets. We present high-resolution imaging of nearly 500 Kepler Objects of Interest (KOIs) obtained using adaptive-optics imaging and nonredundant aperture-mask interferometry on the Keck II telescope. We super-resolve some binary systems to projected separations of under 5 AU, showing that planets might form in these dynamically active environments. However, the full distribution of projected separations for our planet-host sample more broadly reveals a deep paucity of binary companions at solar-system scales. Our results demonstrate that a fifth of all solar-type stars in the Milky Way are disallowed from hosting planetary systems due to the influence of a binary companion. We now update these results with multi-epoch imaging to reject non-comoving background stars and securely identify even the least massive stellar companions, as well as tracing out the orbital motion of stellar companions. These results are beginning to reveal not just the fraction of binaries that do not host planets, but also potential explanations for planet survival even in some very close, dynamically active binary systems.

Author(s): Adam L. Kraus⁵, Michael Ireland¹, Trent Dupuy³, Andrew Mann², Daniel Huber⁴

Institution(s): 1. Australian National University, 2. Columbia University, 3. Gemini Observatory, 4. University of Hawaii - IfA, 5. UT-Austin

148.13 – Modeled 3-D Biosignatures from the Stratospheres of Proxima Centauri b and M-dwarf Planets

Proxima Centauri b is one of the most promising extrasolar terrestrial planets to search for potential biomarkers due to its proximity to Earth and relatively high planet to stellar luminosity ratio. These factors create a prime target for follow-up characterization efforts by e.g., James Webb Space Telescope and/or directing imaging. High-resolution, 3-D model predictions of atmospheric biosignatures however, are not currently available in the community. Here we use the CESM1 WACCM, a high-top coupled climate-chemistry general circulation model, to simulate the circulation, photochemistry, and stratospheric chemistry of Proxima b. From our equilibrium simulations with boundary conditions consistent with Proxima b observations (i.e., mass, radius, heliocentric distance, etc.) and a stellar spectrum consistent with its host star, we find increased mixing ratios and lifetimes for biogenic compounds (e.g., CH₄, N₂O, and CH₃Cl) in

the stratosphere. Whereas these biogenic gases are typically concentrated at the equator on Earth, they are dispersed across the mid-latitudes and even to the poles of Proxima b. Our initial analysis suggests that these characteristics are the result of a markedly energized stratospheric circulation regime and altered photochemistry, both of which are the consequence of enhanced UV and IR radiative forcing relative to Earth. Model simulated global distribution and longer lifetimes of biomarkers suggest that Proxima b's molecular absorption and observational windows are potentially greater than anticipated. These results indicate that the prospects for detecting signals of life on Proxima b and/or other M-dwarf planets are enhanced – a conclusion consistent with several prior studies using 1-D models.

Author(s): Howard Chen¹, Daniel Horton¹
Institution(s): 1. Department of Earth & Planetary Sciences, Northwestern University

148.14 – The Exoplanet Characterization ToolKit (ExoCTK)

The success of exoplanet characterization depends critically on a patchwork of analysis tools and spectroscopic libraries that currently require extensive development and lack a centralized support system. Due to the complexity of spectroscopic analyses and initial time commitment required to become productive, there are currently a limited number of teams that are actively advancing the field. New teams with significant expertise, but without the proper tools, face prohibitively steep hills to climb before they can contribute. As a solution, we are developing an open-source, modular data analysis package in Python and a publicly facing web interface focused primarily on atmospheric characterization of exoplanets and exoplanet transit observation planning with JWST. The foundation of these software tools and libraries exist within pockets of the exoplanet community. Our project will gather these seedling tools and grow a robust, uniform, and well maintained exoplanet characterization toolkit.

Author(s): Kevin Stevenson¹, Julia Fowler¹, Nikole K. Lewis¹, Jonathan Fraine¹, Laurent Pueyo¹, Jeff Valenti¹, Giovanni Bruno¹, Joseph Filippazzo¹, Matthew Hill¹, Natasha E Batalha¹, Rafia Bushra¹
Institution(s): 1. Space Telescope Science Institute

148.15 – Probing Into the Atmosphere of the Young Exoplanet K2-25b

Planets are most transformative during their early life, yet there remains little research on this developmental stage. In order to construct a more accurate picture of the diversity and evolution of planetary atmospheres, we present Spitzer infrared photometry of five transits both in 3.6 μm and 4.5 μm bands of the young exoplanet, K2-25b (650-800 Myr). To correct for the intra-pixel photometric response, we interpolated high-resolution sensitivity maps. Light curves were then created using a transit model and an MCMC framework to find the planet parameters in each wavelength. In comparison to atmospheric theoretical models, we find K2-25b unlikely to have a solar-metallicity atmosphere. However, observed through a full transmission spectrum, K2-25b is consistent with either a high-metallicity atmosphere or a cloudy/hazy layer. Further HST data would provide significantly more detail on the structure of the atmosphere. In a future project, we plan to apply this same method to a younger planet, K2-33b (11 Myr), to determine if cloudy/hazy atmospheres are primordial.

Author(s): Pa Chia Thao², Andrew Mann¹
Institution(s): 1. Columbia University, 2. Mount Holyoke College

148.16 – Assessing the Habitability of TRAPPIST-1e: MHD Simulations of Atmospheric Loss Due to CMEs and Stellar Wind

Recently, three rocky planets were discovered in the habitable zone of the nearby planetary system TRAPPIST-1. The increasing number of exoplanet detections has led to further research into

the planetary requirements for sustaining life. Habitable zone occupants have, in principle, the capacity to retain liquid water, whereas actual habitability might depend on atmospheric retention. However, stellar winds and photon radiation interactions with the planet can lead to severe atmospheric depletion and have a catastrophic impact on a planet's habitability. While the implications of photoevaporation on atmospheric erosion have been researched to some degree, the influence of stellar winds and Coronal Mass Ejections (CMEs) has yet to be analyzed in detail. Here, we model the effect of the stellar wind and CMEs on the atmospheric envelope of a planet situated in the orbit of TRAPPIST-1e using 3D magnetohydrodynamic (MHD) simulations. In particular, we discuss the atmospheric loss due to the effect of a CME, and the relevance of the stellar and planetary magnetic fields on the sustainability of M-dwarf exoplanetary atmospheres.

Author(s): Laura Marshall Harbach¹, Jeremy J. Drake¹, Cecilia Garraffo¹, Julian D. Alvarado-Gomez¹, Sofia P. Moschou¹, Ofer Cohen²

Institution(s): 1. Harvard-Smithsonian Center for Astrophysics, 2. University of Massachusetts Lowell

148.17 – No Metallicity Correlation Associated with the Kepler Dichotomy

NASA's Kepler mission has discovered thousands of planetary systems, $\sim 20\%$ of which are found to host multiple transiting planets. This relative paucity (compared to the high fraction of single transiting systems) is postulated to result from a distinction in the architecture between multi-transiting systems and those hosting a single transiting planet: a phenomenon usually referred to as the Kepler dichotomy. We investigate the hypothesis that external giant planets are the main cause behind the over-abundance of single- relative to multi-transiting systems, which would be signaled by higher metallicities in the former sample. To this end, we perform a statistical analysis on the stellar metallicity distribution with respect to planet multiplicity in the Kepler data. We perform our analysis on a variety of samples taken from a population of 1062 Kepler main sequence planetary hosts, using precisely determined metallicities from the California-Kepler survey. Contrary to some predictions, we do not find a significant difference between the stellar metallicities of the single- and multiple-transiting planet systems. However, we do find a 43% upper bound for systems with a single non-giant planet that could also host a hidden giant planet, based on metallicity considerations. While the presence of external giant planets might be one factor behind the Kepler dichotomy, our results also favor alternative explanations. We suggest that additional radial velocity and direct imaging measurements are necessary to constrain the presence of gas giants in systems with a single transiting planet.

Author(s): Carlos Eduardo Munoz Romero¹, Eliza Kempton¹
Institution(s): 1. Grinnell College

148.18 – Constraints on Neutral Hydrogen Outflow from the Warm Rocky Planet GJ1132b using Lyman-alpha Transit Observations

GJ1132b is one of the few known Earth-sized planets, and at 12 pc away it is also one of the closest known transiting planets. With an equilibrium temperature of 500 K, this planet is too hot to be habitable but we can use it to learn about the presence and volatile content of rocky planet atmospheres around M dwarf stars. Using Hubble STIS spectra during primary transit, we explore the potential for UV transit detections of GJ1132b. If we were to observe a deep Lyman- α transit, that would indicate the presence of a neutral hydrogen envelope flowing from GJ1132b. On the other hand, ruling out deep absorption from neutral hydrogen may indicate that this planet has either retained its volatiles or lost them very early in the star's life. We carry out this analysis by extracting 1D spectra from the STIS pipeline, splitting the time-tagged spectra into higher resolution samples, and

producing light curves of the red and blue wings of the Lyman- α line. We fit for the baseline stellar flux and transit depths in order to constrain the characteristics of the cloud of neutral hydrogen gas that may surround the planet. Our work extends beyond the transit study into an analysis of the stellar variability and Lyman- α spectrum of GJ1132, a slowly-rotating 0.18 M_{Sun} M dwarf with previously uncharacterized UV activity. Understanding the role that UV variability plays in planetary atmospheres and volatile retention is crucial to assess atmospheric evolution and the habitability of cooler rocky planets.

Author(s): William Waalkes⁶, Zachory Berta-Thompson⁶, David Charbonneau², Jonathan Irwin⁵, Elisabeth Newton³, Jason Dittmann³, Vincent Bourrier⁴, David Ehrenreich⁴, Eliza Kempton¹

Institution(s): 1. Grinnell College, 2. Harvard University, 3. Massachusetts Institute of Technology, 4. Observatoire de Geneve, 5. Smithsonian Astrophysical Observatory, 6. University of Colorado, Boulder

148.19 – Eating a planet and spinning up

One of the predictions of high eccentricity planetary migration is that many planets will end up plunging into their host stars. We investigate the consequence of planetary mergers on their stellar hosts' spin-period. Energy and angular momentum conservation yield that a planet consumption by a star will spin-up of the star. We find that our calculations align with the observed bifurcation in the stellar spin-period in young clusters. After a Sun-like star has eaten a planet, it will then, spin down due to magnetic braking, consistent with the observed lack of fast rotators in old clusters. The agreement between the calculations presented here and the observed spin-period of stars in young clusters provides circumstantial evidence that planetary accretion onto their host stars is a generic feature in planetary-system evolution.

Author(s): Ahmed Qureshi², Smadar Naoz², Evgenya L. Shkolnik¹

Institution(s): 1. ASU, 2. UCLA

148.20 – Moderate Resolution Spectroscopy of Substellar Companion Kappa Andromeda B

Recent direct imaging of exoplanets has revealed a population of Jupiter-like objects that orbit at large separations (~ 10 -100 AU) from their host stars. These planets, with masses of ~ 2 -14 M_{Jup} and temperatures of ~ 500 -2000 K, remain a problem for the two main planet formation models—core accretion and gravitational instability. OSIRIS observations of directly imaged planets have expanded our understanding of their atmospheres, alluded to their formation, and uncovered individual molecular lines. Here, we present OSIRIS K band spectra of the “super-Jupiter,” Kappa Andromeda b. Kappa Andromeda b has a lower mass limit at the deuterium burning limit, but also has an uncertain age which may indicate the source is a higher mass brown dwarf. The spectra reveal resolved molecular lines from water and CO. We will present atmospheric properties of this object derived from comparison to PHOENIX atmosphere models, and measure a best fit C/O ratio for the source. We will compare our results to atmospheric properties of other brown dwarfs and gas giant planets in an effort to improve our knowledge of intricate atmospheres of young, substellar objects.

Author(s): Kielan Wilcomb³, Quinn Konopacky³, Travis Barman⁴, Jessie Brown⁴, Laci Brock⁴, Bruce Macintosh², Jean-Baptiste Ruffio², Christian Marois¹

Institution(s): 1. NRC-Herzberg, 2. Stanford, 3. UC San Diego, 4. University of Arizona

148.21 – Stability of Moons in the Trappist-1 System

In the last 20 years, numerous exoplanets have been discovered and it has become clear that habitable bodies are rare. Exomoons mark the next stage in identifying habitable environs. In our own Solar system, several moons have been identified as having features suitable to sustain life. The Trappist-1 system (Gillon et

al. 2017) is a compact configuration of seven Earth-like planets orbiting a M-type dwarf star. The presence of moons cannot be confirmed in the transit data. Kane et al. (2017) suggests that it would be highly improbable for a moon to maintain a stable orbit around any Trappist-1 planet.

The current study investigates the claim by Kane et al. (2017), examining the stability of the Trappist-1 system in the presence of forming satellites. Moon disks are simulated by distributing 100 bodies, each with mass 5.26×10^{18} kg randomly within 10% - 90% of the exoplanet's Hill sphere. Utilizing N-body simulations, the planets and theoretical moons were tracked for 500 kyrs, allowing for gravitational interactions and mergers. Instabilities in the orbital parameters of the Trappist-1 planets was detected, in agreement with previous authors (Burgasser & Mamajerk 2017). Some of the planets are found to retain at least a single satellite for the same duration as the planetary stability. These data suggest that additional observation of the Trappist-1 system may yield the first detection of an exomoon.

Author(s): John Allen¹, Christopher Becker¹, Christopher Fuse¹

Institution(s): 1. Rollins College

148.22 – The Orbits of Long Period Exoplanets

Directly imaged planet surveys have discovered a class of large mass (5-20 M_{Jup}) substellar companions at separations >100 AU from their host stars. These wide planetary mass companions (PMCs) present a challenge to our understanding of how a planetary system forms around a star - most are too far from their star, and too massive, to be accounted for by current planet formation models, but less massive than typical stellar binary companions. PMCs might form in situ, or at small radii and be scattered out to their current orbit through dynamical interactions. Scattering would leave its mark in the orbit that it is on today. Constraining the orbital parameters allowed by current orbital velocities for this population group can provide insight into their formation pathways. We present the relative astrometry for several wide PMCs obtained using the NIRC2 Adaptive Optics camera at Keck telescope in Hawaii spanning several observation epochs. Our measurements achieved astrometric uncertainties near the NIRC2 systematic limit (~ 1 -2 mas), allowing robust measurement of their tangential orbital velocities. We then present constraints on orbital parameters determined through our modified implementation of the Orbits for the Impatient rejection sampling algorithm (Blunt et al. , 2010.).

Author(s): Logan Pearce¹, Adam L. Kraus¹

Institution(s): 1. University of Texas at Austin

148.23 – The Survivability of Moons Around an Escaping Planet

We examine the survivability of a moon system around a planet that is ejected from its parent star. Planetary systems are simulated using the REBOUND integrator and run forward in time until an escaping planet is generated. A moon system is added before the planet's escape, allowing for the survivability of the planet-moon system to be examined. Preliminary results from the simulations show that moons can remain in orbit around the escaping planet over a range of orbital distances and eccentricities.

Author(s): Ian Rabago¹, Jason H. Steffen¹

Institution(s): 1. University of Nevada, Las Vegas

148.24 – High-Resolution Spectroscopy of β Pictoris b

We present reduction and analysis of high-resolution, spatially separated spectroscopy of the exoplanet β Pictoris b (β Pic b). Our data was taken with NIRSPAO, a near-infrared echelle spectrograph coupled with adaptive optics (AO), on the Keck II 10-meter telescope. Astrometry was previously used to characterize the star-planet system's orbital properties, and a single radial velocity (RV) measurement via spectroscopy

supplemented the astrometric measurements. However, additional and more precise RV measurements of the planet are needed to constrain the individual mass of the planet, true eccentricity, and time of periastron passage. Using cross-correlation with model spectra, our goal is to detect the planet signal in NIRSPAO data and thereby expand the number of RV measurements. With this new RV, we can constrain planetary mass and improve the precision of the planet's orbital properties. This result will assist in constraining the time and likelihood of a Hill-sphere transit of β Pic b.

Author(s): Luis Nunez¹, Quinn Konopacky⁴, Max Millar-Blanchaer², Jeffrey K. Chilcote³

Institution(s): 1. California State Polytechnic University, Pomona, 2. Jet Propulsion Laboratory, 3. Stanford University, 4. University of California, San Diego

148.25 – The Effect of Starspots on Detectability of Exoplanet Atmospheres

Transmission spectroscopy is an effective tool for detecting and characterizing the atmospheres of transiting extrasolar planets. However, the presence of cool spots on a planet's host star can be a source of uncertainty that is difficult to account for. Cool starspots introduce wavelength-dependent features and noise into the transmission spectrum of an orbiting exoplanet. For sufficiently cool stars, especially M dwarfs, this could cause false detections of water and other species in the planet's atmosphere. To understand the extent of this problem, we use a combination of PHOENIX model spectra and the starspot simulation code MACULA to simulate the effects of starspots on observed transmission spectra for a wide variety of stars and spot configurations. By comparing the simulated DoTV (Depth of Transit Variation) due to starspots with models of the expected DoTV from exoplanet atmospheres with a given composition, we can estimate the level of effect the starspots have on the detectability of various atmospheres. For example, our results indicate for TRAPPIST-1's planets that while the large amplitude absorption features from a H/He-rich atmosphere should be easily detectable, a pure water atmosphere would be much harder to distinguish from starspot noise. Consequently, proper characterization of exoplanet atmospheres, especially around cool, active host stars, requires a proper understanding of the star's spot properties and suitable methods for reducing or removing spot-induced brightness fluctuations as a source of noise.

Author(s): Ryan Hofmann¹, Zachory Berta-Thompson¹

Institution(s): 1. University of Colorado Boulder

148.26 – Independent Component Analysis applied to Ground-based observations

Transit measurements of Jovian-sized exoplanetary atmospheres allow one to study the composition of exoplanets, largely independent of the planet's temperature profile. However, measurements of hot-Jupiter transits must archive a level of accuracy in the flux to determine the spectral modulation of the exoplanetary atmosphere. To accomplish this level of precision, we need to extract systematic errors, and, for ground-based measurements, the effects of Earth's atmosphere, from signal due to the exoplanet, which is several orders of magnitude smaller.

The effects of the terrestrial atmosphere and some of the time-dependent systematic errors of ground-based transit measurements are treated mainly by dividing the host star by a reference star at each wavelength and time step of the transit. Recently, Independent Component Analysis (ICA) have been used to remove systematics effects from the raw data of space-based observations (Waldmann, 2014, 2012; Morello et al., 2016, 2015). ICA is a statistical method born from the ideas of the blind-source separations studies, which can be used to de-trend several independent source signals of a data set (Hyvarinen and Oja, 2000). This technique requires no additional prior knowledge of the data set. In addition, this technique has the advantage of requiring no reference star.

Here we apply the ICA to ground-based photometry of the exoplanet XO-2b recorded by the 61" Kuiper Telescope and compare the results of the ICA to those of a previous analysis from Zellem et al. (2015), which does not use ICA. We also simulate the effects of various conditions (concerning the systematic errors, noise and the stability of object on the detector) to determine the conditions under which an ICA can be used with high precision to extract the light curve of exoplanetary photometry measurements

Author(s): Walter Martins-Filho³, Caitlin Griffith², Kyle Pearson², Ingo Waldmann⁴, Alvaro Alvarez-Candal³, Robert Thomas Zellem¹

Institution(s): 1. JPL, 2. Lunar and Planetary Laboratory/UA, 3. Observatorio Nacional, 4. UCL

148.27 – Characterizing Giant Exoplanets through Multiwavelength Transit Observations: XO-1 b

Multiwavelength observations of transiting exoplanets can reveal wavelength dependence of the observed transit depth (or a lack thereof), thereby allowing for thorough characterization of their atmospheres. In support of a larger project performing these characterizations of 12 transiting giant exoplanets through 66 nights of continuous observation at the 2.3 m Wyoming Infrared Observatory (WIRO), we report an updated ephemeris for transiting exoplanet XO-1 b. We carried out an MCMC analysis on photometric data obtained using the standard broad bandpass Sloan filter system. Our data set for XO-1 b is the most limited of those contributing to the larger project, the target having only been successfully observed from the transit midpoint to the egress on one night with limited out-of-transit data available. Exoplanet XO-1 b is a planet transiting star XO-1 (GSC 02041-01657) of type G1 V with $V = 11.19$ McCullough et al. (2006). This work is supported by the National Science Foundation under REU grant AST 1560461.

Author(s): Jackson Lane Cole⁴, Cristilyn N. Gardner¹, Bethany R. Garver⁶, Kyla L Jarka², Aman Kar⁷, Aylin M. McGough⁷, David J. PeQueen³, Daniel Ivan Rivera⁵, David Kasper⁷, Hannah Jang-Condell⁷, Henry Kobulnicky⁷, Daniel Dale⁷

Institution(s): 1. California State University San Bernardino, 2. Colorado College, 3. Embry-Riddle Aeronautical University, 4. Middle Tennessee State University, 5. San Diego State University, 6. Seattle Pacific University, 7. University of Wyoming

148.28 – Mapping the Habitable Zone of Exoplanets with a 2D Energy Balance Model

Traditionally, the habitable zone has been defined as the distance at which liquid water could exist on the surface of a rocky planet. However, different complexity models (simplified and fast:1D, and complex and time-intensive:3D) models derive different boundaries for the habitable zone. The goal of this project was to test a new intermediate complexity 2D Energy Balance model, add a new ice albedo feedback mechanism, and derive the habitable zone boundaries. After completing this first project, we also studied how other feedback mechanisms, such as the presence of clouds and the carbonate-silicate cycle, effected the location of the habitable zone boundaries using this 2D model. This project was completed as part of a 2017 summer REU program hosted by Cornell's Center for Astrophysics and Planetary Science and in partnership with the Carl Sagan Institute.

Author(s): Nicole Taylor Moon¹

Institution(s): 1. Cornell University

Contributing team(s): Dr. Lisa Kaltenegger, Dr. Ramses Ramirez

148.29 – Every Cloud has a Silver Lining: Synthesizing Spectra for Exoplanets with Inhomogeneous Aerosol Coverage

In order to learn about exoplanets, we observe the light coming from their host stars. In particular, we can observe a host star while its planet is in transit. During transit, we are able to observe light from the star that has passed through the planet's atmosphere and isolate that signal in a transmission spectrum. Previous transit observations have suggested that some hot Jupiters have aerosols in their atmospheres. We have calculated the effects that non-uniform aerosol coverage would have on the resulting transmission spectra of hot Jupiters. We used 3D atmospheric models of a planet with varying aerosol coverage to produce synthetic transmission spectra of the planet during full transit. We also produced transmission spectra from the start of transit, ingress, and the end of transit, egress, to determine if we can identify whether atmospheric aerosols are concentrated on the east or west side of the exoplanet. This will help us determine global aerosol structure, as well as indicate whether these planets are dominated by photochemically produced haze or directly condensed clouds. Using these spectra, we will test the feasibility of inferring aerosol coverage on a hot Jupiter using the Hubble Space Telescope.

Author(s): Victoria DiTomasso¹, Eliza Kempton², Emily Rauscher³, Michael Roman³

Institution(s): 1. CUNY Hunter College/AMNH, 2. Grinnell College, 3. University of Michigan

148.30 – Companions in Color: High-Resolution Imaging of Kepler's Sub-Neptune Host Stars

A current problem in astronomy is determining how sub-Neptune-sized exoplanets form in planetary systems. These kinds of planets, which fall between 1 and 4 times the size of Earth, were discovered in abundance by the Kepler Mission and were typically found with relatively short orbital periods. The combination of their size and orbital period make them unusual in relation to the Solar System, leading to the question of how these exoplanets form and evolve. One possibility is that they have been influenced by distant stellar companions. To help assess the influence of these objects on the present-day, observed properties of exoplanets, we conduct a NIR search for visual stellar companions to the stars around which the Kepler Mission discovered planets. We use high-resolution images obtained with the adaptive optics systems at the Lick Observatory Shane-3m telescope to find these companion stars. Importantly, we also determine the effective brightness and distance from the planet-hosting star at which it is possible to detect these companions. Out of the 200 KOIs in our sample, 42 KOIs (21%) have visual companions within 3", and 90 (46%) have them within 6". These findings are consistent with recent high-resolution imaging from Furlan et al. 2017 that found at least one visual companion within 4" for 31% of sampled KOIs (37% within 4" for our sample). Our results are also complementary to Furlan et al. 2017, with only 17 visual companions commonly detected in the same filter. As for detection limits, our preliminary results indicate that we can detect companion stars < 3-5 magnitudes fainter than the planet-hosting star at a separation of ~ 1". These detection limits will enable us to determine the probability that possible companion stars could be hidden within the noise around the planet-hosting star, an important step in determining the frequency with which these short-period, sub-Neptune-sized planets occur within binary star systems.

Author(s): Austin Ware¹, Angie Wolfgang¹, Deepti Kannan²

Institution(s): 1. Pennsylvania State University, 2. Stanford University

148.31 – Characterizing Giant Exoplanets through Multiwavelength Transit Observations: HAT-P-8b

Discovering and characterizing gas giants is important to the search for other life, as gas giants greatly affect the habitability of a solar system. Transits of exoplanets observed in visual photometric bands have been used to characterize their atmospheres and confirm planet parameters. We observed two primary transits of the hot gas giant HAT-P-8b with the Wyoming Infrared Observatory's 2.3-meter telescope. Using multi-filter

photometry in the g, r, i, and z bands (Sloan filters) we were able to update HAT-P-8b's planet parameters and constrain characteristics of its atmosphere. Preliminary findings show that there is wavelength dependence in the depth of the transit observations. An infrared spectroscopic follow up of this candidate could yield more details on its atmospheric composition.

Author(s): Kyla L Jarka², Jackson Lane Cole⁴, Cristilyn N. Gardner¹, Bethany Ray Garver⁶, Aman Kar⁷, Aylin Marie McGough⁷, David Jeffrey PeQueen³, Daniel Ivan Rivera⁵, David Kasper⁷, Hannah Jang-Condell⁷, Henry Kobulnicky⁷, Daniel Dale⁷

Institution(s): 1. California State University San Bernardino, 2. Colorado College, 3. Embry-Riddle Aeronautical University, 4. Middle Tennessee State University, 5. San Diego State University, 6. Seattle Pacific University, 7. University of Wyoming

148.32 – Characterizing Giant Exoplanets through Multiwavelength Transit Observations: HAT-P-57 b

Giant planets have thick atmospheres. By observing transits through multiple filters at different wavelengths, we can make constraints on the atmospheres of those planets. When the planets are observed via transit, Rayleigh scattering can cause the transit depth to vary with wavelength. HAT-P-57 b is a giant exoplanet that is observable using the 2.3-meter telescope at the Wyoming Infrared Observatory. We observed half of a transit of HAT-P-57 b using Sloan filters g, r, i, and z. We present early results showing a variation in calculated radius with wavelength. Further observations are needed to confirm this variation and measure it more accurately. This work is supported by the National Science Foundation under REU grant AST 150461.

Author(s): Bethany Ray Garver⁶, Jackson Lane Cole⁴, Cristilyn N. Gardner¹, Kyla L Jarka², Aman Kar⁷, Aylin M. McGough⁷, David Jeffrey PeQueen³, Daniel Ivan Rivera⁵, David Kasper⁷, Hannah Jang-Condell⁷, Henry Kobulnicky⁷, Daniel Dale⁷

Institution(s): 1. California State University San Bernardino, 2. Colorado College, 3. Embry-Riddle Aeronautical University, 4. Middle Tennessee State University, 5. San Diego State University, 6. Seattle Pacific University, 7. University of Wyoming

148.33 – Dynamical Mass of the Exoplanet Host Star HR 8799

HR 8799 is a young A5 star hosting four giant planets at wide separations (15-70 AU) which are undergoing orbital motion and have been continuously monitored with adaptive optics imaging since their discovery nearly a decade ago. Despite intensive searches for similar systems, this remains the only known star with multiple directly imaged exoplanets and is among the most extensively studied systems in the exoplanet community. Many mass estimates of the host star exist in the literature; however, currently no dynamical mass of HR 8799 has been measured. A dynamical mass of the host star is advantageous because it is independent of models and assumes only Kepler's laws of orbital motion. Furthermore, a dynamical mass can help to break degeneracies in the age and bulk metallicity of the host star. We fit Keplerian orbits to existing astrometry and new unpublished adaptive optics observations of this system from Keck Observatory, treating the orbiting planets as massless test particles. Each planet produces an independent mass constraint, together resulting in a cumulative dynamical mass using a Bayesian framework. This result is twice as precise as previous mass estimates based on spectroscopy and is an important step to clarify the fundamental properties of this peculiar A star.

Author(s): Aldo Sepulveda², Brendan Bowler¹

Institution(s): 1. University of Texas at Austin, 2. University of Texas at San Antonio

148.34 – Realistic Simulations of Coronagraphic Observations with WFIRST

We present a framework to simulate observing scenarios with the WFIRST Coronagraphic Instrument (CGI). The Coronagraph and Rapid Imaging Spectrograph in Python (crispy) is an open-source package that can be used to create CGI data products for analysis and development of post-processing routines. The software convolves time-varying coronagraphic PSFs with realistic astrophysical scenes which contain a planetary architecture, a consistent dust structure, and a background field composed of stars and galaxies. The focal plane can be read out by a WFIRST electron-multiplying CCD model directly, or passed through a WFIRST integral field spectrograph model first. Several elementary post-processing routines are provided as part of the package.

Author(s): Maxime Rizzo², Neil Zimmerman², Aki Roberge², Andrew Lincowski⁵, Giada Arney², Chris Stark⁴, Tiffany Jansen¹, Margaret Turnbull³

Institution(s): 1. Columbia University, 2. NASA GSFC, 3. SETI Institute, 4. STScI, 5. University of Washington

Contributing team(s): WFIRST Science Investigation Team (Turnbull)

148.35 – Characterizing Giant Exoplanets through Multiwavelength Transit Observations: HAT-P-5 b

During the summer of 2017, we observed hot Jupiter-type exoplanet transit events using the Wyoming Infrared Observatory's 2.3 meter telescope. We observed 14 unique exoplanets during transit events; one such target was HAT-P-5 b. In total, we collected 53 usable science images in the Sloan filter set, particularly with the g', r', z', and i' band wavelength filters. This exoplanet transited approximately 40 minutes earlier than the currently published literature suggests. After reducing the data and running a Markov chain Monte Carlo analysis, we present results describing the planetary radius, semi-major axis, orbital period, and inclination of HAT-P-5 b. Characteristics of Rayleigh scattering are present in the atmosphere of this exoplanet. This work is supported by the National Science Foundation under REU grant AST 1560461.

Author(s): David Jeffrey PeQueen³, Jackson Lane Cole⁴, Cristilyn N. Gardner¹, Bethany Ray Garver⁶, Kyla L Jarka², Aman Kar⁷, Aylin M. McGough⁷, Daniel Ivan Rivera⁵, David Kasper⁷, Hannah Jang-Condell⁷, Henry Kobulnicky⁷, Daniel Dale⁷

Institution(s): 1. California State University San Bernardino, 2. Colorado College, 3. Embry-Riddle Aeronautical University, 4. Middle Tennessee State University, 5. San Diego State University, 6. Seattle Pacific University, 7. University of Wyoming

148.36 – Characterizing Giant Exoplanets through Multi-wavelength Transit Observations: TrES-4b

The properties of exoplanets are important to investigate because they provide a better understanding of the formation and evolution of planetary systems outside of our own. TrES-4b was observed over the summer of 2017 for multiple nights in g'r'i'z' bandpasses using the wide-field prime focus imager at Wyoming Infrared Observatory (WIRO) 2.3 m telescope. We performed photometry and statistical analysis on the transit over the range of observed optical wavelengths. Photometric precisions were typically 0.2 to 0.9 mmag. Our initial analysis is suggestive of a cloudy opaque atmosphere.

Author(s): Aylin Marie McGough⁷, Jackson Lane Cole⁴, Cristilyn N. Gardner¹, Bethany Ray Garver⁶, Kyla L Jarka², Aman Kar⁷, David Jeffrey PeQueen³, Daniel Ivan Rivera⁵, David Kasper⁷, Hannah Jang-Condell⁷, Henry Kobulnicky⁷, Daniel Dale⁷

Institution(s): 1. Cal State San Bernardino, 2. Colorado College, 3. Embry-Riddle Aeronautical University, 4. Middle Tennessee State University, 5. San Diego State University, 6. Seattle Pacific University, 7. University of Wyoming

148.37 – Characterizing Giant Exoplanets through Multiwavelength Transit Observations: HAT-P-14 b & TrES-1 b

Much current work focuses on characterizing exoplanets. We observed several known exoplanets using the 2.3 meter Wyoming Infrared Observatory over the course of ten weeks using the ugriz Sloan filters. Our goal was to quantify planet-to-star radius ratio, a ratio that is potentially wavelength dependent due to exoplanet atmospheres. We present the results for exoplanets HAT-P 14 b and TrES-1 b. Complementary data from the literature are utilized to supplement our analysis. This work is supported by the National Science Foundation under REU grant AST 1560461 and PAARE grant AST 1559559.

Author(s): Daniel Ivan Rivera⁵, Jackson Lane Cole⁴, Cristilyn N. Gardner¹, Bethany Ray Garver⁶, Kyla L Jarka², Aman Kar⁷, Aylin Marie McGough⁷, David Jeffrey PeQueen³, David Kasper⁷, Hannah Jang-Condell⁷, Henry Kobulnicky⁷, Daniel Dale⁷

Institution(s): 1. California State University San Bernardino, 2. Colorado College, 3. Embry Riddle Aeronautical University, 4. Middle Tennessee State University, 5. San Diego State University, 6. Seattle Pacific University, 7. University of Wyoming

148.38 – Exploring the Effects of Clouds on Hot Jupiter Atmospheres

Secondary eclipse spectroscopy of transiting exoplanets allows us to probe the atmospheric properties on the daysides of tidally locked planets. Specifically, eclipse spectra combined with atmospheric retrieval models permit constraints on the molecular abundances and vertical thermal profiles of the planetary dayside. Eclipse spectra from HST WFC3 are typically interpreted assuming that all of the near infrared light is due solely to the thermal emission of the planet. However, recent evidence suggests that reflected stellar light from clouds on the planetary daysides might contaminate the near-IR spectrum. Here, we aim to explore how reflected light from clouds within in a simplified cloud framework will alter the shape of the near infrared spectra and how they will influence our determinations of dayside temperatures and abundances. Specifically, we will use atmospheric retrieval tools to determine the biases in abundances and temperature profiles if reflected light is not taken into account. We will explore the influence of reflected light on interpretation of WFC3 spectra of the well-observed exoplanets, HD209458b and WASP-43b. We will then investigate how reflected light in the near-IR will influence our interpretation of JWST spectra.

Author(s): Jenna Robinson¹, Michael Line¹

Institution(s): 1. Arizona State University

148.39 – Modeling Exoplanetary Haze and Cloud Effects for Transmission Spectroscopy in the TRAPPIST-1 System

We present theoretical transmission spectra of the planets TRAPPIST-1d, e, f, and g using a version of the Caltech Inverse Modeling and Retrieval Algorithms (CHIMERA) atmospheric modeling code. We use particle size, aerosol production rates, and aerosol composition inputs from recent laboratory experiments relevant for the TRAPPIST-1 system to constrain cloud and haze behavior and their effects on transmission spectra. We explore these cloud and haze cases for a variety of theoretical atmospheric compositions including hydrogen-, nitrogen-, and carbon dioxide-dominated atmospheres. Then, we demonstrate the feasibility of physically-motivated, laboratory-supported clouds and hazes to obscure spectral features at wavelengths and resolutions relevant to instruments on the Hubble Space Telescope and the upcoming James Webb Space Telescope. Lastly, with laboratory based constraints of haze production rates for terrestrial exoplanets, we constrain possible bulk atmospheric compositions of the TRAPPIST-1 planets based on current observations. We show that continued collection of optical data, beyond the supported

wavelength range of the James Webb Telescope, is necessary to explore the full effect of hazes for transmission spectra of exoplanetary atmospheres like the TRAPPIST-1 system.

Author(s): Sarah E Moran¹, Sarah M. Horst¹, Nikole K. Lewis³, Natasha E Batalha³, Julien de Wit²
Institution(s): 1. Johns Hopkins University, 2. Massachusetts Institute of Technology, 3. Space Telescope Science Institute

148.40 – HabEx and the Search for Biosignatures Around Nearby Stars

The Habitable Exoplanet Imaging mission (HabEx) is one of four flagship mission concepts currently under study for the upcoming 2020 Decadal Survey of Astronomy and Astrophysics. One of HabEx's main goals will be a thorough study of planetary systems in our stellar neighborhood. This will include the characterization of any rocky planets in the habitable zones of these systems. Rocky habitable zone planets are, by definition, worlds with the potential to host global liquid water surface oceans, and therefore the potential to harbor global biospheres. HabEx's characterization of these worlds will include a search for signs of life on these planets. These signatures will be primarily spectroscopic in nature, and result from the suite of gases emitted by biota at the planet's surface. In this poster, we will discuss HabEx's abilities to detect potential biosignature gases, and the extent to which it can discriminate biological sources of these gases from non-biological "false positives."

Author(s): Shawn David Domagal-Goldman¹
Institution(s): 1. NASA Goddard Space Flight Center
Contributing team(s): The Habitable Exoplanet Science and Technology Definition Team

148.41 – WFIRST: The Exoplanet Microlensing Survey Tells Us Where We Can Find the Cool Planets

The WFIRST Exoplanet microlensing survey will complete a demographic survey of all types of planets ranging from ~0.5 AU to planets that have become unbound from the stellar systems of their birth. WFIRST's sensitivity extends down below the mass of Mars (or 0.1 Earth masses), and it is sensitive to analogs of all the planets in the Solar System, except for Mercury. When combined with Kepler's statistical census of hot and warm planets in short period orbits, WFIRST's exoplanet microlensing survey will give us a complete picture the mass and separation distribution of all types of planets. The current plans for this survey are presented, and recent developments relating to the WFIRST exoplanet microlensing survey will be presented, including recent ground-based microlensing results that challenge current theories of planet formation. Opportunities for community involvement in the WFIRST exoplanet microlensing survey will be mentioned.

Author(s): David Bennett¹, B. Scott Gaudi²
Institution(s): 1. NASA Goddard Space Flight Center, 2. The Ohio State University
Contributing team(s): The WFIRST Microlensing Science Investigation Team

148.42 – Predicted Exoplanet Yields for the HabEx Mission Concept

The Habitable Exoplanet Imaging Mission (HabEx) is a concept for a flagship mission to directly image and characterize extrasolar planets around nearby stars and to enable a broad range of general astrophysics. The HabEx Science and Technology Definition Team (STDT) is currently studying two architectures for HabEx. Here we summarize the exoplanet science yield of Architecture A, a 4 m monolithic off-axis telescope that uses a vortex coronagraph and a 72m external starshade occulter. We summarize the instruments' capabilities, present science goals and observation strategies, and discuss astrophysical assumptions. Using a yield optimization code, we predict the yield of potentially Earth-like extrasolar planets that could be detected, characterized, and searched for signs of

habitability and/or life by HabEx. We demonstrate that HabEx could also detect and characterize a wide variety of exoplanets while searching for potentially Earth-like planets.

Author(s): Christopher Stark², Bertrand Mennesson¹
Institution(s): 1. NASA JPL, 2. Space Telescope Science Institute
Contributing team(s): The HabEx STDT

148.43 – WFIRST: Retrieval Studies of Directly Imaged Extrasolar Giant Planets

The typical direct imaging and spectroscopy target for the WFIRST Coronagraph will be a mature Jupiter-mass giant planet at a few AU from an FGK star. The spectra of such planets is expected to be shaped primarily by scattering from H₂O clouds and absorption by gaseous NH₃ and CH₄. We have computed forward model spectra of such typical planets and applied noise models to understand the quality of photometry and spectra we can expect. Using such simulated datasets we have conducted Markov Chain Monte Carlo and MultiNest retrievals to derive atmospheric abundance of CH₄, cloud scattering properties, gravity, and other parameters for various planets and observing modes. Our focus has primarily been to understand which combinations of photometry and spectroscopy at what SNR allow retrievals of atmospheric methane mixing ratios to within a factor of ten of the true value. This is a challenging task for directly imaged planets as the planet mass and radius--and thus surface gravity--are not as well constrained as in the case of transiting planets. We find that for plausible planets and datasets of the quality expected to be obtained by WFIRST it should be possible to place such constraints, at least for some planets. We present some examples of our retrieval results and explain how they have been utilized to help set design requirements on the coronagraph camera and integrated field spectrometer.

Author(s): Mark Marley¹, Roxana Lupu¹, Nikole K. Lewis²
Institution(s): 1. NASA Ames Research Center, 2. Space Telescope Science Institute
Contributing team(s): WFIRST Coronagraph SITs

148.45 – Constraining Exoplanet Habitability with HabEx

The Habitable Exoplanet Imaging mission, or HabEx, is one of four flagship mission concepts currently under study for the upcoming 2020 Decadal Survey of Astronomy and Astrophysics. The broad goal of HabEx will be to image and study small, rocky planets in the Habitable Zones of nearby stars. Additionally, HabEx will pursue a range of other astrophysical investigations, including the characterization of non-habitable exoplanets and detailed observations of stars and galaxies. Critical to the capability of HabEx to understand Habitable Zone exoplanets will be its ability to search for signs of surface liquid water (i.e., habitability) and an active biosphere. Photometry and moderate resolution spectroscopy, spanning the ultraviolet through near-infrared spectral ranges, will enable constraints on key habitability-related atmospheric species and properties (e.g., surface pressure). In this poster, we will discuss approaches to detecting signs of habitability in reflected-light observations of rocky exoplanets. We will also present initial results for modeling experiments aimed at demonstrating the capabilities of HabEx to study and understand Earth-like worlds around other stars.

Author(s): Tyler Robinson¹
Institution(s): 1. Northern Arizona University

148.46 – Broadening of spectral lines of CO₂, N₂O, H₂CO, HCN, and H₂S by pressure of gases dominant in planetary atmospheres (H₂, He and CO₂)

HITRAN^{1,2} is a compilation of spectroscopic parameters that a variety of computer codes use to predict and simulate the transmission and emission of light in planetary atmospheres. The goal of this project is to add to the potential of the HITRAN database towards the exploration of the planetary atmospheres by

including parameters describing broadening of spectral lines by H₂, CO₂, and He. These spectroscopic data are very important for the study of the hydrogen and helium-rich atmospheres of gas giants as well as rocky planets with volcanic activities, including Venus and Mars, since their atmospheres are dominated by CO₂. First step in this direction was accomplished by Wilzewski et al. 3 where this was done for SO₂, NH₃, HF, HCl, OCS and C₂H₂. The molecules investigated in this work were CO₂, N₂O, H₂CO, HCN and H₂S. Line-broadening coefficients, line shifts and temperature-dependence exponents for transitions of these molecules perturbed by H₂, CO₂ and He have been assembled from available peer-reviewed experimental and theoretical sources. The data was evaluated and the database was populated with these data and their extrapolations/interpolations using semi-empirical models that were developed to this end.

Acknowledgements: Financial support from NASA PDART grant NNX16AG51G and the Smithsonian Astrophysical Observatory Latino Initiative Program from the Latino Initiatives Pool, administered by the Smithsonian Latino Center is gratefully acknowledged.

149 – Galaxy Evolution Poster Session

149.01 – Deriving Stellar Masses for the ALFALFA α .100 Sample

For this project, we explore different methods of deriving the stellar masses of galaxies in the ALFALFA (Arecibo Legacy Fast ALFA) α .100 survey. In particular, we measure the effectiveness of SED (Spectral Energy Distribution) on the sample. SED fitting was performed by MAGPHYS (Multi-wavelength Analysis of Galaxy Physical Properties), utilizing a wide range of photometry in the UV, optical, and IR bands. Photometry was taken from GALAX GR6/7 (UV), SDSS DR13 (optical), WISE All-Sky (near-IR), and Herschel PACS/SPIRE (far-IR). The efficiency of SED fitting increases with a broader range of photometry, however detection rates varied significantly across the different bands. Using a more “comprehensive” sample of galaxies, the GSWLC-A (GALAX, SDSS, WISE Legacy Catalog All-Sky Survey), we aimed to measure which combination of bands provided the largest sample return with the lowest amount of uncertainty, which could then be used to estimate the masses of the galaxies in the α .100 sample.

Author(s): Logan Hess¹

Institution(s): 1. UW Stevens Point

Contributing team(s): Cornell 2017 Summer REU

149.02 – Characterizing the origin and impact of the most extreme molecular outflows in the nearby universe

Observations over the last decade have revealed that feedback in the form of molecular gas outflows is ubiquitous in local ultra luminous infrared galaxies (ULIRGs). Such outflows can clear the nuclear environments of gas and dust, quench star formation and active galactic nuclei (AGN) growth, and they are a key step in the evolution of dust-obscured AGN to optically luminous quasars. We here present multi-spectral line observations of feedback in the two most powerful molecular gas outflows in the local universe. We spatially resolve the outflows to determine their kinematics and structure and find that they can drive out the molecular gas and quench star formation within \sim few Myr. Applying mid-IR diagnostics to constrain the relative contributions of AGN and nuclear starburst activity, we find that starburst activity plays a significant role in driving the outflow. We discuss the implications for future studies of feedback in the local universe and obscured AGN at high redshift, which is a key target population for JWST and ALMA over the next decade.

Author(s): Avani Gowardhan¹, Dominik A Riechers¹, Henrik Spoon¹, Duncan Farrah²

Institution(s): 1. Department of Astronomy, Cornell University, 2. Department of Physics, Virginia Tech

References:

1. HITRAN online <http://hitran.org/>
2. Gordon, I.E., Rothman, L.S., Hill, C., Kochanov, R.V., Tan, Y., et al., 2017. The HITRAN2016 Molecular Spectroscopic Database. *J. Quant. Spectrosc. Radiat. Transf.* doi:10.1016/j.jqsrt.2017.06.038
3. Wilzewski, J.S., Gordon, I.E., Kochanov, R. V., Hill, C., Rothman, L.S., 2016. H₂, He, and CO₂ line-broadening coefficients, pressure shifts and temperature-dependence exponents for the HITRAN database. Part 1: SO₂, NH₃, HF, HCl, OCS and C₂H₂. *J. Quant. Spectrosc. Radiat. Transf.* 168, 193–206. doi:10.1016/j.jqsrt.2015.09.003

Author(s): Shanelle Samuels², Iouli Gordon¹, Yan Tan¹

Institution(s): 1. Division of Atomic and Molecular Physics, Harvard-Smithsonian Center for Astrophysics, 2. University of Massachusetts Lowell

149.03 – Spatially Resolved Analysis of the Interstellar Medium in the Cosmic Eye, a Lensed Lyman Break Galaxy at $z=3.074$

The [CII]/[NII] ratio combines the [CII] line, a tracer of photodissociation and HII regions emerging from the neutral and ionized phases of the interstellar medium (ISM), with [NII] emission, which only originates from the ionized ISM. In this, the [CII]/[NII] ratio can be used to separate the fractions of [CII] emission emerging from the different phases of the ISM. We present Atacama Large sub-Millimeter Array (ALMA) observations of the Cosmic Eye, a gravitationally lensed Lyman Break Galaxy (LBG). As an LBG, the Cosmic Eye represents a “normal” star forming galaxy in the $z>2$ universe. LBGs were host to the bulk of star formation during the peak epoch of star formation. Diagnosing star formation in these galaxies provides insight into the evolution of “normal” galaxies in a cosmic sense. The high magnification (30x) allows us to resolve the [CII] 158 μ m and the [NII] 205 μ m lines in detail, allowing for a position-resolved analysis of their ratio. We find variations of the line ratio across the galaxy, suggesting the galaxy’s internal structure affects this ratio. We consider the Cosmic Eye in the context of both higher redshift LBGs and local luminous and ultraluminous infrared galaxies, finding that the Cosmic Eye’s line ratio is similar to those of both higher- and lower- redshift galaxies. The Cosmic Eye’s global [CII]/[NII] ratio sits between two previous measurements of $z>5$ LBGs at low resolution, suggesting that the ratio may correlate more significantly with L_{FIR} than with redshift in this epoch. Furthermore, the Cosmic Eye’s [CII]/[NII] ratio is similar to those of the nearby LIRG/ULIRGs, though we expect local [CII]/[NII] values to be lower due to their different metallicities and dust content. High-resolution studies like this one probe the evolution of [CII]/[NII] over cosmic time by examining the evolution of the ISM’s structure. With a better understanding of the [CII]/[NII] line ratio, we can more effectively use it as a probe of the nature of star formation in high-redshift galaxies. CJB participated in the summer 2017 REU program in the Center for Astrophysics and Planetary Science at Cornell University under NSF award AST-1659264.

Author(s): Catherine Ball², Dominik A Riechers¹, Riccardo Pavesi¹

Institution(s): 1. Cornell University, 2. Macalester College

149.04 – Examining the effect of galaxy evolution on the stellar-halo mass relation in the EAGLE simulation

The EAGLE hydrodynamical simulation was used in Matthee et al. 2016 to examine the scatter in the stellar mass-halo mass relation of central galaxies, finding that the stellar mass (M^*) correlates well with the maximum circular velocity (V_{\max}) of the host halo, but with a substantial scatter that does not correlate significantly with other host halo properties. Here we further

examine the scatter in the stellar mass-halo mass relation of central galaxies in EAGLE, its correlation with other properties, and its origin. We find that at fixed V_{\max} , galaxies with lower concentration have younger stellar populations, as expected from the relationship between concentration and halo assembly time. However, at fixed V_{\max} and halo concentration, galaxies with larger M^* have younger stellar ages, so that combining the two effects, galaxies with younger stellar ages at fixed halo mass have higher stellar masses. The host halos of galaxies with larger M^* at fixed V_{\max} and concentration also contain more gas than those with smaller stellar masses at $z = 0.1$, i.e. the baryon fraction of the halos is larger. There is an even stronger correlation between the scatter in M^* at $z = 0.1$ and the scatter in the baryon fraction of the galaxy's progenitors at $z \sim 1$, such that the latter sets $\sim 50\%$ of the scatter in M^* at $z = 0.1$. We conclude that most of the scatter between V_{\max} and M^* at $z = 0.1$ is set at earlier redshifts by the scatter in the baryon fraction of halos, which in turn is primarily the result of differences in feedback strength within halos.

Author(s): Andrea Kulier³, Nelson Padilla³, Joop Schaye¹, Robert Crain², Matthieu Schaller⁴, Richard Bower⁴, Tom Theuns⁴, Enrique Paillas³

Institution(s): 1. *Leiden University*, 2. *Liverpool John Moores University*, 3. *Pontificia Universidad Católica de Chile*, 4. *University of Durham*

149.05 – Black Hole Masses for Type I Active Galactic Nuclei in the Chandra Cosmos Legacy Survey

Tight local relations between SMBH masses and galaxy properties have established the fundamental connection between SMBHs and their host galaxies. However, in order to better understand the coevolution of SMBHs and their host galaxies over cosmic time, we need measurements of black hole masses, AGN luminosities, and galaxy stellar masses from sizable samples of AGN covering lower luminosities than the brightest quasars spanning a wide redshift range. In this study, we report masses of the SMBHs of 224 Type I AGNs from the Chandra COSMOS Legacy Survey as determined by the line widths of Mg II 2798, H β 4862, and H α 6564 via scaling relations derived from reverberation mapping. Preliminary comparison with host galaxy luminosities and stellar masses suggests an increase in Eddington ratio with redshift, consistent with previous studies. In addition, our derived SMBH masses fall above the local AGN $M_{\text{BH}}-M^*$ (galactic stellar mass) relation from Reines & Volonteri (2015), but it is still not clear whether this results from redshift evolution of the $M_{\text{BH}}-M^*$ relation or from the incompleteness of the spectroscopic surveys available.

The SAO REU program is funded by the National Science Foundation REU and Department of Defense ASSURE programs under NSF Grant AST-1659473, and by the Smithsonian Institution.

Author(s): Gautam Nagaraj², Francesca Fornasini¹, Francesca Maria Civano¹

Institution(s): 1. *Harvard/Smithsonian Center for Astrophysics*, 2. *North Carolina State University*

149.06 – Exploring the Nature of Galaxies with Abundance Gradient Anomalies in the SDSS-IV/MaNGA Survey

Disk galaxies are known to have radial oxygen abundance gradients with their centers being more chemically enriched than their outskirts. The steepness of the abundance gradient has recently been shown to correlate with galaxy stellar mass, on average. However, individual galaxies sometimes show pronounced deviations from the expected trends, such as flatter or steeper slopes than expected for their mass, abrupt changes in slope, or azimuthal asymmetries. Here we report on a systematic search for galaxies with abundance gradient anomalies using 2-D spectroscopy from the Sloan Digital Sky Survey IV MaNGA. We

construct nebular oxygen and nitrogen abundance maps for 300 moderately inclined non-interacting disk galaxies and use visual inspection to identify the most interesting cases. We use this training set to develop an automated pipeline to flag galaxies with abundance anomalies from the larger MaNGA dataset for visual inspection. We combine the metallicity maps with kinematic data and measurements of the galaxies' local environments to better understand the processes that shape the radial abundance gradients of disk galaxies.

Author(s): Celeste Keith¹, Christy Tremonti¹, Zach Pace¹, Adam Schaefer¹

Institution(s): 1. *University of Wisconsin Madison*

149.07 – Emission Line Metallicities from the Faint Infrared Grism Survey

We present the redshifts and line identifications for 71 emission-line galaxies (ELGs) with $z \sim 0.3 - 3$ in the HUDF as part of the Faint Infrared Grism Survey (FIGS). We have calculated gas-phase metallicity for 39 ELGs using the R23 method, and for 14 ELGs for which we have [OIII] $\lambda 4363$ measurements at $S/N > 3$, which enables the direct measurement of metallicity from the [OIII] electron temperature. The ELGs were selected by an automatic search of one-dimensional slitless spectroscopy from the WFC3 G102 grism on the Hubble Space Telescope. We matched the ELG candidate spectra with high-resolution optical spectra from MUSE, which allowed confirmation and identification of single-line FIGS detections and provided lower-wavelength line measurements. Once individual line fluxes were measured, we produced metallicities via the [OIII] $\lambda 4363$ and R23 methods and analyzed the metallicity in relation to mass, star formation rate, and other properties.

Author(s): John Pharo¹, Lise Christensen², Sangeeta Malhotra¹, James Rhoads¹, Mark Smith¹, Santosh Harish¹, huan yang¹

Institution(s): 1. *ARIZONA STATE UNIVERSITY*, 2. *Dark Cosmology Centre, University of Copenhagen*

Contributing team(s): The FIGS Collaboration

149.08 – Figuring Out Gas and Galaxies in Enzo (FOGGIE): Simulating effects of feedback on galactic outflows

The circumgalactic medium (CGM) is the region beyond the galactic disk in which gas is accreted through pristine inflows from the intergalactic medium and expelled from the galaxy by stellar feedback in large outflows that can then be recycled back onto the disk. These gas cycles connect the galactic disk with its cosmic environment, making the CGM a vital component of galaxy evolution. However, the CGM is primarily observed in absorption, which can be difficult to interpret. In this study, we use high resolution cosmological hydrodynamic simulations of a Milky Way mass halo evolved with the code Enzo to aid the interpretation of these observations. In our simulations, we vary feedback strength and observe the effect it has on galactic outflows and the evolution of the galaxy's CGM. We compare the star formation rate of the galaxy with the velocity flux and mass outflow rate as a function of height above the plane of the galaxy in order to measure the strength of the outflows and how far they extend outside of the galaxy.

This work was supported by The Space Astronomy Summer Program at STScI and NSF grant AST-1517908.

Author(s): Melissa Elizabeth Morris⁵, Lauren Corlies¹, Molly Peeples³, Jason Tumlinson³, Brian O'Shea², Britton Smith⁴

Institution(s): 1. *Johns Hopkins University*, 2. *Michigan State University*, 3. *Space Telescope Science Institute*, 4. *University of California, San Diego*, 5. *University of Texas at Austin*

149.09 – Estimating precise metallicity and stellar mass evolution of galaxies

The evolution of galaxies can be conveniently broken down into the evolution of their contents. The changing dust, gas, and stellar

content in addition to the changing dark matter potential and periodic feedback from a super-massive blackhole are some of the key ingredients. We focus on the stellar content that can be observed, as the stars reflect information about the galaxy when they were formed. We approximate the stellar content and star formation histories of unresolved galaxies using stellar population modeling. Though simplistic, this approach allows us to reconstruct the star formation histories of galaxies that can be used to test models of galaxy formation and evolution. These models, however, suffer from degeneracies at large lookback times ($t > 1$ Gyr) as red, low luminosity stars begin to dominate a galaxy's spectrum. Additionally, degeneracies between stellar populations at different ages and metallicities often make stellar population modeling less precise. The machine learning technique diffusion k-means has been shown to increase the precision in stellar population modeling using a mono-metallicity basis set. However, as galaxies evolve, we expect the metallicity of stellar populations to vary. We use diffusion k-means to generate a multi-metallicity basis set to estimate the stellar mass and chemical evolution of unresolved galaxies. Two basis sets are formed from the Bruzual & Charlot 2003 and MILES stellar population models. We then compare the accuracy and precision of these models in recovering complete (stellar mass and metallicity) histories of mock data. Similarities in the groupings of stellar population spectra in the diffusion maps for each metallicity hint at fundamental age transitions common to both basis sets that can be used to identify stellar populations in a given age range.

Author(s): Gregory Mosby¹

Institution(s): 1. NASA Goddard Space Flight Center

149.10 – Effects of Pop III to PopII transition on the lowest metallicity stars in dwarf galaxies

We examine the effects of the enrichments from Population III (Pop III) stars on the formation and properties of the first generation of the Population II (Pop II) stars. Pop III stars begin to transition towards Pop II stars when the metals dispersed in Pop III supernovae pollute the nearby gas. However, details of this transition are still largely unknown. We use dwarf galaxy simulations from the Feedback In Realistic Environments (FIRE) project to identify the star-forming gas that is likely to be pre-enriched by Pop III supernovae and follow the stars that form in such gas. This pre-enrichment will leave the signature in the lowest metallicity stars that can be used to better constrain the details of the Pop III-to-Pop II transition.

Author(s): Yimiao Zhang¹, Dusan Keres¹

Institution(s): 1. University of California, San Diego

Contributing team(s): FIRE Team

149.11 – EXPLORING LOCAL HIGHT z ANALOGS

We have selected a sample of nearby star forming galaxies from the Brown et al 2014 (UV to MIR spectroscopic sample) that successfully fit broad band photometric data of high redshift galaxies ($z > 4$) and, hence, are potential local analogs of high redshift galaxies.

Our aim is to characterize the properties of these local galaxies and determine their star formation history (SFH). In order to serve as local analogs to $z > 4$ galaxies, the analogs must be intrinsically young, with stellar ages ≤ 1 Gyr. We combine Herschel photometric FIR data (70, 100, 160, 250, 350 and 500 μm) with optical/NIR data to characterize the star forming properties and their star formation histories. Some of our data present unresolved sources, so we use the Galaxy Fitting software (GALFIT Peng et al 2010) to perform point source function (PSF) fitting. We are also planning to obtain the distribution and kinematics of the neutral atomic gas through 21cm observations.

Author(s): Skarleth Melissa Motino Flores¹, Tommy Wiklund¹

Institution(s): 1. The Catholic University of America

149.12 – Inferring the Growth of Massive Galaxies Using Bayesian Spectral Synthesis Modeling

The most massive galaxies in the universe are typically found at the centers of massive galaxy clusters. Studying these galaxies can provide valuable insight into the hierarchical growth of massive dark matter halos. One of the key challenges of measuring the stellar mass growth of massive galaxies is converting the measured light profiles into stellar mass. We use Prospector, a state-of-the-art Bayesian spectral synthesis modeling code, to infer the total stellar masses of a pilot sample of massive central galaxies selected from the Sloan Digital Sky Survey. We compare our stellar mass estimates to previous measurements, and present some of the quantitative diagnostics provided by Prospector.

Author(s): Coley Michael Stillman¹, Megan R. Poremba¹, John Moustakas¹

Institution(s): 1. Siena College

149.13 – Clumpy Star Formation in Gravitationally Lensed Galaxies at $0.5 < z < 1$

Star-forming regions or clumps in high redshift ($z > 1$) galaxies are observed to be larger (10-100x) and more luminous (several orders of magnitude) than star-forming regions in nearby ($z \sim 0$) galaxies. It is unclear whether these high redshift star-forming clumps are scaled up versions found locally or if they are undergoing a different mode of star formation. The majority of observational studies of high-redshift star-forming clumps are typically unresolved and limited by their overall sample sizes. To gain in sensitivity and angular resolution, we utilize gravitational lensing from massive galaxy clusters to resolve sub-kiloparsec scales of distant star-forming clumps. We present the sizes and luminosities of gravitationally lensed star-forming clumps at the largely unexplored redshift regime of $0.5 < z < 1$. These sources were selected from Hubble Space Telescope (HST) imaging campaign in the Cluster Lensing and Supernova Survey with Hubble (CLASH). For the first time, utilizing gravitational lensing, we are able to explore the resolved properties and potential evolution of star-forming clumps that span the redshift space between local to distant ($z > 1$) star forming galaxies.

Author(s): Brian Molina Merino², Gregory Walth¹, Shelley Wright¹, Maren Cosens¹

Institution(s): 1. Center for Astrophysics and Space Sciences, UC San Diego, 2. Department of Physics and Astronomy, San Francisco State University

149.14 – The VIMOS Ultra Deep Survey (VUDS): Rest-frame UV Spectroscopy for ~10000 Star-forming Galaxies at $z \sim 2-6$

A comprehensive study of star-forming galaxies (SFGs) at $z \sim 2-6$ using ground-based spectroscopy and multi-wavelength photometry is vital for understanding physical processes that govern star formation and galaxy assembly at these cosmic epochs. Until now, such studies were limited by small samples because of the lack of large area, deep spectroscopic observations at high redshifts. We will present the VIMOS Ultra Deep Survey (VUDS), a spectroscopic survey of ~10000 SFGs observed with VIMOS on the VLT and currently, the largest spectroscopic sample at $2 < z < 6$. VUDS covers about 1 sq. deg in three well observed extragalactic fields (ECDFS, COSMOS, VVDS-02h). These fields have extensive photometry from UV to mid-IR wavelengths. The combination of deep VUDS spectroscopy and ample multi-wavelength photometry enables a range of studies for a large spectroscopically confirmed sample of SFGs at $z \sim 2-6$. We will present recent results from this survey that focuses on investigating physical properties of SFGs to better understand early phases of galaxy formation at $2 < z < 6$. The VUDS sample with clean selection constitute a solid reference of the star-forming population that enables massive follow-up with ALMA and JWST.

Author(s): Nimish Hathi², Olivier Le Fevre¹

Institution(s): 1. LAM, 2. STScI

Contributing team(s): VUDS Team

149.15 – Tidal Tales of Minor Mergers: Star Formation in the Tidal Tails of Minor Mergers

While major mergers and their tidal debris are well studied, equal mass galaxy mergers are relatively rare compared to minor mergers (mass ratio <0.3). Minor mergers are less energetic than major mergers, but more common in the observable universe, and thus likely played a pivotal role in the formation of most large galaxies. Tidal debris regions have large amounts of neutral gas but a lower gas density and may have higher turbulence. We use star formation tracers such as young star cluster populations and H-alpha and CII emission to determine the different factors that may influence star formation in tidal debris. These tracers were compared to the reservoirs of molecular and neutral gas available for star formation to estimate the star formation efficiency (SFE). The SFR in tidal debris can reach up to 50% of the total star formation in the system. The SFE of tidal tails in minor mergers can range over orders of magnitude on both local and global scales, and include several star forming regions with higher than normal SFE. From the tidal debris environments in our study, this variance appears to stem from the formation conditions of the debris. New results from the first survey of molecular hydrogen in minor merger tidal debris will be presented. Current surveys of the 2.12 micron line of molecular hydrogen, CO(1-0), and HI for 15 minor mergers, are providing a larger sample of environments to study the threshold for star formation that can inform star formation models, particularly at low densities.

Author(s): Karen Knierman¹, Jacqueline Monkiewicz¹, Paul Scowen¹, Christopher Groppi¹
Institution(s): 1. Arizona State University

149.16 – Local Analogues: Comparing a 12 inch Telescope to the Hubble

The College of Wooster Campus Observatory is home to two telescopes: an 8 inch and a 12 inch. We aimed to test the limits of the observatory equipment and conditions by targeting nearby galaxies, to determine their morphology based on lower resolution. We suspected that this resolution would be similar to that of the Hubble Telescope (HST) for galaxies with a higher redshift. From our images, we hoped to find various variables related to the morphology of the nearby galaxies. These variables included the Sérsic index, concentration, asymmetry, smoothness, the Gini coefficient, and M20. From here, we hoped that these would allow us to create a comparison between lower resolution galaxies that are nearby and galaxies with a higher redshift with similar resolutions.

Author(s): Nathaniel Moore¹, Laura DeGroot¹
Institution(s): 1. College of Wooster

149.17 – Quenching or Bursting: the Role of Stellar Mass, Environment & Specific Star Formation Rate to $z \sim 1$

Using a novel approach, we study the quenching and bursting of galaxies as a function of stellar mass (M_*), local environment (Σ), and specific star-formation rate (sSFR) using a large spectroscopic sample of GALEX/SDSS ($\sim 123,000$) and GALEX/COSMOS/LEGA-C (~ 440) galaxies to $z \sim 1$. We show that out to $z \sim 1$ and at fixed sSFR and local density, on average, less massive galaxies are quenching, whereas more massive systems are bursting, with a quenching/bursting transition at $\log(M_*/M_\odot) \sim 10.5-11$ and likely a short quenching/bursting timescale (≤ 300 Myr). We find that much of the bursting of star-formation happens in massive ($\log(M_*/M_\odot) \geq 11$), high sSFR galaxies ($\log(\text{sSFR}/\text{Gyr}^{-1}) \geq -2$), particularly those in the field ($\log(\Sigma/\text{Mpc}^{-2}) \leq 0$; and among group galaxies, satellites than centrals). Most of the quenching of star-formation happens in low-mass ($\log(M_*/M_\odot) \leq 9$), low sSFR galaxies ($\log(\text{sSFR}/\text{Gyr}^{-1}) \leq -2$), in particular those located in dense environments ($\log(\Sigma/\text{Mpc}^{-2}) \geq 1$), indicating the combined effects of M_* , sSFR, and Σ in quenching/bursting of galaxies since $z \sim 1$. However, we find that stellar mass and sSFR have stronger effects than environment on recent quenching/bursting of galaxies to $z \sim 1$. At any given M_* , sSFR, and environment, centrals are quencher

(quenching faster) than satellites in an average sense. We also find evidence for the strength of mass quenching (and to a lesser degree environment) being stronger at higher redshifts. Our preliminary results have potential implications for the physics of quenching/bursting in galaxies across cosmic time.

Author(s): Behnam Darvish¹, Christopher Martin¹, Thiago Goncalves⁴, Bahram Mobasher⁵, Nick Scoville¹, David Sobral², Arjen van der Wel³
Institution(s): 1. California Institute of Technology, 2. Lancaster University, 3. Max Planck Institute for Astronomy, 4. Universidade Federal do Rio de Janeiro, 5. University of California, Riverside

149.18 – Implications of Pop III Galaxies in the JWST Era

The first Pop III stars at $z > 20$ will be beyond the reach of even JWST without extremely strong gravitational lensing. However, in the presence of a LW background, a subset of halos which cross the Lyman limit at late times ($z < 15$) may contain pristine gas, allowing either direct collapse to $\sim 10^5 M_\odot$ black holes or the formation of a $10^4-10^5 M_\odot$ cluster of Pop III stars. The latter would be detectable by JWST. We present predictions for the number and detectability of these late forming Pop III galaxies as well as a more general overview of the detectability of Pop II galaxies and early massive black holes with JWST.

Author(s): Mia Sauda Bovill¹, Massimo Stiavelli¹
Institution(s): 1. STScI

149.19 – Study of turbulent and shock heated IGM gas with emission line spectroscopy in the Taffy galaxies

We present our results from optical IFU observations of the Taffy system (UGC 12914/15); named so because of the radio emission that stretches between the two galaxies. The Taffy galaxies are a major merger pair of galaxies where two gas-rich spiral galaxies have collided face on and passed through each other. The pair presents an unusually low IR luminosity ($L_{\text{FIR}} \sim 4.5 \times 10^{10} L_\odot$) and SFR ($\sim 0.23 M_\odot/\text{yr}$) for a typical post merger system. It was also found from Spitzer and Chandra observations that the Taffy "bridge" between the galaxies contains large amounts of warm molecular Hydrogen, $> 4.5 \times 10^8 M_\odot$ at 150-175K, and also shows soft X-ray emission. These results hinted at shock heating as a likely mechanism for heating the large amounts of gas in the Taffy bridge and keeping it at these temperatures, after other sources of heating are ruled out. The data we present in this paper are from the VIRUS-P instrument (now called GCMS) on the Harlan J. Smith 2.7m telescope at McDonald Observatory. We detect ionized gas all throughout the Taffy galaxies and in the bridge between them. Interestingly, the ionized gas shows emission line profiles with two velocity components almost all throughout the system. We also show evidence, through line diagnostic (BPT) diagrams, that the velocity component with lower velocity is likely excited by star formation whereas the velocity component with higher velocity is likely excited by shocks. We also find evidence for post-starburst populations in parts of the Taffy system.

Author(s): Bhavin Joshi¹, Phil Appleton³, Guillermo Blanc⁵, Pierre Guillard², Emily Freeland⁶, Bradley Peterson⁷, Katherine Alatalo⁴
Institution(s): 1. Arizona State University, 2. Institut d'Astrophysique de Paris, 3. IPAC, Caltech, 4. Observatories of the Carnegie Institution of Washington, 5. Observatorio Astronomico Nacional, Universidad De Chile, 6. Stockholm University, 7. University of Wisconsin, Barron County

149.20 – The Evolution of Galaxies Through the Spatial Distribution of Their Globular Clusters: the Brightest Galaxies in Fornax

We present a study of the evolution of the 10 brightest galaxies in the Fornax Cluster, as reconstructed through their Globular Cluster (GC) populations. GCs can be characterized by their

projected two-dimensional (2D) spatial distribution. Over- or under-densities in the GC distribution, can be linked to events in the host galaxy assembly history, and used to constrain the properties of their progenitors. With HST/ACS imaging, we identified significant structures in the GC distribution of the 10 galaxies investigated, with some of the galaxies possessing structures with >10 -sigma significance. GC over-densities have been found within the galaxies, with significant differences between the red and blue GC population. For elongated galaxies, structures are preferentially to be aligned along the major axis. Fornax Cluster galaxies appear to be more dynamically relaxed than the Virgo Cluster galaxies previously investigated with the same methodology by D'Abrusco et al. (2016). However, from these observations, the evident imprints left in the spatial distribution of GCs in these galaxies suggest a similarly intense history of interactions.

The SAO REU program is funded by the National Science Foundation REU and Department of Defense ASSURE programs under NSF Grant AST-1659473, and by the Smithsonian Institution.

Author(s): David Wassie Zegeye¹

Institution(s): 1. Harvard-Smithsonian Center for Astrophysics

149.21 – HI-bearing Ultra Diffuse Galaxies in the ALFALFA Survey

The Arecibo Legacy Fast ALFA (Arecibo L-band Feed Array) extragalactic HI survey, with over 30,000 high significance extragalactic sources, is well positioned to locate gas-bearing, low surface brightness sources missed by optical detection algorithms. We investigate the nature of a population of HI-bearing sources in ALFALFA with properties similar to "ultra-diffuse" galaxies (UDGs): galaxies with stellar masses of dwarf galaxies, but radii of L^* galaxies. These "HI-bearing ultra-diffuse" sources (HUDS) constitute a small, but pertinent, fraction of the dwarf-mass galaxies in ALFALFA. They are bluer and have more irregular morphologies than the optically-selected UDGs found in clusters, and they appear to be gas-rich for their stellar mass, indicating low star formation efficiency. To illuminate potential explanations for the extreme properties of these sources we explore their environments and estimate their halo properties. We conclude that environmental mechanism are unlikely the cause of HUDS' properties, as they exist in environments equivalent to that of the other ALFALFA sources of similar HI-masses, however, we do find some suggestion that these HUDS may reside in high spin parameter halos, a potential explanation for their "ultra-diffuse" nature.

Author(s): Lukas Leisman³, Steven Janowiecki¹, Michael G Jones²

Institution(s): 1. ICRAR, University of Western Australia, 2. Instituto de Astrofísica de Andalucía, 3. Valparaiso University

Contributing team(s): The ALFALFA Almost Darks Team

149.22 – HERA, Methods of Computational Optimization in search for Epoch of Reionization

HERA (Hydrogen Epoch of Reionization Array) is a radio telescope array aimed at detecting intergalactic neutral Hydrogen, HI, before it is ionized by early forming stars. One of the challenges that HERA faces is distinguishing signals from foreground, which may be up to orders of 5 times larger than the signal we are searching for. Instrumental noise and foreground calibration both need models of the expected measured visibility. This modeling is computationally expensive and it would be advantageous to optimize this. The main focus of this project is to reduce the amount of time for the computational model. The two routes that were used to achieve this goal was by reducing the amount of calculation, as well as using multiple processors (i.e. GPUs) to perform calculations simultaneously.

Author(s): Marcus Uriel Benavides¹, Aaron Parsons²

Institution(s): 1. HSU, 2. UCB

Contributing team(s): HERA

149.23 – The Evolution of Neutral Hydrogen in Galaxy Groups

The Illustris suite of simulations is held as the standard of large scale gravitational and hydro-dynamical simulations and allows us to make a better comparisons with physical processes at the gaseous level by providing a higher mass resolution than previously available through the Millenium-II simulation. We present a comparison of an analysis on the HI content and distribution of galaxies in groups as a function of their group dark matter halo to the results of a large scale cosmological simulation. From the simulation we select optical group members above a $M_r = -18$ r-band magnitude and HI group members with HI above $109.5M_{\odot}$. We find that 74% of the HI detected galaxies are in groups or clusters and 84% of the optically detected galaxies are in groups or clusters. In the Hess & Wilcots (2013) paper it was found that as group membership, or group dark matter halo mass, increased, the fraction of galaxies detected in HI decreased and the spatial distribution of galaxies in these groups increased. We show the spatial distributions of galaxies, HI and optically detected, in order to reproduce these results. We find that Illustris qualitatively reproduces these trends, however, the simulation seems to be overestimating the mass of HI gas in all of its galaxies as well as the number of galaxies above the $109.5M_{\odot}$ limit.

Author(s): Kelly Nicole Sanderson¹, Eric Wilcots², Kelley M. Hess²

Institution(s): 1. Old Dominion University, 2. University of Wisconsin

149.24 – An Accurate Census of the Stellar Masses of Massive Central Galaxies

A significant fraction of the stellar mass in brightest cluster galaxies--as much as 50% or more--lies in the low surface brightness and hard-to-detect outer envelope of the galaxy. An accurate census of the integrated stellar masses of central galaxies critically impacts many outstanding problems in galaxy evolution, including measurements of the star formation efficiency in massive halos, the relative importance of supernova and black hole feedback, and the cosmic baryon fraction. We use deep optical and mid-infrared imaging of a sample of more than 35,000 central galaxies obtained as part of the Legacy Survey (<http://legacysurvey.org>) to measure their azimuthally averaged stellar mass profiles and integrated stellar masses. We compare our results with previous measurements of the massive end of the stellar mass function and the stellar mass-halo mass relation, and discuss the implications of our results for numerical simulations of star formation and feedback in massive galaxies.

Author(s): John Moustakas³, Dustin Lang⁷, Kevin Napier³, Coley Michael Stillman³, Megan R. Poremba³, Arjun Dey², Eduardo Rozo⁶, Eli Rykoff⁴, David Schlegel¹, Risa Wechsler⁵

Institution(s): 1. LBNL, 2. NOAO, 3. Siena College, 4. SLAC, 5. Stanford University, 6. University of Arizona, 7. University of Toronto

149.25 – The Faint End of the Lyman Alpha Luminosity Function at $2 < z < 3.8$

Most current models predict that our universe is mostly composed of small, dim galaxies. Due to these galaxies being so faint, it is very difficult to study these types of galaxies outside of our local universe. This is particularly an issue for studying how these small galaxies evolved over their lifetimes. With the benefit of gravitational lensing, however, we are able to observe galaxies that are farther and fainter than ever before possible. In this particular study, we focus on Lyman-Alpha emitting galaxies between the redshifts of 2-3.8, so that we may study these galaxies during the epoch of peak star formation in the universe. We use the McDonald Observatory 2.7, Harlan Smith telescope with the VIRUS-P IFU spectrograph to observe several Hubble Frontier Field lensing clusters to spectroscopically discover faint galaxies over this redshift range. In addition to providing insight into the faint-end slope of the Lyman alpha luminosity function, the spectroscopic redshifts will allow us to better constrain the

mass models of the foreground clusters, such as Abell 370, so that we may better understand lensing effects for this and future studies.

Author(s): Yaswant Devarakonda¹, Rachael Livermore¹, Briana Indahl¹, Isak Wold¹, Dustin Davis¹, Steven Finkelstein¹
Institution(s): 1. University of Texas at Austin

149.26 – Metallicities of $z \sim 2$ Galaxies From the 3D-HST Survey

The metal content of the gas in galaxies as a function of cosmic time is a measure of the exchange of gas between the galaxy and its environment. Understanding its evolution is central to understanding the physical processes that govern the efficiency and timing of star formation in galaxies. Our sample consists of 127 galaxies from the 3D-HST survey with individually detected spectral lines at $z \sim 2$. We perform a comparison of line ratios that serve as proxies for the ionization parameter and oxygen abundance (O32 and R23 respectively) between the 3D-HST sample and SDSS galaxies at $z \sim 0$. We examine the mass-metallicity relation of the 3D-HST sample, deriving the metallicity using O32 and R23, based on the Kobulnicky & Kewley models. Results from the O32 versus R23 comparison in the 3D-HST sample yield a similar distribution to recent high redshift samples. The mass-metallicity (MZ) relation shows the majority of 3D-HST metallicity values fall within previous MZ relation results.

Author(s): Betsy Hernandez¹, Ivelina Momcheva²
Institution(s): 1. American Museum of Natural History, 2. Space Telescope Science Institute
Contributing team(s): 3D-HST team

149.27 – The GBT Discovery of a Massive CO(1-0) Filament Associated with the $z=2.8$ Submillimeter Galaxy SMM J02399-0136

Using the Ka-band receiver on the GBT, we have uncovered a new velocity component in CO(1-0) associated the submillimeter galaxy SMM J02399-0136. Follow-up imaging with ALMA in CO(3-2) shows that this velocity component is associated with a large linear filament covering $8''$ on the sky (60 kpc). This component comprises 50% or more of the total molecular gas mass in the system, and may represent tidal debris from a merger event or represents inflowing cold molecular gas that is fueling the ongoing starburst and AGN activity.

Author(s): David Frayer¹, Ronald Maddalena¹, Paul Vanden Bout², Galen Watts¹
Institution(s): 1. Green Bank Observatory, 2. NRAO

149.28 – Emission line galaxies at $z \sim 2$ from the 3D-HST sample

Emission-line surveys probe a much wider range of the high- z galaxy mass function than is possible with continuum selection methods, and upcoming projects such as EUCLID, WFIRST, and HETDEX will identify many millions of such galaxies. However, it is yet to be understood how properties such as the mass function, bias, and reddening distribution of galaxies selected via their Ly-alpha and rest-frame optical emission lines relate to those of systems identified via continuum-selection techniques. As a first step towards understanding the systematics of different selection techniques in the redshift range $1.9 < z < 2.35$, we present the basic properties of ~ 900 AEGIS, COSMOS, and GOODS-N emission-line galaxies found on 3D-HST grism frames. We give the distribution of stellar masses, sizes, star-formation rates, and stellar reddening of these objects, along with their rough estimates of their [O III] 5007 and H-beta luminosity functions. These data will be used as a control sample in analyses of Lyman-alpha emitters from the HETDEX survey.

Author(s): William P Bowman¹, Greg Zeimann², Robin Ciardullo¹, Caryl Gronwall¹, Adam McCarron¹
Institution(s): 1. The Pennsylvania State University, 2. The University of Texas

149.29 – Modeling Well Sampled Composite Spectral Energy Distributions of Distant Galaxies via an MCMC-driven Inference Framework

Using a novel, MCMC-driven inference framework, we have modeled the stellar and dust emission of 32 composite spectral energy distributions (SEDs), which span from the near-ultraviolet (NUV) to far infrared (FIR). The composite SEDs were originally constructed in a previous work from the photometric catalogs of the NEWFIRM Medium-Band Survey, in which SEDs of individual galaxies at $0.5 < z < 2.0$ were iteratively matched and sorted into types based on their rest-frame UV-to-NIR photometry. In a subsequent work, MIPS 24 μm was added for each SED type, and in this work, PACS 100 μm , PACS160 μm , SPIRE 25 μm , and SPIRE 350 μm photometry have been added to extend the range of the composite SEDs into the FIR. We fit the composite SEDs with the Prospector code, which utilizes an MCMC sampling to explore the parameter space for models created by the Flexible Stellar Population Synthesis (FSPS) code, in order to investigate how specific star formation rate (sSFR), dust temperature, and other galaxy properties vary with SED type. This work is also being used to better constrain the SPS models within FSPS.

Author(s): Imad Pasha², Mariska Kriek², Benjamin Johnson¹, Charlie Conroy¹
Institution(s): 1. Harvard-Smithsonian Center for Astrophysics, 2. University of California, Berkeley

149.30 – Galaxy Zoo: Infrared and Optical Morphology

We present the detailed, visual morphologies of approximately 60,000 galaxies observed by the UKIRT Infrared Deep Sky Survey and then classified by participants in the Galaxy Zoo project. Our sample is composed entirely of nearby objects with redshifts of $z \leq 0.3$, which enables us to robustly analyze their morphological characteristics including smoothness, bulge properties, spiral structure, and evidence of bars or rings. The determination of these features is made via a consensus-based analysis of the Galaxy Zoo project data in which inconsistent and outlying classifications are statistically down-weighted. We then compare these classifications of infrared morphology to the objects' optical classifications in the Galaxy Zoo 2 release (Willett et al. 2013). It is already known that morphology is an effective tool for uncovering a galaxy's dynamical past, and previous studies have shown significant correlations with physical characteristics such as stellar mass distribution and star formation history. We show that majority of the sample has agreement or expected differences between the optical and infrared classifications, but also present a preliminary analysis of a subsample of objects with striking discrepancies.

Author(s): Jesse Carla Shanahan¹, Chris Lintott², Galaxy Zoo²
Institution(s): 1. Galaxy Zoo, 2. Oxford University

149.31 – A Phenomenological Model of Star Formation Efficiency in Dark Matter Halos

The efficiency of star formation in massive dark matter halos is extraordinarily low, less than 10% in $>10^{13} M_{\text{sun}}$ sized halos. Although many physical processes have been proposed to explain this low efficiency, such as feedback from supermassive black halos and massive stars, this question remains one of the most important outstanding problems in galaxy evolution. To explore this problem, we build a simple phenomenological model to predict the variations in gas fraction and star formation efficiency as a function of halo mass. We compare our model predictions to central galaxy stellar masses and halo masses drawn from the literature, and discuss plans for our future work.

Author(s): Daniel Finnegan¹, Ghadeer Alsheshakly¹, John Moustakas¹
Institution(s): 1. Siena College

149.32 – Inhomogeneous galactic chemical evolution of r-process elements

Stars provide a fundamental contribution to the cosmic life cycle. Gas clouds form and collapse to stars, experiencing different evolutionary stages according to their properties like mass and metal content. Small stars like our Sun end their life as planetary nebulae, while more massive stars end their evolution with violent explosions like supernovae or hypernovae, leaving behind either a neutron star or a black hole. These compact objects may also merge, leading to a new ejection of material. Today the origin of the heaviest elements is still matter of debate. The relative contributions of the proposed sources of r-process elements (e.g., Supernovae, Neutron Star Mergers) in the early galaxy as well as in the Sun is one of the main uncertainties. We use the inhomogeneous chemical evolution tool “ICE” [1, 2] to study the role of some of the main parameters of the cosmic life cycle. With ICE's high resolution (≥ 20 parsec/cell) runs, we are able to get converged simulations of the inhomogeneities in the early Galactic evolution stages, and of the observed scatter of r-process elements in metal-poor stars [3].

[1] B. Wehmeyer, M. Pignatari, F.-K. Thielemann, 2015 MNRAS 452, 1970–1981

[2] B. Wehmeyer, M. Pignatari, F.-K. Thielemann, 2016 AIPC 1743, 040009

[3] I. Roederer et al., 2010 ApJ 724:975–993

Author(s): Benjamin Wehmeyer¹

Institution(s): 1. North Carolina State Univ

149.33 – Lyman-alpha fractions in the Hubble Ultra Deep Field at $4 < z < 6$

Lyman-alpha (Ly α) emitting galaxies at high-redshifts serve as a good probe of neutral hydrogen in the intergalactic medium (IGM). Here we present measurements of the Ly α fraction using a sample of Lyman-break galaxies (LBGs) between $4 < z < 6$ with deep HST grism observations from the GRAPES/PEARS projects as well as spectroscopic observations from the MUSE integral-field spectrograph. The sample of LBGs at $z \sim 5$ & 6 are spectroscopically confirmed with deep HST grism data from the GRAPES and PEARs projects. We also measure Ly α fractions using a sample of photometrically-selected LBGs for the same redshift range. In addition, we study the EW distribution in relation to continuum and line luminosities, as well as the relation between photometric and spectroscopic redshift. We find that objects with higher EWs tend to have larger differences between photometric and spectroscopic redshifts.

Author(s): Santosh Harish¹, Sangeeta Malhotra¹, James Rhoads¹, Lise Christensen², Vithal Tilvi¹, Steven Finkelstein³, John Pharos¹

Institution(s): 1. Arizona State University, 2. Niels Bohr Institute, University of Copenhagen, 3. University of Texas at Austin

149.34 – UNDERSTANDING THE STRUCTURE OF THE HOT INTERSTELLAR MEDIUM IN NORMAL EARLY-TYPE GALAXIES.

The hot interstellar medium (ISM) of early-type galaxies (ETG's) provides crucial insight into the understanding of their formation and evolution. Mechanisms such as type Ia supernovae heating, AGN feedback, deepening potential depth through dark matter assembly and ramp-pressure stripping are known to affect the structure of the ISM. By using temperature maps and radial temperature profiles of the hot ISM from ~ 70 ETG's with archival Chandra data, it is possible to classify the galaxy's ISM into common structural types. This is extended by using 3D fitting of the radial temperature profile in order to provide models that further constrain the structural types. Five structural types are present, negative (temperature decreases with radii), positive (temperature increases with radii), hybrid-dip (temperature decreases at small radii and increases at large radii), hybrid-bump (inverse of hybrid-dip) and quasi-isothermal (temperature is constant at all radii). This work will be continued by 1) determining which mechanisms are present in which galaxies and

2) analysing the model parameters between galaxies within each structural type to determine whether each type can be described by a single set of model parameters, indicating that the same physical processes are responsible for creating that structural type.

Author(s): Liam Traynor¹, Dong-Woo Kim¹

Institution(s): 1. Harvard-Smithsonian Center for Astrophysics

Contributing team(s): Chandra Galaxy Atlas

149.35 – Understanding Supermassive Black Hole Growth Mechanisms in the SSA22 Protocluster

The SSA22 protocluster is a collection of galaxies at redshift $z = 3.09$, corresponding to a look back time of 11.6 billion years. Observations of the protocluster allow for the investigation of galaxy properties of such protocluster environments in the early universe, potentially giving insight into the formation and evolution of galaxy clusters visible in the local universe (e.g., the Coma Cluster). Compared to other field galaxies at a similar redshift, a larger fraction of galaxies in SSA22 have been found to possess active galactic nuclei (AGN). This enhanced AGN activity suggests a relationship between the environment within the cluster and the growth of supermassive black holes (SMBHs). I will clarify the role that the protocluster environment at $z = 3.09$ plays in enhancing the growth of SMBHs in the cluster. To accomplish this, we are analyzing recently obtained WFC3 F160W data from the Hubble Space Telescope (HST) in SSA22, and equivalent archival CANDELS data in the Hubble Deep Field-North, to compare the merger rates and stellar mass distributions of galaxies in the SSA22 protocluster and in the field. Our goal is to assess the relative role that mergers play in enhancing the SMBH growth observed in over-dense regions in the $z = 3$ Universe.

Author(s): Brett Bonine¹, Bret Lehmer¹

Institution(s): 1. University of Arkansas

149.36 – Resolving the extended stellar halos of nearby galaxies: the wide-field PISCeS survey

I will present results from the wide-field Panoramic Imaging Survey of Centaurus and Sculptor (PISCeS): the resolved stellar halos of two nearby galaxies (the spiral NGC253 and the elliptical Centaurus A, $D \sim 3.7$ Mpc) are investigated out to a galactocentric radius of 150 kpc with Magellan/Megacam. The survey pushes the limits of near-field cosmology beyond the Local Group, by characterizing the stellar content (ages, metallicities, gradients) of extended halos and their substructures in two environments substantially different from the Local Group, i.e. the loose Sculptor group of galaxies and the Centaurus A group dominated by an elliptical. PISCeS has to date led to the discovery of 11 confirmed satellites as faint as $M_V = -8$ (including Ultra Diffuse Galaxies), streams and tidal substructures with surface brightness limits as low as ~ 32 mag/arcsec², and hundreds of globular cluster/ultra-compact dwarf candidates. The unique strength of PISCeS is the exquisite synergy between the wide-field, ground-based survey and its extensive imaging and spectroscopic follow-up (HST, Keck, VLT, Magellan, AAT), which constitute the first accurate characterization of the past and ongoing accretion processes shaping the halos of these nearby galaxies. Our observational campaign will not only provide crucial constraints to quantitatively inform theoretical models of galaxy formation and evolution, but it also represents a necessary testbed in preparation for future very large datasets stemming from the next generation of ground-based (LSST, TMT, GMT) as well as spaceborne (JWST, WFIRST) telescopes.

Author(s): Denija Crnojevic⁵, David Sand⁶, Kristine Spekkens⁴, Nelson Caldwell¹, Puragra Guhathakurta⁷, Brian McLeod¹, Anil Seth⁹, Joshua D. Simon³, Jay Strader², Elisa Toloba⁸

Institution(s): 1. Harvard-Smithsonian Center for Astrophysics, 2. Michigan State University, 3. Observatories of the Carnegie Institution for Science, 4. Royal Military College of Canada, 5. Texas Tech University, 6. University of Arizona, 7. University of California Santa Cruz, 8. University of the Pacific, 9. University of Utah

149.37 – Extended Star-formation and Disk-like Kinematics in a $z \sim 3$ Massive "Main-Sequence" Galaxy through [CII] Imaging and Multi-J CO Line Observations

Dusty star-forming galaxies (SFG) at high redshifts are the main contributors to the comoving star formation rate (SFR) density, which peaks between the redshift of $z=1-3$ ("Cosmic Noon"). Yet, new insights into their gas dynamics, and thus, structural evolution are awaiting spatially resolved observations. I will present the latest results from our kpc-scale [CII] imaging and multi-J CO line observations obtained with ALMA, CARMA, PdBI, and the VLA in one of the most massive "main-sequence" disk galaxy known. XMM03 ($z=2.9850$) is an extremely IR-luminous galaxy with a SFR of ~ 3000 Msun/yr, but its molecular gas excitation is surprisingly similar to the Milky Way up to $J=5$, which is in stark contrast with most high- z galaxies studied to date. The monotonic velocity gradient seen in the [CII] line emission suggest that it is a rotating disk galaxy. Based on the molecular gas surface density and the far-UV radiation flux determined from photo-dissociation region (PDR) modeling, the star-forming environment of XMM03 is similar to nearby SFGs. These findings together with the ~ 1100 km/s wide CO(1-0) line across the entire disk of ~ 8 kpc in radius showcase the different interstellar medium (ISM) environment that we are probing at the most massive end of galaxies in the early Universe. With a stellar mass of $M^* \sim 10^{12}$, its specific SFR is consistent with an extrapolation of the "star-forming main-sequence" up to $M^* \sim 10^{12}$ Msun at $z \sim 3$. Our findings therefore confirm the prevalence of disk-wide star formation responsible for assembling most of the stellar masses toward the "Cosmic Noon".

Author(s): Tsz Kuk Daisy Leung¹, Dominik A Riechers¹, David Clements⁴, Asantha Cooray⁶, Rob Ivison³, Ismael Perez-Fournon⁵, Julie Wardlow²

Institution(s): 1. Cornell University, 2. Durham University, 3. European Southern Observatory (ESO), 4. Imperial College London, 5. Instituto de Astrofísica de Canarias, 6. UC Irvine

149.38 – Significance of Environmental Density in Shocked Poststarburst Galaxy Evolution

The Shocked Poststarburst Galaxy Survey (SPOGS) comprises 1,066 galaxies undergoing the transformation from blue cloud late-type spirals to red sequence non-star-forming early-type ellipticals and lenticulars. They are selected via spectral analysis of ionized gas line ratios, which indicate shocked objects, and Balmer H- δ equivalent width, which select recently formed stars, but not active star formation. E+A galaxies (Zabludoff et al. 1996), like SPOGs, contain young stars but, unlike SPOGs, no emission lines consistent with star formation. They differ in that the quality used to discern SPOGs, their shocks, produces H- α lines that prevent them from being found via the same criteria as E+As. Thus, SPOGs can be found before being entirely stripped of their gas, and, while E+As are largely red and dead, found leaving the green valley, SPOGs are mostly entering it. The environmental density data for SPOGs was retrieved via the NASA Extragalactic Database (NED) radial velocity constrained cone tool, which provides counts and densities within spheres of radii 1, 5, and 10 Mpc from the center of search as well as relative positions and redshifts of objects. The kinematic morphology-density relation (Cappellari et al. 2011) is employed as a point of comparison for how SPOGs' environmental densities might relate to morphological and spectroscopic factors, including tidal

features, asymmetry, and color, in order to fully understand the role of environmental factors in SPOGS object evolution.

Author(s): Laura Jaliff¹

Institution(s): 1. California Institute of Technology

149.39 – Galaxy morphology and the associated stellar properties in PEARS Survey at $0.6 < z < 1.2$

We explored the D4000 strength and photometrically-derived properties of our sample galaxies with their morphology classification. Our sample of galaxies consist of 350 galaxies with $\log(M_*/M) > 9.44$ at $0.6 < z < 1.2$, utilizing both photometric and spectroscopic data mainly obtained from the *Hubble Space Telescope*. We have identified authentically 'red and dead' galaxies in the (U-V) color vs. (V-J) color (UVJ) diagram based on their D4000 strengths. This spectroscopic identification is in good agreement with their photometrically-derived Specific Star Formation Rates (sSFR). We also studied the morphological dependence of galaxies in the UVJ diagram and found that most (67 out of 70 galaxies, $\sim 96\%$) of these newly identified 'red and dead' galaxies have a visually-identifiable prominent bulge component. However, not all of the bulge-dominant galaxies seem to quench their star formation activity. We explored the correlations between galaxy structure and the stellar properties such as the D4000 strength, stellar mass, sSFR, surface density within the effective radius, and Sérsic index. We discuss the implications of our results in the context of galaxy morphology and the associated stellar properties at intermediate redshift.

Author(s): Keunho Kim¹, Bhavin Joshi¹, James Rhoads¹, Sangeeta Malhotra¹, Anna Pasquali², Ignacio Ferreras³

Institution(s): 1. Arizona State University, 2. Universit at Heidelberg, 3. University College London

Contributing team(s): PEARS team

149.40 – Probing Gas Stripping with Resolved Star-Formation Maps of Virgo Filament Galaxies

We are conducting a multi-wavelength study of the gas in galaxies at a variety of positions in the cosmic web surrounding the Virgo cluster, one of the best studied regions of high density in the Universe. Galaxies are very likely pre-processed in filaments before falling into clusters, and our goal is to understand how galaxies are altered as they move through the cosmic web and enter the densest regions. We present spatially-resolved H-alpha imaging results from the KPNO 0.9-m and INT 2.54-m telescopes for a preliminary sample of 30 galaxies. We will combine the star-formation maps with observations of molecular and atomic gas to calculate gas consumption timescales, characterize multiple phases of the galactic gas, and look for signatures of environmentally-driven depletion.

This work is supported in part by NSF grant AST-1716657.

Author(s): Natasha Collova¹

Institution(s): 1. Siena College

149.41 – The Infrared-Radio Correlation of Dusty Star Forming Galaxies at High Redshift

Far-infrared (FIR) and radio continuum emission in galaxies are related by a common origin: massive stars and the processes triggered during their birth, lifetime, and death. FIR emission is produced by cool dust, heated by the absorption of UV emission from massive stars, which is then re-emitted in the FIR. Thermal free-free radiation emitted from HII regions dominates the spectral energy density (SED) of galaxies at roughly 30 GHz, while non-thermal synchrotron radiation dominates at lower frequencies. At low redshift, the infrared radio correlation (IRC, or qIR) holds as a tight empirical relation for many star forming galaxy types, but until recently, there has not been sensitive enough radio observations to extend this relation to higher redshifts. Many selection biases cloud the results of these analyses, leaving the evolution of the IRC with redshift ambiguous. In this poster, I present CIGALE fitted spectral energy distributions (SEDs) for 24 gravitationally-lensed sources selected in the mm-wave from the South Pole Telescope (SPT)

survey. I fit the IRC from infrared and submillimeter fluxes obtained with Herschel, Atacama Pathfinder Experiment (APEX), and SPT and radio fluxes obtained with ATCA at 2.1, 5.5, 9, and 30 GHz. This sample of SPT sources has a spectroscopic redshift range of $2.1 < z < 5.7$ with an average redshift of $z=4$. In this poster, I will present the results of this study and compare our results to various results in the literature.

Author(s): Sidney Lower¹, Joaquin Daniel Vieira¹, Sreevani Jarugula¹

Institution(s): 1. University of Illinois Urbana-Champaign

149.42 – Spectroscopic Redshifts to 1300 Low-Mass Galaxies with $0.3 \leq z \leq 0.4$ in the COSMOS Field

Recent theoretical models and hydrodynamic simulations of galaxy evolution give predictions for the star-forming properties and sizes of low-mass galaxies. Due to their faintness, there exist few unbiased samples of low-mass galaxies to test these predictions. However, the Hubble Space Telescope's deep observations of the COSMOS field allow for the creation of an unbiased collection of galaxies with stellar masses $10^9 < M < 10^{10}$ solar masses in the redshift range $0.3 < z < 0.4$. In particular, the UltraVISTA catalog (Muzzin et al. 2013) identifies roughly 250,000 objects to $K_s=23.4$ mag (AB) in COSMOS and includes estimates of photometric redshifts for the galaxies. To study the star formation and morphological properties of an unbiased sample of galaxies, we targeted 1131 unique galaxies in the above redshift range with the IMACS spectrograph on the Magellan Baade 6.5m telescope. Using real domain, inverse-variance weighted cross-correlation with galaxy templates from the Sloan Digital Sky Survey, we measure accurate spectroscopic redshifts for 86% of the targeted galaxies. Our work provides a population of low-mass galaxies for which we can measure star formation rates, furthering our understanding of low-mass galaxy evolution.

Author(s): Brian Lorenz², Daniel D Kelson¹

Institution(s): 1. Carnegie Observatories, 2. Pomona College

149.43 – Evolution of the Circumgalactic Medium in a Simulated Dwarf Galaxy

The circumgalactic medium (CGM) evolves through galaxies' expulsion of material into the surroundings. Gas in the CGM also accretes onto the galaxy which it surrounds. The history of these close interactions between a galaxy and the CGM is difficult to study observationally, leading to the use of simulations. This project explores the evolution of the CGM of a simulated dwarf galaxy ($M_{vir} = 1.8 \times 10^{10} M_{\odot}$) from $z = 3$ to $z = 0$. We used two forms of analysis on our simulations. We extracted information such as gas temperature and gas surface density directly from the simulations. Then, in order to mimic data that would be received from observational research, we generated synthetic absorption line spectra along lines of sight. Our analysis shows that the CGM becomes more orderly over time. Gas movement at high redshift has much higher variance than at $z = 0$. We observe that there is a trend towards the reduction of gas temperature over time, which is reflected in the ionization levels of the gas. In addition, since $z = 1$, we see an increase in the amount of metals at large radii. This increased metallicity extends far into the CGM, suggesting high velocity outflowing gas from the galactic disk.

Author(s): Nicole Arredondo¹, Patrick Sheehan-Klenk¹, Charlotte Christensen¹

Institution(s): 1. Grinnell College

149.44 – Quantifying the Role of Environment in Star Formation: ISM masses along the Cosmic Web

The rate of star formation in galaxies is observed to vary with environment across the cosmic web and this relationship evolves with redshift. Local galaxies in dense environments are in a state of passive evolution with little star formation. However, ongoing star formation is found in galaxies in dense environments at higher redshifts. Observations of the interstellar medium (ISM), including the molecular gas, which is the direct fuel for star

formation, are key to determining how long star formation will persist.

We present new ALMA observations of 101 galaxies that span a range of environments at $z \sim 0.7$, when star formation in dense environments was higher than it is today. Using these observations, we calculate the total ISM mass and look for depletion as a function of galaxy density in order to understand the quenching of star formation in galaxies as a function of environment.

Author(s): Sarah Betti⁴, Alexandra Pope⁴, Nick Scoville¹, Herve Aussel², Kartik Sheth³, Min Yun⁴

Institution(s): 1. California Institute of Technology, 2. CEA Saclay, 3. NASA HQ, 4. University of Massachusetts Amherst

149.45 – The Structure and Kinematics of Little Blue Spheroid Galaxies

A population of blue, morphologically early-type galaxies, dubbed "Little Blue Spheroids" (LBSs), has been identified as a significant contributor to the low redshift galaxy population in the GAMA survey. Using deep, high-resolution optical imaging from KiDS and the new Bayesian, two-dimensional galaxy profile modelling code PROFIT, we examine the detailed structural characteristics of LBSs, including low surface brightness components not detected in previous SDSS imaging. We find that these LBS galaxies combine features typical of early-type and late-type populations, with structural properties similar to other low-mass early types and star formation rates similar to low-mass late types. We further consider the environments and SAMI-derived IFU kinematics of LBSs in order to investigate the conditions of their formation and the current state of their dynamical evolution.

Author(s): Amanda J Moffett³, Steven Phillipps², Aaron Robotham¹, Simon Driver¹, Malcolm Bremer²

Institution(s): 1. ICRAR, 2. University of Bristol, 3. Vanderbilt University

Contributing team(s): GAMA survey team, SAMI survey team

149.46 – Ultraviolet to Infrared SED (Spectral Energy Distribution) Analysis of Nearby Late-Stage Merger

We present an analysis of the fundamental properties of nearby merging galaxies based on an in-depth analysis of their spectral energy distributions. The Late-Stage Interacting Galaxy Sample (LSIGS) cross-correlates the Revised IRAS-FSC Redshift Catalogue (Wang et al. 2014) with Galaxy Zoo (Lintott et al. 2008, 2011). LSIGS builds on and extends SIGS (Spitzer Interacting Galaxy Sample; Lanz et al. 2013, Brassington et al. 2015) in two ways. First it enlarges the sample considerably to 453 systems, increasing the statistical power of the analysis significantly. Second, it includes galaxies in the most advanced merger stage, during coalescence, filling a gap in the SIGS sample. We present full ultraviolet (UV) to far-infrared (FIR) aperture photometry for 50 galaxies in this sample, 40 of which are late-stage mergers, selecting based on availability of both UV and SPIRE observations. These have subsequently been fit and analyzed by CIGALE (Code Investigating Galaxy Emission; Burgarella 2005) in order to retrieve key physical properties of the galaxies including star-formation rate (SFR), AGN fraction, dust luminosity, bolometric luminosity, and stellar and gas mass. We use this same analysis on hydrodynamical simulations created with GADGET-3 and using SUNRISE for the radiative transfer. Using the observations in conjunction with the simulations, CIGALE fits the simulated values accurately for $f_{AGN} > 0.3$. Additionally galaxies in the midst of coalescence have significantly increased sSFR compared to both early and late-stage mergers, while finding that the gas mass and alpha significantly increase from early stage mergers to those in coalescence. Furthermore, we find a linear anti-correlation between alpha and both the $\log(60/100\mu\text{m})$ flux, and, more interestingly, the compactness. Lastly we bring forth the idea of

using the best fit age of the oldest stars and the folding time of the stellar population, τ_{main} , in conjunction to predict the likelihood of a galaxy being in a late-stage merger or in the midst of coalescence.

Author(s): Aaron S. Weiner³, Howard A. Smith³, Matthew Ashby³, Juan Rafael Martínez-Galarza³, Andres Ramos Padilla³, Chao-Ling Hung⁴, Jeremy Dietrich⁶, Lauranne Lanz², Christopher Hayward⁵, Lee Rosenthal¹, Steven Willner³, Andreas Zezas³

Institution(s): 1. California Institute of Technology, 2. Dartmouth College, 3. Harvard-Smithsonian Center for Astrophysics, 4. Manhattan College, 5. Simons Center for Computational Astrophysics, 6. University of Arizona

149.47 – Insights into galaxy mass quenching in the IllustrisTNG simulation using global morphological diagnostics

Among massive galaxies, the quenching of star formation is observed to correlate with morphological and structural transformations; however, the internal mechanisms by which quenching occurs are still not well constrained. The structural transformations of galaxies have so far mostly been traced using diagnostics that largely describe their innermost volumes, such as the stellar core density, or the density within 1 kpc, the growth of which reflects the dissipative history of galaxies. We use non-parametric global morphological diagnostics, such as Gini and M_{20} , to demonstrate that structural transformations during quenching are more profound than simply the growth of the core density – indeed, the full structure of galaxies undergoes transformations during quenching. Using the IllustrisTNG simulation we test, for the first time, whether the observed relation between quenching and global morphological transformations also occurs in Λ CDM cosmological simulations. Additionally, we investigate the physical processes driving the transformations and quenching of massive galaxies.

Author(s): Samuel Paul Carman², Elena D'Onghia², Mauro Giavalisco¹, Alisha Kundert²

Institution(s): 1. University of Massachusetts - Amherst, 2. University of Wisconsin - Madison

Contributing team(s): IllustrisTNG Team

149.48 – Elliptical Galaxy in the Making: The Dual AGN Activity and Metal-enriched Halo of Mrk 273

A systematic analysis of the X-ray emission from the nearby ultraluminous infrared galaxy Mrk 273 was carried out by combining new 200 ksec Chandra data with archived 44 ksec data. The AGN associated with the SW nucleus is confirmed by the new data, and a secondary hard X-ray point source is detected, overlapping with the N nucleus seen in the near-infrared. The hard X-ray spectrum of the N nucleus is consistent with a heavily absorbed AGN, making Mrk 273 another example of a dual AGN in a nearby galaxy merger. The data also map the giant X-ray nebula south of the host with unprecedented detail. This nebula extends on a scale of $\sim 40 \text{ kpc} \times 35 \text{ kpc}$, and is not related to the well-known tidal tail seen in the optical. The X-ray emission of the nebula is best described by a single-temperature plasma model, with a temperature of ~ 7 million K and a super-solar α/Fe ratio. Both the temperature and α/Fe ratio show no obvious spatial variations across the nebula. Significant 1-3 keV emission is also found along the outflowing gas traced by the broad [OIII] emission detected in a previous study. The α/Fe abundance of the hot gas in this region is super-solar, indicating a connection between the [O III] outflow and the α -enhanced X-ray emitting material. These results suggest that the southern nebula is heated and enriched by multiple galactic outflows generated by the AGN and/or circumnuclear starburst, on a time scale of $\leq 10^8$ yr. Similar results were derived in the nebulae surrounding two other well-known galaxy mergers, NGC 6240 and Mrk 231. In contrast, extended soft X-ray emitting material with lower temperature and α/Fe ratio is detected northeast of the host, perhaps representing the pre-existing halo gas that has not yet been affected by the outflow.

Author(s): Weizhe Liu⁷, Sylvain Veilleux⁷, Kazushi Iwasawa¹, Stacy Teng², Max Claire⁴, David B. Sanders⁶, Vivian U5, Marcio Melendez³, Francesco Tombesi⁷

Institution(s): 1. ICREA, 2. Institute for Defense Analyses, 3. NASA GSFC, 4. UCSC, 5. University of California, Riverside, 6. University of Hawaii, 7. University of Maryland

149.49 – Multi-Wavelength Statistics of Clumpy Galaxies

We calculated the fraction of 'clumpy' galaxies (f_{clumpy}) for three samples of nearby galaxies. These samples include interacting galaxies with strong tidal features, collisional ring galaxies, and normal spiral galaxies. We defined a 'clumpy' galaxy as a galaxy that has luminous star-forming regions contributing more than 8% of the total flux for the galaxy. We calculated f_{clumpy} for 16 different wavelengths. We found that f_{clumpy} is highest in the ultraviolet, H α , and 24 μm , while f_{clumpy} is the lowest in optical and near-infrared wavelengths. We also see a significant increase in f_{clumpy} for the interacting samples compared to the normal spirals.

Author(s): Isaiah Samuel Cox¹, Beverly J Smith¹

Institution(s): 1. East Tennessee State University

149.50 – Comparing Low-Redshift Compact Dwarf Starbursts in the RESOLVE Survey with High-Redshift Blue Nuggets

We identify and characterize a population of compact dwarf starburst galaxies in the RESOLVE survey, a volume-limited census of galaxies in the local universe, to probe the possibility that these galaxies are related to "blue nuggets," a class of intensely star-forming and compact galaxies previously identified at high redshift. Blue nuggets are thought to form as the result of intense compaction events that drive fresh gas to their centers. They are expected to display prolate morphology and rotation along their minor axes. We report IFU observations of three of our compact dwarf starburst galaxies, from which we construct high-resolution velocity fields, examining the evidence for minor axis or otherwise misaligned rotation. We find multiple cases of double nuclei in our sample, which may be indicative of a merger origin as in some blue nugget formation scenarios. We compare the masses, radii, gas-to-stellar mass ratios, star formation rates, stellar surface mass densities, and environmental contexts of our sample to expectations for blue nuggets.

Author(s): Michael Louis Palumbo⁶, Sheila Kannappan⁶, Elaine Snyder⁵, Kathleen Eckert⁸, Dara Norman³, Luciano Fraga², Bruno Quint⁴, Philippe Amram¹, Claudia Mendes de Oliveira⁷

Institution(s): 1. Laboratoire d'Astrophysique de Marseille, 2. Laboratorio Nacional de Astrofísica Coordinadora de Apoio a Ciência, 3. NOAO, 4. Southern Astrophysical Research (SOAR) Telescope, 5. STScI, 6. UNC Chapel Hill, 7. Universidade de São Paulo, 8. University of Pennsylvania

Contributing team(s): RESOLVE Team

149.51 – WFIRST: Extragalactic Science over Twelve Billion Years of Cosmic History

WFIRST's infrared multiband imaging and spectroscopy from space over thousands of square degrees will revolutionize our understanding of galaxy formation and evolution. When combined with unique guest observer programs that provide ultra-deep IR imaging and spectroscopy over areas $>100\times$ larger than achieved by Hubble Space Telescope, WFIRST will provide the first complete picture of star formation and stellar mass build-up in galaxies over twelve billion years of cosmic history. The WFIRST Extragalactic Potential Observations (WFIRST-EXPO) Science Investigation Team has identified a host of guest observer and archival programs where WFIRST can transform our views of the connections between the star formation, environment, morphology, stellar mass, and dark matter halo properties of galaxies, and determined how WFIRST can singularly probe the connection between early galaxies and the process of cosmic reionization. We present these WFIRST capabilities, and discuss

how the science from WFIRST relates to other major forthcoming space- and ground-based facilities.

Author(s): Mark Dickinson¹, Brant Robertson⁷, Henry C. Ferguson³, Steve Furlanetto⁶, Jenny Greene², Piero Madau⁷, Dan Marrone⁵, Alice Shapley⁶, Daniel P Stark⁵, Risa Wechsler⁴, Stan Woosley⁷

Institution(s): 1. National Optical Astronomy Observatory, 2. Princeton University, 3. Space Telescope Science Institute, 4. Stanford University, 5. University of Arizona, 6. University of California Los Angeles, 7. University of California Santa Cruz

Contributing team(s): The WFIRST-EXPO Science Investigation Team

149.52 – Estimating the Evolution of X-ray Binary Populations in Nearby Galaxies

Recently, we have found, in the Chandra Deep Field-South, that the emission from X-ray binary (XRB) populations in galaxies evolves significantly with cosmic time, most likely due to changes in the physical properties of galaxies like star-formation rate, stellar mass, stellar age, and metallicity. However, it has been challenging to directly show that these same physical properties are connected to XRB populations using data from nearby galaxies. We present a new technique for empirically calibrating how X-ray binary (XRB) populations evolve following their formation in a variety of environments. We first utilize detailed spectral energy distribution modeling of far-UV to far-IR broadband data of the nearby (~8.5 Mpc) face-on spiral galaxies M51 to construct a map of its star-formation history (SFH) on subgalactic scales. Using Chandra data, we then identify the locations of the XRBs and correlate their formation frequencies with local SFH, as characterized by the mean mass-weighted stellar age. I will show first constraints on how the shape and normalization of XRB luminosity function evolves with time based on our analysis of M51. I further discuss how expanding our sample to an archival sample of ~25 face-on spirals will lead to a detailed empirical timeline for how XRBs form and evolve in a variety of environments and throughout cosmic time.

Author(s): Bret Lehmer¹, Rafael Eufrazio¹

Institution(s): 1. University of Arkansas

149.53 – Observational Tracers of Hot and Cold Gas in Isolated Galaxy Simulations

We present results from an analysis comparing simulations of isolated spiral galaxies with recent observations of the circumgalactic medium (CGM). As the interface containing inflows and outflows between the interstellar and intergalactic media, the CGM plays an important role in the composition and evolution of galaxies. Using a set of isolated galaxy simulations over different initial conditions and star formation and feedback parameters, we investigate the evolution of CGM gas. Specifically, in light of recent observational studies, we compute the radial column density profiles and covering fractions of various observable ion species (H I, C IV, O VI, Mg II, Si III) for each simulated galaxy. Taking uniformly random sightlines through the CGM of each simulated galaxy, we find the abundance of gas absorbers and analyze their contribution to the overall column density along each sightline. By identifying the prevalence of high column density absorbers, we seek to characterize the distribution and evolution of observable ion species in the CGM. We also highlight a subset of our isolated galaxy simulations that produce and maintain a stable precipitating CGM that fuels high rates of sustained star formation. This project was supported in part by the NSF REU grant AST-1358980 and by the Nantucket Maria Mitchell Association.

Author(s): Bryan Brzycki¹, Devin Silvia²

Institution(s): 1. Harvard University, 2. Michigan State University

149.54 – Star Formation in Merging Galaxies Using FIRE

Galaxy interactions and mergers are efficient mechanisms to birth stars at rates that are significantly higher than found in our Milky Way galaxy. The Kennicutt-Schmidt (KS) relation is an empirical relationship between the star-forming rate and gas surface densities of galaxies (Schmidt 1959; Kennicutt 1998). Although most galaxies follow the KS relation, the high levels of star formation in galaxy mergers places them outside of this otherwise tight relationship. The goal of this research is to analyze the gas content and star formation of simulated merging galaxies. Our work utilizes the Feedback In Realistic Environments (FIRE) model (Hopkins et al., 2014). The FIRE project is a high-resolution cosmological simulation that resolves star-forming regions and incorporates stellar feedback in a physically realistic way. In this work, we have noticed a significant increase in the star formation rate at first and second passage, when the two black holes of each galaxy approach one other. Next, we will analyze spatially resolved star-forming regions over the course of the interacting system. Then, we can study when and how the rates that gas converts into stars deviate from the standard KS. These analyses will provide important insights into the physical mechanisms that regulate star formation of normal and merging galaxies and valuable theoretical predictions that can be used to compare with current and future observations from ALMA or the James Webb Space Telescope.

Author(s): Adrianna Perez¹, Chao-Ling Hung⁴, Jill Naiman³, Jorge Moreno⁵, Philip Hopkins²

Institution(s): 1. California State University Dominguez Hills, 2. California Technical Institute of Technology, 3. Harvard-Smithsonian Center for Astrophysics, 4. Manhattan College, 5. Pomona College

149.55 – The Effects of Galaxy Interactions on Star Formation

Galaxy interactions are key events in galaxy evolution, and are widely thought to trigger significant increases in star formation. However, the mechanisms and timescales for these increases are still not well understood. In order to probe the effects of mergers, we undertook an investigation based on the Spitzer Interacting Galaxies Survey (SIGS), a sample of 102 nearby galaxies in 48 systems ranging from weakly interacting to near coalescence. Our study is unique in that we use both broadband photometry and a large sample of objects chosen to be statistically meaningful. Our data come from 32 broad bands ranging from the UV to far-IR, and we model spectral energy distributions (SEDs) using the Code for Investigating Galaxy Emission (CIGALE) to estimate physical characteristics for each galaxy. We find marginal statistical correlations between galaxy interaction strength and dust luminosity and the distribution of dust mass as a function of heating intensity. The specific star formation rates, however, do not show any enhancement across the interaction stages. This result challenges conventional wisdom that mergers induce star formation throughout galaxy interaction.

The SAO REU program is funded in part by the National Science Foundation REU and Department of Defense ASSURE programs under NSF Grant no. 1262851, and by the Smithsonian Institution.

Author(s): Aliza Beverage⁴, Aaron Weiner³, Andres Ramos Padilla², Matthew Ashby¹, Howard A. Smith¹

Institution(s): 1. Harvard-Smithsonian Center for Astrophysics, 2. Leiden University, 3. Rensselaer Polytechnic Institute, 4. University of Minnesota - Twin Cities

149.56 – Cosmic Star Formation History and Evolution of the Galaxy UV Luminosity Function for $z < 1$

We present the latest constraints on the evolution of the far-ultraviolet luminosity function of galaxies (1500 Å, UVLF hereafter) for $0 < z < 1$ based on GALEX photometry, with redshift measurements from four spectroscopic and photometric-redshift catalogs: NSA, GAMA, VIPERS, and COSMOS photo-z.

Our final sample consists of ~ 170000 galaxies, which represents the largest sample used in such studies. By integrating wide NSA and GAMA data and deep VIPERS and COSMOS photo- z data, we have been able to constrain both the bright end and the faint end of the luminosity function with high accuracy over the entire redshift range. We fit a Schechter function to our measurements of the UVLF, both to parameterize its evolution, and to integrate for SFR densities. From $z \sim 1$ to $z \sim 0$, the characteristic absolute magnitude of the UVLF increases linearly by ~ 1.5 magnitudes, while the faint end slope remains shallow ($\alpha < 1.5$). However, the Schechter function fit exhibits an excess of galaxies at the bright end, which is accounted for by contributions from AGN. We also describe our methodology, which can be applied more generally to any combination of wide-shallow and deep-narrow surveys.

Author(s): Keming Zhang¹, David Schiminovich¹
Institution(s): 1. Columbia University

149.57 – Outer Disks of Clumpy and Spiral Galaxies in the Hubble Frontier Field Parallels

Local disk galaxies have axial ratio distributions that are approximately constant for all inclinations, down to the lower end limited by the disk thickness. In contrast, disk galaxies observed in the Hubble Ultra Deep Field (UDF) at high redshift have a distribution of axial ratios that falls off towards the high end. This effect may be the result of cosmological dimming, which preferentially affects face-on disks, or it could be from a lack of axially symmetric disks. Stacked images of small spheroidal Lyman Break Galaxies in the UDF previously revealed that they have faint outer disks. Here we use the Hubble Frontier Field Parallels to provide a new sample of galaxies; four of the fields have publicly available catalogues listing photometric redshifts. We identified and classified disk galaxies as spiral or clumpy, and determined their disk scale lengths and radial extents. The galaxies were sorted by redshift and size, deprojected, and stacked. Contours of intensity for the combined images were used to determine azimuthally-averaged radial profiles and disk scale lengths. Comparisons were made between the individual and stacked images as well as between spiral and clumpy galaxies in order to study the limits of their outer disks. These measurements allow us to better understand galaxy morphology at high redshifts.

Author(s): Craig Pellegrino², Debra Elmegreen², Bruce G. Elmegreen¹
Institution(s): 1. IBM T.J. Watson Research Center, 2. Vassar College

149.58 – Ionized and Molecular Gas in IC 860: Evidence for an Outflow

Galaxies at present-day fall predominantly in two distinct populations, as either blue, star-forming spirals or red, quiescent early-type galaxies. Blue galaxies appear to evolve onto the red sequence as star formation is quenched. The absence of a significant population falling in the intermediate ‘green valley’ implies that these transitions must occur rapidly. Identifying the initial properties of and pathways taken by these ‘dying galaxies’ is essential to building a complete understanding of galactic evolution. In this work, we investigate these phenomena in action within IC860 – a nearby, early-type spiral in the initial stages of undergoing a rapid transition in the presence of a powerful AGN-driven molecular outflow. As a shocked, post-starburst galaxy with an intermediate-age stellar population which lies on the blue end of the green valley, IC860 provides a window into the early stages of galaxy transition and AGN feedback. We present Hubble Space Telescope imaging of IC860 showing a violent, dusty outflow originating from a compact core. We find that the mean velocity map of the CO(1-0) from CARMA suggests a dynamically excited bar funneling molecular gas into the galactic center. Finally, we present kinematic maps of ionized gas emission lines

as well as sodium D absorption tracing neutral winds obtained by the Wide-Field Spectrograph.

Author(s): Carson Adams¹, Katherine Alatalo², Anne M Medling¹
Institution(s): 1. California Institute of Technology, 2. Space Telescope Science Institute

149.59 – Bridging the gap: New ALMA observations of lensed dusty galaxies in the Frontier Fields

During much of cosmic time, most star formation activity in galaxies is obscured by dust. In order to complete the census of star formation, we must bridge the gap between optical and infrared galaxy populations. With AzTEC on the Large Millimeter Telescope (LMT), we surveyed two of the HST Frontier Fields in order to exploit the gravitational lensing from foreground clusters to study dust-obscured in galaxies below the nominal confusion limit. We detect millimeter galaxies with magnifications ranging from 1.1-8, allowing us to detect dust-obscured star formation rates in galaxies as low as ~ 10 Msun/year. We present new observations with ALMA in order to localize the millimeter emission of the AzTEC/LMT sources and make unambiguous associations with the optical galaxies in the deep HST images. We investigate the issue of multiplicity within our sample. We discuss the multi-wavelength counterparts of our faint millimeter sources and how they relate to brighter dusty galaxies from previous surveys.

Author(s): Zoe Kearney⁴, Alexandra Pope⁴, Itziar Aretxaga¹, David Hughes¹, Danilo Marchesini³, Alfredo Montana¹, Eric Joseph Murphy², Grant Wilson⁴, Min Yun⁴
Institution(s): 1. INAOE, 2. NRAO, 3. Tufts University, 4. University of Massachusetts

149.60 – E+A Galaxy Properties and Post-Starburst Galaxy Evolution Data through SDSS-IV MaNGA and Illustris: A Co-Analysis

E+A galaxies (Elliptical + A-type stars) are post-starburst galaxies that have experienced a sudden quenching phase. Using previous research methods, 39 candidates out of 2,812 galaxies observed, or 1.4%, were selected from the SDSS-IV MaNGA survey. We then identified morphological characteristics of the 39 galaxies including stellar kinematics, Gini coefficient, gas density and distribution and stellar ages. To study the origin of how E+A galaxies evolved to their present state, galaxy simulation data from the Illustris simulation was utilized to identify similar quenched post-starburst candidates. Seven post-starburst candidates were identified through star formation rate histories of Illustris simulated galaxies. The evolution of these galaxies is studied from 0 to 13.8 billion years ago to identify what caused the starburst and quenching of the Illustris candidates. Similar morphological characteristics of Illustris post-starburst candidates are pulled from before, during, and post-starburst and compared to the same morphological characteristics of the E+A galaxies from SDSS-IV MaNGA. The characteristics and properties of the Illustris galaxies are used to identify the possible evolutionary histories of the observed E+A galaxies. This work was supported by grants AST-1460860 from the National Science Foundation and SDSS FAST/SSP-483 from the Alfred P. Sloan Foundation to the CUNY College of Staten Island.

Author(s): Winonah Ojanen², Raymond Dudley⁴, Kay Edwards³, Andrea Gonzalez³, Amalya Johnson⁴, Nicole Kerrison⁶, Mariarosa Marinelli⁵, Nancy Melchert¹, Charles Liu¹
Institution(s): 1. American Museum of Natural History, 2. College of Saint Scholastica, 3. College of Staten Island, 4. Columbia University, 5. Reynolds Community College, 6. Rutgers University
Contributing team(s): Sloan Collaboration, SDSS-IV MaNGA

150 – Computation, Data Handling, Image Analysis Poster Session

150.01 – A Study of the Efficiency of Spatial Indexing Methods Applied to Large Astronomical

Databases

Spatial indexing of astronomical databases generally uses quadrature methods, which partition the sky into cells used to create an index (usually a B-tree) written as database column. We report the results of a study to compare the performance of two common indexing methods, HTM and HEALPix, on Solaris and Windows database servers installed with a PostgreSQL database, and a Windows Server installed with MS SQL Server. The indexing was applied to the 2MASS All-Sky Catalog and to the Hubble Source catalog. On each server, the study compared indexing performance by submitting 1 million queries at each index level with random sky positions and random cone search radius, which was computed on a logarithmic scale between 1 arcsec and 1 degree, and measuring the time to complete the query and write the output. These simulated queries, intended to model realistic use patterns, were run in a uniform way on many combinations of indexing method and indexing level. The query times in all simulations are strongly I/O-bound and are linear with number of records returned for large numbers of sources. There are, however, considerable differences between simulations, which reveal that hardware I/O throughput is a more important factor in managing the performance of a DBMS than the choice of indexing scheme. The choice of index itself is relatively unimportant: for comparable index levels, the performance is consistent within the scatter of the timings. At small index levels (large cells; e.g. level 4; cell size 3.7 deg), there is large scatter in the timings because of wide variations in the number of sources found in the cells. At larger index levels, performance improves and scatter decreases, but the improvement at level 8 (14 min) and higher is masked to some extent in the timing scatter caused by the range of query sizes. At very high levels (20; 0.0004 arcsec), the granularity of the cells becomes so high that a large number of extraneous empty cells begin to degrade performance. Thus, for the use patterns studied here the database performance is not critically dependent on the exact choices of index or level.

Author(s): Tom Donaldson², G. Bruce Berriman¹, John Good¹, Bernie Shiao²

Institution(s): 1. Caltech/IPAC-NExScI, 2. STScI

150.02 – When Will It Be... USNO Seasons and Apsides Calculator

The turning of the Earth's seasons (solstices and equinoxes) and apsides (perihelions and aphelions) are times often used in observational astronomy and also of interest to the public. To avoid tedious calculations, the U.S. Naval Observatory (USNO) has developed an on-line interactive calculator, *Earth's Seasons and Apsides* to provide information about events between 1600 and 2200. The new data service uses an Application Programming Interface (API), which returns values in JavaScript Object Notation (JSON) that can be incorporated into third-party websites or applications.

For a requested year, the *Earth's Seasons and Apsides* API provides the Gregorian calendar date and time of the Vernal Equinox, Summer Solstice, Autumnal Equinox, Winter Solstice, Aphelion, and Perihelion. The user may specify the time zone for their results, including the optional addition of U.S. daylight saving time for years after 1966.

On-line documentation for using the API-enabled *Earth's Seasons and Apsides* is available, including sample calls (<http://aa.usno.navy.mil/data/docs/api.php>). A traditional forms-based interface is available as well (<http://aa.usno.navy.mil/data/docs/EarthSeasons.php>). This data service replaces the popular *Earth's Seasons: Equinoxes, Solstices, Perihelion, and Aphelion* page that provided a static list of events for 2000–2025.

The USNO also provides API-enabled data services for *Complete Sun and Moon Data for One Day* (http://aa.usno.navy.mil/data/docs/RS_OneDay.php), *Dates of the Primary Phases of the Moon* (<http://aa.usno.navy.mil/data/docs/MoonPhase.php>), *Selected Christian Observances* (<http://aa.usno.navy.mil/data/docs/easter.php>), *Selected Islamic Observances* (<http://aa.usno.navy.mil/data/docs/islamic.php>),

Selected Jewish Observances

(<http://aa.usno.navy.mil/data/docs/passover.php>), *Julian Date Conversion* (<http://aa.usno.navy.mil/data/docs/JulianDate.php>), and *Sidereal Time* (<http://aa.usno.navy.mil/data/docs/siderealtime.php>) as well as its *Solar Eclipse Computer* (<http://aa.usno.navy.mil/data/docs/SolarEclipses.php>).

Author(s): Malynda Chizek Frouard¹, Jennifer Lynn Bartlett¹

Institution(s): 1. US Naval Observatory

150.03 – Comparing the Effectiveness of Online Sunrise/Sunset Calculators

The USNO is responsible for providing information through its website on various types of natural phenomena, including times of sunrise and sunset for any given day and location. Alternative websites were explored to see what options are available in case the USNO can no longer support this on-line tool in the future.

Websites with sunrise/sunset calculators were examined to see what algorithm they cited, if any. A large percentage of the websites took their calculations from three main sources (USNO, Meeus, and Schlyter). For ease of comparison, one website with an Application Programming Interface (API) for each algorithm was used to generate sunrise/sunset times for 2 dates per year for 24 years at latitudes from the equator to each pole along the prime meridian. Additionally, dates on which only one phenomenon was expected (first and last day of polar day and night) were tested to examine how each algorithm would perform for these extreme edge cases.

At mid-latitudes, all of the algorithms agreed within 1 minute of each other but their predictions began to diverge as they approached the poles. Close to the poles, all three differed by more than a minute. While the algorithms diverged well before reaching the poles, Schlyter did so at much lower latitudes compared to the other two. In the edge cases, Schlyter and Meeus did not correctly document the missing sunrise/sunsets.

Until a set of arctic or antarctic observations of sunrise and sunset times can be analyzed, we cannot ascertain which algorithm is the most accurate. However, the USNO algorithm handled cases of continuous day and night better than the others. There currently seems to be no better alternative to provide robust sunrise/set times than the USNO Complete Sun and Moon Data for One Day (http://aa.usno.navy.mil/data/docs/RS_OneDay.php).

Author(s): Alan Philips¹, Teresa Wilson², Malynda Chizek Frouard³, Jennifer Lynn Bartlett³

Institution(s): 1. Langley High School, 2. NREIP/Michigan Technological University, 3. US Naval Observatory

150.04 – A catalog of galaxy morphology and photometric redshift

Morphology carries important information about the physical characteristics of a galaxy. Here we used machine learning to produce a catalog of ~3,000,000 SDSS galaxies classified by their broad morphology into spiral and elliptical galaxies. Comparison of the catalog to Galaxy Zoo shows that the catalog contains a subset of 1.7×10^6 galaxies classified with the same level of consistency as the debiased “superclean” sub-sample. In addition to the morphology, we also computed the photometric redshifts of the galaxies. Several pattern recognition algorithms and variable selection strategies were tested, and the best accuracy of mean absolute error of ~0.0062 was achieved by using random forest with a combination of manually and automatically selected variables. The catalog shows that for redshift lower than 0.085 galaxies that visually look spiral become more prevalent as the redshift gets higher. For redshift greater than 0.085 galaxies that visually look elliptical become more prevalent. The catalog as well as the source code used to produce it is publicly available at

Author(s): Nicholas Paul¹, Lior Shamir¹
Institution(s): 1. Lawrence Technological University

150.05 – Developing Generic Image Search Strategies for Large Astronomical Data Sets and Archives using Convolutional Neural Networks and Transfer Learning

Astronomical instruments produce petabytes of images every year, vastly more than can be inspected by a member of the astronomical community in search of a specific population of structures. Fortunately, the sky is mostly black and source extraction algorithms have been developed to provide searchable catalogs of unconfused sources like stars and galaxies. These tools often fail for studies of more diffuse structures like the interstellar medium and unresolved stellar structures in nearby galaxies, leaving astronomers interested in observations of photodissociation regions, stellar clusters, diffuse interstellar clouds without the crucial ability to search. In this work we present a new path forward for finding structures in large data sets similar to an input structure using convolutional neural networks, transfer learning, and machine learning clustering techniques. We show applications to archival data in the Mikulski Archive for Space Telescopes (MAST).

Author(s): Joshua E. G. Peek¹, Jonathan R. Hargis¹, Craig R. Jones¹
Institution(s): 1. Space Telescope Science Institute

150.06 – Real-Time RFI Mitigation in Pulsar Observations

As the use of wireless technology has increased around the world, Radio Frequency Interference (RFI) has become more and more of a problem for radio astronomers. Preventative measures exist to limit the presence of RFI, and programs exist to remove it from saved data, but the routine use of algorithms to detect and remove RFI as an observation is occurring is much less common. Such a method would be incredibly useful for observations in which the data must undergo several rounds of processing before being saved, as in pulsar timing studies. Strategies for real-time mitigation have been discussed and tested with simulated data (Buch et al., 2016), but ideally the results of any approach would be validated by a detailed comparison of the final data products - for pulsar timing, the variance in the pulse times of arrival (TOAs) - with and without mitigation applied. The goal of this project is to develop an RFI mitigation approach based on the previously suggested strategies and test this program on actual data from the observation of pulsar J1713+0747. We use a Median Absolute Deviation (MAD) filter to identify interference in the observation and replace the compromised data with random Gaussian noise to match a characteristic radio signal from space. In order to verify our results, we analyze the pulsar's TOAs obtained both from the mitigated data and from the unmitigated data processed through offline RFI removal software. Comparing the two, our preliminary findings indicate that our program is able to improve the quality of timing results from the observation.

Author(s): Emily Ramey⁵, Nick Joslyn³, Richard Prestage¹, Mark Whitehead¹, Michael Timothy Lam⁶, Tim Blattner², Luke Hawkins¹, Cedric Viou⁴, Jessica Masson⁴
Institution(s): 1. Green Bank Observatory, 2. National Institute of Standards and Technology, 3. Simpson College, 4. Station de Radioastronomie de Nançay, 5. Washington University in St. Louis, 6. West Virginia University

150.07 – Toward an efficient Photometric Supernova Classifier

The Sloan Digital Sky Survey Supernova Survey (SDSS) discovered more than 1,000 Type Ia Supernovae, yet less than half of these have spectroscopic measurements. As wide-field

imaging telescopes such as The Dark Energy Survey (DES) and the Panoramic Survey Telescope and Rapid Response System (Pan-STARRS) discover more supernovae, the need for accurate and computationally cheap photometric classifiers increases. My goal is to use a photometric classification algorithm based on Snocosmo, a python library for supernova cosmology analysis, to reclassify previously identified Hubble SN and other non-spectroscopically confirmed surveys. My results will be compared to other photometric classifiers such as PSNID and STARDUST. In the near future, I expect to have the algorithm validated with simulated data, optimized for efficiency, and applied with high performance computing to real data.

Author(s): Bradley McClain¹
Institution(s): 1. University of South Carolina

150.08 – SpecOp: Optimal Extraction Software for Integral Field Unit Spectrographs

The Hobby-Eberly Telescope's new low resolution integral field spectrographs, LRS2-B and LRS2-R, each cover a 12"x6" area on the sky with 280 fibers and generate spectra with resolutions between R=1100 and R=1900. To extract 1-D spectra from the instrument's 3D data cubes, a program is needed that is flexible enough to work for a wide variety of targets, including continuum point sources, emission line sources, and compact sources embedded in complex backgrounds. We therefore introduce SpecOp, a user-friendly python program for optimally extracting spectra from integral-field unit spectrographs. As input, SpecOp takes a sky-subtracted data cube consisting of images at each wavelength increment set by the instrument's spectral resolution, and an error file for each count measurement. All of these files are generated by the current LRS2 reduction pipeline. The program then collapses the cube in the image plane using the optimal extraction algorithm detailed by Keith Horne (1986). The various user-selected options include the fraction of the total signal enclosed in a contour-defined region, the wavelength range to analyze, and the precision of the spatial profile calculation. SpecOp can output the weighted counts and errors at each wavelength in various table formats using python's astropy package. We outline the algorithm used for extraction and explain how the software can be used to easily obtain high-quality 1-D spectra. We demonstrate the utility of the program by applying it to spectra of a variety of quasars and AGNs. In some of these targets, we extract the spectrum of a nuclear point source that is superposed on a spatially extended galaxy.

Author(s): Adam McCarron¹, Robin Ciardullo¹, Michael Eracleous¹
Institution(s): 1. The Pennsylvania State University

150.09 – Understanding and Using the Fermi Science Tools

The Fermi Science Support Center (FSSC) provides information, documentation, and tools for the analysis of Fermi science data, including both the Large-Area Telescope (LAT) and the Gamma-ray Burst Monitor (GBM). Source and binary versions of the Fermi Science Tools can be downloaded from the FSSC website, and are supported on multiple platforms. An overview document, the Cicerone, provides details of the Fermi mission, the science instruments and their response functions, the science data preparation and analysis process, and interpretation of the results. Analysis Threads and a reference manual available on the FSSC website provide the user with step-by-step instructions for many different types of data analysis: point source analysis - generating maps, spectra, and light curves, pulsar timing analysis, source identification, and the use of python for scripting customized analysis chains. We present an overview of the structure of the Fermi science tools and documentation, and how to acquire them. We also provide examples of standard analyses, including tips and tricks for improving Fermi science analysis.

Author(s): Joseph Asercion¹
Institution(s): 1. Fermi Science Support Center

150.10 – The Astrophysics Source Code Library by the numbers

The Astrophysics Source Code Library (ASCL, ascl.net) was founded in 1999 by Robert Nemiroff and John Wallin. ASCL editors seek both new and old peer-reviewed papers that describe methods or experiments that involve the development or use of source code, and add entries for the found codes to the library. Software authors can submit their codes to the ASCL as well. This ensures a comprehensive listing covering a significant number of the astrophysics source codes used in peer-reviewed studies. The ASCL is indexed by both NASA's Astrophysics Data System (ADS) and Web of Science, making software used in research more discoverable. This presentation covers the growth in the ASCL's number of entries, the number of citations to its entries, and in which journals those citations appear. It also discusses what changes have been made to the ASCL recently, and what its plans are for the future.

Author(s): Alice Allen¹, Peter Teuben¹⁰, G. Bruce Berriman⁵, Kimberly DuPrie⁹, Jessica Mink⁴, Robert Nemiroff⁷, PW Ryan¹, Judy Schmidt¹, Lior Shamir⁶, Keith Shortridge², John Wallin⁸, Rein Warmels³

Institution(s): 1. *Astrophysics Source Code Library*, 2. *Australian Astronomical Observatory*, 3. *ESO*, 4. *Harvard-Smithsonian Center for Astrophysics*, 5. *IPAC-NEExSci*, *Caltech*, 6. *Lawrence Technological University*, 7. *Michigan Technological University*, 8. *Middle Tennessee State University*, 9. *Space Telescope Science Institute*, 10. *University of Maryland*

150.11 – SOSPEX, an interactive tool to explore SOFIA spectral cubes

We present *SOSPEX* (*SOFIA SPECTRAL EXPLORER*), an interactive tool to visualize and analyze spectral cubes obtained with the *FIFI-LS* and *GREAT* instruments onboard the *SOFIA Infrared Observatory*. This software package is written in Python 3 and it is available either through Github or Anaconda. Through this GUI it is possible to explore directly the spectral cubes produced by the *SOFIA* pipeline and archived in the *SOFIA Science Archive*. Spectral cubes are visualized showing their spatial and spectral dimensions in two different windows. By selecting a part of the spectrum, the flux from the corresponding slice of the cube is visualized in the spatial window. On the other hand, it is possible to define apertures on the spatial window to show the corresponding spectral energy distribution in the spectral window. Flux isocontours can be overlapped to external images in the spatial window while line names, atmospheric transmission, or external spectra can be overplotted on the spectral window. Atmospheric models with specific parameters can be retrieved, compared to the spectra and applied to the uncorrected *FIFI-LS* cubes in the cases where the standard values give unsatisfactory results. Subcubes can be selected and saved as FITS files by cropping or cutting the original cubes. Lines and continuum can be fitted in the spectral window saving the results in Jyson files which can be reloaded later. Finally, in the case of spatially extended observations, it is possible to compute spectral momenta as a function of the position to obtain velocity dispersion maps or velocity diagrams.

Author(s): Dario Fadda¹, Edward T Chambers¹
Institution(s): 1. *USRA*

150.12 – Characterization and Processing of Non-Uniformities in Back-Illuminated CCDs

In astronomical photometry, Charged Coupled Device (CCD) detectors are used to achieve high precision photometry and must be properly calibrated to correct for noise and pixel non-uniformities. Uncalibrated images may contain bias offset, dark current, bias structure and uneven illumination. In addition, standard data reduction is often not sufficient to "normalize" imagery to single-digit millimagnitude (mmag) precision. We are investigating an apparent non-uniformity, or interference pattern, in a back-illuminated sensor, the Alta U-47, attached to a DFM Engineering 41-cm Ritchey-Chretien f/8 telescope. Based

on the amplitude of this effect, we estimate that instrument magnitude peak-to-valley deviations of 50 mmag or more may result. Our initial testing strongly suggests that reflected skylight from high pressure sodium city lights may be the cause of this interference pattern. Our research goals are twofold: to fully characterize this non-uniformity and to determine the best method to remove this interference pattern from our reduced CCD images.

Author(s): Alia D Lemm¹, Devin J Della-Rose¹, Sally Maddocks¹
Institution(s): 1. *US Air Force Academy*

150.13 – Simulating OSIRIS Detector Images for the Purpose of Data Extraction

OSIRIS is a near infrared integral field spectrograph on the Keck telescope capable of obtaining spectral information at each spatial sample. Extracting the spatial-spectral information from raw data is challenging due to overlap and cross talk in detector images. Here I present a discussion of the theory behind and creation of a forward model capable of simulating OSIRIS detector images given hypothetical data. This model is then incorporated into a weighted least squares data extractor which mitigates the challenges of extracting information from the densely packed raw data.

Author(s): Caroline Bright Owen¹, Michael Fitzgerald²
Institution(s): 1. *Middlebury College*, 2. *University of California, Los Angeles*

150.14 – The Montage Image Mosaic Toolkit As A Visualization Engine.

The Montage toolkit has since 2003 been used to aggregate FITS images into mosaics for science analysis. It is now finding application as an engine for image visualization. One important reason is that the functionality developed for creating mosaics is also valuable in image visualization. An equally important (though perhaps less obvious) reason is that Montage is portable and is built on standard astrophysics toolkits, making it very easy to integrate into new environments. Montage models and rectifies the sky background to a common level and thus reveals faint, diffuse features; it offers an adaptive image stretching method that preserves the dynamic range of a FITS image when represented in PNG format; it provides utilities for creating cutouts of large images and downsampled versions of large images that can then be visualized on desktops or in browsers; it contains a fast reprojection algorithm intended for visualization; and it resamples and reprojects images to a common grid for subsequent multi-color visualization.

This poster will highlight these visualization capabilities with the following examples:

1. Creation of down-sampled multi-color images of a 16-wavelength Infrared Atlas of the Galactic Plane, sampled at 1 arcsec when created;
2. Integration into web-based image processing environment: JS9 is an interactive image display service for web browsers, desktops and mobile devices. It exploits the flux-preserving reprojection algorithms in Montage to transform diverse images to common image parameters for display. Select Montage programs have been compiled to Javascript/WebAssembly using the Emscripten compiler, which allows our reprojection algorithms to run in browsers at close to native speed.
3. Creation of complex sky coverage maps: an multicolor all-sky map that shows the sky coverage of the Kepler and K2, KELT and TESS projects, overlaid on an all-sky 2MASS image.

Montage is funded by the National Science Foundation under Grant Number ACI-1642453. JS9 is funded by the Chandra X-ray Center (NAS8-03060) and NASA's Universe of Learning (STScI-509913).

Author(s): G. Bruce Berriman¹, Angela Lerias⁴, John Good¹, Eric Mandel², Joshua Pepper³

Institution(s): 1. Caltech/IPAC-NExScI, 2. Harvard-Smithsonian Center for Astrophysics, 3. Lehigh University, 4. University of California, Riverside

150.15 – A Euclid, LSST and WFIRST Joint Processing Study

Euclid, LSST and WFIRST are the flagship cosmological projects of the next decade. By mapping several thousand square degrees of sky and covering the electromagnetic spectrum from the optical to the NIR with (sub-)arcsec resolution, these projects will provide exciting new constraints on the nature of dark energy and dark matter. The ultimate cosmological, astrophysical and time-domain science yield from these missions, which will detect several billions of sources, requires joint processing at the pixel-level. Three U.S. agencies (DOE, NASA and NSF) are supporting an 18-month study which aims to 1) assess the optimal techniques to combine these, and ancillary data sets at the pixel level; 2) investigate options for an interface that will enable community access to the joint data products; and 3) identify the computing and networking infrastructure to properly handle and manipulate these large datasets together. A Joint Processing Working Group (JPWG) is carrying out this study and consists of US-based members from the community and science/data processing centers of each of these projects. Coordination with European partners is envisioned in the future and European Euclid members are involved in the JPWG as observers. The JPWG will scope the effort and resources required to build up the capabilities to support scientific investigations using joint processing in time for the start of science surveys by LSST and Euclid.

Author(s): Ranga-Ram Chary¹

Institution(s): 1. Caltech/IPAC

Contributing team(s): Joint Processing Working Group

150.16 – Using Velocity Anisotropy to Analyze Magnetohydrodynamic Turbulence in Giant Molecular Clouds

Structure function (SF) analysis is a strong tool for gaging the Alfvénic properties of magnetohydrodynamic (MHD) simulations, yet there is a lack of literature rigorously investigating limitations in the context of radio spectroscopy. This study takes an in depth approach to studying the limitations of SF analysis for analyzing MHD turbulence in giant molecular cloud (GMC) spectroscopy data. MHD turbulence plays a critical role in the structure and evolution of GMCs as well as in the formation of sub-structures known to spawn stellar progenitors. Existing methods of detection are neither economical nor robust (e.g. dust polarization), and nowhere is this more clear than in the theoretical-observational divide in current literature. A significant limitation of GMC spectroscopy results from the large variation in methods used for extracting GMCs from survey data. Thus, a robust method for studying MHD turbulence must correctly gauge physical properties regardless of the data extraction method used. While SF analysis has demonstrated strong potential across a range of simulated conditions, this study finds significant concern regarding its feasibility as a robust tool in GMC spectroscopy.

Author(s): Alecio Madrid¹, Audra Hernandez¹

Institution(s): 1. University of Wisconsin-Madison

150.17 – Combining Single Dish and Interferometric data: a new tool in CASA

The basic mapping and deconvolution techniques used for (radio) interferometric data only works well for spatial scales that are sampled by the interferometer. Since interferometers cannot sample below a certain spacing, this implies spatial scales above a certain scale are not sampled. Our new tool converts the short spacings represented by a single dish map into a virtual radio interferometric dataset, and then performs a joint deconvolution

of all spatial scales to recover a high fidelity image. Using recent ALMA data we will illustrate how this works.

Author(s): Peter Teuben², Jin Koda¹

Institution(s): 1. Stony Brook University, 2. University of Maryland

150.18 – Learning a Novel Detection Metric for the Detection of O’Connell Effect Eclipsing Binaries

With the advent of digital astronomy, new benefits and new challenges have been presented to the modern day astronomer. No longer can the astronomer rely on manual processing, instead the profession as a whole has begun to adopt more advanced computational means. Here we focus on the construction and application of a novel time-domain signature extraction methodology and the development of a supporting supervised pattern detection algorithm for the targeted identification of eclipsing binaries which demonstrate a feature known as the O’Connell Effect. A methodology for the reduction of stellar variable observations (time-domain data) into Distribution Fields (DF) is presented. Push-Pull metric learning, a variant of LMNN learning, is used to generate a learned distance metric for the specific detection problem proposed. The metric will be trained on a set of a labelled Kepler eclipsing binary data, in particular systems showing the O’Connell effect. Performance estimates will be presented, as well the results of the detector applied to an unlabeled Kepler EB data set; this work is a crucial step in the upcoming era of big data from the next generation of big telescopes, such as LSST.

Author(s): Kyle Johnston¹, Rana Haber¹, Matthew Knotte¹, Saida Maria Caballero-Nieves¹, Adrian Peter¹, Véronique Petit²

Institution(s): 1. Florida Institute of Technology, 2. University of Delaware

150.19 – Slaying Hydra: A Python-Based Reduction Pipeline for the Hydra Multi-Object Spectrograph

We present a Python-based data reduction pipeline for the Hydra Multi-Object Spectrograph on the WIYN 3.5 m telescope, an instrument which enables simultaneous spectroscopy of up to 93 targets. The reduction steps carried out include flat-fielding, dynamic fiber tracing, wavelength calibration, optimal fiber extraction, and sky subtraction. The pipeline also supports the use of sky lines to correct for zero-point offsets between fibers. To account for the moving parts on the instrument and telescope, fiber positions and wavelength solutions are derived in real-time for each dataset. The end result is a one-dimensional spectrum for each target fiber. Quick and fully automated, the pipeline enables on-the-fly reduction while observing, and has been known to outperform the IRAF pipeline by more accurately reproducing known RVs. While Hydra has many configurations in both high- and low-resolution, the pipeline was developed and tested with only one high-resolution mode. In the future we plan to expand the pipeline to work in most commonly used modes.

Author(s): Richard Seifert², Andrew Mann¹

Institution(s): 1. Columbia University, 2. University of Texas at Austin

150.20 – Spectacle and SpecViz: New Spectral Analysis and Visualization Tools

A new era of spectroscopic exploration of our universe is being ushered in with advances in instrumentation and next-generation space telescopes. The advent of new spectroscopic instruments has highlighted a pressing need for tools scientists can use to analyze and explore these new data. We have developed Spectacle, a software package for analyzing both synthetic spectra from hydrodynamic simulations as well as real COS data with an aim of characterizing the behavior of the circumgalactic medium. It allows easy reduction of spectral data and analytic line generation capabilities. Currently, the package is focused on automatic determination of absorption regions and line identification with custom line list support, simultaneous line fitting using Voigt profiles via least-squares or MCMC methods,

and multi-component modeling of blended features. Non-parametric measurements, such as equivalent widths, delta v₉₀, and full-width half-max are available. Spectacle also provides the ability to compose compound models used to generate synthetic spectra allowing the user to define various LSF kernels, uncertainties, and to specify sampling.

We also present updates to the visualization tool SpecViz, developed in conjunction with the JWST data analysis tools development team, to aid in the exploration of spectral data. SpecViz is an open source, Python-based spectral 1-D interactive visualization and analysis application built around high-performance interactive plotting. It supports handling general and instrument-specific data and includes advanced tool-sets for filtering and detrending one-dimensional data, along with the ability to isolate absorption regions using slicing and manipulate spectral features via spectral arithmetic. Multi-component modeling is also possible using a flexible model fitting tool-set that supports custom models to be used with various fitting routines. It also features robust user extensions such as custom data loaders and support for user-created plugins that add new functionality.

This work was supported in part by HST AR #13919, HST GO #14268, and HST AR #14560.

Author(s): Nicholas Earl¹, Molly Peeples¹
Institution(s): 1. *Space Telescope Science Institute*
Contributing team(s): JDADF Developers

150.21 – CIAO: CHANDRA/X-RAY DATA ANALYSIS FOR EVERYONE

Eighteen years after the launch of Chandra, the archive is full of scientifically rich data and new observations continue. Improvements in recent years to the data analysis package CIAO (Chandra Interactive Analysis of Observations) and its extensive accompanying documentation make it easier for astronomers without a specialist background in high energy astrophysics to take advantage of this resource.

The CXC supports hundreds of CIAO users around the world at all levels of training from high school and undergraduate students to the most experienced X-ray astronomers. In general, we strive to provide a software system which is easy for beginners, yet powerful for advanced users.

Chandra data cover a range of instrument configurations and types of target (pointlike, extended and moving), requiring a flexible data analysis system. In addition to CIAO tools using the familiar FTOOLS/IRAF-style parameter interface, CIAO includes applications such as the Sherpa fitting engine which provide access to the data via Python scripting.

In this poster we point prospective (and existing!) users to the high level Python scripts now provided to reprocess Chandra or other X-ray mission data, determine source fluxes and upper limits, and estimate backgrounds; and to the latest documentation including the CIAO Gallery, a new entry point featuring the system's different capabilities.

This work has been supported by NASA under contract NAS 8-03060 to the Smithsonian Astrophysical Observatory for operation of the Chandra X-ray Center.

Author(s): Jonathan McDowell¹
Institution(s): 1. *Harvard-Smithsonian Center for Astrophysics*
Contributing team(s): CIAO Team

150.22 – CRKSPH: A new meshfree hydrodynamics method with applications to astrophysics

The study of astrophysical phenomena such as supernovae, accretion disks, galaxy formation, and large-scale structure formation requires computational modeling of, at a minimum,

hydrodynamics and gravity. Developing numerical methods appropriate for these kinds of problems requires a number of properties: shock-capturing hydrodynamics benefits from rigorous conservation of invariants such as total energy, linear momentum, and mass; lack of obvious symmetries or a simplified spatial geometry to exploit necessitate 3D methods that ideally are Galilean invariant; the dynamic range of mass and spatial scales that need to be resolved can span many orders of magnitude, requiring methods that are highly adaptable in their space and time resolution. We have developed a new Lagrangian meshfree hydrodynamics method called Conservative Reproducing Kernel Smoothed Particle Hydrodynamics, or CRKSPH, in order to meet these goals. CRKSPH is a conservative generalization of the meshfree reproducing kernel method, combining the high-order accuracy of reproducing kernels with the explicit conservation of mass, linear momentum, and energy necessary to study shock-driven hydrodynamics in compressible fluids. CRKSPH's Lagrangian, particle-like nature makes it simple to combine with well-known N-body methods for modeling gravitation, similar to the older Smoothed Particle Hydrodynamics (SPH) method. Indeed, CRKSPH can be substituted for SPH in existing SPH codes due to these similarities. In comparison to SPH, CRKSPH is able to achieve substantially higher accuracy for a given number of points due to the explicitly consistent (and higher-order) interpolation theory of reproducing kernels, while maintaining the same conservation principles (and therefore applicability) as SPH. There are currently two coded implementations of CRKSPH available: one in the open-source research code Spheral, and the other in the high-performance cosmological code HACC. Using these codes we have applied CRKSPH to a number of astrophysical scenarios, such as rotating gaseous disks, supernova remnants, and large-scale cosmological structure formation. In this poster we present an overview of CRKSPH and show examples of these astrophysical applications.

Author(s): John Michael Owen¹, Cody Raskin¹, Nicholas Frontiere²
Institution(s): 1. *Lawrence Livermore National Laboratory*, 2. *University of Chicago*

150.23 – Updated O-C Diagrams for Several Bright HW Vir Binaries Observed with the Evryscope

HW Vir systems are eclipsing, post-common-envelope binaries consisting of a hot subdwarf star and a cooler M dwarf or brown dwarf companion. They show a strong reflection effect and have characteristically short orbital periods of only a few hours, allowing observers to detect multiple eclipses per night. Observed minus calculated (O-C) studies allow one to measure minuscule variations in the orbital periods of these systems by comparing observed eclipse timings to a calculated ephemeris. This technique is useful for detecting period changes due to secular evolution of the binary, gravitational wave emission, or reflex motion from an orbiting circumbinary object. Numerous eclipse timings obtained over several years are vital to the proper interpretation and analysis of O-C diagrams. The Evryscope – an array of twenty-four individual telescopes built by UNC and deployed on Cerro Tololo – images the entire Southern sky once every two minutes, producing an insurmountable amount of data for objects brighter than 16th magnitude. The cadence with which Evryscope exposes makes it an unparalleled tool for O-C analyses of HW Vir binaries; it will catalogue thousands of eclipses over the next several years. Here we present updated O-C diagrams for several HW Vir binaries using recent measurements from the Evryscope. We also use observations of AA Dor, an incredibly stable astrophysical clock, to characterize the accuracy of the Evryscope's timestamps.

Author(s): Kyle A Corcoran¹, Brad Barlow¹, Hank Corbett², Octavi Fors², Ward S Howard², Nicholas Law², Jeff Ratzloff²
Institution(s): 1. *High Point University*, 2. *University of North Carolina at Chapel Hill*

150.24 – LINEAR:

We present a new paradigm for extracting one-dimensional spectra from a collection of slitless spectroscopic images obtained at multiple position angles. We compute the optimal spectrum for each object simultaneously by computing all of the transformations from the direct image to each dispersed image at the wavelengths of interest. This approach has several key advantages over standard extraction-based techniques by (1) removing the need for contamination corrections, (2) improving signal-to-noise without loss of spectral resolution, and (3) extracting sources that overlap in the direct image (such as bulge/disk or annular sectors). We present a series of simulated HST/WFC3 data to test the accuracy of our method. We will also show high-redshift sources from various deep fields as illustrations of our technique.

Author(s): Russell Ryan¹, Stephano Casertano¹, Nor Pirzkal¹
Institution(s): 1. *Space Telescope Science Institute*

150.25 – Software Development for Asteroid and Variable Star Research

The process of collecting and analyzing light curves from variable stars and asteroids is almost identical. In 2016 a collaboration was created to develop a simple fundamental way to study both asteroids and variable stars using methods that would allow the process to be repeated by middle school and high school students.

Using robotic telescopes at Cerro Tololo (Chile), Yerkes Observatory (US), and Stone Edge Observatory (US) data were collected on RV Del and three asteroids. It was discovered that the only available software program which could be easily installed on lab computers was MPO Canopus. However, after six months it was determined that MPO Canopus was not an acceptable option because of the steep learning curve, lack of documentation and technical support.

Therefore, the project decided that the best option was to design our own python based software. Using python and python libraries we developed code that can be used for photometry and can be easily changed to the user's needs. We accomplished this by meeting with our mentor astronomer, Tyler Linder, and in the beginning wrote two different programs, one for asteroids and one for variable stars. In the end, though, we chose to combine codes so that the program would be capable of performing photometry for both moving and static objects.

The software performs differential photometry by comparing the magnitude of known reference stars to the object being studied. For asteroids, the image timestamps are used to obtain ephemeris of the asteroid from JPL Horizons automatically.

Author(s): Teaghen Sweckard², Timothy Clason², Jessica Kenney², Wolfgang Wuerker², Sage Palser², Tucker Giles², Tyler Linder¹, Richard Sanchez³
Institution(s): 1. *Astronomical Research Institute*, 2. *Buffalo High School*, 3. *Johnson County School District*

150.26 – Simulations of Polarization Leakage and Ionospheric Attenuation in Visibility Measurements for the HERA and PAPER Experiments

The HERA and PAPER experiments that aim to detect the power spectrum of the 21cm brightness temperature during the Epoch of Reionization (EoR) are planned with the expectation that foregrounds will be separated from the cosmological signal by a clearly demarcated boundary in Fourier space. Polarized foregrounds with complex frequency structure present a potential systematic as their mixing into unpolarized signal by the polarized response of an instrument's beam may be confused for the unpolarized EoR signal. There are two factors we believe will mitigate this systematic to the point that it will not impede the detection of the cosmological power spectrum in the foreground avoidance scheme. First, variation in the ionospheric plasma density observed between different days produces attenuation of the effective polarized power on the sky when visibilities are

averaged coherently over many days. Second, the absolute level of polarization leakage can be suppressed through careful design of the instrument. We have performed detailed visibility simulations to investigate both effects, and present the results of these simulations for both the HERA and PAPER instruments.

Author(s): Zachary Martinot¹, Saul Kohn¹, James Aguirre¹, Immanuel Washington¹
Institution(s): 1. *University of Pennsylvania*
Contributing team(s): HERA Collaboration, PAPER Collaboration

150.27 – The Search for Transients and Variables in the LSST Pathfinder Survey

This research was completed during participation in the NSF-REU program at University of Wisconsin-Madison. Two fields of a few square degrees, close to the galactic plane, were imaged on the WIYN 3.5 meter telescope during the commissioning of the One Degree Imager (ODI) focal plane. These images were taken with repeated, shorter exposures in order to model an LSST-like cadence. This data was taken in order to identify transient and variable light sources. This was done by using Source Extractor to generate a catalog of all sources in each exposure, and inserting this data into a larger photometry database composed of all exposures for each field. A Python code was developed to analyze the data and isolate sources of interest from a large data set. We found that there were some discrepancies in the data, which lead to some interesting results that we are looking into further. Variable and transient sources, while relatively well understood, are not numerous in current cataloging systems. This will be a major undertaking of the Large Synoptic Survey Telescope (LSST), which this project is a precursor to. Locating these sources may give us a better understanding of where these sources are located and how they impact their surroundings.

Author(s): Mary Katherine Gorsuch¹, Ralf Kotulla²
Institution(s): 1. *Colorado Mesa University*, 2. *University of Wisconsin-Madison*

150.28 – Schroedinger's code: Source code availability and transparency in astrophysics

Astronomers use software for their research, but how many of the codes they use are available as source code? We examined a sample of 166 papers from 2015 for clearly identified software use, then searched for source code for the software packages mentioned in these research papers. We categorized the software to indicate whether source code is available for download and whether there are restrictions to accessing it, and if source code was not available, whether some other form of the software, such as a binary, was. Over 40% of the source code for the software used in our sample was not available for download.

As URLs have often been used as proxy citations for software, we also extracted URLs from one journal's 2015 research articles, removed those from certain long-term, reliable domains, and tested the remainder to determine what percentage of these URLs were still accessible in September and October, 2017.

Author(s): PW Ryan¹, Alice Allen¹, Peter Teuben²
Institution(s): 1. *Astrophysics Source Code Library*, 2. *University of Maryland*

150.29 – Using Deep Learning to Analyze the Voices of Stars.

With several new large-scale surveys on the horizon, including LSST, TESS, ZTF, and Evryscope, faster and more accurate analysis methods will be required to adequately process the enormous amount of data produced. Deep learning, used in industry for years now, allows for advanced feature detection in minimally prepared datasets at very high speeds; however, despite the advantages of this method, its application to astrophysics has not yet been extensively explored. This dearth may be due to a lack of training data available to researchers. Here we generate synthetic data loosely mimicking the properties

of acoustic mode pulsating stars and compare the performance of different deep learning algorithms, including Artificial Neural Networks, and Convolutional Neural Networks, in classifying these synthetic data sets as either pulsators, or not observed to vary stars.

Author(s): Thomas Macaulay Boudreaux¹
Institution(s): 1. High Point University

150.30 – The Use of the Time Average Visibility for Analyzing HERA-19 Commissioning Data

The Hydrogen Epoch of Reionization Array (HERA) is a radio telescope that will be observing large structure throughout the cosmic reionization epoch. This will allow us to characterize the evolution of the 21 cm power spectrum to constrain the timing and morphology of reionization, the properties of the first galaxies, the evolution of large-scale structure, and the early sources of heating. We develop a simple and robust observable for the HERA-19 commissioning data, the Time Average Visibility (TAV). We compare both redundantly and absolutely calibrated visibilities to detailed instrument simulations and to analytical expectations, and explore the signal present in the TAV. The TAV has already been demonstrated as a method to reject poorly performing antennas, and may be improved with this work to allow a simple cross-check of the calibration solutions without imaging.

Author(s): Samavarti Gallardo¹, Roshan Benefo², Paul La Plante², James Aguirre²
Institution(s): 1. California State University Los Angeles, 2. University of Pennsylvania
Contributing team(s): HERA Collaboration

150.31 – The Use of the Time Average Visibility for Analyzing HERA-19 Commissioning Data: Effects of Non-Redundancy

The Hydrogen Epoch of Reionization Array (HERA) is a radio telescope situated in South Africa designed to observe the universe from redshifts 13 through 6, in order to detect the emission of the 21 cm line from the hydrogen spin-flip transition. We perform 21 cm cosmology due to its relation with reionization; by detecting this emission line, we can identify the timing of reionization, and understand more about the nature of the universe during the birth of the first stars and galaxies. With that, we can understand the heating conditions of the initial universe, providing us a larger picture of the conditions that created the large-scale structure of the universe we observe today. The HERA array currently consists of 19 antennas, spaced in a hexagonal grid pattern. We consider a robust observable, the time-averaged visibility (TAV), which is in principle sensitive to variations in the beam pattern between antenna elements and is easier to measure than the beam pattern itself. We use this TAV to explore the non-redundancy of baselines in the HERA array due either to cross-coupling between antennas (probed by antenna location in the array) or non-uniformity in their manufacture. The TAV may provide a simple way of verifying improvements in antenna element redundancy.

Author(s): Roshan Benefo², Samavarti Gallardo¹, James Aguirre², Paul La Plante²
Institution(s): 1. California State University Los Angeles, 2. University of Pennsylvania
Contributing team(s): HERA Collaboration

150.32 – Polarized Power Spectra from HERA-19 Commissioning Data: Instrument Stability

The Epoch of Reionization (EoR) is a key period in the universe's history, containing the formation of the first galaxies and large scale structures. Foreground emission is the limiting factor in detecting the 21 cm emission from the Epoch of Reionization (EoR). The HERA-19 low frequency radio interferometer aims to reduce the obfuscation from the foreground emission with its dish shaped antennae. We generate polarized 2D (cylindrically averaged) power spectra from seven days of observation from the

HERA-19 2016 observation season in each of the four Stokes parameters I, Q, U, and V. These power spectra serve as a potent diagnostic tool that allow us to understand the instrument stability by comparison between nominally redundant baselines, and between observations of nominally the same astrophysical sky on successive days. The power spectra are expected to vary among nominally redundant measurements due to ionosphere fluctuations and thermal changes in the electronics and instrument beam patterns, as well as other factors. In this work we investigate the stability over time of these polarized power spectra, and use them to quantify the variation due to these effects.

Author(s): Austin Fox Fortino², Paul Chichura², Amy Igarashi¹, Saul Kohn², James Aguirre²
Institution(s): 1. San Diego State University, 2. University of Pennsylvania
Contributing team(s): HERA Collaboration

150.33 – First Polarized Power Spectra from HERA-19 Commissioning Data: Comparison with Simulations

The Hydrogen Epoch of Reionization Array (HERA) is a radio telescope whose primary goal is the detection of redshifted 21-cm line radiation produced from the spin-flip transition of HI during the Epoch of Reionization (EoR). HERA is currently under construction in South Africa, and will eventually be an array of 350 14-m antennas. HERA aims for a statistical detection of the power spectrum of this emission, using the so-called delay spectrum technique (Parsons et al 2012). We examine a first season of commissioning data from the first 19 elements (HERA-19) to characterize Galactic and extragalactic foregrounds. We compare the delay spectrum for HERA-19 constructed from data to those constructed from simulations done using a detailed instrument electromagnetic model and using the unpolarized Global Sky Model (GSM2008). We compare the data and simulations to explore the effects of Stokes-I to Q and U leakage, and further examine whether statistical models of polarization match the observed polarized power spectra.

Author(s): Amy Igarashi¹, Paul Chichura¹, Austin Fox Fortino¹, Saul Kohn¹, James Aguirre¹
Institution(s): 1. University of Pennsylvania
Contributing team(s): HERA Collaboration, CHAMP

150.34 – Polarized Power Spectra from HERA-19 Commissioning Data: Effect of Calibration Techniques

Studying the Epoch of Reionization (EoR) is crucial for cosmologists as it not only provides information about the first generation of stars and galaxies, but it may also help answer a number of fundamental astrophysical questions. The Hydrogen Epoch of Reionization Array (HERA) is doing this by examining emission from the 21cm hyperfine transition of neutral hydrogen, which has been identified as a promising probe of reionization. Currently, HERA is still in its commissioning phase; 37 of the planned 350 dishes have been constructed and analysis has begun for data received from the first 19 dishes built. With the creation of fully polarized power spectra, we investigate how different data calibration techniques affect the power spectra and whether or not ordering these techniques in different ways affects the results. These calibration techniques include using both non-imaging redundant measurements within the array to calibrate, as well as more traditional approaches based on imaging and calibrating to a model of sky. We explore the degree to which the different calibration schemes affect leakage of foreground emission to regions of Fourier space where EoR the power spectrum is expected to be measurable.

Author(s): Paul Chichura², Amy Igarashi¹, Austin Fox Fortino², Saul Kohn², James Aguirre²
Institution(s): 1. San Diego State University, 2. University of Pennsylvania
Contributing team(s): HERA Collaboration

150.35 – JWST Wavefront Sensing and Control: Operations Plans, Demonstrations, and Status

After JWST launches and unfolds in space, its telescope optics will be aligned through a complex series of wavefront sensing and control (WFSC) steps to achieve diffraction-limited performance. This iterative process will comprise about half of the observatory commissioning time (~ 3 out of 6 months). We summarize the JWST WFSC process, schedule, and expectations for achieved performance, and discuss our team's activities to prepare for an effective & efficient telescope commissioning. During the recently-completed OTIS cryo test at NASA JSC, WFSC demonstrations showed the flight-like operation of the entire JWST active optics and WFSC system from end to end, including all hardware and software components. In parallel, the same test data were processed through the JWST Mission Operations Center at STScI to demonstrate the readiness of ground system components there (such as the flight operations system, data pipelines, archives, etc). Moreover, using the Astronomer's Proposal Tool (APT), the entire telescope commissioning program has been implemented, reviewed, and is ready for execution. Between now and launch our teams will continue preparations for JWST commissioning, including further rehearsals and testing, to ensure a successful alignment of JWST's telescope optics.

Author(s): Marshall Perrin², D. Scott Acton¹, Charles-Philippe Lajoie², J. Scott Knight¹, Carey Myers², Chris Stark²
Institution(s): 1. *Ball Aerospace*, 2. *STScI*
Contributing team(s): JWST Wavefront Sensing & Control Team

150.36 – Tiny Tim vs ePSF: A Study of PSF Models for Hubble's Advanced Camera for Surveys

This study compares the Tiny Tim PSF against an empirically-derived PSF (Anderson & King 2006) for the HST Advanced Camera for Surveys/Wide Field Channel imaging. We manipulate the Tiny Tim PSF FITS files into a format that can be utilized by the ePSF FORTRAN photometry code. Then we perform PSF photometry on globular cluster NGC 6397 and analyze the photometry and astrometry results. We find that the ePSF models outperform the Tiny Tim PSFs in every measurement of stellar sources in this field.

Author(s): Samantha Hoffmann¹, Jay Anderson¹
Institution(s): 1. *Space Telescope Science Institute*

150.37 – HiCAT Software Infrastructure: Safe hardware control with object oriented Python

High contrast imaging for Complex Aperture Telescopes (HiCAT) is a testbed designed to demonstrate coronagraphy and wavefront control for segmented on-axis space telescopes such as envisioned for LUVOIR. To limit the air movements in the testbed room, software interfaces for several different hardware components were developed to completely automate operations. When developing software interfaces for many different pieces of hardware, unhandled errors are commonplace and can prevent the software from properly closing a hardware resource. Some fragile components (e.g. deformable mirrors) can be permanently damaged because of this. We present an object oriented Python-based infrastructure to safely automate hardware control and optical experiments. Specifically, conducting high-contrast imaging experiments while monitoring humidity and power status along with graceful shutdown processes even for unexpected errors. Python contains a construct called a "context manager" that allows you define code to run when a resource is opened or closed. Context managers ensure that a resource is properly closed, even when unhandled errors occur. Harnessing the context manager design, we also use Python's multiprocessing library to monitor humidity and power status without interrupting the experiment. Upon detecting a safety problem, the master process sends an event to the child process that triggers the context managers to gracefully close any open resources. This infrastructure allows us to queue up several experiments and safely operate the testbed without a human in the loop.

Author(s): Christopher Moriarty¹, Keira Brooks¹, Remi Soummer¹
Institution(s): 1. *Space Telescope Science Institute*

150.38 – COS2025: Extending the Lifetime of the FUV channel of the Cosmic Origins Spectrograph to 2025

The Hubble Space Telescope's Cosmic Origins Spectrograph (COS) Far-Ultraviolet (FUV) microchannel plate detector's efficiency at converting incoming photons into detectable events decreases with usage. This depletion of the detector's gain (i.e. gain sag) results in unusable regions of the COS/FUV detector. In order to mitigate this gain sag, a number of strategies have been employed over the past 8 years of operations, ranging from moving to different lifetime positions, to managing the high voltage to extract a smaller amount of charge, to re-distributing the cenwave usage so that Ly-alpha does not produce a gain-sag hole in a given location. We are now at a point where none of the strategies above will, without any other changes, allow us to continue operating the COS/FUV detector to 2025. To address this a new COS2025 policy was developed, with the goal of retaining full science capability of COS/FUV to 2025. We present an overview of the COS2025 policy, which places restrictions on the G130M cenwaves allowed at Lifetime Position 4 (LP4). We also present a tool which allows users to visualize the COS/FUV wavelength ranges to help users prepare their proposals in the light of the restrictions on the G130M cenwaves.

Author(s): Marc Rafelski¹, Gisella De Rosa¹, William J. Fischer¹, Mees Fix¹, Andrew Fox¹, Nick Indriolo¹, Bethan James¹, Camellia Magness¹, Cristina M. Oliveira¹, Steven V. Penton¹, Rachel Plesha¹, Julia Roman-Duval¹, David J. Sahnou¹, Ravi Sankrit¹, Elaine M Snyder¹, Joanna M. Taylor¹, James White¹
Institution(s): 1. *Space Telescope Science Institute*

150.39 – Exploring Algorithms for Stellar Light Curves With TESS

The Kepler and K2 missions have produced tens of thousands of stellar light curves, which have been used to measure rotation periods, characterize photometric activity levels, and explore phenomena such as differential rotation. The quasi-periodic nature of rotational light curves, combined with the potential presence of additional periodicities not due to rotation, complicates the analysis of these time series and makes characterization of uncertainties difficult. A variety of algorithms have been used for the extraction of rotational signals, including autocorrelation functions, discrete Fourier transforms, Lomb-Scargle periodograms, wavelet transforms, and the Hilbert-Huang transform. In addition, in the case of K2 a number of different pipelines have been used to produce initial detrended light curves from the raw image frames.

In the near future, TESS photometry, particularly that deriving from the full-frame images, will dramatically further expand the number of such light curves, but details of the pipeline to be used to produce photometry from the FFIs remain under development. K2 data offers us an opportunity to explore the utility of different reduction and analysis tool combinations applied to these astrophysically important tasks. In this work, we apply a wide range of algorithms to light curves produced by a number of popular K2 pipeline products to better understand the advantages and limitations of each approach and provide guidance for the most reliable and most efficient analysis of TESS stellar data.

Author(s): Derek Buzasi¹
Institution(s): 1. *Florida Gulf Coast University*

150.40 – WFIRST: Simulating and Analyzing Wide Field, High-Resolution Images of Nearby Galaxies

The large field of view, high sensitivity, and high spatial resolution of WFIRST at 0.5~2.0 μ m will enable the study of the stellar contents and halo substructures of galaxies at 1~10 Mpc in unprecedented detail. We are producing realistic simulated multi-

band WFI imaging data by combining synthetic stellar population and observed background galaxy catalogs. We use these catalogs as input to the the Space Telescope Image Product Simulator (STIPS) to produce images with the detector and optics characteristics expected for the Wide Field Imager. Furthermore, we are developing software to measure the photometric properties of the simulated objects in the STIPS images using DOLPHOT. This suite of tools is beginning to provide end-to-end simulations of WFIRST nearby galaxy observations and analysis. We present preliminary evaluations of WFIRST's scientific capabilities based on statistical analysis of early simulations, and

151 – Catalogs Poster Session

151.01 – Classifying Variable Sources in SDSS Stripe 82

SDSS (Sloan Digital Sky Survey) Stripe 82 is a well-documented and researched region of the sky that does not have all of its ~67,500 variable objects labeled. By collecting data and consulting different catalogs such as the Catalina Survey, we are able to slowly cross-match more objects and add classifications within the Stripe 82 catalog. Such matching is performed either by pairing SDSS identification numbers, or by converting and comparing the coordinates of every object within the Stripe 82 catalog to every object within the classified catalog, such as the Catalina Survey catalog. If matching is performed with converted coordinates, a follow-up check is performed to ascertain that the magnitudes of the paired objects are within a reasonable margin of error and that objects have not been mismatched. Once matches have been confirmed, the light curves of classified objects can then be used to determine features that most effectively separate the different types of variable objects in feature spaces. By classifying variable objects, we can construct a reference for subsequent large research surveys, such as LSST (the Large Synoptic Survey Telescope), that could utilize SDSS data as a training set for its own classifications.

Author(s): Christina Willecke Lindberg¹

Institution(s): 1. *University of Washington*

151.02 – A Search to Uncover the Infrared Excess (IRXS) Sources in the Spitzer Enhanced Imaging Products (SEIP) Catalog

The Spitzer Enhanced Imaging Products catalog (SEIP) is a collection of nearly 42 million point sources obtained by the Spitzer Space Telescope during its 5+ year cryogenic mission. Strasburger et al (2014) isolated sources with a signal-to-noise ratio (SNR) >10 in five infrared (IR) wavelength channels (3.6, 4.5, 5.8, 8 and 24 microns) to begin a search for sources with infrared excess (IRXS). They found 76 objects that were never catalogued before. Based on this success, we intend to dig deeper into the catalog in an attempt to find more IRXS sources, specifically by lowering the SNR on the 3.6, 4.5, and 24 micron channels. The ultimate goal is to use this large sample to seek rare astrophysical sources that are transitional in nature and evolutionarily very important.

Our filtering of the database at SNR > 5 yielded 461,000 sources. This was further evaluated and reduced to only the most interesting based on source location on a [3.6]-[4.5] vs [4.5]-[24] color-color diagram. We chose a sample of 985 extreme IRXS sources for further inspection. All of these candidate sources were visually inspected and cross-referenced against known sources in existing databases, resulting in a list of highly reliable IRXS sources.

These sources will prove important in the study of galaxy and stellar evolution, and will serve as a starting point for further investigation.

discuss the advantages of simultaneously developing image simulation and data analysis capabilities as WFIRST's instrumental designs are finalized.

Author(s): Rubab Khan¹, Benjamin F. Williams¹, Julianne Dalcanton¹

Institution(s): 1. *University of Washington*

Contributing team(s): WFIRST Infrared Nearby Galaxies Survey (WINGS)

Author(s): Jamie Lynn Rowe¹, Gary Duranko⁴, Varoujan Gorjian³, Howard Lineberger², Laura Orr⁵, Ayomikun Adewole⁴, Eric Bradford², Alea Douglas⁵, Steven Kohl², Lillia Larson², Gus Lascola², Quinton Orr⁵, Mekai Scott², Joseph Walston², Xian Wang⁴

Institution(s): 1. *Bethlehem Central High School*, 2. *Durham Academy Upper School*, 3. *JPL/Caltech*, 4. *Oak Hill Academy*, 5. *Ukiah High School*

151.03 – Digitizing Villanova University's Eclipsing Binary Card Catalogue

Villanova University's Department of Astrophysics and Planetary Science has years of hand-written archival data on Eclipsing Binaries at its disposal. This card catalog began at Princeton in the 1930's with notable contributions from scientists such as Henry Norris Russel. During World War II, the archive was moved to the University of Pennsylvania, which was one of the world centers for Eclipsing Binary research, consequently, the contributions to the catalog during this time were immense. It was then moved to University of Florida at Gainesville before being accepted by Villanova in the 1990's. The catalog has been kept in storage since then. The objective of this project is to digitize this archive and create a fully functional online catalog that contains the information available on the cards, along with the scan of the actual cards. Our group has built a database using a python-powered infrastructure to contain the collected data. The team also built a prototype web-based searchable interface as a front-end to the catalog. Following the data-entry process, information like the Right Ascension and Declination will be run against SIMBAD and any differences between values will be noted as part of the catalog. Information published online from the card catalog and even discrepancies in information for a star, could be a catalyst for new studies on these Eclipsing Binaries. Once completed, the database-driven interface will be made available to astronomers worldwide. The group will also acquire, from the database, a list of referenced articles that have yet to be found online in order to further pursue their digitization. This list will be comprised of references in the cards that were neither found on ADS nor online during the data-entry process. Pursuing the integration of these references to online queries such as ADS will be an ongoing process that will contribute and further facilitate studies on Eclipsing Binaries.

Author(s): Giannina Guzman¹, Briana Dalton¹, Kyle Conroy¹, Andrej Prsa¹

Institution(s): 1. *Villanova University*

151.04 – A Transdimensional Approach to Modeling the Cosmic X-ray Background

Cataloging astrophysical sources is a fundamental operation in astronomy. While simple in principle, cataloging becomes more complicated for images with low signal to noise and degeneracies across different emission components. We analyze Chandra Deep Field - South (CDF-S) data using a novel method called probabilistic cataloging, which extracts information by sampling from the catalog space, i.e. the space of different point source configurations consistent with a given image. By employing a reversible-jump Markov Chain Monte Carlo (RJMCMC) sampling method, we are able to infer the flux and color distribution for Active Galactic Nuclei (AGN) in the region. We are also able to infer the number of AGN by marginalizing over faint members below the detection threshold. To validate our method, we use

simulated deep Chandra exposures and show that the isotropic background emission can be constrained at the 10% level. This result takes into account its covariance with unresolved AGN and the particle background of Chandra. We then present results of probabilistic cataloging applied to the CDF-S 2Ms, 4Ms, and 7Ms datasets in order to evaluate the fidelity of our method. Furthermore, by incorporating auxiliary redshift information from the COMBO Survey within our framework, we present the first three-dimensional probabilistic catalog of AGN and discuss possible implications for AGN synthesis models.

Author(s): Richard Feder¹, Tansu Daylan¹
Institution(s): 1. *Harvard University*

151.05 – The VLITE Post-Processing Pipeline

A post-processing pipeline to adaptively extract and catalog point sources is being developed to enhance the scientific value and accessibility of data products generated by the VLA Low-band Ionosphere and Transient Experiment (VLITE; <<http://vlite.nrao.edu/>>) on the Karl G. Jansky Very Large Array (VLA). In contrast to other radio sky surveys, the commensal observing mode of VLITE results in varying depths, sensitivities, and spatial resolutions across the sky based on the configuration of the VLA, location on the sky, and time on source specified by the primary observer for their independent science objectives. Therefore, previously developed tools and methods for generating source catalogs and survey statistics are not always appropriate for VLITE's diverse and growing set of data. A raw catalog of point sources extracted from every VLITE image will be created from source fit parameters stored in a queryable database. Point sources will be measured using the Python Blob Detector and Source Finder software (PyBDSF; Mohan & Rafferty 2015). Sources in the raw catalog will be associated with previous VLITE detections in a resolution- and sensitivity-dependent manner, and cross-matched to other radio sky surveys to aid in the detection of transient and variable sources. Final data products will include separate, tiered point source catalogs grouped by sensitivity limit and spatial resolution.

Author(s): Emily E. Richards¹, Tracy Clarke¹, Wendy Peters¹, Emil Polisensky¹, Namir E Kassim¹
Institution(s): 1. *Naval Research Laboratory*

151.06 – Initial results from the Arecibo Galaxy Environment Survey in the Pegasus Cluster

As part of the Arecibo Galaxy Environment Survey (AGES), we have covered a 5deg x 4deg region centered on the Pegasus Cluster and its principal member, the elliptical galaxy NGC 7619, in the 21-cm line of neutral hydrogen. The survey takes in the full redshift range of the cluster and the volume behind it out to 18,000 km/s. In the cluster and the volume we detect over 500 sources, many of which are previously uncataloged. These include five sources without obvious optical counterparts (three within the redshift range of the cluster, which are assumed to be members); of these, four (two within the cluster) have possible low surface-brightness counterparts identified on stacked and/or smoothed SDSS images, while the third remains without an optical counterpart. We also detect three low surface-brightness ultra-diffuse galaxies from the catalog of Shi et al. (2017) in HI for the first time, and find fourteen other HI sources where both a UDG and other potential counterparts are present in the beam, making an unambiguous association with the UDG not possible on the basis of this data alone. In addition to these, we detect N objects with HI and stellar streams.

Author(s): Robert Minchin¹, Rhys Taylor²
Institution(s): 1. *Arecibo Observatory*, 2. *Czech Academy of Sciences*
Contributing team(s): AGES Collaboration

151.07 – OSIRIS-REx Asteroid Sample Return Mission Image Analysis

152 – Instrumentation: Ground Based or Airborne Poster Session

NASA's Origins Spectral Interpretation Resource Identification Security-Regolith Explorer (OSIRIS-REx) mission constitutes the "first-of-its-kind" project to thoroughly characterize a near-Earth asteroid. The selected asteroid is (101955) 1999 RQ36 (a.k.a. Bennu). The mission launched in September 2016, and the spacecraft will reach its asteroid target in 2018 and return a sample to Earth in 2023. The spacecraft that will travel to, and collect a sample from, Bennu has five integrated instruments from national and international partners. NASA's OSIRIS-REx asteroid sample return mission spacecraft includes the Touch-And-Go Camera System (TAGCAMS) three camera-head instrument. The purpose of TAGCAMS is to provide imagery during the mission to facilitate navigation to the target asteroid, confirm acquisition of the asteroid sample and document asteroid sample stowage. Two of the TAGCAMS cameras, NavCam 1 and NavCam 2, serve as fully redundant navigation cameras to support optical navigation and natural feature tracking. The third TAGCAMS camera, StowCam, provides imagery to assist with and confirm proper stowage of the asteroid sample. Analysis of spacecraft imagery acquired by the TAGCAMS during cruise to the target asteroid Bennu was performed using custom codes developed in MATLAB. Assessment of the TAGCAMS in-flight performance using flight imagery was done to characterize camera performance. One specific area of investigation that was targeted was bad pixel mapping. A recent phase of the mission, known as the Earth Gravity Assist (EGA) maneuver, provided images that were used for the detection and confirmation of "questionable" pixels, possibly under responsive, using image segmentation analysis. Ongoing work on point spread function morphology and camera linearity and responsivity will also be used for calibration purposes and further analysis in preparation for proximity operations around Bennu. Said analyses will provide a broader understanding regarding the functionality of the camera system, which will in turn aid in the fly-down to the asteroid, as it will allow the pick of a suitable landing and sample location.

Author(s): Lee Roger Chevres Fernandez², Brent Bos¹
Institution(s): 1. *NASA Goddard Space Flight Center*, 2. *University of Puerto Rico*

151.08 – Real-time Automatic Search for Multi-wavelength Counterparts of DWF Transients

The Deeper Wider Faster (DWF) survey aims to find and classify the fastest transients in the Universe. DWF utilizes the Dark Energy Camera (DECam), collecting a continuous sequence of 20s images over a 3 square degree field of view.

Once an interesting transient is detected during DWF observations, the DWF collaboration has access to several facilities for rapid follow-up in multiple wavelengths (from gamma to radio).

An online web tool has been designed to help with real-time visual classification of possible astrophysical transients in data collected by the DWF observing program. The goal of this project is to create a python-based code to improve the classification process by querying several existing archive databases. Given the DWF transient location and search radius, the developed code will extract a list of possible counterparts and all available information (e.g. magnitude, radio fluxes, distance separation). Thanks to this tool, the human classifier can make a quicker decision in order to trigger the collaboration rapid-response resources.

Author(s): Christopher Murphy², Antonino Cucchiara², Igor Andreoni¹, Jeff Cooke¹, Sarah Hegarty¹
Institution(s): 1. *Swinburne University*, 2. *University of the Virgin Islands*

152.01 – "Slit Mask Design for the Giant Magellan Telescope Multi-object Astronomical and Cosmological Spectrograph"

The Giant Magellan Telescope Multi-object Astronomical and Cosmological Spectrograph (GMACS) is currently in development for the Giant Magellan Telescope (GMT). GMACS will employ slit masks with a usable diameter of approximately 0.450 m for the purpose of multi-slit spectroscopy. Of significant importance are the design constraints and parameters of the multi-object slit masks themselves as well as the means for mapping astronomical targets to physical mask locations. Analytical methods are utilized to quantify deformation effects on a potential slit mask due to thermal expansion and vignetting of target light cones. Finite element analysis (FEA) is utilized to simulate mask flexure in changing gravity vectors. The alpha version of the mask creation program for GMACS, GMACS Mask Simulator (GMS), a derivative of the OSMOS Mask Simulator (OMS), is introduced.

Author(s): Darius Williams¹, Jennifer L Marshall², Luke M Schmidt², Travis Prochaska², Darren L DePoy²

Institution(s): 1. Case Western Reserve University, 2. Texas A&M University

152.02 – Astronomical Research at the U.S. Air Force Academy Observatory

The U.S. Air Force Academy (USAFA) Observatory houses 61-cm and 41-cm Ritchey-Chrétien (RC) reflecting telescopes, and serves as the hub for a world-wide network of 50-cm RC reflectors known as the Falcon Telescope Network (FTN). Since the 1970s, the USAFA Observatory has hosted a wide range of student and faculty research projects including variable star photometry, exoplanet light curve and radial velocity studies, near-Earth object astrometry, and "lucky imaging" of manmade spacecraft. Further, the FTN has been used extensively for LEO through GEO satellite photometry and spectroscopy, and for exoplanet photometry. Future capabilities of our observatory complex include fielding several new FTN observatory sites and the acquisition of a 1-meter RC fast-tracking telescope at the USAFA Observatory.

Author(s): Devin J Della-Rose¹, Randall E Carlson¹, Francis K Chun¹, Timothy W Giblin¹, Steven J Novotny¹, Daniel E Polsgrove¹

Institution(s): 1. United States Air Force Academy

152.03 – Determining the Optimal Design for a New ADR Mechanical Support

ZEUS-2 is a grating spectrometer that is used to observe emission lines in submillimeter wavelengths. It is capable of detecting redshifted fine structure lines of galaxies over a wide redshift range. ZEUS-2 can observe carbon, nitrogen, and oxygen lines, which will in turn allow for modeling of optically thick molecular clouds, provide information about star temperatures, and help gain insight about the interstellar medium and gases from which stars form. The detections collected by ZEUS-2 can provide a glimpse into star formation in the early universe and improve the current understanding of the star formation process.

ZEUS-2 utilizes an Adiabatic Demagnetization Refrigerator (ADR) to cool its detectors to around 100 mK. Copper rods connect the salt pills within the ADR and the mechanical supports. These supports are comprised of three main pieces: a base member, an inner member, and a guard member. On two separate mechanical supports, the Kevlar strands have broken. This led to thermal contact between the three members, preventing the detector from reaching its final operating temperature. It is clear that a replacement mechanical support system is necessary for operation.

Author(s): Kelly Waldvogel¹, Gordon Stacey¹, Thomas Nikola¹, Stephen Parshley¹

Institution(s): 1. Cornell University

152.04 – Updated Astrometric Calibration of the Gemini Planet Imager: Application to the Theta1 Orionis B System

The Gemini Planet Imager (GPI), housed on the 8-meter Gemini South telescope in Chile, is an instrument designed to detect Jupiter-like extrasolar planets by direct imaging. It relies on adaptive optics to correct the effects of atmospheric turbulence, along with an advanced coronagraph and calibration system. One of the scientific goals of GPI is to measure the orbital properties of the planets it discovers. Because these orbits have long periods, precise measurements of the relative position between the star and the planet (relative astrometry) are required. In this poster, I will present the astrometric calibration of GPI. We constrain the plate scale and orientation of the camera by observing different binary star systems with both GPI and another well-calibrated instrument, NIRC2, at the Keck telescope in Hawaii. We measure their separations with both instruments and use that information to calibrate the plate scale. By taking these calibration measurements over the course of three years, we have measured the plate scale to 0.05% and shown that it is stable across multiple epochs. One of the calibrators for GPI is Theta1 Orionis B, one of the star systems in the Trapezium Cluster in Orion. Using GPI and Keck measurements taken over the past several years combined with astrometry from the literature spanning two decades, we can place new constraints on the orbital properties of this massive multiple system. We will present the best fit orbital properties for these objects, including updated mass estimates for the components.

Author(s): Debby Tran¹, Quinn Konopacky¹

Institution(s): 1. University of California San Diego

Contributing team(s): GPIES Team

152.05 – Milliarcsecond Astronomy with the CHARA Array

The Center for High Angular Resolution Astronomy offers 50 nights per year of open access time at the CHARA Array. The Array consists of six telescopes linked together as an interferometer, providing sub-milliarcsecond resolution in the optical and near-infrared. The Array enables a variety of scientific studies, including measuring stellar angular diameters, imaging stellar shapes and surface features, mapping the orbits of close binary companions, and resolving circumstellar environments. The open access time is part of an NSF/MSIP funded program to open the CHARA Array to the broader astronomical community. As part of the program, we will build a searchable database for the CHARA data archive and run a series of one-day community workshops at different locations across the country to expand the user base for stellar interferometry and encourage new scientific investigations with the CHARA Array.

Author(s): Gail Schaefer², Theo ten Brummelaar², Douglas Gies¹, Jeremy Jones¹, Christopher Farrington²

Institution(s): 1. Georgia State University, 2. Georgia State University - CHARA

152.06 – Design and Construction of a Light Box for Flat Fielding in Photometry

Flat fielding in photometry is a necessary part of the procedure to reduce error in data. One method to accomplish consistent flat fields is by using a light box and mounting it on the telescope. This achieves the same effects as dome flats but more reliably, as it is a self-contained system. I detail the procedure I went through to build my first light box and upon discovering issues, the subsequent improvements to the light box. This procedure may prove useful for amateur astronomers who wish to improve their own photometry data, or just for those who wish to redesign how they do flat fielding.

Author(s): Alexander Gable¹

Institution(s): 1. Ithaca College

152.07 – Expected Science Performance of the Square Kilometre Array Phase 1 (SKA1)

The Square Kilometre Array (SKA) will be the world's largest radio telescope when Phase 1 (SKA1) is completed in the next decade. The past few years have seen great progress toward this goal, through extensive design activities, with construction to start before the end of this decade, and early operations anticipated to begin around 2026. This poster describes the SKA and presents the expected performance and capabilities of SKA1 based on the modelling and proto-typing to date.

Author(s): Tyler Bourke¹, Robert Braun¹, Anna Bonaldi¹, Cristina Garcia-Miro¹, Evan Keane¹, Jeff Wagg¹

Institution(s): 1. SKA Organisation

Contributing team(s): SKAO Science Team

152.08 – NEID Port Adapter: Design and Verification Plan

The NEID spectrograph is an optical (380–930 nm), fiber-fed, precision Doppler spectrograph currently in development for the 3.5 m WIYN Telescope at Kitt Peak National Observatory. Designed to achieve a radial velocity precision of <30 cm/s, NEID will be sensitive enough to detect terrestrial-mass exoplanets around low-mass stars. Light from the target stars is focused by the telescope to a bent-Cassegrain port at the edge of the primary mirror mechanical support. The specialized NEID “Port Adapter” system is mounted at this bent-Cassegrain port and is responsible for delivering the incident light from the telescope to the NEID fibers. In order to provide stable, high-quality images to the science instrument, the Port Adapter houses several subcomponents designed to acquire the target stars, correct for atmospheric dispersion, stabilize the light onto the science fibers, and calibrate the spectrograph by injecting known wavelength sources such as a laser frequency comb. Here we describe the overall design of the Port Adapter and outline the development of calibration tools and an on-sky test plan to verify the performance of the atmospheric dispersion corrector (ADC). We also discuss the development of an error budget and test requirements to ensure high-precision centroiding onto the NEID science fibers using a system of coherent fiber bundles.

Author(s): Sarah E. Logsdon⁴, Michael McElwain⁴, Michael W. McElwain⁴, Qian Gong⁴, Chad Bender⁷, Samuel Halverson⁸, Fred Hearty⁶, Emily Hunting⁵, Kurt Jaehnig⁹, Ming Liang⁵, Suvrath Mahadevan⁶, A. J. Monson⁶, Jeffrey Percival⁹, Jayadev Rajagopal⁵, Lawrence Ramsey⁶, Arpita Roy², Fernando Santoro¹, Christian Schwab³, Michael Smith⁹, Marsha Wolf⁹, Jason Wright⁶

Institution(s): 1. ASTRO LLC., 2. Caltech, 3. Macquarie University, 4. NASA Goddard Space Flight Center, 5. National Optical Astronomy Observatory, 6. The Pennsylvania State University, 7. University of Arizona, 8. University of Pennsylvania, 9. University of Wisconsin-Madison

152.09 – The Binary Offset Effect in CCDs: an Anomalous Readout Artifact Affecting Most Astronomical CCDs in Use

We discovered an anomalous behavior of CCD readout electronics that affects their use in many astronomical applications, which we call the “binary offset effect”. Due to feedback in the readout electronics, an offset is introduced in the values read out for each pixel that depends on the binary encoding of the previously read-out pixel values. One consequence of this effect is that a pathological local background offset can be introduced in images that only appears where science data are present on the CCD. The amplitude of this introduced offset does not scale monotonically with the amplitude of the objects in the image, and can be up to 4.5 ADU per pixel for certain instruments. Additionally, this background offset will be shifted by several pixels from the science data, potentially distorting the shape of objects in the image. We tested 22 instruments for signs of the binary offset effect and found evidence of it in 16 of them, including LRIS and DEIMOS on the Keck telescopes, WFC3-UVIS and STIS on HST, MegaCam on CFHT, SNIFS on the UH88 telescope, GMOS on the Gemini telescopes, HSC on Subaru, and FORS on VLT. A large amount of archival data is therefore affected by the binary offset

effect, and conventional methods of reducing CCD images do not measure or remove the introduced offsets. As a demonstration of how to correct for the binary offset effect, we have developed a model that can accurately predict and remove the introduced offsets for the SNIFS instrument on the UH88 telescope. Accounting for the binary offset effect is essential for precision low-count astronomical observations with CCDs.

Author(s): Kyle Robert Boone⁵, Gregory Aldering⁴, Yannick Copin², Samantha Dixon⁵, Rachel Domagalski⁶, Emmanuel Gangler³, Emmanuel Pecontal¹, Saul Perlmutter⁵

Institution(s): 1. Centre de Recherche Astronomique de Lyon, Université Lyon 1, 2. Institut de Physique Nucleaire de Lyon, Université de Lyon, 3. Laboratoire de Physique Corpusculaire de Clermont-Ferrand, 4. Lawrence Berkeley National Laboratory, 5. University of California, Berkeley, 6. University of Toronto

Contributing team(s): Nearby Supernova Factory Collaboration

152.10 – The CHARIS Integral Field Spectrograph with SCEXAO: Data Reduction and Performance

We summarize the data reduction pipeline and on-sky performance of the CHARIS Integral Field Spectrograph behind the SCEXAO Adaptive Optics system on the Subaru Telescope. The open-source pipeline produces data cubes from raw detector reads using a X^2 -based spectral extraction technique. It implements a number of advances, including a fit to the full nonlinear pixel response, suppression of up to a factor of ~ 2 in read noise, and deconvolution of the spectra with the line-spread function. The CHARIS team is currently developing the calibration and postprocessing software that will comprise the second component of the data reduction pipeline. Here, we show a range of CHARIS images, spectra, and contrast curves produced using provisional routines. CHARIS is now characterizing exoplanets simultaneously across the J, H, and K bands.

Author(s): N. Jeremy Kasdin³, Tyler Groff², Timothy Brandt⁶, Thayne Currie⁵, Maxime Rizzo², Jeffrey K. Chilcote⁴, Olivier Guyon⁷, Nemanja Jovanovic¹, Julien Lozi⁵, Barnaby Norris⁸, Motohide Tamura⁹

Institution(s): 1. California Institute of Technology, 2. Goddard Space Flight Center, 3. Princeton University, 4. Stanford University, 5. Subaru Telescope, 6. UC Santa Barbara, 7. University of Arizona, 8. University of Sydney, 9. University of Tokyo

152.11 – Constructing a dispersed fringe sensor prototype for the Giant Magellan Telescope

The Giant Magellan Telescope (GMT) will be the world's largest telescope upon completion. The GMT employs seven 8 m primary mirror segments and seven 1 m secondary mirror segments. One challenge of the GMT is keeping the seven pairs of mirror segments on the GMT in phase. In this project, we developed and began assembly on a design for a dispersed fringe sensor prototype consisting of an optical and basic mechanical layout. The prototype design will be tested on the Magellan Clay Telescope as an experiment for future phasing methods to be used on the GMT.

Author(s): Danielle Frostig¹, Brian McLeod²

Institution(s): 1. Harvard University, 2. Harvard-Smithsonian Center for Astrophysics

Contributing team(s): AGWS Team

152.12 – Improved Weather Forecasting for the Dynamic Scheduling System of the Green Bank Telescope

The Robert C Byrd Green Bank Telescope (GBT) uses a software system that dynamically schedules observations based on models of vertical weather forecasts produced by the National Weather Service (NWS). The NWS provides hourly forecasted values for ~ 60 layers that extend into the stratosphere over the observatory. We use models, recommended by the Radiocommunication Sector of the International Telecommunications Union, to derive

the absorption coefficient in each layer for each hour in the NWS forecasts and for all frequencies over which the GBT has receivers, 0.1 to 115 GHz. We apply radiative transfer models to derive the opacity and the atmospheric contributions to the system temperature, thereby deriving forecasts applicable to scheduling radio observations for up to 10 days into the future. Additionally, the algorithms embedded in the data processing pipeline use historical values of the forecasted opacity to calibrate observations.

Until recently, we have concentrated on predictions for high frequency (> 15 GHz) observing, as these need to be scheduled carefully around bad weather. We have been using simple models for the contribution of rain and clouds since we only schedule low-frequency observations under these conditions. In this project, we wanted to improve the scheduling of the GBT and data calibration at low frequencies by deriving better algorithms for clouds and rain.

To address the limitation at low frequency, the observatory acquired a Radiometrics Corporation MP-1500A radiometer, which operates in 27 channels between 22 and 30 GHz. By comparing 16 months of measurements from the radiometer against forecasted system temperatures, we have confirmed that forecasted system temperatures are indistinguishable from those measured under good weather conditions. Small mis-calibrations of the radiometer data dominate the comparison. By using recalibrated radiometer measurements, we looked at bad weather days to derive better models for forecasting the contribution of clouds to the opacity and system temperatures. We will show how these revised algorithms should help us improve both data calibration and the accuracy of scheduling low-frequency observations.

Author(s): Kari Henry², Ronald Maddalena¹
Institution(s): 1. *Green Bank Observatory*, 2. *Oswego College*

152.13 – Simulated Guide Stars: Adapting the Robo-AO Telescope Simulator to UH 88”

Robo-AO is an autonomous adaptive optics system that is in development for the UH 88” Telescope on the Mauna Kea Observatory. This system is capable of achieving near diffraction limited imaging for astronomical telescopes, and has seen successful deployment and use at the Palomar and Kitt Peak Observatories previously. A key component of this system, the telescope simulator, will be adapted from the Palomar Observatory design to fit the UH 88” Telescope. The telescope simulator will simulate the exit pupil of the UH 88” telescope so that the greater Robo-AO system can be calibrated before observing runs. The system was designed in Code V, and then further improved upon in Zemax for later development. Alternate design forms were explored for the potential of adapting the telescope simulator to the NASA Infrared Telescope Facility, where simulating the exit pupil of the telescope proved to be more problematic. A proposed design composed of solely catalog optics was successfully produced for both telescopes, and they await assembly as time comes to construct the new Robo-AO system.

Author(s): Jaren Ashcraft², Christoph Baranec¹
Institution(s): 1. *Institute for Astronomy - University of Hawaii*, 2. *University of Rochester*

152.14 – Building an Experimental Setup to Characterize an H4RG-15

The Teledyne Imaging Sensors H4RG-15 infrared detector is designed for the next era of extremely large telescopes. Characterization of individual H4RG-15 detectors are critical for future astronomical use. ULBcam, a former UH88 IR camera and remnant test dewar for H2RG characterization, was previously modified for H4RG-15 characterization. During the summer, this system was further upgraded with a baffle tube to a blackbody illumination source to allow controlled field illumination. This baffle tube, designed in OpenSCAD, was constructed in the IfA machine shop. Specific placements of the 50-micron aperture and

scatter restrictive baffling was designed in Zemax. Four separate data sets were acquired to look into detector persistence, dark current, read noise, and charge gain. With the illumination source set at 450 K, ten ramps of 90/90 read frames were taken to pass saturation values. These tests were repeated at 500K to show results at over saturated conditions. Five ramps of 136/136 read frames were taken with a blank shutter applied. The persistence results showed expected results with signals settling from the third ramp. Dark current results showed higher than Teledyne stated values at 0.06 electrons/second, a factor of 6 higher than expected, which exposes systematic ULBcam dark testing capabilities. The read noise resulted with an expected value of 0.014 electrons. The charge gain showed 0.02 electrons/ADU where the expected value is 2 electrons/ADU. Data analysis using reference frame subtraction will be done for future work.

Author(s): Mickie Hirata¹, K. Hodapp¹, Donald N.B. Hall¹, Sean B. Goebel¹, Shane M. Jacobson¹
Institution(s): 1. *University of Hawaii Institute for Astronomy*

152.15 – Argus+ : The Future of Wide-Field, Spectral-Line Imaging at 3-mm with the Green Bank Telescope

The Robert C Byrd Green Bank Telescope has met its design goal of providing high-quality observations at 115 GHz. Observers also have access to the new, 16-pixel, 3-mm Argus receiver, which is providing high-dynamic range images over wide fields for the multitude of spectral lines between 85 and 115 GHz, including CO, ¹³CO, C¹⁸O, SiO, HCN, HCO⁺, HNC, N₂H⁺, and CS.

The small number of pixels in Argus limits its ability to map many of the most interesting objects whose extent exceeds many arc-minutes. The successful performance of Argus, and its modular design, demonstrates that receivers with many more pixels could be built for the GBT. A 12 x 12 array of the Argus design would have mapping speeds about nine times faster than Argus without suffering any degradation in performance for the outer pixels in the array.

We present our plans to build the next-generation Argus instrument (Argus+) with 144-pixels, a footprint 5'x5', and 7" resolution at 110 GHz. The project will be a collaboration between the Green Bank Observatory and university groups, who will supply key components. The key science drivers for Argus+ are studies of molecular filaments in the Milky Way, studies of molecular clouds in nearby galaxies, and the observations of rapidly evolving solar system objects.

Author(s): Ronald Maddalena¹, David Frayer¹, Felix Lockman¹, Karen O'Neil¹, Steven White¹
Institution(s): 1. *Green Bank Observatory*
Contributing team(s): Argus+ Collaboration

152.16 – Charge Gain, Voltage Gain, and Node Capacitance of the SAPHIRA Detector Pixel by Pixel

The University of Hawai'i Institute for Astronomy has partnered with Leonardo (formerly Selex) in the development of HgCdTe linear mode avalanche photodiode (L-APD) SAPHIRA detectors. The SAPHIRA (Selex Avalanche Photodiode High-speed Infra-Red Array) is ideally suited for photon-starved astronomical observations, particularly near infrared (NIR) adaptive optics (AO) wave-front sensing. I have measured the stability, and linearity with current, of a 1.7-um (10% spectral bandpass) infrared light emitting diode (IR LED) used to illuminate the SAPHIRA and have then utilized this source to determine the charge gain (in e-/ADU), voltage gain (in uV/ADU), and node capacitance (in fF) for each pixel of the 320x256@24um SAPHIRA. These have previously only been averages over some sub-array. Determined from the ratio of the temporal averaged signal level to variance under constant 1.7-um LED illumination, I present the charge gain pixel-by-pixel in a 64x64 sub-array at the center of the active area of the SAPHIRA (analyzed separately as four 32x32 sub-arrays) to be about 1.6 e-/ADU ($\sigma=0.5$ e-/ADU).

Additionally, the standard technique of varying the pixel reset voltage (PRV) in 10 mV increments and recording output frames for the same 64x64 subarray found the voltage gain per pixel to be about 11.7 uV/ADU ($\sigma=0.2$ uV/ADU). Finally, node capacitance was found to be approximately 23 fF ($\sigma=6$ fF) utilizing the aforementioned charge and voltage gain measurements. I further discuss the linearity measurements of the 1.7- μ m LED used in the charge gain characterization procedure.

Author(s): Izabella M. Pastrana³, Donald N.B. Hall², Ian M. Baker¹, Shane M. Jacobson², Sean B. Goebel²

Institution(s): 1. Leonardo Company, 2. University of Hawai'i Institute for Astronomy, 3. Washington University in St. Louis

152.17 – Transformative Science for the Next Decade with the Green Bank Observatory

With new instruments and improved performance, the 100m Green Bank Telescope is now demonstrating its full potential. On this 60th anniversary of the groundbreaking for the Green Bank Observatory, we can look forward to the future of the facility for the next 5, 10, and even 20 years. Here we describe the results from a recent workshop, "Transformative Science for the Next Decade with the Green Bank Observatory: Big Questions, Large Programs, and New Instruments," and describe the scientific plans for our facility.

Author(s): Karen O'Neil¹, David Frayer¹, Frank Ghigo¹, Felix Lockman¹, Ryan Lynch¹, Ronald Maddalena¹, Anthony minter¹, Richard Prestage¹

Institution(s): 1. Green Bank Observatory

152.18 – The Habitable Zone Planet Finder: Precision NIR Radial Velocities during Testing & Commissioning

The Habitable Zone Planet Finder (HPF) is a fiber-fed near-infrared (0.8 to 1.24 microns) spectrometer designed for high stability for precision Doppler radial velocity surveys using the 10m Hobby Eberly Telescope. We discuss results obtained during the lab testing and commissioning phase that show the solar spectrum and the key parameters of the instrument, and demonstrate that the HPF fibers track each other to sub-meter per second relative Doppler radial velocity precision. We will also discuss the capabilities of HPF, as well as the reduction challenges in the infrared, and our solutions to these challenges.

Author(s): Joe Philip Ninan⁴, Arpita Roy¹, Ryan Terrien³, Kyle Kaplan⁵, Chad Bender⁵, Andy Monson⁴, Paul Robertson⁶, Gudmundur Stefansson⁴, Shubham Kanodia⁴, Sam Halverson⁷, Suvrath Mahadevan⁴, Fred Hearty⁴, Jason T Wright⁴, Lawrence Ramsey⁴, Scott Blakeslee⁴, Tyler Anderson⁴, Christian Schwab²

Institution(s): 1. California Institute of Technology, 2. Macquarie University, 3. National Institute of Standards & Technology, 4. The Pennsylvania State University, 5. University of Arizona, 6. University of California, 7. University of Pennsylvania

152.19 – Characterization of Kilopixel TES detector arrays for PIPER

The Primordial Inflation Polarization ExploreR (PIPER) is a balloon-borne instrument optimized to measure the polarization of the Cosmic Microwave Background (CMB) at large angular scales. It will map 85% of the sky in four frequency bands centered at 200, 270, 350, and 600 GHz to characterize dust foregrounds and constrain the tensor-to-scalar ratio, r . The sky is imaged on to 32x40 pixel arrays of time-domain multiplexed Transition-Edge Sensor (TES) bolometers operating at a bath temperature of 100 mK to achieve background-limited sensitivity. Each kilopixel array is indium-bump-bonded to a 2D superconducting quantum interference device (SQUID) time-domain multiplexer (MUX) chip and read out by warm electronics. Each pixel measures total incident power over a frequency band defined by bandpass filters in front of the array,

while polarization sensitivity is provided by the upstream Variable-delay Polarization Modulators (VPMs) and analyzer grids. We present measurements of the detector parameters from the laboratory characterization of the first kilopixel science array for PIPER including transition temperature, saturation power, thermal conductivity, time constant, and noise performance. We also describe the testing of the 2D MUX chips, optimization of the integrated readout parameters, and the overall pixel yield of the array. The first PIPER science flight is planned for June 2018 from Palestine, Texas.

Author(s): Rahul Datta⁴, Peter Ade¹, Dominic Benford⁴, Charles Bennett⁵, David Chuss¹¹, Nicholas Costen³, Kevin Coughlin¹⁰, Jessie Dotson⁶, Joseph Eimer⁵, Dale Fixsen⁴, Natalie Gandilo⁵, Mark Halpern⁹, Thomas Essinger-Hileman⁴, Gene Hilton⁷, Gary Hinshaw⁹, Kent Irwin⁸, Christine Jhabvala³, Mark Kimball², Al Kogut⁴, Justin Lazear⁵, Luke Lowe⁴, George Manos³, Jeff McMahon¹⁰, Timothy Miller², Paul Mirel⁴, Samuel Harvey Moseley⁴, Samuel Pawlyk⁴, Samelys Rodriguez⁴, Elmer Sharp⁴, Peter Shirron², Johannes G Staguhn⁵, Dan Sullivan², Eric Switzer⁴, Peter Taraschi⁴, Carole Tucker¹, Alexander Walts⁴, Edward Wollack⁴

Institution(s): 1. Cardiff University, 2. Code 552, NASA Goddard Space Flight Center, 3. Code 553, NASA Goddard Space Flight Center, 4. Code 665, NASA Goddard Space Flight Center, 5. Johns Hopkins University, 6. NASA Ames Research Center, 7. National Institute of Standards and Technology, 8. Stanford University, 9. University of British Columbia, 10. University of Michigan, 11. Villanova University

152.20 – Constraining foreground spectrum with the projection-induced polarization for the cosmological global 21-cm experiments

Detecting the cosmological global (sky-averaged) 21-cm spectrum as a function of observed frequency will provide a powerful tool to study the thermal history of intergalactic medium (IGM) in the high-redshift Universe (~ 400 million years after the Big Bang). The biggest challenge in conventional ground-based total-power global 21-cm experiments is the removal of the Galactic and extragalactic synchrotron foreground ($\sim 1e4$ - $1e5$ K) to uncover the weak cosmological signal (~ 10 - 100 mK). The foreground is further corrupted by the frequency-dependent instrumental systematics. We have developed a new polarimetry-based observational approach that aims to measure the foreground emission by modulating it as a function of time through its circumpolar motion. Due to geometry, the projection of the anisotropic foreground sources onto the dual-polarized antenna induces a net foreground polarization, which is distinct from the much weaker intrinsic polarization of synchrotron sources. Instead of pointing the radio antenna at the zenith as in the conventional experiments, we point the antenna at the North Celestial Pole (NCP) and measure the projection-induced polarization modulated by the foreground's circumpolar diurnal periodicity. This temporal signature allows us to separate the dynamic foreground spectrum from the static cosmological background. In this presentation, we describe the design, construction, and initial results from the "Cosmic Twilight Polarimeter" (CTP) as a proof-of-concept implementation of this technique. The instrument consists of a dual-polarized broadband antenna (60-120 MHz) with a two-stage thermally stabilized front-end electronics, tilted toward the NCP. The instrument is currently being evaluated at a site near Charlottesville, VA. Ultimately, the instrument will be relocated to an RFI-quiet site closer to the Geographic North Pole (GNP) to mitigate sky obstruction due to the horizon at a lower latitude.

Author(s): Bang D. Nhan², Richard F. Bradley¹, Professor O. Burns²

Institution(s): 1. National Radio Astronomy Observatory - Central Development Laboratory, 2. University of Colorado at Boulder

152.21 – HAWC+/SOFIA Instrumental Polarization Calibration

HAWC+ is a new far-infrared polarimeter for the NASA/DLR SOFIA (Stratospheric Observatory for Infrared Astronomy) telescope. HAWC+ has the capability to measure the polarization of astronomical sources with unprecedented sensitivity and angular resolution in four bands from 50-250 microns. Using data obtained during commissioning flights, we implemented a calibration strategy that separates the astronomical polarization signal from the induced instrumental polarization. The result of this analysis is a map of the instrumental polarization as a function of position in the instrument's focal plane in each band. The results show consistency between bands, as well as with other methods used to determine preliminary instrumental polarization values.

Author(s): Joseph M. Michail⁴, David Chuss⁴, Charles D. Dowell¹, Fabio Santos³, Javad Siah⁴, John Vaillancourt²
Institution(s): 1. Jet Propulsion Laboratory, 2. MIT Lincoln Laboratory, 3. Northwestern University, 4. Villanova University
Contributing team(s): HAWC+ Instrument Team

152.22 – bRing: An observatory dedicated to monitoring the β Pictoris b Hill sphere transit

The bRing experiment (“ β Pic b Ring”) consists of twin two-camera instruments originally designed to be part of an international campaign to monitor the bright star β Pictoris throughout the 2017-2018. bRing was designed to detect obscuration due to the transit of any circumplanetary dust orbiting within the Hill sphere of the exoplanet β Pic b. bRing was also designed with a large field of view to monitor for photometric variations and events for most of the bright stars ($V \sim 4-8$ mag) in the southern sky. The 2017-2018 β Pic b transit season represents the first time that a directly imaged exoplanet will be monitored coming close to passing in front of its star. This event is the best opportunity yet for observational constraints on the late stages of gas giant planet formation and the nature of circumplanetary disks, which may spawn exomoons. We present an overview of the instrument and its data products.

Author(s): Samuel Mellon⁶, Remko Stuik³, Jeb Bailey³, Patrick Dorval³, Geert Jan Talens³, Iva Laginja⁵, Blaine B. D. Lomberg⁴, Steve Crawford⁴, Michael Ireland¹, Matthew Kenworthy³, Eric Mamajek²

Institution(s): 1. Australian National University, 2. Jet Propulsion Laboratory, 3. Leiden Observatory, 4. South African Astronomical Observatory, 5. Space Telescope Science Institute, 6. University of Rochester

152.23 – Investigating the Bright End of LSST Photometry

The Large Synoptic Survey Telescope (LSST) will begin operations in 2022, conducting a wide-field, synoptic multiband survey of the southern sky. Some fraction of objects at the bright end of the magnitude regime observed by LSST will overlap with other wide-sky surveys, allowing for calibration and cross-checking between surveys. The LSST is optimized for observations of very faint objects, so much of this data overlap will be comprised of saturated images. This project provides the first in-depth analysis of saturation in LSST images. Using the PhoSim package to create simulated LSST images, we evaluate saturation properties of several types of stars to determine the brightness limitations of LSST. We also collect metadata from many wide-field photometric surveys to provide cross-survey accounting and comparison. Additionally, we evaluate the accuracy of the PhoSim modeling parameters to determine the reliability of the software. These efforts will allow us to determine the expected useable data overlap between bright-end LSST images and faint-end images in other wide-sky surveys. Our next steps are developing methods to extract photometry from saturated images.

This material is based upon work supported in part by the National Science Foundation through Cooperative Agreement 1258333 managed by the Association of Universities for Research

in Astronomy (AURA), and the Department of Energy under Contract No. DE-ACO2-76SF00515 with the SLAC National Accelerator Laboratory. Additional LSST funding comes from private donations, grants to universities, and in-kind support from LSSTC Institutional Members.

Thanks to NSF grant PHY-135195 and the 2017 LSSTC Grant Award #2017-UG06 for making this project possible.

Author(s): Elle Ojala², Joshua Pepper¹
Institution(s): 1. Lehigh University, 2. Western Washington University
Contributing team(s): LSST Collaboration

152.24 – NRES: The Network of Robotic Echelle Spectrographs

Las Cumbres Observatory (LCO) is building the Network of Robotic Echelle Spectrographs (NRES), which will consist of four (up to six in the future) identical, optical (390 - 860 nm) high-precision spectrographs, each fiber-fed simultaneously by up to two 1-meter telescopes and a Thorium-Argon calibration source. We plan to install one at up to 6 observatory sites in the Northern and Southern hemispheres, creating a single, globally-distributed, autonomous spectrograph facility using up to ten 1-m telescopes. Simulations suggest we will achieve long-term radial velocity precision of 3 m/s in less than an hour for stars brighter than $V = 11$ or 12 once the system reaches full capability. Acting in concert, these four spectrographs will provide a new, unique facility for stellar characterization and precise radial velocities.

Following a few months of on-sky evaluation at our BPL test facility, the first spectrograph unit was shipped to CTIO in late 2016 and installed in March 2017. After several more months of additional testing and commissioning, regular science operations began with this node in September 2017. The second NRES spectrograph was installed at McDonald Observatory in September 2017 and released to the network after its own brief commissioning period, extending spectroscopic capability to the Northern hemisphere. The third NRES spectrograph was installed at SAAO in November 2017 and released to our science community just before year's end. The fourth NRES unit shipped in October and is currently en route to Wise Observatory in Israel with an expected release to the science community in early 2018.

We will briefly overview the LCO telescope network, the NRES spectrograph design, the advantages it provides, and development challenges we encountered along the way. We will further discuss real-world performance from our first three units, initial science results, and the ongoing software development effort needed to automate such a facility for a wide array of science cases.

Author(s): Robert Siverd³, Tim Brown³, Todd Henderson³, John Hygelund¹, Stuart Barnes⁶, Jon de Vera³, Jason Eastman², Annie Kirby³, Cary Smith³, Brook Taylor³, Joseph Tufts⁵, Julian van Eyken⁴

Institution(s): 1. Arthrex California Technology, Inc, 2. Harvard-Smithsonian Center for Astrophysics, 3. Las Cumbres Observatory, 4. NExScI, 5. Semiconductor Technology Associates, Inc., 6. Stuart Barnes Optical Design

152.25 – Design of FHiRE: the Fiber High Resolution Echelle Spectrograph

The enormous success of the Kepler mission in the discovery of transiting exoplanets implies that the majority of stars have planetary systems. NASA's upcoming Transiting Exoplanet Survey Satellite (TESS) is designed to survey the brightest stars over the entire sky, systems that are accessible to spectroscopic follow-up with mid-sized telescopes. We have undertaken the development of a precision radial velocity spectrograph with the goal of providing ground-based support for TESS. The instrument, known as FHiRE (Fiber High Resolution Echelle spectrograph), is being developed in collaboration with Indiana University and will be deployed at the 2.3-meter telescope of the

Wyoming InfraRed Observatory (WIRO). FHiRE features a traditional white pupil echelle design with $R \sim 60,000$ that is fed via two optical fibers from the telescope. Both the science fiber and a simultaneously sampled Thorium-Argon comparison fiber will make use of double mode scramblers. FHiRE itself will be housed within a vacuum enclosure in order to minimize any temperature variations of the instrument and maximize its radial velocity precision. Together, these two features should enable FHiRE to reach a long-term velocity precision of < 1 m/s. We present the design of FHiRE and its expected performance. In a companion poster (Jang-Condell et al.) we will present the exoplanet science goals of the project.

Author(s): Michael J Pierce², Jacob N McLane², C. A. Pilachowski¹, Henry Kobulnicky², Hannah Jang-Condell²
Institution(s): 1. Indiana University, 2. University of Wyoming

152.26 – The CHARA Array Database

We are building a searchable database for the CHARA Array data archive. The Array consists of six telescopes linked together as an interferometer, providing sub-milliarcsecond resolution in the optical and near-infrared. The Array enables a variety of scientific studies, including measuring stellar angular diameters, imaging stellar shapes and surface features, mapping the orbits of close binary companions, and resolving circumstellar environments. This database is one component of an NSF/MSIP funded program to provide open access to the CHARA Array to the broader astronomical community. This archive goes back to 2004 and covers all the beam combiners on the Array. We discuss the current status of and future plans for the public database, and give directions on how to access it.

Author(s): Jeremy Jones¹, Gail Schaefer¹, Theo ten Brummelaar¹, Douglas Gies¹, Christopher Farrington¹
Institution(s): 1. GSU/CHARA

152.27 – Detecting Exoplanets and Characterizing their Orbital Properties with Fringe Nulling

Detecting exoplanets and characterizing their orbital properties is a difficult task, due to their proximity and brightness ratio relative to their host stars. Here we present an interferometric fringe nulling technique, aimed at solving these issues. This

153 – Cosmology Poster Session

153.01 – The Effect of Antenna Position Errors on Redundant-Baseline Calibration of HERA

HERA (the Hydrogen Epoch of Reionization Array) is a large, highly-redundant radio interferometer in South Africa currently being built out to 350 14-m dishes. Its mission is to probe large scale structure during and prior to the epoch of reionization using the 21 cm hyperfine transition of neutral hydrogen. The array is designed to be calibrated using redundant baselines of known lengths. However, the dishes can deviate from ideal positions, with errors on the order of a few centimeters. This potentially increases foreground contamination of the 21 cm power spectrum in the cleanest part of Fourier space. The calibration algorithm treats groups of baselines that should be redundant, but are not due to position errors, as if they actually are. Accurate, precise calibration is critical because the foreground signals are 100,000 times stronger than the reionization signal. We explain the origin of this effect and discuss weighting strategies to mitigate it.

Author(s): Naomi Orosz², Joshua Dillon², Aaron Ewall-Wice¹, Aaron Parsons²
Institution(s): 1. Massachusetts Institute of Technology, 2. University of California, Berkeley
Contributing team(s): HERA Collaboration

153.02 – Cosmological Origins of Water

Recent models indicate that the sun's protoplanetary disk provided insufficient pathways for water formation, as evidenced by $[D/H]_{H_2O}$ measurements in asteroids and Earth's oceans. It is therefore likely that the early universe contained sites conducive

to water chemistry. This research tracks the timeline and abundance rates of water using cosmological simulations in Enzo. A 64 Mpc cube of space is evolved from $z = 200$ to $z = 2$. Simulations are then centered on a massive halo, and a 26-species reaction network is applied using operator split to track water formation rates. Density projection plots with metallicity contours predict regions of water formation, which are then compared to simulated abundances at both galactic and extragalactic scales. Observational signatures of formation sites are further discussed, and allow for additional validation of the simulations used.

Author(s): Henrique R. Schmitt¹, Ellyn Baines¹, J. Thomas Armstrong¹, Sergio Restaino¹
Institution(s): 1. Naval Research Laboratory

152.28 – WFIRST: Principal Components Analysis of H4RG-10 Near-IR Detector Data Cubes

The Wide Field Infrared Survey Telescope's (WFIRST) Wide Field Instrument (WFI) incorporates an array of eighteen Teledyne H4RG-10 near-IR detector arrays. Because WFIRST's science investigations require controlling systematic uncertainties to state-of-the-art levels, we conducted principal components analysis (PCA) of some H4RG-10 test data obtained in the NASA Goddard Space Flight Center Detector Characterization Laboratory (DCL). The PCA indicates that the Legendre polynomials provide a nearly orthogonal representation of up-the-ramp sampled illuminated data cubes, and suggests other representations that may provide an even more compact representation of the data in some circumstances. We hypothesize that by using orthogonal representations, such as those described here, it may be possible to control systematic errors better than has been achieved before for NASA missions. We believe that these findings are probably applicable to other H4RG, H2RG, and H1RG based systems.

Author(s): Bernard Rauscher¹
Institution(s): 1. NASA/GSFC

to water chemistry. This research tracks the timeline and abundance rates of water using cosmological simulations in Enzo. A 64 Mpc cube of space is evolved from $z = 200$ to $z = 2$. Simulations are then centered on a massive halo, and a 26-species reaction network is applied using operator split to track water formation rates. Density projection plots with metallicity contours predict regions of water formation, which are then compared to simulated abundances at both galactic and extragalactic scales. Observational signatures of formation sites are further discussed, and allow for additional validation of the simulations used.

Author(s): Alexander Gagliano¹, Morgan Taylor¹, William Black¹, Joseph Smidt¹, Brandon K Wiggins¹
Institution(s): 1. Los Alamos National Laboratory

153.03 – WFIRST: Science from Deep Field Surveys

WFIRST will enable deep field imaging across much larger areas than those previously obtained with Hubble, opening up completely new areas of parameter space for extragalactic deep fields including cosmology, supernova and galaxy evolution science. The instantaneous field of view of the Wide Field Instrument (WFI) is about 0.3 square degrees, which would for example yield an Ultra Deep Field (UDF) reaching similar depths at visible and near-infrared wavelengths to that obtained with Hubble, over an area about 100-200 times larger, for a comparable investment in time. Moreover, wider fields on scales of 10-20 square degrees could achieve depths comparable to large HST surveys at medium depths such as GOODS and CANDELS, and would enable multi-epoch supernova science that could be

matched in area to LSST Deep Drilling fields or other large survey areas. Such fields may benefit from being placed on locations in the sky that have ancillary multi-band imaging or spectroscopy from other facilities, from the ground or in space. The WFIRST Deep Fields Working Group has been examining the science considerations for various types of deep fields that may be obtained with WFIRST, and present here a summary of the various properties of different locations in the sky that may be considered for future deep fields with WFIRST.

Author(s): Anton Koekemoer¹, Ryan Foley²
Institution(s): 1. Space Telescope Science Institute, 2. UC Santa Cruz
Contributing team(s): WFIRST Deep Field Working Group

153.04 – Analysis of the Best-Fit Sky Model Produced Through Redundant Calibration of Interferometers

21 cm cosmology provides unique insights into the formation of stars and galaxies in the early universe, and particularly the Epoch of Reionization. Detection of the 21 cm line is challenging because it is generally 4-5 magnitudes weaker than the emission from foreground sources, and therefore the instruments used for detection must be carefully designed and calibrated. 21 cm cosmology is primarily conducted using interferometers, which are difficult to calibrate because of their complex structure. Here I explore the relationship between sky-based calibration, which relies on an accurate and comprehensive sky model, and redundancy-based calibration, which makes use of redundancies in the orientation of the interferometer's dishes. In addition to producing calibration parameters, redundant calibration also produces a best fit model of the sky. In this work I examine that sky model and explore the possibility of using that best fit model as an additional input to improve on sky-based calibration.

Author(s): Dara Storer¹, Jonathan Pober¹
Institution(s): 1. Brown University

153.05 – Removing the Impact of Baluns from Measurements of a Novel Antenna for Cosmological HI Measurements

The Hydrogen Epoch of Reionization Array (HERA) is a low-frequency radio interferometer aiming to detect redshifted 21 cm emission from neutral hydrogen during the Epoch of Reionization at frequencies between 100 and 200 MHz. Extending HERA's performance to lower frequencies will enable detection of radio waves at higher redshifts, when models predict that gas between galaxies was heated by X-rays from the first stellar-mass black holes. The isolation of foregrounds that are four orders of magnitude brighter than the faint cosmological signal presents an unprecedented set of design specifications for our antennas, including sensitivity and spectral smoothness over a large bandwidth. We are developing a broadband sinuous antenna feed for HERA, extending the bandwidth from 50 to 220 MHz, and we are verifying antenna performance with field measurements and simulations. Electromagnetic simulations compute the differential S-parameters of the antenna. We measure these S-parameters through a lossy balun attached to an unbalanced vector network analyzer. Removing the impact of this balun is critical in obtaining an accurate comparison between our simulations and measurements. I describe measurements to characterize the baluns and how they are used to remove the balun's impact on the antenna S-parameter measurements. Field measurements of the broadband sinuous antenna dish at MIT and Green Bank Observatory are used to verify our electromagnetic simulations of the broadband sinuous antenna design. After applying our balun corrections, we find that our field measurements are in good agreement with the simulation, giving us confidence that our feeds will perform as designed.

Author(s): Vincent Trung¹, Aaron Michael Ewall-Wice², Jianshu Li¹, Jacqueline Hewitt¹, Daniel Riley¹, Richard F. Bradley³, Krishna Makhija⁵, Sierra Garza⁴
Institution(s): 1. MIT Kavli Institute for Astrophysics and Space Research, 2. NASA Postdoctoral Fellow at NASA Jet Propulsion Laboratory, 3. National Radio Astronomy Observatory, 4. Riverside City College, 5. University of Virginia
Contributing team(s): HERA Collaboration

153.06 – A Search for Cosmic String Loops Using GADGET-2 Cosmological N-Body Simulator

Cosmic string loops are an extremely elusive hypothetical entity that have eluded the grasp of physicists and astronomers since their existence was postulated in the 1970's. Finding evidence of their existence could be the first empirical evidence of string theory.

Simulating their basic motion in a cold dark matter background using GADGET-2 allows us to predict where they may cluster during large scale structure formation (if they cluster at all). Here, we present our progress in placing cosmic strings into GADGET-2 with their basic equations of motion to lay a ground work for more complex simulations to find where these strings cluster. Ultimately, these simulations could lay a groundwork as to where future microlensing and gravitational wave observatories should look for cosmic strings.

Author(s): William Braverman³, Bryce Cousins², Hewei Jia¹
Institution(s): 1. Cornell, 2. Indiana University, 3. The College of New Jersey

153.07 – The Science and Prospects of Astrophysical Observations with New Horizons

Astrophysical observation from the outer solar system provides a unique and quiet vantage point from which to understand our cosmos. If properly designed, such observations enable several niche science cases that are difficult or impossible to perform near Earth. NASA's New Horizons mission includes several instruments with ~10cm telescopes that provide imaging capability from UV to near-IR wavelengths with moderate spectral resolution. A carefully designed survey can optimize the expendable propellant and limited data telemetry bandwidth to allow several unique measurements, including a detailed understanding of the cosmic extragalactic background light in the optical and near-IR, studies of the local and extragalactic UV background, measurements of the properties of dust and ice in the outer solar system, searches for moons and other faint structures around exoplanets, and determinations of the mass of planets far from their parent stars using gravitational microlensing. New Horizons is currently in an extended mission, that will conclude in 2021, designed to survey distant objects in the Kuiper Belt at high phase angles and perform a close flyby of KBO 2014 MU69. Afterwards, the astrophysics community will have a unique, generational opportunity to use this mission for astronomical observations at heliocentric distances beyond 50 AU. In this poster, we present the science case for an extended 2021 - 2026 astrophysics mission, and discuss some of the practical considerations that must be addressed to maximize the potential science return.

Author(s): Chi Nguyen², Michael Zemcov², Asantha Cooray⁴, Carey Lisse¹, Andrew Poppe³
Institution(s): 1. Johns Hopkins University Applied Physics Laboratory, 2. Rochester Institute of Technology, 3. University of California at Berkeley, 4. University of California at Irvine

153.08 – Photometric Redshift Calibration Strategy for WFIRST Cosmology

In order for WFIRST and other Stage IV Dark energy experiments (e.g. LSST, Euclid) to infer cosmological parameters not limited by systematic errors, accurate redshift measurements are needed. This accuracy can only be met using spectroscopic subsamples to calibrate the full sample. In this poster, we employ the machine

leaning, SOM based spectroscopic sampling technique developed in Masters et al. 2015, using the empirical color-redshift relation among galaxies to find the minimum spectra required for the WFIRST weak lensing calibration. We use galaxies from the CANDELS survey to build the LSST+WFIRST lensing analog sample of ~36k objects and train the LSST+WFIRST SOM. We show that 26% of the WFIRST lensing sample consists of sources fainter than the Euclid depth in the optical, 91% of which live in color cells already occupied by brighter galaxies. We demonstrate the similarity between faint and bright galaxies as well as the feasibility of redshift measurements at different brightness levels. 4% of SOM cells are however only occupied by faint galaxies for which we recommend extra spectroscopy of ~200 new sources. Acquiring the spectra of these sources will enable the comprehensive calibration of the WFIRST color-redshift relation.

Author(s): Shoubaneh Hemmati¹

Institution(s): 1. Caltech

Contributing team(s): WFIRST, WFIRST-HLS-COSMOLOGY

153.09 – eGSM: A extended Sky Model of Diffuse Radio Emission

Both cosmic microwave background and 21cm cosmology observations must contend with astrophysical foreground contaminants in the form of diffuse radio emission. For precise cosmological measurements, these foregrounds must be accurately modeled over the entire sky. Ideally, such full-sky models ought to be primarily motivated by observations. Yet in practice, these observations are limited, with data sets that are observed not only in a heterogeneous fashion, but also over limited frequency ranges. Previously, the Global Sky Model (GSM) took some steps towards solving the problem of incomplete observational data by interpolating over multi-frequency maps using principal component analysis (PCA).

In this poster, we present an extended version of GSM (called eGSM) that includes the following improvements: 1) better zero-level calibration 2) incorporation of non-uniform survey resolutions and sky coverage 3) the ability to quantify uncertainties in sky models 4) the ability to optimally select spectral models using Bayesian Evidence techniques.

Author(s): Doyeon Kim², Adrian Liu², Eric Switzer¹

Institution(s): 1. NASA Goddard, 2. University of California, Berkeley

153.10 – Probing Inflation Using Galaxy Clustering On Ultra-Large Scales

A detailed understanding of curvature perturbations in the universe is necessary to constrain theories of inflation. In particular, measurements of the local non-gaussianity parameter, f_{locNL} , enable us to distinguish between two broad classes of inflationary theories, single-field and multi-field inflation. While most single-field theories predict $f_{\text{locNL}} \approx -5/12$ (ns -1), in multi-field theories, f_{locNL} is not constrained to this value and is allowed to be observably large. Achieving $\sigma(f_{\text{locNL}}) = 1$ would give us discovery potential for detecting multi-field inflation, while finding $f_{\text{locNL}}=0$ would rule out a good fraction of interesting multi-field models. We study the use of galaxy clustering on ultra-large scales to achieve this level of constraint on f_{locNL} . Upcoming surveys such as Euclid and LSST will give us galaxy catalogs from which we can construct the galaxy power spectrum and hence infer a value of f_{locNL} . We consider two possible methods of determining the galaxy power spectrum from a catalog of galaxy positions: the traditional Feldman Kaiser Peacock (FKP) Power Spectrum Estimator, and an Optimal Quadratic Estimator (OQE). We implemented and tested each method using mock galaxy catalogs, and compared the resulting constraints on f_{locNL} . We find that the FKP estimator can measure f_{locNL} in an unbiased way, but there remains room for improvement in its precision. We also find that the OQE is not computationally fast, but remains a promising option due to its ability to isolate the power spectrum at large scales. We plan to extend this research to study alternative methods, such as pixel-

based likelihood functions. We also plan to study the impact of general relativistic effects at these scales on our ability to measure f_{locNL} .

Author(s): Roohi Dalal¹, Roland de Putter¹, Olivier Dore¹

Institution(s): 1. California Institute of Technology

153.11 – Cosmological parameter constraints with the Deep Lens Survey using galaxy-shear correlations and galaxy clustering properties

The Deep Lens Survey (DLS), a precursor to the Large Synoptic Survey Telescope (LSST), is a 20 sq. deg survey carried out with NOAO's Blanco and Mayall telescopes. The strength of the survey lies in its depth reaching down to ~27th mag in BVRz bands. This enables a broad redshift baseline study and allows us to investigate cosmological evolution of the large-scale structure. In this poster, we present the first cosmological analysis from the DLS using galaxy-shear correlations and galaxy clustering signals. Our DLS shear calibration accuracy has been validated through the most recent public weak-lensing data challenge. Photometric redshift systematic errors are tested by performing lens-source flip tests. Instead of real-space correlations, we reconstruct band-limited power spectra for cosmological parameter constraints. Our analysis puts a tight constraint on the matter density and the power spectrum normalization parameters. Our results are highly consistent with our previous cosmic shear analysis and also with the Planck CMB results.

Author(s): Mijin Yoon², Myungkook James Jee², Tony Tyson¹

Institution(s): 1. UC Davis, 2. Yonsei University

153.12 – Beyond δ : Tailoring marked statistics to reveal modified gravity

Models which attempt to explain the accelerated expansion of the universe through large-scale modifications to General Relativity (GR), must satisfy the stringent experimental constraints of GR in the solar system. Viable candidates invoke a "screening" mechanism, that dynamically suppresses deviations in high density environments, making their overall detection challenging even for ambitious future large-scale structure surveys. We present methods to efficiently simulate the non-linear properties of such theories, and consider how a series of statistics that reweight the density field to accentuate deviations from GR can be applied to enhance the overall signal-to-noise ratio in differentiating the models from GR. Our results demonstrate that the cosmic density field can yield additional, invaluable cosmological information, beyond the simple density power spectrum, that will enable surveys to more confidently discriminate between modified gravity models and Λ CDM.

Author(s): Georgios Valogiannis¹, Rachel Bean¹

Institution(s): 1. Cornell University

153.13 – HERA Broadband Feed Design for Low-Frequency Radio Astronomy

As part of the Hydrogen Epoch of Reionization Array (HERA) project, we are designing a broadband low-frequency radio feed to extend the bandwidth from 100-200 MHz to 50-220 MHz. By extending the lower-limit to 50 MHz, we hope to detect the signatures of the first black holes heating the hydrogen gas in the intergalactic medium.

The isolation of a very faint signal from vastly brighter foregrounds sets strict requirements on antenna spectral smoothness, polarization purity, forward gain, and internal reflections. We are currently working to meet these requirements with a broad-band sinuous antenna feed suspended over the 14-m parabolic HERA dish, using a combination of measurements and simulations to verify the performance of our design. A sinuous feed has been designed and simulated with Computer Simulation Technology (CST) software. We will present the construction of a prototype sinuous antenna and measurements of its reflection coefficient, S11, including laboratory characterization of baluns. Our measurements agree well with the

CST simulations of the antenna's performance, giving us confidence in our ability to model the feed and ensure that it meets the requirements of a 21cm cosmology measurement.

Author(s): Sierra Garza⁴, Vincent Trung⁵, Aaron Michael Ewall-Wice², Jianshu Li¹, Jacqueline Hewitt¹, Daniel Riley¹, Richard F. Bradley³, Krishna Makhija⁶

Institution(s): 1. *Massachusetts Institute of Technology*, 2. *NASA Jet Propulsion Laboratory*, 3. *National Radio Astronomy Observatory*, 4. *Riverside City College*, 5. *San Jose State University*, 6. *University of Virginia*

153.14 – Exploring Proposals for Resolving the Initial Conditions and Multiverse Problems in Inflation

The theory of cosmic inflation with the plateau-like potentials for the scalar field is very successful in predicting standard cosmological parameters. However, if the quantum effects are included, the theory inherently contains serious problems, namely, the multiverse problem and the initial conditions problem. It has been suggested in Mukhanov 2015 and Deen et al. 2016 to add a potential wall to the potential, so that the field never reaches the self-reproduction point. We examine these two proposals by varying the positions of the potential wall as well as varying the initial ratios of kinetic energy, potential energy and curvature. We demonstrate that both proposals are fine-tuned, at best, as they suffer from the drift in the predictions of the spectral tilt (n_s) and the tensor-to-scalar ratio (r).

Author(s): Nondh Panithanpaisal¹, Paul Steinhardt¹

Institution(s): 1. *Princeton University*

153.15 – A Bayesian approach to truncated data sets: An application to Malmquist bias in Supernova Cosmology

A problem commonly encountered in statistical analysis of data is that of truncated data sets. A truncated data set is one in which a number of data points are completely missing from a sample, this is in contrast to a censored sample in which partial information is missing from some data points. In astrophysics this problem is commonly seen in a magnitude limited survey such that the survey is incomplete at fainter magnitudes, that is, certain faint objects are simply not observed. The effect of this 'missing data' is manifested as Malmquist bias and can result in biases in parameter inference if it is not accounted for. In Frequentist methodologies the Malmquist bias is often corrected for by analysing many simulations and computing the appropriate correction factors. One problem with this methodology is that the corrections are model dependent. In this poster we derive a Bayesian methodology for accounting for truncated data sets in problems of parameter inference and model selection. We first show the methodology for a simple Gaussian linear model and then go on to show the method for accounting for a truncated data set in the case for cosmological parameter inference with a magnitude limited supernova Ia survey.

Author(s): Marisa Cristina March¹

Institution(s): 1. *University of Pennsylvania*

153.16 – Exploring the Effect of a Curved Reheating Surface on the Transition to Eternal Inflation

This work tests the volume bound in slow roll inflation for the case of a curved reheating surface, expanding upon Dubovsky et al's 2001 paper. Previous works have shown that the transition to eternal inflation begins when the average volume of the reheating surface, in terms of the number of classical e-foldings, reaches $\langle V \rangle = e^{6N} c$. The volume reaches this size and the transition occurs when $\Omega = 1$, as expected, and the distribution diverges when $\Omega < 1$. At the transition, the probability of producing finite volumes falls below one and there is some non-zero probability of producing an infinite volume, i.e. a non-terminating inflation. In the case of a curved reheating surface, we have found that there are no analytic expressions for the average volume distribution. We proceed numerically and find

that the curved reheating surface volume distribution in the non-eternal regime is not peaked around the classical volume value, even when Ω is well within finite volume range. Further, the average volume distribution doesn't appear to peak at any specific range of values. This result is unexpected, and negates the universality of the bound that has previously been shown. Further testing of this result is needed, but this work could provide insight into a general case for multi-field slow roll inflation.

Author(s): Carrie Filion¹

Institution(s): 1. *Bryn Mawr College*

Contributing team(s): Carrie Filion

153.17 – Constraining the evolution of the Hubble Parameter using cosmic chronometer

The Lambda-CDM model of Big Bang cosmology relies heavily on the assumption that two components - dark energy and dark matter - encompass 95% of the energy density of the Universe. Despite the dominant influence of these components, their nature is still entirely unknown.

We present the initial results from a project that aims to provide new insights regarding the Dark Energy component. We do this by deriving independent constraints on the time-evolution of the Hubble parameter (H_0) using the "cosmic chronometer" method.

By analyzing the HST NIR spectra from a large archival sample of passively evolving galaxies in distinct redshift bins between 1.3 and 2 we measure the typical stellar population ages (A) for the galaxies in each bin. The differential evolution of stellar population age with redshift (dA/dz) can be used to infer the corresponding evolution of H_0 which will provide important constraints on the nature of Dark Energy and its equation of state.

Author(s): Claudia Scarlata¹, Hugh Dickinson¹

Institution(s): 1. *University of Minnesota*

153.18 – Complete Calibration of the Color-Redshift Relation (C3R2): A Critical Foundation for Weak Lensing Cosmology with Euclid and WFIRST

A primary objective of both WFIRST and Euclid is to provide a 3D map of the distribution of matter across a significant fraction of the universe from the weak lensing shear field. Doing so will require accurate redshifts to the billions of galaxies that comprise the weak lensing samples of these surveys; achieving the required accuracy is a "tall pole" challenge for both missions. Here we present the ongoing Complete Calibration of the Color-Redshift Relation (C3R2) survey, designed specifically to calibrate the empirical galaxy color-redshift relation to Euclid depth. C3R2 is an ambitious Keck spectroscopy program, with a survey design based on a machine learning technique that allows us to optimally select the most important galaxies to sample the full range of galaxy colors. C3R2 is a multi-center program with time from all the primary Keck partners (Caltech, UC, Hawaii, and NASA), with a total of 34.5 Keck nights allocated to this project. Data Release 1, including 1283 high-confidence spectroscopic redshifts, is published as Masters, Stern, Cohen, Capak, et al. (2017), and we are currently completing Data Release 2, which will include >2000 additional high-confidence spectroscopic redshifts (Masters et al., in prep.). We will discuss current results and prospects for the survey going forward.

Author(s): Daniel C Masters², Daniel Stern², Judy Cohen¹, Peter Capak¹

Institution(s): 1. *Caltech*, 2. *Jet Propulsion Laboratory*

153.19 – Cluster mislocation in kinematic Sunyaev-Zel'dovich (kSZ) effect extraction

We investigate the impact of a variety of analysis assumptions that influence cluster identification and location on the kSZ pairwise momentum signal and covariance estimation. Photometric and spectroscopic galaxy tracers from SDSS, WISE, and DECaLS, spanning redshifts $0.05 < z < 0.7$, are considered in combination with CMB data from Planck and WMAP. With two complementary techniques, analytic offset modeling and direct

comparisons of redMaPPer brightest and central catalog samples, we find that miscentering uncertainties average to 0.4-0.7 σ for the Planck kSZ statistical error budget obtained with a jackknife estimator. We also show that jackknife covariance estimates are significantly more conservative than those obtained by CMB rotation methods. Using redMaPPer data, we concurrently compare uncertainties for photometric redshift errors and miscentering and find them comparable for separations $< \sim 50$ Mpc where the kSZ signal is largest.

For the next generation of CMB and LSS surveys the statistical and photometric errors will shrink markedly. Our results demonstrate that uncertainties introduced through using galaxy proxies for cluster locations will need to be fully incorporated, and actively mitigated, for the kSZ to reach its full potential as a cosmological constraining tool for dark energy and neutrino physics.

Author(s): Victoria Rose Calafut¹, Rachel Bean¹, Byeonghee Yu²

Institution(s): 1. Cornell University, 2. University of California, Berkeley

153.20 – Improving the Calibration of the SN Ia Anchor Datasets with a Bayesian Hierarchical Model

Inter-survey calibration remains one of the largest systematic uncertainties in SN Ia cosmology today. Ideally, each survey would measure their system throughputs and observe well characterized spectrophotometric standard stars, but many important surveys have not done so. For these surveys, we calibrate using tertiary survey stars tied to SDSS and Pan-STARRS. We improve on previous efforts by taking the spatially variable response of each telescope/camera into account, and using improved color transformations in the surveys' natural instrumental photometric system. We use a global hierarchical model of the data, automatically providing a covariance matrix of magnitude offsets and bandpass shifts which reduces the systematic uncertainty in inter-survey calibration, thereby providing better cosmological constraints.

Author(s): Miles Currie¹, David Rubin¹

Institution(s): 1. Space Telescope Science Institute

153.21 – High-Redshift SNe with Subaru and HST

High-redshift type Ia supernovae are crucial for constraining any time variation in dark energy. Here, we present the first discoveries and light curves from the Subaru Supernovae with Hubble Infrared (SUSHI) program, which combines high-redshift SN discoveries from the Subaru Strategic Program (SSP, as well as other Subaru time) with HST WFC3 IR followup. This program efficiently uses the wide field and high collecting area of Subaru Hyper Suprime-Cam for optical light curves, but still obtains a precision NIR color. We are on track to double the number of well-measured SNe Ia at $z > 1.1$, triggering on 23 SNe Ia in our first season.

Author(s): David Rubin¹¹, Nao Suzuki⁵, Nicolas Regnault⁴, Gregory Aldering⁹, Rahman Amanullah¹⁵, Pierre Antilogus⁴, Pierre Astier⁴, Kyle Barbary⁹, Marc Betoule⁴, Kyle Robert Boone⁹, Miles Currie¹¹, Susana Deustua¹¹, Mamoru Doi¹⁶, Andrew Fruchter¹¹, Ariel Goobar¹⁵, Brian Hayden⁹, Francois Hazenberg⁴, Isobel Hook⁸, Xiaosheng Huang¹⁷, Jian Jiang¹⁶, Takahiro Kato¹⁶, Alex Kim⁹, Marek Kowalski², Chris Lidman¹, Eric Linder⁹, Keiichi Maeda⁷, Tomoki Morokuma¹⁶, Jakob Nordin³, Reynald Pain⁴, Saul Perlmutter¹³, Pilar Ruiz-Lapuente¹⁴, Masao Sako¹², Clare Myers Saunders⁴, Anthony L Spadafora⁹, Masaomi Tanaka¹⁰, Nozomu Tominaga⁶, Naoki Yasuda⁵, Naoki Yoshida⁵

Institution(s): 1. Australian Astronomical Observatory, 2. DESY, 3. Humboldt, 4. IN2P3, 5. IPMU, 6. Konan University, 7. Kyoto University, 8. Lancaster University, 9. Lawrence Berkeley National Laboratory, 10. NAOJ, 11. Space Telescope Science Institute, 12. U Penn, 13. UC Berkeley, 14. University of Barcelona, 15. University of Stockholm, 16. University of Tokyo, 17. USF

153.22 – Exploring the Pulse Structure of the Gamma-Ray Bursts from the Swift Burst Alert Telescope

Gamma-ray bursts (GRBs) are one of the brightest and most intense explosions in our universe. For this project, we studied the shape of 400 single pulse GRBs using data gathered from Swift's Burst Alert Telescope (BAT). Hakkila et al. (2015) have discovered a mathematical Model that describes the GRB's pulse shapes. Following the method in Hakkila et al. (2015), we fit GRB pulses with the Norris function and examined the residual in the fitting, to see whether the results are consistent with the one reported in Hakkila et al. (2015).

Author(s): Juan-Carlos Martinez¹

Institution(s): 1. NASA Goddard

Contributing team(s): Team 1: Jon Hakkila, Amy Lien, Judith, Racusin, Team 2: Antonino Cucchiara, David Morris

153.23 – Gamma-ray Burst X-ray Flares Light Curve Fitting

Gamma Ray Bursts (GRBs) are the most luminous explosions in the Universe. These electromagnetic explosions produce jets demonstrated by a short burst of prompt gamma-ray emission followed by a broadband afterglow. There are sharp increases of flux in the X-ray light curves known as flares that occurs in about 50% of the afterglows. In this study, we characterized all of the X-ray afterglows that were detected by the Swift X-ray Telescope (XRT), whether with flares or without. We fit flares to the Norris function (Norris et al. 2005) and power laws with breaks where necessary (Racusin et al. 2009). After fitting the Norris function and power laws, we search for the residual pattern detected in prompt GRB pulses (Hakkila et al. 2014, 2015, 2017), that may indicate a common signature of shock physics. If we find the same signature in flares and prompt pulses, it provides insight into what causes them, as well as, how these flares are produced.

Author(s): Jonisha Aubain¹

Institution(s): 1. University of the Virgin Islands

153.24 – Tackling The Dragon: Investigating Lensed Galaxy Structure

Galaxies have been seen to have a rapid decrease in star formation beginning at a redshift of around 1-2 up to the present day. To understand the processes underpinning this change, we need to observe the inner structure of galaxies and understand where and how the stellar mass builds up. However, at high redshifts our observable resolution is limited, which hinders the accuracy of the data. The lack of resolution at high redshift can be counteracted with the use of gravitational lensing. The magnification provided by the gravitational lens between us and the galaxies in question enables us to see extreme detail within the galaxies. To begin fine-tuning this process, we used Hubble data of Abell 370, a galaxy cluster, which lenses a galaxy known as "The Dragon" at $z=0.725$. With the increased detail provided by the gravitational lens we provide a detailed analysis of the galaxy's spatially resolved star formation rate, stellar age, and masses.

Author(s): Alexander Fortenberry², Rachael Livermore¹

Institution(s): 1. University of Texas at Austin, 2. University of the Virgin Islands

155 – CosmoQuest and NITARP: Two Examples of Engaging Students, Teachers, and Lifelong Learners in Astronomy Poster Session

155.01 – CosmoQuest: Making the public your students and collaborators

CosmoQuest is a second generation citizen science project that makes it possible for NASA Subject Matter Experts to engage the public as both learners and collaborators in research. Engaging the public in publishable science is termed “Citizen Science.” This is a powerful technique for accomplishing research projects and tasks that require many minds and eyes to complete. While some projects may use undergraduates for help, others simply have too many images or too much data for a small population to sort through. CosmoQuest is a platform that enables scientists to take advantage of already existing science tools to engage the public in their research and to acquire the data analysis they need. Citizen scientists, like students, need their experience properly scaffolded to their understanding, and they require mentoring and training to succeed.

This presentation focuses on methods for focusing research projects for successful citizen science engagement, and determining what scaffolding must be built to support citizen education and engagement.

This presentation will help you understand how to transform your research project into a successful citizen science engagement. We will also present a flowchart to help you define: what is required, how to focus on what science does and doesn't work, and what support your project requires. The content presented will allow you to successfully implement a project within the CosmoQuest facility, and determine what educational support you should provide or request aid to provide.

Author(s): Pamela Gay¹, Sanlyn Buxner², Jennifer Grier², Matthew Richardson²

Institution(s): 1. *Astronomical Society of the Pacific*, 2. *Planetary Science Institute*

Contributing team(s): CosmoQuest Team

155.02 – CosmoQuest: A Glance at Citizen Science Building

CosmoQuest is a virtual research facility focused on engaging people - citizen scientists - from across the world in authentic research projects designed to enhance our knowledge of the cosmos around us. Using image data acquired by NASA missions, our citizen scientists are first trained to identify specific features within the data and then requested to identify those features across large datasets. Responses submitted by the citizen scientists are then stored in our database where they await for analysis and eventual publication by CosmoQuest staff and collaborating professional research scientists.

While it is clear that the driving power behind our projects are the eyes and minds of our citizen scientists, it is CosmoQuest's custom software, Citizen Science Builder (CSB), that enables citizen science to be accomplished. On the front end, CosmoQuest's CSB software allows for the creation of web-interfaces that users can access to perform image annotation through both drawing tools and questions that can accompany images. These tools include: using geometric shapes to identify regions within an image, tracing image attributes using freeform line tools, and flagging features within images. Additionally, checkboxes, dropdowns, and free response boxes may be used to collect information. On the back end, this software is responsible for the proper storage of all data, which allows project staff to perform periodic data quality checks and track the progress of each project. In this poster we present these available tools and resources and seek potential collaborations.

Author(s): Matthew Richardson², Jennifer Grier², Pamela Gay¹, Cory Lehan¹, Sanlyn Buxner²

Institution(s): 1. *Astronomical Society of the Pacific*, 2. *Planetary Science Institute*

Contributing team(s): CosmoQuest Team

155.03 – CosmoQuest: Measuring Audience Needs to Obtain Better Science

The CosmoQuest Virtual Research Facility provides a place for scientists to recruit people to aid in their science projects via citizen science. Just as students need training to be effective researchers, so do citizen scientists, but their needs are different. In this presentation, we present the results of surveys of members of the CosmoQuest community, including both citizen scientists and educators using citizen science in their classrooms. For all members of the community, we investigated the types of projects that respondents enjoyed doing, the level of difficulty they were willing to engage in, and the amount of time they spent doing citizen science projects. We also investigated what other science-related activities respondents were engaged in, other opportunities they were interested in, and what support and resources they needed to be successful in completing projects. For educators, we investigated the types of projects they wanted to engage in with their students, the ideal length of time for citizen science projects to be used in their classrooms, and the resources they needed to be able to engage students in citizen science projects effectively.

Author(s): Sanlyn Buxner², Maya Bakerman², Pamela Gay¹, Alison Reiheld³

Institution(s): 1. *Astronomical Society of the Pacific*, 2. *Planetary Science Institute*, 3. *Southern Illinois University Edwardsville*

Contributing team(s): CosmoQuest Team

155.04 – NITARP: Bridging the Gap Between the Traditional Science Classroom and Authentic Research

In this poster, the differences between what occurs in the traditional secondary science classroom and what happens in the actual research world is examined. Secondary classroom teachers generally have limited, if any, research experience beyond what is presented through their undergraduate college lab coursework. A disparity exists between classroom laboratory work and professional research. Opportunities like NITARP provide research elements that bridge this gap. NITARP teams are in a unique situation, joining a small team working alongside Caltech researchers on cutting edge investigations in astrophysics. In this poster it is shown how the NITARP program provides key components and experiences to expand the skill sets that teachers bring to their classrooms, bridging the gap between the typical secondary classroom and the world of the professional researcher. The NASA/IPAC program immerses participating teachers into a year-long training experience via online and face-to-face learning that translates into enhanced instruction at the secondary level. This work was made possible through the NASA/IPAC Teacher Archive Research Program (NITARP) and was funded by NASA Astrophysics Data Program.

Author(s): Olivia K. Stalnaker³, Sam Evans⁴, Thomas Rutherford⁵, John Taylor², Luisa Rebull¹

Institution(s): 1. *Caltech-IPAC/IRSA*, 2. *Elkhart Memorial High School*, 3. *Lake Dallas Middle School*, 4. *Maumee High School*, 5. *Sullivan South High School*

155.05 – NITARP: An Example of Effective Data-Based Research in the Classroom

The use of data in the classroom is a core component of both project based learning and STEM based education. Authentic student driven research using real-world data is a primary focus

of both teaching strategies. To make the educational outcome effective and long lasting, the type and quality of data used in the lessons is important. The NASA/IPAC Teacher Archive Research Program (NITARP) program encapsulates this in very meaningful ways by providing both teachers and students the opportunity to ask deep meaningful questions, collaborate with peers, and arrive at meaningful conclusions. Teachers trained in the use of scientific archives and the application of those archives for authentic research is critical for this type of learning to be successful.

In this study we use the NITARP program as an example of effective STEM project based learning using archived scientific data. We explore the components of the program that are most effective, the effects on teacher competency and ease of use with students, and use in the classroom. For each area we also explore alternate sources of teacher support, data archives, and techniques for implementation in classrooms for various topics and skill levels.

Author(s): Laura Orr⁵, Jamie L Rowe¹, Howard Lineberger², Gary Duranko⁴, Varoujan Gorjian³

Institution(s): 1. Bethlehem Central High School, 2. Durham Academy, 3. JPL/Caltech, 4. Oak Hill Academy, 5. Ukiah High School

155.06 – An Authentic Research Experience in an Astronomy Education Professional Development Program: An Analysis of 8 Years of Data on the NASA/IPAC Teacher Archive Research Program (NITARP)

The NASA/IPAC Teacher Archive Research Program (NITARP) partners small groups of educators with a research astronomer for a year-long authentic research project. This program aligns well with the characteristics of high-quality professional

156 – Professional Development for Teachers, Grads, Postdocs, and College Instructors Poster Session

156.01 – Visualizing Gaia Data with Science Teachers at AMNH

The American Museum of Natural History is an accredited graduate school and offers an innovative Master of Arts in Teaching (MAT) degree that leverages its unique scientific resources and long history of leadership in teacher education and professional development. The MAT program consists of 15-months of intensive mentoring, classroom experience, lab work, and professional development with AMNH scientists and educators. It is then followed by a 4 year commitment by all degree awardees to teach at an in needs New York high school. During the second summer of their first 15 months of the program, students are paired with a scientific mentor to obtain an REU like experience in Astronomy, Geology or Paleontology. During the summer of 2017 five teachers worked on incorporating a subset of the Tycho Gaia Astrometric Survey into the Partiview open source software. The result is an interactive experience where we can fly live through all of TGAS and highlight nearby clusters and associations. The tool is (1) a demonstration of the power of Partiview at visualizing a vast dataset such as Gaia, and (2) an extremely powerful instrument for teaching science through visualization.

Author(s): Jacqueline K Faherty¹, Deion Desir¹, Kristina Coker¹, Olivia Nelson¹, Chelsea Vasquez¹, Iliya Smithka¹

Institution(s): 1. American Museum of Natural History

156.02 – Twenty Years of One Astronomy Teacher Professional Development - The EXES Teacher Associate Program at UT Austin

The Astronomy Department and McDonald Observatory at the University of Texas at Austin has and continues to offer a suite of different astronomy based K-12 teacher professional development programs. One of our longest running, and most successful programs, is reaching its 20th anniversary, the EXES Teacher

development (PD) programs and has worked with a total of 103 educators since 2005. In this poster, we explore surveys obtained from 74 different educators, at up to four waypoints during the course of 13 months, incorporating data from the class of 2010 through the class of 2017. The reasons educators participate are mapped onto a continuum ranging from more inward-focused to more outward-focused; NITARP has had more outward-focused educators than inward-focused, though there is a bias against the extremes on either end of the continuum. This insight into teacher motivations has implications for how the educators are supported during the NITARP year. Three-quarters of the educators self-report some or major changes in their understanding of the nature of science. The program provides educators with experience collaborating with astronomers and other educators, and forges a strong link to the astronomical research community; the NITARP community of practice encourages and reinforces these linkages. During the experience, educators get comfortable with learning complex new concepts, with ~40% noting in their surveys that their approach to learning has changed. Educators are provided opportunities for professional growth; at least 12% have changed career paths substantially in part due to the program, and 11% report that the experience was “life changing.” At least 60% are including richer, more authentic science activities in their classrooms. This work illuminates what benefits the program brings to its participants, and serves as a model for similar PD programs in other STEM subjects.

Author(s): Luisa Rebull¹, Tracy Roberts¹, Wendi Laurence², Michael Fitzgerald³, Debbie French⁵, Varoujan Gorjian⁴, Gordon Squires¹

Institution(s): 1. Caltech-IPAC, 2. Create-osity, 3. Edith Cowan Institute for Education Research, 4. JPL, 5. Wilkes University

Associate Program, which was started in 1998. The EXES Teacher Associate program features sustained and continued professional development opportunities for K-12 science and math educators. It consists of 6 times per year day-long meetings, coupled with other professional development opportunities provided at various times. In total, there are approximately 30 active members of the group currently, but more than 90 teachers have participated in this group over its 20 year history. The program has had astronomy education as its focus throughout its history, but different partnerships and collaborations with other programs have supported the group and have allowed for a variety of professional development opportunities and themes for educators to engage in. We will give an overview of this program, present evaluation data and teacher feedback related to program success and student impact, and highlight a few specific program opportunities that are unique and have been shown to be most impactful for participants.

Author(s): Keely Finkelstein², Mary Kay Hemenway², Chris Sneden², John Lacy², Matthew J. Richter¹

Institution(s): 1. University of California at Davis, 2. University of Texas at Austin

Contributing team(s): EXES Teacher Associates

156.03 – The Lowell Observatory Predoctoral Scholar Program

Lowell Observatory is pleased to solicit applications for our Predoctoral Scholar Fellowship Program. Now beginning its tenth year, this program is designed to provide unique research opportunities to graduate students in good standing, currently enrolled at Ph.D. granting institutions. Lowell staff research spans a wide range of topics, from astronomical instrumentation, to icy bodies in our solar system, exoplanet science, stellar populations, star formation, and dwarf galaxies. Strong collaborations, the new Ph.D. program at Northern Arizona University, and cooperative links across the greater Flagstaff

astronomical community create a powerful multi-institutional locus in northern Arizona. Lowell Observatory's new 4.3 meter Discovery Channel Telescope is operating at full science capacity and boasts some of the most cutting-edge and exciting capabilities available in optical/infrared astronomy. Student research is expected to lead to a thesis dissertation appropriate for graduation at the doctoral level at the student's home institution. For more information, see <http://www2.lowell.edu/rsch/predoc.php> and links therein. Applications for Fall 2018 are due by May 1, 2018; alternate application dates will be considered on an individual basis.

Author(s): Lisa Prato¹, Larissa Nofi¹
Institution(s): 1. Lowell Observatory

156.04 – Postdoctoral Mentoring at the Space Telescope Science Institute

The Space Telescope Science Institute (STScI) has, on average, about 30 postdoctoral researchers. This group is funded primarily by individual grants but includes independent Fellows (Giacconi, Lasker, and Hubble Fellows) and postdocs based at neighboring Johns Hopkins University but with supervisors based at STScI. Our mentoring program aims to support the intellectual and career development of this entire group, outside of the scientific and career mentoring they receive from their direct supervisors or fellowship sponsors.

Our mentoring program consists of two parts. First and foremost, each postdoc has a mentor (someone on the research staff) with whom they meet regularly. Ideally, the mentor is not someone with whom the postdoc collaborates scientifically and can therefore provide an outside, independent, fresh perspective. As different postdocs require different kinds of mentoring, we try to best pair postdocs and mentors according to the postdocs' needs and the mentors' backgrounds, skills, and mentoring styles.

Second, we conduct several career guidance seminars and related events throughout the year. These have included proposal writing workshops, formalized practice talks, academic job application seminars, and discussion sessions on career paths outside of

158 – The Sun, Extrasolar Planets and Stars iPoster Session

158.02 – WFIRST: Discovery and characterization of planets in the habitable zone with the CGI

The WFIRST coronagraph instrument (CGI) will be the first coronagraph with wavefront control in space, with an expected instrumental raw contrast of 3×10^{-9} at 150 milliarcseconds in the V band. The CGI will be capable of directly imaging and characterizing mature exoplanets in reflected light for the first time, with a prime focus on stars with known radial velocity (RV) planets. The majority of these RV planet hosting stars are at relatively far distances for coronagraphic imaging of their inner habitable zone. However, the recent discovery of four radial velocity planets around the near G-type star Tau Ceti (3.7 pc), including two potential super-Earths located at the edges of its habitable zone, provides a great new opportunity for direct imaging with the WFIRST/CGI. This underscores the importance of the continued search for radial velocity planets around nearby host stars, as it may reveal additional discoveries of planets in the habitable zone which then can be characterized by the WFIRST/CGI. Finally, the CGI may also detect habitable zone planets through blind searches around the very nearest stars (<5pc), and we also examine this potential here.

Author(s): Jason Rhodes², Tiffany Meshkat¹, Margaret Frerking², Bertrand Mennesson², Margaret Turnbull⁴, Bruce Macintosh⁵, Jeremy Kasdin³
Institution(s): 1. IPAC, 2. NASA JPL, 3. Princeton University, 4. SETI Institute, 5. Stanford University

158.03 – WFIRST: Exoplanet Data Challenge. Atmospheric retrieval results

academia (featuring colleagues who are no longer in academia). These workshops have the added benefit of providing the postdocs with a wider support network of staff members.

Finally, we have begun to conduct an annual survey of the postdocs to gauge their experience and integration at STScI, the efficacy of the mentoring program, and to collect feedback on how to improve postdoctoral life at the Institute.

Author(s): Molly Peeples¹
Institution(s): 1. Space Telescope Science Institute

156.05 – Science Thought and Practices: A Professional Development Workshop on Teaching Scientific Reasoning, Mathematical Modeling and Data Analysis

The NSF-supported "AstroCom NYC" program, a collaboration of the City University of New York and the American Museum of Natural History (AMNH), has developed and offers hands-on workshops to undergraduate faculty on teaching science thought and practices. These professional development workshops emphasize a curriculum and pedagogical strategies that uses computers and other digital devices in a laboratory environment to teach students fundamental topics, including: proportional reasoning, control of variables thinking, experimental design, hypothesis testing, reasoning with data, and drawing conclusions from graphical displays. Topics addressed here are rarely taught in-depth during the formal undergraduate years and are frequently learned only after several apprenticeship research experiences. The goal of these workshops is to provide working and future faculty with an interactive experience in science learning and teaching using modern technological tools.

Author(s): Dennis Robbins², K.E.Saavik Ford¹
Institution(s): 1. Borough of Manhattan Community College, 2. Hunter College

We present the results of the Exoplanet Data Challenge for its first 2016/17 cycle and the current cycle 2. Some input spectra for extra-solar systems are processed through the WFIRST IFS instrument model, producing simulated data representative of the flight data. Atmospheric properties are then recovered using complex atmospheric models and multidimensional optimization. The results inform about WFIRST CGI ability to characterize exoplanetary atmospheres.

Author(s): Sergi Hildebrandt¹, Margaret Turnbull²
Institution(s): 1. California Institute of Technology, 2. Carl Sagan Center for the Study of Life in the Universe
Contributing team(s): Exoplanet Data Challenge Team

158.04 – WFIRST: Microlensing Parallax Observations from K2 in the Exoplanet Microlensing Field

The recent explosion in our understanding of exoplanetary systems has been driven primarily by the Kepler mission, which has replaced radial velocities as our main planet discovery method. While Kepler has provided a large sample of planets that will allow a robust statistical determination of the properties of exoplanets in close orbits about their host stars, the Kepler mission was stopped shortly after the start of its 5th year. This led to the Kepler 2 (K2) mission, which could observe up to 18 different fields in the ecliptic plane, including a fraction of the WFIRST microlensing field. The K2 mission has focused on lower mass host stars and spending one observing campaign in the Galactic bulge to make use of Kepler's orbit to determine the masses and distances to microlensing systems via the microlensing parallax effect. These K2 Campaign 9 observations help to develop the microlensing planet detection method, which will be employed by the WFIRST mission that will extend the

statistical census of exoplanets to include low-mass planets in wide orbits. While the photometric light curve of a microlensing event observed from the ground provides important constraints on the lens physical parameters, in many cases the lens mass and distance from Earth remain degenerated. The poster will show how simultaneous space- and ground-based observations can break this mass-distance degeneracy. This method will be used for a fraction of the events observed by WFIRST. Finally, the poster will present a new method to correct the K2 photometry from the correlated systematic noise. This investigation helps in characterizing the properties of the lens stars and source stars in one WFIRST field with high extinction.

Author(s): Clement Ranc¹

Institution(s): 1. NASA Goddard Space Flight Center

Contributing team(s): Radek Poleski, David Bennett, K2C9 Microlensing Science Experiment Team

158.05 – WFIRST – UKIRT Microlensing Survey as a Pathfinder

Gravitational microlensing as a method of exoplanet detection is best suited to detecting planets of all masses located just beyond the snow line. This region of parameter space is largely unexplored, and it is necessary to detect many more planets via large microlensing surveys in order to understand these understudied planets. Our project utilizes the ground-based United Kingdom Infrared Telescope (UKIRT) as the first near infrared (NIR) microlensing survey to explore this parameter space. Preliminary results from Shvartzvald et al. 2017 presented five highly extinguished UKIRT microlensing events near the Galactic bulge (i.e. where $|b| < 2$) and provided initial constraints to the NIR event rate. As a follow up to this study, we inject a multitude of mock stars with simulated microlensing signals into real UKIRT observations taken between 2015 and 2017. We then utilize a modified UKIRT pipeline to extract the light curves of these mock stars, from which we aim to derive the UKIRT detection efficiency and eventually the NIR event rate per square degree to a precision of $\sim 10\%$. Information on event rates in the NIR is crucial for informing mission design specifications, and prepares for the upcoming Wide Field Infrared Survey Telescope (WFIRST).

Author(s): Savannah Renee Jacklin³, Yossi Shvartzvald², Geoff Bryden², Sebastiano Calchi Novati¹

Institution(s): 1. California Institute of Technology, 2. NASA Jet Propulsion Laboratory, 3. Vanderbilt University

158.06 – WFIRST: Microlensing Analysis Data Challenge

WFIRST will produce thousands of high cadence, high photometric precision lightcurves of microlensing events, from which a wealth of planetary and stellar systems will be discovered. However, the analysis of such lightcurves has historically been very time consuming and expensive in both labor and computing facilities. This poses a potential bottleneck to deriving the full science potential of the WFIRST mission. To address this problem, the WFIRST Microlensing Science Investigation Team designing a series of data challenges to stimulate research to address outstanding problems of microlensing analysis. These range from the classification and modeling of triple lens events to methods to efficiently yet thoroughly search a high-dimensional parameter space for the best fitting models.

Author(s): Rachel Street¹

Institution(s): 1. Las Cumbres Observatory

Contributing team(s): WFIRST Microlensing Science Investigation Team

158.07 – Multi-wavelength Observations of Solar Acoustic Waves Near Active Regions

Active region areas on the Sun are abundant with a variety of waves that are both acoustically helioseismic and magnetohydrodynamic in nature. The occurrence of a solar flare

can disrupt these waves, through MHD mode-mixing or scattering by the excitation of these waves. We take a multi-wavelength observational approach to understand the source of these waves by studying active regions where flaring activity occurs. Our approach is to search for signals within a time series of images using a Fast Fourier Transform (FFT) algorithm, by producing multi-frequency power map movies. We study active regions both spatially and temporally and correlate this method over multiple wavelengths using data from NASA's Solar Dynamics Observatory. By surveying the active regions on multiple wavelengths we are able to observe the behavior of these waves within the Solar atmosphere, from the photosphere up through the corona. We are able to detect enhancements of power around active regions, which could be acoustic power halos and of an MHD-wave propagating outward by the flaring event. We are in the initial stages of this study understanding the behaviors of these waves and could one day contribute to understanding the mechanism responsible for their formation; that has not yet been explained.

Author(s): Teresa Monsue³, Dean Pesnell¹, Frank Hill²

Institution(s): 1. NASA Goddard Space Flight Center, 2. The National Solar Observatory, 3. Vanderbilt University

158.09 – Timing Exoplanet Occultations from the Towson University 0.4m Telescope

We present observations of transits of exoplanets KIC 4150611 and KIC 11180361. These were observed with the TU 0.4m telescope in the fall of 2017. Long term observation of shifts between the predicted and observed occultation times can be used to constrain the presence of additional bodies in these systems.

Author(s): Alex Storrs², Hayley Clark¹

Institution(s): 1. Chesapeake HS, 2. Towson Univ.

158.10 – Simulations of Tidally Driven Formation of Binary Planet Systems

In the last decade there have been hundreds of exoplanets discovered by the Kepler, CoRoT and many other initiatives. This wealth of data suggests the possibility of detecting exoplanets with large satellites. This project seeks to model the interactions between orbiting planets using the FLASH hydrodynamics code developed by The Flash Center for Computational Science at University of Chicago. We model the encounters in a wide variety of encounter scenarios and initial conditions including variations in encounter depth, mass ratio, and encounter velocity and attempt to constrain what sorts of binary planet configurations are possible and stable.

Author(s): R. Zachary P Murray¹, James Guillochon²

Institution(s): 1. Cornell University, 2. Harvard University

158.11 – Simulations of Magnetic Flux Emergence in Cool, Low-Mass Stars: Toward Linking Dynamo Action with Starspots

Starspots are windows into a star's internal dynamo mechanism. However, the manner by which the dynamo-generated magnetic field traverses the stellar interior to emerge at the surface is not especially well understood. Establishing the details of magnetic flux emergence plays a key role in deciphering stellar dynamos and observed starspot properties. In the solar context, insight into this process has been obtained by assuming the magnetism giving rise to sunspots consists partly of idealized thin flux tubes (TFTs). Here, we present three sets of TFT simulations in rotating spherical shells of convection: one representative of the Sun, the second of a solar-like rapid rotator, and the third of a fully convective M dwarf. Our solar simulations reproduce sunspot observables such as low-latitude emergence, tilting action toward the equator following the Joy's Law trend, and a phenomenon akin to active longitudes. Further, we compare the evolution of rising flux tubes in our (computationally inexpensive) TFT simulations to buoyant magnetic structures that arise naturally in a unique global simulation of a rapidly rotating Sun. We comment

on the role of rapid rotation, the Coriolis force, and external torques imparted by the surrounding convection in establishing the trajectories of the flux tubes across the convection zone. In our fully convective M dwarf simulations, the expected starspot latitudes deviate from the solar trend, favoring significantly poleward latitudes unless the differential rotation is sufficiently prograde or the magnetic field is strongly super-equipartition. Together our work provides a link between dynamo-generated magnetic fields, turbulent convection, and observations of starspots along the lower main sequence.

Author(s): Maria Ann Weber², Matthew Browning³, Nicholas Nelson¹

Institution(s): 1. California State University, Chico, 2. University of Chicago, 3. University of Exeter

158.12 – The Possibility That M dwarfs are Gamma Ray Emitters

M dwarfs are the most abundant class of stars in our galaxy, ensuring that there are many nearby. Moreover, some are even found to be a source of x-ray and radio emission, predominantly the younger M dwarfs because of their fast spin, which generates strong magnetic fields. The same magnetic fields may also be accountable for accelerating particles to near the speed of light, generating gamma radiation. Gamma rays are photons of the highest energies (~100 MeV and higher), which are useful to study the most energetic processes in astrophysics. Using data from the Fermi Large Area Telescope (LAT), we create, combine, and analyze maps of over 50 nearby and young M dwarfs. If these M dwarfs are detected, we can add them to the rare class of objects that emit gamma rays.

Author(s): Francis Rivera¹, Timothy Paglione²

Institution(s): 1. CUNY Lehman College, 2. CUNY York College

158.13 – Completeness and Bias Tests of Small Flares in gPhoton M Dwarfs

gPhoton is a time-tagged database of more than one trillion calibrated ultraviolet photon events from the ten-year GALEX mission. With the open-source gPhoton software, users can construct images and light curves at user-defined temporal and spatial scales. We have been working on a project to detect stellar flares on M dwarfs observed in GALEX data, with particular focus on smaller flares that have durations between 30 seconds and 30 minutes, and energies between 10^{27} and 10^{29} ergs. This parameter space is still largely unconstrained in the UV/optical, even with Kepler/K2 data, due to their short durations. We present completeness and reliability tests we are conducting to be able to account for selection and detection bias in our sample, including stellar type, instrument artifacts, sampling bias, and signal-to-noise. The bias-corrected occurrence rate of such flares, which are exponentially more frequent than larger flares already characterized by Kepler and ground-based studies, can be included in future calculations of exoplanet habitability.

Author(s): Scott W. Fleming³, Chase Million², Clara Brasseur³, Rachel A. Osten³, Bernie Shiao³, Luciana Bianchi¹

Institution(s): 1. Johns Hopkins, 2. Million Concepts, Inc., 3. STScI

158.14 – The Backyard Worlds: Planet 9 Citizen Science Project

In February of 2017 our team launched a new citizen science project entitled Backyard Worlds: Planet 9 to scan the cosmos for fast moving stars, brown dwarfs, and even planets. This Zooniverse website, BackyardWorlds.org, invites anyone with a computer or smartphone to flip through WISE images taken over a several year baseline and mark any point source that appears to move. This “blinking technique” is the same that Clyde Tombaugh discovered Pluto with over 80 years ago. In the first few days of our program we recruited over 30,000 volunteers. After 3/4 of a year with the program we have completed 30% of the sky and our

participants have identified several hundred candidate movers. These include (1) over 20 candidate Y-type brown dwarfs, (2) a handful of new co-moving systems containing a previously unidentified low mass object and a known nearby star, (3) over 100 previously missed M dwarfs, (4) and more than 200 candidate L and T brown dwarfs, many of which occupy outlier positions on reduced proper motion diagrams. Our first publication credited four citizen scientists as co-authors. The Backyard Worlds: Planet 9 project is both scientifically fruitful and empowering for any mind across the globe that has ever wanted to participate in a discovery-driven astronomy research project.

Author(s): Jacqueline K Faherty², Marc Kuchner⁶, Adam Schneider³, Aaron Meisner⁸, Jonathan Gagné⁴, Joeseeph Filippazzo⁷, Laura Trouille¹, Backyard Worlds: Planet 9 Collaboration⁵

Institution(s): 1. Adler Planetarium, 2. American Museum of Natural History, 3. Arizona State University, 4. Carnegie Institution of Washington, 5. Citizen Science, 6. NASA Goddard, 7. STScI, 8. UC Berkeley

Contributing team(s): Jacqueline Faherty

158.15 – The True Ultracool Binary Fraction Using Spectral Binaries

Brown dwarfs bridge the gap between stars and giant planets. While the essential mechanisms governing their formation are not well constrained, binary statistics are a direct outcome of the formation process, and thus provide a means to test formation theories. Observational constraints on the brown dwarf binary fraction place it at 10 – 20%, dominated by imaging studies (85% of systems) with the most common separation at 4 AU. This coincides with the resolution limit of state-of-the-art imaging techniques, suggesting that the binary fraction is underestimated. We have developed a separation-independent method to identify and characterize tightly-separated (< 5 AU) binary systems of brown dwarfs as spectral binaries by identifying traces of methane in the spectra of late-M and early-L dwarfs. Imaging follow-up of 17 spectral binaries yielded 3 (18%) resolved systems, corroborating the observed binary fraction, but 5 (29%) known binaries were missed, reinforcing the hypothesis that the short-separation systems are undercounted. In order to find the true binary fraction of brown dwarfs, we have compiled a volume-limited, spectroscopic sample of M7-L5 dwarfs and searched for T dwarf companions. In the 25 pc volume, 4 candidates were found, three of which are already confirmed, leading to a spectral binary fraction of $0.95 \pm 0.50\%$, albeit for a specific combination of spectral types. To extract the true binary fraction and determine the biases of the spectral binary method, we have produced a binary population simulation based on different assumptions of the mass function, age distribution, evolutionary models and mass ratio distribution. Applying the correction fraction resulting from this method to the observed spectral binary fraction yields a true binary fraction of $27 \pm 4\%$, which is roughly within 1 σ of the binary fraction obtained from high resolution imaging studies, radial velocity and astrometric monitoring. This method can be extended to identify giant planet companions to young brown dwarfs.

Author(s): Daniella Bardalez Gagliuffi¹, Adam J. Burgasser⁵, Sarah J. Schmidt⁴, Jonathan Gagné², Jacqueline K Faherty¹, Kelle Cruz¹, Chris Gelino³

Institution(s): 1. American Museum of Natural History, 2. Carnegie Institution of Washington - Department of Terrestrial Magnetism, 3. Infrared Processing and Analysis Center - California Institute of Technology, 4. Leibniz-Institute for Astrophysics Potsdam (AIP), 5. UC San Diego

158.16 – The Ultracool Typing Kit - An Open-Source, Qualitative Spectral Typing GUI for L Dwarfs

The Ultracool Typing Kit (UTK) is an open-source graphical user interface for classifying the NIR spectral types of L dwarfs, including field and low-gravity dwarfs spanning L0-L9. The user

is able to input an NIR spectrum and qualitatively compare the input spectrum to a full suite of spectral templates, including low-gravity beta and gamma templates. The user can choose to view the input spectrum as both a band-by-band comparison with the templates and a full bandwidth comparison with NIR spectral standards. Once an optimal qualitative comparison is selected, the user can save their spectral type selection both graphically and to a database. Using UTK to classify 78 previously typed L dwarfs, we show that a band-by-band classification method more accurately agrees with optical spectral typing systems than previous L dwarf NIR classification schemes. UTK is written in python, released on Zenodo with a BSD-3 clause license and publicly available on the BDNyc Github page.

Author(s): Ellianna Schwab¹, Kelle Cruz⁴, Alejandro Núñez², Adam J. Burgasser⁶, Emily Rice³, Neill Reid⁵, Jacqueline K Faherty¹

Institution(s): 1. American Museum of Natural History, 2. Columbia University, 3. CUNY - College of Staten Island, 4. CUNY - Hunter College, 5. Space Telescope Science Institute, 6. University of California, San Diego

Contributing team(s): BDNyc

200 – AAS Prize Presentations by AAS President Christine Jones (Harvard-Smithsonian, CfA)

200 Plenary Session: Prize Presentations: AAS Weber Award (Ian McLean, UCLA), LAD Prize, and Buchalter Cosmology Prize

201 – Plenary Talk: Unveiling the Low Surface Brightness Stellar Peripheries of Galaxies, Annette Ferguson (University of Edinburgh)

201.01 – Unveiling the Low Surface Brightness Stellar Peripheries of Galaxies

The low surface brightness peripheral regions of galaxies contain a gold mine of information about how minor mergers and accretions have influenced their evolution over cosmic time. Enormous stellar envelopes and copious amounts of faint tidal debris are natural outcomes of the hierarchical assembly process and the search for and study of these features, albeit highly challenging, offers the potential for unrivalled insight into the mechanisms of galaxy growth. Over the last two decades, there has been burgeoning interest in probing galaxy outskirts using resolved stellar populations. Wide-field surveys have uncovered vast tidal debris features and new populations of very remote globular clusters, while deep Hubble Space Telescope photometry has provided exquisite star formation histories back to the earliest epochs. I will highlight some recent results from studies within and beyond the Local Group and conclude by briefly discussing the great potential of future facilities, such as JWST, Euclid, LSST and WFIRST, for major breakthroughs in low surface brightness galaxy periphery science. cosmic time. Enormous stellar envelopes

257 – Stellar Topics, Galaxies iPoster Session

257.01 – On Stellar Flash Echoes from Circular Rings

A flash -- or any episode of variability -- that occurs in the vicinity of a circular ring might be seen several times later, simultaneously, as echoes on the ring. Effective images of the flash are created and annihilated in pairs, with as many as four flash images visible concurrently. Videos detailing sequences of image pair creation, tandem motion, and subsequent image annihilation are shown, given simple opacity and scattering assumptions. It is proven that, surprisingly, images from a second pair creation event always annihilate with images from the first. Caustic surfaces between flash locations yielding two and four images are computed. Although such ring echos surely occur, their practical detection might be difficult as it could require dedicated observing programs involving sensitive photometry of extended objects. Potential flash sources include planetary and interstellar gas and dust rings near and around variable stars, flare stars, novae, supernovae, and GRBs. Potentially recoverable information includes size, distance, temporal history, and angular isotropy of both the ring and flash.

158.17 – Imaging Analysis and Spectroscopy of Resolved Very Low Mass Binary Systems.

Low-mass stars and brown dwarfs are among the most common objects in the Milky Way Galaxy, but theories of their formation and evolution remain poorly constrained. Binary systems are important for understanding the formation of these objects and for making direct orbit and mass measurements to validate evolutionary theories. We present SpeX observations of three new binary systems. In each case, near-infrared spectroscopy indicates late-M spectral types, in one case nearly identical M7 twins. By modeling the imaging data, we measured the separations, position angles and relative brightnesses of the systems, and used our spectroscopic analysis to estimate their distances, projected separations and tangential velocities. We also performed atmosphere model fits to assess their physical properties. We place this set of binaries in context with other widely-separated late M dwarf binaries.

Author(s): Elizabeth Moreno Hilario², Adam J. Burgasser¹
Institution(s): 1. UC San Diego, 2. University of Guanajuato

and copious amounts of faint tidal debris are natural outcomes of the hierarchical assembly process and the search for and study of these features, albeit highly challenging, offers the potential for unrivalled insight into the mechanisms of galaxy growth. Over the last two decades, there has been burgeoning interest in probing galaxy outskirts using resolved stellar populations. Wide-field surveys have uncovered vast tidal debris features and new populations of very remote globular clusters, while deep Hubble Space Telescope photometry has provided exquisite star formation histories back to the earliest epochs. I will highlight some recent results from studies within and beyond the Local Group and conclude by briefly discussing the great potential of future facilities, such as JWST, Euclid, LSST and WFIRST, for major breakthroughs in low surface brightness galaxy periphery science.

Author(s): Annette Ferguson¹, Annette M. N. Ferguson
Institution(s): 1. University of Edinburgh

Author(s): Robert Nemiroff¹, Oindabi Mukherjee¹
Institution(s): 1. Michigan Technological University

257.02 – Time-series photometry of FO Aquarii's 2016 and 2017 low states

For decades prior to 2016, the intermediate polar FO Aquarii had been observed exclusively in a state of high mass transfer, but in two separate low states in 2016 and 2017, the mass-transfer rate plummeted, causing the system to fade by over 2 magnitudes in the first event and 1 magnitude in the second. During the nine months separating the two low states, the system's brightness stabilized at $V \sim 13.75$, approximately 0.25 mag fainter than it was before the 2016 event. Power spectral analysis shows that during the first low state, the dominant short-term modulation was at twice the spin-orbit beat frequency, implying that a substantial fraction of the accretion occurred via direct interaction between the accretion stream and the white dwarf's magnetosphere. Near the end of the recovery from the low state, there was a pronounced transition back to the spin-pulse-dominated light curve normally seen in the high state. During the subsequent low state in 2017, the strongest signal in the power spectrum was the

beat frequency itself. Furthermore, in both low states, the light curves exhibit irregular flaring episodes that correlate with changes in the power spectrum. Finally, we examine how the eclipse profile became narrower and shallower during the two faint states.

Author(s): Colin Littlefield², Peter Garnavich², Mark Kennedy¹

Institution(s): 1. University College Cork, 2. University of Notre Dame

Contributing team(s): American Association of Variable Star Observers

257.03 – Photometry of High-Redshift Gravitationally Lensed Type Ia Supernovae

Out of more than 1100 well-identified Type Ia Supernovae, only roughly 10 of them are at $z > 1.5$. High redshift supernovae are hard to detect but this is made easier by taking advantage of the effects of gravitational lensing, which magnifies objects in the background field of massive galaxy clusters. Supernova Nebra ($z \sim 1.8$), among others, was discovered during observations taken as part of the RELICS survey, which focused on fields of view that experience strong gravitational lensing effects. SN Nebra, which sits behind galaxy cluster Abell 1763, is magnified and therefore appears closer and easier to see than with HST alone. Studying high-redshift supernovae like SN Nebra is an important step towards creating cosmological models that accurately describe the behavior of dark energy in the early Universe. Recent efforts have been focused on improving photometry and the building and fitting of preliminary light curves.

Author(s): Anastasia Haynie¹

Institution(s): 1. University of South Carolina

257.04 – Recent Hubble Space Telescope Imaging of the Light Echoes of Supernova 2016adj in Centaurus A

Light echoes are one of the most powerful and efficient probes of the structure and composition of dust in circumstellar and interstellar environments. Observations of light echoes provide exact three dimensional (3-D) positions of dust while constraining its density, grain-size and chemical make-up. These can be used to study the evolutionary history of supernova (SN) progenitors, produce high-resolution maps of the structure and composition of interstellar media (ISM), and geometrically measure extragalactic distances. Here we report on our progress with analyzing our ongoing campaign of Hubble Space Telescope (HST) observations of the light echoes of SN 2016adj in Centaurus A. SN 2016adj was discovered on 08 Feb 2016 and identified as a core-collapse SN of either Type Ib or Type IIb. All observers agreed the SN was highly reddened, suffering $A_V = 2-4$ mags of extinction, which is consistent with its location within the famous dust lane of its elliptical host galaxy. The light echo first reported by Sugerman & Lawrence (2016) from the earliest epoch of WFC3 imaging with marked N-S asymmetry has expanded into a complete ring that is fairly well-centered on the SN. The ring is azimuthally non-uniform in brightness, but less dramatically so than at early times. By day 395 it has expanded to radii ranging from $0.62''$ (NW)– $0.76''$ (SE). Adopting a distance of 3.42 Mpc, this indicates a sheet of ISM dust at foreground distances of 160–240 pc. These observations and analysis are supported by STScI grants 14146, 14487 and 14700.

Author(s): Ali Hyder¹, Stephen Lawrence¹, Ben Sugerman²

Institution(s): 1. Hofstra University, 2. Space Science Institute

257.05 – Supernovae Discovery Efficiency

Abstract:

We present supernovae (SN) search efficiency measurements for recent Hubble Space Telescope (HST) surveys. Efficiency is a key component to any search, and is important parameter as a correction factor for SN rates. To achieve an accurate value for efficiency, many supernovae need to be discoverable in surveys. This cannot be achieved from real SN only, due to their scarcity,

so fake SN are planted. These fake supernovae—with a goal of realism in mind—yield an understanding of efficiency based on position related to other celestial objects, and brightness. To improve realism, we built a more accurate model of supernovae using a point-spread function. The next improvement to realism is planting these objects close to galaxies and of various parameters of brightness, magnitude, local galactic brightness and redshift. Once these are planted, a very accurate SN is visible and discoverable by the searcher. It is very important to find factors that affect this discovery efficiency. Exploring the factors that effect detection yields a more accurate correction factor. Further inquires into efficiency give us a better understanding of image processing, searching techniques and survey strategies, and result in an overall higher likelihood to find these events in future surveys with Hubble, James Webb, and WFIRST telescopes. After efficiency is discovered and refined with many unique surveys, it factors into measurements of SN rates versus redshift. By comparing SN rates vs redshift against the star formation rate we can test models to determine how long star systems take from the point of inception to explosion (delay time distribution). This delay time distribution is compared to SN progenitors models to get an accurate idea of what these stars were like before their deaths.

Author(s): Colin John¹

Institution(s): 1. University of South Carolina

257.06 – Are narrow-line Seyfert 1 galaxies highly accreting low M_{BH} AGNs?

In this work, we test the hypothesis that the nuclei of narrow-line Seyfert 1 galaxies (NLS1s) are active galactic nuclei in their early phase, in other words, that they are younger and more active than the more common broad-line Seyfert 1 galaxies (BLS1s). If that is true, then NLS1s should, on average, have lower black hole (BH) masses and higher accretion rates than BLS1s. To test this, we use a sample of 35 NLS1s and 54 BLS1s with similar X-ray luminosity distributions and good XMM-Newton observations. To determine the BH mass, we apply an X-ray scaling method, which is independent of any assumption on the broad line region dynamics and of the inclination of the objects. The X-ray method depends on a comparison with a Galactic BH (GBH) of known mass and distance, so we use three different reference GBHs to test the consistency of the results. Using all three GBHs, we find that NLS1s, on average, do have smaller BH masses and higher accretion rates than do BLS1s, and the differences are statistically significant.

Author(s): James K. Williams¹, Mario Gliozzi¹, Ross Ruzdinsky²

Institution(s): 1. George Mason University, 2. University of California Berkeley

257.07 – An Outflow-shaped Magnetic Field Toward the Class o Protostellar Source Serpens SMM1

The results from the polarization system at the Atacama Large Millimeter/submillimeter Array (ALMA) have begun both to expand and to confound our understanding of the role of the magnetic field in low-mass star formation. Here we show the highest resolution and highest sensitivity polarization images made to date toward the very young, intermediate-mass Class o protostellar source Serpens SMM1, the brightest source in the Serpens Main star-forming region. These ALMA observations achieve ~ 140 AU resolution, allowing us to probe dust polarization—and thus magnetic field orientation—in the innermost regions surrounding the protostar. By complementing these observations with polarization observations from the Submillimeter Array (SMA) and archival data from the Combined Array for Research in Millimeter-wave Astronomy (CARMA) and the James Clerk Maxwell Telescopes (JCMT), we can compare the magnetic field orientations at different spatial scales. We find major changes in the magnetic field orientation between large (~ 0.1 pc) scales—where the magnetic field is oriented E–W, perpendicular to the major axis of the dusty filament where

SMM1 is embedded—and the intermediate and small scales probed by CARMA (~1000 au resolution), the SMA (~350 au resolution), and ALMA. The ALMA maps reveal that the redshifted lobe of the bipolar outflow is clearly shaping the magnetic field in SMM1 on the southeast side of the source. High-spatial-resolution continuum and spectral-line observations also reveal a tight (~130 au) protobinary system in SMM1-b, the eastern component of which is launching an extremely high-velocity, one-sided jet visible in both CO(2-1) and SiO(5-4); however, that jet does not appear to be shaping the magnetic field. These observations show that with the sensitivity and resolution of ALMA, we can now begin to understand the role that feedback (e.g., from protostellar outflows) plays in shaping the magnetic field in very young, star-forming sources like SMM1.

Author(s): Charles Hull⁵, Josep M. Girart², Lukasz Tychoniec⁴, Ramprasad Rao¹, Paulo Cortés⁶, Riwaj Pokhrel³, Qizhou Zhang³, Martin Houde¹², Michael Dunham⁸, Lars Kristensen¹⁰, Shih-Ping Lai⁷, Zhi-Yun Li¹¹, Richard Plambeck⁹
Institution(s): 1. ASIAA, 2. CSIC-IEEC, 3. Harvard-Smithsonian Center for Astrophysics, 4. Leiden Observatory, 5. NAOJ/ALMA, 6. NRAO/ALMA, 7. NTHU, 8. SUNY Fredonia, 9. UC Berkeley, 10. University of Copenhagen, 11. University of Virginia, 12. University of Western Ontario

257.08 – Hydrogen Cyanide In Protoplanetary Disks

The chemistry behind star and planet formation is extremely complex and important in the formation of habitable planets. Life requires molecules containing carbon, oxygen, and importantly, nitrogen. Hydrogen cyanide, or HCN, one of the main interstellar nitrogen carriers, is extremely dangerous here on Earth. However, it could be used as a vital tool for tracking the chemistry of potentially habitable planets. As we get closer to identifying other habitable planets, we must understand the beginnings of how those planets are formed in the early protoplanetary disk. This project investigates HCN chemistry in different locations in the disk, and what this might mean for forming planets at different distances from the star. HCN is a chemically diverse molecule. It is connected to the formation for other more complex molecules and is commonly used as a nitrogen tracer. Using computational chemical models we look at how the HCN abundance changes at different locations. We use realistic and physically motivated conditions for the gas in the protoplanetary disk: temperature, density, and radiation (UV flux). We analyze the reaction network, formation, and destruction of HCN molecules in the disk environment. The disk environment informs us about stability of habitable planets that are created based on HCN molecules. We reviewed and compared the difference in the molecules with a variety of locations in the disk and ultimately giving us a better understanding on how we view protoplanetary disks.

Author(s): Ashley L. Walker¹, Karin Oberg², L. Ilse-dore Cleves²
Institution(s): 1. Chicago State University, 2. Harvard Smithsonian Center for Astrophysics

257.09 – Exploring the Internal Dynamics of Globular Clusters

Exploring the Internal Dynamics of Globular Clusters

The formation histories and structural properties of globular clusters are imprinted on their internal dynamics. Energy equipartition results in velocity differences for stars of different mass, and leads to mass segregation, which results in different spatial distributions for stars of different mass. Intermediate-mass black holes significantly increase the velocity dispersions at the centres of clusters. By combining accurate measurements of their internal kinematics with state-of-the-art dynamical models, we can characterise both the velocity dispersion and mass profiles of clusters, tease apart the different effects, and understand how clusters may have formed and evolved.

Using proper motions from the Hubble Space Telescope Proper Motion (HSTPROMO) Collaboration for a set of 22 Milky Way globular clusters, and our discrete dynamical modelling techniques designed to work with large, high-quality datasets, we are studying a variety of internal cluster properties. We will present the results of theoretical work on simulated clusters that demonstrates the efficacy of our approach, and preliminary results from application to real clusters.

Author(s): Laura L Watkins¹, Roeland van der Marel¹, Andrea Bellini¹, Nora Luetzgendorf¹
Institution(s): 1. Space Telescope Science Institute
Contributing team(s): HSTPROMO Collaboration

257.11 – GalMod: the last frontier of Galaxy population synthesis models

We present a novel Galaxy population synthesis model: GalMod (Pasetto et al. 2016, 2017a,b) is the only star-count model featuring an asymmetric bar/bulge as well as spiral arms as directly obtained by applying linear perturbative theory to self-consistent distribution function of the Galaxy stellar populations. Compared to previous literature models (e.g., Besancon, Trilegal), GalMod allows to generate full-sky mock catalogue, M31 surveys and provides a better match to observed Milky Way (MW) stellar fields.

The model can generate synthetic mock catalogs of visible portions of the MW, external galaxies like M31, or N-body simulation initial conditions. At any given time, e.g., a chosen age of the Galaxy, the model contains a sum of discrete stellar populations, namely bulge/bar, disk, halo. The disk population is itself the sum of subpopulations: spiral arms, thin disk, thick disk, and gas component, while the halo is modeled as the sum of a stellar component, a hot coronal gas, and a dark matter component. The Galactic potential is computed from these subpopulations' density profiles and used to generate detailed kinematics by considering the first few moments of the Boltzmann collisionless equation for all the stellar subpopulations. The same density profiles are then used to define the observed color-magnitude diagrams within an input field of view from an arbitrary solar location. Several photometric systems have been included and made available on-line, e.g., SDSS, Gaia, 2MASS, HST WFC3, and others. Finally, we model the extinction with advanced ray tracing solutions. The model's web page (and tutorial) can be accessed at www.GalMod.org.

Author(s): Stefano Pasetto², Juna Kollmeier², Eva K. Grebel¹, cesare chiosi³
Institution(s): 1. Astronomisches Rechen-Institut: Zentrum für Astronomie, 2. Carnegie Observatories, 3. University of Padua

257.12 – Characterizing the 300 km/s Stream Near Segue 1

The characterization of stellar streams in the Milky Way halo can provide important observational constraints on the Λ CDM cosmological model, which posits that galaxies form via the accretion of smaller satellites. One such stream, the 300 km/s stellar stream near the dwarf galaxy Segue 1 (300S), was detected in narrow-field spectroscopic surveys, but its photometric counterpart has not been identified. In this study, we search for members of 300S in wide-field survey data to map out the stream's extent and further characterize its progenitor. We add to the existing catalog of 300S members by finding new members of 300S in SEGUE-1, SEGUE-2, and APOGEE-2 surveys, and confirm the kinematic association of 300S with an elongated substructure found in both SDSS and PanSTARRS photometric data. The 300S stars display a mean metallicity of $[Fe/H] = -1.42 \pm 0.26$, and have chemical abundance patterns similar to that of Local Group dwarf galaxies, as well as that of the Milky Way halo. Using the open-source code *galpy* to model a preliminary orbit of the stream, we suggest that the progenitor of 300S experienced one major tidal disruption event on its most recent pericentric passing. We conclude that the progenitor of the stream is a dwarf

galaxy that is probably similar to the satellites that were accreted to build the present-day Milky Way halo.

Author(s): Wanying Fu⁵, Joshua D. Simon⁴, Jo Bovy⁷, CARLOS ALLENDE PRIETO³, Timothy Beers⁶, Paul Harding¹, Inese I. Ivans⁸, Richard Lane²

Institution(s): 1. Case Western Reserve University, 2. Instituto de Astrofísica at Pontificia Universidad Católica de Chile, 3. Instituto de Astrofísica de Canarias, 4. Observatories of the Carnegie Institution of Washington, 5. Pomona College, 6. University of Notre Dame, 7. University of Toronto, 8. University of Utah

Contributing team(s): APOGEE-2

257.13 – The Smallest Galaxies in the Universe: Investigating the Origins of Ultra-faint Galaxies

One outstanding question in cosmology is, what are the smallest galaxies that can form? The answer to this question can tell us much about galaxy formation, and even of the properties of dark matter itself. A candidate for the smallest galaxies that can form are the ultrafaint galaxies. The star formation of ultrafaints appears to have been shut off during the epoch of reionization, when radiation from the first stars ionized all the free hydrogen in the universe. This would imply ultrafaints should exist everywhere in the universe. However, we can only observe ultrafaints as satellites of the Milky Way, due to their low brightness. This will change with the next generation of telescopes such as the Large Synoptic Survey Telescope (LSST). The focus of this work is to predict the number of ultrafaints that should be seen with future surveys. To that end, we use the ELVIS suite, which contains 14 dark matter only simulations of Local Group like systems containing a Milky Way and Andromeda-like galaxy and the substructure out to around 1 Mpc of the barycenter. We mock observe the simulations in order to mimic current surveys such as the Sloan Digital Sky Survey (SDSS), and the Dark Energy Survey (DES), and use the population of galaxies found by those surveys to project the population of dwarf galaxies out beyond the virial radius of either galaxy. This number will depend sensitively on the formation mechanism of ultrafaint dwarfs, and comparisons of future surveys to this work could help rule out certain formation scenarios.

Author(s): Yuewen Qi¹, Andrew Graus¹, James Bullock¹
Institution(s): 1. University of California, Irvine

257.14 – Effects of gas on the formation and evolution of a bar in Milky-Way sized galaxies

To study the effects of a gas component on the formation and evolution of a stellar bar, we run fully self-consistent three-dimensional simulations of isolated barred galaxies similar to the Milky Way. Our models consider feedbacks from star formation and accretion to a black hole, but neglect the effects of magnetic fields. We vary the gas fraction in the disk as well as the Toomre stability parameter Q in the stellar disk. In models with $Q=1.2$, the presence of gas tends to delay the bar formation and make a bar weaker since the gas disk does not actively participate in a bar-forming large-scale gravitational instability. In models with $Q=1.0$, on the other hand, the gas rapidly turns into stars with low velocity dispersions, which cools down the stellar disk and thus promotes the bar formation. While gas-free disks are subject to buckling instability, disks with the gas fraction more than 5% are found to thicken secularly without undergoing the buckling instability. A stellar bar that forms is efficient in redistributing the gas in the bar regions and produces a star-forming nuclear ring. The ring is very small when it first forms and grows in size over time. The bars and nuclear rings formed in our models have properties similar to the central molecular zone in the Milky Way.

Author(s): Woo-Young Seo², Woong-Tae Kim², Philip Hopkins¹
Institution(s): 1. Caltech, 2. Seoul National University

257.15 – A gravitationally lensed starburst galaxy at $z=1.03$ detected by SOFIA/HAWC+

We present a high S/N \sim 20 detection at 89 micron (in 15 mins) of the Herschel-selected gravitationally lensed starburst galaxy HATLASJ1429-0028 with the High-resolution Airborne Wideband Camera-plus (HAWC+) onboard the Stratospheric Observatory for Infrared Astronomy (SOFIA). The spectacular lensing system consists of an edge-on foreground disk galaxy at $z=0.22$ and a nearly complete Einstein ring of an intrinsic ultra-luminous infrared galaxy at $z=1.03$. Is this high luminosity powered by pure star formation (SF) or an active galactic nucleus (AGN)? Previous nebular line diagnostics indicate that it is star-formation dominated. SOFIA/HAWC+ allows the broad-band spectral energy distribution of the galaxy to be studied between 20 - 100 micron, which is an important wavelength range for further constraining the fractional AGN contribution to the total IR luminosity. Multi-wavelength SED modeling constrains the AGN fraction to be $< 1\%$. The detection of a source at z of 1 shows the potential of utilizing SOFIA/HAWC+ for distant galaxy studies and the potential to decompose SF/AGN that cannot be obtained with other current facilities.

Author(s): Arianna Brown¹, Jingzhe Ma¹, Asantha Cooray¹, Hooshang Nayyeri¹, Nicholas Timmons¹
Institution(s): 1. UC Irvine

257.16 – Tracing Cold Molecular Gas in Starburst Galaxies

We use hydrodynamical simulations of isolated galaxies and galaxy mergers to probe the efficiency and completeness of CO as a tracer of cold molecular gas in outflows. Our simulations were run using the Feedback In Realistic Environments (FIRE) model which accounts for gravity, hydrodynamics, radiative gas cooling, star formation, and feedback associated with star formation. A multi-phase ISM naturally develops in these simulations, where cold-dense star forming molecular gas is continually formed via gas cooling, but is also continually destroyed via feedback. We study the extent to which CO traces the total molecular gas budget, with a focus on how CO can be used to trace the cold gas budget in galactic outflows.

Author(s): Michael Bueno¹, Paul Torrey², Desika Narayanan⁴, Jorge Moreno³
Institution(s): 1. Haverford College, 2. MIT Kavli Institute for Astrophysics & Space Research, 3. Pomona College, 4. University of Florida

257.17 – Using CO as a Physical Probe of the SF Activity in the Planck-Herschel Selected Hyper Luminous Infrared Galaxies

Multi-J CO line studies are essential for quantifying the physical properties of the star-forming ISM, yet it is observationally expensive to detect those faint CO emission lines at high redshift. Our eight Planck-Herschel selected galaxies, with apparent $L_{\text{IR}} > 10^{13-14} L_{\odot}$, serve as the best laboratories to conduct such a CO spectral line energy distribution analysis at high- z . Using our GBT and LMT ($J_{\text{up}} = 1-3$) measurements, we trace the bulk molecular gas mass, finding relatively large star formation efficiencies (as traced by the $L_{\text{IR-to-}L'_{\text{CO}(1-0)}}$ ratio) consistent with a starburst mode of activity. With our mid-J ($J_{\text{up}} = 4-8$) CO line measurements, obtained with the IRAM 30m telescope, we find gas excitation conditions ranging from sub-thermal SMGs to highly excited local starbursts out to $J_{\text{up}} = 5-8$. The consistently high velocity-integrated line intensities at $J_{\text{up}} = 5-8$ indicates the presence a warm/dense component responsible for exciting the higher-J CO lines, therefore we use coupled non-LTE large velocity gradient and dust radiative transfer models to begin characterising the two-component molecular ISM in these strongly lensed systems.

Author(s): Kevin Harrington¹
Institution(s): 1. Max Planck Institut für Radioastronomie/Argelander Institut für Astronomie

257.18 – Broadband Photometric Reverberation Mapping Analysis on SDSS-RM and Stripe 82 Quasars

We extended the broadband photometric reverberation mapping (PRM) code, JAVELIN and test the availability to get broad line region (BLR) time delays that are consistent with spectroscopic reverberation mapping (SRM) projects. Broadband light curves of SDSS-RM quasars produced by convolution with system transmission curve were used in the test. We find that under similar sampling conditions (evenly and frequently sampled), the key factor determining whether the broadband PRM code can yield lags consistent with spectroscopic projects is the flux ratio of line to the reference continuum, which is in line with the findings in Zu et al. (2016). We further find a crucial line-to-continuum flux ratio, above which the mean of the ratios between the lags from PRM and SRM becomes closer to unity, and the scatter is pronouncedly reduced. Based on this flux ratio criteria, we selected some of the quasars from Hernitschek et al. (2015) and carry out broadband PRM on this subset. The performance of damped random walking (DRW) model and power-law (PL) structure function model on broadband PRM are compared using mock light curves with high, even cadences and low, uneven ones, respectively. We find that DRW model performs better in carrying out broadband PRM than PL model both for high and low cadence light curves with other data qualities similar to SDSS-RM quasars.

Author(s): Haowen Zhang¹, Qian Yang¹, Xuebing Wu¹, Yue Shen²

Institution(s): 1. Peking University, 2. UIUC

257.19 – Unraveling the Physics of FR II Jets Using HST Polarimetry

Polarization is a critical parameter for understanding jet flows, as their radio to optical emission is produced by synchrotron radiation, which is naturally polarized, with the inferred magnetic field direction indicating the magnetic field direction in the emission region. Polarization has proven essential in characterizing the physics of FR I jets, where it has helped us map out their magnetic field and energetic structure and the relationship of this structure to the high-energy emission and particle acceleration. To date, high-quality HST polarimetry has been analyzed for just one FR II jet, that of PKS 1136-135. To rectify this, we have obtained new HST polarimetry observations of two key FR II jets, 3C 273 and 1150+497, with future observations of PKS 0637-752 scheduled. These new observations allow for the determination of the magnetic field structure and confirmation of which emission mechanisms are operating to create the observed optical to X-ray emission, and will allow us to greatly advance modeling efforts for these jets and nail down their kinetic power, a key parameter for understanding quasars and their cosmological effects. With this project we hope to bring our understanding of their unique physics more in line with that of the FR Is.

Author(s): Devon Clautice², Eric S. Perlman², Mihai Cara¹⁰, Sebastian Jester⁶, Markos Georganopoulos¹⁴, Klaus Meisenheimer⁶, Richard Perley⁷, Stefi Baum¹³, Mitchell C. Begelman¹², John A. Biretta¹, Mark Birkinshaw¹¹, Chi C. Cheung⁸, Paolo Coppi¹⁵, Jean Eilek⁷, Herman L. Marshall⁵, Andre Martel¹⁰, Christopher P. O'Dea¹³, Rita M. Sambruna³, William B. Sparks¹⁰, Lukasz Stawarz⁴, Yasunobu Uchiyama⁹, Meg Urry¹⁵, Diana M. Worrall¹¹

Institution(s): 1. Eureka Scientific, 2. Florida Institute of Technology, 3. George Mason University, 4. Jagiellonian University, 5. Massachusetts Institute of Technology, 6. Max-Planck-Institut für Astronomie, 7. National Radio Astronomy Observatory, 8. Naval Research Laboratory, 9. Rikkyo University, 10. Space Telescope Science Institute, 11. University of Bristol, 12. University of Colorado Boulder, 13. University of Manitoba, 14. University of Maryland Baltimore County, 15. Yale University

257.20 – Investigating Possible Outliers in the Fermi Blazar AGN Sample

The Fermi Gamma-Ray Space Telescope (*Fermi*) has cataloged over 3000 gamma-ray (>100 MeV) point sources of which more than 1100 are likely AGN. These AGN are predominantly among the radio-loud “blazar” subclass. Recently however, a significant sample of bright ($F_{15\text{GHz}} > 1.5$ Jy), radio selected AGN was found to overlap with Fermi at only the $\sim 80\%$ level (Lister et al., 2015). This could be a result of some selection bias or it could be due to deficient Doppler boosting among that $\sim 20\%$. Additionally, a recent survey of high-latitude gamma-ray sources by Schinzel et al. (2017) reveals a sample of ~ 100 objects which are not detected in the 4-10 GHz radio band to a limiting flux of about 2mJy. This apparent lack of radio flux is puzzling, and may indicate either an extreme Compton-dominated sample, or copious gamma-ray emission from a heretofore unknown population such as a subclass of radio-quiet AGN. Speculatively, these radio-loud/gamma-quiet and gamma-loud/radio quiet samples could be odd cases of the blazar phenomena which reside outside of the well-known blazar sequence. To explore this problem further we have undertaken a study to construct or constrain individual source SEDs as a first step towards their classification. In this contribution we present results from our search for emission in the Swift-BAT 15-100-keV hard X-ray band for each of these samples.

Author(s): Chris Shrader¹

Institution(s): 1. NASA GSFC

257.21 – Exploring the Dynamics of Exoplanetary Systems in a Young Stellar Cluster

I describe a dynamical simulation of planetary systems in a young star cluster. One rather arbitrary aspect of cluster simulations is the choice of initial conditions. These are typically chosen from some standard model, such as Plummer or King, or from a “fractal” distribution to try to model young clumpy systems. Here I adopt the approach of realizing an initial cluster model directly from a detailed magnetohydrodynamical model of cluster formation from a 1000-solar-mass interstellar gas cloud, with magnetic fields and radiative and wind feedback from massive stars included self-consistently. The N-body simulation of the stars and planets starts once star formation is largely over and feedback has cleared much of the gas from the region where the newborn stars reside. It continues until the cluster dissolves in the galactic field. Of particular interest is what would happen to the free-floating planets created in the gas cloud simulation. Are they captured by a star or are they ejected from the cluster? This method of building a dynamical cluster simulation directly from the results of a cluster formation model allows us to better understand the evolution of young star clusters and enriches our understanding of extrasolar planet development in them. These simulations were performed within the AMUSE simulation framework, and combine N-body, multiples and background potential code.

Author(s): Jonathan Daniel Thornton¹, Joseph Paul Glaser¹, Joshua Edward Wall¹

Institution(s): 1. Drexel University

257.22 – TYCHO: Simulating Exoplanets Within Stellar Clusters

Recent surveys exploring nearby open clusters have yielded noticeable differences in the planetary population from that seen in the Field. This is surprising, as the two should be indistinguishable given currently accepted theories on how a majority of stars form within the Galaxy. Currently, the existence of this apparent deficit is not fully understood. While detection bias in previous observational surveys certainly contributes to this issue, the dynamical effects of star-star scattering must also be taken into account. However, this effect can only be investigated via computational simulations and current solutions of the multi-scale N-body problem are limited and drastically simplified.

To remedy this, we aim to create a physically complete computational solution to explore the role of stellar close encounters and interplanetary interactions in producing the observed exoplanet populations for both open cluster stars and Field stars. To achieve this, TYCHO employs a variety of different computational techniques, including: multiple n-body integration methods; close-encounter handling; Monte Carlo scattering experiments; and a variety of observationally-backed initial condition generators. Herein, we discuss the current state of the

202 – Sustainability at Professional Societies: best Practices in Environmental Stewardship

The AAS Sustainability Committee will host this special session in a panel forum format with 5-6 panelists. Our goal is to learn about best practices in sustainability at our sister professional societies, and to share our own experiences with them. What institutional structures or barriers exist that affect the society's environmental impact? Does the society have a sustainability committee and/or policy (the AAS has both)? What kind of sustainability outreach and education efforts does the society offer? What activities of the society and its members cause the largest environmental impact, e.g. greenhouse gas emissions associated with air travel, and what can be or is being done to mitigate that impact? Note: session will be panel forum format, not a sequence of speakers. Confirmed panelists: Kay Kane, Instructional Design Specialist, U.S. Green Building Council. Ed Liebow, Executive Director, American Anthropological Association Chris McEntee, Executive Director, American Geophysical Union Doug Richardson, Executive Director, American Association of Geographers Kevin Marvel, Executive Officer, American Astronomical Society

203 – IGM and QSO Absorption Line Systems I

203.01 – Atomic Data Revisions for Improving Absorption Line Studies of the Interstellar, Circumgalactic, and Intergalactic Medium

Surveying and studying galaxies at different epochs is essential to understanding how galaxies evolve. Atomic spectroscopy is used to study the gas in and around galaxies by means of the absorption features in the spectra of background quasars. Element abundances derived from the measurement of observed lines in these quasar absorption systems rely on accurate atomic data such as the oscillator strength of electric dipole transitions. We have produced a compilation of recommended oscillator strengths for 576 key transitions for wavelengths longward of 911.753 Angstroms (the H I Lyman limit). This compilation focuses on the recent findings from numerous theoretical and experimental physicists for ions of astrophysical interest that have been observed in the interstellar medium (ISM), the circumgalactic medium (CGM), and the intergalactic medium (IGM), for selected elements ranging from C to Pb. Differences between the former and the newly recommended values are greater than 25% for approximately 22% of lines with updated oscillator strength values. We encourage future absorption line studies of the ISM, CGM, and IGM medium to use this compilation.

This work was supported in part by NSF-AST/1108830, NASA/STScI support for HST GO-12536, and a NASA/SC Space Grant graduate fellowship.

Author(s): Frances Cashman², Varsha Kulkarni², Romas Kisielius³, Gary Ferland¹, Pavel Bogdanovich³
Institution(s): 1. University of Kentucky, 2. University of South Carolina, 3. Vilnius University

203.02D – Quasars Probing Quasars: the Circumgalactic Medium Surrounding $z \sim 2$ Quasars

Understanding the circumgalactic medium--the gaseous halo surrounding a galaxy, is an integral part to understanding galaxy evolution. The $z \sim 2-3$ universe is interesting as this is when the star formation rate and AGN activity peak. My thesis concludes the decade-long Quasars Probing Quasars survey designed for studying massive galaxy formation and quasar feedback. I use

code's implantation within the AMUSE framework and its applications towards present exoplanet surveys.

Author(s): Joseph Paul Glaser¹, Jonathan Thornton¹, Aaron M Geller², Stephen McMillan¹
Institution(s): 1. Drexel University, 2. Northwestern University

– Kevin Marvel, Executive Officer, American Astronomical Society

– Doug Richardson, Executive Director, American Association of Geographers

– Chris McEntee, Executive Director, American Geophysical Union

– Ed Liebow, Executive Director, American Anthropological Association

– Kay Kane, Instructional Design Specialist, U.S. Green Building Council.

background quasar sightlines that pass close to foreground quasars to study the circumgalactic medium of quasar-host galaxies in absorption. My sample of 149 quasar pairs involve spectra taken with 17 different optical and near IR instruments.

I present results on the statistical and physical properties of the circumgalactic medium. The circumgalactic medium is enriched even beyond the virial radius. The alpha/Fe abundance ratio is enhanced, suggesting enrichment from core-collapse supernovae. The cool gas mass within the virial radius is enough to fuel star formation for another Gyr, and may account for 1/3 of the baryonic budget of the galaxy halo. The ionization state increases with projected distance from the quasar, which implies the quasar does not dominate the ionizing radiation flux. However, detection of fluorescent Lyman-alpha emission and NV absorption imply these transverse absorbers are partially illuminated by the quasar. In one peculiar case, the absorbing clump has density $>100 \text{ cm}^{-3}$ and sub-parsec size. The average absorption in the circumgalactic medium exhibits large velocity widths, and is asymmetric about the systemic redshift of the galaxies. The widths are consistent with gravitational motions and Hubble flow, and outflows are not required to explain them. The asymmetry can be explained if the ionizing radiation from the quasar is anisotropic or intermittent and the gas is not in inflow.

My results pose challenges for cosmological hydrodynamic simulations to produce a substantial cool gas reservoir surrounding quasars, that is also enriched and shows extreme kinematics.

Author(s): Marie Lau¹
Institution(s): 1. University of California, Santa Cruz
Contributing team(s): The Quasars Probing Quasars survey

203.03 – "Resolving" the Problems of the Circumgalactic Medium

Galactic gas accretion drives the formation and evolution of every galaxy. The circumgalactic medium, the tenuous gas surrounding a galaxy, acts as a direct probe of star formation, stellar feedback, and gas accretion, all responsible for a galaxy's fate. To date, attempts to model the multiphase CGM have failed to adequately match observations, leaving many unanswered questions

regarding its origin, distribution, and kinematics. In this talk I will present synthetic observations of the CGM from the FIRE simulations and the TempestCGM simulations, two sets of state-of-the-art cosmological hydrodynamic zoom-in simulations with extremely high spatial resolution. For the first time, these models are able to reproduce many of the CGM observational samples (e.g. COS-Halos), and they indicate that the size of the physical structures of the CGM are smaller than previously simulated (< 1 kpc).

Author(s): Cameron Hummels¹

Institution(s): 1. *California Institute of Technology*

203.04D – Constraining the Intergalactic and Circumgalactic Media with Lyman-Alpha Absorption

Lyman-alpha (Ly- α) absorption features detected in quasar spectra in the redshift range $0 < z < 6$ are a powerful tool to probe the intergalactic and circumgalactic media (IGM/CGM) and, consequently, to constrain models of galaxy formation and cosmology. In the first part of my thesis, I overcome numerical challenges posed by cosmological hydrodynamic simulations by developing a novel semi-analytic technique to predict various statistics of Ly- α absorption in the IGM with large N-body cosmological simulations. The technique developed is more accurate than previous attempts in the literature, and can be applied to Gpc-scale N-body simulations, allowing an accurate investigation of the Ly- α absorption on unprecedentedly large scales. In the second part of my thesis, I compare predictions of state-of-the-art hydrodynamic cosmological simulations with observations of the mean Ly- α absorption around foreground quasars, damped Ly- α absorbers, and Lyman-break galaxies, at different transverse distances (~ 20 kpc– 20 Mpc) from background quasars. Far from galaxies > 2 Mpc, the simulations asymptotically match the observations, because the Λ CDM model successfully describes the ambient IGM. This represents a critical advantage of studying the mean absorption profile. However, significant differences between the simulations, and between simulations and observations are present on scales 20 kpc– 2 Mpc, illustrating the challenges of accurately modeling and resolving galaxy formation physics. It is noteworthy that these differences are observed as far out as ~ 2 Mpc, indicating that the 'sphere-of-influence' of galaxies could extend to approximately ~ 20 times the halo virial radius (~ 100 kpc). Current observations are very precise on these scales and can thus strongly discriminate between different galaxy formation models. I demonstrate that the Ly- α absorption profile is primarily sensitive to the underlying temperature-density relationship of diffuse gas around galaxies, and argue that it thus provides a fundamental test of galaxy formation models. With near-future high-precision observations of Ly- α absorption, the tools developed in my thesis set the stage for even stronger constraints on models of galaxy formation and cosmology.

Author(s): Daniele Sorini², Jose Onorbe², Joseph F Hennawi³, Zarija Lukic¹

Institution(s): 1. *Lawrence Berkeley National Laboratory*, 2. *Max Planck Institute for Astronomy*, 3. *University of California Santa Barbara*

203.05 – Element abundance measurements in gas-rich galaxies at $z \sim 5$

Element abundances in high-redshift galaxies offer key constraints on models of the chemical evolution of galaxies. The chemical composition of galaxies at $z > \sim 5$ are especially important since they constrain the star formation history in the first ~ 1 Gyr

204 – Detection of Extrasolar Planets II

204.01 – Technology Required to Image and Characterize an exo-Earth from Space

NASA's Exoplanet Exploration Program (ExEP) guides the development of technology that enables the direct imaging and characterization of exo-Earths in the habitable zone of Sun-like stars with future space observatories. Here we present the 2018

after the Big Bang and the initial mass function of early stars. Observations of damped Lyman-alpha (DLA) absorbers in quasar spectra enable robust measurements of the element abundances in distant gas-rich galaxies. In particular, abundances of volatile elements such as S, O and refractory elements such as Si, Fe allow determination of the dust-corrected metallicity and the depletion strength in the absorbing galaxies. Unfortunately measurements for volatile (nearly undepleted) elements are very sparse for DLAs at $z > 4.5$. We present abundance measurements of O, C, Si and Fe for three gas-rich galaxies at $z \sim 5$ using observations from the Very Large Telescope (VLT) X-shooter spectrograph and the Keck Echelle Spectrograph and Imager. Our study has doubled the existing sample of measurements of undepleted elements at $z > 4.5$. After combining our measurements with those from the literature, we find that the cosmological mean metallicity of $z \sim 5$ absorbers is consistent with the prediction based on $z < 4.5$ DLAs within $< 0.5 \sigma$. Thus, we find no significant evidence of a sudden drop in metallicity at $z > 4.7$ as reported by prior studies. Some of the absorbers show evidence of depletion of elements on dust grains, e.g. low [Si/O] or [Fe/O]. These absorbers along with other $z \sim 5$ absorbers from the literature show some peculiarities in the relative abundances, e.g. low [C/O] in several absorbers and high [Si/O] in one absorber. We also find that the metallicity vs. velocity dispersion relation of $z \sim 5$ absorbers may be different from that of lower-redshift absorbers.

We acknowledge support from NASA grant NNX14AG74G and NASA/STScI support for HST programs GO-12536, 13801 to the Univ. of South Carolina.

Author(s): Suraj Poudel², Varsha Kulkarni², Sean Morrison¹, Celine Peroux¹, Debopam Som¹, Hadi Rahmani¹, Samuel Quiret¹
Institution(s): 1. *Laboratoire d'Astrophysique de Marseille*, 2. *University of South Carolina*

203.06 – Constraining local reionization histories with 21 cm observations

Several low-frequency radio instruments are poised to detect faint signatures of the Epoch of Reionization through the redshifted HI 21 cm line, while near-infrared (NIR) observations continue to push studies of galactic properties to higher redshifts. With ongoing upgrades to radio facilities and the imminent launch of JWST, both fields are on the verge of revolutionary advances in the characterization of the EoR. But there remains an open question of how to marry these observations in a way that will fully exploit their complementary nature. NIR observations will reveal how galaxies formed and evolved, while 21 cm observations will trace the impact early galaxies had on their large scale environments. Simultaneous observation of these two physical processes is difficult owing to the disparate scales probed by the instruments. I will present a method for using images of large-scale 21 cm brightness temperature to constrain the reionization history of a given region of cosmological volume, thereby providing environmental context to galaxy observations in the same region. This framework is complicated by foreground contamination in 21 cm EoR images, but can be mitigated with filtering techniques and useful information is still recoverable. By adding local reionization history to NIR surveys, we will be able to distinguish between galaxies in a variety of environments. This has the potential to enhance expected signatures such as the flattening of the luminosity function at high redshift, or reveal new observables altogether.

Author(s): Adam Beardsley¹

Institution(s): 1. *Arizona State University*

ExEP Technology Gap List, an annual update to ExEP's list of technologies, to be advanced in the next 1-5 years. Key technology gaps are starlight suppression with a coronagraph (internal occulters) or a starshade (external occulters), enabling imaging at extreme contrast (more than 10 billion) by blocking on-axis starlight, while allowing the reflected light of off-axis exoplanets to be detected. Building and operating a space coronagraph capable

of imaging an exo-Earth will require new technologies beyond those of WFIRST, the first high-contrast coronagraph in space. A starshade has never been used in a space mission and requires new capabilities in precision deployment of large structures, starlight suppression, and in formation sensing and control. We review the current state-of-the-art in coronagraph and starshade technology and the performance level that must be achieved to discover and characterize Earth analogs.

Author(s): Brendan Crill¹

Institution(s): 1. Jet Propulsion Laboratory

204.02D – Examining the Potential of LSST to Contribute to Exoplanet Discovery

The Large Synoptic Survey Telescope (LSST), currently under construction in Chile with scheduled first light in 2019, will be one of the major sources of data in the next decade and is one of the top priorities expressed in the last Decadal Survey. As LSST is intended to cover a range of science questions, and so the LSST community is still working on optimizing the observing strategy of the survey. With a survey area that will cover half the sky in 6 bands providing photometric data on billions of stars from 16th to 24th magnitude, LSST has the ability to be leveraged to help contribute to exoplanet science. In particular, LSST has the potential to detect exoplanets around stellar populations that are not normally usually included in transiting exoplanet searches. This includes searching for exoplanets around red and white dwarfs and stars in the galactic plane and bulge, stellar clusters, and potentially even the Magellanic Clouds. In probing these varied stellar populations, relative exoplanet frequency can be examined, and in turn, LSST may be able to provide fresh insight into how stellar environment can play a role in planetary formation rates.

Our initial work on this project has been to demonstrate that even with the limitations of the LSST cadence, exoplanets would be recoverable and detectable in the LSST photometry, and to show that exoplanets indeed worth including in discussions of variable sources that LSST can contribute to. We have continued to expand this work to examine exoplanets around stars in belonging to various stellar populations, both to show the types of systems that LSST is capable of discovering, and to determine the potential exoplanet yields using standard algorithms that have already been implemented in transiting exoplanet searches, as well as how changes to LSST's observing schedule may impact both of these results.

Author(s): Michael B Lund², Joshua Pepper¹, Savannah Jacklin², Keivan G Stassun²

Institution(s): 1. Lehigh University, 2. Vanderbilt University

204.03 – Occurrence of giant planets around stars with dusty debris disks

Debris disks may be the signposts of recent planet formation. The dust, which is generated in collisional cascades of asteroids and comets, is enhanced by the gravitational stirring of gas giant planets. Thus bright debris disk systems are natural targets for imaging searches for planets, as it indicates that the host star likely possesses some kind of planetary system. In this work, we describe a joint high contrast imaging survey for planetary mass companions at Keck and VLT of the last significant sample of debris disks identified by the Spitzer Space Telescope. No new substellar companions were discovered in our survey of Spitzer-selected targets. We combine these observations with from three published surveys, to put constraints on the frequency of planets around debris disk stars in the largest sample to date. We also obtained published data on stars that do not show infrared excesses for a control sample. We assume a double power law distribution of the form $f(m,a) = C m^\alpha a^\beta$ for this population of companions. We find that the frequency of giant planets with masses 5-20 MJup and separations 10-1000 au around stars with debris disks is 6.3% (68% confidence interval 3.7-9.8%), compared to 0.7% (68% confidence interval 0.2-1.8%) for the control sample of stars without disks. For the first time, we show that the occurrence of young giant planets around stars with

debris disks is higher than those without debris disks at the 88% confidence level, tentatively suggesting that these distributions are distinct.

Author(s): Tiffany Meshkat¹, Dimitri Mawet¹, Marta Bryan¹, Sasha Hinkley⁶, Brendan Bowler⁷, Karl Stapelfeldt³, Konstantin Batygin¹, Deborah Padgett³, Farisa Morales³, Eugene Serabyn³, Valentin Christiaens⁵, Timothy Brandt⁴, Zahed Wahhaj²

Institution(s): 1. Caltech, 2. European Southern Observatory, 3. Jet Propulsion Laboratory, 4. Princeton, 5. Universidad de Chile, 6. University of Exeter, 7. University of Texas at Austin

204.04 – The Kepler and K2 Near-Infrared Transit Survey (KNITS)

NASA's Kepler mission discovered a plethora of transiting exoplanets after observing a single region of the Galaxy for four years. After a second reaction wheel failed, NASA's Kepler spacecraft was repurposed as K2 to observe different fields along the ecliptic in ~80 day campaigns. To date, K2 has discovered ~130 exoplanets along with another ~400 candidates. The exoplanets that have been confirmed or validated from Kepler and K2 have been primarily subject to spectroscopic observations, high-resolution imaging, or statistical methods. However, most of these, along with all the remaining candidate exoplanets, have had no follow-up transit photometry. In addition, recent studies have shown that for single-planet systems, statistical validation alone can be unreliable and additional follow-up observations are required to reveal the true nature of the system. I will present the latest results from an ongoing program to use the 3.5-meter WIYN telescope at Kitt Peak National Observatory for near-infrared transit photometry of Kepler and K2 exoplanets and candidates. Our program of high-precision, high-cadence, high-spatial-resolution near-infrared transit photometry is providing new measurements of the transit ephemerides and planetary radii as well as weeding out false positives lurking within the candidate lists. To date, 25 K2 and 5 Kepler targets have been observed with WIYN. I will also describe upcoming observations with WIYN that will take place in January 2018 as part of a campaign to observe exoplanet transits in the near-infrared simultaneously with the Kepler spacecraft during K2 Campaign 16. Our program ultimately provides a vetted sample of exoplanets that could be targeted in the future by NASA's James Webb Space Telescope (JWST) and also demonstrates WIYN's capabilities for observations of exoplanets to be discovered by NASA's all-sky Transiting Exoplanet Survey Satellite (TESS).

Data presented herein were obtained at the WIYN Observatory from telescope time allocated to NN-EXPLORE through the scientific partnership of the National Aeronautics and Space Administration, the National Science Foundation, and the National Optical Astronomy Observatory.

Author(s): Knicole Colon³, Joseph E. Rodriguez¹, Geert Barentsen², Jose Vinicius de Miranda Cardoso², Andrew Vanderburg⁴

Institution(s): 1. Harvard-Smithsonian Center for Astrophysics, 2. NASA Ames Research Center, 3. NASA Goddard Space Flight Center, 4. University of Texas at Austin

204.05 – Fast cadence planet-searches with the all-sky, gigapixel-scale Evryscope

The Evryscope is a 24-camera robotic telescope that continuously images 8,000 square degrees in 2-minute exposures, that has been collecting data continuously since deployment to CTIO in mid-2015. The telescope provides the fast cadence observations necessary for detecting minute to tens-of-minute time-scale exoplanet transits, which would occur around small, compact host stars including White Dwarfs and Hot Subdwarfs. We are conducting target surveys for each of these types of stars searching for potential planet transit signals. Our surveys will be the largest performed to date with several thousand targets in each group and years of observations, and the only surveys with minute-scale cadence. We present the status of the surveys, our

estimated detection ability, interesting candidates, and preliminary results.

Author(s): Jeff Ratzloff¹, Nicholas Law¹
Institution(s): 1. UNC Chapel Hill

204.06 – Constraining the Population of Small Close-in Planets Around Evolved Intermediate Mass Stars

Intermediate mass stars ($> 1.3 M_{\text{Sun}}$) have high occurrence rates of Jupiter mass planets in predominately long period orbits (~ 1.0 AU). There is a prominent planet gap, known as the 'Planet Desert', for low mass planets (Super-Earth, Neptune) < 0.5 AU from subgiants, the evolved counterpart to intermediate mass stars. Thus far, using current radial velocity methods, we have not been able to detect short period planets around subgiants due to noise from p-mode oscillations perhaps mimicking radial velocity signals (~ 5 m/s) in this planetary regime. Here we present techniques and preliminary results with regards to finding low mass, short period planets around subgiants and its implications for the Planet Desert.

Author(s): Amber Medina¹, John Asher Johnson¹
Institution(s): 1. Harvard Smithsonian Center for Astrophysics

201.07 – Hubble Observations of the Exomoon Candidate Kepler-1625b I

The exomoon candidate Kepler-1625b I was identified by the Hunt for Exomoons with Kepler (HEK) collaboration in August 2016 following an extensive program to characterize the occurrence rate of exomoons. Follow-up observations of the candidate for the purpose of validating the existence of the moon and constraining its properties were carried out on the Hubble Space Telescope on October 28th-29th 2017, using slitless spectroscopy on Wide Field Camera 3. We report preliminary results of that observation.

205 – AGN, QSO, Blazars III

205.01 – Polarization Observations of the Fermi blazars

Ever since the revolutionary discovery by the Fermi mission that active galactic nuclei (AGN) produce copious amounts of high-energy emission, its origin has remained elusive. Using high-frequency radio interferometry (VLBI) polarization imaging, we could probe the magnetic field topology of the compact high-energy emission regions in blazars. A case study for blazar 3C 279 reveals presence of multiple gamma-ray emission regions. The observed anti-correlation between gamma-ray flux and percentage polarization at optical bands challenges the current high-energy emission models. In addition to the turbulent component responsible for gamma-ray flares, our analysis suggests the presence of a steady polarized component having with its polarization direction aligned along the jet axis. The steady polarized component could possibly be the toroidal component of the helical magnetic field. To better understand the acceleration processes in jets, high-energy polarization missions are of great importance.

Author(s): Bindu Rani¹
Institution(s): 1. NASA GSFC
Contributing team(s): S. Jorstad, A. P. Marscher (BU, USA), K. Sokolovsky (IAASARS, Greece), I. Agudo (CSIC, Spain)

205.02 – Effects of Magnetic Field Geometry on the Broadband Emission of Blazars

The knowledge of the structure of the magnetic field inside a blazar jet, as deduced from polarization observations at radio to optical

Author(s): Alexander Teachey¹, David Kipping¹, Guillermo Torres⁴, Gaspar A Bakos³, David Nesvorný⁵, Lars Buchhave⁶, Chelsea Xu Huang², Joel D Hartman³
Institution(s): 1. Columbia University, 2. Dunlap Institute, University of Toronto, 3. Princeton University, 4. Smithsonian Institution Astrophysical Observatory, 5. Southwest Research Institute, 6. University of Copenhagen, Niels Bohr Institute

201.08 – Project Blue: Optical Coronagraphic Imaging Search for Terrestrial-class Exoplanets in Alpha Centauri

Project Blue is a coronagraphic imaging space telescope mission designed to search for habitable worlds orbiting the nearest Sun-like stars in the Alpha Centauri system. With a 45-50 cm baseline primary mirror size, Project Blue will perform a reconnaissance of the habitable zones of Alpha Centauri A and B in blue light and one or two longer wavelength bands to determine the hue of any planets discovered. Light passing through the off-axis telescope feeds into a coronagraphic instrument that forms the heart of the mission. Various coronagraph designs are being considered, such as phase induced amplitude apodization (PIAA), vector vortex, etc. Differential orbital image processing techniques will be employed to analyze the data for faint planets embedded in the residual glare of the parent star. Project Blue will advance our knowledge about the presence or absence of terrestrial-class exoplanets in the habitable zones and measure the brightness of zodiacal dust around each star, which will aid future missions in planning their observational surveys of exoplanets. It also provides on-orbit demonstration of high-contrast coronagraphic imaging technologies and techniques that will be useful for planning and implementing future space missions by NASA and other space agencies. We present an overview of the science goals, mission concept and development schedule. As part of our cooperative agreement with NASA, the Project Blue team intends to make the data available in a publicly accessible archive.

Author(s): Jon Morse¹
Institution(s): 1. BoldlyGo Institute
Contributing team(s): Project Blue team

wavelengths, is closely related to the formation and propagation of relativistic jets that result from accretion onto supermassive black holes. However, a largely unexplored aspect of the theoretical understanding of radiation transfer physics in blazar jets has been the magnetic field geometry as revealed by the polarized emission and the connection between the variability in polarization and flux across the spectrum.

Here, we explore the effects of various magnetic geometries that can exist inside a blazar jet: parallel, transverse, oblique, toroidal, helical, and tangled. We investigate the effects of changing the orientation of the magnetic field, according to the above-mentioned geometries, on the resulting high-energy spectral energy distributions (SEDs) and spectral variability patterns (SVPs) of a typical blazar. We use the MUlti-ZOne Radiation Feedback (MUZORF) model to carry out this study and to relate the geometry of the field to the observed SEDs. One of the goals of the study is to address the issue of the reason for the appearance of some of the gamma-ray "orphan flares" observed in a few blazars. This can be associated with the directionality of the magnetic field, which creates a difference in the radiation field as seen by an observer versus that seen by the electrons in the emission region.

This research was supported in part by NASA through Fermi grants NNX10AO59G, NNX08AV65G, and NNX08AV61G, NASA through Swift grants NNX09AR11G, NNX10AL13G, and NNX10AF88G, and by NSF grant AST-0907893.

Author(s): Manasvita Joshi¹, Alan Marscher¹, Markus Boettcher²

Institution(s): 1. Boston University, 2. North West University

205.03D – Modeling Blazar Spectra by Solving an Electron Transport Equation

Blazars are luminous active galaxies across the entire electromagnetic spectrum, but the spectral formation mechanisms, especially the particle acceleration, in these sources are not well understood. We develop a new theoretical model for simulating blazar spectra using a self-consistent electron number distribution. Specifically, we solve the particle transport equation considering shock acceleration, adiabatic expansion, stochastic acceleration due to MHD waves, Bohm diffusive particle escape, synchrotron radiation, and Compton radiation, where we implement the full Compton cross-section for seed photons from the accretion disk, the dust torus, and 26 individual broad lines. We used a modified Runge-Kutta method to solve the 2nd order equation, including development of a new mathematical method for normalizing stiff steady-state ordinary differential equations. We show that our self-consistent, transport-based blazar model can qualitatively fit the IR through *Fermi* g-ray data for 3C 279, with a single-zone, leptonic configuration. We use the solution for the electron distribution to calculate multi-wavelength SED spectra for 3C 279. We calculate the particle and magnetic field energy densities, which suggest that the emitting region is not always in equipartition (a common assumption), but sometimes matter dominated. The stratified broad line region (based on ratios in quasar reverberation mapping, and thus adding no free parameters) improves our estimate of the location of the emitting region, increasing it by ~5x. Our model provides a novel view into the physics at play in blazar jets, especially the relative strength of the shock and stochastic acceleration, where our model is well suited to distinguish between these processes, and we find that the latter tends to dominate.

Author(s): Tiffany Lewis¹, Justin Finke², Peter A. Becker¹

Institution(s): 1. George Mason University, 2. Naval Research Laboratory

205.04 – Characteristic Variability Timescales in the Gamma-ray Power Spectra of Blazars

We study the gamma-ray variability of 13 bright blazars observed with the Fermi Large Area Telescope in the 0.2-300 MeV band over 7.8 years.

We find that continuous-time autoregressive moving average

206 – Multimessenger Astronomy in light of LIGO-Virgo Discoveries

address over this time frame? What are the main challenges? How did this picture change with the multimessenger discovery of the binary neutron star merger GW170817? The 2018 AAS Winter meeting is well-timed to take stock of the opportunities the future holds for the broad astronomical community. The Special Session adopts a panel format, and includes three panel discussions with leaders of gravitational wave, electromagnetic and astroparticle/neutrino observational efforts. Panel I: Gravitational wave observations and facilities Panelists: Barry Barish (Caltech), Marica Branchesi (Urbino), Jocelyn Read (Fullerton), Leo Singer (NASA) Panel II: Electromagnetic observations Panelists: Philip Cowperthwaite (Harvard), Wen-fai Fong (Arizona), Raffaella Margutti (Northwestern) and Brian Metzger (Columbia) Panel III: High-energy

207 – Exoplanet Characterization Through Emission Spectroscopy: A Roadmap To Detecting Biosignatures

In recent years, the most prominent form of exoplanet atmospheric characterization has been the transmission spectroscopy technique. However, successfully unraveling the composition of a given planet with this method relies critically on the lack of obscuring aerosols that often dampen the strength of molecular features. Emission spectroscopy measures photons directly emanating from a planet's dayside and, thus, the detection of molecular absorption features is less impacted by the presence of aerosols. Furthermore, this technique provides

(CARMA) models provide adequate fits to the blazar light curves, and using the models we constrain the power spectral density (PSD) of each source.

We also perform simulations to test the ability of CARMA modeling to recover the PSDs of artificial light curves with our data quality.

Seven sources show evidence for a low-frequency break at an average timescale of ~1 year, with five of these sources showing evidence for an additional high-frequency break at an average timescale of ~7 days.

We compare our results to previous studies, and discuss the possible physical interpretations of our results.

Author(s): James Lee Ryan², Aneta Siemiginowska¹,

Malgorzata Sobolewska¹, Jonathan E Grindlay¹

Institution(s): 1. Harvard Smithsonian Center for Astrophysics, 2. UCLA

205.05 – X-ray Reverberation Mapping in Active Galactic Nuclei

Active Galactic Nuclei can produce as much or more electromagnetic and kinetic luminosities than the combined stellar luminosity of an entire galaxy. The energy output from AGN comes from the gravitational potential energy of the infalling material and the rotational energy of the black hole, both of which are released very close to the black hole. Therefore, probing the relativistic region of the inner accretion flow is essential to understanding how AGN work and effect their environments. In this talk, I will present a new technique for probing these relativistic environments: X-ray reverberation mapping. Similar to Optical reverberation mapping, where time delays of days or weeks between the continuum and Broad Line Region lines map out centiparsec scales, X-ray reverberation reveals time delays of tens of seconds, which map out microparsec scales in the accretion flow—well beyond the spatial resolution power of any instrument. This technique has been discovered in the past decade, so I will give a brief overview of how the measurements are made, and highlight some recent discoveries, which allow us to map the gas falling on to the black hole and measure the effects of strongly curved spacetime close to the event horizon.

Author(s): Erin Kara¹

Institution(s): 1. University of Maryland

astroparticle/neutrino observations Panelists: Chad Finley (Stockholm), Francis Halzen (UW Madison), Kara Hoffman (Maryland)

– **Panel I: Gravitational wave observations and facilities**

– **Panel II: Electromagnetic observations**

– **Panel III: High-energy astroparticle/neutrino observations**

constraints on a planet's thermal profile. In this session, speakers will present the latest theoretical models and emission spectroscopy and photometry results from current space-based telescopes (including HST and Spitzer) with an emphasis on discussing the big open questions that will allow us to take the crucial next steps in our understanding of exoplanet atmospheres. Looking forward to JWST and other potential future space-based missions, the goal is to stimulate new lines of discussion that focus on the development of new observational and modeling

strategies that will be necessary as we push towards smaller and cooler exoplanets and, ultimately, search for biosignatures in potentially-habitable worlds.

207.01 – A Statistical Approach to Exoplanetary Molecular Spectroscopy Using Spitzer Eclipses

Secondary eclipses of exoplanets observed using the Spitzer Space Telescope measure the total emission emergent from exoplanetary atmospheres integrated over broad photometric bands. Spitzer photometry is excellent for measuring day side temperatures, but is less well suited to the detection of molecular absorption or emission features. Even for very hot exoplanets, it can be difficult to attain the accuracy on eclipse depth that is needed to unambiguously interpret the Spitzer results in terms of molecular absorption or emission. However, a statistical approach, wherein we seek deviations from a simple blackbody planet as a function of the planet's equilibrium temperature, shows promise for defining the nature and strength of molecular absorption in ensembles of planets. In this paper, we explore such an approach using secondary eclipses observed for tens of hot exoplanets during Spitzer's Cycles 10, 12, and 13. We focus on the possibility that the hottest planets exhibit molecular features in emission, due to temperature inversions.

Author(s): Drake Deming⁴, Emily Garhart⁴, Adam Burrows², Jonathan Fortney³, Heather Knutson¹, Kamen Todorov⁵

Institution(s): 1. Caltech, 2. Princeton University, 3. UC Santa Cruz, 4. Univ. of Maryland, 5. University of Amsterdam

207.02 – Beyond hot Jupiters: Characterizing exoplanets below 1000 K with Spitzer and JWST emission spectroscopy

Most thermal emission spectra of exoplanets to date have been obtained for the hot Jupiters with equilibrium temperatures above ~1500K due to their favorable eclipse depth in the NIR. Emission spectroscopy of colder planets, however, provides us with the important opportunity to understand cloud formation and atmospheric chemistry near the CH₄/CO transition. In this talk, we will demonstrate JWST's unique capabilities for these planets and discuss results from our ongoing Spitzer effort to study warm Neptunes and Jupiters.

Author(s): Björn Benneke¹

Institution(s): 1. Université de Montréal

Contributing team(s): Université de Montréal, Caltech, University of Arizona, Space Science Institute, UCSC, Harvard University

207.03 – Prospects for Detecting Thermal Emission from Terrestrial Exoplanets with JWST

A plethora of nearby, terrestrial exoplanets has been discovered recently by ground-based surveys. Excitingly, some of these are in the habitable zones of their host stars, and may be hospitable for life. However, all the planets orbit small, cool stars and have considerably different irradiation environments from the Earth, making them vulnerable to atmospheric escape, erosion and collapse. Atmosphere characterization is therefore critical to assessing the planets' habitability. I will discuss possible JWST thermal emission measurements to determine the atmospheric properties of nearby terrestrial planets. I will focus on prospects for detecting physically motivated atmospheres for planets orbiting LHS 1140, GJ 1132, and TRAPPIST-1. I will also discuss the potential for using phase curve observations to determine whether an atmosphere has survived on the non-transiting planet Proxima b.

Author(s): Laura Kreidberg¹

Institution(s): 1. Harvard University

207.04 – Optimal Strategies for Probing Terrestrial Exoplanet Atmospheres with JWST

It is imperative that the exoplanet community determines the feasibility and the resources needed to yield high fidelity

atmospheric compositions from terrestrial exoplanets. In particular, LHS 1140b and the TRAPPIST-1 system, already slated for observations by JWST's Guaranteed Time Observers, will be the first two terrestrial planets observed by JWST. I will discuss optimal observing strategies for observing these two systems, focusing on the NIRSpec Prism (1-5 μ m) and the combination of NIRISS SOSS (1-2.7 μ m) and NIRSpec G395H (3-5 μ m). I will also introduce currently unsupported JWST readmodes that have the potential to greatly increase the precision on our atmospheric spectra. Lastly, I will use information content theory to compute the expected confidence interval on the retrieved abundances of key molecular species and temperature profiles as a function of JWST observing cycles.

Author(s): Natasha E Batalha², Nikole K. Lewis², Michael Line¹

Institution(s): 1. Arizona State University, 2. Space Telescope Science Institute

207.05 – Thermal emission measurements with FINESSE in the era of JWST

FINESSE (Fast Infrared Exoplanet Spectroscopy Survey Explorer) is a candidate Medium-Class Explorer (MIDEX) mission dedicated to performing a statistical census of transiting exoplanet atmospheres. The objectives of FINESSE are to test theories of planetary origins and climate, enable comparative planetology, and open up discovery space on atmospheric chemistry, planetary evolution, and other topics. The baseline design for FINESSE is a 75 cm telescope observing from L2. The FINESSE instrument is a high throughput spectrometer with continuous coverage from 0.5 to 5.0 microns in a single shot. FINESSE will survey on order of 1000 exoplanets with a combination of transmission, dayside emission, and phase-resolved emission spectroscopy during a two year mission. FINESSE is currently being developed as part of a Phase A concept study. I will present an overview of FINESSE with a particular emphasis on the thermal emission measurements and their importance in the era of JWST.

Author(s): Jacob Bean¹

Institution(s): 1. University of Chicago

Contributing team(s): FINESSE Science Team

207.06 – Transit Spectroscopy of Biosignature Gases: Prospects and Challenges

Transit spectroscopy should provide astronomers with their first opportunities to search for signs of life on exoplanets: first with JWST, then with ground-based extremely large telescopes, and eventually with purpose-designed missions such as the Origins Space Telescope. However, given this exciting opportunity, there are challenges to observing these signatures. The transit observation technique will carry observational biases towards planets orbiting cool (M-type) stars. These planets have challenges for habitability, including the potential for tidal locking and for planetary atmospheres to be lost to high-energy radiation from the host star. These observations will also have a bias towards spectral information from the uppermost of planetary atmospheres, where strictly abiotic photochemical processes can efficiently produce some biosignature gases, in particular as oxygen and ozone. Here, we will discuss these challenges, and how future missions/telescopes can account for them in their instrument design and observation strategies. We will also discuss how, even if some of the concerns above are warranted, such observations are justified astrobiological explorations of rocky planets around other stars.

Author(s): Shawn David Domagal-Goldman¹, Giada Arney¹, Victoria Meadows²

Institution(s): 1. NASA Goddard Space Flight Center, 2. University of Washington

Contributing team(s): Virtual Planetary Laboratory, Sellers Exoplanet Environments Collaboration

207.07 – Characterizing Exoplanet Habitability with Emission Spectroscopy

Results from NASA's *Kepler* mission and other recent exoplanet surveys have demonstrated that potentially habitable exoplanets are relatively common, especially in the case of low-mass stellar hosts. The next key question that must be addressed for such planets is whether or not these worlds are *actually* habitable, implying they could sustain surface liquid water. Only through investigations of the potential habitability of exoplanets and through searches for biosignatures from these planets will we be able to understand if the emergence of life is a common phenomenon in our galaxy. Emission spectroscopy for transiting exoplanets (sometimes called secondary eclipse spectroscopy) is a powerful technique that future missions will use to study the atmospheres and surfaces of worlds orbiting in the habitable zones of nearby, low-mass stars. Emission observations that span the mid-infrared wavelength range for potentially habitable exoplanets provide opportunities to detect key habitability and life signatures, and also allow observers to probe atmospheric and surface temperatures. This presentation will outline the case for using emission spectroscopy to understand if an exoplanet can sustain surface liquid water, which is believed to be a critical precursor to the origin of life.

Author(s): Tyler Robinson¹

Institution(s): 1. Northern Arizona University

207.08 – Detecting Atmospheric Biosignatures of Transiting Exoplanets in the Mid-IR

For the first time in human history, our generation will have the technology needed to answer one of the longest-standing questions: "Are we alone?" Only recently have planet-hunting programs (such as TRAPPIST, MEarth, and Kepler) confirmed the first Earth analogues orbiting M dwarfs. However, it is unknown whether planets orbiting the most ubiquitous stars in

208 – HAD V: Genealogy, History, and Technology

208.01 – AstroGen: A Progress Report

Since early 2014 a small group of volunteers has been compiling the world's astronomy-related doctoral dissertations. Working almost entirely with data available online, we have now listed more than 24,000 such theses, including nearly complete coverage of 21 countries: the United States (14,183), United Kingdom (3699), Spain (1091), Netherlands (982), Canada (872), Australia (738), Sweden (375), Greece (239), Argentina (182), Finland (165), Denmark (110), Ireland (103), South Africa (97), New Zealand (87), Norway (79), Chile (42), Iran (25), Mauritius (5), Iceland (3), Pakistan (2), and Ethiopia (1). These numbers are as of mid-September 2017 and subject to revision. For each country we go back to the beginning of the modern Ph.D. or equivalent. Fully half of the doctorates have been earned since 1999. For each thesis we try to include the author (with links to a website or obituary), awarding institution, year of degree, thesis title, link to the thesis if online (about 64% are), translation of title if necessary, advisor(s), and other mentors.

Our goal is to emulate the Mathematics Genealogy Project (MGP: <http://www.genealogy.ams.org/>) with a website having a page for each person with links to that person's advisor(s) and students, if any. We will also have a page for each university. We have posted some introductory material on the website (<https://astrogen.aas.org/>), and are waiting for help from the AAS IT department to convert our data, currently in spreadsheets, to a database and then a website. We expect this to occur in early 2018.

I will present some summaries of our results to date and conduct a discussion of how we can expand our database. We have people currently working on France, Russia, and India, but we need volunteers with linguistic ability and, preferably, familiarity with the academic cultures, to take on Germany, Italy, and nearly all the countries of Asia.

our galaxy can support life. I will discuss the challenges and opportunities of looking for biosignatures in transiting exoplanet atmospheres at mid-infrared wavelengths and argue that the only way to ascertain the truth is to make a measurement. I will also present how a survey of nearby mid-to-late M dwarfs could empirically determine the fraction of habitable-zone planets that develop life.

Author(s): Kevin Stevenson¹

Institution(s): 1. Space Telescope Science Institute

207.09 – Using thermal phase curves to probe the climate of potentially habitable planets

Thermal phase-curve observations probe the variation in emitted flux of a planet with phase, or longitude. When conducted spectroscopically, they allow us to probe the two-dimensional temperature structure in both longitude and altitude, which directly relate to the planet's circulation and chemistry. In the case of small, potentially habitable exoplanets, spectroscopic phase-curve observations can provide us with direct evidence that the planet is capable of sustaining liquid water from measurements of its brightness temperature, and allow us to distinguish between a 'airless' body and one that has an appreciable atmosphere. In this talk I will summarize efforts to characterize exoplanets smaller than Neptune with phase-curve observations and emission spectroscopy using the Spitzer and Hubble Space Telescopes. I will then discuss how these 'lessons learned' can be applied to future efforts to characterize potentially habitable planets with phase-curve observations using JWST and future facilities such as the Origins Space Telescope (OST).

Author(s): Tiffany Kataria¹

Institution(s): 1. JPL/Caltech

Author(s): Joseph S. Tenn¹

Institution(s): 1. Sonoma State University

Contributing team(s): The AstroGen Team

208.02 – Mighty Oaks from Little Acorns Grow

In 1935 John Stanley Plaskett (and his colleague Joseph Pearce) established that the Milky Way is a mass of 165 billion stars and interstellar material rotating about a centre 10 000 parsecs away in Sagittarius—a model that held in its broad details for the rest of the twentieth century. This brief presentation will explore the great uncertainties in the mass and size of the Galaxy in the prior decade and how small but timely suggestions from Kapteyn and Schlesinger as well as contact with Oort proved to be fruitful in producing Plaskett's robust results.

Author(s): Peter Broughton¹

Institution(s): 1. Retired

208.03 – The Observatory as Laboratory: Spectral Analysis at Mount Wilson Observatory

This paper will discuss the seminal changes in astronomical research practices made at the Mount Wilson Observatory in the early twentieth century by George Ellery Hale and his staff. Hale's desire to set the agenda for solar and stellar astronomical research is often described in terms of his new telescopes, primarily the solar tower observatories and the 60- and 100-inch telescopes on Mount Wilson. This paper will focus more on the ancillary but no less critical parts of Hale's research mission: the establishment of associated "physical" laboratories as part of the observatory complex where observational spectral data could be quickly compared with spectra obtained using specialized laboratory equipment. Hale built a spectroscopic laboratory on the mountain and a more elaborate physical laboratory in Pasadena and staffed it with highly trained physicists, not classically trained astronomers. The success of Hale's vision for

an astronomical observatory quickly made the Carnegie Institution's Mount Wilson Observatory one of the most important astrophysical research centers in the world.

Author(s): Ronald Brashear¹

Institution(s): 1. *Chemical Heritage Foundation*

208.04 –

All Over the World: Mid-Twentieth Century Radio Astronomy and the Origin of the International SETI Network

Cold War mythology is rife with stories about secrecy, competition, espionage, and animosity. Yet the history behind the myth-- the overlooked scientists collaborating outside of the aims of the state-- also tells an interesting story. This paper examines the challenges of international scientific collaboration during the Cold War, focusing especially on a case study concerning Soviet radio astronomer Iosif Samuilovich Shklovskii and U.S. astrophysicist Carl Sagan, and their collaborative work on the search for extraterrestrial intelligence (SETI). Despite the hyper-politics that instigated and fueled the Space Race, SETI was held up as an ideal internationalist science, with the lofty goal of uniting all of humanity by situating it within a cosmic community. Although the internationalism of SETI discourse is not entirely unfounded due to its roots in international collaboration, further research indicates that such internationalism was in reality instilled with geopolitics, international conflict, and even espionage. That said, however, the cultural and philosophical perspectives of individual SETI scientists led them to operate within the tensions between national and ideological restraints and their own personal philosophical perspectives. In reviewing the letters of correspondence, conference proceedings, interviews, transcripts of lectures, and autobiographical writings of early-

209 – Supernovae I

209.02D –

Impact of Stellar Convection Criteria on the Nucleosynthetic Yields of Population III Supernovae.

A grid of 15-80 solar mass $Z=0$ stellar models are evolved to pre-core collapse using the stellar evolution code BRAHAMA. Each initial zero-age main sequence mass model star is evolved with two different convection criteria, Ledoux and Schwarzschild. The choice of convection produces significant changes in the evolutionary model tracks on the HR diagram, mass loss, and interior core and envelope structures. At onset of core collapse, a SNe explosion is initiated using a one-dimensional radiation-hydrodynamics code and followed for 400 days. The explosion energy is varied between 1-10 foe depending on the model as there are no observationally determined energies for population III supernovae. Due to structure differences, the Schwarzschild models resemble Type II-P SNe in their lightcurve while the Ledoux models resemble SN1987a, a Type IIpec. The nucleosynthesis is calculated using TORCH, a 3,208 isotope network, in a post process method using the hydrodynamic history. The Ledoux models have, on average, higher yields for elements above Fe compared to the Schwarzschild. Using a Salpeter IMF and other recently published population III IMF's, the net integrated yields per solar mass are calculated and compared to published theoretical results and to published observations of extremely metal poor halo stars of $[Fe/H] < -3$. Preliminary results show the lower mass models of both criteria show similar trends to the extremely metal poor halo stars but more work and analysis is required.

Author(s): Jacob Teffs², Tim Young², Tim Lawlor¹

Institution(s): 1. *Penn State Brandywine*, 2. *University of North Dakota*

209.03 – Near-infrared SN Ia Cosmology

Observations of SN Ia in the near infrared (NIR) are a promising way to construct an accurate cosmic expansion history to

SETI radio astronomers, this paper ultimately argues that, although SETI was not the ideal internationalist science it was portrayed as, SETI pioneers were able to connect and form international networks within a contentious system which often centred on the restriction of free information and international collaboration through their mutual unconventional scientific interests, and facilitated by their personal utopian futurist philosophies.

Author(s): Rebecca Charbonneau¹

Institution(s): 1. *University of Oxford*

208.05 – Advanced Technologies and Instrumentation at the National Science Foundation

Over its more than thirty-year history, the Advanced Technologies and Instrumentation (ATI) program within the Division of Astronomical Sciences has provided grants to support the development and deployment of detectors and instrumentation for ground-based astronomy. This program has enabled scientific advances in diverse fields from solar physics to exoplanets to cosmology. ATI has provided instrumentation for both small and large observatories from radio through visible wavebands. It has played a role in the early development of major initiatives such as the Large Synoptic Survey Telescope. Technology development for astronomy unfolds over a longer period than the lifetime of a single grant. This review will consider ATI from an historical perspective to assess its impact on astronomy.

Author(s): Peter Kurczynski¹, James E. Neff¹

Institution(s): 1. *National Science Foundation*

constrain the properties of dark energy. SN Ia are more nearly standard candles in NIR than in optical bands, while dust absorption is less of a problem at NIR wavelengths. This allows us to investigate the dark energy properties in a way that is less sensitive to systematic errors due to the variations in the intrinsic brightness of SN Ia or the properties of dust in their host galaxies. In this talk, I present preliminary results from our RAISIN 1 (HST GO-13046) and RAISIN 2 (HST GO-14216) programs with the Hubble Space Telescope, where we have constructed a Hubble diagram combining optical + NIR photometric data using a sample of low and high redshift SN Ia. I will discuss our current results, challenges, and the advantage of using optical + NIR data to derive accurate cosmic distances and improve knowledge of the dark energy equation of state. This research is supported by NSF grants AST-156854 and AST-1211196.

Author(s): Arturo Avelino², Robert Kirshner¹, Kaisey

Mandel⁴, Peter Challis², Andrew Friedman³

Institution(s): 1. *Gordon and Betty Moore Foundation*, 2. *Harvard University*, 3. *University of California, San Diego*, 4. *University of Cambridge*

Contributing team(s): RAISIN Team

209.04 – Finale of a Quartet: Hints on Supernova Formation

The origin of Type Ia Supernovae (SNe) is not well understood. Two most popular hypotheses are the single-degenerate scenario, where one white dwarf (WD) accretes matter from its giant companion until the Chandrasekhar limit is reached, and the double-degenerate scenario, where two WDs merge and explode. We focus on the second scenario. It has long been realized that binary WD systems normally take extremely long time to merge via gravitational waves and it is still unclear whether WD mergers can fully account for the observed SN Ia rate. Recent effort has been devoted to the effects of introducing a distant tertiary to the binary system. The standard "Kozai-Lidov" mechanism can lead to high eccentricities of the binary WDs, which could lead to direct collisions or much efficient energy dissipation. Alternatively, we investigate the long-term evolution of the

hierarchical quadruple systems, i.e. WD binary with a binary companion, which are basically unexplored, yet they should be numerous. We explore their interesting dynamics and find that the fraction of reaching high eccentricities is largely enhanced, which hints on a higher WD merger rate than predicted from triple systems with the same set of secular and non-secular effects considered. Considering the population of quadruple stellar systems, the quadruple scenario might contribute significantly to the overall rate of Ia SNe.

Author(s): Xiao Fang¹, Todd A. Thompson¹, Christopher M. Hirata¹
Institution(s): 1. *The Ohio State University*

209.05D – Probing Late-Stage Stellar Evolution through Robotic Follow-Up of Nearby Supernovae

Many of the remaining uncertainties in stellar evolution can be addressed through immediate and long-term photometry and spectroscopy of supernovae. The early light curves of thermonuclear supernovae can contain information about the nature of the binary companion to the exploding white dwarf. Spectra of core-collapse supernovae can reveal material lost by massive stars in their final months to years. Thanks to a revolution in technology—robotic telescopes, high-speed internet, machine learning—we can now routinely discover supernovae within days of explosion and obtain well-sampled follow-up data for months and years. Here I present three major results from the Global Supernova Project at Las Cumbres Observatory that take advantage of these technological advances. (1) SN 2017cbv is a Type Ia supernova discovered within a day of explosion. Early photometry shows a bump in the *U*-band relative to previously observed Type Ia light curves, possibly indicating the presence of a nondegenerate binary companion. (2) SN 2016bkv is a low-luminosity Type IIP supernova also caught very young. Narrow emission lines in the earliest spectra indicate interaction between the ejecta and a dense shell of circumstellar material, previously observed only in the brightest Type IIP supernovae. (3) Type Ibn supernovae are a rare class that interact with hydrogen-free circumstellar material. An analysis of the largest-yet sample of this class has found that their light curves are much more homogeneous and faster-evolving than their hydrogen-rich counterparts, Type IIn supernovae, but that their maximum-light spectra are more diverse.

Author(s): Griffin Hosseinzadeh¹
Institution(s): 1. *Las Cumbres Observatory*

209.06 – The Interplay of Opacities and Rotation in Promoting the Explosion of Core-Collapse Supernovae

For over five decades, the mechanism of explosion in core-collapse supernovae has been a central unsolved problem in astrophysics, challenging both our computational capabilities and our understanding of relevant physics. Current simulations often produce explosions, but they are at times underenergetic. The neutrino mechanism, wherein a fraction of emitted neutrinos is absorbed in the mantle of the star to reignite the stalled shock, remains the dominant model for reviving explosions in massive stars undergoing core collapse. We present here a diverse suite of

210 – Galaxy Formation and Evolution III

210.01 – Exploring the Origin of Kinematically Irregular Galaxies with MaNGA

Deviations from normal rotation in galaxies may have a number of potential drivers, including tidal interactions, gas inflows/outflows, spiral structure, bar/oval distortions, or other internally generated instabilities. Thanks to new massive IFU surveys like MaNGA, we can now characterize the gas and stellar kinematics of thousands of galaxies in the local universe, enabling statistical analyses on the frequency of disturbed kinematics, their origin, and their impact on their host galaxies. We present a census of kinematics in MaNGA using a modified version of the Radon transform to map radial variations in kinematic position

2D axisymmetric simulations produced by FORNAX, a highly parallelizable multidimensional supernova simulation code. We explore the effects of various corrections, including the many-body correction, to neutrino-matter opacities and the possible role of rotation in promoting explosion amongst various core-collapse progenitors.

Author(s): David Vartanyan¹, Adam Burrows¹, David Radice¹
Institution(s): 1. *Princeton University*

209.07 – The Dependence of Type Ia Supernova Luminosity on Host Galaxy Properties from a Sample without the Local-Global Difference in Star Formation

Recent studies suggest that the difference between local and global properties of galaxies might play an important role in the Type Ia supernova (SN Ia) host galaxy studies. Obtaining local spectroscopic measurements for hosts at high redshift, however, is difficult. Here we will introduce a more efficient way to infer the local properties from global galaxy measurements. We find that when the globally star-forming galaxies are restricted to a low-mass subset ($\leq 10^{10} M_{\odot}$), a sample without the local-global difference in star formation is efficiently selected. From this sample, we confirm that SNe Ia in locally star-forming environments are 0.080 ± 0.018 mag fainter (4.4σ) than those in locally passive environments. Our results are, however, statistically more significant than previous results, because of ~ 5 times larger sample across a wider redshift range. Considering the significant difference in the mean stellar population age between these environments, the result would imply a possible luminosity evolution of SNe Ia.

Author(s): Younglo Kim², Mathew Smith¹, Mark Sullivan¹, Young-Wook Lee²
Institution(s): 1. *University of Southampton*, 2. *Yonsei University*

209.08 – Kilonova Counterparts of Binary Neutron Star Mergers

The merger of a binary neutron star is accompanied by the ejection of neutron-rich matter into space at velocities up to several tenths that of light, which synthesizes rare heavy isotopes through the rapid neutron capture process (*r*-process). The radioactive decay of these nuclei was predicted by Metzger et al. (2010) to power an optical transient roughly 1000 times more luminous than a classical nova (a "kilonova"), which is among the most promising electromagnetic counterparts to accompany gravitational wave signal from the merger. I will describe how the luminosities, color, and spectra of the kilonova emission inform the properties of the merging binary (neutron star masses/radii and inclination angle) and the long sought origin of the heaviest elements in the Universe. Results will be discussed in the context of recent discoveries by Advanced LIGO/Virgo.

Author(s): Brian Metzger¹
Institution(s): 1. *Columbia University*

angles (PA). We discuss the frequency of kinematically irregular disks, and describe commonly observed patterns in radial PA profiles. In order to constrain the drivers of these kinematic signatures, we analyze how they correlate with galaxy mass, environment, star formation history, and gas-phase metallicity.

Author(s): David Vincent Stark⁴, Kevin Bundy⁹, Kyle Westfall⁹, Matthew Bershady¹³, Edmond Cheung⁴, Juan Soler³, Jarle Brinchmann⁵, Roberto Abraham¹², Dmitry Bizyaev¹, Karen Masters², Anne-Marie Weijmans¹¹, Yanmei Chen⁷, Yifei Jin⁷, Niv Drory⁶, Alexandre Roman Lopes¹⁰, David Law⁸

Institution(s): 1. Apache Point Observatory, 2. Institute of Cosmology & Gravitation, University of Portsmouth, 3. Institut d'Astrophysique Spatiale, 4. Kavli IPMU, 5. Leiden Observatory, Leiden University, 6. McDonald Observatory, The University of Texas at Austin, 7. Nanjing University, 8. Space Telescope Science Institute, 9. UCO/Lick Observatory, University of California, Santa Cruz, 10. Universidad de La Serena, 11. University of St Andrews, 12. University of Toronto, 13. University of Wisconsin-Madison

210.02D – The Lyman-alpha signature of the first galaxies

Radiation from the first stars and galaxies initiated the dramatic phase transition marking an end to the cosmic dark ages. The emission and absorption signatures from the Lyman-alpha (Ly α) transition of neutral hydrogen have been indispensable in extending the observational frontier for high-redshift galaxies into the epoch of reionization. Ly α radiative transfer provides clues about the processes leading to Ly α escape from individual galaxies and the subsequent transmission through the intergalactic medium. Cosmological simulations incorporating Ly α radiative transfer enhance our understanding of fundamental physics by supplying the inferred spectra and feedback on the gas. In this talk, I will discuss the dynamical impact of Ly α radiation pressure on galaxy formation throughout cosmic reionization with the first fully coupled Ly α radiation-hydrodynamics simulations. Based on a suite of spherically symmetric models and high-resolution ab initio cosmological simulations we find that Ly α radiation pressure is dynamically important during the assembly of direct collapse black holes (DCBHs), which may be the seeds of the first supermassive black holes in the universe. Finally, I will discuss recent advances in Ly α modeling based on current state-of-the-art simulations and observational insights.

Author(s): Aaron Smith¹

Institution(s): 1. University of Texas at Austin

210.03 – Mapping UV Properties Throughout the Cosmic Horseshoe: Lessons from VLT-MUSE

Mapping the rest-frame UV spectra of galaxies has often been problematic due to limited aperture size and poor-sensitivity. As a result, many questions concerning the outflow properties of star-forming galaxies have remained unanswered. With VLT-MUSE, such studies are now within reach for galaxies at $z=2-3$. Here we present the first spatially-resolved rest-frame UV study of the famous gravitationally lensed galaxy, the 'Cosmic Horseshoe' (J1148+1930). Our gravitational lens model shows that the system is made up of four star-forming regions, each $\sim 15-30$ kpc² in size. We define and extract four spatially exclusive regional spectra from our VLT-MUSE observations and map the interstellar and photospheric absorption lines, along with CIII] doublet emission lines, in each of these regions to investigate any variation in emission/absorption line properties. The emission line redshifts show distinct kinematical structure - with velocity offsets of 150 km/s between regions, suggestive of a merging system. Our observations reveal a range of outflow velocities across the system, with gas outflowing between $-200 < v$ (km/s) < -50 relative to the systemic velocity of that region. We do not, however, detect any variation in the star-formation rates across the system (ranging between 8-16 M \odot /yr), owing mostly to large uncertainties in reddening estimates. As such, the outflows appear to be 'global' rather than 'locally' sourced. We measure an average electron density of $N_e \sim 23,000$ cm⁻³, which again does not vary within the large uncertainties. We demonstrate that such high densities are typical when measured using with the CIII] doublet due to its large critical density. Finally, we find no change in the optical depth of the interstellar absorption lines across the system, which may be due to the absorbing gas lying far in-front of the UV emitting regions. Overall, our observations demonstrate

that either the majority of properties traced by the UV continuum do not exhibit large variations or the variations are of level so subtle that observations of much higher S/N are required. This study provides important lessons for the spatially-resolved rest-frame UV studies expected with future observatories, such as JWST.

Author(s): Bethan James³, Matthew Auger², Max Pettini², Daniel P Stark⁴, Vasily Belokurov², Stefano Carniani¹

Institution(s): 1. Cavendish Laboratories, 2. Institute of Astronomy, 3. STScI, 4. University of Arizona

210.04D – Probing galaxy growth through metallicity scaling relations over the past 12 Gyr of cosmic history

A primary goal of galaxy evolution studies is to understand the processes governing the growth of the baryonic content of galaxies over cosmic history. Observations of galaxy metallicity scaling relations and their evolution with redshift, in combination with chemical evolution models, provide unique insight into the interplay between star formation, gas accretion, and feedback/outflows. I present measurements of the stellar mass-gas phase metallicity relation and its evolution over the past 12 Gyr from $z=0$ to $z\sim 3.5$, utilizing data from the Mosfire Deep Evolution Field survey that uniquely provides rest-frame optical spectra of >1000 uniformly-selected galaxies at $z=1.3-3.8$. We find evolution towards lower metallicity at fixed stellar mass with increasing redshift that is consistent with current cosmological simulations including chemical evolution, with a large evolution of ~ 0.3 dex from $z=0$ to $z\sim 2.5$ and minor evolution of < 0.1 dex from $z\sim 2.5$ to $z\sim 3.5$. We unambiguously confirm the existence of star-formation rate dependence of the mass-metallicity relation at high redshift for the first time. A clear view of cosmic chemical evolution requires accounting for systematic biases in galaxy metallicity measurements at both low and high redshifts. We use a set of empirically-based models to correct for diffuse ionized gas contamination that biases metallicity estimates from $z=0$ global galaxy spectra. Evolving properties of ionized gas such as electron density, ionization parameter, hardness of the ionizing spectrum, and chemical abundance patterns may render locally-calibrated metallicity estimators unreliable at high redshifts. Using strong-line ratios alone, it is extremely difficult to break degenerate solutions between pure metallicity evolution and additional evolution of the ionization parameter and/or shape of the ionizing spectrum. Temperature-sensitive auroral-line measurements provide a way to directly and independently measure metallicities, breaking these degeneracies. We present measurements of auroral [OIII]4363 and direct-method metallicities at $z>2$, and discuss the potential of current and next-generation observational facilities to obtain statistical auroral-line samples at high redshifts.

Author(s): Ryan Sanders¹

Institution(s): 1. University of California, Los Angeles
Contributing team(s): The MOSDEF team

210.05 – CHILES: Resolved HI morphology and galaxy environment at $z=0.12$ and $z=0.17$

We present an HI study of galaxies in different environments from the first 178 hours of observing the COSMOS HI Large Extragalactic Survey (CHILES). CHILES is a single deep pointing with the Very Large Array (VLA) in the COSMOS field designed to resolve HI in over 300 galaxies over a continuous redshift range out to $z = 0.45$. We use the COSMOS 20k group catalogue to assign group membership, and the Discrete Persistent Structures Extractor (DisPerSE) to identify filamentary structure in two volumes at $z = 0.12$ and $z = 0.17$. We discuss our findings from testing the automated spectral line source finder, SoFiA, on CHILES data cubes. We present resolved HI total intensity maps, and discuss correlations between observed HI morphology and overall gas content with both the local environment and with the large-scale structure.

Author(s): Kelley Hess², Nick Lubert¹, Ximena Fernandez⁴, Hansung Gim⁵, Emmanuel Momjian³, Jacqueline van Gorkom¹
Institution(s): 1. Columbia University, 2. Kapteyn Astronomical Institute, 3. NRAO, 4. Rutgers University, 5. UMass Amherst
Contributing team(s): CHILES

210.06 – Figuring Out Gas in Galaxies In Enzo (FOGGIE): Resolving the Inner Circumgalactic Medium

Cosmological hydrodynamical simulations using every common numerical method have struggled to reproduce the multiphase nature of the circumgalactic medium (CGM) revealed by recent observations. However, to date, resolution in these simulations has been aimed at dense regions – the galactic disk and in-falling satellites – while the diffuse CGM never reaches comparable

211 – Extrasolar Planets III

211.01 – WASP-121b: An ultrahot gas-giant exoplanet with a stratosphere

Stratospheres are ubiquitous in the atmospheres of solar system planets, and provide crucial information about an atmosphere's chemical composition, vertical temperature structure, and energy budget. While it has been suggested that stratospheres could form in highly irradiated exoplanets, the extent to which this occurs has so far been unresolved both theoretically and observationally. Here we present secondary eclipse observations of the ultra-hot ($T_{\text{eq}} \sim 2500$ K) gas giant exoplanet WASP-121b made using HST/WFC3 in spectroscopic mode across the 1.12-1.64 micron wavelength range. The spectrum is inconsistent with an isothermal atmosphere and has spectrally-resolved water features in emission, providing a detection of an exoplanet stratosphere at 5-sigma confidence. WASP-121b is one of the standout exoplanets available for atmospheric characterization, both in transmission and emission, due to its large radius (1.8 R_{Jup}), high temperature, and bright host star ($H=9.4$ mag). As such, we will also discuss follow-up observations of WASP-121b with HST and JWST to probe the longitudinal extent of its stratosphere, and the molecular absorbers that may produce it.

Author(s): Tiffany Kataria¹, Thomas M Evans³, David Sing³, Jayesh Goyal³, Nikolay Nikolov³, Hannah R Wakeford³, Drake Deming⁴, Mark S Marley²
Institution(s): 1. JPL/Caltech, 2. NASA Ames Research Center, 3. Univ. of Exeter, 4. Univ. of Maryland
Contributing team(s): PanCET Team

211.02 – Probing Planet Formation with APOGEE: A Dichotomy in Planet Orbital-Periods and Stellar Metallicities

The Apache Point Observatory Galactic Evolution Experiment (APOGEE) is a near-infrared (1.5-1.7 microns), high resolution ($R \sim 22,500$), high S/N (>100), spectroscopic survey as part of the Sloan Digital Sky Survey (SDSS). Among the goals of this survey is multi-epoch monitoring of exoplanetary systems discovered by the Kepler mission, resulting in very high S/N (typically a few hundred) observations of Planet-hosting stars. The combined visits and sensitivity of the Sloan 2.5-meter telescope yield stellar parameters for a large number of planet-hosting systems with higher precision (e.g., $\sigma_{[\text{Fe}/\text{H}]} < 0.05$ dex), and deeper observations ($H < 14$) than many other spectroscopic surveys of similar scale. We have combined this rich dataset with orbital and planetary properties from the Kepler mission to reveal a correlation with stellar metallicity and planet orbital period in close-in ($P < 100$ days), small ($R_p < 20 R_{\text{Earth}}$) exoplanetary systems. In particular, we find that planets with orbital periods $P \leq 8.5$ days have statistically more metal-enriched hosts than planets with $P > 8.5$ days. This dichotomy implies that there may be different formation histories between these two populations. For example, there may be a protoplanetary disk inner-radius (such as the gas co-rotation radius or the dust-sublimation radius) with a metallicity-dependence at the time of planet formation that allows small, rocky planets to either form or

levels of refinement. Taking advantage of the flexible grid structure of the adaptive mesh refinement code Enzo, we force refinement in a region of the CGM of a Milky Way-like galaxy to the same spatial resolution as that of the disk. In this talk, I will present how the physical and structural distributions of the circumgalactic gas change dramatically as a function of the resolution alone. I will also show the implications these changes have for the observational properties of the gas in the context of the observations.

Author(s): Lauren Corlies¹, Molly Peeples³, Jason Tumlinson³, Brian O'Shea², Britton Smith⁴
Institution(s): 1. Johns Hopkins University, 2. Michigan State University, 3. Space Telescope Science Institute, 4. University of California, San Diego

migrate closer in to their host star in metal-rich conditions. In addition, based on previous work about the "Evaporation Valley", there is theoretical support that this critical period of 8.5 days may be tied to the bulk composition of the two exoplanet populations.

Author(s): Robert Forrest Wilson⁹, Johanna Teske⁴, Steven R Majewski⁹, Katia Cunha⁵, Verne Smith³, Diogo Souto⁵, Chad Bender⁷, Suvrath Mahadevan⁶, Nicholas Troup⁹, CARLOS ALLENDE PRIETO², Keivan G Stassun¹⁰, Michael Skrutskie⁹, ANDRES ALMEIDA⁸, Jonathan Brinkmann¹
Institution(s): 1. Apache Point Observatory, 2. Instituto de Astrofísica de Canarias, 3. National Optical Astronomy Observatory, 4. Observatories of the Carnegie Institution for Science, 5. Observatorio Nacional, Rua General Jose Cristino, 6. Pennsylvania State University, 7. Steward Observatory, University of Arizona, 8. Universidad de La Serena, 9. University of Virginia, 10. Vanderbilt University
Contributing team(s): APOGEE

211.03 – Evidence for a Dayside Thermal Inversion and High Metallicity for the Hot Jupiter WASP-18b

Hot Jupiters have been vital in revealing the structural and atmospheric diversity of gas-rich planets. Since they are exposed to extreme conditions and relatively easy to observe through transit and eclipse spectroscopy, hot Jupiters provide a window into a unique part of parameter space, allowing us to better understand both atmospheric physics and planetary structure. Additionally, constraints on the structure and composition of exoplanetary atmospheres allow us to test and generalize planetary formation models. We find evidence for a strong thermal inversion in the dayside atmosphere of the highly irradiated hot Jupiter WASP-18b ($T_{\text{eq}}=2400$ K, $M=10M_{\text{J}}$) based on Hubble Space Telescope secondary eclipse observations and *Spitzer* eclipse photometry. We report a 4.7σ detection of CO, and a non-detection of water vapor as well as all other relevant species (e.g., TiO, VO). The most probable atmospheric retrieval solution indicates a C/O ratio of 1 and an extremely high metallicity ($C/H \sim 283x$ solar). If confirmed with future observations, WASP-18b would be the first example of a planet with a non-oxide driven thermal inversion and an atmospheric metallicity inconsistent with that predicted for Jupiter-mass planets.

Author(s): Kyle Sheppard⁴, Avi M Mandell², Patrick Tamburo¹, Siddarth Gandhi³, Arazi Pinhas³, Nikku Madhusudhan³, Drake Deming⁴
Institution(s): 1. Boston University, 2. NASA GSFC, 3. University of Cambridge, 4. University of Maryland

211.04D – Gravitational Instabilities in a Young Protoplanetary Disk with Embedded Objects

Gravitational Instabilities (GIs), a mechanism for angular momentum transport, are more prominent during the early phases of protoplanetary disk evolution when the disk is relatively massive. In my dissertation work, I performed radiative 3D

hydrodynamics simulations (by employing the code, CHYMER) and extensively studied GIs by inserting different objects in the 'control disk' (a 0.14 M_{\odot} protoplanetary disk around a 1 M_{\odot} star).

Studying planetary migration helps us better constrain planet formation models. To study the migration of Jovian planets, in 9 separate simulations, each of the 0.3 MJ, 1 MJ, and 3 MJ planets was inserted near the Inner and Outer Lindblad Resonances and the Corotation Radius (CR) of the dominant GI-induced two-armed spiral density wave in the disk. I found the migration timescales to be longer in a GI-active disk when compared to laminar disks. The 3 MJ planet controls its own orbital evolution, while the migration of a 0.3 MJ planet is stochastic in nature. I defined a 'critical mass' as the mass of an arm of the dominant two-armed spiral density wave within the planet's Hill diameter. Planets above this mass control their own destiny, and planets below this mass are scattered by the disk. This critical mass could provide a recipe for predicting the migration behavior of planets in GI-active disks.

To understand the stochastic migration of low-mass planets, I performed a simulation of 240 zero-mass planet-tracers (hereafter, planets) by inserting these at a range of locations in the control disk (an equivalent of 240 simulations of Saturn-mass or lower-mass objects). I calculated a Diffusion Coefficient (3.6 AU²/1000 yr) to characterize the stochastic migration of planets. I analyzed the increase in the eccentricity dispersion and compared it with the observed exoplanet eccentricities. The diffusion of planets can be a slow process, resulting in the survival of small planetary cores. Stochastic migration of planets is dynamically similar to the radial migration of stars in the Milky Way (MW). In MW, the CR of transient spiral arms can cause radial migration of stars.

Also, to determine the effects of a companion, I studied GIs in a circumbinary disk with a 0.2 M_{\odot} brown dwarf companion.

Author(s): Karna M. Desai¹, Thomas Y Steiman-Cameron¹, Richard H Durisen¹

Institution(s): 1. Indiana University Bloomington

211.05 – Searching for polarized thermal emission from sub-stellar companions with GPI and SPHERE

Clouds are ubiquitous in the atmospheres of brown dwarfs and gas giant exoplanets, but their physical properties have proven difficult to constrain from the available photometric and spectroscopic data. Observing the linear polarization of sub-stellar objects' thermal emission, however, can give new insights into key properties such as cloud grain size distributions and structures. Here, we discuss our on-going, multi-year observing program to detect polarized thermal emission from sub-stellar companions using the Gemini Planet Imager (GPI) and Spectro-Polarimetric High-contrast Exoplanet REsearch (SPHERE). Our preliminary results indicate that these instruments are well-suited to analyzing dust particles in sub-stellar atmospheres with imaging polarimetry.

Author(s): Rebecca Jensen-Clem⁵, Max Millar-Blanchaer², Dimitri Mawet¹, James Graham⁵, Heather Knutson¹, Marshall Perrin³, Sloane Wiktorowicz⁴

Institution(s): 1. California Institute of Technology, 2. Jet Propulsion Laboratory, 3. Space Telescope Science Institute, 4. The Aerospace Corporation, 5. UC Berkeley

Contributing team(s): GPI Team

211.06 – Weird planets and odd relations: Atmospheric Circulation on Hot Jupiters

We extract phase curves from Spitzer photometry for the highly irradiated hot Jupiter WASP-33b and the unusually dense Saturn-mass planet HD 149026b. To do so, we develop a new variant of Pixel Level Decorrelation that is effective at removing intrapixel sensitivity variations for long observations (> 10 hours)

where the position of the star can vary by a significant fraction of a pixel. Using this algorithm, we derive eclipse depths, phase amplitudes, and phase offsets for both planets at 3.6 μm and 4.5 μm . We use a simple toy model to show that WASP-33b's phase offset, albedo, and heat recirculation efficiency are largely similar to those of other hot Jupiters despite its very high irradiation. On the other hand, our fits for HD 149026b prefer a very high albedo and an unusually high recirculation efficiency. We also compare our results to predictions from GCM models, and find that while neither provide a good match to the data, the discrepancies for HD 149026b are unusually large. We speculate that this may be related to its high bulk metallicity, which could lead to enhanced atmospheric opacities and the formation of reflective cloud layers in localized regions of the atmosphere. We then place these two planets in a broader context by exploring relationships between the temperatures, albedos, efficiencies, and phase offsets of all planets with published thermal phase curves. We find a striking relationship between phase offset and irradiation temperature--the former dips with temperature until around 3300 K, and rises thereafter. Although some aspects of this trend are mirrored in GCM models, there are notable differences that provide important clues for future modeling efforts.

Author(s): Michael Zhang¹, Heather Knutson¹, Tiffany

Kataria², Adam Burrows³, Jonathan Fortney⁴

Institution(s): 1. Caltech, 2. Jet Propulsion Laboratory, 3. Princeton University, 4. UCSC

211.07 – Bayesian Analysis of Hot Jupiter Radius Anomalies Points to Ohmic Dissipation

The cause of the unexpectedly large radii of hot Jupiters has been the subject of many hypotheses over the past 15 years and is one of the long-standing open issues in exoplanetary physics. In our work, we seek to examine the population of 300 hot Jupiters to identify a model that best explains their radii. Using a hierarchical Bayesian framework, we match structure evolution models to the observed giant planets' masses, radii, and ages, with a prior for bulk composition based on the mass from Thorngren et al. (2016). We consider various models for the relationship between heating efficiency (the fraction of flux absorbed into the interior) and incident flux. For the first time, we are able to derive this heating efficiency as a function of planetary T_{eq} . Models in which the heating efficiency decreases at the higher temperatures (above ~1600 K) are strongly and statistically significantly preferred. Of the published models for the radius anomaly, only the Ohmic dissipation model predicts this feature, which it explains as being the result of magnetic drag reducing atmospheric wind speeds. We interpret our results as evidence in favor of the Ohmic dissipation model.

Author(s): Daniel Thorngren¹, Jonathan Fortney¹

Institution(s): 1. University of California, Santa Cruz

211.08 – Precise Masses & Radii of the Planets Orbiting K2-3 and GJ3470

We report improved masses, radii, and densities for two planetary systems, K2-3 and GJ3470, derived from a combination of new radial velocity and transit observations. Both stars are nearby, early M dwarfs. K2-3 hosts three super-Earth planets between 1.5 and 2 Earth-radii at orbital periods between 10 and 45 days, while GJ 3470 hosts one 4 Earth-radii planet with a period of 3.3 days. Furthermore, we confirmed GJ3470's rotation period through multi-year ground-based photometry; RV analysis must account for this rotation signature. Due to the planets' low densities (all < 4.2 g/cm³) and bright host stars, they are among the best candidates for transmission spectroscopy with JWST and HST in order to characterize their atmospheric compositions.

Author(s): Molly Kosiarek⁶, Ian Crossfield³, Kevin Hardegree-Ullman⁹, John Livingston⁸, Andrew Howard¹, Benjamin Fulton¹, Lea Hirsch⁵, Howard Isaacson⁵, Erik Petigura¹, Evan Sinukoff⁷, Lauren Weiss⁴, Heather Knutson¹, Xavier Bonfils², Björn Benneke⁴, Charles Beichman¹, Courtney Dressing⁵

Institution(s): 1. *California Institute of Technology*, 2. *Institut de Planétologie et d'Astrophysique de Grenoble*, 3. *Massachusetts Institute of Technology*, 4. *Université de Montréal*, 5. *University of California, Berkeley*, 6. *University of California, Santa Cruz*, 7. *University of Hawaii, Manoa*, 8. *University of Tokyo*, 9. *University of Toledo*

212 – Milky Way and Galactic Center I

212.01 – Photometric detection of a candidate low-mass giant binary system at the Milky Way Galactic Center

We present the discovery of a new periodic variable star at the Milky Way Galactic Center (GC). This study uses laser guide-star adaptive optics data collected with the W. M. Keck 10 m telescope in the K'-band (2.2 μm) over 35 nights spanning an 11 year time baseline, and 5 nights of additional H-band (1.6 μm) data. We implemented an iterative photometric calibration and local correction technique, resulting in a photometric uncertainty of $\Delta m_{K'} \sim 0.03$ to a magnitude of $m_{K'} \sim 16$.

The periodically variable star has a 39.42 day period. We find that the star is not consistent with known periodically variable star classes in this period range with its observed color and luminosity, nor with an eclipsing binary system. The star's color and luminosity are however consistent with an ellipsoidal binary system at the GC, consisting of a K-giant and a dwarf component with an orbital period of 78.84 days. If a binary system, it represents the first detection of a low-mass giant binary system in the central half parsec of the GC. Such long-period binary systems can easily evaporate in the dense environment of the GC due to interactions with other stars. The existence and properties of a low-mass, long-period binary system can thus place valuable constraints on dynamical models of the GC environment and probe the density of the hypothesized dark cusp of stellar remnants at the GC.

Author(s): Abhimat Krishna Gautam³, Tuan Do³, Andrea Ghez³, Shoko Sakai³, Mark Morris³, Jessica Lu², Gunther Witzel³, Siyao Jia², Eric Eric Becklin³, Keith Matthews¹

Institution(s): 1. *California Institute of Technology*, 2. *University of California, Berkeley*, 3. *University of California, Los Angeles*

212.02 – The Galactograph

The Galactograph is a proposal for a dedicated facility for galactic archeology using a multi-object robotic fiber spectrograph on the 3.8 meter UKIRT telescope on Mauna Kea. With a 0.9m hyperboloid secondary mirror, a 1 degree FOV can be imaged at the cassigrain focus on an aspheric surface 0.8 meters in diameter. A DESI type robotic fiber system could have 5000 robotic fibers over the 1 degree FOV. With four dual arm spectrographs with eight 10k CCD cameras, a resolution of 10,000 from 3400 to 10000Å is possible with 0.3Å/pixel. With 30 minute exposures, 20 exp/night, 200 nights/year, a 5 year program could obtain spectra of 100 Million stars. Combined with GAIA parallaxes and proper motions, this would produce a transformative data set for galactic archaeology, stellar evolution, stellar populations and stellar evolution, galactic structure and dynamics, and near field cosmology.

Author(s): Kenneth Chambers¹

Institution(s): 1. *University of Hawaii*

212.03D – Stellar streams and the galaxies they reside in

As galaxies collide, as smaller galaxies are disrupted by larger galaxies, or as clusters of stars orbit a galaxy, a gravitational tidal interaction unfolds and the systems tear apart into distinct

morphological and kinematic structures. In my thesis, I have exploited these structures to understand various components of galaxies, such as the baryon cycle in dwarf galaxy interactions (Pearson et al. 2016, Pearson et al. 2017b). In this talk, I will focus on my thesis work related to the stellar stream emerging from the old, globular cluster, Palomar 5 (Pal 5), orbiting our own Milky Way. As the stellar stream members were once closely tied together in energy and angular momentum space, we can use their distribution in phase space to trace back where they were once located and what affected them along their paths. In particular, I will show that the mere existence of Pal 5's thin stream can rule out a moderately triaxial potential model of our Galaxy (Pearson et al. 2015) and that the debris of Pal 5-like streams will spread much further in space in a triaxial potential (a mechanism which I dubbed "stream fanning"). Additionally, I will show that the Milky Way's Galactic bar, can punch holes in stellar streams and explain the recently discovered length asymmetry between Pal 5's leading and trailing arm (Pearson et al. 2017a). These holes grow and have locations along stellar streams dependent on the Galactic bar orientation, mass and rotational speed, which provides an intriguing methodology for studying our own Milky Way's Galactic bar in more detail. The fact that the bar can create under densities in stellar streams, further demonstrates that we should be careful when interpreting gaps in stellar streams as indirect evidence of the existence of dark matter subhalos in our Galaxy.

Author(s): Sarah Pearson¹

Institution(s): 1. *Columbia University*

212.04 – Can we measure the halo mass of the Milky Way accurately?

The halo mass of the Milky Way is considered fundamental in the cosmological interpretation of Galactic observations. A large family of MW mass measurements rely on steady-state modelling of the tracer dynamics. We demonstrate that such measurements can be biased due to unnecessary and unjustified assumptions about the distribution function of tracers. To avoid such biases, we develop a first-principle method that involves minimal assumptions. Applying this method to a large sample of simulated haloes, we show that stars in galactic haloes are not in a steady-state, leading to a systematic uncertainty up to a factor of three in the halo mass measurement.

Author(s): Jiaxin Han², Wenting Wang², Shaun Cole¹, Carlos Frenk¹

Institution(s): 1. *ICC, Durham University*, 2. *Kavli IPMU (WPI), UTIAS, The University of Tokyo*

212.05 – Stellar Streams in the Dark Energy Survey

We present a search for Galactic stellar streams in the Dark Energy Survey (DES), using three years of optical data taken across 5000 sq. degrees of the southern sky. The wide-field, uniform DES photometry provides unprecedented sensitivity to the stellar density field in the southern hemisphere, allowing for the detection of faint stellar populations. We follow the "Field of Streams" procedure developed in the Sloan Digital Sky Survey (Belokurov et al., 2006) to identify stellar density features such as dwarf galaxies, globular clusters, and the stellar streams resulting from the tidal disruption of these objects. Improved analysis techniques applied to the DES data enable the discovery of new

stellar streams, and provide added insight into the origin and stellar populations of previously identified objects. An increased sample size together with detailed characterization of individual stellar streams and their progenitors can inform our understanding of the formation of the Milky Way stellar halo, as well as the large and small scale distribution of dark matter in the Milky Way.

Author(s): Nora Shipp², Alex Drlica-Wagner¹, Eduardo Balbinot³

Institution(s): 1. *Fermi National Accelerator Laboratory, 2. University of Chicago, Department of Astronomy & Astrophysics, 3. University of Surrey, Department of Physics*

Contributing team(s): The DES Collaboration

212.06 – The Sagittarius Stream: Probing the Outer Halo Potential

The Sagittarius Stream should be the premier probe of the outer Milky Way halo potential. Instead it has generated a series of puzzles that have frustrated modelers and prevented us from measuring the halo forces. The latest such puzzle is the factor of two difference between leading and trailing apocenter distances, seen most clearly in a recent sample of RR Lyraes from PS1. Using a set of dynamical models, we explain how to match this feature. The key element are that the debris at apocenter should be dynamically young, originating from the last two pericentric passages only. We also explain the important roles played by the mass profile of the halo, dynamical friction, and departures from sphericity. The models show that the separate components already visible in the PS1 data should separate clearly once velocities are obtained, and the youngest component should probe the potential even beyond the observed distances of $>\sim 100$ kpc. We explain what observations would be useful to eliminate remaining degeneracies in the models and fulfill the promise of the stream for understanding the Milky Way.

Author(s): Mark Fardal¹

Institution(s): 1. *STScI*

Contributing team(s): HSTPROMO

212.07 – Characterizing Milky Way Tidal Streams and Dark Matter with MilkyWay@home

MilkyWay@home is a 0.5 PetaFLOPS volunteer computing platform that is mapping out the density substructure of the Sagittarius Dwarf Tidal Stream, the so-called bifurcated portion of the Sagittarius Stream, and the Virgo Overdensity, using turnoff stars from the Sloan Digital Sky Survey. It is also using the density of stars along tidal streams such as the Orphan Stream to constrain properties of the dwarf galaxy progenitor of this stream, including the dark matter portion. Both of these programs are

213 – Computation, Data Science, and Image Analysis

213.01 – Improvement in the accuracy of flux measurement of radio sources by exploiting an arithmetic pattern in photon bunching noise

A hierarchy of statistics of increasing sophistication and accuracy is proposed, to exploit an interesting and fundamental arithmetic structure in the photon bunching noise of incoherent light of large photon occupation number, with the purpose of suppressing the noise and rendering a more reliable and unbiased measurement of the light intensity. The method does not require any new hardware, rather it operates at the software level, with the help of high precision computers, to reprocess the intensity time series of the incident light to create a new series with smaller bunching noise coherence length. The ultimate accuracy improvement of this method of flux measurement is limited by the timing resolution of the detector and the photon occupation number of the beam (the higher the photon number the better the performance). The principal application is accuracy improvement in the bolometric flux measurement of a radio source.

enabled by a specially-built optimization package that uses differential evolution or particle swarm methods to find the optimal model parameters to fit a set of data. To fit the density of tidal streams, 20 parameters are simultaneously fit to each 2.5-degree-wide stripe of SDSS data. Five parameters describing the stellar and dark matter profile of the Orphan Stream progenitor and the time that the dwarf galaxy has been evolved through the Galactic potential are used in an n-body simulation that is then fit to observations of the Orphan Stream. New results from MilkyWay@home will be presented. This project was supported by NSF grant AST 16-15688, the NASA/NY Space Grant fellowship, and contributions made by The Marvin Clan, Babette Josephs, Mani Limlami, and the 2015 Crowd Funding Campaign to Support Milky Way Research.

Author(s): Heidi Jo Newberg¹, Siddhartha Shelton¹, Jake Weiss¹

Institution(s): 1. *Rensselaer Polytechnic Institute*

212.08 – Interstellar Matters: Neutral Hydrogen and the Galactic Magnetic Field

The physics of the interstellar medium was revolutionized by the observations of the Galactic Arecibo L-Band Feed Array (GALFA) HI survey done at the Arecibo Observatory. The high-resolution, high-sensitivity, high-dynamic-range images show complex, tangled, extended filaments, and reveal that the fabric of the neutral interstellar medium is deeply tied to the structure of the ambient magnetic field. This discovery prompts an obvious question – how exactly is the interstellar neutral hydrogen being affected by the galactic magnetic field? We look into this question by examining a set of GALFA-HI data in great detail. We have chosen a long, straight filament in the southern galactic sky. This structure is both close by and isolated in velocity space. Gaussian analysis of profiles both along and across the filament reveal internal structure – braided strands that can be traced through the simplest part, but become tangled in more complex segments. These braids do not resemble in any way the old spherical HI clouds and rudimentary pressure balance models that were used to explain the pre-GALFA-HI interstellar medium. It is clear that these structures are created, constrained, and dominated by magnetic fields. Like many subfields of astronomy before it, e.g., physics of the solar coronal, extragalactic radio jets, and pulsar environment, scientists are confronted with observations that simply cannot be explained by simple hydrodynamics and are forced to consider magneto-hydrodynamics.

Author(s): Gerrit Verschuur¹, Joan T. Schmelz¹, M. Asgari-Targhi asgari-Targhi²

Institution(s): 1. *Arecibo Observatory, 2. Harvard Smithsonian Ctr for Astrophysics*

Author(s): Richard Lieu¹

Institution(s): 1. *University of Alabama in Huntsville*

213.02 – Source / component separation with NMF and scarlet

Astronomical data are often superpositions of multiple source signals. I will introduce the open-source analysis framework scarlet, based on the Non-negative Matrix Factorization (NMF), that achieves efficient source separation and enables flexible constraints or priors on the shape of the signals and/or the signal amplitude across multiple observations.

I will demonstrate scarlet's capabilities of separating multi-component photo-z distributions, AGN jets from host galaxies, and more generally: crowded extragalactic fields in the HSC survey. I will also discuss extensions for joint pixel-level deblending with images from LSST and WFIRST, and for hyperspectral or grism data.

Author(s): Peter Melchior¹, Fred Moolekamp¹
Institution(s): 1. Princeton University
Contributing team(s): LSST Data Management, WFIRST Preparatory Science

213.03 – Here Be Dragons: Effective (X-ray) Timing with the Cospectrum

In recent years, the cross spectrum has received considerable attention as a means of characterising the variability of astronomical sources as a function of wavelength. While much has been written about the statistics of time and phase lags, the cospectrum—the real part of the cross spectrum—has only recently been understood as means of mitigating instrumental effects dependent on temporal frequency in astronomical detectors, as well as a method of characterizing the coherent variability in two wavelength ranges on different time scales. In this talk, I will present recent advances made in understanding the statistical properties of cospectra, leading to much improved inferences for periodic and quasi-periodic signals. I will also present a new method to reliably mitigate instrumental effects such as dead time in X-ray detectors, and show how we can use the cospectrum to model highly variable sources such as X-ray binaries or Active Galactic Nuclei.

Author(s): Daniela Huppenkothen², Matteo Bachetti¹
Institution(s): 1. INAF-Osservatorio Astronomico di Cagliari, 2. University of Washington Seattle

213.04 – Fast Computation of the Two-Point Correlation Function in the Age of Big Data

We present a new code which quickly computes the two-point correlation function for large sets of astronomical data. This code combines the ease of use of Python with the speed of parallel shared libraries written in C. We include the capability to compute the auto- and cross-correlation statistics, and allow the user to calculate the three-dimensional and angular correlation functions. Additionally, the code automatically divides the user-provided sky masks into contiguous subsamples of similar size, using the HEALPix pixelization scheme, for the purpose of resampling. Errors are computed using jackknife and bootstrap resampling in a way that adds negligible extra runtime, even with many subsamples. We demonstrate comparable speed with other clustering codes, and code accuracy compared to known and analytic results.

Author(s): Andrew Pellegrino¹, John Timlin¹
Institution(s): 1. Drexel University

213.05D – ANNA: A Convolutional Neural Network Code for Spectroscopic Analysis

We present ANNA, a Python-based convolutional neural network code for the automated analysis of stellar spectra. ANNA provides a flexible framework that allows atmospheric parameters such as temperature and metallicity to be determined with accuracies comparable to those of established but less efficient techniques. ANNA performs its parameterization extremely quickly; typically several thousand spectra can be analyzed in less than a second. Additionally, the code incorporates features which greatly speed up the training process necessary for the neural network to measure spectra accurately, resulting in a tool that can easily be run on a single desktop or laptop computer. Thus, ANNA is useful in an era when spectrographs increasingly have the capability to collect dozens to hundreds of spectra each night. This talk will cover the basic features included in ANNA and demonstrate its performance in two use cases: an open cluster abundance analysis involving several hundred spectra, and a metal-rich field star study. Applicability of the code to large survey datasets will also be discussed.

Author(s): Donald Lee-Brown¹, Barbara J Anthony-Twarog¹, Bruce A Twarog¹
Institution(s): 1. University of Kansas

213.06 – Anomalous Stars and Where to Find Them

The sky is now extensively mapped by imaging surveys in wavelengths that span the electromagnetic spectrum, ranging from Fermi and GALEX down to WISE, Planck, and radio surveys like FIRST and VLSS. Individual public catalogs now contain on order hundreds of millions of distinct sources. Recent progress in image analysis techniques makes possible great increases in the efficiency, sensitivity, and reliability of measurements that combine imaging data from multiple probes with heterogeneous properties. This is especially true for the identification of anomalous sources: traditional methods for finding ‘outliers’ typically rely on making hard cuts on noisy catalog properties, greatly restricting the potential discovery space. Cross-catalog matches confine investigation to objects that occur at signal-to-noise ratios sufficient to be independently detectable in a subset of all the available multi-wavelength coverage. The process of merging the latest analyses with existing data is severely hampered, however, by the fractured way in which these data are processed and stored, limitations of data access, the data volume involved, and the computation power required. This has left archive data far from fully exploited. Stellar anomalies present the best place to start: joint distributions of stellar colors and magnitudes have finer structures than extended sources, and modelling of point sources is computationally cheaper than for galaxies. We present a framework to solve the problem of applying new algorithms to old data while overcoming the limitations described above, in the search for the undiscovered anomalous.

Author(s): Demitri Muna², Eric Huff¹
Institution(s): 1. Jet Propulsion Laboratory, 2. Ohio State University

213.07 – Investigating the Cosmic Web with Topological Data Analysis

Data exhibiting complicated spatial structures are common in many areas of science (e.g. cosmology, biology), but can be difficult to analyze. Persistent homology is a popular approach within the area of Topological Data Analysis that offers a new way to represent, visualize, and interpret complex data by extracting topological features, which can be used to infer properties of the underlying structures. In particular, TDA may be useful for analyzing the large-scale structure (LSS) of the Universe, which is an intricate and spatially complex web of matter. In order to understand the physics of the Universe, theoretical and computational cosmologists develop large-scale simulations that allow for visualizing and analyzing the LSS under varying physical assumptions. Each point in the 3D data set represents a galaxy or a cluster of galaxies, and topological summaries ("persistent diagrams") can be obtained summarizing the different ordered holes in the data (e.g. connected components, loops, voids).

The topological summaries are interesting and informative descriptors of the Universe on their own, but hypothesis tests using the topological summaries would provide a way to make more rigorous comparisons of LSS under different theoretical models. For example, the received cosmological model has cold dark matter (CDM); however, while the case is strong for CDM, there are some observational inconsistencies with this theory. Another possibility is warm dark matter (WDM). It is of interest to see if a CDM Universe and WDM Universe produce LSS that is topologically distinct.

We present several possible test statistics for two-sample hypothesis tests using the topological summaries, carryout a simulation study to investigate the suitability of the proposed test statistics using simulated data from a variation of the Voronoi foam model, and finally we apply the proposed inference framework to WDM vs. CDM cosmological simulation data.

Author(s): Jessi Cisewski-Kehe⁶, Mike Wu⁴, Brittany Fasy³, Wojciech Hellwing⁵, Mark Lovell¹, Alessandro Rinaldo², Larry Wasserman²

Institution(s): 1. Max-Planck-Institut, 2. Carnegie Mellon University, 3. Montana State University, 4. Stanford, 5. University of Portsmouth, 6. Yale

214 – Star Formation II

214.01 – What drives the formation of massive stars and clusters?

Galaxy-wide surveys allow to study star formation in unprecedented ways. In this talk, I will discuss our analysis of the Large Magellanic Cloud (LMC) and the Milky Way, and illustrate how studying both the large and small scale structure of galaxies are critical in addressing the question: what drives the formation of massive stars and clusters?

I will show that ‘turbulence-regulated’ star formation models do not reproduce massive star formation properties of GMCs in the LMC and Milky Way: this suggests that theory currently does not capture the full complexity of star formation on small scales. I will also report on the discovery of a massive star forming complex in the LMC, which in many ways manifests itself as an embedded twin of 30 Doradus: this may shed light on the formation of R136 and ‘Super Star Clusters’ in general. Finally, I will highlight what we can expect in the next years in the field of star formation with large-scale sky surveys, ALMA, and our JWST-GTO program.

Author(s): Bram Ochsendorf⁶, Margaret Meixner⁵, Julia Roman-Duval⁵, Neal J. Evans II², Mubdi Rahman⁶, Hans Zinnecker⁴, Omnarayani Nayak⁶, John Bally¹, Olivia C. Jones⁵, Remy Indebetouw³

Institution(s): 1. Astrophysical and Planetary Sciences Department, University of Colorado, 2. Department of Astronomy, University of Texas, 3. Department of Astronomy, University of Virginia, 4. Deutsches SOFIA Institut, University of Stuttgart, 5. STScI, 6. The Johns Hopkins University

214.02D – Starless Clumps and the Earliest Phases of High-mass Star Formation in the Milky Way

High-mass stars are key to regulating the interstellar medium, star formation activity, and overall evolution of galaxies, but their formation remains an open problem in astrophysics. In order to understand the physical conditions during the earliest phases of high-mass star formation, I report on observational studies of dense starless clump candidates (SCCs) that show no signatures of star formation activity. I identify 2223 SCCs from the 1.1 mm Bolocam Galactic Plane Survey, systematically analyze their physical properties, and show that the starless phase is not represented by a single timescale, but evolves more rapidly with increasing clump mass. To investigate the sub-structure in SCCs at high spatial resolution, I study the 12 most high-mass SCCs within 5 kpc using ALMA. I report previously undetected low-luminosity protostars in 11 out of 12 SCCs, fragmentation equal to the thermal Jeans length of the clump, and no starless cores exceeding 30 solar masses. While uncertainties remain concerning the star formation efficiency in this sample, these observational facts are consistent with models where high-mass stars form from initially low- to intermediate-mass protostars that accrete most of their mass from the surrounding clump.

Author(s): Brian Svoboda¹

Institution(s): 1. University of Arizona

214.03 – Bipolar Molecular Outflows within 1pc of Sgr A*:

Evidence for Low-mass Star Formation Activity

The 4 million solar mass black hole, Sgr A*, is expected to suppress star formation because the measured density of the cloud is insufficient for self-gravity to overcome tidal disruption by the black hole’s gravitational field. Nevertheless, objects resembling dust-enshrouded young stars and photo-evaporative flows from their disks have been identified within 2pc of Sgr A*. Clear identification of the nature of these objects has been

hampered by the Galactic center’s distance, 30 magnitudes of foreground extinction, and stellar crowding. Here, we report the discovery of 11 bipolar molecular outflows using ALMA within a projected distance of one pc from Sgr A*. These unambiguous signatures of young protostars manifest as approaching and receding lobes of dense gas swept up by the jets created during the formation and early evolution of low-mass stars. The mean dynamical age of the outflow sources and the rate of star formation are estimated to be ~6500 years and $\sim 5 \times 10^{-4}$ solar mass per year, respectively. These measurements suggest that star formation could take place in the immediate vicinity of supermassive black holes in the nuclei of external galaxies.

Author(s): Farhad Yusef-Zadeh², Mark Wardle¹, Devaki Kunneriath³, Marc Royster², Al Wootten³, Douglas Roberts²

Institution(s): 1. Macquarie University, 2. Northwestern University, 3. NRAO

214.04D – Radiation hydrodynamics of super star cluster formation

Throughout the history of the Universe, the nuclei of super star clusters represent the most active sites for star formation. The high densities of massive stars within the clusters produce intense radiation that imparts both energy and momentum on the surrounding star-forming gas. Theoretical claims based on idealized geometries have claimed the dominant role of radiation pressure in controlling the star formation activity within the clusters. In order for cluster formation simulations to be reliable, numerical schemes have to be able to model accurately the radiation flows through the gas clumps at the cluster nuclei with high density contrasts. With a hybrid Monte Carlo radiation transport module we developed, we performed 3D radiation hydrodynamical simulations of super star cluster formation in turbulent clouds. Furthermore, our Monte Carlo radiation treatment provides a native capability to produce synthetic observations, which allows us to predict observational indicators and to inform future observations. We found that radiation pressure has definite, but minor effects on limiting the gas supply for star formation, and the final mass of the most massive cluster is about one million solar masses. The ineffective forcing was due to the density variations inside the clusters, i.e. radiation takes the paths of low densities and avoids forcing on dense clumps. Compared to a radiation-free control run, we further found that the presence of radiation amplifies the density variations. The core of the resulting cluster has a high stellar density, about the threshold required for stellar collisions and merging. The very massive star that form from the stellar merging could continue to gain mass from the surrounding gas reservoir that is gravitationally confined by the deep potential of the cluster, seeding the potential formation of a massive black hole.

Author(s): Benny Tsz Ho Tsang¹

Institution(s): 1. The University of Texas at Austin

Contributing team(s): Milos Milosavljevic

214.05D – The Initial Mass Function of the Arches Cluster

The Arches star cluster is only 26 pc (in projection) from Sgr A*, the supermassive black hole at the Galactic Center. This young massive cluster allows us to examine the impact of the extreme Galactic Center environment on the stellar Initial Mass Function (IMF). However, measuring the IMF of the Arches is challenging due to the highly variable extinction along the line of sight, which makes it difficult to separate cluster members from the field stars. We use high-precision proper motion and photometric measurements obtained with the Hubble Space Telescope to calculate cluster membership probabilities for stars down to ~2

M_sun out to the outskirts of the cluster (3 pc). In addition, we measure the effective temperatures of a small sample of cluster members in order to calibrate the mass-luminosity relationship using Keck OSIRS K-band spectroscopy. We forward model these observations to simultaneously constrain the cluster IMF, age, distance, and extinction. We obtain an IMF that is shallower than what is observed locally, with a higher fraction of high-mass stars to low mass stars (i.e., “top-heavy”). We will compare the IMF of the Arches to similar clusters in the Galactic disk and quantify the effect of the GC environment on the star formation process.

Author(s): Matthew Hosek⁴, Jessica Lu², Jay Anderson¹, Andrea Ghez³, Mark Morris³, Tuan Do³, William Clarkson⁵, Sandra Albers², Daniel Weisz²

Institution(s): 1. *Space Telescope Science Institute*, 2. *University of California, Berkeley*, 3. *University of California, Los Angeles*, 4. *University of Hawaii at Manoa*, 5. *University of Michigan-Dearborn*

214.06 – Tracing Star Formation and Molecular Cloud Evolution with Pre-main Sequence Stars in the SMC

The Southwest Bar region in the Small Magellanic Cloud (SMC) contains star-forming molecular clouds sampling a wide range of evolutionary states: from quiescent pre-star-forming regions to evolved HII region hosts. We use deep, panchromatic, high spatial resolution Hubble Space Telescope imaging obtained as part of the SMIDGE survey (PI: K. Sandstrom) to identify young, pre-main sequence stars that trace recent and ongoing star formation within these clouds. We characterize a color-selected sample (and H α line-emitting subsample) of pre-main sequence stars via SED fitting and analyze their association with the local ISM, inferred from observations of CO and dust emission. These low-mass stars serve as robust star formation tracers not tied to

215 – Instrumentation: Ground Based and Airborne I

215.01 – The Path from VLITE to ngLOBO: A Roadmap for Evolving a Low Frequency Commensal System from the JVLA to the ngVLA

The VLA Low-band Ionosphere and Transient Experiment (VLITE, <<http://vlite.nrao.edu/>>) is a commensal observing system on the NRAO Karl G. Jansky Very Large Array (VLA). The separate optical path of the prime-focus sub-GHz dipole feeds and the Cassegrain-focus GHz feeds provided an opportunity to expand the simultaneous frequency operation of the VLA through joint observations across both systems. 16 VLA antennas are outfitted with dedicated samplers and use spare fibers to transport the 320-384 MHz band to the VLITE CPU-based correlator. Initial goals included exploring the scientific potential of a commensal low frequency system for ionospheric remote sensing, astrophysics and transients. VLITE operates at nearly 70% wall time with roughly 6200 hours of VLA time recorded each year.

Several papers at this meeting review VLITE science and early results. Here we consider how the project could evolve in the future. Over the next 10 years, a straightforward evolutionary path calls for an expansion of VLITE to all 27 VLA antennas and to the maximum available low band receiver bandwidth (224-480 MHz). The GPU-based correlator for this Low Band Observatory (LOBO) would also incorporate lower frequency signals from the new VLA 74 MHz system, including from VLA dishes (60-80 MHz) and standalone Long Wavelength Array (LWA) aperture array stations (20-80 MHz).

In the longer term, we look towards leveraging the vast infrastructure of the ngVLA to include a commensal low frequency capability, called ngLOBO. As described in our community white paper (Taylor et al. 2018; arXiv:1708.00090), ngLOBO has three primary scientific missions: (1) Radio Large Synoptic Survey Telescope (Radio-LSS): one naturally wide beam, commensal with ngVLA, will conduct a continuous

synoptic survey of large swaths of the sky for both slow and fast transients; (2) This same commensal beam will provide complementary low frequency images of all ngVLA targets when such data enhances their value. (3) Independent beams from the ngLOBO-Low aperture array will conduct research in astrophysics, Earth science and space weather applications, engaging new communities and attracting independent resources. We describe our developing ngLOBO technical concept.

Author(s): L. Clifton Johnson¹

Institution(s): 1. *Northwestern University*

Contributing team(s): SMIDGE Team

synoptic survey of large swaths of the sky for both slow and fast transients; (2) This same commensal beam will provide complementary low frequency images of all ngVLA targets when such data enhances their value. (3) Independent beams from the ngLOBO-Low aperture array will conduct research in astrophysics, Earth science and space weather applications, engaging new communities and attracting independent resources. We describe our developing ngLOBO technical concept.

Author(s): Namir E Kassim⁴, Tracy Clarke⁴, Simona Giacintucci⁴, Joseph Helmboldt⁴, Paul S Ray⁴, Wendy Peters⁴, Emil Polisensky⁴, Brian C hicks⁴, Walter Brisken², Scott D hyman⁵, Julia Deneva¹, Matthew T Kerr⁴, Gregory Taylor⁶, Jayce Dowell⁶, Frank K. Schinzel³

Institution(s): 1. *George Mason University (resident at NRL)*, 2. *Long Baseline Observatory*, 3. *National Radio Astronomy Observatory*, 4. *Naval Research Laboratory*, 5. *Sweet Briar College*, 6. *University of New Mexico*

215.02D – Design and Performance of the Multiplexed SQUID/TES Array at Ninety Gigahertz

We present the array performance and astronomical images from early science results from MUSTANG-2, a 90 GHz feedhorn-coupled, microwave SQUID-multiplexed TES bolometer array operating on the Robert C. Byrd Green Bank Telescope (GBT). MUSTANG-2 was installed on the GBT on December 2, 2016 and immediately began commissioning efforts, followed by science observations, which are expected to conclude June 2017. The feedhorn and waveguide-probe-coupled detector technology is a mature technology, which has been used on instrument including the South Pole Telescope, the Atacama Cosmology Telescope, and the Atacama B-mode Search telescope. The microwave SQUID readout system developed for MUSTANG-2 currently reads out 66 detectors with a single coaxial cable and will eventually allow thousands of detectors to be multiplexed. This microwave SQUID multiplexer combines the proven abilities of millimeterwave TES

detectors with the multiplexing capabilities of KIDs with no degradation in noise performance of the detectors. Each multiplexing device is read out using warm electronics consisting of a commercially available ROACH board, a DAC/ADC card, and an Intermediate Frequency mixer circuit. The hardware was originally developed by the UC Berkeley Collaboration for Astronomy Signal Processing and Electronic Research (CASPER) group, whose primary goal is to develop scalable FPGA-based hardware with the flexibility to be used in a wide range of radio signal processing applications. MUSTANG-2 is the first on-sky instrument to use microwave SQUID multiplexing and is available as a shared-risk/PI instrument on the GBT. In MUSTANG-2's first season 7 separate proposals were awarded a total of 230 hours of telescope time.

Author(s): Sara Stanchfield¹, Peter Ade¹, James Aguirre¹, Justus A. Brevik¹, Hsiao-Mei Cho¹, Rahul Datta¹, Mark Devlin¹, Simon R. Dicker¹, Bradley Dober¹, Shannon M. Duff¹, Dennis Egan¹, Pam Ford¹, Gene Hilton¹, Johannes Hubmayr¹, Kent Irwin¹, Kenda Knowles¹, Paul Marganian¹, Brian Scott Mason¹, John A.B. Mates¹, Jeff McMahon¹, Melinda Mello¹, Tony Mroczkowski¹, Charles Romero¹, Jonathon Sievers¹, Carole Tucker¹, Leila R. Vale¹, Michael Vissers¹, Steven White¹, Mark Whitehead¹, Joel Ullom¹, Alexander Young¹
Institution(s): 1. *University of Pennsylvania*

215.03 – Phase Synchronization for the Mid-Frequency Square Kilometre Array Telescope

The Square Kilometre Array (SKA) project is an international effort to build the world's most sensitive radio telescope operating in the 50 MHz to 14 GHz frequency range. Construction of the SKA has been divided into phases, with the first phase (SKA1) accounting for the first 10% of the telescope's receiving capacity. During SKA1, a low-frequency aperture array comprising over a hundred thousand individual dipole antenna elements will be constructed in Western Australia (SKA1-low), while an array of 197 parabolic-dish antennas, incorporating the 64 dishes of MeerKAT, will be constructed in South Africa (SKA1-mid).

Radio telescope arrays such as the SKA require phase-coherent reference signals to be transmitted to each antenna site in the array. In the case of the SKA1-mid, these reference signals will be generated at a central site and transmitted to the antenna sites via fiber-optic cables up to 175 km in length. Environmental perturbations affect the optical path length of the fiber and act to degrade the phase stability of the reference signals received at the antennas, which has the ultimate effect of reducing the fidelity and dynamic range of the data.

Since 2011, researchers at the University of Western Australia (UWA) have led the development of an actively-stabilized phase-synchronization system designed specifically to meet the scientific needs and technical challenges of the SKA telescope. Recently this system has been selected as the official phase synchronization system for the SKA1-mid telescope. The system is an evolution of Atacama Large Millimeter Array's distributed 'photonic local oscillator system', incorporating key advances made by the international frequency metrology community over the last decade, as well as novel innovations developed by UWA researchers.

In this presentation I will describe the technical details of the system; outline how the system's performance was tested using metrology techniques in a laboratory setting, on 186 km of overhead fibre at the South African SKA site, and verified using existing astronomical radio interferometers; and how the system can enhance the astronomical performance of the SKA1-mid telescope.

Author(s): Sascha Schediwy¹, David Gozzard¹, Simon Stobie¹, Charles Gravestock¹, Richard Whitaker², Bassem Alachkar², Sias Malan⁴, Paul Boven³, Keith Grainge²
Institution(s): 1. *International Centre for Radio Astronomy Research, The University of Western Australia*, 2. *Jodrell Bank Centre for Astrophysics, The University of Manchester*, 3. *Joint Institute for VLBI in Europe*, 4. *SKA South Africa*

215.04D – Observing the Cosmic Microwave Background Polarization with Variable-delay Polarization Modulators for the Cosmology Large Angular Scale Surveyor

The search for inflationary primordial gravitational waves and the optical depth to reionization, both through their imprint on the large angular scale correlations in the polarization of the cosmic microwave background (CMB), has created the need for high sensitivity measurements of polarization across large fractions of the sky at millimeter wavelengths. These measurements are subjected to instrumental and atmospheric 1/f noise, which has motivated the development of polarization modulators to facilitate the rejection of these large systematic effects.

Variable-delay polarization modulators (VPMs) are used in the Cosmology Large Angular Scale Surveyor (CLASS) telescopes as the first element in the optical chain to rapidly modulate the incoming polarization. VPMs consist of a linearly polarizing wire grid in front of a moveable flat mirror; varying the distance between the grid and the mirror produces a changing phase shift between polarization states parallel and perpendicular to the grid which modulates Stokes U (linear polarization at 45°) and Stokes V (circular polarization). The reflective and scalable nature of the VPM enables its placement as the first optical element in a reflecting telescope. This simultaneously allows a lock-in style polarization measurement and the separation of sky polarization from any instrumental polarization farther along in the optical chain.

The Q-Band CLASS VPM was the first VPM to begin observing the CMB full time in 2016. I will be presenting its design and characterization as well as demonstrating how modulating polarization significantly rejects atmospheric and instrumental long time scale noise.

Author(s): Kathleen Harrington¹
Institution(s): 1. *Johns Hopkins University*
Contributing team(s): The CLASS Collaboration

215.05 – Second-generation Micro-Spec: a medium-resolution spectrometer-on-a-chip for submillimeter astronomy

This work reports on the design of a second-generation Micro-Spec (μ -Spec), a direct-detection spectrometer which integrates all the components of a diffraction-grating spectrometer onto a $\sim 10\text{-cm}^2$ chip by means of superconducting microstrip transmission lines on a monocrystalline silicon substrate. The second-generation μ -Spec is designed to operate with a resolving power of 512 over the 500-1000 μm (300-600 GHz) wavelength range, a band of interest for several spectroscopic applications in astrophysics and the study of the early ($z > 8$) Universe. High-altitude balloon missions would provide the first testbed to demonstrate the μ -Spec technology in a space-like environment and would represent an economically viable venue for multiple observation campaigns.

A brief overview of each instrument subsystem will be provided. Emphasis will be given to the design of the spectrometer's two-dimensional diffractive region, through which the light of different wavelengths is focused on the kinetic inductance detectors along the focal plane. An optical design optimized for balloon missions through an optimization process that satisfies specific requirements on spectrometer's size, operating spectral range and optical performance is presented in terms of geometric layout, spectral purity and efficiency.

Author(s): Giuseppe Cataldo¹, Emily M. Barrentine¹, Berhanu T. Bulcha¹, Negar Ehsan¹, Larry A. Hess¹, Omid Noroozian², Thomas R. Stevenson¹, Kongpop U-Yen¹, Edward Wollack¹, Samuel Harvey Moseley¹

Institution(s): 1. NASA Goddard Space Flight Center, 2. National Radio Astronomy Observatory

215.06 – Large aperture wide field multi-object spectroscopy for the 2020s: the science and status of the Maunakea Spectroscopic Explorer.

Numerous international reports have recently highlighted the need for fully dedicated, large aperture, highly multiplexed spectroscopy at a range of spectral resolutions in the OIR wavelength range. Such a facility is the most obvious missing link in the emerging network of international multi-wavelength, astronomy facilities, and enables science from reverberation mapping of black holes to the nucleosynthetic history of the Galaxy, and will follow-up discoveries from the optical through to the radio with facilities such as LSST. The only fully dedicated large aperture MOS facility that is in the design phase is the

216 – Preparing Our Next Generation: Education Research and Practice from High School Through the Major

216.01 – A Bridge to the Stars: A Model High School-to-College Pipeline for Encouraging Positive STEM Identities

The need to grow and diversify the STEM workforce remains a critical national challenge. Research shows that STEM identity (how one views herself/himself with respect to STEM) is an important factor for success or failure. A Bridge to the Stars (ABtS) offers URM and low-income high-school students a high impact exposure to science through innovative experiential learning with a professional scientist in freshmen astronomy at UMKC, an urban research university. Showing students who traditionally do not self-identify with high-tech careers that they can succeed in a university science course is a promising way to help build positive STEM identities and aspirations during the critical bridge between high school and college. In five years, we have awarded 45 ABtS scholarships; 93% of these 15-17 year-old students have passed the course satisfactorily with an average grade of 80%. Remarkably, the ABtS scholar performance is on par with that of 600 UMKC students enrolled in the same courses over 8 semesters. Long-term tracking of former scholars shows positive attitudes regarding ABtS and persistence in STEM aspirations at promising rates based on small-number statistics. I will describe the implementation of this unique STEM immersion program offering extended and inclusive engagement in astronomy, arguably the most accessible window to science. I will share classroom and near-peer mentoring innovations, and a new third ABtS tier in which previous scholars can enroll in a freshmen science laboratory experience for UMKC credit. This novel course introduces novices to scientific research and Big Data science through authentic hands-on experiences centered on their own exploration of data from McIntosh's actual research. The long-term mission of ABtS is to see urban educational institutions across the U.S. adopt similar pipelines in all STEM disciplines built on the ABtS model. Adopting programs like ABtS for freshmen STEM majors, especially in urban colleges and universities, is a key step to overcoming the dire national deficit in URM and low-income STEM majors.

Author(s): Daniel H. McIntosh¹, Derrick H. Jennings¹

Institution(s): 1. U. Missouri-Kansas City

216.02 – “Big Data” Teen Astronomy Cafes at NOAO

The National Optical Astronomy Observatory has designed and implemented a prototype educational program designed to test and understand best practices with high school students to promote an understanding of modern astronomy research with its emphasis on large data sets, data tools, and visualization tools. This program, designed to cultivate the interest of talented youth in astronomy, is based on a teen science café model developed at

Maunakea Spectroscopic Explorer (MSE), an 11.4m segmented mirror prime focus telescope with a 1.5 square degree field of view that has 3200 fibers at low (R~2500) and moderate (R~6000) resolution, and 1000 fibers at high (R=20/40000) resolution. I will provide an overview of MSE, describing the science drivers and the current design status, as well as the international partnership, and the results of multiple, newly completed, external reviews for the system and subsystems. The anticipated cost and timeline to first light will also be presented.

Author(s): Daniel Devost¹, Alan McConnachie³, Kenneth Chambers², Sarah Gallagher⁴

Institution(s): 1. Canada-France-Hawaii Telescope, 2. Institute for Astronomy, 3. Project office, Maunakea Spectroscopic Explorer, 4. Western University

Contributing team(s): Maunakea Spectroscopic Explorer Project office, MSE Science Advisory group, MSE Science Team

Los Alamos as the Café Scientifique New Mexico. In our program, we provide a free, fun way for teens to explore current research topics in astronomy on Saturday mornings at the NOAO headquarters. The program encourages stimulating conversations with astronomers in an informal and relaxed setting, with free food of course. The café is organized through a leadership team of local high school students and recruits students from all parts of the greater Tucson area. The high school students who attend have the opportunity to interact with expert astronomers working with large astronomical data sets on topics such as killer asteroids, the birth and death of stars, colliding galaxies, the structure of the universe, gravitational waves, gravitational lensing, dark energy, and dark matter. The students also have the opportunity to explore astronomical data sets and data tools using computers provided by the program. The program may serve as a model for educational outreach for the 40+ institutions involved in the LSST.

Author(s): Stephen Pompea¹, Constance E. Walker¹

Institution(s): 1. National Optical Astronomy Observatory

216.03 – The Community Mentoring REU: A Novel Paradigm for Research Experiences for Undergraduates Programs

Research Experience for Undergraduates programs were conceived to promote entry of college students into STEM disciplines. Evidence suggests that participating in REUs increases interest in STEM, conveys skills leading to STEM jobs and graduate study, increases science self-efficacy, builds professional networks for young scientists, and cultivates identity as a scientist. Nevertheless, the factors that mediate desired outcomes are still poorly understood, and persistence of negative mentoring experiences among REU participants motivates the design and study of novel approaches to preparing future STEM professionals. During five summers spanning 2012-2016 we implemented a "Community Mentoring" paradigm at the University of Wyoming's 10-week Astronomy REU program. In contrast to "traditional model (TM)" REUs that pair a single senior scientist mentor with a single junior mentee, community mentoring (CM) unites 6-8 undergraduates with 3-5 faculty (perhaps assisted by a graduate student or postdoc) on a collaborative team addressing a single science goal. In CM, students have access to a pool of mentors and a peer group reading the same literature, working in a common location, sharing equipment (in this case the WIRO 2.3 meter telescope), sharing data, and learning the same analysis skills. The community interacts daily, modeling the highly collaborative nature of modern scientific teams. Our study used an electronic survey consisting of 24 questions to compare a cohort of 28 CM students to a national control group of 77 students who conducted REUs elsewhere during the same period, typically under the TM.

CM students report a significantly higher level of "learning from their peers", "learning to work on a science team", and "sense of community" compared to the TM cohort. The CM cohort also reports a higher overall level of satisfaction with the REU and a lower level of negative experiences, such as finding it difficult to get time with a mentor. This talk will review other lessons learned in five years of community mentoring as it describes an alternative paradigm for REUs.

Author(s): Henry Kobulnicky¹, Lara Maierhofer¹, Carol Kobulnicky¹, Daniel A. Dale¹

Institution(s): 1. *University of Wyoming*

216.04 – Public Science Education and Outreach as a Modality for Teaching Science Communication Skills to Undergraduates

The Alan Alda Center for Communicating Science at Stony Brook University is working with Carthage College, Dartmouth College, and Smith College, in partnership with the Appalachian Mountain Club, to develop and disseminate curriculum to incorporate science communication education into undergraduate science programs. The public science education and outreach program operating since 2012 as a partnership between Carthage and the Appalachian Mountain Club is being used as the testbed for evaluating the training methods. This talk will review the processes that have been developed and the results from the first cohort of students trained in these methods and tested during the summer 2017 education and outreach efforts, which reached some 12,000 members of the public. A variety of evaluation and assessment tools were utilized, including surveys of public participants and video recording of the interactions of the students with the public. This work was supported by the National Science Foundation under grant number 1625316.

Author(s): Douglas Arion¹, Christine OConnell⁴, James Lowenthal³, Ryan C. Hickox², Daniel Lyons¹

Institution(s): 1. *Carthage College*, 2. *Dartmouth College*, 3. *Smith College*, 4. *Stony Brook University*

216.05 – Actively Encouraging Learning and Degree Persistence in Advanced Astrophysics Courses

The need to grow and diversify the STEM workforce remains a critical national challenge. Less than 40% of college students interested in STEM achieve a bachelor's degree. These numbers are even more dire for women and URMs, underscoring a serious concern about the country's ability to remain competitive in science and tech. A major factor is persistent performance gaps in rigorous 'gateway' and advanced STEM courses for majors from diverse backgrounds leading to discouragement, a sense of exclusion, and high dropout rates. Education research has clearly demonstrated that interactive-engagement ('active learning') strategies increase performance, boost confidence, and help build positive 'identity' in STEM. Likewise, the evidence shows that traditional science education practices do not help most students gain a genuine understanding of concepts nor the necessary skill

261 – Cosmology II

261.01 – In Defense of an Accelerating Universe: Model Insensitivity of the Hubble Diagram

A recently published paper by Nielsen, Guffanti & Sarkar (*Sci. Rep.* **6**, 35596, Oct. 2016) argues that the evidence for cosmic acceleration is marginal and that a coasting universe - the "Milne Universe" - fits the same supernovae data in a Hubble diagram nearly as well. Other papers have since jumped on the bandwagon. The Milne Universe has negative spatial curvature, but is Riemann-flat. Nevertheless, we confirm that the Milne model fits the data just as well as LCDM. We show that this unexpected result points to a weakness in the Hubble diagram rather than to a failure in LCDM. It seems the Hubble diagram is insensitive to spatial curvature. To be specific, the spatial curvature dependences of the comoving radius in the luminosity distance nearly exactly cancel the energy density differences. That is, $r(\text{LCDM}) = \sinh[r(\text{Milne})]$. By transforming the distance

set to succeed in their disciplines. Yet, lecture-heavy courses continue to dominate the higher-ed curriculum, thus, reinforcing the tired notion that only a small percentage of 'special' students have the inherent ability to achieve a STEM degree. In short, very capable students with less experience and confidence in science, who belong to groups that traditionally are less identified with STEM careers, are effectively and efficiently 'weeded out' by traditional education practices. I will share specific examples for how I successfully incorporate active learning in advanced astrophysics courses to encourage students from all backgrounds to synthesize complex ideas, build bedrock conceptual frameworks, gain technical communication skills, and achieve mastery learning outcomes all necessary to successfully complete rigorous degrees like astrophysics. By creating an inclusive and active learning experience in junior-level extragalactic and stellar interiors/atmospheres courses, I am helping students gain fluency in their chosen major and the ability to 'think like a scientist', both critical to improving STEM degree retention and degree-completion rates. My long-term mission is to see STEM degree programs at U.S. colleges and universities adopt active learning strategies as the curricular norm. Understanding the benefits of this evidence-based best practice is a key step to increasing and diversifying the national STEM degree recipient pool.

Author(s): Daniel H. McIntosh¹

Institution(s): 1. *U. Missouri-Kansas City*

216.06 – Listening to the solar eclipse with an educational tool for the blind and visually impaired

The Great American Solar Eclipse took place on August 21, 2017 and swept through 14 of the United States. This was a highly publicized event and much of the world took notice. We live in a time where everything is accessible via the internet as it is happening. Many people, even those outside of the eclipse path, wanted to experience the event in real-time. We built a device, using an Arduino compatible microcontroller, that converts sunlight to sound so that the blind and visually impaired community could experience the eclipse live with the rest of the world. The device has a high dynamic range light sensor and an audio output that connects to a webcam and a computer. The event was successfully streamed to YouTube from Jackson Hole, Wyoming and people from all around the world connected to listen as the sun was temporarily dimmed by the eclipse of the moon. This device is inexpensive to reproduce (< \$40 per device) and can be used as a teaching tool in a lab or classroom setting. Students can learn to build and write code for these devices as well. This is a tool with great potential for human development.

Author(s): Allyson Bieryla¹, Wanda Diaz-Merced², Daniel Davis¹, Robert Hart¹

Institution(s): 1. *Harvard University*, 2. *Office of Astronomy for Development at the South African Astronomical Observatory*

modulus vs. redshift data to scale factor vs. cosmological time data, for each curvature, $k = \{+1, 0, -1\}$, the curvature dependence of the data is effectively separated thus permitting a more precise fit of the Omega parameters to the scale factor data to decide the correct model. Here we present the data and both models in a scale factor vs. cosmological time plot. The difference of the means of the $k = 0$ and $k = -1$ data separate at a 2-sigma confidence level. The LCDM fit to the $k = 0$ data are consistent with an accelerating universe to 99% confidence. The Milne universe fits the $k = -1$ data to no better than about 70% confidence. This is consistent with independent CMB and BAO observations supporting a flat universe.

Author(s): Harry I Ringermacher¹, Lawrence R Mead¹

Institution(s): 1. *U. of Southern Mississippi*

261.02D – Cosmology with CLASS

The Cosmology Large Angular Scale Surveyor (CLASS) will use large-scale measurements of the polarized cosmic microwave background (CMB) to constrain the physics of inflation, reionization, and massive neutrinos. The experiment is designed to characterize the largest scales, which are inaccessible to most ground-based experiments, and remove Galactic foregrounds from the CMB maps. In this dissertation talk, I present simulations of CLASS data and demonstrate their ability to constrain the simplest single-field models of inflation and to reduce the uncertainty of the optical depth to reionization, τ , to near the cosmic variance limit, significantly improving on current constraints. These constraints will bring a qualitative shift in our understanding of standard Λ CDM cosmology. In particular, CLASS's measurement of τ breaks cosmological parameter degeneracies. Probes of large scale structure (LSS) test the effect of neutrino free-streaming at small scales, which depends on the mass of the neutrinos. CLASS's τ measurement, when combined with next-generation LSS and BAO measurements, will enable a 4σ detection of neutrino mass, compared with 2σ without CLASS data. I will also briefly discuss the CLASS experiment's measurements of circular polarization of the CMB and the implications of the first-such near-all-sky map.

Author(s): Duncan Watts¹

Institution(s): 1. Johns Hopkins University

Contributing team(s): CLASS Collaboration

261.03D – Integrated Approach to Cosmology

Recent progress in observational cosmology and the establishment of Λ CDM have relied on the combination of different cosmological probes. These probes are not independent, since they all measure the same physical fields. The resulting cross-correlations allow for a robust test of the cosmological model through the consistency of different physical tracers and for the identification of systematics. Integrated analyses taking into account both the auto- as well as the cross-correlations between cosmological probes therefore present a promising analysis method for both current as well as future data.

In this talk, I will present an integrated analysis of CMB temperature anisotropies, CMB lensing, galaxy clustering and weak lensing as well as background probes. I will describe the cosmological probe combination framework, the obtained results and illustrate how this analysis has provided a confirmation of Λ CDM through the consistency of different probes. Furthermore, I will discuss possible tensions between the derived constraints on cosmological parameters and existing ones.

Author(s): Andrina Nicola¹, Alexandre Refregier¹, Adam Amara¹

Institution(s): 1. ETH Zuerich

261.04D – Modeling of the response of the POLARBEAR bolometers with a continuously rotating half-wave plate

262 – HEAD II: GW170817/GRB 170817A: Multi-messenger Astrophysics from a Neutron Star Merger

262.01 – Gravitational wave discovery and characterization of the binary neutron star inspiral GW170817

On August 17, 2017 the Advanced LIGO and Advanced Virgo gravitational-wave detectors observed a binary neutron star inspiral. The source, GW170817, was the closest, loudest, and best localized gravitational-wave observation to date and was part of the spectacular multi-messenger observing campaign including the associated gamma-ray burst, a transient counterpart discovered in the optical, and late-time X-ray and radio emission. This talk will overview the discovery of GW170817 and what has been learned about the source from the gravitational-wave observations.

The curly pattern, the so-called B-mode, in the polarization anisotropy of the cosmic microwave background (CMB) is a powerful probe to measure primordial gravitational waves from the cosmic inflation, as well as the weak lensing due to the large scale structure of the Universe. At present, ground-based CMB experiments with a few arcminutes resolution such as POLARBEAR, SPTpol, and ACTPol have successfully measured the angular power spectrum of the B-mode only in sub-degree scales, though these experiments also have potential to measure the inflationary B-modes in degree scales in absence of the low-frequency noise (1/f noise). Thus, techniques of polarization signal modulation such as a continuously rotating half-wave plate (CRHWP) are widely investigated to suppress the 1/f noise and also to reduce instrumental systematic errors. In this study, we have implemented a CRHWP placed around the prime focus of the POLARBEAR telescope and operated at ambient temperatures. We construct a comprehensive model including half-wave plate synchronous signals, detector non-linearities, beam imperfections, and all noise sources. Using this model, we show that, in practice, the 1/f noise and instrumental systematics could remain even with the CRHWP. However, we also evaluate those effects from test observations using a prototype CRHWP on the POLARBEAR telescope and find that the residual 1/f noise is sufficiently small for POLARBEAR to probe the multipoles about 40. We will also discuss prospects for future CMB experiments with better sensitivities.

Author(s): Satoru Takakura¹

Institution(s): 1. KEK

Contributing team(s): POLARBEAR collaboration

261.05D – The Cosmology Large Angular Scale Surveyor (CLASS)

The Cosmology Large Angular Scale Surveyor (CLASS) is an array of telescopes that observe Cosmic Microwave Background (CMB) polarization over $\sim 65\%$ of the sky from the Atacama Desert, Chile in frequency bands at 40 GHz, 90 GHz, 150 GHz, and 220 GHz. Multi-frequency observation enables CLASS to distinguish CMB from galactic foregrounds. CLASS is making large angular scale CMB polarization measurements as part of a five-year survey that will constrain the tensor-to-scalar ratio at the 0.01 level by measuring both the reionization and recombination peaks. CLASS will measure the optical depth to last scattering to near the cosmic variance limit, significantly improving on current constraints. Combining the CLASS optical depth measurement with higher resolution data will improve constraints on the sum of neutrino masses. CLASS will also provide the deepest wide-sky-area Galactic microwave polarization maps for Galactic studies. CLASS has been observing for over one year at 40 GHz frequency band. In my talk, I will introduce the science, design, and current status of the CLASS experiment.

Author(s): Zhilei Xu¹

Institution(s): 1. University of Pennsylvania

Contributing team(s): CLASS Collaboration

Author(s): Tyson Littenberg¹

Institution(s): 1. NASA Marshall Space Flight Center

Contributing team(s): LIGO Scientific Collaboration and Virgo Collaboration

262.02 – The First Unambiguous Electromagnetic Counterpart to a Gravitational-Wave Signal: GRB 170817A and GW170817

On 2017 August 17 at 12:41:06 UTC the Fermi Gamma-ray Burst Monitor (GBM) detected and triggered on the short gamma-ray burst (GRB) 170817A. Approximately 2 s prior to this GRB, the LIGO gravitational-wave observatory triggered on a binary compact merger candidate associated with the GRB. This is the

first unambiguous coincident observation of gravitational waves and electromagnetic radiation from a single astrophysical source and marks the start of gravitational-wave multi-messenger astronomy. We report the GBM observations and analysis of this short GRB and the joint science that results from this discovery.

Author(s): Adam Goldstein¹

Institution(s): 1. *Universities Space Research Association*

262.03 – Discovery, Follow-up, and Implications of the Optical/Infrared Counterpart to GW170817

On August 17th, 2017, the field of multi-messenger, gravitational-wave, astronomy was born. On this date, Advanced LIGO and Advanced Virgo observed gravitational waves from the coalescence of a neutron star binary with a false alarm probability of 1 per 10000 years and electromagnetic counterparts were subsequently identified across the entire electromagnetic spectrum. In this talk, I will give a broad review of the optical and infrared emission associated with the binary neutron star merger, GW170817. I will describe the process of the discovery and localization of the optical counterpart, and review the extensive follow-up observations obtained over the following three weeks. Finally, I will place these results in context. I will discuss the implications of these observations on our understanding of the ejecta from neutron star mergers, the origin of r-process elements, and the prospects for the identification of similar transients in upcoming surveys.

217 – Plenary Talk: The Stormy Life of Galaxy Clusters, Larry Rudnick (Minnesota Institute for Astrophysics)

217.01 – The Stormy Life of Galaxy Clusters

Galaxy clusters, the largest gravitationally bound structures, hold the full history of their baryonic evolution, serve as important cosmological tools and allow us to probe unique physical regimes in their diffuse plasmas. With characteristic dynamical timescales of 10⁷-10⁹ years, these diffuse thermal and relativistic media continue to evolve, as dark matter drives major mergers and more gentle continuing accretion. The history of this assembly is encoded in the plasmas, and a wide range of observational and theoretical investigations are aimed at decoding their signatures. X-ray temperature and density variations, low Mach number shocks, and "cold front" discontinuities all illuminate clusters' continued evolution. Radio structures and spectra are passive

219 – Dark Energy Survey: Results and Data Release

219.01 – The Dark Energy Survey First Data Release

In this talk I will announce and highlight the main components of the first public data release (DR1) coming from the Dark Energy Survey (DES).

In January 2016, the DES survey made available, in a simple unofficial release to the astronomical community, the first set of products. This data was taken and studied during the DES Science Verification period consisting on roughly 250 sq. degrees and 25 million objects at a mean depth of $i=23.7$ that led to over 80 publications from DES scientist.

The DR1 release is the first official release from the main survey and it consists on the observations taken during the first 3 seasons from August 2013 to February 2016 (about 100 nights each season) of the survey which cover the entire DES footprint. All of the Single Epoch Images and the Year 3 Coadded images distributed in 10223 tiles are available for download in this release. The catalogs provide astrometry, photometry and basic classification for near 400M objects in roughly 5000 sq. degrees on the southern hemisphere with a approximate mean depth of $i=23.3$. Complementary footprint, masking and depth information is also available. All of the software used during the generation of these products are open sourced and have been made available through the Github DES Organization. Images, data and other sub products have been possible through the international and collaborative effort of all 25 institutions involved in DES and are available for exploration and download

Author(s): Maria Drout¹

Institution(s): 1. *Carnegie Observatories*

262.04 – The Firework of Electromagnetic Counterparts from GW170817

The gravitational-wave signal of the binary neutron star merger GW170817 was followed by a firework of electromagnetic transients across the entire electromagnetic spectrum. The gamma-ray emission has provided strong evidence for the association of short gamma-ray bursts (SGRBs) with binary neutron star mergers and the ultraviolet, optical, and near-infrared emission is consistent with a kilonova indicative of the formation of heavy elements in the merger ejecta by the rapid neutron capture process (r-process). In this talk, I will discuss and review theoretical scenarios to interpret the gamma-ray, X-ray, and radio observations. I will present recent results from general-relativistic magnetohydrodynamic simulations and discuss possible scenarios and mass ejection mechanisms that can give rise to the observed kilonova features. In particular, I will argue that massive winds from neutrino-cooled post-merger accretion disks most likely synthesized the heavy r-process elements in GW170817.

Author(s): Daniel Siegel¹

Institution(s): 1. *Columbia University*

indicators of merger shocks, while radio galaxy distortions reveal the complex motions in the intracluster medium. Deep in cluster cores, AGNs associated with brightest cluster galaxies provide ongoing energy, and perhaps even stabilize the intracluster medium. In this talk, we will recount this evolving picture of the stormy ICM, and suggest areas of likely advance in the coming years.

Author(s): Lawrence Rudnick¹

Institution(s): 1. *University of Minnesota*

through the interfaces provided by a partnership between NCSA, NOAO and LineA.

Author(s): Matias Carrasco Kind¹

Institution(s): 1. *NCSA/University of Illinois*

219.02 – Cosmological Constraints from Galaxy Clustering and Weak Lensing

The Dark Energy Survey (DES) is a five-year, 5000 sq. deg. observing program using the Dark Energy Camera on the 4m Blanco telescope at CTIO. I will describe the cosmological analysis of large-scale structure in the Universe using 1321 sq. deg. of data taken in the first year of DES operations. The analysis combines unprecedented measurements of weak gravitational lensing and the clustering of galaxies over the redshift range 0.2 to 1.3 to derive the most precise such cosmological constraints to date. These DES results from the low-redshift Universe are consistent with those from the cosmic microwave background (CMB) and support the standard cosmological model, Λ CDM. In the coming years, DES will produce significantly tighter constraints on cosmology through similar and additional analyses using observations over more than three times the sky-area and more than twice the integrated exposure time per object as these results.

Author(s): Michael Troxel¹

Institution(s): 1. *Ohio State University*

Contributing team(s): DES Collaboration

219.03 – DES cluster cosmology results

DES detects thousands of galaxy clusters across its footprint, reaching out to redshift $z \approx 1$. In addition, its weak-lensing program allows us to weigh those clusters with unprecedented accuracy. The combinations of these two efforts enables powerful constraints of the cosmological model. I will describe the approach we take regarding measurements, calibrations, and theoretical models; discuss the benefits of combining DES with X-ray and Sunyaev-Zel'dovich observations; and present the first cosmological results from galaxy clusters in the DES Year-1 data.

Author(s): Peter Melchior¹

Institution(s): 1. Princeton University

Contributing team(s): DES Weak Lensing Working Group, DES Cluster Working Group

219.04 – Cosmological Parameter Constraints from the Dark Energy Survey Supernova Program Three Year Spectroscopic Sample.

We present cosmological parameter constraints from 251 spectroscopically confirmed Type Ia Supernovae ($0.02 < z < 0.9$) discovered during the first 3 years of the Dark Energy Survey Supernova Program (DESSN). The photometric calibration, scene modeling photometric pipeline, additional low- z supernovae samples ($z < .1$), as well as the final cosmological results and systematics analysis are discussed.

Author(s): Dillon Brout¹

Institution(s): 1. University of Pennsylvania

219.05 – Milky Way Science with the Dark Energy Survey

220 – Results from the August 21, 2017, Total Solar Eclipse

The total solar eclipse that crossed the United States from Oregon to South Carolina on August 21, 2017, was a spectacular event seen by tens of millions. Scientific measurements were made by many, including not only professional but also citizen-science projects. At this special session, we will have reports on (and preliminary reduction of) a wide variety of types of observations taken inside the 70-mile-wide band of totality as well as comments on the public effects of and reaction to the partial eclipse across the whole United States. We will include results from airborne platforms and simultaneous observations from satellites.

220.01 – Eclipse Across America: Through the Eyes of NASA

Monday, August 21, 2017, marked the first total solar eclipse to cross the continental United States coast-to-coast in almost a century. NASA scientists and educators, working alongside many partners, were spread across the entire country, both inside and outside the path of totality. Like many other organizations, NASA prepared for this eclipse for several years. The August 21 eclipse was NASA's biggest media event in recent history, and was made possible by the work of thousands of volunteers, collaborators and NASA employees. The agency supported science, outreach, and media communications activities along the path of totality and across the country. This culminated in a 3 1/2-hour broadcast from Charleston, SC, showcasing the sights and sounds of the eclipse – starting with the view from a plane off the coast of Oregon and ending with images from the International Space Station as the Moon's inner shadow left the US East Coast. Along the way, NASA shared experiments and research from different groups of scientists, including 11 NASA-supported studies, 50+ high-altitude balloon launches, and 12 NASA and partner space-based assets. This talk shares the timeline of this momentous event from NASA's perspective, describing outreach successes and providing a glimpse at some of the science results available and yet to come.

Author(s): C. Alex Young¹

Institution(s): 1. NASA Goddard Space Flight Center

Contributing team(s): The Heliophysics Education Consortium

The Dark Energy Survey (DES) offers the deepest, wide-area view of the southern sky to date, providing an unprecedented opportunity to study faint and/or distant stellar populations. I will describe several ongoing studies of the Milky Way environment using DES, including searches for Milky Way satellite galaxies, outer halo star clusters, stellar streams, and variable stars. In combination with an extensive spectroscopic follow-up campaign, DES has helped shed light on the missing satellites problem and the origin of the heavy elements. At the same time, the proximity of the DES footprint to the Magellanic Clouds has raised several new questions about the influence of the Milky Way's largest neighbors on the formation of the local environment. With additional imaging and improved data quality, DES promises to become an even more powerful tool to probe near-field cosmology and Galactic archeology in the years to come.

Author(s): Alex Drlica-Wagner¹

Institution(s): 1. Fermilab

Contributing team(s): DES Collaboration

219.06 – DES Gravitational Wave Follow-up Program

We present latest results from the DES/DECam program of searches for optical counterparts of gravitational wave events triggered by LIGO/Virgo detectors.

Author(s): Marcelle Soares-Santos¹

Institution(s): 1. Brandeis University

220.02 – Preparing a Nation for the Eclipse of a Generation -

On August 21st 2017, there was a total solar eclipse visible from a vast swath of the US.

In preparation for that event, the American Astronomical society created a taskforce charged with planning for the eclipse for the entire nation. The preparations included interfacing with the public, the media, non-profit organizations and governmental organizations. Preliminary data suggests that nearly 90% of American adults watched the eclipse either directly or via live streams. Moreover, there were no major problems associated with the event, in spite of valiant attempts from, e.g. improper solar viewing materials. The eclipse offered opportunities for many scientific experiments within and beyond astronomy. Here we present on the work of the taskforce, and the lessons learned as well as lesser known science experiments undertaken during the eclipse.

Author(s): Angela Speck⁹, Shadia Habbal⁸, Richard Tresch Fienberg¹, Michael Kentrianakis¹, Andrew Fraknoi⁵, Tyler Nordgren¹⁰, Matthew Penn⁷, Jay M. Pasachoff¹¹, Michael Bakich³, Henry Winter⁴, Pamela Gay², Mario Motta⁶

Institution(s): 1. American Astronomical Society, 2. Astronomical Society of the Pacific, 3. Astronomy Magazine, 4. CfA, 5. Foothill College, 6. Massachusetts General Hospital, 7. National Solar Observatory, 8. University of Hawaii, 9. University of Missouri, 10. University of Redlands, 11. Williams College

220.03 – Eclipse Megamovie 2017: How did we do?

The Eclipse Megamovie program, as set up for the Great American Eclipse of 21 August 2017, achieved a massive volunteer participation, making maximal use existing equipment but with coordinated training. Everything worked fine, and the archive entered the public domain on Friday, October 6. It comprises about 800 GB of data from DSLR cameras and telescopes. An additional 200 GB of data were obtained by smartphone cameras operating a dedicated free app. The massive oversampling made possible by the many (about 2500) volunteer observers has

opened new parameter space for tracking coronal and chromospheric time development. Fortunately some solar activity appeared during the 90-minute period of totality, including a C-class flare and an ongoing CME. At the smartphone level, with the advantage of precise GPS timing, we have data on solar structure via the timing of Baily's Beads at the 2nd and 3rd contacts. The Megamovie archive is an historical first, and we hope that it has already been a springboard for citizen-science projects. We discuss the execution of the program, presenting some of the 2017 science plans and results. We expect that the eclipse of 2024 will be better still.

Author(s): Hugh Hudson⁵, Mark Bender², Braxton Collier⁴, Calvin Johnson³, Justin Koh³, David Konerding³, Juan Carlos Martinez Oliveros⁵, Laura Peticolas⁵, Vivian White¹, Dan Zevin⁵
Institution(s): 1. ASP, 2. Eclipse over America, 3. Google, 4. Ideum, 5. UC Berkeley

220.04 – The Award Winning Black Suns

Black Suns: An Astrophysics Adventure is a documentary film focusing on the annular and total solar eclipses of 2012. We made a different kind of astronomy documentary showing the human aspects rather than just focusing on pretty astronomy pictures. The film combines personal stories with science. Our heroes are Hakeem Oluseyi and Alphonse Sterling, who valiantly travel to study the solar corona during total solar eclipses. The goals of the film included presenting three dimensional scientists, to show their paths to becoming astrophysicists, and to show them as they collect data and work as scientists. Drama and tension surround taking data during the small window of time during totality. The Black Suns was filmed in Tokyo, Cairns, Tucson, and Melbourne Florida. Uniquely, the film began through a Kickstarter campaign to fund travel and filming in Tokyo. Many American Astronomical Society members donated to the film! Black Suns won the Jury Prize at the 2017 Art of Brooklyn Film Festival. Black Suns will be screening in full on ???.

Author(s): Jarita Holbrook¹
Institution(s): 1. National Science Foundation

220.05 – First results from the Citizen CATE Experiment from August 2017

The Citizen Continental-America Telescopic Eclipse Experiment deployed 68 identical telescope/detector systems across the path of totality for the August 2017 solar eclipse. The sites were located from Oregon to South Carolina, and while at any one site the solar corona was observed for just 2 minutes, the combined data set reveals evolution of the corona for 93 minutes of time. CATE aims to measure the acceleration of the fast solar wind in polar plumes, which is currently unknown as the inner solar corona is not observed from space and difficult to observe at high signal to noise from the ground. With radial velocities ranging from 1 to 100 km/s, density enhancements in the wind in the polar plumes should be observed to move across the CATE field of view in about 1 hour.

On 21 Aug 2017, the CATE network had fantastic luck, collecting data from more than 56 of the 68 sites, and excellent data was collected at the first and last sites, maximizing the time coverage. Several of the volunteers from 27 universities, 22 high schools and 19 amateur astronomers uploaded one high-dynamic range image on eclipse day and an initial movie of the coronal evolution has been made (<https://citizencate.org>). Polar plumes are observed in the CATE data to the edge of the field above both north and south polar coronal holes. Slow evolution of low-lying coronal loops is seen, and large-scale motions are visible in a coronal streamer on the south-east solar limb. An ejection event is observed in the southern coronal hole, but with just 1% of the data analyzed so far, the signal to noise ratio is currently not sufficient to track steady solar wind flows.

CATE was funded with a collaboration of federal, corporate and private groups. CATE training was funded by NASA, and CATE equipment was funded by Daystar, Mathworks, Celestron, colorMaker, NSF and a dozen smaller donors. The funding was

organized so that all 68 CATE groups are keeping their equipment, and CATE is now seeking other types of citizen science projects in astronomy. Please bring your project ideas to the talk!

Author(s): Matthew Penn¹
Institution(s): 1. National Solar Observatory
Contributing team(s): The Citizen CATE Experiment 2017 Team

220.06 – Early Science Results from the Williams College Eclipse Expedition

We describe our first cut of data reduction on a wide variety of observations of the solar corona and of the effect of the penumbra and umbra on the terrestrial atmosphere, carried out from our eclipse site on the campus of Willamette University in Salem, Oregon. Our team of faculty, undergraduate students, graduate students, and other colleagues observed the eclipse, taking images and spectra with a variety of sensors and telescopes. Equipment included frame-transfer cameras observing at 3 Hz in 0.3 nm filters at the coronal green and red lines to measure the power spectrum of oscillations in coronal loops or elsewhere in the lower corona; 3 spectrographs; a variety of telescopes and telephotos for white-light imaging; a double Lyot system tuned at Fe XIV 530.3 nm (FWHM 0.4 nm) and Fe X 637.4 nm (FWHM 0.5 nm); and a weather station to record changes in the terrestrial atmosphere. We are comparing our observations with predictions based on the previous mapping of the photospheric magnetic field, and preparing wide-field complete coronal imaging incorporating NOAA/NASA GOES-16 SUVI and NRL/NASA/LASCO for the corona outside our own images (which extend, given the completely clear skies we had, at least 4 solar radii), and NASA SDO/AIA and NOAA/NASA GOES-16 SUVI for the solar disk. One of our early composites appeared as Astronomy Picture of the Day for September 27:

<https://apod.nasa.gov/apod/ap170927.html>
Our expedition was supported in large part by grants from the Committee for Research and Exploration of the National Geographic Society and from the Solar Terrestrial Program of the Atmospheric and Geospace Sciences Division of the National Science Foundation, with additional student support from the STP/AGS of NSF, the NASA Massachusetts Space Grant Consortium, the Sigma Xi honorary scientific society, the Clare Booth Luce Foundation studentship and the Freeman Foote Expeditionary Fund at Williams College, other Williams College funds, and U. Pennsylvania funds.

Author(s): Jay M. Pasachoff¹², Michael J Person⁴, Ron Dantowitz³, Christian A. Lockwood¹², Tim Nagle-McNaughton¹², Erin N Meadors¹², Cielo C. Perez¹², Connor J Marti¹², Ross Yu¹², Brendan Rosseau¹², Declan M. Daly¹², Charles A. Ide¹², Allen B. Davis¹³, Muzhou Lu⁸, David Sliski¹⁰, John Seiradakis¹, Aris Voulgaris¹, Vojtech Rusin², Marcos A. Peñaloza-Murillo¹¹, Michael Roman⁷, Daniel B. Seaton⁵, Amy Steele⁹, Duane M. Lee⁴, Marcus J. Freeman⁶
Institution(s): 1. Aristotle U., Dept. Physics, 2. Astron. Inst., Slovakian Acad. Sci., 3. Clay Center Obs., Dexter Southfield School, 4. MIT, 5. NOAA, 6. RIT, 7. U Michigan, 8. U. Colorado, Boulder, 9. U. Maryland, 10. U. Pennsylvania, 11. Universidad los Andes, 12. Williams College, 13. Yale U.

220.07 – Observations of the Dynamics and Thermodynamics of the Corona during the 21 August 2017 Total Solar Eclipse

The visible wavelength range, encompassing forbidden coronal emission lines, offers unique diagnostic tools for exploring the physics of the solar corona, such as its chemical composition and the dynamics of its major and minor constituents. These tools are best exploited during total solar eclipses, when the field of view spans several solar radii, starting from the solar surface. This spatial span is currently untenable from any observing platform. Imaging and spectroscopic eclipse observations, including the 2017 August 21 event, are shown to be the first to yield the temperature distribution in the corona as a function of solar cycle.

They are also the first to lead to the discovery of cool prominence material at less than 10,000 to 50,000 K, within more than a radius above the solar surface, streaming away from the Sun, while maintaining its compositional identity. These data underscore the importance of capturing emission from coronal forbidden lines with the next generation space-based instrumentation to address the general problem of coronal heating.

Author(s): Shadia Rifai Habbal³, Adalbert Ding², Miloslav Druckmüller¹

Institution(s): 1. Brno University of Technology, 2. Institute for Optics and Atomic Physics, 3. University of Hawaii

Contributing team(s): The Solar Wind Sherpas

220.08 – Physical Conditions in the Solar Corona Derived from the Total Solar Eclipse Observations obtained on 2017 August 21 Using a Polarization Camera

We present preliminary results obtained by observing the solar corona during the 2017 August 21 total solar eclipse using a polarization camera mounted on an eight-inch Schmidt-

221 – Beyond the Academy: Panel Discussion on Entering Non-Academic Careers

More of our astronomy colleagues are choosing meaningful careers in industry, and yet very little information trickles back into academia about what those careers are like, what skills transferred from astronomy training, or even how to make the career transition. The lack of solid information and mentoring can make any career path beyond the academy seem daunting. We propose to fill this information gap in a continuation of the Employment Committee's professional development workshops and seminars at the annual winter meeting of the American Astronomical Society (AAS). In partnership with the American Institute of Physics (AIP), we propose to have two complimentary sessions on careers beyond academia. This first session is designed to provide an inside look at the types of projects tackled

222 – AGN, QSO, Blazars IV

222.01 – Measuring the ISM Content of Optically Luminous Type 2 Quasars

There is a connection between black holes (BH) and the surrounding bulge stars. Measuring the cold interstellar medium (ISM) content of host galaxies is essential to understand the coevolution of galaxies and BHs. The ISM measurement is important because gas constitutes the raw material from which BHs grow and stars form. Quasars are extremely luminous active galaxies fueled by accreting supermassive black holes. Type 2 quasars have narrow spectral lines whereas type 1 quasars have broad spectral lines. Not only can the ISM measurements provide empirical data to help further clarify quasar models but it is also crucial in distinguishing the physical differences between type 1 and type 2 quasars. Observations of twenty type 2 quasars were made using IRAM, a single dish 30 meter radio telescope, to measure ^{12}CO (1-0) and ^{12}CO (2-1) emission. We used line widths to constrain the dynamical mass and gravitational potential of the host galaxy. Star formation rate (SFR) measured in the infrared (IR) and SFR derived from optical spectra were used to estimate star formation efficiency and gas depletion time scale ($M \text{ H}_2/\text{star formation rate}$). Preliminary analysis suggests that star formation efficiency in type 2 quasars is slightly higher than in type 1 quasars.

Author(s): Jameeka Marshall⁵, Andreea Petric³, Nicolas Flagey¹, Mark Lacy⁴, Alain Omont²

Institution(s): 1. Canada-France-Hawaii Telescope Corporation, 2. Institut d'Astrophysique de Paris, 3. Institute for Astronomy/Canada-France-Hawaii Telescope Corporation, 4. National Radio Astronomy Observatory, 5. University of Hawaii at Hilo

222.02D – The Evolution of AGN Obscuration: A Result of Dusty Nuclear Starburst Disks

Cassegrain telescope. The observations were made from Madras Oregon during 17:19 to 17:21 UT. Total and polarized brightness images were obtained at four wavelengths (385, 398.5, 410, and 423 nm). The polarization camera had a polarization mask mounted on a 2048x2048 pixel CCD with a pixel size of 7.4 microns. The resulting images had a size of 975x975 pixels because four neighboring pixels were summed to yield the polarization and total brightness images. The ratio of 410 and 385 nm images is a measure of the coronal temperature, while that at 423 and 398.5 nm images is a measure of the coronal flow speed. We compared the temperature map from the eclipse observations with that obtained from the Solar Dynamics Observatory's Atmospheric Imaging Assembly images at six EUV wavelengths, yielding consistent temperature information of the corona.

Author(s): N. Gopalswamy¹, Seiji Yashiro², Nelson Reginald², Neeharika Thakur², Barbara J Thompson¹, Qian Gong¹

Institution(s): 1. NASA Goddard Space Flight Center, 2. The Catholic University of America

and skills needed in a variety of rewarding and intellectually challenging careers. Through a series of invited talks from astronomers who are currently in the professional, entrepreneurial, and government sectors, we will learn about their career trajectories, what they do day-to-day, and why they recommend this path, as well as the growth opportunities and challenges in their fields. Showcasing these real-world examples of astronomers in successful careers will provide tangible recognition of the rich variety of career paths available beyond academia.

A significant number of active galactic nuclei (AGNs) are observed to be obscured by dust and gas. The distribution of obscured AGNs (f_2), especially the fraction of Compton thick AGNs, plays an important role in modeling the cosmic X-ray background (CXB). Moreover, this f_2 seems to be dependent on the redshift and the AGN luminosity with various mechanisms and physical conditions potentially responsible for the observed obscuration. One of the possible explanations for the obscuration in Seyfert galaxies at intermediate redshift is dusty starburst disks. In this work, we compute the 2D hydrostatic structure of 768 nuclear starburst disks (NSDs) which spans a wide range of physical conditions (e.g., size of a disk, gas fraction, & black hole mass) to compute the evolution of the obscuring N_{H} distribution. The major findings are: (1) the obscured fraction increases with the redshift for all N_{H} , (2) the N_{H} distribution always peaks near $10^{23.5} \text{ cm}^{-2}$, and (3) the obscured AGN has a stronger evolution with increasing N_{H} . I will also go through the predicted cosmic X-ray background as well as the AGN number counts in 2-8 keV and 8-24 keV bands.

Author(s): Raj Gohil¹, David Ballantyne¹

Institution(s): 1. Georgia Institute of Technology

222.03 – The Curious Molecular Gas Conditions in a $z=2.6$ Radio-loud Quasar

Theoretical work suggests that AGN play an important role in quenching star formation in massive galaxies. In addition to molecular outflows observed in the local universe, emission from very high- J CO rotational transitions has been one of the key pieces of evidence for AGN directly affecting the molecular gas reservoirs that fuel star formation. However, very few observations of $J_{\text{upper}} > 9$ transitions exist for galaxies in the early universe. Here we will present the peculiar molecular gas conditions in MG 0414+0534 (MG 0414 hereafter), one of the few high- z galaxies with very high- J CO detections. MG 0414 is a strongly lensed IR-bright radio-loud quasar with broad H α

emission at $z=2.6390$. We recently confirmed the CO(3–2) detection from Barvainis et al. (1998), but were unable to detect the CO(1–0) line. The 3 σ lower limit on the 3–2/1–0 line ratio (in units of brightness temperature) is $r_{3,1} > 5.72$, which is significantly higher than the $r_{3,1} \leq 1$ typical for thermalized optically thick emission in other $z \sim 2-3$ AGN host galaxies. In addition, the CO(11–10) line was detected to high significance using the Atacama Large Millimeter/submillimeter Array, and the CO(11–10) line FWHM is nearly double that of the CO(3–2) line. We will discuss possible explanations for the peculiar line ratios in MG 0414 (such as optically thin emission, molecular outflows, and differential lensing) and what the origin of these ratios imply for molecular gas observations of other high- z AGN host galaxies.

Author(s): Chelsea Sharon⁴, Dominik A Riechers², Tsz Kuk Leung², Axel Weiss⁵, Fabian Walter⁶, Chris Carilli⁷, Kirsten Kraiburg Knudsen¹, Jacqueline Hodge³

Institution(s): 1. Chalmers University of Technology, 2. Cornell University, 3. Leiden Observatory, 4. McMaster University, 5. MPI für Radioastronomie, 6. MPIA, 7. NRAO

222.04 – Star Formation of Merging Disk Galaxies with AGN Feedback Effects

We studied the star formation of merging disk galaxies using numerical hydrodynamics simulations. Including gas accretion onto supermassive black holes and active galactic nucleus (AGN) feedback in our model, we performed idealized merger simulations with various parameters such as mass ratios, inclinations, orbits, galaxy structures and morphologies. We confirmed that star formation is suppressed more efficiently by AGN in merging galaxies than in isolated galaxies. Furthermore, we found that AGN effect is more significant in major mergers than in minor mergers. Contrary to the previous simulations without AGN feedback, we found that enhancement of star formation does not show significant difference in galaxies with different primary bulge-to-total ratios. We discuss the gap between our results made with AGN prescriptions and observations.

Author(s): Jongwon Park¹, Rory Smith¹, Sukyoung ken Yi¹
Institution(s): 1. Yonsei University

222.05D – Revealing the Star-Forming Hosts of Luminous Quasars at $z \sim 2$: A Multi-Wavelength Study

Quasars are thought to govern many fundamental processes within galaxies, from quenching star formation to shaping the galaxy itself. In an evolutionary picture of quasars, the most luminous systems ($L_{\text{bol}} \sim 10^{47}$ erg) are thought to evolve from merger-driven starbursts, appearing heavily obscured during their transition to UV-luminous quasars as dust from the decaying starburst is being cleared out of the galaxy. Understanding the connection between dust obscuration, black

223 – Data Driven Discoveries in Serendipitous X-ray Catalogs

For the past ~ 17 years, Chandra and XMM Newton have been observing selected regions of the sky in the 0.5 - 10 keV band. These observations have resulted in a wealth of publications on targeted sources. Collectively, the observations cover 1800 deg² of the sky with a total of 550 Ms of exposure time, resolving 100% of the cosmic XRB in point sources. These data have been mined by the Chandra and XMM-Newton teams to extract catalogs that include all of the serendipitous sources in the field of view of given targets, as well as the targets themselves. These catalogs include almost a million X-ray sources, in wildly different environments. Most of the catalog sources have not undergone specific investigation and represents, for this reason, an untapped reservoir of discovery that could shed new light on the X-ray Universe. Some of the questions we will seek to address are: What new can be learnt from an open ended exploration of the X-ray sky making use of these catalogs? What are the X-ray-specific diagnostics and exploration techniques that will open the field to new, unexpected discoveries? What challenges are posed by mining these X-ray catalogs in conjunction with other wavelength repositories? The speakers in this session will guide us through

hole accretion and star formation in luminous quasars undergoing this transition is therefore an important test of such evolutionary models. Host galaxy studies of the most massive and luminous quasars at $z > 1.5$ remain challenging, particularly in the rest-frame UV where a quasar will typically outshine its host galaxy by several orders of magnitude. I will present the first rest-frame UV study for a population of obscured type-1 quasars at $z \sim 2$ - a peak epoch in both star formation and black hole accretion. By combining deep ground-based imaging from the Dark Energy Survey (DES) with near infra-red observations, I exploit dust obscuration towards the quasar to isolate host galaxy emission, finding obscured quasars to reside in prodigiously star-forming hosts at $z \sim 2$, with the most actively star-forming galaxies appearing to host the most luminous quasars. Combining these results with new sub-mm observations from SCUBA2, I will present a direct comparison of the unobscured and obscured star formation in this population of dusty quasar hosts.

Author(s): Clare Wethers¹, Manda Banerji¹, Paul Hewett¹
Institution(s): 1. University of Cambridge
Contributing team(s): Dark Energy Survey (DES)

222.06 – Photoionization Modelling of the Giant Broad-Line Region in NGC 3998.

Prior high angular resolution spectroscopic observations of the low-ionization nuclear emission-line region in NGC 3998 obtained with the Space Telescope Imaging Spectrograph aboard the Hubble Space Telescope revealed a rich UV-visible spectrum consisting of broad permitted and broad forbidden emission lines. The photoionization code XSTAR is employed together with reddening-insensitive emission line diagnostics to constrain a dynamical model for the broad-line region (BLR) in NGC 3998. The BLR is modelled as a large H⁺ region ~ 7 pc in radius consisting of dust-free, low density $\sim 10^4$ cm⁻³, low metallicity $\sim 0.01 Z/Z_{\odot}$ gas. Modelling the shape of the broad H α emission line significantly discriminates between two independent measures of the black hole mass, favouring the estimate of de Francesco (2006). Interpreting the broad H α emission line in terms of a steady-state spherically symmetric inflow leads to a mass inflow rate of 1.4×10^{-2} M \odot /yr, well within the present uncertainty of calculations that attempt to explain the observed X-ray emission in terms of an advection-dominated accretion flow (ADAF). Collectively, the model provides an explanation for the shape of the H α emission line, the relative intensities and luminosities for the H Balmer, [OIII], and potentially several of the broad UV emission lines, as well as refining the initial conditions needed for future modelling of the ADAF.

Author(s): Nicholas Devereux¹
Institution(s): 1. Embry-Riddle Aeronautical University

the XMM and Chandra catalogs, present the recently released Chandra Source Catalog version 2 (source properties, pipeline and public interfaces), talk about new ways to use the available datasets to address the above questions, and the synergies between X-rays and other wavelengths source catalogs (including SDSS, WISE, Pan-STARRS, etc...). Moreover, we will include a discussion on how the studies on current catalogs can inform what can be done and planned in the near and far future with data from the upcoming large field, large collecting area X-ray telescopes (eRosita, Athena, Lynx, etc).

223.01 – Doing Science with the Chandra Source Catalog

The excellent spatial resolution (~ 1 arcsecond on-axis) of the Chandra X-ray Observatory, combined with a reasonable field of view and low instrumental backgrounds, allow detection of serendipitous X-ray sources with a high detectable-source density with low confusion. The aim of the Chandra Source Catalog (CSC) is to disseminate this wealth of information to the user community in a form that is immediately usable for scientific

investigation, and the catalog is intended to satisfy the needs of a broad-based group of scientists, including those who may be less familiar with astronomical data analysis in the X-ray regime.

The second major release of the catalog, CSC 2.0, will be made available to the user community in early 2018, and preliminary lists of detections and sources are available now. CSC 2.0 will roughly triple the size of the current version of the catalog to an estimated 375,000 detections, corresponding to ~315,000 unique X-ray sources on the sky. For each detected X-ray source, the catalog provides a detailed set of properties including the source position and associated position error ellipse, source extent, multi-band aperture photometry probability density functions, spectral fits using several source models, hardness ratios, and intra- and inter-observation temporal variability measures. All numerical measures have associated two-sided confidence intervals. In addition to tabular data, the catalog provides FITS data products that are immediately suitable for further user analysis, including per-field and per-source images, photon event lists, responses, spectra, and light curves.

We describe the content and organization of the catalog in more detail, discuss the analyses that were performed to extract the measured source properties, and demonstrate how the catalog content can be immediately and effectively utilized for scientific investigations.

This work has been supported by NASA under contract NAS 8-03060 to the Smithsonian Astrophysical Observatory for operation of the Chandra X-ray Center.

Author(s): Ian N Evans¹

Institution(s): 1. *Smithsonian Astrophysical Observatory*

Contributing team(s): The Chandra Source Catalog Team

223.02 – Variable X-ray sources in the 3XMM catalogue

The current version of the XMM-Newton serendipitous source catalogue, 3XMM-DR7, was released on 1st June 2017. It contains 727790 X-ray detections, of which 499266 are unique sources, detected as many as 59 times. This catalogue produced by the Survey Science Centre (SSC) provides a variety of information for each detection, the position and its associated error, a measure of the reliability, as well as count rates and fluxes in 7 different bands, 4 hardness ratios, the probability of the source being constant over an observation and a cross correlation of the detection with more than 200 other catalogues, providing possible multi-wavelength identification. This elaborate catalogue can be searched for sources varying over one observation of up to 36 hours in duration or spanning as much as 16 years in time. We present the 3XMM catalogue and describe some of the rare and interesting objects discovered within it, including accreting stellar mass compact objects, intermediate mass black holes, tidal disruption events and extreme AGN.

Author(s): Natalie A. Webb¹

Institution(s): 1. *Institut de Recherche en Astrophysique et Planétologie*

Contributing team(s): XMM-Newton Survey Science Centre

223.03 – The NuSTAR Serendipitous Survey and Archival X-ray Data

The Nuclear Spectroscopic Telescope Array (NuSTAR) provides an improvement in sensitivity at energies above 10 keV by two orders of magnitude over non-focusing satellites, making it possible to probe deeper into the Galaxy and Universe. Lansbury and collaborators recently completed a catalog of 497 sources serendipitously detected in the 3–24 keV band using 13 square degrees of NuSTAR coverage. With NuSTAR alone, the "serendips" have error circles with radii of 14–22 arcseconds, which is not accurate enough to identify optical or near-IR counterparts that would allow the sources to be classified. Thus,

X-ray data, including catalogs and archival data, have been used extensively to classify the NuSTAR serendips. In some cases, the catalogs provide immediate source classification, while in other cases, the improved positions allow for classification via follow-up ground-based optical spectroscopy. In this talk, we describe the procedures that have been used to classify a large percentage of the serendips, highlighting the use of the X-ray catalogs and archives. We also describe the scientific results, which include new information about populations of Active Galactic Nuclei as well as Galactic sources such as High-Mass X-ray Binaries.

Author(s): John Tomsick¹

Institution(s): 1. *UC Berkeley*

Contributing team(s): The NuSTAR Extragalactic and Galactic Surveys Groups

223.04 – One of a Handful in the Universe: Confirming a Wolf Rayet X-ray Binary Candidate in NGC 253

With Chandra, we have discovered a candidate Wolf Rayet X-ray Binary (WR XRB) in NGC 253 as part of a NuSTAR-Chandra campaign. WR XRBs represents a rarely-observed instance of an progenitor system for a BH-BH merger of the type that emits gravitational waves detectable by Advanced LIGO. This particular source was present in an archival Chandra dataset and had previously not been recognized as a WR XRB candidate. We discuss the implications for this source as well as serendipitous searches for time-variable X-ray phenomena.

Author(s): Ann Hornschemeier⁵, T. J. Maccarone⁷, Mihoko Yukita², Daniel Wik⁹, Vallia Antoniou⁶, Keith Bechtol⁴, Fiona Harrison¹, Bret Lehmer⁸, Andrew Ptak⁵, Daniel Stern³, Tonia Venters⁵, Andreas Zezas⁶

Institution(s): 1. *Caltech*, 2. *Johns Hopkins University*, 3. *JPL/Caltech*, 4. *LSSST - Stanford*, 5. *NASA GSFC*, 6. *Smithsonian Astrophysical Observatory*, 7. *Texas Tech University*, 8. *University of Arkansas*, 9. *University of Utah*

223.05 – X-ray-ing the Low Luminosity Supermassive Black Hole Accretion: the Crucial Role of Public Serendipitous Catalogs.

For most of the nearby active galaxies, a mix of processes including emission from star-forming regions, other ionization sources (shocks, turbulence, etc.), nuclear obscuration, as well as host galaxy starlight obfuscate the true nature of their dominant ionization mechanism. X-ray emission is one of the most reliable primary signatures of accretion activity, and with the advent of the public catalogs, it became one of the most effective diagnostics as well. Working with large and significantly less biased samples that only serendipitous X-ray catalogs are able to provide, we were able to: 1) provide the most accurate estimates of the AGN fraction as a function of a diverse set of parameters; 2) confirm with X-rays a sequence from star-forming to active to passive galaxies that matches trends in both optical host galaxy characteristics and in the large scale environment; 3) discover intriguing similarities between accretion onto supermassive and stellar size black holes, with direct consequences for the physical significance of the Gamma-L/Ledd relation for AGN of both type I and II in the local universe. This presentation will summarize these exciting results, and will also report on novel extended efforts to decipher the link between the water megamaser emission and galactic nuclear activity, which are made possible only by the availability of the large sample statistics of carefully curated X-ray measurements uniquely offered by the combined Chandra and XMM catalogs.

Author(s): Anca Constantin², Paul Green¹, Daryl Haggard³

Institution(s): 1. *Harvard-Smithsonian Center for Astrophysics*, 2. *James Madison University*, 3. *McGill University*

223.06 – Serendipitous X-Ray Catalogs: A View from Infrared and Time-Domain Studies

Serendipitous X-ray catalogs from Chandra and XMM have provided an important legacy for multi-wavelength studies. I will

discuss a few uses we have made of this resource for studies of extreme AGN identified from mid-IR and/or optical time-domain studies -- specifically, from the WISE satellite and/or the Catalina Real-time Transient Survey (CRTS). Specifically, I will discuss Assef et al. (2016; ApJ, 819, 111), which reports on a deep (170 ks) archival Chandra observation of an extremely luminous AGN with extremely red mid-IR colors, i.e., a so-called "Hot, Dust-Obscured Galaxy" or HotDOG. The deep, public X-ray data allowed unique insight into this rare source class. I will also discuss archival X-ray observations of several quasars with extreme optical and/or mid-IR light curves.

Author(s): Daniel Stern¹

Institution(s): 1. Jet Propulsion Laboratory/California Institute of Technology

223.07 – Active galactic nuclei as cosmological probes.

I will present the latest results on our analysis of the non-linear X-ray to UV relation in a sample of optically selected quasars from the Sloan Digital Sky Survey, cross-matched with the most recent XMM-Newton and Chandra catalogues. I will show that this correlation is not only very tight, but can be potentially even tighter by including a further dependence on the emission line full-width half maximum.

This result implies that the non-linear X-ray to optical-ultraviolet luminosity relation is the manifestation of an ubiquitous physical mechanism, whose details are still unknown, that regulates the energy transfer from the accretion disc to the X-ray emitting corona in quasars. I will discuss what the perspectives of AGN in the context of observational cosmology are. I will introduce a

224 – Gravitational Waves and EM Counterparts II

224.01 – Using gravitational-wave data to constrain dynamical tides in neutron star binaries

We discuss the role of dynamical tidal effects for inspiralling neutron star binaries, focusing on features that may be considered "unmodelled" in gravitational-wave searches. In order to cover the range of possibilities, we consider i) individual oscillation modes becoming resonant with the tide, ii) the elliptical instability, where a pair of inertial modes exhibit a nonlinear resonance with the tide, and iii) the non-resonant p-g instability which may arise as high order p- and g-modes in the star couple nonlinearly to the tide. In each case, we estimate the amount of additional energy loss that needs to be associated with the dynamical tide in order for the effect to impact on an observed gravitational-wave signal. We discuss to what extent the involved neutron star physics may be considered known and how one may be able to use observational data to constrain theory.

Author(s): Wynn C.G. Ho¹, Nils Andersson¹

Institution(s): 1. University of Southampton

224.02 – Optical follow-up of gravitational wave triggers by the TOROS collaboration

We present the results of the followup of several gravitational-wave alerts provided by the LIGO VIRGO Collaboration to the TOROS "Transient Optical Robotic Observatory of the South" Collaboration. TOROS was organized in 2013 to participate in the worldwide effort to search for the electromagnetic counterparts of these events. Our goal is to establish a wide-field optical telescope on Cordón Macon in northwestern Argentina while using other facilities provided by its members based on opportunity and availability.

We present the results of our observations since the initial LIGO detection in September 2015 during the first observational campaign, and also provide a report on observations conducted during the second observational campaign O2 which ended August 25, 2017.

Additionally we give a progress update on the TOROS telescope.

novel technique to test the cosmological model using quasars as "standard candles" by employing the non-linear X-ray to UV relation as an absolute distance indicator.

Author(s): Elisabeta Lusso¹, Guido Risaliti²

Institution(s): 1. Durham University, 2. University of Florence

223.08 – Future prospects with the Chandra and XMM source catalogs: Setting the stage for Lynx

Lynx is a NASA concept X-ray mission that will probe the distant Universe to extremely faint fluxes and with superb angular resolution. I will discuss how the *Chandra* and *XMM* X-ray source catalogs will enable important progress on our understanding of AGN populations and will inform the preparations for the *Lynx* survey program. The wide areas covered by these serendipitous surveys enable a census of the X-ray Universe that includes low-luminosity AGN such as low-Eddington and dwarf systems, as well as rare sources such as super-Eddington AGN and mergers. Characterizing these AGN provides a view of the populations that, at high redshifts, will be uniquely detected and characterized with *Lynx*. The *XMM* and *Chandra* source catalogs also provide important constraints on the evolution of the quasar luminosity function, allowing more accurate predictions for the number of lower-luminosity, high redshift sources that may be detected with *Lynx* as it probes the formation of black holes in the early Universe.

Author(s): Ryan C. Hickox¹

Institution(s): 1. Dartmouth College

224 – Gravitational Waves and EM Counterparts II

Author(s): Mario Claudio Diaz¹

Institution(s): 1. The University of Texas RIO GRANDE VALLEY

Contributing team(s): TOROS Collaboration

224.03D – Modeling Gravitational Wave Sources For Pulsar Timing Arrays

Pulsar Timing Arrays (PTAs) are galactic-scale low-frequency (nHz - μ Hz) gravitational wave (GW) observatories, which aim to directly detect GWs from binary supermassive black holes (SMBHs) ($\geq 10^7 M_{\odot}$). Binary SMBHs are predicted products of galaxy mergers, and are a crucial step in galaxy formation theories. Understanding the link between binary SMBHs and the gravitational radiation detected by PTAs is crucial to the community's capability of making meaningful scientific statements using PTA observations. Recent PTA upper limits on the gravitational radiation in the nanohertz frequency band are impacting our understanding of the binary SMBH population. But as upper limits grow more constraining, what can be implied about galaxy evolution? In this talk, I will provide insights into this question with investigations into which astrophysical parameters have the largest impact on GW predictions, direct translations between PTA limits and measured values for the parameters of galaxy evolution, and explorations into how the use of different galaxy evolution parameters affects the characterization of the GW signal.

The inspiral of binary SMBHs creates extended interaction between the black holes and their host galaxy, and there is the potential for many electromagnetic tracers to accompany the binary's evolution. This talk will also highlight work incorporating models of electromagnetic radiation from binary SMBHs to investigate the potential for jointly detecting a binary's electromagnetic and gravitational radiation. The detection of a single 'multi-messenger' source would provide a unique window into a pivotal stage of galaxy evolution, and would revolutionize the understanding of late-stage galaxy evolution.

Author(s): Joseph Simon¹

Institution(s): 1. Jet Propulsion Laboratory

224.04 – Matter in compact binary mergers

Mergers of binary neutron stars or neutron-star/black-hole systems are promising targets for gravitational-wave detection. The dynamics of merging compact objects, and thus their gravitational-wave signatures, are primarily determined by the mass and spin of the components. However, the presence of matter can make an imprint on the final orbits and merger of a binary system. I will outline efforts to understand the impact of neutron-star matter on gravitational waves, using both theoretical and computational input, so that gravitational-wave observations can be used to measure the properties of source systems with neutron-star components.

Author(s): Jocelyn Read¹

Institution(s): 1. CSU Fullerton

Contributing team(s): LIGO Scientific Collaboration, Virgo Scientific Collaboration

224.05 – LIGO and Virgo searches for continuous gravitational waves

While short signals from binary black hole mergers were the first gravitational waves detected, long-lived continuous waves from rapidly rotating neutron stars will bring us more information once they are detected. I summarize results from Advanced LIGO and Virgo searches for known pulsars and other sources of continuous gravitational waves, and sketch ongoing analyses.

Author(s): Benjamin Owen¹

Institution(s): 1. Texas Tech University

Contributing team(s): LIGO Scientific Collaboration, Virgo Collaboration

224.06 – Increasing Pulsar Timing Array Sensitivity Through Addition of Millisecond Pulsars

Siemens et al. (2013) and Taylor et al. (2016) demonstrated the importance of increasing the number of millisecond pulsars (MSPs) in pulsar timing arrays (PTAs) in order to increase the sensitivity of the array and decrease the time-to-detection of a gravitational wave background (GWB). In particular, they predict that adding four MSPs per year to the NANOGrav and International PTAs will likely yield a GWB detection in less than a decade. A more even distribution of MSPs across the sky is also important for discriminating a GWB signal from a non-quadrupolar background (Sampson et al., in prep). Pulsar surveys and targeted searches have consistently led to additions of 4 or more MSPs per year to PTAs. I will describe these ongoing efforts, particularly in the context of the Green Bank North Celestial Cap pulsar survey and Fermi-guided searches at Green Bank and

225 – Applied Statistical Methods in Astronomy: Gaussian Processes and Machine Learning

Modern telescopes provide challenging data, not only in quantity but also quality, demanding new methods and techniques for scientific inference. New algorithms specific to astronomical problems are being developed and brought to the community by a new generation of scientists. This special session will focus on statistical methods that were published within the last year. This proposal originates from the AAS Working Group on Astroinformatics and Astrostatistics (<https://aas.org/comms/working-group-astroinformatics-and-astrostatistics-wgaa>) and the CHASC International Center for Astrostatistics (<http://hea-www.harvard.edu/AstroStat/>). We have organized many well attended sessions at the past AAS meetings. Interest in the community in advanced/applied statistical methods has been increasing steadily over the last decade as indicated by workshops and focused meetings on the analysis of astronomical data. The goal of this special session is to review advances in the newly popular methods of gaussian processes and machine learning, to present applications to data, and to discuss current issues and future perspectives. These methods have applications across the entire spectrum of astronomical research and are being rapidly developed. They have to be presented at large forums to make the community aware of

Arecibo that seek to find MSPs in low-pulsar-density regions of the sky.

Author(s): Megan E. DeCesar⁴, Fronefield Crawford², Elizabeth Ferrara⁵, Ryan Lynch⁷, Chiara Mingarelli¹, Lina Levin Preston³, Scott Ransom⁷, Joseph Romano¹⁰, Joseph Simon⁶, Renee Spiewak⁹, Kevin Stovall⁸, Joe Swiggum¹¹, Stephen Taylor⁶

Institution(s): 1. Flatiron Institute, 2. Franklin & Marshall College, 3. Jodrell Bank Centre for Astrophysics, University of Manchester, 4. Lafayette College, 5. NASA/Goddard, 6. NASA/JPL, 7. NRAO, 8. NRAO, 9. Swinburne University of Technology, 10. UT Rio Grande Valley, 11. UW-Milwaukee

Contributing team(s): Green Bank North Celestial Cap Pulsar Survey, Fermi LAT Collaboration, Fermi Pulsar Search Consortium

224.07 – O2 Results from the Low-Latency GstLAL Search for Compact Binaries

Advanced LIGO's second observing run, lasting 9 months, concluded August 25th. While collecting data, the LIGO Scientific Collaboration searches for gravitational waves in low-latency for rapid identification of signals which are shared with follow-up partners to look for multimessenger counterparts. One type of search run in low-latency looks for gravitational waves from the merger of compact binaries, such as binary black holes and binary neutron stars. In this talk, I will present a short overview of the low-latency GstLAL-based inspiral pipeline, one of the compact binary searches, followed by a summary of the results.

Author(s): Alan Weinstein¹, Cody Messick²

Institution(s): 1. California Institute of Technology, 2. Penn State University

224.08 – LIGO and Virgo Observations of Binary Black Hole Mergers

Advanced LIGO's first and second observing runs have revealed a wide range of binary black hole (BBH) masses. I present astrophysical context and source parameters of select BBH systems among LIGO and Virgo's observational repertoire.

Author(s): Eve Chase¹

Institution(s): 1. Northwestern University

Contributing team(s): LIGO Scientific Collaboration, Virgo Collaboration

the rapid progress being made in this field. The specific invited talks (with 5 speakers already confirmed) include discussion of application of gaussian processes to time-series spectra in exoplanet research, machine learning techniques to quantify variability states of a micro-quasar, machine learning application in cosmology, and handling multi-catalogs source detection. We also intend to have an associated poster session allowing contributions from the entire community. The session schedule will allow for a discussion, questions and input from the audience.

225.01 – An astronomer's introduction to Gaussian Processes

Gaussian Processes (GPs) are a class of stochastic models that have become widely used in astronomy. A general introduction to GP modeling can be mystifying so, in this talk, I will introduce GP modeling with a focus on applications from the astronomy literature. I will summarize the basic theory and motivate the broad applicability of these methods. Finally, I will discuss some of the computational limitations of simple implementations of GP models and describe some recent developments that make these models more broadly tractable.

Author(s): Daniel Foreman-Mackey¹
Institution(s): 1. Flatiron Institute

225.02 – Using Gaussian Processes to Construct Flexible Models of Stellar Spectra

The use of spectra is fundamental to astrophysical fields ranging from exoplanets to stars to galaxies. In spite of this ubiquity, or perhaps because of it, there are a plethora of use cases that do not yet have physics-based forward models that can fit high signal-to-noise data to within the observational noise. These inadequacies result in subtle but systematic residuals not captured by any model, which complicates and biases parameter inference. Fortunately, the now-prevalent collection and archiving of large spectral datasets also provides an opening for empirical, data-driven approaches. We introduce one example of a time-series dataset of high-resolution stellar spectra, as is commonly delivered by planet-search radial velocity instruments like TRES, HIRES, and HARPS. Measurements of radial velocity variations of stars and their companions are essential for stellar and exoplanetary study; these measurements provide access to the fundamental physical properties that dictate all phases of stellar evolution and facilitate the quantitative study of planetary systems. In observations of a (spatially unresolved) spectroscopic binary star, one only ever records the composite sum of the spectra from the primary and secondary stars, complicating photospheric analysis of each individual star. Our technique “disentangles” the composite spectra by treating each underlying stellar spectrum as a Gaussian process, whose posterior predictive distribution is inferred simultaneously with the orbital parameters. To demonstrate the potential of this technique, we deploy it on red-optical time-series spectra of the mid-M-dwarf eclipsing binary LP661-13, which was recently discovered by the MEarth project. We successfully reconstruct the primary and secondary stellar spectra and report orbital parameters with improved precision compared to traditional radial velocity analysis techniques.

Author(s): Ian Czekala¹
Institution(s): 1. Stanford University

225.03 – Classifying Black Hole States with Machine Learning

Galactic black hole binaries are known to go through different states with apparent signatures in both X-ray light curves and spectra, leading to important implications for accretion physics as well as our knowledge of General Relativity. Existing frameworks of classification are usually based on human interpretation of low-dimensional representations of the data, and generally only apply to fairly small data sets. Machine learning, in contrast, allows for rapid classification of large, high-dimensional data sets. In this talk, I will report on advances made in classification of states observed in Black Hole X-ray Binaries, focusing on the two sources GRS 1915+105 and Cygnus X-1, and show both the successes and limitations of using machine learning to derive physical constraints on these systems.

Author(s): Daniela Huppenkothen¹
Institution(s): 1. University of Washington Seattle

226 – Cosmology III

226.01 – Strong Lensing Science Results from the Hyper Suprime-Cam Survey

Strong gravitational lenses are valuable objects for studying galaxy structure and cosmology. Lensing is a unique probe of the dark matter structure of galaxies, groups, and clusters, as well as an independent tool for constraining cosmological parameters. Lensing also magnifies the background source population, allowing for detailed studies of their properties at high resolution. However, strong lenses are rare and difficult to find, requiring deep wide-area high-resolution imaging surveys. With data from the ongoing Hyper Suprime-Cam (HSC) Subaru Strategic Program, we have discovered over 100 new strong lenses at the

225.04 – Dynamical Mass Measurements of Contaminated Galaxy Clusters Using Support Distribution Machines

We study dynamical mass measurements of galaxy clusters contaminated by interlopers and show that a modern machine learning (ML) algorithm can predict masses by better than a factor of two compared to a standard scaling relation approach. We create two mock catalogs from Multidark’s publicly available N-body MDPL1 simulation, one with perfect galaxy cluster membership information and the other where a simple cylindrical cut around the cluster center allows interlopers to contaminate the clusters. In the standard approach, we use a power-law scaling relation to infer cluster mass from galaxy line-of-sight (LOS) velocity dispersion. Assuming perfect membership knowledge, this unrealistic case produces a wide fractional mass error distribution, with a width $E=0.87$. Interlopers introduce additional scatter, significantly widening the error distribution further ($E=2.13$). We employ the support distribution machine (SDM) class of algorithms to learn from distributions of data to predict single values. Applied to distributions of galaxy observables such as LOS velocity and projected distance from the cluster center, SDM yields better than a factor-of-two improvement ($E=0.67$) for the contaminated case. Remarkably, SDM applied to contaminated clusters is better able to recover masses than even the scaling relation approach applied to uncontaminated clusters. We show that the SDM method more accurately reproduces the cluster mass function, making it a valuable tool for employing cluster observations to evaluate cosmological models.

Author(s): Michelle Ntampaka², Hy Trac¹, Dougal Sutherland⁴, Sebastien Fromenteau³, Barnabas Pocz¹, Jeff Schneider¹
Institution(s): 1. Carnegie Mellon University, 2. Harvard University, 3. Instituto de fisica UNAM, 4. University College London

225.05 – Sub-Band Image Reconstruction using DCR

Refraction by the atmosphere causes the astrometric positions of sources to depend on the airmass through which an observation was taken. This shift is dependent on the underlying spectral energy of the source and the filter or bandpass through which it is observed. Wavelength-dependent refraction within a single passband is often referred to as differential chromatic refraction (DCR). With a new generation of astronomical surveys undertaking repeated observations of the same part of the sky over a range of different airmasses and parallactic angles DCR should be a detectable and measurable astrometric signal. Here we introduce a novel procedure that uses this subtle signal to infer the underlying spectral energy distribution of a source; we solve for multiple latent images at specific wavelengths via a generalized deconvolution procedure built on robust statistics.

Author(s): Tamas Budavari¹, Matthias Lee¹, Andrew Connolly²
Institution(s): 1. The Johns Hopkins University, 2. University of Washington

galaxy and group scale to expand the sample of lensing systems, particularly at redshifts $z > 0.5$, where there have previously been relatively few known lenses. We present a summary of the latest strong lensing science results from the HSC survey data taken through the S17A semester.

Author(s): Kenneth Wong¹
Institution(s): 1. National Astronomical Observatory of Japan
Contributing team(s): HSC SSP Strong Lens Working Group

226.02D – What Can Galaxies Tell Us About The Epoch of Reionization?

The reionization of neutral hydrogen in the intergalactic medium (IGM) in the universe's first billion years ($z > 6$) was likely driven by the first stars and galaxies, and its history encodes information about their properties. But the timeline of reionization is not well-measured and it is still unclear whether galaxies alone can produce the required ionizing photons. I will describe two key ways in which galaxies at our current observational frontiers can constrain reionization.

One tool is the UV luminosity function (LF), which traces the evolution of star-forming galaxies and their ionizing photons. I will describe a Bayesian technique to account for gravitational lensing magnification bias in galaxy surveys to produce accurate LFs. I will then describe a simple, but powerful, model for LF evolution and its implications for reionization and $z > 10$ galaxy surveys with JWST. Secondly, Lyman alpha (Ly α) emission from galaxies is a potential probe of the IGM ionization state as Ly α photons are strongly attenuated by neutral hydrogen, but requires disentangling physics on pc to Gpc scales. I will introduce a new forward-modeling Bayesian framework which combines cosmological IGM simulations with models of interstellar medium conditions to infer the IGM neutral fraction from observations of Ly α emission. I will present our new measurement of the neutral fraction at $z \sim 7$ and place it in the context of other constraints of the reionization history. I will describe ongoing efforts to build larger samples of Ly α emitting galaxies for more accurate measurements with the HST survey GLASS, and will describe future prospects with JWST.

Author(s): Charlotte Mason¹

Institution(s): 1. UCLA

Contributing team(s): GLASS, BoRG

226.03 – Cosmological Simulations with Molecular Astrochemistry: Water in the Early Universe

Water is required for the rise of life as we know it throughout the universe, but its origin and the circumstances of its first appearance remain a mystery. The abundance of deuterated water in solar system bodies cannot be explained if all the water in the solar system were created in the protoplanetary disk (Cleeves et al. 2014), suggesting that as much as half of Earth's water predates the Sun. Water has been observed as early as one sixth the current universe's age in MG J0414+0534 (Imprellizzeri et al. 2008). It was recently shown that water could, in principle, appear in hot halos barely enriched with heavy elements such as oxygen and carbon (Bialy et al. 2015). So far, no self-consistent calculation of cosmology physics carried out in line with a large chemical reaction network has been carried out to study the first sites of water formation in the universe. We present initial results the first such series of cosmological calculations with a 26 species low metallicity molecular chemical reaction network with Enzo (Bryan et al. 2014) to understand the role of hydrodynamics and radiative feedback on molecule formation in the early universe and to shed light on the cosmological history of this life-giving substance.

Author(s): Brandon K Wiggins², Joseph Smidt¹

Institution(s): 1. Los Alamos National Laboratory, 2. Southern Utah University

226.04 – On the Treatment of l-changing Proton-hydrogen Rydberg Atom Collisions

Energy-conserving, angular momentum-changing collisions between protons and highly excited Rydberg hydrogen atoms are important for precise understanding of the primordial

227 – Galaxy Formation and Evolution IV

227.01 – Why do Galaxies Stop Forming Stars? New Evidence for the Role of AGN-feedback in Driving Galaxy Bimodality

One of the most striking features of the population of local galaxies is that the distributions of several key galaxy properties are highly bimodal (e.g. color and star formation rate). In general, high mass galaxies in dense environments, with bulge-dominated

recombination cascade, and the elemental abundance.

Early approaches to l-changing collisions used perturbation theory for only dipole-allowed ($\Delta l = \pm 1$) transitions. An exact non-perturbative quantum mechanical treatment is possible, but it comes at computational cost for highly excited Rydberg states. In this note we show how to obtain a semi-classical limit that is accurate and simple, and develop further physical insights afforded by the non-perturbative quantum mechanical treatment.

Author(s): Daniel Vranceanu², Roberto Onofrio³, Hossein Sadeghpour¹

Institution(s): 1. Harvard-Smithsonian Center for Astrophysics, 2. Texas Southern University, 3. Universita di Padova

226.05D – Approaching reionization from two directions: high-redshift Lyman-alpha emitters and local analogs

The dark ages that followed the recombination of the universe ended with the appearance of metal-free stars and the subsequent formation of numerous low-mass, metal-poor galaxies. The collective ionizing background from these newly-forming galaxies is thought to be responsible for the reionization of the diffuse hydrogen in the intergalactic medium between redshifts 10 and 6.5. The progression of the reionization history depends on the nature of these first sources -- their number densities, luminosities, clustering, and production rates of ionizing photons -- which is currently the subject of considerable observational and theoretical efforts.

I will present results of a two-pronged approach to studying the Epoch of Reionization: a systematic search for Lyman-alpha emitting galaxies at redshifts greater than 6, and an analysis of high S/N spectra of a sample of local galaxies that are potential analogs to those responsible for the reionization. Selected for their large [OIII]/[OII] ratios and high H-alpha equivalent widths, the local galaxies have very low masses and are consistent with photoionization by stars with effective temperatures of 10^4 K. Both the emission lines and continua of the spectra are spatially extended, allowing for an analysis of galaxy properties such as gas temperature, elemental abundance, and ionizing power at different radii.

Author(s): Micaela Bagley¹

Institution(s): 1. University of Minnesota

226.06 – Radial Acceleration Relation in SDSS Spherical Galaxies

The observed aperture velocity dispersions of nearly spherical, disk-less SDSS galaxies are compared with the velocity dispersions predicted by the observed stellar mass distributions. The ratio of the squared velocity dispersions as a function of radial acceleration or surface density exhibits a characteristic shape. Construction of an ensemble of models for each galaxy under the cold dark matter paradigm using a host of empirical results on galaxies and dark halos reveals a remarkable correlation between radial accelerations by baryons and dark matter. We present the results and discuss implications.

Author(s): Kyu-Hyun Chae¹, Mariangela Bernardi², Ravi K Sheth²

Institution(s): 1. Sejong University, 2. University of Pennsylvania

morphologies and pressure supported kinematics are more frequently passive (non-star forming) than lower mass galaxies in low density environments, with disc-dominated morphologies and rotationally supported kinematics. Understanding which, if any, of these correlations is causally related to the 'quenching' of star formation in galaxies remains an active and hotly debated area of investigation in modern astrophysics.

Theoretically, a wealth of physical processes have been evoked to account for central galaxy quenching, including halo mass quenching from virial shocks, feedback from active galactic nuclei (AGN; in either the quasar or radio mode), stabilizing torques from central mass concentrations, feedback from supernovae, or even magnetic fields interacting with the hot gas halo.

I will present strong new statistical evidence which suggests that the quenched fraction of local central galaxies is primarily related to their central kinematics (Bluck et al. 2016; 2017 in prep.). I will show that this is broadly consistent with quenching from AGN feedback, through a detailed comparison with a semi-analytic model and a cosmological hydrodynamical simulation.

Using a sample of over half a million local galaxies from the SDSS DR7, we go on to develop a number of sophisticated techniques, including machine learning with artificial neural networks, to rank the importance of galaxy properties to quenching (Teimoorinia, Bluck & Ellison 2016). We find that properties closely correlated with the central supermassive black hole are highly favoured statistically to predict whether a galaxy will be star forming or not. Perhaps surprisingly, stellar mass and halo mass have no impact on star formation activity in central galaxies selected at a fixed black hole mass; and environment is totally uncorrelated to quenching in centrals.

I will conclude by assessing which physical mechanisms for quenching are viable in light of our new results.

Author(s): Asa Bluck¹, Hossen Teimoorinia², Sara L. Ellison⁴, Trevor Mendel³

Institution(s): 1. *ETH Zurich*, 2. *HIA*, 3. *MPE*, 4. *University of Victoria*

227.02 – Identifying and Tracing the Stellar Mass Growth of Brightest Cluster Galaxy Ancestors

The most massive galaxies in the present-day universe are the Brightest Cluster Galaxies (BCGs), which formed through a complex process of mergers and star formation episodes yet to be fully understood. The age and high total mass of their stellar populations hint toward intense star formation episodes long ago, with the further delivery of additional stars through galaxy mergers. To investigate when this high redshift in-situ mass growth occurs, I use the constant and evolving number density methods to identify progenitors of low redshift BCGs. I use publicly available multiwavelength observations from the COSMOS survey to construct a SED for each ancestor candidate, which is then fit to stellar, dust, and AGN models when appropriate. By tracing the specific star formation and stellar mass of BCG ancestors in the early universe, we gain a new understanding of when the largest individual structures in the universe formed their stars.

Author(s): Kevin C. Cooke¹, Jeyhan Kartaltepe¹, Krystal Tyler¹

Institution(s): 1. *Rochester Institute of Technology*

Contributing team(s): COSMOS Collaboration

227.03 – On the evolution of early-type galaxy rotation in the Horizon-AGN simulation

Recent IFU surveys, providing an additional dimension of galaxy data, have reinvigorated the study of galaxy kinematics. IFU surveys have repeatedly shown that rotational properties and internal kinematics of early-type galaxies (ETGs) vary as much as or even more than their morphologies do. Theoretical studies have investigated the origin of the widely varying galactic rotations using cosmological simulations, and an agreement seems to be made that mergers are important in general. However, using the Horizon-AGN simulation data, we find that the relative importance of mergers and non-merger processes strongly depends on the environment. Slow rotators at the centers of large halos had gone through numerous mergers. But much more slow rotators near large halos are results of frequent tidal interactions, rather than mergers. These slow rotating satellite

ETGs were initially fast rotators or late-type galaxies before their infall into the halo potential. In this study, we consider only massive ETGs ($M^* > 10^{10} M_{\odot}$) due to the resolution limit, similar to previous studies based on other cosmological simulations. We will also discuss the prospect for revealing a more thorough view covering more ETGs at the lower mass end with next-generation simulations.

Author(s): Hoseung Choi², Yohan Dubois¹, Taysun Kimm², Sukyoung Ken Yi²

Institution(s): 1. *Institut d'Astrophysique de Paris*, 2. *Yonsei University*

227.04 – Integral Field Spectroscopy of the Merger Remnant NGC 7252

The merging of galaxies is a key aspect of the hierarchical Λ CDM Universe. The formation of massive quiescent elliptical galaxies may be explained through the merger of two star-forming disc galaxies. Despite nearly a century of effort, our understanding of this complex transformational process remains incomplete and requires diligent observational study.

NGC 7252 is one of the nearest starbursting major-merger galaxy remnants, formed about 1 Gyr after the collision of presumably two disc galaxies. It is therefore an ideal laboratory to study the underlying processes involved in transformation of two disc galaxies to an elliptical galaxy via a merger.

We obtained wide-field IFU spectroscopy with the VLT-VIMOS integral-field spectrograph covering the central $50'' \times 50''$ of NGC 7252 to map the stellar and ionized gas kinematics, and the distribution and conditions of the ionized gas, revealing the extent of ongoing star formation and recent star formation history.

Contrary to previous studies we find the inner gas disc not to be counter-rotating with respect to the overall stellar angular momentum. However, the stellar kinematics appear to be complex with a superposition of at least two nearly perpendicular angular momentum components. The host galaxy is still blue with $g - i \sim 0.8$ with an ongoing star formation rate of $2.2 \pm 0.6 M_{\text{sun}}/\text{yr}$, placing NGC 7252 close to the blue cloud of galaxies and consistent with a disc-like molecular depletion time of ~ 2 Gyr.

Although NGC 7252 appears as a fading starburst galaxy at the center, the elliptical-like major merger remnant appears to active, inconsistent with a fast quenching scenario. NGC 7252 may take several Gyr to reach the red sequence of galaxies unless star formation becomes quenched by either AGN feedback or inefficient gas conversion, leading to an H I-rich elliptical galaxy.

Author(s): John Weaver³, Bernd Husemann², Harald Kuntschner¹, Ignacio Martín-Navarro²

Institution(s): 1. *ESO*, 2. *Max-Planck-Institut für Astronomie*, 3. *University of St Andrews*

227.05D – The Role of Environment on Active Galactic Nuclei Triggering

Active galactic nuclei (AGN) play a role in regulating galactic star formation and transitioning a galaxy from star forming to passive. However, the mechanisms triggering AGN are still debated and can depend on both environmental and secular processes. The dense, rich environment of galaxy clusters provides a unique regime in which to study the impact of large-scale environmental factors on AGN triggering. We present analysis of AGN in 2300 galaxy clusters from the Massive and Distant Clusters of WISE Survey (MaDCoWS) at redshift $z \sim 1$. With MaDCoWS, we significantly improve the statistical precision of cluster AGN studies during an epoch of major assembly of the cluster and intracluster medium. We use literature catalogs of AGN selected via optical+infrared (OIR), mid-infrared (MIR), and radio data to isolate populations of majority unobscured, dust-obscured, and

radio-loud AGN, respectively, and crossmatch with Spitzer images of MaDCoWS clusters. The fraction of cluster galaxies that host OIR- and MIR-selected AGN is comparable to that of the field at all cluster radii. We find no statistically significant dependence of the OIR- and MIR-selected AGN fraction upon cluster mass, implying that environment is at most a second order factor for OIR and MIR AGN triggering. In contrast, the radio-selected AGN fraction is ~ 2 times that of the field in cluster cores. While the total overdensity of radio-selected AGN increases with cluster mass, we also find that the fraction of cluster galaxies hosting radio-selected AGN is greatest in low mass clusters. Our results are consistent with a picture in which environmental factors do play a role in influencing the fueling of radio-mode AGN. We also conduct a study of radio sources in MaDCoWS clusters to investigate the properties of these radio sources and how they impact their surrounding environment. We find that clusters with central radio source have more central OIR- and MIR-selected AGN than radio-inactive clusters, implying that central cluster radio activity and AGN triggering are somehow linked.

Author(s): Wenli Mo¹

Institution(s): 1. *University of Florida*

Contributing team(s): MaDCoWS Collaboration

227.06 – Black Holes and Neutron Stars in Nearby Galaxies: Insights from NuSTAR

With the launch of the first focusing hard X-ray ($E > 10$ keV) telescope, *NuSTAR*, critical diagnostics can be applied outside the Milky Way in this crucial bandpass. Determining the ratio of X-ray binaries (XRBs) that are black holes or neutron stars reveals clues about the formation and evolution of binary systems in different galactic environments. However, identifying the compact object types of extragalactic XRBs is problematic due to the similarity and/or degeneracy of their spectra. We analyze a *NuSTAR*-selected sample of 12 nearby galaxies within 5 Mpc that represent a range of star formation rates ($0.1 - 10 M_{\odot} \text{ yr}^{-1}$) and stellar masses ($10^9 - 10^{11} M_{\odot}$). Using X-ray color-color and color-intensity diagnostics we classify sources by their accretion states and compact object types. We find that most sources are black holes accreting in the intermediate state. We study the 4-25 keV and 12-25 keV X-ray luminosity functions of our sample scaled by specific star formation rate and compare with the 0.5-8 keV analogues from *Chandra* and *XMM-Newton*. The combined 12-25 keV X-ray luminosity function shows a break above $10^{39} \text{ erg s}^{-1}$ indicating the ultraluminous X-ray source regime. We also present the relationship between the 12-25 keV X-ray point source luminosities and specific star formation rates of our galaxy sample.

Author(s): Neven Vulic², Ann Hornschemeier², Daniel Wik⁶, Mihoko Yukita¹, Andreas Zezas³, Andrew Ptak², Bret Lehmer⁵, Valsamo Antoniou³, Thomas J. Maccarone⁴, Ben Williams⁷

Institution(s): 1. *John Hopkins University*, 2. *NASA GSFC*, 3. *Smithsonian Astrophysical Observatory*, 4. *Texas Tech University*, 5. *University of Arkansas*, 6. *University of Utah*, 7. *University of Washington*

227.07 – Characterizing bursty star formation

An ongoing area of research in galaxy evolution is the efficiency of star formation as a function of galaxy halo mass. At low mass, it is

228 – Extrasolar Planets IV

228.01 – Observationally Constraining Gas Giant Composition via Their Host Star Abundances

While the photospheric abundances of the Sun match many rock-forming elemental abundances in the Earth to within 10 mol%, as well as in Mars, the Moon, and meteorites, the Solar System giant planets are of distinctly non-stellar composition — Jupiter's bulk metallicity (inferred from its bulk density, measured from spacecraft data) is $\sim x5$ -10 solar, and Saturn is $\sim x10$ -20 solar. This knowledge has led to dramatic advances in understanding models of core accretion, which now match the heavy element enrichment of each of the Solar System's giant planets. However,

believed that supernova feedback can expel gas from the galaxy and shut down star formation. However, there are still significant uncertainties in how the momentum/energy of the supernova couple with the gas and the efficiency with which it drives winds. Particularly uncertain are the parameters of the resulting bursts of star formation — amplitudes, durations, and periods — with important implications for interpreting observations of dwarf galaxies. Some hydrodynamical simulations predict order of magnitude bursts (and quenching) on very short (< 10 Myr) timescales in dwarf galaxies at all redshifts. Here, we use star formation indicators of dwarf galaxies (H-alpha and ultraviolet luminosities) that trace star formation on different time scales (~ 5 Myr and ~ 20 Myr, respectively), as well as their relation to the average galaxies of similar stellar mass, to better constrain the parameters of the star formation bursts. We find that the burst amplitude increases with decreasing stellar mass, with amplitudes ranging two orders of magnitude at stellar masses of 10^7 . We also find that the star formation is quenched very rapidly, with e-folding times less than 10 Myr in galaxies with stellar masses less than $10^{7.5}$. We conclude by comparing our results to recent hydrodynamical simulations and discussing the effects of stochastic sampling of the stellar initial mass function.

Author(s): Najmeh Emami¹

Institution(s): 1. *UC Riverside*

227.08 – The ULIRG Monster Mash: The Evolution of Massive Mergers Since $z \sim 1$

Theoretical models and observations in the local Universe indicate there is a clear progression from merger-induced star-formation (SF) to QSO activity via Ultraluminous Infrared Galaxies (ULIRGs), systems with $L_{8-1000 \mu\text{m}} \geq 10^{12} L_{\text{Sun}}$. Not all mergers are ULIRGs, but all local ULIRGs are mergers, and likely the progenitors of QSO host galaxies. At earlier epochs, this relationship is less well accepted. Here, we first present an overview of how the dynamical properties of local ($z < 0.4$) ULIRGs are statistically indistinguishable from Radio Loud and Radio Quiet QSOs. Then, transition to the critical redshift range $0.4 < z < 1.0$, where the star-formation rates, gas fractions, and masses of galaxies are believed to be significantly higher than in the local universe. ULIRGs at these redshifts begin to dominate the SF activity and are responsible for up to 70% of the co-moving IR density. We use rest-frame UV & optical imaging and spectra to apply the same techniques used for local ULIRGs to a sample of "classically" selected (i.e via integrated 12, 25, 60 and 100 μm fluxes) systems at $0.4 < z < 1.0$. Although, in general, galaxies at $z > 0.4$ are not the same as those in the local Universe, these intermediate redshift ULIRGs are dynamically similar, but more powerful, than their local counterparts. Furthermore, they show evidence of merging, while containing a powerful AGN hosted within a massive galaxy.

Author(s): Barry Rothberg¹, Jacqueline Fischer², Nor Pirzkal⁴, Myriam Rodrigues³

Institution(s): 1. *Large Binocular Telescope Observatory*, 2. *Naval Research Laboratory*, 3. *Observatoire de Paris GEPI*, 4. *Space Telescope Science Institute*

we have thus far lacked similar data for exoplanets to use as a check for formation and composition models over a much larger parameter space. Here we present a study of the host stars of a sample of cool transiting gas giants with measured bulk metal fractions (as in Thorngren et al. 2016) to better constrain the relation $Z_{\text{planet}}/Z_{\text{star}}$ — giant exoplanet metal enrichment relative to the host star. We add a new dimension of chemical variation, measuring C, O, Mg, Si, Ni, and well as Fe (on which previous $Z_{\text{planet}}/Z_{\text{star}}$ calculations were based). Our analysis provides the best constraints to date on giant exoplanet interior composition and how this relates to formation environment, and

make testable predictions for JWST observations of exoplanet atmospheres.

Author(s): Johanna Teske¹, Daniel Thorngren², Jonathan Fortney²

Institution(s): 1. Carnegie Institution for Science, Department of Terrestrial Magnetism, 2. University of California Santa Cruz

228.02D – Exoplanet Meteorology: Characterizing the Atmospheres of Directly Imaged Sub-Stellar Objects

I study the structure, composition and dynamic evolution of directly imaged exoplanet and brown dwarf atmospheres, using spectrophotometric data collected from a range of ground and space based instrumentation. As part of my dissertation, I led studies exploring the atmospheres of brown dwarfs to search for weather variations, and characterized the near and mid infrared SEDs of imaged exoplanets to estimate their fundamental parameters.

To understand the evolution of weather on brown dwarfs we conducted a multi-epoch study monitoring of 4 ultracool, T₅ - Y₀, brown dwarfs in the J-band to search for photometric variability. These cool brown dwarfs are predicted to have salt and sulfide clouds condensing in their upper atmosphere. The study found that cool brown dwarfs, fit with higher opacity clouds, were more likely to be variable. Through data taken with the *Hubble Space Telescope* and Gemini telescope we characterized the atmospheres of directly imaged exoplanets. For HR 8799, in near IR wavelengths unobservable from the ground, we constrained the presence of clouds in the outer planets. As a member of the Gemini Planet Imager Exoplanet Survey team, I analyzed archival *HST* data and examined the near-infrared colors of HD 106906b as seen with GPI, concluding that the companion shows weak evidence of a circumplanetary dust disk or cloud. Finally, by combining data spanning 1 - 5 μ m for the low mass Jupiter-like exoplanet, 51 Eri b, we found a cool effective temperature best fit by a patchy cloud atmosphere. This makes the planet an excellent candidate for future variability studies with the *James Webb Space Telescope*.

Author(s): Abhijith Rajan¹

Institution(s): 1. Space Telescope Science Institute

Contributing team(s): Gemini Planet Imager, Extrasolar Planets and Systems Imaging Group

228.03 – Trends in Atmospheric Properties of Neptune-Size Exoplanets

Short-period planets with sizes 2-6 Earth radii and extremely common, yet until recently few have been subjected to detailed atmospheric scrutiny. I will discuss recent efforts to discover new planets in this class suitable for atmospheric characterization, and the results of recent and ongoing atmospheric studies of these planets. I will also discuss the prospects for characterization of the large numbers of new planets expected to be found by TESS.

Author(s): Ian Crossfield², Laura Kreidberg¹

Institution(s): 1. Harvard/CfA, 2. MIT

228.04 – Monitoring the High-Energy Radiation Environment of Exoplanets Around Low-mass Stars with SPARCS (Star-Planet Activity Research CubeSat)

Roughly seventy-five billion M dwarfs in our galaxy host at least one small planet in the habitable zone (HZ). The stellar ultraviolet (UV) radiation from M dwarfs is strong and highly variable, and impacts planetary atmospheric loss, composition and habitability. These effects are amplified by the extreme proximity of their HZs (0.1–0.4 AU). Knowing the UV environments of M dwarf planets will be crucial to understanding their atmospheric composition and a key parameter in discriminating between biological and abiotic sources for observed biosignatures. The Star-Planet Activity Research CubeSat (SPARCS) will be a 6U CubeSat

devoted to photometric monitoring of M stars in the far-UV and near-UV, measuring the time-dependent spectral slope, intensity and evolution of M dwarf stellar UV radiation. For each target, SPARCS will observe continuously over at least one complete stellar rotation (5 - 45 days). SPARCS will also advance UV detector technology by flying high quantum efficiency, UV-optimized detectors developed at JPL. These Delta-doped detectors have a long history of deployment demonstrating greater than five times the quantum efficiency of the detectors used by GALEX. SPARCS will pave the way for their application in missions like LUVOIR or HabEx, including interim UV-capable missions. SPARCS will also be capable of 'target-of-opportunity' UV observations for the rocky planets in M dwarf HZs soon to be discovered by NASA's TESS mission, providing the needed UV context for the first habitable planets that JWST will characterize.

Acknowledgements: Funding for SPARCS is provided by NASA's Astrophysics Research and Analysis program, NNH16ZDA001N.

Author(s): Evgenya L. Shkolnik¹, David Ardila², Travis Barman⁵, Matthew Beasley⁴, Judd D Bowman¹, Varoujan Gorjian², Daniel Jacobs¹, April Jewell², Joe Llama³, Victoria Meadows⁶, Shouleh Nikzad², Paul Scowen¹, Mark Swain², Robert Zellem²

Institution(s): 1. Arizona State University, 2. Jet Propulsion Laboratory, 3. Lowell Observatory, 4. Planetary Resources, 5. University of Arizona, 6. University of Washington

228.05 – pyLIMA : The first open source microlensing modeling software

Microlensing is highly sensitive to planets beyond the snowline and distributed along the line of sight towards the Galactic Bulge. The WFIRST-AFTA mission should detect about 3000 of these planets and significantly improves our knowledge of planet formation and statistics, complementing results found by transit and radial velocity methods. However, the modeling of microlensing event is challenging on different aspects leading to a highly time consuming analysis. After a quick summarize of these different challenges, I will present pyLIMA, the first open source microlensing modeling software. The aimed goal of this software are to be flexible, powerful and user friendly. This presentation will focus on various case and early results.

Author(s): Etienne Bachelet², Rachel Street², Valerio Bozza¹

Institution(s): 1. Dipartimento di Fisica "E.R. Caianiello", Università di Salerno, 2. Las Cumbres Observatory

228.06 – Patterns in exoplanet count and eccentricity distributions

The distribution of exoplanets contains an unexpected level of features, starting with an unexpected gap the splits the main pileup of much of the planet population. In the population of planets of metal-rich sunlike single stars (SLSS objects), which comprises 40% of planets found by the radial velocity method, when counting logarithmic periods the main pileup of planets with periods longer than 100 days is split into two peaks separated by a significant gap. There is a wide region which has so few planets that none are found in the current data set. We show that this gap is extremely unlikely to occur by random. Because this gap is well-filled among planets of low surface gravity and low metallicity stars with 31 objects, it is unlikely that the bimodal nature of the metal rich SLSS population is due to observational effects. Comparisons of eccentricity of the metal-rich and metal-poor SLSS populations depend strongly on the two-peak-gap structure of counts of the metal-rich SLSS (rSLSS) population. Consideration of these features is essential to properly study the correlations of eccentricity with other planet-system parameters given how the eccentricity of rSLSS objects is highest in the two peaks of the rSLSS population.

Author(s): Stuart F. Taylor¹

Institution(s): 1. Participation Worldscape/Okapi Architecture

228.07 – Results and lessons from the GMOS survey of transiting exoplanet atmospheres

We present results from the first comprehensive survey program dedicated to probing transiting exoplanet atmospheres using transmission spectroscopy with a multi-object spectrograph (MOS). Our four-years survey focussed on ten close-in giant planets for which the wavelength dependent transit depths in the visible were measured with Gemini/GMOS. We present the complete analysis of all the targets observed (50 transits, 300 hours), and the challenges to overcome to achieve the best spectrophotometric precision (200-500 ppm / 10 nm). We also present the main results and conclusions from this survey. We show that the precision achieved by this survey permits to distinguish hazy atmospheres from cloud-free ones. We discuss the challenges faced by such an experiment, and the lessons learnt for future MOS survey. We lay out the challenges facing future ground based MOS transit surveys aiming for the atmospheric characterization of habitable worlds, and utilizing the next generation of multi-object spectrographs mounted on extremely large ground based telescopes (ELT, TMT).

Author(s): Kamen Todorov⁴, Jean-Michel Desert⁴, Catherine Huitson⁶, Jacob Bean⁵, Jonathan Fortney³, Marcel Bergmann¹, Kevin Stevenson²

Institution(s): 1. NOAO and Gemini Observatory, 2. Space Telescope Science Institute, 3. UCSC, 4. University of Amsterdam, 5. University of Chicago, 6. University of Colorado

229 – Circumstellar Disks II

229.01 – The evolution of inner disk winds from a large survey of high-resolution [OI] spectra

Current theoretical work suggests that protoplanetary disk evolution and dispersal could be driven by radially extended disk winds. I will present new observational results on the evolution of inner disk winds as linked to jets and to the dispersal of disks. The analysis is based on a large survey of forbidden emission from oxygen ([OI]) as observed in the optical (5577 and 6300 ang) at the spectral resolution of ~ 7 km/s, and it is part of a large recent effort (Rigliaco et al. 2013, Simon et al. 2016) to study winds at higher resolution than in the past. Past work identified two largely distinct components in [OI] emission: a high-velocity-component (HVC) that has been related to collimated jets, and a low-velocity-component (LVC) that has been attributed to slow disk winds (MHD and/or photoevaporative). The larger sample, high resolution, and improved correction for photospheric absorption now allow us to find new important clues, in particular in terms of the evolution of line blue-shifts and of 5577/6300 line flux ratios in the LVC. I will discuss these findings in the context of the properties and evolution of wind process(es) that are proposed to produce them.

Author(s): Andrea Banzatti², Illaria Pascucci², Suzan Edwards¹

Institution(s): 1. Smith College, 2. University of Arizona

229.02D – Probing Protoplanetary Disks: From Birth to Planets

Disks are very important in the evolution of protostars and their subsequent planets. How early disks can form has implications for early planet formation. In the youngest protostars (i.e., Class 0 sources) magnetic fields can control disk growth. When the field is parallel to the collapsing core's rotation axis, infalling material loses angular momentum and disks form in later stages. Sub-/millimeter polarization continuum observations of Class 0 sources at ~ 1000 au resolution support this idea. However, in the inner (~ 100 au), denser regions, it is unknown if the polarization only traces aligned dust grains. Recent theoretical studies have shown that self-scattering of thermal emission in the disk may contribute significantly to the polarization. Determining the scattering contribution in these sources is important to disentangle the magnetic field. At older times (the Class II phase), the disk structure can both act as a modulator and signpost of

228.08 – Fomalhaut's Stellar Companions as the Driver of its Morphology

Fomalhaut A is among the most well-studied nearby stars and has been discovered to possess a putative planetary object as well as a remarkable eccentric dust belt. This eccentric dust belt has often been interpreted as the dynamical signature of one or more planets that elude direct detection. However, the system also contains two other stellar companions residing $\sim 100,000$ AU from Fomalhaut A. Using numerical simulations of the system's dynamical evolution, we find that close encounters between Fomalhaut A and B are expected, with a $\sim 25\%$ probability that the two stars have passed within at least 400 AU of each other at some point. Although the outcomes of such encounter histories are extremely varied, these close encounters nearly always excite the eccentricity of Fomalhaut A's dust belt and occasionally yield morphologies very similar to the observed belt. With these results, we argue that close encounters with Fomalhaut A's stellar companions should be considered a plausible mechanism to explain its eccentric belt, especially in the absence of detected planets capable of sculpting the belt's morphology. More broadly, we can also conclude from this work that very wide binary stars may often generate asymmetries in the stellar debris disks they host.

Author(s): Nathan Kaib², Ethan White², Andre Izidoro¹

Institution(s): 1. Univ. Estadual Paulista, 2. University of Oklahoma

planet formation, if there is enough of a mass reservoir. In my dissertation talk, I will present results that bear on disk evolution at both young and late ages. I will present 8 mm polarization results of two Class 0 protostars (IRAS 4A and IC348 MMS) from the VLA at ~ 50 au resolution. The inferred magnetic field of IRAS 4A has a circular morphology, reminiscent of material being dragged into a rotating structure. I will show results from SOFIA polarization data of the area surrounding IRAS 4A at ~ 4000 au. I will also present ALMA 850 micron polarization data of ten protostars in the Perseus Molecular Cloud. Most of these sources show very ordered patterns and low ($\sim 0.5\%$) polarization in their inner regions, while having very disordered patterns and high polarization patterns in their extended emission that may suggest different mechanisms in the inner/outer regions. Finally, I will present results from our ALMA dust continuum survey of protoplanetary disks in Rho Ophiuchus; we measured both the sizes and fluxes of 49 pre main-sequence stellar systems and detected either gaps or cavities in ~ 6 of these sources. Combined, these results build upon how early protoplanetary disks can form around young protostars and thus how early planets can begin to form.

Author(s): Erin Guilfoil Cox¹

Institution(s): 1. University of Illinois

229.03 – Forward modelling techniques for spectra retrieval of circumstellar debris disks

The Gemini Large and Long Program studying circumstellar disks using the Gemini Planet Imager (GPI) is aiming at better constraining the properties of the circumstellar dust, specifically, measuring the near-infrared total intensity and polarization fraction colors, and searching for solid-state spectral features of nearby beta Pic-like disks. This program has already observed 16 disks in one or several of the bandwidths allowed by this instruments. These observations will allow us to break the degeneracy among the particle properties such as composition, size, porosity, and shape. An important step towards this achievement would be to be able to retrieve accurate spectra of the observed debris disks in all the bands of the Integral Field Spectrograph (IFS).

Several differential imaging techniques (ADI, SDI) have been developed to improve a posteriori the contrast of the images taken using an IFS. These aggressive techniques, although

necessary to detect point-like or extended objects, have important effects on the shape of these objects and their photometry. We present here the forward-modelling technique we developed to remove these effects and obtain accurate spectra of the extended objects in the IFS data. Finally, we present the first results of this technique using the data of the LLP disk program.

Author(s): **Johan Mazoyer**¹, Pauline arriaga⁴, Christine Chen², Laurent Pueyo², Charles Poteet², Jason Jinfei Wang³, Marshall Perrin²

Institution(s): 1. *Johns Hopkins University*, 2. *Space Telescope Science Institute*, 3. *UC Berkely*, 4. *UCLA*

229.04D – The Evolution of CO in Protoplanetary Disks During Planet Formation

CO has long been used as a tracer of gas mass. However, recent observations have revealed a low CO to dust mass ratio in numerous protoplanetary disks. In at least some of these systems it is the CO, rather than the total gas mass, which is missing. During my PhD I have used models of protoplanetary disk chemistry as well as millimeter observations to explore the causes and extent of CO depletion in disks. My ALMA observations of CO isotopologues in the TW Hya protoplanetary disk revealed that CO is under-abundant in that system by nearly two orders of magnitude, failing to return to ISM abundances even inside the midplane CO snow line. I have also explored the physical conditions needed to remove carbon from gas phase CO via chemically process using a large grid of chemical models. My analysis reveals that in the warm molecular layer, a wide range of physical conditions can result in an order of magnitude reduction of CO in the outer disk. In the inner disk, ionization, such as from cosmic rays, is needed for chemical reprocessing to occur.

230 – ISM II

230.01 – Resolving the substructure of molecular clouds in the LMC

We present recent wide-field CO and ¹³CO mapping of giant molecular clouds in the Large Magellanic Cloud with ALMA. Our sample exhibits diverse star-formation properties, and reveals comparably diverse molecular cloud properties including surface density and velocity dispersion at a given scale. We first present the results of a recent study comparing two GMCs at the extreme ends of the star formation activity spectrum. Our quiescent cloud exhibits 10 times lower surface density and 5 times lower velocity dispersion than the active 30 Doradus cloud, yet in both clouds we find a wide range of line widths at the smallest resolved scales, spanning nearly the full range of line widths seen at all scales. This suggests an important role for feedback on sub-parsec scales, while the energetics on larger scales are dominated by clump-to-clump relative velocities. We then extend our analysis to four additional clouds that exhibit intermediate levels of star formation activity.

Author(s): **Tony Wong**³, Annie Hughes², Kazuki Tokuda¹, Remy Indebetouw⁴, Evan Wojciechowski³, Jeffrey Bandurski³
Institution(s): 1. *Osaka Prefecture University*, 2. *Université de Toulouse*, 3. *University of Illinois, Urbana-Champaign*, 4. *University of Virginia*

Contributing team(s): MC3 Collaboration

230.02D – HST Ultraviolet Spectroscopy of the Dusty, Molecular Gas in Planck Cold Clumps

The Planck Catalogue of Galactic Cold Clumps (PGCC) has provided a wealth of information about the cold, dusty ISM across the entire sky, identifying regions ranging from relatively diffuse cold clouds to pre-stellar cores in giant molecular clouds. This catalogue uses sub-millimeter emission arising from cold dust to determine the physical properties, morphology, and temperature of these regions. By combining this data with existing Hubble Space Telescope high-resolution UV spectra, we can probe the gas within these objects with the diagnostic capabilities of absorption line spectroscopy. Using data from Planck, Gaia, and CO emission studies, we have identified 22 stars which lie behind a PGCC region, and thus whose sightlines probe the cold gas associated

with these objects. Here we report results from our studies of these sightlines, comparing the dust depletion to previous work done in studies of the diffuse ISM. In particular, we find that the dust depletion decreases as projected distance from the centers of nearby PGCCs increases. Furthermore, we investigate the CO content of the cold gas using the numerous CO absorption bands in the UV. Additionally, by using neutral chlorine as a fiducial for H₂, we calculate the CO-to-H₂ ratio and explore the abundance of CO-dark gas. Finally, we compare the ¹²CO/¹³CO ratio to previous all-sky surveys, finding that our sightlines tend to show higher ¹²CO/¹³CO ratios when compared to other samples of Galactic sightlines.

Author(s): **Kamber Schwarz**¹, Edwin Bergin¹, Edwin Bergin¹
Institution(s): 1. *University of Michigan*

229.05 – [OI] in circumstellar disks

In the far-infrared, [OI] 63 micron is the most sensitive probe of gas in protoplanetary disks and has even been detected in several young debris disks.

We have now obtained velocity resolved spectra (velocity resolution 0.1 km/s) using the heterodyne receiver GREAT on the Stratospheric Observatory for Infrared Astronomy (SOFIA) of five of the brightest circumstellar disks in the [OI] 63 micron line. Four of these are protoplanetary disks (AB Aur, HL Tau, HD 100546 and HD 97048), while one is a disk around an FS CMa star, HD 50138. Since all the stars are surrounded by disks in Keplerian rotation, our observations allow us to explore where the [OI] emission originates and the physical conditions of the [OI] emitting layers. In this presentation we present preliminary results of our findings.

Author(s): **Goran Sandell**¹
Institution(s): 1. *USRA*

with these objects. Here we report results from our studies of these sightlines, comparing the dust depletion to previous work done in studies of the diffuse ISM. In particular, we find that the dust depletion decreases as projected distance from the centers of nearby PGCCs increases. Furthermore, we investigate the CO content of the cold gas using the numerous CO absorption bands in the UV. Additionally, by using neutral chlorine as a fiducial for H₂, we calculate the CO-to-H₂ ratio and explore the abundance of CO-dark gas. Finally, we compare the ¹²CO/¹³CO ratio to previous all-sky surveys, finding that our sightlines tend to show higher ¹²CO/¹³CO ratios when compared to other samples of Galactic sightlines.

Author(s): **Cody Dirks**¹
Institution(s): 1. *Northwestern University*

230.03 – Global Infrared–Radio Spectral Energy Distributions of Galactic Massive Star-Forming Regions

We present a multiwavelength study of 30 Galactic massive star-forming regions. We fit multicomponent dust, blackbody, and power-law continuum models to 3.6 μm through 10 mm spectral energy distributions obtained from *Spitzer*, *MSX*, *IRAS*, *Herschel*, and *Planck* archival survey data. Averaged across our sample, ~20% of Lyman continuum photons emitted by massive stars are absorbed by dust before contributing to the ionization of H II regions, while ~50% of the stellar bolometric luminosity is absorbed and reprocessed by dust in the H II regions and surrounding photodissociation regions. The most luminous, infrared-bright regions that fully sample the upper stellar initial mass function (ionizing photon rates $N_C \geq 10^{50} \text{ s}^{-1}$ and total infrared luminosity $L_{\text{TIR}} \geq 106.8 L_{\odot}$) have higher percentages of absorbed Lyman continuum photons (~40%) and dust-reprocessed starlight (~80%). The monochromatic 70-μm luminosity L_{70} is linearly correlated with L_{TIR} , and on average $L_{70}/L_{\text{TIR}} = 50\%$, in good agreement with extragalactic studies. Calibrated against the known massive stellar content in our sampled H II regions, we find that star formation rates based on L_{70} are in reasonably good agreement with extragalactic calibrations, when corrected for the smaller physical sizes of the Galactic regions. We caution that absorption of Lyman

continuum photons prior to contributing to the observed ionizing photon rate may reduce the attenuation-corrected H α emission, systematically biasing extragalactic calibrations toward lower star formation rates when applied to spatially-resolved studies of obscured star formation.

This work was supported by the National Science Foundation under award CAREER-1454333.

Author(s): Matthew Samuel Povich¹, Breanna Arlene Binder¹

Institution(s): 1. *Cal Poly Pomona*

230.04D – Examining Sites of Recent Star Formation in the Galactic Center: A Closer Look at the Arched Filaments and H III Regions

In this dissertation presentation, we analyze mid-infrared imaging of the Arched Filaments and H III regions in the Galactic center taken with the Faint Object Infrared Camera for the SOFIA Telescope (FORCAST). Examining these regions are of great interest because they provide insights on star formation in the Galactic center and the interactions massive stars have with the ISM. The Arched Filaments are a collection of molecular cloud ridges which are ionized by the nearby Arches star cluster, and give the appearance of large (~25 pc) arch-like structures. The H III regions are a collection of H II regions just to the west of the Arches cluster (~5-15 pc). The origin of the stars powering the H III regions is uncertain, as they may have formed in a nearby molecular cloud or could be ejected members of the Arches cluster. FORCAST observations of these regions were used to study the morphology and heating structure of the H II regions, as well as constrain their luminosities.

Color-temperature maps of the Arched Filaments created with the FORCAST data reveals fairly uniform dust temperatures (~70-100 K) across the length filaments. The temperature uniformity of the clouds can be explained if they are heated by the Arches cluster but are located at a larger distance from the cluster than they appear. The density of the Arched Filaments clouds was estimated from the FORCAST data and was found to be below the threshold for tidal shearing, indicating that that the clouds will be destroyed by the strong tidal field near the Galactic center. To the west of the Arched Filaments, there is an interesting collection of H II regions, referred to as the H III regions. These regions are likely heated by massive O/B type stars, and the morphology of the dust emission associated with these objects indicate a mixture of potential in situ formation mechanisms and interlopers. Interestingly, FORCAST imaging of the H III regions also reveal several compact sources, which may be young embedded stars. We discuss these sources in the context of star formation scenarios in the Galactic center.

Author(s): Matthew Hankins³, Terry Herter³, Ryan Lau², Mark Morris⁴, Elisabeth Mills¹

Institution(s): 1. *Boston University*, 2. *Caltech*, 3. *Cornell University*, 4. *UCLA*

230.05D – More Than Filaments and Cores: Statistical Study of Structure Formation and Dynamics in Nearby Molecular Clouds

In the past decade, multiple attempts at understanding the connection between filaments and star forming cores have been made using observations across the entire spectrum. However,

231 – Surveys and Large Programs I

231.01 – The Breakthrough Listen Search for Intelligent Life

The \$100M, 10-year philanthropic "Breakthrough Listen" project is driving an unprecedented expansion of the search for intelligent life beyond Earth. Modern instruments allow ever larger regions of parameter space (luminosity function, duty cycle, beaming fraction, frequency coverage) to be explored, which is enabling us to place meaningful physical limits on the prevalence of transmitting civilizations. Data volumes are huge, and preclude long-term storage of the raw data products, so real-

time and machine learning processing techniques must be employed to identify candidate signals as well as simultaneously classifying interfering sources. However, the Galaxy is now known to be a target-rich environment, teeming with habitable planets.

the filaments and the cores are usually treated as predefined--and well-defined--entities, instead of structures that often come at different sizes, shapes, with substantially different dynamics, and inter-connected at different scales. In my dissertation, I present an array of studies using different statistical methods, including the dendrogram and the probability distribution function (PDF), of structures at different size scales within nearby molecular clouds. These structures are identified using observations of different density tracers, and where possible, in the multi-dimensional parameter space of key dynamic properties--the LSR velocity, the velocity dispersion, and the column density. The goal is to give an overview of structure formation in nearby star-forming clouds, as well as of the dynamics in these structures. I find that the overall statistical properties of a larger structure is often the summation/superposition of sub-structures within, and that there could be significant variations due to local physical processes. I also find that the star formation process within molecular clouds could in fact take place in a non-monolithic manner, connecting potentially merging and/or transient structures, at different scales.

Author(s): How-Huan Chen¹, Alyssa Goodman¹

Institution(s): 1. *Harvard University*

230.06 – The GBT Diffuse Ionized Gas Survey (GDIGS)

Diffuse ionized gas in the Galactic mid-plane known as the "Warm Ionized Medium" (WIM) makes up ~20% of the gas mass of the Milky Way and >90% of its ionized gas. It is the last major component of the interstellar medium (ISM) that has not yet been studied at high spatial and spectral resolution, and therefore many of its fundamental properties remain unclear. The Green Bank Telescope (GBT) Diffuse Ionized Gas Survey (GDIGS) is a new large survey of the Milky Way disk at C-band (4-8 GHz). The main goals of GDIGS are to investigate the properties of the WIM and to determine the connection between the WIM and high-mass star formation over the Galactic longitude and latitude range of $32^\circ < l < 5^\circ$, $|b| < 0.5^\circ$. We use the new VEGAS spectrometer to simultaneously observe 22 H α -alpha radio recombination lines, 25 H β -beta lines, 8 H γ -gamma lines, and 9 molecular lines (namely CH₃OH and H₂CO), and also continuum at ~60 frequencies. We average the H α -alpha lines to produce Nyquist-sampled maps on a spatial grid of 1 arcmin, a velocity resolution of 0.5 km/s and rms sensitivities of ~3 mJy per beam. GDIGS observations are currently underway and are expected to be completed by late 2018. These data will allow us to: 1) Study for the first time the inner-Galaxy WIM unaffected by confusion from discrete H II regions, 2) determine the distribution of the inner Galaxy WIM, 3) investigate the ionization state of the WIM, 4) explore the connection between the WIM and H II regions, and 5) analyze the effect of leaked photons from H II regions on ISM dust temperatures.

Author(s): Matteo Luisi⁴, Loren Dean Anderson⁴, Bin Liu⁴, Thomas Bania¹, Dana Balsler², Trey Wenger², Lawrence Matthew Haffner³

Institution(s): 1. *Boston University*, 2. *National Radio Astronomy Observatory*, 3. *University of Wisconsin-Madison*, 4. *West Virginia University*

time and machine learning processing techniques must be employed to identify candidate signals as well as simultaneously classifying interfering sources. However, the Galaxy is now known to be a target-rich environment, teeming with habitable planets.

Data from Breakthrough Listen can also be used by researchers in other areas of astronomy to study pulsars, fast radio bursts, and a range of other science targets. Breakthrough Listen is already underway in the optical and radio bands, and is also engaging with facilities across the world, including Square Kilometer Array

precursors and pathfinders. I will give an overview of the technology, science goals, data products, and roadmap of Breakthrough Listen, as we attempt to answer one of humanity's oldest questions: Are we alone?

Author(s): Steve Croft¹, Andrew Siemion¹, David De Boer¹, J. Emilio Enriquez¹, Griffin Foster¹, Vishal Gajjar¹, Greg Hellbourg¹, Jack Hickish¹, Howard Isaacson¹, Matt Lebofsky¹, David MacMahon¹, Daniel Price¹, Dan Werthimer¹
Institution(s): 1. UC Berkeley

231.02 – Radio Transients in 1333 deg² of the VLA Sky Survey Pilot

The VLA Sky Survey (VLASS) is an ongoing project by the NRAO to map ~34,000 deg² of the sky at 3GHz, over 3 epochs spanning 6 years. In preparation for the full survey, a set of fields covering 2480 deg² was recently observed as the VLASS pilot project. We searched 1333 deg² of the VLASS pilot for radio transients with characteristic decay timescales between weeks and years, such as the synchrotron afterglows of supernovae, tidal disruption events, and long/short gamma ray bursts. These radio afterglows are thought to be roughly isotropic and extinction-free, allowing us to observe transients that would be missed by optical/high energy surveys due to obscuration or off-axis jetting.

Within the searched area, we identified 215 VLASS sources that have no counterpart in the FIRST survey and have a projected distance of < 50kpc from the nearest galaxy by angular distance in the CLU and GWENs galaxy catalogs. By selection, these targets are predominantly located near low redshift ($z < 0.05$) galaxies, allowing us to study their host environments with a sub-kiloparsec spatial resolution. Prioritizing based on visual association with SDSS galaxies, we imaged and/or took spectra of the host environment of 60 targets with the Low Resolution Imaging Spectrometer (LRIS) on Keck 1. In this talk, we present the radio and optical results for the most exciting VLASS transients.

Author(s): Dillon Dong¹, Gregg Hallinan¹, Steven T. Myers², Kunal Mooley³
Institution(s): 1. Caltech, 2. NRAO, 3. University of Oxford
Contributing team(s): VLASS Survey Team, VLASS Survey Science Group (SSG)

231.03 – The XMM-SERVS Survey: first results in the 5 deg² XMM-LSS region

We present an X-ray source catalog obtained with XMM-Newton in the XMM-LSS region as part of the X-SERVS survey (XMM-SERVS-LSS), which aims to expand the parameter space of current X-ray surveys with medium-deep X-ray observations in multiple large fields with superb multiwavelength coverage. Within the 5 deg² XMM-SERVS-LSS field, we combine the 1.3 Ms XMM observations allocated at XMM AO-15 with archival data, and identified 5218 X-ray sources of which 2400 are new sources. We reach 1.2×10^{-15} erg s⁻¹ cm⁻² for 50% of the area, which is comparable to the XMM-COSMOS survey but with 2.5 times more sources. We also present multiwavelength identifications, basic photometric properties, and spectroscopic redshifts obtained from the literature. These data, combined with the existing data from COSMOS, will enable a wide range of science on AGN evolution, including studying SMBH growth across the full range of cosmic environments and minimizing cosmic variance.

Author(s): Chien-Ting Chen², William Brandt², Bin Luo¹
Institution(s): 1. Nanjing University, 2. The Pennsylvania State University
Contributing team(s): the X-SERVS team

231.04D – Characterizing the Supernova Host Galaxy Population with ASAS-SN

The goal of the All-Sky Automated Survey for Supernovae (ASAS-SN) is to provide the astronomical community with a complete

record of the optically accessible night sky. ASAS-SN uses a global array of telescopes to monitor the entire sky on a nightly cadence. Due to the nearby volume probed by ASAS-SN, our survey excels at discovering bright transient events. The events we discover can be studied in great detail and monitored well into the late phases of evolution with only modest observational resources. ASAS-SN has discovered a plethora of interesting transient events, and has also amassed a large sample of supernovae (SNe). Not only are the statistical properties of these SNe interesting in their own right, but the galaxies that host these events are also of great scientific interest. I will present the initial results of our SNe host galaxy census, and highlight some systems that would have been missed by traditional SN surveys. Finally I will discuss how this dataset will be used to improve our understanding of the SNe-host galaxy connection.

Author(s): Jonathan Brown¹
Institution(s): 1. The Ohio State University
Contributing team(s): The ASAS-SN Team

231.05 – GUSTO: Gal/Xgal U/LDB Spectroscopic Stratospheric TeraHertz Observatory

GUSTO is a recently selected NASA Explorer mission that will map in unprecedented detail the structure, dynamics, energy balance, and evolution of the interstellar medium within the Milky Way and Large Magellanic Cloud. GUSTO is a balloon-borne, 0.85-m on-axis telescope that will observe in three important interstellar lines: [CII], [OI], and [NII] at 158, 63, and 205 microns, respectively. With its 60" angular resolution, high-velocity resolution, and efficient "On-The-Fly" mapping strategy, GUSTO will address key unanswered questions about the stellar life cycle and provide new insights into the birth and evolution of stars and galaxies. From its Ultra-Long-Duration Balloon (ULDB) platform at an altitude of 33 km, GUSTO will survey ~100 deg² of the Milky Way and 24 deg² of the LMC at 60" angular resolution using three 8-pixel heterodyne array receivers. The GUSTO receivers provide sub-km/s velocity resolution and bandwidths sufficiently wide to track all clouds orbiting in the Milky Way and LMC. GUSTO will detect and locate in three dimensions every important interstellar cloud ($A_V > 0.5-1$) in the surveyed regions. The baseline mission of 100 days can be completed in one ULDB Antarctic balloon flight, and an extended mission of up to 169 days is possible. GUSTO's observing campaign comprises three distinct surveys: GPS: A Galactic Plane Survey (42 days); LMCS: An LMC Survey (36 days); TDS: Targeted Deep Surveys of selected regions in the Galaxy and LMC (18 days). In our presentation we will discuss both the science goals of GUSTO and the mission implementation.

Author(s): Christopher Kidd Walker⁹, Craig Kulesa⁹, Paul Goldsmith⁴, Christopher Groppi¹, Frank Helmich⁸, David Hollenbach⁷, Jonathan Kawamura⁴, William Langer⁴, Gary Melnick³, David Neufeld⁵, Jorge Pineda⁴, Gordon Stacey², Antony Stark³, Alexander Tielens⁶, Mark Wolfire¹⁰, Harold Yorke¹¹, Erick Young¹¹
Institution(s): 1. Arizona State University, 2. Cornell University, 3. Harvard-Smithsonian Center for Astrophysics, 4. Jet Propulsion Laboratory, 5. Johns Hopkins University, 6. Leiden University, 7. SETI Institute, 8. SRON, 9. University of Arizona, 10. University of Maryland, 11. USRA

231.06 – Rapid All-Sky Transient Discovery and Analysis with Evryscope

The Evryscope is an array of 24 small telescopes on a common mount, capable of observing the entire visible sky down to $g' \sim 16$ with a two-minute cadence. Each exposure covers 8000 square degrees over 691 MPix and requires minimal readout time, providing 97% continuous coverage of the night sky. The system's large field of view and rapid cadence enable exploration of a previously inaccessible parameter space of bright and fast transients, including nearby microlensing events, supernovae, and kilonovae GW counterparts. The first instrument, located at CTIO in Chile, was deployed in mid-2015 and is currently in production creating multi-year light curves with percent-level

precision. A second identical system is on track for deployment at Mount Laguna Observatory in California in early 2018. Once operational, the two sites will provide simultaneous two-color photometry over a 4000 square degree overlapping region accessible to both instruments, operating as a combined discovery and follow-up network for transient phenomena on all nearby stars and many nearby galaxies. I will present recent science results from the Evryscope and an overview of our data reduction pipeline.

Author(s): Henry T Corbett¹, Nicholas Law¹, Octavi Fors¹, Jeff Ratzloff¹, Erin Goeke¹, Ward S Howard¹

Institution(s): 1. University of North Carolina at Chapel Hill

231.07 – LADUMA: Looking At the Distant Universe with the MeerKAT Array

The cosmic evolution of galaxies' neutral atomic gas content is a major science driver for the Square Kilometre Array (SKA), as well as for its Australian (ASKAP) and South African (MeerKAT) precursors. Among the HI surveys planned for ASKAP and MeerKAT, the deepest and narrowest tier of the "wedding cake" will be defined by the approved 3424-hour Looking At the Distant Universe with the MeerKAT Array (LADUMA) survey, which will probe HI in emission within a single "cosmic vuvuzela" that extends to $z = 1.4$, when the universe was only a third of its present age. Through a combination of individual and stacked detections (the latter relying on extensive multiwavelength studies of the survey's target field), LADUMA will study the redshift evolution of the baryonic Tully-Fisher relation and the cosmic HI density, the variation of the HI mass function with redshift and environment, and the connection between HI content and the properties of galaxies' stars (mass, age, etc.). The survey will also build a sample of OH megamaser detections that can be used to trace the cosmic merger history. This talk will introduce the science potential of LADUMA and plans for its execution starting in 2018.

Author(s): Andrew J. Baker¹, Sarah Blyth², Benne W. Holwerda³

Institution(s): 1. Rutgers, The State University of NJ, 2. University of Cape Town, 3. University of Louisville

Contributing team(s): LADUMA team

231.08 – The VLA Sky Survey (VLASS): Overview and First Results

232 – Astronomy Outreach: From Large Observatory to Memorable Music

232.01 – Weaving a Webb story: Communicating Science for JWST

NASA's next great observatory is an impressive and complex mission with many tales to tell. Science is a collection of stories and Webb will be a storytelling machine. How are we preparing to share the scientific news to come from this amazing telescope? From news releases to multimedia content to a vast online presence, the stories of the James Webb Space Telescope will require crafting in order to impact the widest audience. We discuss the art of storytelling based on messaging, goals, mediums, and audience, and how you can apply the same principles to communicating your own research.

Author(s): Alexandra Lockwood¹

Institution(s): 1. Space Telescope Science Institute

232.02 – Showing Complex Astrophysical Settings Through Virtual Reality

The James Webb Space Telescope (JWST), NASA's next great observatory launching in spring 2019, will routinely showcase astrophysical concepts that will challenge the public's understanding. Emerging technologies such as virtual reality bring the viewer into the data and the concept in previously unimaginable immersive detail. For example, we imagine a spacefarer inside a protoplanetary disk, seeing the accretion

The VLA Sky Survey (VLASS) is a 5520 hour spectropolarimetric synoptic survey covering the 33885 square degrees of the sky above Declination -40 degrees from 2-4 GHz at 2.5" angular resolution using the upgraded Karl G. Jansky Very Large Array (VLA). Over the survey duration of 7 years, each area of the sky will be covered in 3 epochs spaced 32 months apart, to a projected depth of 0.12mJy/beam rms noise per epoch and 0.07mJy/beam for 3 epochs combined. The VLASS employs on-the-fly mosaicking (OTFM) to rapidly scan the sky with a net speed of approximately 20 sq. degrees per hour. The high-level science goals for the survey include the identification and precise location of radio transients, the measurement of magnetic fields in our galaxy and beyond, and the study of radio emission from galaxies and active galactic nuclei throughout the Universe. The ability of the VLASS to see through dust allows us to unveil phenomena such as hidden cosmic explosions, emission from deep within our galaxy, and supermassive black holes buried within host galaxies.

The VLASS was proposed in 2014 by our community-led Survey Science Group (SSG). VLASS Pilot observations were taken in mid-2016, and the first epoch covering half the area (VLASS1.1) commenced in September 2017. The raw data from the VLASS are available in the NRAO archive immediately with no proprietary period. The Basic Data Products (BDP) that will be produced by the survey team are public and will additionally include: calibrated visibility data, quick-look continuum images (with a goal of posting to the archive within 1 week of observation), single-epoch and cumulative combined-epoch images, spectral image cubes, and basic object catalogs. Single-epoch and cumulative images are in intensity and linear polarization (Stokes IQU). In addition to the BDP provided by NRAO and served through the NRAO archive, there are plans for Enhanced Data Products and Services to be provided by the community in partnership with the VLASS team.

In this presentation we describe the science goals, survey design, and technical implementation for the VLASS, and highlight results from the Pilot and the first epoch observations taken so far.

Author(s): Steven T. Myers¹

Institution(s): 1. National Radio Astronomy Observatory

Contributing team(s): VLASS Survey Team, Survey Science Group (SSG)

process directly. STScI is pioneering some tools related to JWST for showcasing at AAS, and in local events, which I highlight here. If we develop materials properly tailored to this medium, we can reach more diverse audiences than ever before.

Author(s): Joel Green¹, Denise Smith¹, Louis Chad Smith¹, Brandon Lawton¹, Alexandra Lockwood¹, Hussein Jirdeh¹

Institution(s): 1. Space Telescope Science Institute

232.03 – Local Community Advocacy for the Thirty Meter Telescope on the Big Island of Hawai'i

The Thirty Meter Telescope project is a next-generation ground-based optical/infrared telescope planned for construction on Mauna Kea. It is also a prominent social issue in Hawai'i, touching upon a wide range of island-specific issues, including economic/educational opportunities and justice, Hawaii's long and proud history of astronomy/navigation, the cultural significance of Mauna Kea to some Hawaiians, and Hawaiian sovereignty. In this talk, we describe local community outreach carried out by Hawai'i island resident members of our group, Yes2TMT, and also by the pro-TMT Hawaiian group P.U.E.O based in Hilo. We have cultivated a substantial social media community and persistent on-the-ground advocacy that addresses the many misconceptions about TMT while providing an outlet for concerns from our neighbors. Since early 2016 and thanks to the efforts of many on Hawai'i, support for TMT has

3 4 1 2 3

1 2 5 2
1 3 4 4
2

12

1 1 1 1

234 – Stars and Friends II

1 2 2

1

2
5

7

3

6

4

1

1

2

3

1

1

1

2

2

3

1

1

236 – HEAD Bruno Rossi Prize: Gravitational Waves Astrophysics, Gabriela Gonzalez (Louisiana State University for the LIGO Scientific Collaboration and the Virgo Collaboration)

1

237 – The Milky Way & The Galactic Center Poster Session

2

1

3

4

1

2

4

1

1

1
1

1

1

1

1

1

1

1
1

2
3

3

2
1

2
3

6

2
5

4
1

3
2

1

2

1

1

9 7 **2** 5 1 6 4 8 3 3

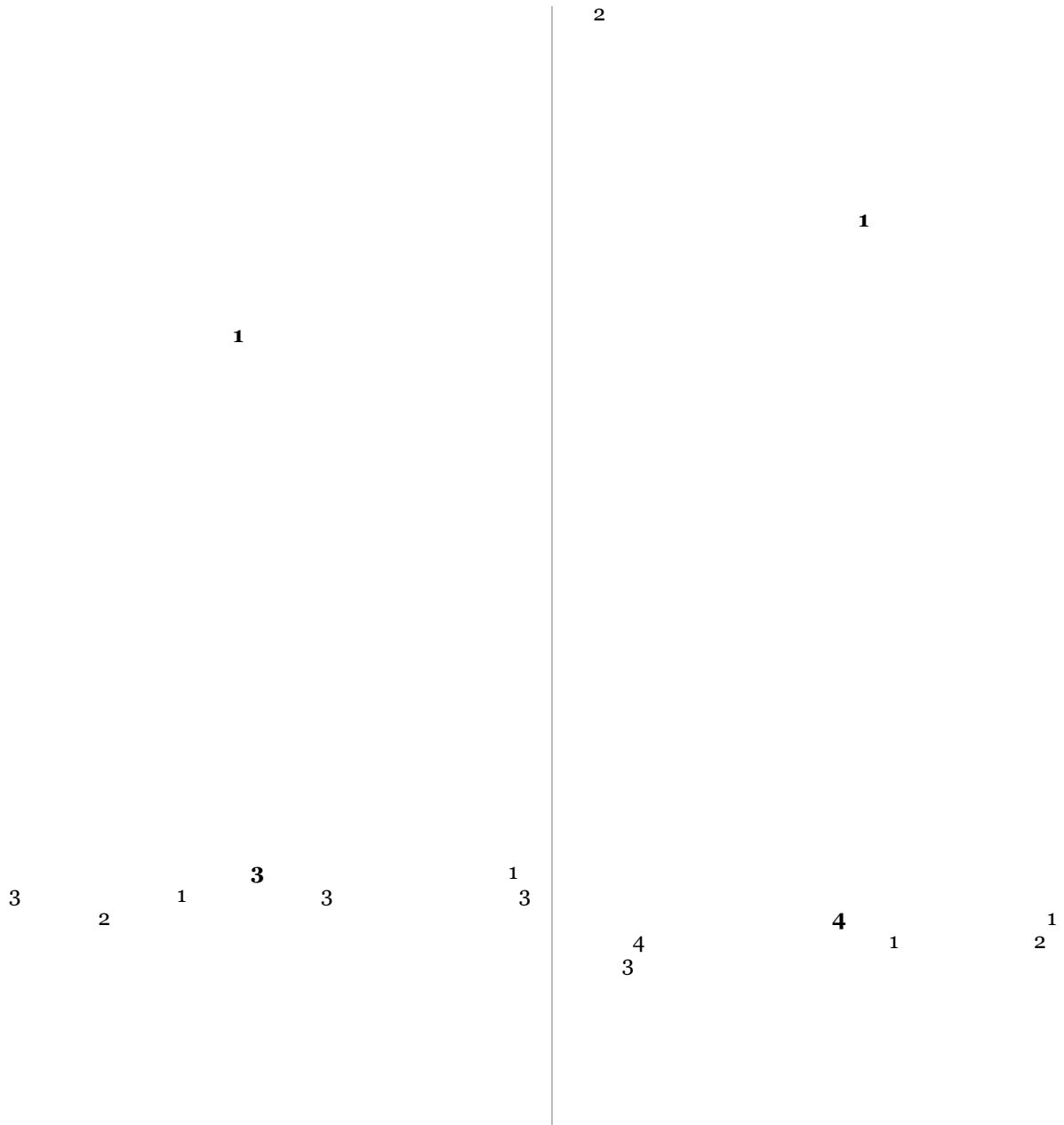
2 1 **2**

1 **1** 2

200
2 1 **2** 2 2 2

1

2 2



238 – Data Driven Discoveries in Serendipitous X-ray Catalogs Poster Session

4
4 1 4
4 4 4 4
4 4 4 4 4
4 4 4 4 4 4
4 2 4 4 4 4 4
4 4 4 4 4 4 4
4 4 4 4 4 4 4

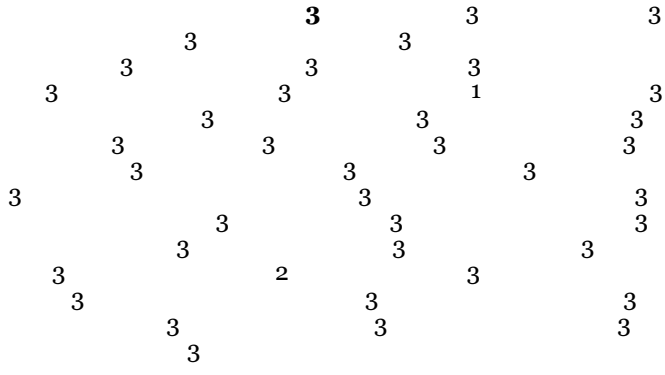
3
3 3 3
3 3 3 3
3 3 3 3 3
3 3 3 3 3 3
3 3 3 3 3 3 3
3 3 3 3 3 3 3 3
3 3 3 3 3 3 3 3 3
3 3 3 3 3 3 3 3 3 3

3
3 3 3 3 3
3 3 3 3 3 3
3 3 3 3 3 3 3
3 3 3 3 3 3 3 3
3 3 3 3 3 3 3 3 3
3 3 3 3 3 3 3 3 3 3
3 3 3 3 3 3 3 3 3 3 3
3 3 3 3 3 3 3 3 3 3 3 3

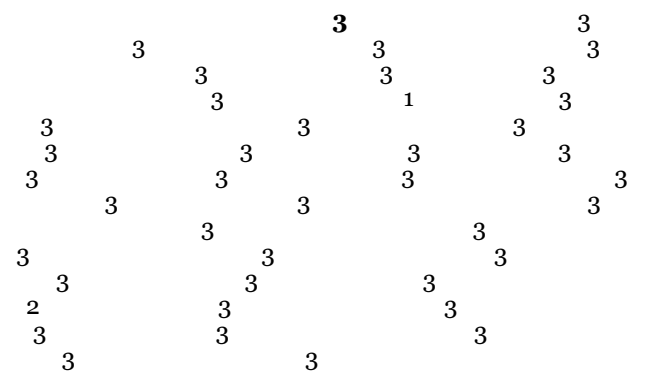
3 3 3 1 3 3 3 3 3 3
 3 3 3 3 3 3 3 3 3 3
 3 3 3 2 3 3 3 3 3 3
 3 3 3 3 3 3 3 3 3 3

3 3 3 3 3 3 3 3 3 3
 3 1 3 3 3 3 3 3 3 3
 3 3 3 2 3 3 3 3 3 3
 3 3 3 3 3 3 3 3 3 3

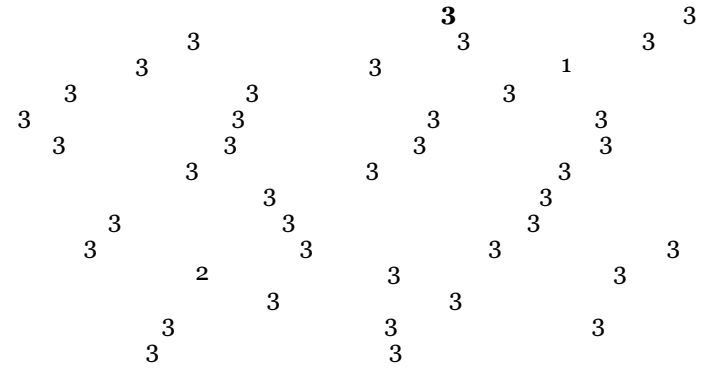
3 3 3 3 3 3 3 3 3 3
 3 3 3 3 3 3 3 3 3 3
 3 3 3 2 3 3 3 3 3 3
 3 3 3 3 3 3 3 3 3 3



1 1 1 1



2



3 3
3 1
3 3
3 3
3 3
3 3
3 2
3 3

3
3
3 3
3 3
3 3
3 3
3 3

3
3
3 3
3
3 3

3
3
3 3
3
3 3

3 3
3
3 3
3 3
3 3
3 3

1

1

1

1

1

1

3

2

2

3 1 1
 2 2 4

239 – Applied Statistical Methods in Astronomy: Gaussian Processes and Machine Learning Poster Session

1 1 2

1 1

1 1

2 2 3 1

2 4 2 3 5 1

241 – Planetary Nebulae and SNRs Poster Session

2
4 2 7 **3** 5 4 2
6 1

2 1 **2** 2

1 **1** 1
1

3 4 **2** 1 7
5 6

2

2

2

2

2

2

2

2

2
2 -1

2

2

5

4

1

4

2

3

2 1 1

1 1 3 2 1

2 1 1

3 1 2 4 2 1
1

1 3 3 3 2 4

1 5 4 3 5 1 5
2

1

2 2 2 1

1 1 1

○

+3 +

2 2 3 2 4
1

242 – Results from the August 21, 2017, Total Solar Eclipse Poster Session

1 1

2 1

1 2 3 2 2 2 2
2

1

2

3

1

1

2

2

2

2
1

2

2

3

3

1

4

3

2²
2

3⁴

2¹

1

2¹

1

2
1

1¹

1

1

1¹

1

1

1

3 **3** 2
 1

1

st

4 **4** 2 2
3 2 2 1
 4

1

1

1

1

243 – Neutron Stars (Pulsars, Magnetars, Pulsar Wind Nebulae) Poster Session

1

5
2

5

4

3

1

1

2

1

11

2

1

1

1

2 1

1 4 **3** 3 3 2

4 2 **4** 3 1

r γ

r γ

r γ

2 1

1 1 **2** 1 1

4 5 2 **3** 4 6 7 1

3 1 4 2

2 1 1

11 5 14 2 3 1 13 5 7
15 1 1 12 5 1
13 4 5 6 10
8 13 9 10
1

6 10 5
9 2 7 1
8 2 4 2 3 1

3 **2** 2 3 3
1

3 **2** 1

4 5 **1** 2 3

5 **9** 1 5 5 4
8 4 2 7 5 5 3
5 6 5 9

2 7 **9** 8 9
9 1 4 3 6 3 10
5

4 6 **1** 3 5 2
6

244 – Binary Stars Poster Session

2

2

1

1

1

2

c c

2

1

3

1

1

Sun

Sun

1

1

1

1

2

2

1

1

2

2

1

2

2

2

1

1 2

1

2

1

2

2 1

1 2

o

3

5

4

1

2

1

1

1

1

2 1 2 1

4 1 3
 2

1 1

2 3 5 1 4

7 3 8 8 6
 4 2 1 5

1

1

1
1

1

1

1

1

1

1

1

2

1

1 1 2

2 2 3 1

1 2 1 1

245 – Supernovae Poster Session

1 1

5 1 4 4
3 1 6 2

3 1 2

3 2 2 2 2 1

1 1 3 2 2 1

2 1 1 3 10 12 5 7 1 8 9 11 2

2

4 4 3 4 2 1 3 4

2 1 2 2 1

1 1

1 2 1

2 2 2 1

1

2 3 1 3

1

1

HI ^{-2}C \odot

1 2 1 1
1

246 – Extrasolar Planets: Detection Poster Session

o o

2 4 1 6 7
5 4 6 6 3

1 1 1

1 1

1 1

1 1

1 **1** 1
 1

4 3 **3** 5 2 3 2 1 3

8 9 8 8
 1 8 12 8 12 8
8 12 10 11 9 7 12
9 4 7 5 5 7 9
5 9 9 9 10 9
9 11 6 2 5 3 9
 6 5 9 9

2 **3** 1

2 **1** 2 1
 2

2

1
1

1

1

1

1

6

6

7

2

8

5

2

4
3

1

1

1

1

2

2

2

1

1 1 1 1
 1
 1

1 2

1 1

1 1 1 1 1
 1 1 1 1

1

4 1 **5** 2 3

1 1 **3** 2

2 3 1 **7** 1 **5**
4 6 1 1

1 1 **1** 1 1

1 1 1 **1** 1 1 1

3
1

2 **2**
2 2

4 2 2
2 2

2

5 5 5 **5** 6 5 1 5

2 5 3 4 5 4 5 7 5

5 5 1 5 5 5 5 3

1 1

-9

1 1 **1** 1 1

1 **1** 1 1

1

1 4
4 4
2 4 4
4 3

2 2 3 1 3 3
1 1

1 1 1 1 1 1
1

3 1 4 1 5 2

4 2 5 1 3 1

4 4 4 4 4 4
4 2 4 6 5 4 5 1
3 4 4 7

3 2 3 2 4
2 2 1 2

1 1 1 1 2

247 – ISM, HII Regions and Molecular Clouds Poster Session

2 2

1 3 2 2 2 6
2 4 5

2 2 1 1

1 1 1

1

2 1

1 1 1 1

2 5 3 4
1

1

1

1

3

1

2

2

1

3

2

1

1
1

1

V V

1 2

3 1 3 2 2

o

1 1

1 1 1 1

13 + 13 2 3 + 2 + 2

22 -2

2

2

1

2

1 1

4 2
4 1 3 4 3 3

4 7

3 2 2 1

1 2 1 1

13

12

1 1 1 1 1 1

1 2 1

2 7 1 5 4 3 1
1 1 1 6

9 1 9 6 3 8 7
2 5 1 4 9

4 6 8 7 9
9 1 2 3 5

1 1 1

1 2 1 1

V

+ 2

3 k 2 2 H -

12 13 +

1 2 3 2
4 4

1 1

1 2 2

8 4 9 1 2 5 4 7 9 9 8 3 6

1 1 1

2 1

2

248 – Spiral Galaxies Poster Session

1 2 2 1

3 2 1 1

1 1

1 1

1 2

2

2
1

1

4

4

1

2
3

4

4

1

1

1

1

249 – Elliptical Galaxies Poster Session

1

1

1

1

1

250 – AGN, QSO, Blazars Poster Session

24 -2

5
6

1
3

1
4 2

1
7

H

1

2

1

1

1

1

1

2

1

2

2

1 2 **3** 2

2 2 1

1 1 **1** 1 1

-6.58

2 **1** 1 1 4
 1 5 3

2 2 **1** 1

2

1

3

1

1

1

1
1

1 **1**

2

2

2

1 **2**

2

1

1

1 1 1 1 1

2 1 1

1 2 3 1

1

1

1 3 2

2 1 4 3

1

1 1

OX OX

OX
Edd

OX OX

5
8
3

9
10
4

11
8

1

2
6

7

OX

Edd

2

3

1

1

1 1

-1

1 1 1

4 3 2 1 4

1 1 1

1 2

1 1 1

1 1 **3** 2

1 4 1 1 1 3
 2

v 42 -1

2 1 1

4 3 1 2 2

6 8 1 2 1
 4 7 5 3

-1

1

2

2

1

1

7

6

5

3

4

3

6

1

2

5

2

2

5

2

3

4

5

1

2

1

1

2

2

1

2

1

1

1 1

1 4 1

2 3

1 2

1 1

3 1

1

1 1

4

1

1

1

3

1

1

1

251 – Starburst Galaxies Poster Session

1

2

3

1

1

1

2

1 1 1

1 4 3 1 2
2

3 4 5 2 2 2
1

1 1 1

solar

1 1

3 5 5 5
2 4 1

*

⊙

2 3 2 2 4 1 2

* 8 11 ⊙

5 10 ⊙ 7.8 ⊙

7 ⊙

1 2

252 – Galaxy Clusters Poster Session

2

2 1

3
6
3

3
1

5

4
2

4

7

1

1

1 2 **3** 1 3
 X X
 X X
 X
 X
 3 5 5 **6** 4 3 2 4 5
 1

2 1 5 3 1 1 4
 1 1 1

3 1 **3** 2

1 **2** 3

-2 -2

2

2

1

2
2

1

2

1

2

1

2

1

1

1

1

1

1

1

1

1

1

1

3

2
1

2
1

2

2

1

1

2

1

2

2

HI

2

3 4

4 1

253 – Laboratory Astrophysics Poster Session

1

1

4

3

2

3

5

3

1

2

2

4

2

3

4

1

254 – Gamma Ray Bursts Poster Session

1

255 – Gravitational Waves, Relativistic Astrophysics and Related Topics Poster Session

1

1

2

1

2

-12

-5

-12

2

-11

2

1

1

1

3

2

1

1

1

1

1

1

1

2

4

1

6

3

1

5

2

1

1

2

1

1

2 2 1 2

2 1 2 1

-1 -3

45 46 -13 8²
8 ⊙ -13 8³
2 2 -13 -13 3
1 2 3

-3

2 1 1

1 1

4 2 4 2 5 4 1
4 2 3

1

1

2 1 1 4
6 5 7 3

1

1

1

1

1

1

1

1

1

1

1

1

1

1

1

1

1

258 – Galaxies, Cosmology iPoster Session

1

13 5 11 10 10 10
 2 9 7 10 1
 7 12 7 7 13
 8 4 6 7
 3

1

1

8 4 1 6 2 9 7 5 3 1 1 1

2

1

1

1

3

4

2
5
4

6¹

4

44 -1

X

2

4
1

3

2

1

1

1

1

1

2

1
2

1

2

1

2

4
3

1

⊙

K

K

⊙

10

⊙

12

⊙

⊙

$10^{0.15}$

m

⊙

⊙

10

K

⊙

⊙

IGM

14

3 3 1 3 2 3 2

1 1 1

1

1 6 7 1 3 7 2 1 4 2 6 5

1 2 1 3

300 – Plenary Talk: Venus: Our Misunderstood Sister, Darby Dyar (Planetary Science Institute)

2

1

361 – Dark Matter, Instrumentation and Other Topics iPoster Session

2

1

1

1

1

1

2

1

3 5
3 4
2 3
6 1

1

1

3 2 4 1

1 1 1 1 2 1 1
1 1 1 2 1 1

4 1 1 7 1 7
 8 2 6 9 2
 2 3 5

1 1

1

2

1

5 4 4 4 2 3 4 4 1

2 2 2 1 2 1

8 1 4 2 6 1 7 1 4 3 1 5 6 3 1

301 – Water, Water, Everywhere

1

1

1

302 – IGM and QSO Absorption Line Systems II

90

-2

6
2

3

2

4

2

6

1

7

5

1

1

4

2
4

1

2

3

1

1

1

1

1

1

3
1

6
5

3

4
2

5 6

1 1 1

2 1 2 2

 1

1 1 1

1 1

1 1 3 2 4

1 8 **3** 4
7 2 5 5
6 2 9 2

2 7 **2** 2 4
6 5 3 9 8 1

1 1 **1** 2

304 – AGN, QSO, Blazars V

2

5 8 **12** 6 9
13 18 7 18 17
15 14 16 10
4 18 1 2
3 5 11

2
1 1 1

1 1

1 2 3

1 1
5 1 1 3
2 4

4 5 10 3 4 11 6 8 2
1 4 7 4 4 4 9

4 5 1 2 6 3

305 – Multi-messenger Observations of Intermediate Mass Black Holes with LISA

1

4 3 2 1

2 4 3 1

306 – Galaxy Clusters I

3 4 6 3 6 6 5 3 1 4 6 2 4
4 6 3 1 1

2

s

s

1

1

1

4 7 5 2 8 3 8 7
6 9 9 6 1 8

1 2 2

307 – Astronomy Software Publishing: Community Roles and Services

1 2

1

1

1

1

1

1

1

1

2

308 – Supernovae II

3

4

3

1

2

6

2

5

1

1

2

2

2

2

3

1

o

a

o

a

w^{CC}

w^{disp}

		8	9	3
	7	2	2	9
	8	8	5	3
	2	10	10	10
1		10	10	10
	10	1	10	
	6	10	6	4
		6	6	

1

309 – Galaxy Formation and Evolution V

1 1 1

rot g

rot g

3

1

1

2

4

1

1

2

1

1

1

1

310 – Extrasolar Planets V

1

6
1

4

5

6
2

6
3

1

1
1

1
1

1

1

3

2

2 1 1

2 3 1

1 1

1 2 3

311 – Milky Way and Galactic Center II

1

3 3 3 3 3 3 3
3 3 3 2 3 3
1

1 1

1 1

1

2 5 3 1 6 3 4
5

312 – Dwarf and Irregular Galaxies I

1 2 3 1

1

4 4 1 2 1 4 3

3 1 2 4

h

h

*

4

h

1

313 – Star Formation III

bol submm
bol bol submm
12 13 13 + 2
up 12 2

2 1

1 1 1

1

3 1 1 2 4 1

1

4 1 3 2

4 8 ○

1
2

1
1

1

1

3

314 – Instrumentation: Ground Based and Airbourne II

1 1 1 1 1 1
2 1 2 2 2 1 1 1
3

2 4 3 **2** 1 2 4
4

2 2 **1** 2
1 1

1 **1** 1

4 4 2 3 3
9 3 3 7 1 3
5 3 7 6 3 8 3
3 3 3 3 3 3 3
3 3 3 3 3 3 3
2 3 3 3 3 3 3

2 1

th

2

315 – The Sun

1

1

1

1

1

1

1

1

2 1 **3** 3

1

1

1

316 – Gen. Ed. Astronomy Education: Research, Resources, and Practice

2

1

2

1

1

2

1

1

1

1

1

1

1

1

1

1

1

365 – Status of the Astronomy Workforce

1

1

1

1

3
1

2

3 1 2
 4 1

317 – Plenary Talk: Astro Data Science: The Next Generation, Chris Mentzel (Moore Foundation)

1

320 – New Results on Nearby AGN with Swift BAT

2 4 5 1 1
3 1 6 1 5
-1 -12 -1 -2 -12
-2

1

4 3 2 4
6 4 4 5 4
 1 6 5

X Edd

Edd

x

Edd

x x
x Edd
Edd

BH

BH

Edd

x

2

6

3
5

1

6

2
7

4

2

7

1

2

4

5

3

6

2

4

4

7

8

4

1

9

1

7

1

2

2

2

3

1

1

2

5 1 **1** 3 2 1 4

1 2 **2** 2

321 – The Very Large Array Today and Tomorrow: First Molecules to Life on Exoplanets

1

1

1

1

1

1

322 – New Views of the Universe from 1 to 115 GHz with the Green Bank Telescope

1

2

1

2 + 2 +

+

4 3 **2** 1 2

		6	10		
13	8	9	14	1	3
2				10	8
	8	8	13		
6		11	5	12	
	4			9	7

			11	1		11
	6		8	5		11
3	11		6		6	
8	3	9	6	3	6	7
	6		10		3	
1	2		4	6	9	3
	3	6		6	11	
		6				

1 1

323 – AGN, QSO, Blazars VI

eff

OX

1

1 **2** 2

2 3 1 **3** 2 3

1

2

3

3

1

1

1

1

1

1

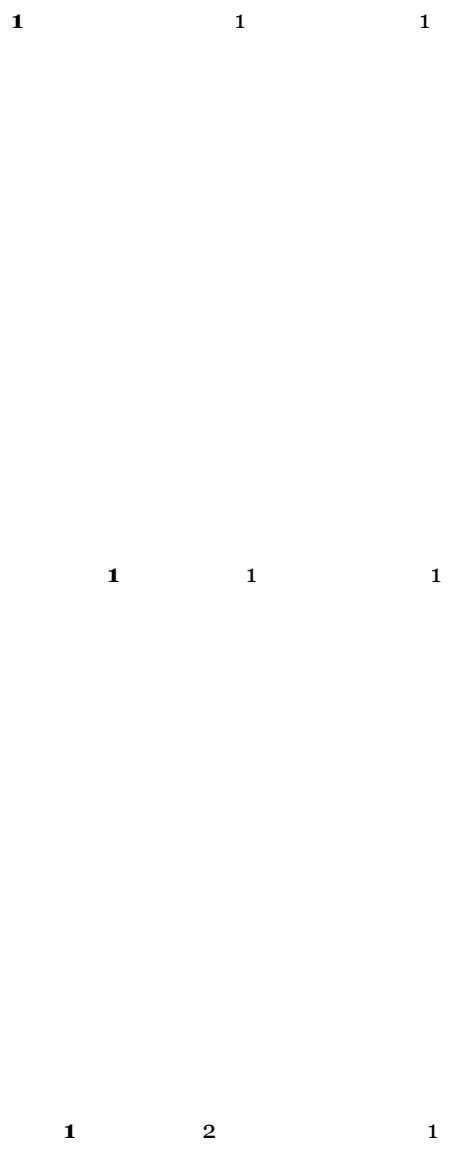
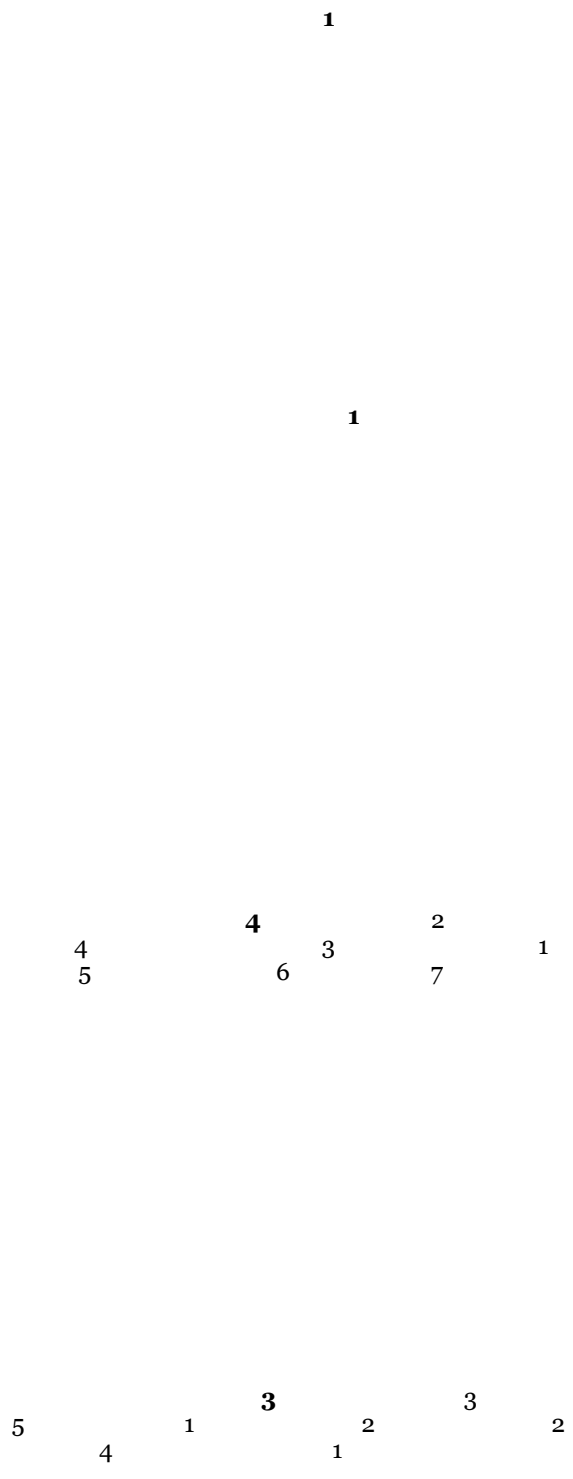
1

1

324 – Astronomy Visualization in Research, Outreach, and Entertainment

325 – Gravitational Waves and EM Counterparts III

1



1 2
1 3 3 1

1 2 2

1

3 1 1 3 2 3

1

1

327 – Cosmology IV

1

1

1

1

19 17 19 19 16 14 10
22 19 18 18 7 18
5 18 25
27 17 24 30
28 11 9 10 10
4 29 32 15
16 2 10 4 12 16
19 3 26 16
1 18 23 19
10 12 7 19 6
13 20 9 31
21 16 19

1 1
 1 1

1

3 4 1 1
 2

1

0

0

0 -1

-1

0

0

0

1

2

2

5

3

1

4

1

2

3

2

3

3

3
1

3

2

1

12.5-13 ☉

4 1 8 6 7 8 2 4 5 3

329 – Extrasolar Planets VI

1 6 8 10 1 1
7 1 4 3 6 2
4 5 8 1
3 3 1 12 3 1
3 11 8 11 3 9
7 13

1 1 1

1 1 1
1

5 2 4 4
3 3 1 6

3 3 4 1 4
5 2 2 3 4
2

1 1

330 – Circumstellar Disks III

1

1

2

3

2
1

2 ²
2

2

1

2

1

2
1

2

1 **1** **2** **2**
 3

1 **2** **2** **1**

1

331 – ISM III

2 4 **2** 1 3

10 9 8 7
3 5 1 6 4
2 10

2 1 1

13 + 13 13 + 13
2 + 2 +

5 3 2 1 4 6 2

-1 -1

1 3 3 2
3 3

GC

3 4 1
1 1 4 1 2
1 5

332 – Surveys and Large Programs II

1

1

2

1

1

7

5

4

3

2

6

2

1
2

2

2

2

1

2

2

1

2

2

1

1

1

3

4

3

2

2

3

2

1

5

1

2

5

6

5

3

4

1

2

3

334 – Stars and Friends III

2

2

3

1

1

3

1

2

1

2

2

2

1

1

1 1 **1** 2

1 2 2

2 ³ 2 **2** ¹ 2 ² ² ²

2 2 **3** ¹ ⁴

335 – The AAS Committee on the Status of Women: Then and Now and Where Do We Go from Here?

1 2

336 – Helen B. Warner Prize: The Evolution of Stars & Galaxies, Charlie Conroy (Harvard University)

1

337 – Henry Norris Russell Lectureship: Fifty-four Years of Adventures in Infrared Astronomy, Eric Becklin (University of California, Los Angeles)

1

338 – The Sun Poster Session

1

2

1

1

1

1

1

2

4

3

2

1

2

1

2

1

2

1

1

1

1

2

Jup

1

4 3 4 2 1 2 6 5
4 2 2 4 2

2

2

2

3 + 2 2
2 2 2
2 -9 -8 2
2 2

3 5 2 3 1 5 5
1 5 1 5 1 5 5
5 3 4 1 3 5 5
3 4 3 4 5 5

1

1

2

1

2

2

1

1

1

1

2

1

2

2

1

2

2

1

1

1

2

2

2

2

1

2

2

2

4

1

5

2

3

2

2

340 – Dwarf and Irregular Galaxies Poster Session

2

2

1

2

3

1

1

2

1

3 2 **3**
 1

2 1 3
 3 3

5 6 7 8
 ⊙ ⊙

3 4 1 3
2 2 5

0

1 2 **2** 1 1

5 5 4 5
6 5 2

1 3

1 2 4 3 1 3

2 1 2

2 5 1 3 4

1

4 5 2 6 3
5 5 1

1
3 2 4 3 1

2 1 1

1 2 2

2 3 4 1

eff

eff

eff

eff eff eff

1 2

orb

J

1 3 1

2 1 1 1

4 ⊙ d d -6 ⊙ IR
eq

2 2 1 2

**342 – The Very Large Array Today and Tomorrow: First Molecules to Life on Exoplanets
Poster Session**

1

1 1

1 1 1

1 1 1

1

2

1

1

1

1

1

1

1

1
1

1

1

3

-4

-4

-4

3

-4

2.6

1 1 1 1 1

1 1 1 1 1

1 1 1 1

4 4 3 3 4
5 4 4 1 4
4 2 5 2 4

1

1

2

2

2

2

1

5

3
4

1

2

3

2

1

1

1

1

1
4

5
4

4

3

6

4

2

V

3

3

3

2

1

2

1

1

1

1

4 4 7 6 **1** 2 3 5

5 6 4 **4** 1 4 4²
1 3 7 4 4

9 4 8 **10** 2 10 5
1 7 3 3

2 **2** 2 3 1

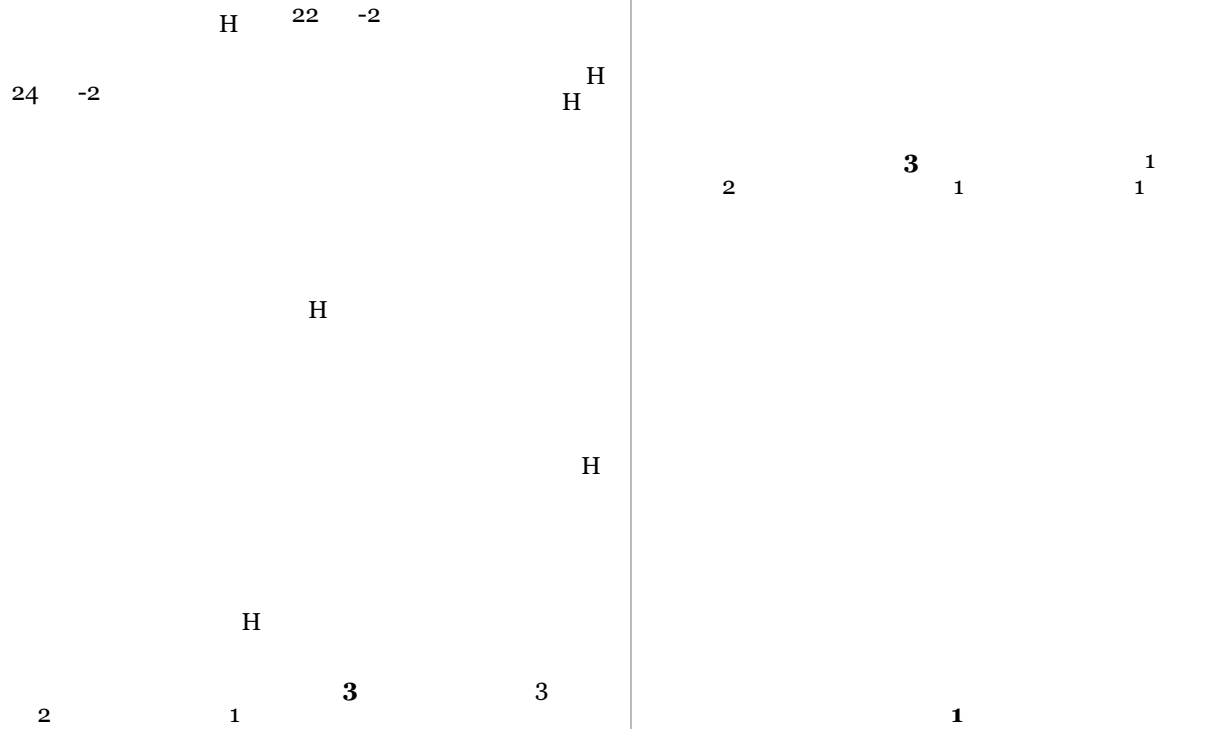
4 8 4 6
2 7 1 7 7
9 8 11 12 3 12
10 5

2 7 1 4 2 5
3 6 2

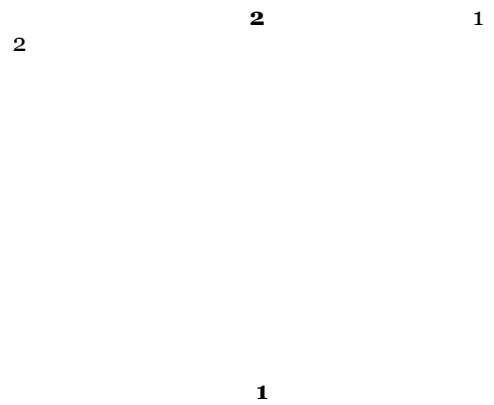
3 2 2 2 1
2

2 1 3

343 – New Results on Nearby AGN with Swift BAT Poster Session



344 – Star Clusters and Associations Poster Session



3

1

2

1

1

4

2

4

3

4

4

4

4

4

3

0

1

3

2

2

1

2

3

2

1

2

3

1

2

2

1

2

2

2

1

2

3 8
7

2 1
5 4

7 8 2
6 7

2

3
3
5

2

3
4

1 3
6

1

1

2

1

1

6

2

5

3

4

4

5

3

2

3

1

2

1

2

1

1

1

1

1

1

347 – Black Holes Poster Session

2

1

4
6

1

3

1
2
5

1
7

2

1

1

1

1

1

1

1

2

3

2

6

5

4

7

2

1

1

1

8

6

2

4

4

5

4

3

7

1

1

1

1

1

1

3 4 1 2 1 2

X age

1 1 1

1 1 1

1 2

1 1 1

X Edd 8^{-7}
BH 8 sun

1

2

2

1

2

3

1

1

1

2²
2

2²
2

1
3

4

1

2

2

⊙

-5/3

12 16 14
peak
1 1 1

3 1 **2** 3 3

3 3 **2** 1

1 6 5 7 8 **3** 7 4 2 6

348 – Stellar Evolution, Stellar Populations Poster Session

1 2 3

2 **1** 3 2
2

1

1

1

1

1

2

1
2

3 **2**

4 **2**

2

1

1

1

1

1

1

1

2

3

3

1

1

2

60

3

1

4

2

init crit

init crit

1

1

0

0

0

2

1

1

2

1

1

2

2

2

2

2

1

2

2

2

1

1

349 – Stars, Cool Dwarfs, Brown Dwarfs Poster Session

3

2

1

2

1

1

2

2

2

2

1

1

1 1 1 1 **2** 1 1

1 3 2 4 4 4 6
1 5



Jup

Jup

3 7 2 6 5 5 4
5 2 8 7 1 7

2 1 2 3 2

1 6 1 6 4 6 6
1 3 2 5

36

34

4 1 2 4 4 3
1 1

3 2 2
1

2

2 2 1 2

2 1 3 2 1

1

2

1

1

1

T

1

1

4
3

2

4

5

1

6

7

4

1

2

5

3

2

2 1 2 2

1 1 2

5 3 1 4 2

8 1 1

3 1 2 4

5 2 1 4 3 6
6

2

2

1

-1

Jup

1

1

1

1

1

3

1

3

2

1

1

2

2

1

4

5

3

3

6

35

35 37

1 1

2 1 1 1

2 6 3 6 5 3
7 8 7 5 1

2 5 4 3 5 1

Jup

2 1

2

1
2

3

1

1

1

2

3
4

1

1

2

1

1

2

3

350 – Dust Poster Session

1

2

2

1

2

2

1

1

1

1

3

2

3 4 **1**
3 2 2

4 2 3

1 1

org
2 4 1 3 **6** 3 5

351 – Large Scale Structure, Cosmic Distance Scale Poster Session

1 **1** 1

1 1

3 **1** 2

1

1

2

2

1

2

1

3 4

4 1

2

1

1

1

6 ☉

1

1

2

3

4
3

1

2

2

2
1

2
2

3

2

4

**353 – Observatory Site Protection, Light Pollution, Radio Interference, and Space Debris
Poster Session**

354 – Surveys and Large Programs Poster Session

5 2 1 2 **2** 1 3 4 1

1

i

r

1

2

1

1 1 4 3 3 1 1 2 3 1 3 1 3

1

2

1	5	7	9	2	10	8
7	6	3	4	11	7	7

2

2 1 1

3	2	1	3	2
		2	3	

2 1

1	1	2	1
---	---	---	---

4 3 3 3 3 2
3 3 5 3 4 3
3 4 4 3 3

2 2 2 1 2 2 2

1 1 1 1 1

AB
AB
2 1 1 2
3 3 1 2 1 4 1 1 2

3 4 2 4 4 2 4 4 1 5

1

3 3 2 3 2 4
4 4 4 4 3 3
3 1 3 3 2 3 4

1

1

1

2

3
1

3

1

1

2

1

1

1

1

1

1

1

2

2

1

1 1 1 1 1 1 1
1 1 1 1 1 1 1

1 1 2 2 1 2
1 1 1 1 2 2

1

1

2 1 1 4 5
2 2 2 2 2 3
2 2 2 2 2 3

9
12 8
1
1 1 1 1 1 1 1
2 3 2
1 1 1
1

1 1 1
1 1 1
1 1 1

1 1 1

2 2 2
1 2 2
3

1

1
2

3

4

2

1

1

1

2

1
2

3

2

3

3

2
3

3

1

7 11
10 8
11 1 3 8
5
11 4 10 2 8
9 6 3

2 3 4 4 1 4
1 3 4 4 4

8 2 1 5 7 6 4
9 9 4 3

7
2
2
+ + 3 +

1 2 1 1

4 1 3 1 2 1

 1 1 1 1 1
1 1 1 1 1

1 1 2 1

 3 4 1 2

1 1 1 1 1

1 1 1 1

1

1

1

4 5

3 1

3

2

5

1

1

1

1

2

2

1

th

1

3

1

2

2

1

1

1

1

1

1

1

1

3 6
 6
 5
 8

2 6
 1
 6
 7
 4

8 7 6 6
 6 6 6 6
 9 6 6 3

1

1

1

1

1

5 2 1 2
 4 3 3 3
 2 2 3
 4 4 4
 6 2 4

3 3 1 2 5 4
 3 3 2 5

1

2

2 2 2 2 2 2
 1 2 1 2 1 2

1

1

1		1		1		1		1		1
1			1		1		1		1	
	1			1			1			1

®

2

1

			1			1
1	1	1		1	1	1
		1			1	

2

1

1

			1			1
1	1	1		1	1	1
		1			1	

1

2

1 1 1 1 1 1 1

1

1 1 1 1 2 1 1 2

1

3

2

1

1

1

2

3

1

2

1

1

6 5 5 5 5 5 6 5 4 5 5 5 5 2 3 5 4 1

2

3

3

1

1

1

2

2

1

2

356 – CMB, Dark Matter & Dark Energy Poster Session

1

1

1

1

1

baryon

o

dm

o

2

5

1

1

1

3

2

1

3

357 – IGM, QSO Absorption Lines Poster Session

3

1

2

2

1

1

17.5

20.3

-2

1

2

1

1

1

1

1

1

2

4

3

1

3

6

1

6

2

9

6

10

6

10

1

5

4

10

8

10

1

6

1

3

7

358 – Cataclysmic Variables Poster Session

6
4

2
5

5

3
5

5

1

2

3
1

4

5

1

1

2

1

1

1

1

1

2

1

2

2

1

1

4

1

2

3

1

3

5

4

3

2

1

⊙

⊙

2

3

2

3

1

V

V

7

7

7

7

7

7

1

2

3

2

4

7

7

12

7

7

7

7

6

4

5

1

3

2

1

Evaluation, and Curriculum Poster Session

1

2

3

3

1

6 6 7 5 7 4 5 2 3
3 3 7 4 5 3 9 8

10

1

4

4

7

5

5

5

5

5

5

5

5

5

5

5

5

5

5

5

5

5

5

5

5

5

5

5

5

5

5

5

5

5

5

1

1

1 2 1 1

1 1

1 1

1 1

1 1

1 2 3 4 5 2
2 2

th

st

1 3 5 5 4
5 5 2

1

4 2 3 1

5 4 **2** 1 3 4

1 1 1 1 1 1 1 1 1
1 1 1 1 1 1 1 1 1

3 **2** 2 1

1

3 5 **2** 4 1

362 – Surveys, Data, Computation and Lab Astro iPoster Session

1

1

1

1

1

2

1

3

1

1

3

2

2

2

2

2

2

1

2

3

2 2 2 2
1 1 2 2 1 3

1 2 1

2 1

3 2 3 1 3 2

2 1 1

1

1

2

2

2

1

4

3

2

1

2

1

1

st

1 1 2 1

1 1 1 1 1
1 1 1 1
1 1 1

3 1 2

1 2 4 3 1 2

400 – Plenary Talk: Illuminating Gravitational Waves, Mansi Kasliwal (California Institute of Technology)

1

401 – Astrobiology

2

1

2

1

1

1

3

1

1

1

402 – Instrumentation: Space Missions I

1

2

10 14 14 1 6
 11 15 17 8
 7 5 6 3
 2 6 2 4 12
9 2 13 6 7
4 15 6 16 4

1 **2** 1 2 2

1 1 1 **1** 2 1 1

-4

1 2 **1** 1 1 1

3 2 4 1

-13 -2

		1		1	
1		1		1	1
1		1		1	

		2		2	
1		1		2	2

403 – Detection of Extrasolar Planets IV

		2		2	
3		1		1	1

			th
th	th		

1		1		1
----------	--	----------	--	----------

1

1

2

1
3
3

3
1
1

1
1

4

2

4
3

2

2

2

1

1

4

3

3

3

4

2

404 – AGN, QSO, Blazars VII

45 46

1

2

2

2

1

2

2

2

1

7
2

5 3

6
8 4

1
3

H

s

4
1

3

3

5

2

405 – Black Holes I

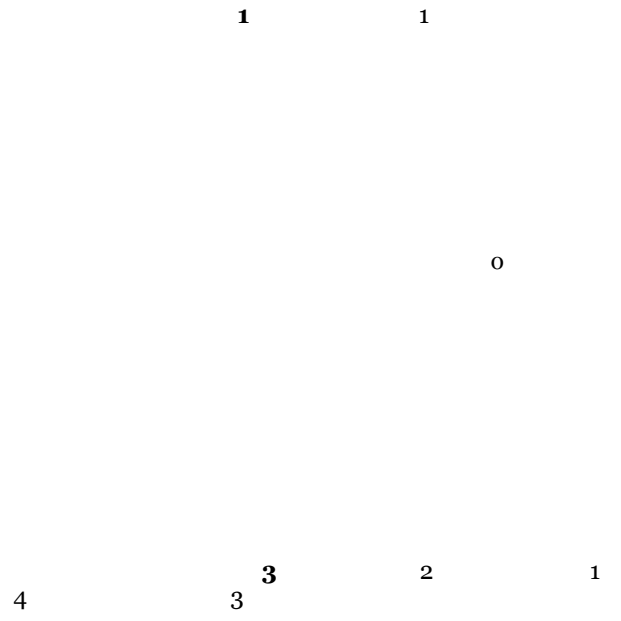
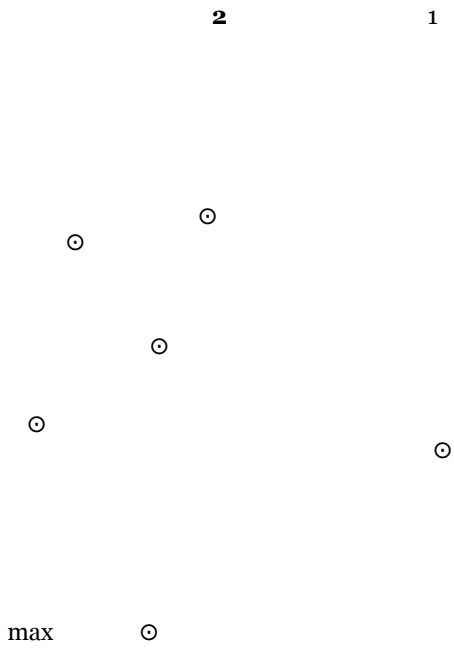
1 **3** 1 3 2
 1 1

2 1 **2** 2

1 2 **2** 2 2

3 2 **1** 1 1

3 4 **1** 2 2



406 – Galaxy Clusters II

1

1 1 1 3
1 6 5 2 6
1 4 3

3

2

1

1

1

3

3

1

2

3

3

3

1

1

1

1

2

2

2

5

3

4

5

1

407 – AAS Public Policy Panel: The Ongoing Evolution of the WFIRST Mission and Implications for Future Flagship Missions

1

408 – Supernovae III

2

1

2

2

1

5

3

4

1

4

2

2

2

3

2

2 1 1 1
 1 1 1

4 3 1 2

 2 2 2
 2 2 3
 1 4 3

1

1 2 1 1
 1

409 – Galaxy Formation and Evolution VII

1

1

1

1

2

1,2
1,2

1,2

1,2

1,2
1,2

3

2

2

2

2
1

2

2

1 1 1

1 1

410 – Extrasolar Planets VII

8 5 7 5 4
3 2 9 5 6 1 7

1 1 1

1 3 2

2

2

2

3

2

1

1

g

g

1

1

4

2

2

1

3

411 – Milky Way and Galactic Center III

1 4 **3** 4 7
 1 5 2
 7 6

1 **2** 2 3
 4

4 9 8 **3** 6 3 6 6
 5 7 2
 7 1

1 1 2 1 **4** 3 1 1

412 – Dwarf and Irregular Galaxies II

6 sun

BH

7 * 9 sun

7 sun

*

2

5

5
1

4
3

1

Sun

5

6 Sun

2

1

1

8 ☉

10-10.5

4

2

3

3

3

1

3

☉

1

2

1

2

1

413 - Star Clusters

4 ☉

☉

☉

-2

1

2
1

2

2

1

1

4

3

2

6

1

5

2

1

1

3

2

1

3

1
4
4

5

1
4
3

4

2

2

4

4
1
4

414 – Various Stellar Topics

4

2
4

7
1

6

8³

5
7

2

3
1

4

2

1

3 **3** 1
 2 4 5

1 3 **1** 2

1 3 2 4 1 4

3 1 4 **3** 3 2

415 – Gravitational Lenses

c t

1

1

2

3

3

1

1

2

1

3

3 3 4 4
2 2 1 6
5 7

1

2 3 1

417 – Plenary Talk: The Fate of Exploding White Dwarfs, Rob Fisher (University of Massachusetts, Dartmouth)

1

434 – Binary Stars (Late) Poster Session

5 4 1 4 2 3

-2 H 12 22

1 1

2

1

1 3

2

4

3

1 2

3

4

2

3

2

1

4

3 3

5

1

1

1

435 – Black Holes (Late) Poster Session

1

2

1

1

1

1

3

1

1

2

2

1

1

1

1

1

436 – Catalogs, Surveys, Computation, Etc. (Late) Poster Session

5

4

5

5

2

5

5

6

3

4

4

1

1

1

1

1

1

1

1

1

0

0

2

3 1 1 4 1 1 1
5 2 5

1 2

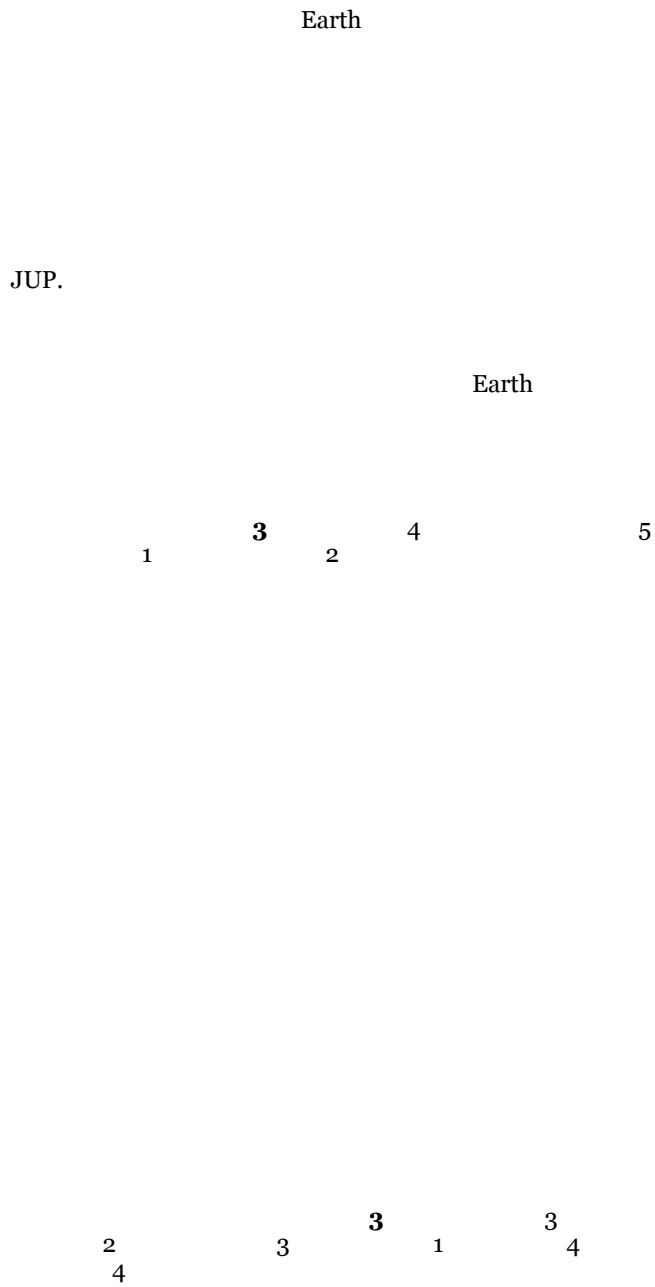
1 1

1 1 1 1 1 1 1
1 1 1 1 1

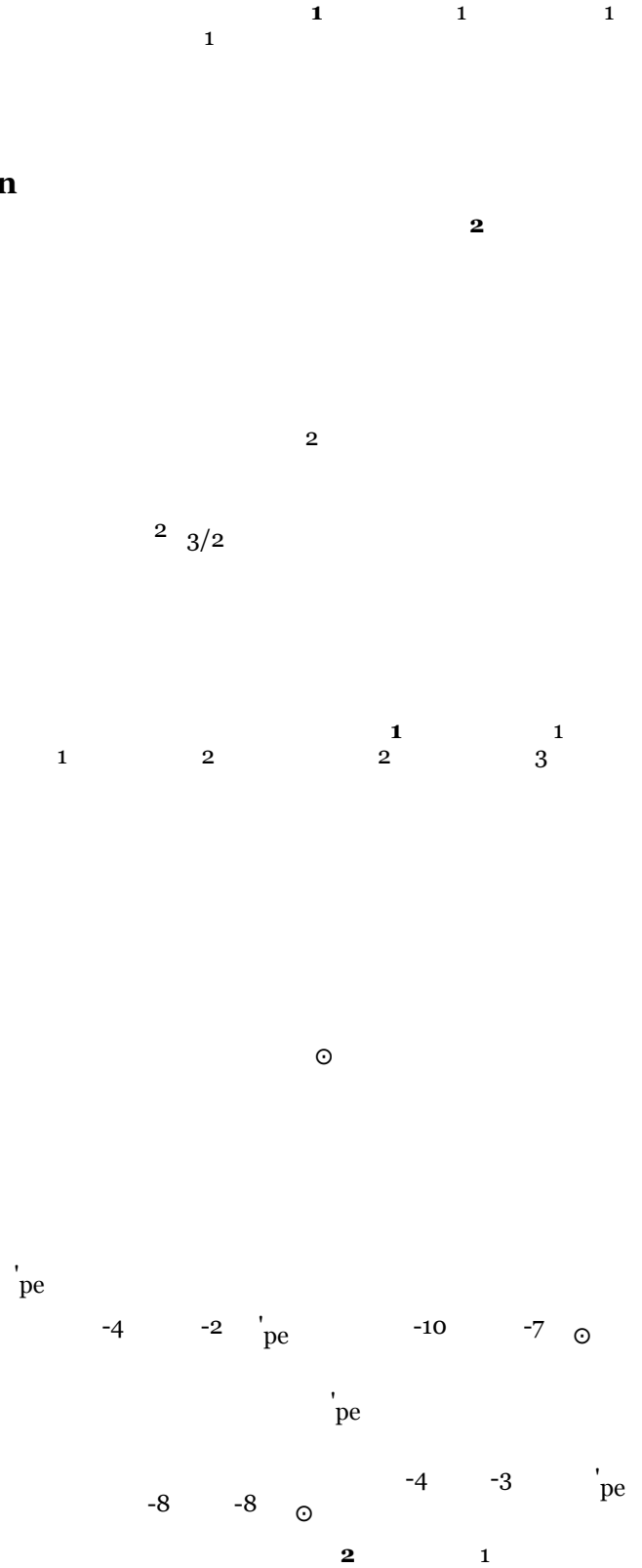
1 2 2

1

437 – Circumstellar Disks (Late) Poster Session



438 – Cosmology Etc. (Late) Poster Session



1

2

1

1

2

1

1

4

1

1

1

1

1

1

1

2

2

1

1

2/3

1

1

1

1

1

1

1

1

1

1

2

1

1

1

90

2

8 5 5 8 5 4 5
8 8 8 9 3 1 11 3
7 9 2 6 2 7
10 10 11 6 2 7

439 – Extrasolar Planets (Late) Poster Session

2 1

4 4 **1** 3 **1** 2

1

1 1 1 1

1

1 1 1 1 1

2 3 2 1 2 3
1 3 1 3

1 1 1 1

1 1 1 2 2 1

6 12 5 2 5 7 3
10 1 10 1 1 11
8 3 9 13 4
5

1 1 1

1

1 1 1

1 1

1

1

3
2

3
2

3

2

1

1

1

3

3
2

1

1

1

E

E

E

2

2

1

3 **2** 1 4 3

1 **1** 2 1 1

2 4

4 2

4 2 4 4

2 4 2 4
4 4 4

1 3 **3** 2

1 2

440 – Galaxies, AGN & Friends (Late) Poster Session

1

1

1

⊙ -1

2⁵

5⁵
1⁵

3⁵

4

1

1

1

1

1

1

2

2

1

3

1

2

1 1 1 1

1 2 1 1 2
1 1 1 1 1
1 1 1 1 1

1 1

2 1 1 4 3 4

2 1

1 1 1

rest

3

4

2

1

2

2

2

1

1

1

1

1

2

5

2

3

4

1

2 2 **2** 2 1

9 ☉

1 2 **3** 3

2 **2** 1

48

1 1 1

441 – Galaxy Clusters & Large Scale Structure (Late) Poster Session

2 1 1 1 1 1

1 1 1 1

1

1

1

1

1

2

1
3

5

2

4

-1

-1

-1

-1

2

1

442 – Instrumentation on the Ground and in the Air (Late) Poster Session

4

3

1

2

4

4

4

4

4

4

4

4

1 1 1 1 1 1

1 1

1

1 5 5 1 3 1 5
2 4 2 4 1 5

3 2 3 2 2 1 2

1 4 4 2
 4 3

1

1

443 – Laboratory Astrophysics (Late) Poster Session

2 1 2 2

444 – Light Pollution & Education (Late) Poster Session

1 2 3 3

1

1

1

1

1

1

1

1

1

1

2

2

1

1

1

1

1

1

1

1

1

4

3

2

1

1

1

1

1

1

1

1

1 2 1 1 5 4 3

3 2 1 1

445 – Molecular Clouds, ISM and Dust (Late) Poster Session

2 1 4 2 4 3

2 3 4 1 4

1

1

2

1

1

1

2

3

2

4

1

4

1

2

1

1

1 1

1

1 1

2 3 1

1 5 5 1 5 3
1 1 1 1 1 4
5 3 2 1 1

1 1 2

1 1 1 2 1 2 4
3 1 1 5 6 7

3 1 2 1

1

1

2 2
2 11
12 3 3
13 13 3
1 13 8 12
9 10 6 13
4 5 7

7 5 9
8 1 8
6 5 3 3 4 2 7
3 4 8

1

56 56

1 **1**

Ch

9 3

1

4

2

2

3

1

1

1

-1

2

1

3

2

1

2

2

1

-1

-1

1 1 1 1 1

447 – Space Missions Instrumentation (Late) Poster Session

-20

1

6

3

1

1

1

1

1 1 1 2 1
1 1 3 1 1

1

1

448 – Star Associations & Clusters (Late) Poster Session

1

2

1

2

1

2

1

1

1

1

1

449 – Star Formation and YSOs (Late) Poster Session

1

3
2

1

1

3

3

2

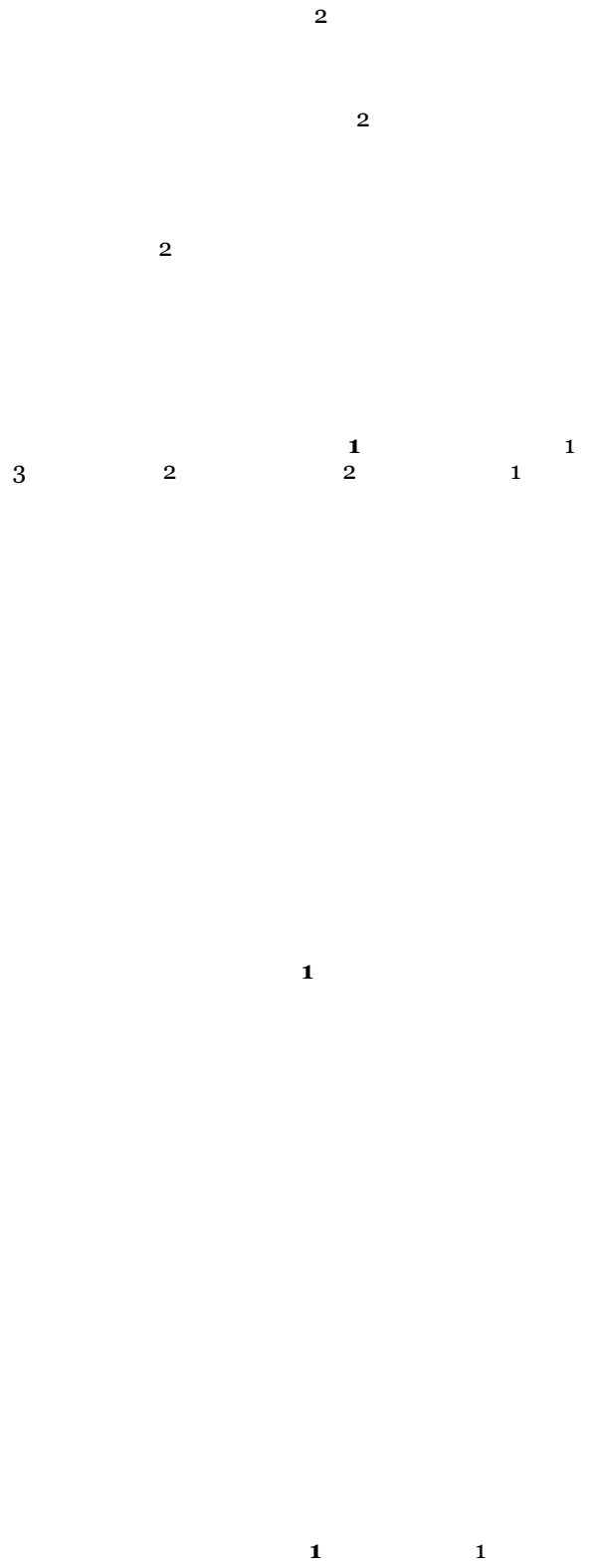
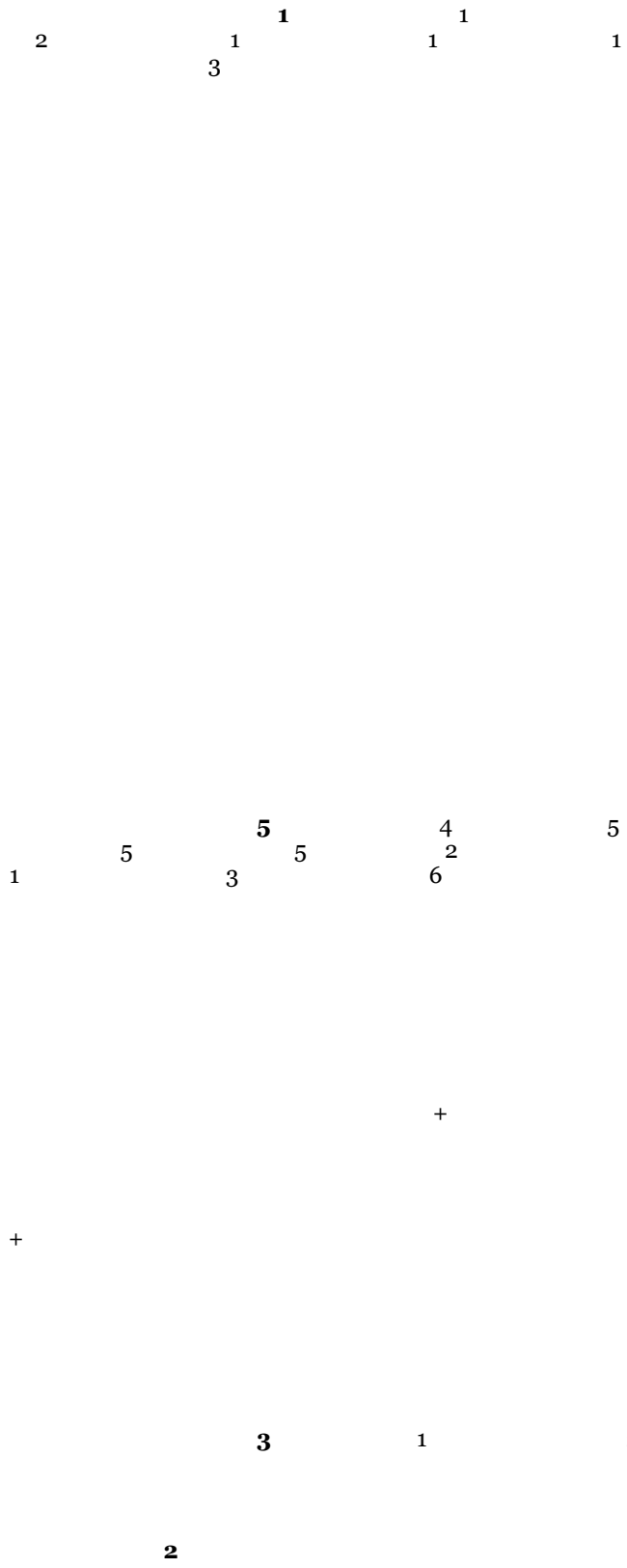
1

2

2

1

4 8 ⊙



450 – Stars and Stellar Evolution (Late) Poster Session

1

1

5

6

4
1

5

6

3

2

1

2

1

1

1

1

eff

1

1

1

4

3

3
1

2

3

1

1 1 1 1 1

2 2 2 1

2 1 6 5 2
3 4 2 2

⊙

2 1

eff

1 1

5 1 6 7 9
 9 10 2 7
 3 13 8 4 7
 7

451 – The Milky Way (Late) Poster Session

-1

10 ☉ ☉
 1 2

2 1 1

1

-1

452 – The Sun, the Solar System and Astrobiology (Late) Poster Session

1

2

1
3

2
2

3²
3

3

2

4

3

3 8

3 6

3

2 2

6
2

4

5

3

2

1

1

1
1

1

1

2

3

3

3

3

1

2

1

1

1

1

1
2

4

1

1

3
1

1 1 1 1 1

453 – White Dwarfs, Neutron Stars (Late) Poster Session

1 1

1 1

1 1 2

3 3 2 3
1

3 4 1 2 4 4
5 6 6 6 6

2 0 -1
33 -1

3 1 3 3
3 2 3 3

1

2

1 2 2 1

5 6 3 4
2 4 1 6 7

2 1 2 2
 1 4 3

1 2 3 2
 1

7 6 5 4 1 5 6 6
 2 3

3 6 2 5 4
 6 4 1 6

1 2

454 – Galaxy Evolution (Late) Poster Session

1

1

7 ⊙

1

3

2

200

200

3
2

1 4

2

1

2 2

1

2 **3**

1 1 1

1 1 1

1

2

2

2

1

8 8 8 8 8 8 15
13 15 13 15 13 13 13 15
2 13 2 2 14 2 8
8 3 6 3 3 1 8
1 12 12 3 12 9 11
9 9 12 10 13 9 13
7 4 8 4 13 5 13

1

1

1

1

7 5 5 5 5
8 7 11 9 10
5 5 2 10 3
3 4 8 11 7 2
11 12 8 6 1 2

3
4

3
6

2

5
1

2

3

1 2 1 3 3 1 3 4

1

1

3 2 1 1 3

5
3
3
3
2

4

7
3
3
3
3

8
10
3

6
3
3
3

2
3
3

9

7
3

3
1

1
1

1
1

1

1

1

1

3

3

1

3

1

2

420 – Large Scale Structure

2

1

1

1

2

3

1

1

1

1

4258 LMC

r

sys

4 2 6 4 4
 2 5 3 5 7
 2 1

421 – Binary Stars

1 1

1 3 3
 3 2

1 1

b

1 2 2

2 2 2 1
 2 2

32

1

2

3

2

1

2

422 – AGN, QSO, Blazars VIII

3

4

1

2

1

-γ

0

2

1

1

1

423 – Black Holes II

1

1

3

1

2

1

BH

BH

BH

BH

BH

BH

2

1

1

3

8 ⊙

1

1

2

2

1

1

1

1

1

1

1

1

1

2
2

2

1

1

1

1

6

1

2

7

5

4

3

3
7

1

5

1

6

4

4

2

4

1

425 – Spiral Galaxies

1

9.5 -9.5 -1

1

1

1

1

1

1

1

1

1

3

2

1

426 – Galaxy Formation and Evolution VIII

1

1

1

1

1

3 5 4 5 3 6
 1 6 6 2

9 ○

3 1 5 5
 2 4 6

1

1

1

1

3 1 **2** 1

9 17 **6** 15 2
1 5
11 3 13
12 11 4 8 16
10 3 18 14 7
11 11 11

3 **1** 2 1

2 7 **8** 7 5
4 2 1 3 6

1 **3** 2 2

1 **2** 2

2.26
 2 2 2 1
 4 2 4
 2 2 2 4
 4 4
 4

4 2
 2 2 2 11
 4 4 2 -
 4 4 -4 2
 2 1 1
 5

1 3 9 8 6
 2 5 7 7 7

1 2 3

428 – Circumstellar Disks IV

1

1

2

2

1

1

1

1

1

429 – ISM IV

1

6 6

5
7

7 6 5

5

1

7 2
6

4 1

7 1
3

5 1
5

H α

-6

1

1

2

1

1
2

1

1

2

1

2

430 – Cosmology V

1

1

1

1

1

1

1

1

431 – Detection of Extrasolar Planets V

1

1

1

1

1

1

1

1

432 – Plenary Talk: Science Policy Plenary Talk--The Politics of Science Funding: Is the Fault in Our Stars, David Goldston (MIT)

1

433 – Lancelot M. Berkeley Prize: The Instruments that Launched Gravitational-wave Astronomy, Peter Fritschel (MIT Kavli Institute) for LIGO

1

Authors Index

- Aarnio, Alicia: **315.02**, 362.18, **365.01**, 365.04
Abdeen, Mohammad Shameer: 409.03
Abe, Taisei: 446.08
Abel, Nicholas: 250.10
Abraham, Peter: 147.17
Abraham, Roberto: 210.01
Abrams, Daniel: 144.10
Accomazzi, Alberto: **307.09**, **362.17**
Acebron, Ana: 454.10, 454.12
Acharya, Kinsuk: 247.01
Achterberg, Richard: 452.03
Acquaviva, Viviana: 239.02, 359.03
Acton, D. Scott: 150.35
Ádámkovics, Máté: 449.09
Adams, Angela: 242.14
Adams, Arthur: 450.05
Adams, Carson: **149.58**
Adams, Elizabeth: 340.06, **354.04**
Adams, Fred: 427.03
Adams, Mitzi: 242.14, 452.01
Adams, Steven Cade.: **449.09**
Ade, Peter: 112.02D, 152.19, 215.02D, 314.05D, 322.05, 419.05
Adebahr, Björn: 354.04
Adewole, Ayomikun: 151.02
Adil, Arsalan: **438.06**
Adkins, Ally: **147.01**
Adler-Levine, Ryan: **250.06**
Agol, Eric: 410.02D
Agostino, James: **354.18**
Agüeros, Marcel: 344.07, **349.21**, 359.03
Aguilar, Jonathan: 414.07
Aguilar, Laura: 445.03
Aguirre, James: 150.26, 150.30, 150.31, 150.32, 150.33, 150.34, 215.02D, 322.05, **328.04**
Ajello, Marco: 123.04, 242.18
Akerib, Daniel: 361.02
Akeson, Rachel: 246.08, 329.01, **354.29**, 354.36, 355.25, 414.05D
Akitaya, Hiroshi: 446.03, 446.08
Akiyama, Eiji: 449.08
Akiyama, Kazunori: 347.11, 347.16
Alachkar, Bassem: 215.03
Alam, Md Faisal.: 333.05
Alarcon, Alex: **440.01**
Alatalo, Katherine: **105.05**, 149.19, 149.58, 342.28
Alavi, Anahita: 328.03D, **426.05**
Alberding, Brian G.: 349.05
Albers, Sandra: 214.05D
Albert, Loic: 128.06
Alberts, Sean: **344.21**
Alberts, Stacey: 105.03
Albin, Edward: **444.07**
Alcolea, Javier: 241.07
Aldering, Gregory: 152.09, 153.21, 245.14, 327.02
Aldoroty, Lauren: 355.34
Alexander, Kate Denham.: **107.04D**
Alexandroff, Rachael: **250.35**, 304.01
Alexov, Anastasia: **436.12**
Ali-Dib, Mohamad: 115.08
Allan, Gregory: 402.04
Allard, France: 120.03
Allen, Alice: **150.10**, 150.28, **307.10**
Allen, Christopher E.: 238.01, 238.02, 238.03, 238.04, 238.05, 238.06, 238.07, 238.09, 238.10, 238.11
Allen, Gabrielle: 255.14
Allen, John: **148.21**
Allen, Lori E.: **142.08**, **246.08**
Allen, Magdalena: **157.07**
ALLENDE PRIETO, CARLOS: 211.02, 257.12
Aller, Kimberly: 137.01, 349.26
Allevato, Viola: 304.01
ALMEIDA, ANDRES: 211.02
Almeida, Triana: **422.03D**
Alonso Garcia, Javier: 413.03
Alpaslan, Mehmet: 306.04
Alsheshakly, Ghadeer: 149.31
Alvarado-Gomez, Julian D.: 148.16
Alvarez, Gabriella: 441.01
Alvarez-Candal, Alvaro: 148.26
Amanullah, Rahman: 153.21, 327.02
Amara, Adam: 261.03D
Amaro, Rachael Christina.: **246.09**
Amatucci, Edward: 354.33
amini, rashied: 140.11
Amiri, Mandana: 112.02D
Amram, Philippe: 149.50
Amy, Paul: 237.03
An, Hongjun: **453.07**
An, Xin: 246.18
Ananna, Tonima Tasnim.: 304.01
Anbar, Ariel: **113.07**, 256.04
Anchordoqui, Luis: 359.03
Andersen, Bridget: **147.10**
Andersen, Morten: 331.02D, 349.32, **354.30**
Anderson, Craig S.: 238.01, 238.02, 238.03, 238.04, 238.05, 238.06, 238.07, 238.09, 238.10, 238.11
Anderson, Jay: 150.36, 214.05D
Anderson, Loren: 247.07, 247.16, 247.25, **408.08**, 445.04
Anderson, Loren Dean.: 230.06, 247.11, 247.18, 247.31, 331.02D
Anderson, Richard I.: **327.07**, 420.07
Anderson, Teddy: 144.09
Anderson, Tyler: 152.18, 355.44, 355.46
Andersson, B-G: 247.13, 247.24, **414.04**
Andersson, Nils: 224.01
Andrade-Santos, Felipe: 406.06, 454.10, 454.12
Andreoni, Igor: 151.08
Andretta, Vincenzo: 234.02
Andrews, Sean: 129.01, 129.06, 147.13, 147.15, 147.17, 147.18, 339.06, 339.08, 437.01
Angelo, Isabel: **111.03**
Anguiano, Borja: **436.06**
Angus, Charlotte: 245.10
Angus, Ruth: 349.23
Aning, Isaac: 256.03
Annibali, Francesca: 241.02
Ansdell, Megan: 133.06
Anthony-Twarog, Barbara J.: 213.05D, 344.06
Antilogus, Pierre: 153.21
Antoni, Andrea: **244.01**
Antonioni, Vallia: 223.04, 333.01, **421.08**
Antonioni, Valsamo: 227.06
Antwi-Danso, Jacqueline: 411.01
Apai, Dániel: 359.06
Apala, Elizabeth: 258.11, 357.04
Aparicio, Antonio: 414.07
Apollo, Peter: 355.29
Apple, Stephen: **402.06**, 419.06
Applebaum, Elaad: 237.13
Appleton, Phil: 149.19, 361.21
Aragon-Calvo, Miguel: 258.13
Arav, Nahum: **250.50**, 250.51, 250.52
Arcavi, Iair: 304.07, **325.06**, 325.07, 325.08
Archibald, Anne: **233.02**, 233.05D, 243.13, 243.18, 453.15
Ardila, David: 228.04
Arenberg, Jonathan: **355.22**
Arendt, Richard: 408.04
Aretxaga, Itziar: 149.59
Argiroffi, Costanza: 133.01
Argo, Megan: 245.09, 340.11
Arion, Douglas: **144.02**, **216.04**
Armentrout, William Paul.: 247.16, 247.18, 247.25, **331.02D**, **445.04**
Armstrong, J. Thomas.: **442.06**
Armstrong, J. Thomas: 152.27, 157.01
Armstrong, James: 104.04
Armus, Lee: 127.06, 251.07, 354.29, 354.36, **355.05**, 355.11, 355.50
Arney, Giada: 148.34, 207.06, 246.21, **427.08**, 439.23
Arnold, Lauren: 104.07
Arras, Phil: 128.07, 421.06
Arredondo, Nicole: **149.43**
arriaga, Pauline: 229.03, 329.04D
Artigau, Étienne: 349.37
Artkop, Kyle: **438.14**
Arulanantham, Nicole: **147.11**, 349.06
Arzoumanian, Zaven: 140.06, 157.11, 157.13, 243.17, 333.03, **333.07**, 341.01, 347.01, 453.05, 453.11
Ascensio-Torres, Ruben: 303.07
Asercion, Joseph: **150.09**
asgari-Targhi, M. Asgari-Targhi.: 212.08
Ashby, Matthew: 125.07, 149.46, 149.55
Ashcraft, Jaren: **152.13**
Ashcraft, Teresa: 354.14
Assani, Korash: 449.07
Assef, Roberto: 304.06
Astier, Pierre: 153.21
Atkinson, David: 144.01
Atteia, Jean-Luc: 107.08
Aubain, Jonisha: **153.23**
Aubin, Sam: 250.16
Auchetl, Katie: 241.09
Audi, Clayton Moses: **436.15**
Auger, Matthew: 210.03, 415.04D
Augustine, Carlyn: **446.05**
Aussel, Herve: 149.44
Avachat, Sayali: **440.07**
Avelino, Arturo: **209.03**
Avila, Roberto J.: 411.04, 454.10, 454.12
Avilez, Ian: 147.07, 339.12, 360.01
Awan, Humna: 239.03
Axelrod, Tim: 354.17
Ayers, Megan: **347.18**
Baar, Stefan: 446.08
Babb, James: 111.08
Babb, James F.: **445.06**
Babler, Brian: 237.15
Bachellet, Etienne: **228.05**
Bachetti, Matteo: 213.03, 453.09
Backman, Dana Edward.: **131.05**
Badenes, C.: 408.05
Badenes, Carles: 241.11, 244.16, 326.05D, 421.08
Bae, Jaehan: **129.05**
Baer, Rudolf Erik.: **405.08**
Bagley, Micaela: **226.05D**
Bai, Xue-Ning: 129.01
Bailey, Jeb: 152.22, 344.17
Bailey, Vanessa P.: 361.18
Bailin, Jeremy: **344.04**
Baines, Ellyn: 152.27, **157.01**, 442.06
Baker, Andrew J.: **231.07**
Baker, Ian M.: 152.16
Baker, John: **255.15**, 350.04, 405.04
Baker, William: **157.15**
Bakerman, Maya: 155.03, 360.06
Bakerman, Maya Nona.: **444.15**
Bakich, Michael: 220.02
Bakos, Gaspar A.: 148.02, 201.07
Balasubramanian, Kunjithapatham: 246.18, 246.33, 246.44
Balbinot, Eduardo: 212.05, 413.07
Baldassare, Vivienne: **105.06**
Baldwin, Jack: 241.01
Balick, Bruce: 241.07
Ball, Catherine: **149.03**
Ballantyne, David: 140.06, **140.08**, 222.02D
Ballard, Sarah: 148.01, 329.05
Ballhausen, Ralf: 243.11, 333.01
Bally, John: 147.17, 214.01, 247.24
Balokovic, Mislav: 140.08, 320.04
Balsler, Dana: 230.06, 237.04, **247.05**, 247.07, 247.18, 247.25, 247.31, 331.02D, 445.04

Bambic, Christopher J.: **252.16**
 Bamford, Steven: 110.07
 Bandurski, Jeff Brian.: **247.26**
 Bandurski, Jeffrey: 230.01, 247.08
 Banerji, Manda: 222.05D
 Banfield, Donald: 144.01
 Bania, Thomas: 230.06, 247.05, 247.07, 247.18, 247.25, 247.31, 331.02D, 344.11, 445.04
 Bannister, Michele T.: 115.03
 Banzatti, Andrea: **229.01**
 Baraffe, Isabelle: 326.04
 Baran, Andrzej: 146.04, 146.16
 Baranec, Christoph: 128.05, 152.13, 349.13
 Barbary, Kyle: 153.21, 327.02
 Barclay, Thomas: 303.06, 326.01, 334.07, 349.08, **403.08**, 439.10
 Bard, Deborah: 239.05
 Bardalez Gagliuffi, Daniella: **158.15**
 Barentine, John: **142.01**
 Barentsen, Geert: 204.04, 303.06, **431.01**, 439.07, 439.10
 Barger, Amy: 328.02
 Barger, Kat: 340.04, 411.01
 Baring, Matthew: 333.06
 Barker, Brandon L.: **255.06**
 Barker, Thurburn: 349.14
 Barkhouse, Wayne: 306.05D
 Barkhouser, Robert: 402.01
 Barlow, Brad: 146.03, 150.23, 354.12, 453.04
 Barman, Travis: 148.20, 228.04, 329.07, 334.05
 Barnes, Derek: 402.04
 Barnes, Kate L.: 248.02
 Barnes, Rory: 403.01
 Barnes, Stuart: 152.24
 Barnes, Thomas G.: 109.05
 Baronchelli, Ivano: 355.12
 Barone-Nugent, Robert: 306.04
 Barr, Alex: 361.01
 Barr, Robert: 362.01
 Barrentine, Emily M.: 215.05, 447.01
 Barret, Didier: 453.08
 Barrett, Paul: 340.11
 Barrientos, L. Felipe: 250.41
 Barro, Guillermo: 127.01
 Barron, Darcy: **356.02**, **359.04**
 Barrow, Kirk Stuart Simeon.: **327.05D**
 Barrows, R. Scott.: 440.05
 Barthelmy, Scott D.: 320.03, 343.02
 Bartlett, James: 402.01
 Bartlett, Jennifer Lynn.: 150.02, 150.03, **242.17**, **246.01**, 362.08
 Bartolone, Lindsay: 242.21
 Bartz, Allison: **338.07**
 Barua, Prachurjya: 444.13
 Bassa, Ceas: 233.05D, 453.15
 Basten, Fabienne: 246.08
 Bastian, Timothy: **342.19**
 Bastien, Fabienne: 303.03
 Basu-Zych, Antara: **251.10**, 354.10
 Batalha, Natalie Marie.: 403.06, **427.04**
 Batalha, Natasha E.: 148.14, 148.39, **207.04**, 439.17
 Bates, Jennifer: 247.23
 Batiste, Merida: 422.07, **422.08**
 Batta, Aldo: 435.01
 Battersby, Cara: **125.06**, 125.07, 136.07, **355.07**
 Battye, Richard: 251.06
 Batygin, Konstantin: 204.03, 329.01
 Bauer, Amanda: **444.06**
 Bauer, Dr. Amanda: 444.02
 Bauer, Franz Erik.: 245.09, 250.38, 320.05
 Bauer, James: **355.17**
 Bauer, James M.: 144.15
 Baum, Stefi: 257.19
 Baumgartner, Wayne H.: 320.03
 Bayliss, Daniel: 104.04
 Bayliss, Matt: 250.41
 Bayyari, Ammar: 449.07
 Bazzano, Angela: 438.19
 Beaky, Matthew: 244.23
 Beale, Luca: 360.01
 Bean, Jacob: 128.06, **207.05**, 228.07, 310.04, 410.01, 427.04
 Bean, Rachel: 153.12, 153.19
 Beardsley, Adam: **203.06**
 Beasley, Anthony: **342.03**
 Beasley, Matthew: 228.04
 Beaton, Rachael L.: 146.14, 344.01
 Beaton, Rachael Lynn.: **351.05**
 Beatty, Thomas: **234.04**, 427.01
 Bechtol, Keith: 223.04, 340.07, 413.07
 Beck, Melanie: 362.03
 Beck, Sara: 362.15
 Becker, Andrew: 144.08
 Becker, Christopher: 148.21
 Becker, Juliette: 427.03, 434.06
 Becker, Peter A.: 132.07, 205.03D, 243.11, **333.04**
 Beckey, Jacob: **255.05**
 Becklin, Eric Eric.: 212.01, 237.06, **337.01**
 Bedard, A.: 145.02
 Beeler, Doreen: **350.03**
 Beers, Timothy: 257.12
 Begelman, Mitchell C.: 257.19, 423.03
 Behar, Ehud: 404.04, 405.05
 Beheshtipour, Banafsheh: **323.07**
 Beichman, Charles: 211.08, **246.46**, 310.06, 329.01, 330.02, 355.10
 Beifiori, Alessandra: 306.01D
 Bektesevic, Dino: 144.08
 Belczynski, Krzysztof: 325.04
 Belikov, Ruslan: 246.02, 402.02, 402.07
 Bell, Cameron: 355.10
 Bell, Eric F.: 110.03, 409.02D
 Belles, A.: 344.09
 Belles, Alexander: **247.30**
 Bellini, Andrea: 257.09, **361.10**
 Bellis, Matthew: 351.02
 Bellm, Eric: 362.04
 Bellovary, Jillian: **305.01**, 325.05, 340.10, 347.13, 347.15, 359.03
 Belokurov, Vasily: 210.03
 Beltre, Chasity: 444.14
 Beltz, Hayley: **357.02**
 Benavides, Marcus Uriel.: **149.22**
 Bendek, Eduardo: 402.02, **402.07**
 Bender, Chad: 152.08, 152.18, 211.02, 244.16, 246.08, 246.45
 Bender, Edward: 444.01
 Bender, Mark: 220.03
 Bender, Ralf: 306.01D
 Benecchi, Susan: 115.03
 Benedict, George Frederick.: **109.05**
 Benefo, Roshan: 150.30, **150.31**
 Benford, Dominic: 152.19, 304.06, 314.05D, 419.05
 Beniamini, Paz: 243.07
 Benjamin, Robert A.: 237.15, 237.16, **247.22**, 402.01, 429.03, 429.04D
 Benjamin, Telvin: **344.14**
 Benneke, Björn: 104.07, **207.02**, 211.08, 329.01, 427.04
 Bennett, Charles: 152.19, 314.05D, 419.05
 Bennett, David: **148.41**, 246.17
 Bennett, Lee: 354.29, 354.36
 Benson, Andrew: **354.08**
 Benson, James A.: 157.01, 442.06
 Bentley, Rory: **241.01**
 Bento, Joao: 104.04
 Bentz, Misty C.: 422.07, 422.08
 BenZvi, Segev: 250.05
 Berg, Michelle: 248.09
 Berger, Clara: **340.03**
 Berger, Edo: 234.03, 308.06, 349.10
 Bergeron, Eddie: 106.03
 Bergeron, P.: 145.02
 Bergin, Edwin: 229.04D, 229.04D, **301.03**, 355.11, 355.11, **355.13**, 355.20, 355.20
 Bergmann, Marcel: 228.07
 Berkeley, Matthew R.: **445.11**
 Berlind, Perry: 104.04, 334.06
 Bermeo, Alberto: 252.04
 Bernard, Stephanie: 349.32
 Bernardi, Mariangela: 226.06
 Bernstein, Alexandra E.: 339.05
 Bernstein, Gary: 354.28
 Bernstein, Rebecca: 413.07
 Berriman, G. Bruce.: 150.10, **150.14**
 Berriman, G. Bruce: 150.01
 Bershad, Matthew: 112.05, 210.01
 Berta-Thompson, Zach: 427.04
 Berta-Thompson, Zachory: 111.05, 148.18, 148.25, 349.13, **427.09**
 Berti, Emanuele: 325.04
 Bertoldi, Frank: 304.03
 Best, Philip N.: 328.05D
 Best, William M J.: **137.01**, 349.07, **349.19**, 349.26
 Bestenlehner, Joachim: 413.05D
 Betoule, Marc: 153.21
 Betti, Sarah: **149.44**
 Bettis, Wyatt: 316.06
 Beuther, Henrik: 408.08
 Beverage, Aliza: **149.55**
 Bhalerao, Jayant: 241.11
 Bhargava, Sunayana: 252.04
 Bhatawdekar, Rachana: 306.04
 Bhattacharya, Aparna: **148.10**
 Biancardi, Rochelle: 250.13
 Bianchi, Luciana: **140.12**, 158.13, **362.01**
 Bianco, Federica: 239.01
 Bichon, Luis: **434.04**
 Bicknell, Geoff: 342.28
 Biddle, Lauren: 339.12
 Biederman, Moriah: 245.14
 Bieryla, Allyson: 104.04, **216.06**, 244.12, 303.05, 439.13
 Biferno, Anya A.: 131.03
 Bigiel, Frank: 125.07, 322.04
 Bihl, Simon: 408.08
 Bildsten, Lars: **235.01**
 Bilinski, Christopher: 245.07
 Bilous, Anna: 243.09
 Binder, Breanna Arlene.: 230.03, 339.07
 Binks, Alex: 349.29
 Bird, Jonathan: 411.02D
 Bird, Justin: 252.13
 Biretta, John A.: 257.19
 Birkinshaw, Mark: 257.19, 404.01
 Birky, Jessica Lua.: **349.25**
 Bittle, Lauren: **429.05D**
 Bittle, Lauren E.: 360.01
 Bizyaev, Dmitry: 210.01
 Bjoraker, Dr. Gordon: 144.17
 Bjorkman, Jon E.: 434.06
 Bjorkman, Karen: 157.06, 434.06
 Black, Kevin: 157.11, 355.55
 Black, William: 153.02
 Blackman, Eric: 244.05
 Blackwell, Annie E.: **244.21**
 Blagorodnova, Nadia: 405.02D
 Blair, William Patrick.: **248.03**
 Blake, Cullen: 246.08
 Blakeslee, Scott: 152.18, 246.08
 Blanc, Guillermo: 149.19
 Blanco Cuaresma, Sergi: 362.17
 Bland-Hawthorn, Joss: 237.05
 Blandford, Roger: 330.05
 Blattner, Tim: 150.06
 Bleacher, Lora: 242.08, 360.06
 Blecha, Laura: 123.05, 250.02, 250.10, 250.26, **305.04**
 Blecic, Jasmina: 148.02, 148.08, 410.04, 439.18
 Blitz, Leo: 130.01, 340.09, 426.04D
 Blondin, John: 241.03, 244.22
 Bloodgood, Felise: 349.27
 Bloom, Joshua: 420.07
 Bluck, Asa: **227.01**
 Blundell, Katherine: 342.29
 Blundell, Raymond: **125.01**
 Blunt, Sarah: **439.22**
 Blyth, Sarah: 231.07
 Bochenek, Christopher: **245.01**
 Bock, James: **354.21**
 Bodewits, Dennis: **452.04**
 Boehler, Keith: 442.01
 Boër, Michel: 107.08
 Boettcher, Erin: **429.04D**
 Boettcher, Markus: 205.02
 Bogdan, Akos: 347.04
 Bogdanov, Slavko: 233.05D, 243.17, **453.15**

Bogdanovic, Tamara: 250.26, 347.22
 Bogdanovich, Pavel: 203.01
 Bohlin, Ralph: 354.17, 355.27, 355.34
 Bohringer, Hans: 327.02
 Boissay Malaquin, Rozenn: **440.13**
 Boisvert, John: **104.06D**
 Boizelle, Benjamin: **423.02D**
 Bolatto, Alberto: 130.07, 241.08, 247.19, 322.04, 355.05
 Bolatto, Alberto D.: 130.01, 342.25, 426.04D
 Bolcar, Matthew R.: 246.37
 Bolejko, Krzysztof: **420.05**
 Bolton, Scott: **101.01**
 Bonaca, Ana: **411.03**
 Bonaldi, Anna: 152.07
 Bonamigo, Mario: 438.15
 Bond, Howard E.: **145.02**
 Bonev, Boncho: 144.13
 Bonfils, Xavier: 211.08
 Bonidie, Victoria: 333.05
 Bonine, Brett: **149.35**
 Bonnefois, Aurélie: 355.53
 Bonnell, Jerry: 242.13
 Bonvin, Vivien: 440.10
 Boogert, Adwin: 247.01
 Bookbinder, Jay: 338.02
 Boone, David: **250.27**
 Boone, Kyle Robert.: **152.09**, 153.21, 327.02
 Boorman, Peter Gregory.: **343.01**
 Booth, Mark: 147.08
 Boquien, Médéric: 454.04
 Borden, Jeremy: 357.08
 Bordenave, David: 360.01
 Bordoloi, Rongmon: 237.05
 Borissova, Jordanka: 136.08
 Borkowski, Kazik: 241.03, 244.22
 Boryta, Mark: 144.14
 Bos, Brent: 151.07
 Bose, Maitrayee: 358.11
 Bostroem, K. Azalee.: **245.16**, 413.05D
 Bouchy, Francois: 104.04
 Boudreaux, Thomas Macaulay.: **150.29**
 Bouma, Luke: 128.06
 Bouman, Katherine: 347.21
 Bouquin, Daina: **143.03**
 Bourdin, Herve: 441.01
 Bouret, Jean-Claude: **419.01**
 Bourke, Tyler: **152.07**
 Bourrier, Vincent: 148.18
 Bouvier, Jerome: 109.01
 Boven, Paul: 215.03
 Bovill, Mia Sauda.: **149.18**
 Bovy, Jo: 257.12
 Bowen, Dennis B.: 124.07
 Bower, Geoffrey C.: **125.02**, 132.02, 243.18, **342.31**
 Bower, Richard: 149.04
 Bowers, Charles: 355.18
 Bowler, Brendan: 104.02, 148.33, 204.03, 349.04, 349.07, **349.09**
 Bowman, Judd D.: 116.02D, 116.04, 228.04, 312.05D
 Bowman, William P.: **149.28**
 Bowyer, Rachel: **252.10**
 Boyajian, Tabettha: 450.05
 Boyce-Jacino, Katherine: **126.03**
 Boyd, Patricia: 244.26, 250.09, 304.05, 326.01
 Boyer, Amy: 362.03
 Boylan-Kolchin, Michael: 313.06, 356.05, 449.06
 Boyle, Richard P.: **344.05**
 Boyle, Robert J.: **144.17**
 Boyles, Jason: 243.13
 Bozza, Valerio: 228.05, 246.16, 255.12
 Bozzo, Enrico: 140.06, 438.19
 Braatz, James: 123.03D, 351.07
 Bracey, Georgia: 444.15
 Brachet, Frank: 419.01
 Bradac, Marusa: 454.10, 454.12
 bradford, charles: 355.50
 Bradford, Charles Matt.: 251.07, 355.05, **355.48**
 Bradford, Eric: 151.02
 Bradley, Damon: 354.33
 Bradley, Larry: 454.10, 454.12
 Bradley, Richard F.: 152.20, 153.05, 153.13
 Brady, Greg: 355.53
 Brady, Gregory: 246.36
 Brady, Kristin: 242.03
 Brady, Patrick: 361.20
 Brainerd, Tereasa: **415.01**
 Brammer, Gabriel: 355.12, 355.19, 454.08, 454.12
 Brandt, Soren: 140.06, 438.19
 Brandt, T.J.: 344.14
 Brandt, Timothy: 152.10, 204.03, 303.07
 Brandt, William: 231.03, 250.36
 Branton, Doug: 355.01, 355.42
 Brashear, Ronald: **208.03**
 Brasseur, Clara: 158.13
 Braude, Ashwin: 115.04
 Braun, Robert: 152.07
 Braun, Timothy Trent.: **248.07**
 Braverman, William: **153.06**, 258.15
 Bray, Evan: 355.15, **355.28**, 355.35, 355.44, 355.46
 Brazier, Adam: **255.18**
 Breckinridge, James Bernard.: **439.04**
 Breet, Jessica: **248.10**
 Bregman, Joel N.: **237.17**, 357.06, **407.01**, 451.02
 Breiding, Peter: 323.02, **323.04D**
 Breivik, Katelyn: **124.04D**
 Bremer, Malcolm: 149.45
 Brennan, Ryan: 347.03
 Brennan, Sean: 255.11
 Brenneman, Laura: 140.06, **237.19**, 237.20
 Bres, Luis: 442.01
 Brevik, Justus A.: 215.02D, 322.05
 Brewer, Janesse: 232.04
 Brewer, John: 120.03, 450.05
 Breysse, Patrick C.: **327.04**
 Briceno, Cesar: **339.04**
 Brickhouse, Nancy S.: **237.20**, 253.03
 Bridge, Carrie: 304.06
 Bridge, Joanna: 349.32
 Briggs, Michael: 361.14
 Bright, Jane: **157.08**
 Brill, Ari: 440.23
 Brinchmann, Jarle: 210.01, 402.01
 Brinkman, Casey: 132.02
 Brinkman-Traverse, Casey Lynn.: **354.05**
 Brinkmann, Jonathan: 211.02
 Brinkworth, Carolyn: 246.13
 Brisbin, Drew: 112.02D, 251.05
 Brisken, Walter: 215.01, 342.30, 354.11
 Bristow, Makennah: 104.07, **439.02**, 439.13
 Brito, Arturo: 246.36
 Britt, Christopher T.: **453.06**
 Brittain, Sean: 242.18, 437.03, 449.09
 Brocious, Dan: 142.08
 Brock, Laci: 148.20
 Brodwin, Mark: 327.02
 Brogan, Crystal: **342.20**, 342.21, 449.01
 Brogi, Matteo: 349.09
 Bromley, Benjamin: 144.09
 Brooks, Alyson: 237.13, 340.10
 Brooks, Derek: **358.01**
 Brooks, Keira: 150.37, **246.36**
 Broos, Patrick: 339.07
 Broughton, Peter: **208.02**
 Brout, Dillon: **219.04**
 Brown, Alexander: 111.05
 Brown, Ari D.: 447.01
 Brown, Arianna: **257.15**
 Brown, Daniel: 255.05
 Brown, Jessie: 148.20
 Brown, Jonathan: **231.04D**
 Brown, Jonathon: **252.07**
 Brown, Michael J.L.: 425.02D
 Brown, Peter: 408.02
 Brown, Steven W.: 349.05
 Brown, Thomas M.: 411.04
 Brown, Tim: 152.24
 Brownell, Eric: 143.03
 Browning, Matthew: 133.03, 158.11
 Bruck Syal, Megan: 115.09
 Bruenjes, Fred: 126.08
 Bruno, Giovanni: 148.14
 Brusa, Marcella: 304.01
 Bruton, Sean Tyler.: **441.02**
 Bruursema, Justice: 436.04, **446.15**
 Bryan, Marta: **111.06D**, 204.03, 349.09, 427.03
 Bryden, Geoff: 158.05
 Bryson, Steve: **403.06**
 Brzycki, Bryan: **149.53**
 Bublitz, Jesse: **241.07**
 Buchhave, Lars: 201.07, 427.03
 Buckner, Spencer L.: 242.14
 Budavari, Tamas: **225.05**, 362.16
 Budynkiewicz, Jamie A.: 238.01, 238.02, 238.03, 238.04, 238.05, 238.06, 238.07, 238.09, 238.10, 238.11
 Bueno, Michael: **257.16**
 Bugg, Adam Garth.: **146.12**
 Bujarrabal, Valentín: 241.07
 Bulbul, Esra: 347.07, 441.01
 Bulcha, Berhanu T.: 215.05
 Bullock, James: 257.13
 Bult, Peter: 157.13, 243.17, 333.03
 Bundy, Kevin: 210.01, 250.46, 406.03
 Bunn, Emory: 438.06, 438.07, 438.08, 438.09
 Buote, David: 252.05
 Burchett, Joseph: 357.08
 Burchett, Joseph N.: **302.05**
 Burgasser, Adam J.: 158.15, 158.16, 158.17, 349.10, 349.25
 Burge, Jim: 140.13
 Burgett, William: 308.06
 Burke, Christopher: 403.06
 Burke, Douglas: 238.01, 238.02, 238.03, 238.04, 238.05, 238.06, 238.07, **238.08**, 238.09, 238.10, 238.11
 Burke-Spoloar, Sarah: **250.26**, 323.06
 Burkhardt, Andrew Michael.: **360.01**, **429.02D**
 Burnam-Fink, Michael: 359.06
 Burns, Eric: **107.05**
 Burns, Keaton: 234.03
 Burns, Professor O.: **116.01**, 152.20
 Burrows, Adam: 148.09, 207.01, 209.06, 211.06, 234.04
 Burrows, Dave: 241.11, 355.28
 Burrows, David N.: 245.08, 355.15, 355.35, 355.44, 355.46, 447.05
 Burtnyk, Kimberly: 360.08
 Burton, Michael G.: 241.05
 Burtscher, Leonard: 320.09
 Buscher, David F.: 314.03
 Bushouse, Howard: 436.12
 Bushra, Rafia: 148.14
 Buson, Sara: 250.29, **440.18**
 Bustard, Chad: 251.04, 251.08
 Butler, Bryan: **342.09**
 Butler, Bryan J.: 342.14
 Butterfield, Natalie: 311.06, **445.01**
 Buxner, Sanlyn: 113.02, 113.03, 113.05, **113.06**, 139.02, 155.01, 155.02, **155.03**, 316.01, **360.06**, 444.15
 Buzasi, Derek: **150.39**
 Byeon, Seoyeon: 442.03
 Byrne, Lindsey: **136.03**
 Byrne, Ruby: 247.27
 Caballero-Nieves, Saida Maria.: 150.18, 362.09, **413.05D**, 424.04D
 Caceres, Gabriel: 246.34, **431.03D**
 Cackett, Ed: 157.13, 347.01, 347.05, 347.07
 Cackett, Edward: **453.08**
 Cadelano, Mario: 243.09
 cady, eric: 246.18, 355.47, 361.13
 Cahoy, Kerri: 355.14, 402.04
 Cahoy, Kerri L.: 419.08
 Cai, Qijie: **444.05**
 Calafut, Victoria Rose.: **153.19**
 Calahan, Jenny: **136.01**, **360.11**
 Calamida, Annalisa: 354.17, 411.04
 Calchi Novati, Sebastiano: 158.05
 Caldwell, Nelson: 149.36, 344.17

Cale, Bryson L.: **246.13**
 Caler, Michelle A.: **441.06**
 Calkins, Mike: 104.04, 334.06
 Callas, John: 246.08
 Calvén, Emilia: **446.01**
 Calvet, Nuria: 339.09
 Calzetti, Daniela: **106.02**,
 114.02D
 Cameron, Andrew: 104.04,
 148.02
 Camp, Jordan: **121.05**
 Campanelli, Manuela: 124.07
 Campbell, David: 454.02
 Cancino, Adolfo A.: 133.07
 Cancino, Adolfo Andrew.:
349.34
 Cane, Thomas: 351.13
 Cann, Jenna: **250.10**
 Cannon, John M.: 340.06,
 340.08
 Cantello, Matteo: 255.09,
307.02
 Cao, Yixian: **426.04D**
 Capak, Peter: 153.18, 332.04
 Cappellari, Michele: 306.01D
 Cappelluti, Nico: 110.06,
238.13, 320.06
 Capps, Richard W.: 246.08
 Caprioli, Damiano: 326.05D
 Caputo, Regina: **355.49**, 361.14
 Cara, Mihai: 257.19
 Cardamone, Carolin: **110.06**,
 110.07, 304.01, **316.03**
 Cargile, Phillip: 354.06
 Carilli, Chris: 222.03, 252.08,
 342.09, 342.10, 342.25, 342.26
 Carini, Michael: 250.21
 Carlberg, Joleen K.: 246.43,
355.01, 355.42
 Carleton, Timothy: **412.05**
 Carlin, Jeffrey: 237.02, 340.07
 Carlin, Jeffrey L.: **237.12**
 Carlson, Randall E.: 152.02
 Carlton, Ashley: 355.14, 419.08
 Carman, Samuel Paul.: **149.47**
 Carmichael, Theron: **246.03**
 Carniani, Stefano: 210.03
 Caron, Laura: **126.02**
 Carpenter, John: 147.15, 147.18
 Carpenter, Ken G.: 341.08,
 348.16, **348.17**
 Carr, Brandon: 340.08
 Carr, John S.: 437.03, 449.09
 Carrasco, Daniela: 454.10,
 454.12
 Carrasco, Eleazar: 309.06D
 Carrasco Damele, Eleazar
 Rodrigo.: **258.08**
 Carrasco Kind, Matias: **219.01**
 Carroll, Christopher M.: 105.01
 Carroll, Joseph: 314.07
 Carter, David: 344.16
 Carter, Evan: **147.15**, 147.18
 Carter, Ruth: 354.33, 354.35,
355.24
 Casado, Johanna: 362.18
 Casar, Caitlin: 401.01
 Casertano, Stephano: 150.24,
 355.12, 355.45, 420.07
 Casetti, Dana: 411.01
 Casey, Caitlin M.: 251.06,
 252.06, 252.07, 328.01, 342.25,
342.26
 Casey-Clyde, J. Andrew: 237.14
 Cash, Jennifer: 242.18
 Cashman, Frances: **203.01**,
 357.05
 Caspi, Amir: 402.03D
 Castelaz, Michael: , 242.03,
349.14
 Castelli, Fiorella: 157.05
 Castillo, Brandon: **145.03**
 Castro, Daniel: **408.07**
 Castro, Norberto: 434.06
 Castro-Carrizo, Arancha: 241.01
 Cataldo, Giuseppe: **215.05**
 Catinella, Barbara: 309.03
 Caton, Daniel Bruce.: **142.05**,
244.03, 244.10, 434.03
 Cen, Renyue: 357.01
 Cenko, Bradley: 124.06,
 243.08, 247.10, 320.03,
 343.02, 347.22, 405.02D
 Cernis, Kazimieras: 344.05
 Cerny, Catherine: 454.10,
 454.12
 Ceverino, Daniel: 127.02
 Chaboyer, Brian: **344.10**
 Chae, Kyu-Hyun: **226.06**
 Chael, Andrew: **311.04**, 347.21
 Chakrabarti, Sukanya: 451.01
 Chakrabarti, Supriya: 246.41,
 355.03, **355.08**
 Chakrabarty, Deepto: 140.06,
157.13, **160.04**, 233.06,
 233.06, 243.17, 243.17, 333.03
 Chalifour, Matthieu: **349.29**
 Challener, Ryan: 148.02,
410.04
 Challener, Ryan C.: 148.08
 Challinor, Anthony: 327.01
 Challis, Peter: 209.03, 308.06
 Chamberlain, Heather: 244.10,
434.03
 Chamberlin, Phil: 338.01
 Chambers, Edward T.: 150.11
 Chambers, Kenneth: **102.01**,
 115.05, **212.02**, 215.06, 308.06
 Champagne, Jaclyn: 342.26
 Chan, Jeffrey C C.: 306.01D
 Chance, Quadry: **148.01**
 Chanchaiworawit, Krittapas:
406.04D
 Chandar, Rupali: 313.05
 Chandler, Claire J.: 342.14,
 342.21
 Chang, Tzu-Ching: **140.01**
 Chaplin, William J.: 450.13
 Chapman, Scott: 251.06
 Chappell, Samantha: 311.02
 Charbonneau, David: 148.18,
 334.02, 334.06
 Charbonneau, Rebecca:
208.04
 Charbonnier, Aldée: 440.03
 Charlton, Jane: 250.42, 250.44,
 302.04, 412.02D
 Charnley, Steven: 136.11
 Chary, Ranga-Ram: **150.15**,
 402.01
 Chase, Eve: **224.08**, 243.06
 Chastain, Sarah: **243.03**
 Chatterjee, Shami: 132.02,
 132.06, 243.01, 243.10, 243.18,
 342.31, **453.16**
 Chatterjee, Sourav: 344.15,
 423.07, **439.15**
 Chatterjee, Suchetana: 342.27
 Chattopadhyay, Tanmoy:
 355.15, 355.28, **355.35**, 355.44,
 355.46
 Chatzopoulos, Emmanouil:
 157.02
 Chawla, Pragya: 243.13
 Cheatham, Diana M.: 243.11
 Chee, Zoe: 242.21
 Chen, Brian: 348.08
 Chen, C.-H. Rosie.: 136.11
 Chen, Cheng: **144.12**
 Chen, Chien-Ting: **231.03**
 Chen, Christine: 147.19, 229.03
 Chen, How-Huan: **230.05D**
 Chen, Howard: **148.13**, 439.15
 Chen, Jingjing: 439.20
 Chen, Judy C.: 238.01, 238.02,
 238.03, 238.04, 238.05,
 238.06, 238.07, 238.09,
 238.10, 238.11
 Chen, Kai-Feng: 406.03
 Chen, Mike: 342.22
 Chen, Peter C.: **361.07**
 Chen, Xinyi: **252.04**
 Chen, Yanmei: 210.01
 Chen, Zhou: 311.07
 Chen, Zhuo: **237.06**
 Chenevez, Jerome: 157.13,
 438.19
 Cheng, Eric: **348.08**
 Chernoff, David: 258.15
 Chernyakova, Masha: 233.04
 Cheshire, Ishani: 453.02
 Cheung, Chi C.: 257.19
 Cheung, Chi C (Teddy):
255.16
 Cheung, Edmond: 210.01,
 250.46
 Chevalier, Roger: 245.01
 Chevres Fernandez, Lee Roger:
151.07
 Chiang, Eugene: 147.15, 147.18
 Chiang, Yi-Kuan: 252.06
 Chiboucas, Kristin: **344.16**,
 354.30
 Chibueze, James: 342.21
 Chichura, Paul: 150.32, 150.33,
150.34
 Chilcote, Jeffrey K.: 148.24,
 152.10, 303.07, 329.04D,
 361.18
 Child, Sierra: 339.05
 Chilton, Andrew: **402.05**,
 402.06, 419.06
 chiosi, cesare: 257.11
 Chirenti, Cecilia: **421.01**
 Chiu, I-non: 406.03
 Chizek Frouard, Malynnda:
150.02, 150.03, **242.16**,
 362.08
 Chizek Frouard, Malynnda R.:
 242.17
 Cho, Hsiao-Mei: 112.02D,
 215.02D, 322.05
 Cho, Hyejeon: **252.09**
 Chogi, Maiko: 446.08
 Choi, Changsu: 442.03
 Choi, Ena: 347.03
 Choi, Hoseung: **227.03**
 Choi, Hyunseop: 250.14
 Choi, Jaeho: **442.04**
 Choi, Philip: 314.01
 Choi, Yumi: 157.06
 Chojnowski, Drew: 244.16
 Chomiuk, Laura: 250.26,
 326.05D, 342.32, 414.02,
 453.06
 Choquet, Elodie: **147.12**,
 246.36, 330.02, 355.53
 Chornock, Ryan: 308.06
 Christensen, Charlotte: 136.03,
 149.43, 340.10
 Christensen, Lars: 360.10,
 360.13
 Christensen, Lise: 149.07,
 149.33, 357.03, 357.07
 Christensen, Robert: 246.08
 Christiaens, Valentin: 204.03
 Christian, Tiffany: **348.09**
 Christiansen, Jessie: 104.07,
303.06, 329.01, 403.06,
 439.08
 Christophersen, Marc: 140.06
 Chu, Devin S.: **311.02**
 Chun, Francis K.: 152.02
 Churazov, Eugene: 406.05
 Church, Sara: 322.03
 Church, Sarah: 322.04
 Churchill, Christopher: 302.04
 Churchwell, Edward: 247.31
 Churnetski, Kristen: 241.02
 Chuss, David: 152.19, 152.21,
247.24, 314.05D, 354.33,
 419.05, 445.11
 Chyla, Roman: 362.17
 Ciani, Giacomo: 402.05,
 402.06, 419.06
 Ciardi, David: 104.04, 104.07,
 128.01, 329.01, 410.03,
 414.05D, 439.08, 439.13
 Ciardullo, Robin: 149.28,
 150.08, 241.10
 Ciaschi, Cody: 127.02
 Cibirka, Nathália: 454.10,
 454.12
 Cid, Aurora: **349.35**, 349.39
 Cieplak, Agnieszka: **420.01**
 Cieza, Lucas: 349.09, 437.01
 Cimatti, Andrea: 357.07, 402.01
 Cisewski-Kehe, Jessi: **213.07**
 Civano, Francesca Maria.:
 149.05, 238.01, 238.02, 238.03,
 238.04, 238.05, 238.06,
 238.07, 238.08, 238.09,
238.10, 238.11, 238.12, 304.01,
412.01
 Claire, Max: 149.48
 Clancy, Pdraig: **434.08**
 Clark, Beth Ellen.: 452.05
 Clark, Catherine: 349.31
 Clark, Coral: 131.05
 Clark, Hayley: 158.09
 Clark, James R.: **419.08**
 Clarke, John: 355.36, 361.06
 Clarke, Seth: **348.05**
 Clarke, Tracy: 151.05, 215.01,
 243.14, 342.29, 342.30, **354.11**,
 354.15
 Clarkson, William: 214.05D
 Clarkson, William I.: 348.07,
411.04
 Clason, Timothy: 150.25
 Clautice, Devon: **257.19**
 Clayton, Geoffrey C.: 145.04,
157.02
 Cleary, Colleen: 305.01, **347.13**
 Cleary, Joseph: **356.01**
 Cleary, Kieran: 322.04
 Cleeves, L. Ilsedore: 257.08,
 339.03
 Cleeves, Lauren Ilsedore.:
428.06

Clément, Benjamin: 112.03
 Clements, David: 149.37
 Cline, J. Donald.: **242.03**
 Close, Laird: 303.02
 Clowes, Roger G.: 357.08
 Cobb, Bethany E.: 316.03, **316.04**
 Cobos, Aracely Susan.: **252.11**
 Coburn, William: 354.11
 Cochran, Anita: 144.13
 Cochran, William: 104.04, 109.05
 Cocroft, Daven: **136.13**
 Cody, Ann Marie: 439.07, 439.10, 439.13
 Coe, Dan: **454.10**, 454.12
 Coerver, Anna: **453.10**
 Cohen, David: 424.04D
 Cohen, Judy: 153.18
 Cohen, Ofer: 148.16
 Cohen, Roger: 344.10, **413.03**
 Cohen, Seth: 354.14
 Cohn, Jonathan: **110.05**
 Coil, Alison: 258.05
 Coker, Kristina: 156.01
 Colbert, James: 354.29, 354.36, **355.12**
 Colditz, Sebastian: 445.12
 Cole, Brent: 442.01
 Cole, Jackson L.: 111.07, 148.07
 Cole, Jackson Lane.: 148.11, **148.27**, 148.31, 148.32, 148.35, 148.36, 148.37
 Cole, Shaun: 212.04
 Colebaugh, Alexander: **249.01**
 Colgan, Sean: 237.01, 247.01
 Collaboration, Backyard Worlds: Planet 9: 158.14
 Collier, Braxton: 220.03
 Collins, Karen: 104.04, **307.07**, **439.08**
 Collova, Natasha: **149.40**
 Colon, Knicole: 104.04, **204.04**, 431.01
 Combes, Francoise: 241.01
 Comeau, Tom: 246.36
 Comerford, Julia: **440.05**
 Comerford, Julie: 250.26, 320.05, 323.03
 Cominsky, Lynn: 131.03
 Condon, James: 123.03D, 342.10, 342.11
 Coneglian, Michele: 402.05
 Conklin, John: 402.05, 402.06
 Conklin, John W.: **419.06**
 Conn, Tracie Renea.: **338.02**
 Connaughton, Valerie: 361.14
 Connolly, Andrew: 144.08, 225.05
 Connolly, Brian: 304.06
 Connour, Kyle: 452.09
 Conroy, Charlie: 149.29, 237.10, **336.01**, 354.06, 402.01, 411.03
 Conroy, Kyle: 151.03, 244.07, **244.25**
 Conselice, Christopher: 258.01, **306.04**, 354.14
 Constantin, Anca: 123.05, **223.05**, 250.02, 440.04
 Conti, Alberto: 355.22
 Contopoulos, Ioannis: 404.04
 Conway, Matthew: 258.11, **357.04**
 Cook, Ben: 444.10
 Cook, David O.: **332.06**, 361.20
 Cook, Joshua S.: 258.01
 Cook, Therese: 104.02, 246.42
 Cook, Timothy: 246.41, 355.08, **355.16**
 Cooke, Jeff: 151.08
 Cooke, Kevin C.: **227.02**
 Cooper, Ellie: 444.13
 Cooper, Michael: 412.05
 Cooray, Asantha: **103.01**, **121.10**, 149.37, 153.07, 257.15, **354.27**, 354.33, 355.11, 355.52
 Copin, Yannick: 152.09
 Coppejans, Deanne: 245.13
 Coppi, Paolo: 257.19, 304.01
 Corbally, Christopher: 142.08
 Corbet, Robin: 333.01
 Corbett, Hank: 150.23, 354.12
 Corbett, Henry T.: **231.06**, 310.03
 Corcoran, Kyle A.: **150.23**
 Corcoran, Michael: 349.12
 Corcoran, Michael Francis.: **341.01**, 450.09
 Cordes, James: 132.06, 243.01, 255.18, 342.31
 Cordes, Jim: 132.02, 243.18
 Córdova Rosado, Rodrigo Eduardo Lope.: **157.14**
 Corlies, Lauren: 149.08, **210.06**
 Cornelis, Juliette: 444.12
 Cornell, Hunter: 438.10
 Corrales, Lia: 130.03, 350.01, 350.03, **429.06**
 Corsi, Alessandra: **124.01**, 438.14
 Cortes, Jorge: **246.19**
 Cortés, Paulo: 257.07
 Cortes, Rosemary: **252.18**
 Cortese, Luca: 309.03
 Cosens, Maren: 112.03, 149.13
 Cosentino, Richard: **144.06**
 Cosner, Christopher M.: 355.03
 Costa, Allison: **130.05D**
 Costen, Nicholas: 152.19
 Costeraste, Josiane: 419.01
 Côté, Patrick: 127.05D
 Cotera, Angela: 142.08, 237.01
 Cotter, Cory: **251.04**
 Cotton, William: 342.10, 342.11, 342.30
 Coughlin, Eric Robert.: **308.05**
 Coughlin, Jeffrey: 403.06, **431.02**
 Coughlin, Kevin: 152.19
 Coughlin, Michael William.: **124.05**
 Coughlin, Scott: 243.06
 Courbin, Fredric: 440.10
 Court, Travis: **351.04**
 Courtney, Sol: **362.02**
 Courvoisier, T. J.-L.: 438.19
 Cousins, Bryce: 153.06, **258.15**
 Covarrubias, Ricardo A.: **442.08**
 Covey, Kevin: 244.16, 246.43
 Covino, Elvira: 234.02
 Cowan, John J.: 157.03
 Cowan, Nicolas: 427.02
 cowie, lennox: 328.02
 Cowley, Charles: **157.05**
 Cowperthwaite, Philip: **325.02D**
 Cox, Erin Guilfoil.: **229.02D**
 Cox, Isaiah Samuel.: **149.49**
 Cracraft, Misty: 106.03
 Craig, David: 351.08
 Craig, Peter: **451.01**
 Crain, Robert: 149.04
 Cranmer, Miles: **436.13**
 Crawford, Fronefield: 224.06, **333.05**
 Crawford, Steve: 112.05, 152.22, 237.05
 Creech-Eakman, Michelle J.: **314.03**
 Creighton, Teviet: 442.01
 Crenshaw, D. Michael: 250.45, 250.48, 404.05
 Crepp, Justin: 329.01, 439.01, 439.19, 450.05
 Crill, Brendan: **204.01**
 Crnojevic, Denija: **149.36**
 Crocker, Alison: 136.05, 247.17
 Croft, Steve: 132.02, **231.01**, **342.24**
 Cromartie, H. Thankful: **243.15**
 Croke, John: **146.16**
 Crosley, Michael K.: **334.03D**, 342.18
 Crossfield, Ian: 104.04, 104.07, 211.08, **228.03**, 246.07, 303.06, 329.01, 403.05, 410.03, 427.04, 439.08, 439.13
 Croton, Darren J.: 258.01
 Crouzet, Nicolas: 427.04
 Crowe, Cassie: **440.16**
 Crowley, Chelsea: **347.11**
 Crowther, Paul: 411.01, 413.05D
 Crum, Ryan Matthew.: **245.08**
 Cruz, Kelle: 158.15, 158.16, 349.23, **349.33**, 349.35, 349.39, 359.03
 Cubillos, Patricio: **439.18**
 Cubillos, Patricio E.: 148.02, 148.08, 410.04
 Cucchiara, Antonino: 151.08, 247.10, 442.07
 Cudworth, Kyle: 344.12
 Cui, Bingyi: **233.03D**, 243.13
 Cui, Isaac: 314.01
 Cui, Xiaohong: 253.03
 Cuillandre, Jean-Charles: 127.05D
 Cukierman, Ari: **419.04D**
 Culliton, Chris: 250.42
 Cumbee, Renata S.: 253.03, **253.04**
 Cummings, Jeffrey: **233.01**, 344.10
 Cunha, Carlos: 327.02
 Cunha, Katia: 211.02, 344.13, 424.03
 Cunningham, Devin: 249.01, **436.08**
 Cunningham, Emily: 453.02
 Cunningham, Nichol: 247.20
 Cunningham, Virginia A.: **243.08**
 Currie, Miles: **153.20**, 153.21, 327.02
 Currie, Thayne: 152.10, **232.03**, **303.07**, **360.09**, 428.07
 Curtis, Jason: **133.04**, 234.04
 Cushing, Michael: 427.06
 Cutini, Sara: 440.18
 Cutler, Sam Edward.: **356.03**
 Cybulski, Ryan: 328.01
 Cyganowski, Claudia: 342.21, 449.01
 Cyr-Racine, Francis-Yan: 327.03D, **415.03**
 Czakon, Nicole: 454.10
 Czarnatowicz, Alexis: **344.20**
 Czekala, Ian: **129.03**, **225.02**, 339.08
 D'Abusco, Raffaele: 238.01, 238.02, 238.03, 238.04, 238.05, 238.06, 238.07, **238.09**, 238.10, 238.11, 238.12
 D'Ammando, Filippo: 440.18
 D'Andrea, Christopher: **245.10**
 D'Angelo, Caroline: 233.05D, 453.15
 d'Ascoli, Stephane: 124.07
 D'Onghia, Elena: 149.47, 411.01
 Dabbieri, Collin: **250.14**
 Dabney, David: 347.08
 Daddi, Emanuele: 402.01
 Dahiwalé, Aishwarya: 242.13
 Dahle, Håkon: 250.41
 Dahlstrom, Eric: 115.06
 Dahm, Scott: **436.04**
 Dahn, Conard C.: 157.10
 Dai, Xinyu: 441.02
 Dai, Zhibin: 414.01
 Dalal, Roohi: **153.10**
 Dalba, Paul: **128.02**
 Dalcanton, Julianne: 150.40, 157.06, 340.08
 Dale, Daniel: 148.11, 148.27, 148.31, 148.32, 148.35, 148.36, 148.37, **248.02**
 Dale, Daniel A.: 111.07, 148.07, 216.03
 Daley, Cail: 147.15, 147.17, **147.18**
 Dalton, Briana: 151.03
 Daly, Declan M.: 220.06
 Dame, Thomas: 331.02D
 Damon, James: 143.03
 Dana, Ryan: **253.01**
 Danchi, William: 140.09, 140.13, **140.16**
 Danekkar, Ashkbiz: **241.12**
 Daniel, Jonathan: **361.02**
 Daniel, Kathryn J.: 248.10, **425.05**
 Dannerbauer, Helmut: 252.07
 Dantowitz, Ron: 220.06
 Darling, Jeremy: 430.03D
 Dartez, Louis: **442.01**
 Darvish, Behnam: **149.17**, 328.05D
 Das, Debjani: 444.13
 Dashtamirova, Dzhuliya: **250.45**, 250.48, 404.05
 Datta, Rahul: **152.19**, 215.02D, 314.05D, 322.05, 419.05
 Dauser, Thomas: 237.22, 435.05
 Dave, Romeel: 342.26, 355.54
 Davenport, James: 234.04, **326.06**
 David, Trevor: 439.13, **450.12**
 David, Trevor J.: 104.07
 David-Uraz, Alexandre: 424.04D
 Davidson, Kris: 341.04

Davies, Richard: 320.09, 323.03
 Davies, Roger L.: 306.01D
 Davila, Joseph M.: 338.03
 Davis, Allen B.: 220.06
 Davis, Benjamin L.: 409.03
 Davis, Brian: **241.10**
 Davis, Daniel: 216.06
 Davis, Dustin: 149.25
 Davis, Lindsey E.: 342.14
 Davis, Shane: 409.05
 Dawson, Bekki: 147.19
 Dawson, Joanne: 247.25, 331.02D
 Dawson, Kyle: 144.09
 Dawson, Sandra: 232.04
 Dawson, William: 239.05, 454.10, 454.12
 Day, Brian: 360.06
 Daylan, Tansu: 151.04, **327.03D**, 354.01
 de Blok, Willem J. G.: 354.04
 De Boer, David: 132.02, 231.01
 de Cia, Annalisa: 408.02
 de Gouvêa, André: 255.03
 de la Vega, Alexander: 127.01
 De Lee, Nathan Michael.: 244.16, **246.43**, 403.04
 De Marchi, Guido: **247.12**
 De Marco, Eugenia: 255.10
 De Marco, Orsola: 241.04
 de Miranda Cardoso, Jose Vinicius: 204.04, **439.07**, 439.10
 de Nolfo, Georgia: 361.14
 De Pree, Christopher G.: **247.23**
 de Putter, Roland: 153.10
 De Rosa, Gisella: 150.38, 355.40
 De Rosa, Robert J.: 329.04D, 349.07
 de Vera, Jon: 152.24
 de Wit, Julien: 128.08, 148.39
 Deacon, Niall: 137.01
 Deam, Sophie: 316.06
 Debattista, Victor P.: 411.04
 Debes, John: 147.04, **147.19**, 355.01
 debes, John Henry.: 147.12, 330.04, 355.42, 428.07
 Decarli, Roberto: 342.25, 342.26
 DeCesar, Megan E.: **224.06**, 243.13
 Deger, Sinan: **409.01**
 DeGroot, Laura: 149.16
 Dehghanfar, Arezu: 237.06
 Deich, Alex: **435.02**
 Deighan, Justin: 452.09
 Dekel, Avishai: 258.01
 del Ser, Daniel: 310.03
 Delacroix, Christian: 246.06, 246.11
 DeLisle, Tim: 242.03
 Deliyannis, Constantine P.: 344.06, 344.09
 Della-Rose, Devin J.: 150.12, **152.02**
 Deller, Adam: 233.05D, 243.10, 453.15
 Dello Russo, Neil: 144.13
 Delorme, Jacques: 442.02
 Delrez, Laetitia: 427.09
 Delsanti, Audrey C.: 115.03
 Delvecchio, Ivan: 304.03
 DeMarcy, Bryan: **250.42**
 Demers, Richard: 246.32
 Deming, Drake: 111.04, 128.06, **207.01**, 211.01, 211.03, 246.23, 410.01, 410.04, 427.02
 Demorest, Paul: 243.12, 255.18, 342.31, 453.09
 Demory, Brice-Olivier: 427.09
 Den Hartog, Elizabeth: 362.13
 Deneva, Julia: **157.11**, 215.01, 243.14, 354.11, 453.05
 DeNigris, Natalie: 250.16, 323.04D
 Denneau, Larry: 109.04
 Dennis, Brian R.: 402.03D
 Denny, Lucas: **248.09**
 Dent, Bill: 147.15, 147.18
 DePoy, Darren L.: 152.01, 413.07
 DeRosa, Alessandra: 140.06
 Derosa, Ryan: 255.10
 Derr, Nicholas James.: 452.08
 Desai, Abhishek A.: **123.04**
 Desai, Karna M.: **211.04D**
 Desch, Steven: 147.02, 359.06, 428.05, 439.23
 Desert, Jean-Michel: 228.07, 427.04
 Desir, Deion: 156.01
 Desjacques, Vincent: 420.03
 Despalì, Giulia: 415.04D
 Dessauges, Miroslava: 112.03
 Deustua, Susana: 106.03, 153.21, 327.02, **349.05**, 354.17, 355.19, 355.34
 Devarakonda, Yaswant: **149.25**
 Devereux, Nicholas: **222.06**
 Devlin, Mark: 215.02D, 322.05
 DeVorkin, David: **126.04**
 Devost, Daniel: **215.06**
 Devour, Brian: **409.02D**
 Devriendt, Julien: 110.01, 127.07
 DeWitt, Curtis: 241.15
 Dexter, Jason: 342.31
 Dey, Arjun: 139.01, 149.24, 332.05
 Dhabal, Arnab: **331.05D**
 Dhara, Atirath: **351.11**
 Dhawan, Vivek: 115.01
 Di Francesco, James: 147.09, 147.17, **342.22**
 Di Gennaro, Gabriella: **406.06**
 Di Teodoro, Enrico M.: 237.07, 331.03
 Diamond, Tiara: **446.11**
 Diamond-Lowe, Hannah: 427.09
 Diamond-Stanic, Aleksandar: 258.05
 Diaz, Mario Claudio.: **224.02**
 Diaz, Rosa: 436.12
 Diaz Rivero, Ana: 327.03D
 Diaz-Merced, Wanda: 216.06, 365.01
 Diaz-Merced, Wanda Liz.: **362.18**, 365.04
 Diaz-Santos, Tanio: 127.06
 Dicenzo, Brooke: **341.05**
 Dicker, Simon R.: 215.02D, 322.05
 Dickey, John M.: 247.25, 331.02D
 Dickinson, Hugh: **110.07**, 153.17, 362.03
 Dickinson, Mark: **149.51**, 354.07, 402.01
 Dickson-Vandervelde, Annie: 129.06
 Dickson-Vandervelde, Dorothy: **147.13**
 Didier, Brian: 351.03
 Dieck, Christopher: **440.21**
 Diego, Jose: 306.04
 Diehl, R.: 438.19
 Dieterich, Sergio: 349.17, **349.18**
 Dietrich, Jeremy: 149.46
 Dillon, Joshua: 153.01
 Dillon, Thomas: 246.36
 Dincer, Tolga: 157.09
 Dinerstein, Harriet L.: **241.15**
 Ding, Adalbert: 220.07
 Dingus, Brenda: 453.10
 DiPirro, Michael: 354.35, 355.24
 DiPompeo, Michael A.: 105.01
 Dirienzo, William: **247.14**, **316.05**
 Dirks, Cody: **230.02D**
 DiSanti, Michael: 144.13
 Disher, Grace M.: **252.02**
 DiTomasso, Victoria: **148.29**
 Dittmann, Alexander: **250.04**
 Dittmann, Jason: 148.18
 Dixon, Christopher: 249.01
 Dixon, Samantha: 152.09, **245.17**, 327.02
 Dixon, Van: 355.12, 355.34
 Djordjevic, Julie: **331.04D**
 Do, Tuan: 212.01, 214.05D, 237.06, 311.02
 Doan, Anh Nguyen Duy.: **347.09**
 Dober, Bradley: 215.02D, 322.05
 Doctor, Zoheyr: **124.03**
 Dodson, Kelly: 140.13
 Doe, Stephen M.: 238.01, 238.02, 238.03, 238.04, 238.05, 238.06, 238.07, 238.09, 238.10, 238.11
 Doeleman, Sheperd: 157.14, 347.21
 Doi, Mamoru: 153.21
 Dokter, Erin: 316.01
 Dolch, Timothy: 255.18, 442.01
 Dolphin, Andrew: 340.08
 Domagal-Goldman, Shawn David.: **148.40**, **207.06**, 246.30, 329.03, **401.05**, 427.08, 439.23
 Domagalski, Rachel: 152.09
 Domingo, A.: 438.19
 Domingue, Donovan: 136.06
 Dominguez, Alberto: 123.04
 Donahue, Megan: 402.01
 Donaldson, Jessica: 428.07
 Donaldson, Tom: **150.01**
 Donavan, Sophia: 333.06
 Dong, Dillon: **231.02**
 Donor, John: 344.13
 Donovan, Benjamin: **355.04**
 Donovan Meyer, Jennifer: **454.13**
 Dore, Olivier: 153.10, **354.23**, 402.01
 Dorland, Bryan: 436.02, 436.04
 Dorn-Wallenstein, Trevor: **250.28**
 Dorodnitsyn, Anton: 250.43
 Dorval, Patrick: 152.22
 Dotson, Jessie: 152.19, 314.05D, 419.05, 431.01
 Douglas, Alea: 151.02
 Douglas, Ewan S.: 147.19, **355.14**, 402.04, 419.08
 Douglas, Stephanie: 344.07, 344.08, 349.22
 Dowd, Tara: 112.06, **251.09**
 Dowell, Charles D.: 130.04, 152.21, 247.24
 Dowell, Jayce: 215.01
 Doyle, Timothy: 450.06
 Dragomir, Diana: 104.04, 329.05, **403.05**, 439.08
 Drake, Jeremy J.: 148.16, 421.08
 Drake, Stephen: 341.01, 349.12
 Drake, Stephen A.: **450.09**
 Draper, Peter: 308.06
 Dressing, Courtney: 104.07, 211.08, 303.06, **329.01**
 Dressler, Alan: 237.10
 Driver, Simon: 149.45, 306.04
 Drlica-Wagner, Alex: 212.05, **219.05**, 413.07
 Drory, Niv: 210.01
 Drouot, Maria: **102.07**, **262.03**, 444.10
 Druckmuller, Miloslav: 220.07
 Du, Xinnan: **130.02D**
 Dubois, Yohan: 227.03
 Duchene, Gaspard: **109.01**, 147.19, 330.04, 449.04
 Dudley, Raymond: 149.60, 251.12, 454.15
 Duff, Shannon M.: 215.02D, 322.05
 Dulz, Shannon: 439.01
 Dulz, Shannon D.: **439.19**
 Duncan, Douglas: 242.12
 Dunham, David W.: **126.08**, **144.11**
 Dunham, Joan B: 144.11
 Dunham, Michael: **125.05**, 147.10, 257.07, 339.10
 Dunn, Brianne: **440.02**
 Dunn, Marina Madeline.: **247.21**
 Dupke, Renato: 309.06D
 Dupont, Marcus: **338.06**
 DuPrie, Kimberly: 150.10
 Dupuis, Christopher Michael.: **145.01**
 Dupuy, Trent: 133.06, **133.07**, 148.12, 349.07, 349.19, 349.34
 Durand, S.: 342.06
 Duranko, Gary: 151.02, 155.05
 Durbin, Meredith: 157.06
 Duriscoe, Dan: 122.03
 Durisen, Richard H.: 211.04D
 Dusenbery, Paul: 242.12
 Dussault, Mary E.: **444.09**
 Dutan, Ioana: 404.03
 Dvorkin, Cora: 327.03D
 Dwarkadas, Vikram: 245.01, 245.08
 Dwek, Eli: **408.04**
 Dyar, Darby: **300.01**
 Dye, Simon: 436.04
 Eakins, Emma: 339.05
 Earl, Nicholas: **150.20**

Early, Laura: 248.09
 Eastman, Jason: **111.01**, 128.01, 152.24, 303.08, 314.02D, 314.04
 Ebeling, Harald: 112.03
 Eckart, Mega E.: 331.06
 Eckersley, Jared: 354.30
 Eckert, Kathleen: 149.50, **354.28**
 Eckleholm, Elliot: 258.13
 Edgar, Roman: 362.08
 Edge, Alastair: 342.29
 Ednie, Michaela: **349.15**
 Edson, Shauna Elizabeth.: **242.20**
 Edwards, Charlotte: 359.10
 Edwards, Kay: 149.60, 251.12, 454.15
 Edwards, Suzan: 229.01
 Efsits, Gabriel: 339.02
 Efstathiou, Andreas: 304.06
 Efstathiou, George: 327.01
 Egami, Eiichi: 112.03
 Egan, Dennis: 215.02D, 322.05
 Egron, Sylvain: 246.36, 355.53
 Ehrenreich, David: 148.18
 Ehsan, Negar: 215.05
 Eidelman, Dave: 361.01
 Eilek, Jean: 257.19
 Eimer, Joseph: 152.19
 Eisenhamer, Jonathan: 436.12
 Eisenhardt, Peter: 304.06, 327.02, 402.01
 Eisenstein, Daniel: 351.01
 Elert, Julia T.: 339.05
 Elitzur, Moshe: 250.22
 Ellis, Justin: 453.09
 Ellis, Richard: 340.09
 Ellison, Sara L.: 123.05, 227.01, 250.02, 357.05
 Elmegreen, Bruce: 248.01, 340.02
 Elmegreen, Bruce G.: **114.06**, 149.57
 Elmegreen, Debra: 149.57, 340.02
 Elowitz, Mark: **452.07**
 Elsworth, Yvonne: 450.13
 Ely, Todd A.: 314.01
 Emami, Najmeh: **227.07**
 Emmons, Ben: 360.13
 Emonts, Bjorn: 342.28
 Eney, Brian: 242.11
 Engelmann-Suissa, Gabrielle: **439.20**
 Engle, Scott: 146.09, 146.15, 148.05, 244.11, **349.36**
 English, Tom: 126.07
 Ennico, Kimberly: 144.03, 355.06
 Enoto, Teruaki: 333.01, 333.07, 450.09, 453.05, **453.11**
 Enriquez, J. Emilio: 132.02, 231.01, **401.02**
 Eracleous, Michael: 150.08, 250.42, 347.09, 347.22
 Erasmus, Nicolas: 115.06
 Erickson, Alan: 354.11
 Erickson, Kristen: 131.01
 Erickson, Mary: **146.15**
 Eriksen, Kristoffer: 446.14
 Errando, Manel: 434.02
 Errani, Raphael: 412.05
 Espallat, Catherine: 339.09
 Espinoza, Néstor: 104.04
 Espinoza Galeas, David
 Abraham.: **347.17**
 Esposito, Massimiliano: 234.02
 Esposito, Thomas M.: 349.07
 Esquerdo, Gil: 104.04, 334.06
 Essick, Reed: 128.07
 Essinger-Hileman, Thomas: 152.19, 314.05D, 419.05
 Estrada, Paul: 147.03
 Etienne, Zachariah: 255.15, 405.04
 Eufrasio, Rafael: 149.52, 347.12
 Evan, Rubyet A.: 127.02
 Evans, Aaron: 320.05
 Evans, Ian N.: **223.01, 238.01**, 238.02, 238.03, 238.04, 238.05, 238.06, 238.07, 238.09, 238.10, 238.11
 Evans, Janet D.: 238.01, 238.02, 238.03, 238.04, 238.05, 238.06, 238.07, 238.09, 238.10, 238.11
 Evans, Nancy: 109.05, **146.09**
 Evans, Sam: 155.04, **339.02**
 Evans, Thomas M.: 211.01
 Evans II, Neal J.: 214.01
 Everett, Mark: 109.02
 Evrard, August: 252.04
 Ewall-Wice, Aaron: 153.01
 Ewall-Wice, Aaron Michael.: 153.05, 153.13
 Ewing, Becca Elizabeth.: **255.04**
 Fabbiano, Giuseppina: 238.01, 238.02, 238.03, 238.04, 238.05, 238.06, 238.07, 238.09, 238.10, 238.11, 238.12, 412.01
 Faber, Sandra M.: 110.03
 Fabian, Andy: 157.13, 241.01, 342.29, 347.01, 347.05, 347.07, 406.07
 Fajb, Gaia: **250.18**, 250.34
 Fabritius, Joseph M.: **252.13**
 Fabrycky, Daniel: 439.25
 Factor, Samuel: 147.17
 Fadda, Dario: **150.11**, 445.12
 Fagan, Ben: 242.14
 Faherty, Jacqueline K.: **156.01, 158.14**, 158.15, 158.16, 349.23, 349.33, 349.37, 444.13
 Faisst, Andreas: 354.08
 Falco, Emilio: 142.08, 440.10, 440.14
 Falcone, Abraham: 355.15, 355.28, 355.35, 355.44, 447.05
 Falkner, Sebastian: 243.11
 Fan, Haoyu: 331.01
 Fan, Xiaohui: 258.17, 304.02D, 440.11
 Fang, Xiao: **209.04**
 Fanning, William Charles.: **148.03**
 Farahi, Arya: 252.04
 Fardal, Mark: **212.06**
 Farner, William: **448.03**
 Farnham, Tony: 452.04
 Farnocchia, Davide: 115.07
 Farrah, Duncan: 149.02, 304.01, **304.06**
 Farrington, Christopher: 152.05, 152.26
 Fassbender, Rene: 327.02
 Fassnacht, Christopher: 415.04D
 Fasy, Brittany: 213.07
 Faucher-Giguère, Claude-André: 136.04
 Faulkner, Danny R.: 244.03, 244.10
 Fausnaugh, Michael: **439.09**, 439.11, 439.12
 Featherstone, Nicholas A.: 133.03
 Fecteau-Beaucage, David: 342.29
 Feder, Richard: **151.04**
 Feigelson, Eric: **246.34**
 Feigelson, Eric D.: 136.08
 Feigenson, Thomas: 157.03
 Feinberg, Lee: 355.29, 419.08
 Feinstein, Adina: **104.07**
 Fekel, Francis: 453.14
 Feldman, Paul: 355.34, 450.07
 Feldmeier, John: 241.10
 Felfeli, Zineb: 111.08
 Felton, Ryan: **439.23**
 Feng, Katherina: 410.01
 Feng, Xiaotong: 440.11
 Feng, Yuting: **252.15**
 Ferdman, Robert: 255.18
 Ferguson, Annette: **201.01**
 Ferguson, Annette M N.: **201.01**
 Ferguson, Henry C.: 149.51, 258.01, 402.01
 Ferguson, Jason: 123.05, **440.04**
 Ferkinhoff, Carl: 112.02D, 251.05
 Ferland, Gary: 203.01, 241.01
 Fernandes, Alexandre Giongo.: **237.15**
 Fernandes, Rachel: 437.02, 449.08
 Fernandez, Rodrigo: 308.05
 Fernandez, Ximena: 210.05, 441.03
 Fernandez de Castro, Patricia: **359.05**
 Fernandez-Trincado, Jose: 250.36, 411.02D
 Feroci, Marco: 140.06
 Ferrara, Elizabeth: 224.06
 Ferrarese, Laura: 127.05D
 Ferrari, Marc: 355.53
 Ferrari, Tiberio: 436.07
 Ferraro, Nicholas: **247.18**
 Ferreira, Denelis: 444.12
 Ferreras, Ignacio: 149.39, 357.07
 Ferrigno, Carlo: 243.11, 438.19
 Feuille, Diane: 411.02D
 Fey, Alan: 436.02, 440.20
 Fienberg, Richard Tresch.: 220.02
 Figura, Charles: **114.04**
 Filion, Carrie: **153.16**
 Filippazzo, Joeseeph: 158.14
 Filippazzo, Joseph: 148.14, 349.33
 Filippenko, Alexei: 245.01
 Finch, C.: 246.01, 349.17
 Findlay, Joseph: **250.07**
 Finkbeiner, Douglas: 327.03D, 350.02, 354.01
 Finke, Justin: 123.04, 132.07, 140.10, 205.03D, **250.19**
 Finkelstein, Keely: **156.02**, 357.07
 Finkelstein, Steven: 127.03D, 149.25, 149.33, 258.17, 328.02, 357.07
 Finn, Dr. Rose: 354.18
 Finn, Molly: 360.01
 Finn, Susanna: 246.41, 355.16
 Finnegan, Daniel: **149.31**
 Finney, Elizabeth E.: **351.12**
 Finoguenov, Alexis: 304.03
 Fiore, William: **255.01**
 Firebaugh, Ariel: 360.01
 Fischer, Chrisitan: 445.12
 Fischer, Christian: 450.07
 Fischer, Jacqueline: 227.08
 Fischer, Travis: **250.41**, 250.45, 250.48, 404.05
 Fischer, William J.: 150.38, 355.40
 Fish, Vincent: 347.11, 347.16
 Fishbach, Maya: **405.07**
 Fisher, Robert: **417.01**, 446.07
 Fisher, Ryan Patrick.: **255.07**
 Fitts, Alex: 356.05
 Fitzgerald, Michael: 150.13, 155.06
 Fitzpatrick, Michael: 362.05
 Fix, Mees: 145.05, 150.38, 355.40
 Fixsen, Dale: 152.19, 314.05D, 419.05
 Flagey, Nicolas: 222.01, **445.03**
 Flaherty, Kevin: **129.01**, 147.09, 147.15, 147.17, 147.18
 Flasar, F. M.: 452.03
 Fleming, Scott W.: **158.13**
 Fletcher, Corinne: **424.04D**
 Flewelling, Heather: **102.02**, 308.06, **436.01**
 Flohic, Helene M L G.: 347.09
 Flores, Anel: 354.33
 Flores, Anthony M.: **440.22**
 Flores, Jose Antonio.: **136.04**
 Florez, Lina Maria.: **362.07**
 Florian, Michael: 250.41
 Flury, Sophia: **250.40**
 Fogarty, Kevin: 246.39, **403.02**
 Fogle, Bryan: 242.18
 Foley, Michael: **408.01**
 Foley, Ryan: 153.03, 308.06, 408.01
 Folkner, William M.: 115.01
 Follette, Katherine: **303.02, 316.01**, 349.15
 Fonseca, Emmanuel: 243.13
 Fonseca, Gloria: 354.13
 Foott, Bettymaya: 142.01
 Forbrich, Jan: 125.07
 Ford, Amanda Brady.: 302.05
 Ford, K.E. Saavik.: **421.05**
 Ford, K.E.Saavik: 156.05, 250.18, 250.34, 325.05, 359.03
 Ford, Pam: 215.02D, 322.05
 Foreman-Mackey, Daniel: **225.01**
 Forman, William: 252.03, 252.05, 406.05, 406.06, 441.01
 Formanek, Martin: 113.02, 113.03, 113.06, **139.02**
 Fornasini, Francesca: 149.05
 Forrest, Ben: **110.02D**, 110.05
 Fors, Octavi: 150.23, 231.06, 310.03, 354.12
 Forster, Francisco: 446.06

Fortenberry, Alexander: **153.24**
Fortin, Pascal: 142.08
Fortino, Austin Fox.: **150.32**, 150.33, 150.34
Fortney, Jonathan: 207.01, 211.06, 211.07, 228.01, 228.07, 329.08, 410.01, 439.17, 439.24, 450.04
Fortson, Lucy: 110.07, **362.03**
Forveille, Thierry: 129.06, 147.13
Fossati, Luca: 349.06
Foster, Adam: 237.20, **253.03**, 338.06
Foster, Griffin: 231.01
Fowler, Julia: 148.14, **355.19**
Fox, Andrew: 150.38, 237.05, 355.40, **411.01**
Fox, Ori: 245.01, 245.02, **308.07**, 408.04
Fraga, Luciano: 149.50
Fragkos, Anastasios: 251.10
Frail, Dale: 124.02, 354.15
Fraire, Jonathan: 111.04, 148.14, 427.04
Fraire, Jonathan D.: **410.01**
Fraknoi, Andrew: 220.02, **242.12**
France, Kevin: 111.05, 147.11, 234.01, **349.06**, 445.05
Franczowski, Anna: 255.01
Frank, Juhan: 157.02
Frank, Kari A.: 245.08
Fraser, Wesley C.: 115.03, 402.01
Frayer, David: **149.27**, 152.15, 152.17, 247.20, 322.03, 322.04
Frazer, Chris: **311.03D**
Frederick, Sara: **250.39**
Freeland, Emily: 149.19
Freeman, Marcus J.: 220.06
Freire, Paulo: 243.09, 243.16
Freise, Andreas: 255.05
French, David M.: **302.03D**
French, Debbie: 155.06
Frenk, Carlos: 212.04, 454.02
Frerking, Margaret: 158.02
Frerking, Margaret A.: **246.32**, 361.13
Frey, Grace: 339.05
Frey, Katie: 143.03
Friedman, Andrew: 209.03
Friel, Eileen D.: 348.04
Fries, Logan B.: 127.02
Friesen, Rachel: **322.02**, 342.21
Frimann, Søren: 147.10
Frinchaboy, Peter: **344.13**
Fritschel, Peter: **433.01**
Fritze, Hannah: **347.10**, 354.13
Fröhlich, Carla: 408.03D
Fromenteau, Sebastien: 225.04
Froning, Cynthia S.: **111.05**
Frontiere, Nicholas: 150.22
Frostig, Danielle: **152.11**
Frouard, Julien: **436.02**, 440.20
Fruchter, Andrew: 153.21, 327.02, 347.22, **405.06**
Frye, Brenda: 306.04, 354.14, 454.10, 454.12
Fu, Guangwei: **111.04**
Fu, Hai: 316.06
Fu, Wanying: **257.12**
Fu, Yuming: 440.11
Fuerst, Felix: 243.11
Fukui, Yasuo: 136.11
Fukumura, Keigo: 404.04, **405.05**
Fulda, Paul: **255.10**
Fullard, Andrew G.: 341.02
Fulmer, Leah M.: **348.02**
Fulton, Benjamin: 104.04, 104.07, 211.08, 329.01, 439.13, 439.22
Furlanetto, Steve: 149.51, 354.07
Fusco, Thierry: 246.40
Fuse, Christopher: **144.16**, 148.21
Gabaldon, Charris: **247.04**
Gable, Alexander: **152.06**
Gabor, Paul: 142.08
Gaetz, Terrance: 241.14
Gagliano, Alexander: **153.02**
Gagné, Jonathan: 158.14, 158.15, **235.06**, 246.13, 349.37
Gaidos, Eric: 133.06, 349.40
Gajjar, Vishal: **132.02**, 231.01, 243.18, 243.19, 354.05
Galache, J. L.: 115.06
Galamez, Audrey: 306.01D
Galan, Cezary: 453.14
Galaz, Gaspar: **425.01**
Galeazzi, Massimiliano: 331.06
Gall, E.E.E.: 308.06
Gallagher, John S.: 348.02, 429.04D
Gallagher, Molly: 322.04
Gallagher, Sarah: 215.06, 250.24
Gallant, Margaret A.: 452.08
Gallardo, Samavarti: **150.30**, 150.31
Gallego, Angelina Ramona.: **360.14**
Gallego, Laly: 237.06, 311.07
Gallegos, Monica: **347.19**
Gallo, Elena: 105.06, 349.24
Galvan-Madrid, Roberto: 247.23
Gandhi, Poshak: 343.01
Gandhi, Pratik Jigish.: **438.15**
Gandhi, Siddarth: 211.03
Gandilo, Natalie: 152.19, **314.05D**
Ganel, Opher: 355.02
Ganesh, Shivani: 351.03
Gangler, Emmanuel: 152.09
Gangolli, Nakul: **255.03**
Ganguly, Rajib: 250.42, 250.44
Gao, Feng: 123.03D
Gao, Peter: 246.13, **427.05**
Garani, Jasmine I.: **349.07**
Garaud, Pascale: 450.02
Garcia, Beatriz: 362.18
Garcia, Cedar: 351.09
Garcia, Javier: 140.08, **435.05**
Garcia, Rafael A.: 450.13
Garcia Perez, Ana: 424.03
Garcia Soto, Aylin: 238.14, **244.12**
Garcia-Benito, Rubén: 130.01
Garcia-Miro, Cristina: 152.07
Gardner, Cristilyn N.: 111.07, **148.07**, 148.11, 148.27, 148.31, 148.32, 148.35, 148.36, 148.37
Gardner, Jonathon: 355.34
Garhart, Emily: 207.01
Garland, Ryan: **133.05**
Garnavich, Peter: 245.12, 257.02, 358.04, **358.09**, 408.01, 414.01, 446.06
Garner, Ray: **312.03**
Garofali, Kristen: **109.06D**
Garraffo, Cecilia: 148.16
Garrett, Daniel: **246.04**, 246.06, 246.11
Garsden, Hugh: 436.13
Garver, Bethany R.: 111.07, 148.07, 148.27
Garver, Bethany Ray.: 148.11, 148.31, **148.32**, 148.35, 148.36, 148.37
Garver-Daniels, Nathaniel: 255.18
Garza, Sierra: 153.05, **153.13**
Gastaldello, Fabio: 252.05
Gatkine, Pradip: **247.10**
Gaudi, B. Scott.: **103.03**, 148.41, 246.07, 246.30, **310.08**, 314.02D, 355.36, 361.06, 403.05
Gaunt, Caleb: 250.13
Gautam, Abhimat: 237.06, 311.07
Gautam, Abhimat Krishna.: **212.01**, 311.02
Gavin, Andrew: **442.05**
Gawiser, Eric: 239.02, 426.03, **426.06**
Gay, Pamela: **113.01**, **155.01**, 155.02, 155.03, 220.02, **242.15**, 436.16
gburek, Timothy: 426.05
Ge, Jian: 302.01, 302.02, 349.02
Ge, Mingyu: 243.02
Geach, James: 258.05
Geballe, Tom: 354.30
Gebhardt, Henry: **420.06**
Geers, Vincent C.: 342.14
Geha, Marla: 237.10, 354.07
Gehrels, Neil: 320.03
Gehrz, Robert D.: 424.02D
Geiger, Nicole P.: **440.20**
Geis, Gena: **144.05**
Geis, Norbert: 445.12
Geisler, Doug: 344.10, 413.03, 450.11
Geist, Emily: **244.23**
Gelino, Chris: 158.15
Geller, Aaron M.: 257.22
Gendon-Marsolais, Marie-Lou: 406.07
Gendre, Bruce: 107.08, 442.07
Gendreau, Keith C.: 140.06, 157.11, 157.13, **160.01**, 243.17, 333.03, 341.01, 347.01, 347.05, 347.07, 349.12, 453.05, 453.11
Gendron-Marsolais, Marie-Lou: **306.03D**, **342.29**
Generozov, Aleksey: 422.05, **423.04D**
Genier, Fred: **351.02**
Gennaro, Mario: 411.04
Gentile, Peter: 157.12
Genus, Amelia: **359.09**
Geogdzhayeva, Maria: 444.14
Georganopoulos, Markos: 250.16, 250.30, 257.19, 323.02, 323.04D, 440.17
Gerber, Jeffrey M.: **348.04**
Gerdes, David: 144.04
Gerin, Maryvonne: 355.13
Gerosa, Davide: 325.04
Gersh-Range, Jessica: 246.18, 246.44
Getman, Konstantin V.: 136.08
Gezari, Suvi: **102.06**, 105.02D, 347.18, 347.22, 405.02D, 405.03
Ghavamian, Parviz: 157.15, **408.05**, 446.12
Ghez, Andrea: 212.01, 214.05D, 237.06, 311.02, 311.07
Ghigo, Frank: 152.17
Ghosh, Tapasi: 245.19
Giacintucci, Simona: 215.01, 342.30, 354.11, 354.15
Giacomazzo, Bruno: 255.15, 405.04
Giampapa, Mark S.: **234.02**
Giannetti, Andrea: 114.04
Giavalisco, Mauro: 149.47
Gibb, Erika: 144.13
Gibbs, Aidan: 360.11
Gibbs, John C.: 339.05
Gibbs II, Danny G.: 238.01, 238.02, 238.03, 238.04, 238.05, 238.06, 238.07, 238.09, 238.10, 238.11
Giblin, Timothy W.: 152.02, 442.07
Gibson, Coyne Andrew.: 442.03
Gibson, Neale: 427.04
Gibson, Rose: **344.07**
Gies, Douglas: 152.05, 152.26, 244.04, **244.24**
Gilbert, Karoline: 354.07
Gilbert, Karoline M.: **354.32**
Gilbertson, Woodrow: **347.12**
Gilda, Sankalp: **349.02**
Giles, Daniel: **332.03**
Giles, Tucker: 150.25
Gilfanov, M.: 408.05
Gill, Ajay: **342.08**
Gilligan, Christina: 344.10
Gillon, Michael: 427.09
Gilmer, Matthew: **408.03D**
Gim, Hansung: 210.05
Ginsburg, Adam: 136.15, 445.01
Giorla Godfrey, Paige A.: 349.22
Giovannelli, Riccardo: 340.06
Girardi, Leo: 362.01
Girart, Josep M.: 257.07
Giryanskaya (Morozova), Viktoriya: 245.16, **308.03**
Given, Gabriel: **356.04**
Gizis, John E.: 349.10
Gladders, Michael: 250.41, 327.02
Gladysz, Wojciech: 325.04
Glaser, Joseph Paul.: 257.21, **257.22**
Glazer, Kelsey Samantha.: 242.11, **359.10**
Glazer, Stuart: 355.29
Glenn, Jason: **121.02**, 247.09
Glennon, Derek Ray.: **255.14**
Glesener, Lindsay: 414.08
Glidden, Ana: 439.09, 439.11, **439.12**
Glikman, Eilat: 304.01
Gliozzi, Mario: 123.05, 250.02, 250.10, 257.06
Glotfelty, Kenny J.: 238.01, 238.02, 238.03, 238.04,

238.05, 238.06, 238.07,
 238.09, 238.10, 238.11
 Gnilka, Crystal L.: 250.45,
 250.48, **404.05**
 Godfrey, Paige: **256.05**
 Godon, Patrick: 358.05
 Godwin, Caleb: **248.05**
 Goebel, Sean B.: 152.14, 152.16
 Goeke, Erin: 231.06
 Goetz, Eric: **438.07**
 Goffrey, Tom: 326.04
 Gogus, Ersin: 333.06
 Goh, Tze: **258.13**
 Gohil, Raj: **222.02D**
 Goicoechea, Luis: 440.14
 Goldberg, David: 252.13
 Goldsmith, Ben: 242.03
 Goldsmith, Paul: **130.06**,
 231.05, 247.02, 322.03
 Goldsmith, Stephen: 142.01
 Goldstein, Adam: **107.07**,
 140.06, **262.02**
 Goldston, David: **432.01**
 Golimowski, David A.: 147.12
 Golish, Dathon: 452.05
 Golovich, Nathan: 252.03
 Gomez, Anay: 444.12
 Gomez, Facundo: 454.02
 Gomez, Jose: 404.03
 Gomez, Sebastian: 423.06
 Gomez, Thomas: **452.02**
 Goncalves, Thiago: 149.17,
 440.03
 Gong, Nathaniel: 339.05
 Gong, Qian: 152.08, 220.08,
246.20, 355.47
 Gonzales, Eileen: 349.33,
349.37
 Gonzales, Erica Jasmine.:
 329.01, **410.03**, 439.13
 Gonzalez, Andrea: 149.60,
 251.12, 454.15
 Gonzalez, Anthony: 327.02
 González, Gabriela: **236.01**
 Gonzalez Quiles, Junellie:
354.09
 Goobar, Ariel: 153.21, 327.02
 Good, John: 150.01, 150.14
 Goodman, Alyssa: 125.07,
 230.05D
 Goodman, Jordan: 453.10
 Goodwin, Adelle: 309.03
 Goodwin, Simon: 109.01
 Gopalswamy, N.: **220.08**
 Gordon, Brian: 246.18
 Gordon, Iouli: 148.46
 Gordon, Karl D.: 127.01, 355.10
 Gordon, Michael S.: 348.13
 Gordon, Michael Scott.:
424.02D
 Gorjian, Varoujan: 151.02,
 155.05, 155.06, 228.04, 329.01
 Gorsuch, Mary Katherine:
150.27
 Gorti, Uma: 129.06, 133.01,
 147.03, 147.13, 358.02, 437.04
 Gosnell, Natalie M.: 244.06,
 344.08
 Goss, Miller: 247.23
 Gotthelf, Eric: 453.10
 Gottlieb, Amy M.: 243.11
 Gottlieb, Carl: 408.06
 Gottlieb, Sophia: **258.05**
 Gourджи, Kelly: 243.18, 243.19
 Gowardhan, Avani: **149.02**
 Goyal, Jayesh: 211.01
 Gozzard, David: 215.03
 Grabowski, Kathleen: 146.13
 Grady, Carol: 437.02, 449.07
 Graessle, Dale E.: 238.01,
 238.02, 238.03, 238.04,
 238.05, 238.06, **238.07**,
 238.09, 238.10, 238.11
 Graham, James: 211.05,
 329.04D
 Graham, John: **107.01**
 Graham, Matthew: **354.16**,
 362.04
 Graham, Peter: 255.16
 Graham, Sean: 339.12
 Grainge, Keith: 215.03
 Grammer, Wes: 342.06, 342.09
 Granados Contreras, Agueda
 Paula.: **410.05D**
 Grand, Robert: 454.02
 Granot, Jonathan: 333.06
 Grant, Carolyn S.: 362.17
 Grasha, Kathryn: **114.02D**
 Graus, Andrew: 257.13
 Gravestock, Charles: 215.03
 Greaves, Jane: 342.17
 Grebel, Eva K.: 257.11, 413.01
 Green, Gregory M.: 102.04,
 354.01
 Green, Gregory Maurice.:
350.02
 Green, Joel: **232.02**, 313.01
 Green, Paul: 157.04, 223.05
 Green, Richard F.: **122.03**,
 440.11
 Greenbaum, Alexandra Z.:
 355.10
 Greenberg, Adam: 115.06
 Greene, Jenny: 105.06,
 123.03D, 149.51, 250.35,
 440.05, 440.21
 Greene, Thomas P.: 355.10
 Greenhill, Lincoln: 436.13
 Greer, Frank: 246.18
 Grefenstette, Brian: 414.08
 Greisen, Eric: 247.15
 Grell, Gabriel: 148.03
 Grier, Catherine: **250.25**,
 250.36, 440.16
 Grier, Jennifer: 155.01, 155.02
 Grier, John D.: 238.01, 238.02,
 238.03, **238.04**, 238.05,
 238.06, 238.07, 238.09,
 238.10, 238.11
 Griessmeier, Jean-Mathias:
 310.05D
 Griffin, Elizabeth:
 Griffin, Sean: **361.09**
 Griffith, Caitlin: 148.26
 Griffiths, Alex: 306.04
 Grillmair, Carl J.: **344.02**
 Grillo, Claudio: 438.15
 Grin, Daniel: 356.04, 438.05
 Grindlay, Jonathan:
 Grindlay, Jonathan E.: 205.04,
423.06
 Grocholski, Aaron: 344.10
 Groenewegen, M. A T.: 109.07,
 348.10
 Groff, Tyler: 152.10, 303.07,
355.47
 Grogin, Norman: 354.14,
 355.33, 357.07
 Groh, Jose: 157.16
 Gromadzki, Mariusz: 136.08
 Gronwall, Caryl: 149.28
 Groom, Steven: 362.04
 Groppi, Christopher: 149.15,
 231.05
 Grove, J. Eric.: **355.51**
 Groves, Brent: 125.07
 Grudic, Michael: **313.06**,
449.06
 Grudich, Michael: 114.03D
 Grundy, William M.: 144.03
 Grunwald, Warren: **402.04**
 Guainazzi, Matteo: 123.01
 Guarracino, Daniel: 143.03
 GUDIEL, ANDREA: **314.07**
 Guedel, Manuel: 136.14
 Guenther, H. Moritz: 146.09,
 237.22
 Guerras, Eduardo: 441.02
 Guerrero, Natalia: 439.09,
439.11, 439.12
 Güesten, Rolf: 112.02D
 Gugliucci, Nicole: 444.15
 Guhathakurta, Puragra:
 127.05D, 149.36, 252.15,
 258.07, **306.02**, 351.11, 453.02
 Guillard, Pierre: 149.19
 Guillemot, Lucas: 243.05
 Guillochon, James: 158.10
 Guillot, Sebastien: 157.13,
 243.17
 Guinan, Edward: 146.09,
 146.15, 148.05, 244.11
 Guinan, Edward Francis.:
 349.36, **401.06**
 Guiriec, Sylvain: **107.02**
 Gull, Theodore: **108.04**,
348.11
 Gullede, Deborah Jean.:
145.05
 Gully-Santiago, Michael A.:
 439.07, 439.10
 Gültekin, Kayhan: 347.14
 Gundersen, Joshua: 322.04
 Gunshefski, Linda: **348.15**
 Guo, Xueying: **329.05**
 Guo, Yicheng: **110.03**, 127.02
 Gupta, Anshu: **406.02D**
 Gupta, Arvind F.: **344.01**
 Gupta, Harshal: 408.06
 Gupta, Nandita: 453.02
 Gurvich, Alex: 136.04
 Gurwell, Mark: 125.07
 Gusinskaia, Nina: 233.02
 Guszejnov, David: **114.03D**,
 313.06, 449.06
 Gutierrez, Elizabeth: **136.07**
 Guver, Tolga: 157.13, 453.11
 Guy, Michael: 338.05
 Guyon, Olivier: 152.10, 303.07,
 419.08
 Guzik, Joyce A.: 315.01
 Guzman, Giannina: **151.03**
 Guzman, Rafael: 406.04D
 Gwyn, Stephen: 127.05D
 Ha, Richard: 232.03, 360.09
 Haas, J. Patrick.: 361.07
 Haas, Roland: 255.14
 Haas, Sean: **147.03**
 Habbal, Shadia: 220.02
 Habbal, Shadia Rifai.: **220.07**
 Haber, Rana: 150.18
 Habertzettl, Lutz G.: 357.08
 Hack, Warren: 436.12
 Hadley, Kathryn: 330.01
 Haffner, L. Matthew.: 237.16,
 247.22, **429.03**
 Haffner, Lawrence Matthew.:
 230.06, 247.31, 340.04
 Hagan, James Brendan.: 147.12
 Hagen, Cedric: 349.24
 Haggard, Daryl: 223.05
 Haider, Syed Jibrán: **440.08**
 Hailey, Charles: 435.06, 453.10
 Hailey-Dunsheath, Steven:
 251.05
 Haiman, Zoltan: 325.05
 Hain, Roger: 238.01, 238.02,
 238.03, 238.04, 238.05,
238.06, 238.07, 238.08,
 238.09, 238.10, 238.11
 Hainaut, Olivier R.: 102.08
 Hainline, Kevin N.: 105.01
 Haji, Umran: **237.13**
 Hala, Fnu: **362.14**
 Hales, Chris: 251.06
 Hall, Diane M.: 238.01, 238.02,
 238.03, 238.04, 238.05,
 238.06, 238.07, 238.09,
 238.10, 238.11
 Hall, Donald NB.: 152.14,
 152.16
 Hall, Jeffrey C.: **122.07**,
142.04, 142.08
 Hall, Patrick: 250.36
 Hall, Ryan: 351.13
 Hallenbeck, Gregory: 351.13
 Hallinan, Gregg: 124.02, 231.02
 Halpern, Jules P.: 347.09,
 453.06
 Halpern, Mark: 112.02D,
 152.19, 314.05D, 419.05
 Halverson, Sam: 152.18,
 246.08, 246.45
 Halverson, Samuel: 152.08
 Hamaguchi, Kenji: 341.01,
349.12, 450.09
 Hamann, Fred: 250.35
 Hamann, Wolf-Rainer: 348.02
 Hambleton, Kelly: 146.01,
 244.20
 Hamden, Erika: 446.17
 Hamill, Colin: **258.11**, 357.04
 Hamilton, Douglas: 115.02
 Hamilton, Kathleen: **361.01**
 Hammerstein, Erica: **347.14**
 Han, Jiabin: **212.04**
 Han, Jiwon: **351.07**
 Han, Xianming: 244.14
 Hanany, Shaul: **121.01**, 140.17,
 140.18
 Hanayama, Hidekazu: 446.08
 Hancock, Daniel A.: 246.24
 Hancock, Danielle: 360.01
 Hand, Kevin: 106.03
 Haniff, Chris A.: 314.03
 Hankins, Matthew: **230.04D**
 Hanley, Jeffrey: 355.29
 Hanlon, L.: 438.19
 Hansen, Stephanie: 452.02
 Hansen, Terese: 413.07
 Harada, Nanase: 125.07, 237.14
 Harbach, Laura Marshall.:
148.16
 Harbo, Peter N.: 238.01,
 238.02, 238.03, 238.04,
 238.05, 238.06, 238.07,
 238.09, 238.10, 238.11
 Hardcastle, Martin: 123.01

Hardegree-Ullman, Kevin: 211.08, 329.01, **427.06**
 Hardegree-Ullman, Melody: 360.11
 Hardegree-Ullman, Michael: 360.11
 Harding, Alice: 243.05, 243.17, 333.06, 453.05, 453.11
 Harding, Pat: 140.10
 Harding, Paul: 257.12
 Hare, Jeremy: **238.15**, 333.02, **358.03**
 Hargis, Jonathan R.: 150.05
 Harish, Santosh: 149.07, **149.33**
 Harker, David E.: 350.06
 Harl, Linda: 339.02
 Harman, Pamela: 131.05, **131.06**
 Harmer, Dianne: 241.04
 Harmon, Robert: **349.27**
 Harness, Anthony: 439.05
 Harper, Doyal: 247.24
 Harriett, Edward: **244.07**
 Harrington, Joseph: 148.02, **148.08**, 410.04, 439.18
 Harrington, Kathleen: **215.04D**
 Harrington, Kevin: **257.17**
 Harris, Andrew: 322.04, 359.07
 Harris, Hugh C.: 157.10
 Harris, James Austin.: 446.02
 Harris, Madison: **453.02**
 Harrison, Fiona: 223.04, 320.04, 343.01, 435.05, 440.05
 Harrison, Matthew F.: 354.18
 Harrison, Thomas E.: 109.05
 Hart, Robert: 216.06
 Hart, Steve: 444.01
 Hartkopf, William: 434.01
 Hartman, Joel D.: 148.02, 201.07, 246.12
 Hartman, Katherine: **146.14**
 Hartman, Zachary: **244.15**
 Hartmann, Dieter: 123.04, 140.06, 242.18, 404.03, **419.02**
 Hartmann, Lee: 114.05, 136.02
 Harvey, Adam: **440.17**
 harvey, david: 355.47
 Harwood, Jeremy: 342.28
 Hasan, Farhanul: **136.05**
 Hasan, Hashima: **131.01**
 Hasinger, Guenther: 250.11, 436.04
 Hasselfield, Matthew: 112.02D
 Hasselquist, Sten: **411.02D**, 424.03
 Hathi, Nimish: **149.14**, 258.01, 354.14, 357.07
 Haughton, Jared: **239.04**
 Häußler, Boris: 127.02
 Hawkins, Keith: 443.01
 Hawkins, Luke: 150.06
 Hawkins, Steven: 255.18
 Hayden, Brian: 153.21, **327.02**
 Hayes-Gehrke, Melissa: **359.07**, **359.08**
 Haynes, Martha P.: 252.18, 340.06, 351.08, 351.12, 351.13, 354.19, 359.05
 Haynie, Anastasia: **257.03**
 Hayward, Christopher: 136.04, 149.46
 Hayward, Thomas L.: 361.18
 Haywood, Raphaelle: 427.03
 Hazelton, Bryna: 247.27
 Hazenberg, Francois: 153.21
 Heald, George: 243.18
 Heap, Sara: **121.04**, 140.09, 140.13, 140.16, **355.30**
 Hearty, Fred: 152.08, 152.18, 246.08, 246.45, 411.02D
 Heckman, Timothy M.: 309.02D
 Hedges, Christina: 431.01
 Hedges, Christina L.: 439.07, **439.10**
 Hedlund, Audrey R.: 339.05
 Hees, Aurelien: 237.06, 311.02
 Hegarty, Sarah: 151.08
 Heger, Mairead: 326.05D
 Heida, Marianne: 341.07
 Heilmann, Ralf: **355.26**
 Heintz, Tyler: **246.16**
 Heinz, Sebastian: **130.03**, 350.01, 350.03, 429.06
 Heinze, Aren Nathaniel.: **109.04**
 Heitsch, Fabian: 311.03D
 Hejazi, Neda: **349.20**
 Hekker, Saskia: 450.13
 Helgason, Kari: 123.04
 Hellbourg, Greg: 132.02, 231.01, 342.24
 Hellier, Coel: 410.04, 427.09
 Hellinger, Doug: 258.13
 Hellwing, Wojciech: 213.07
 Helmboldt, Joseph: 215.01, **242.04**, 354.11
 Helmich, Frank: 231.05
 Helou, George: 354.29, 354.36, 362.04, 402.01
 Helton, Andrew: 358.02, 446.01
 Hemenway, Mary Kay: 156.02
 Hemler, Zachary: **250.36**
 Hemmati, Shoubaneh: 136.16, **153.08**, 328.05D
 Hempel, Maren: 413.03
 Hemphill, Paul B.: 243.11
 Hemphill, Paul Britton.: **233.06**
 Hendel, David: **412.04D**
 Henderson, Calen: **310.06**
 Henderson, Todd: 152.24
 Hendrix, Amanda: 452.07
 Henkel, Christian: 123.03D
 Hennawi, Joseph F.: 203.04D
 Henneken, Edwin: 143.03, 362.17
 Hennessey, Ryan: **347.16**
 Henny, Kiana: **247.27**
 Henrici, Andrew: **247.03**
 Henry, Alaina: 355.12
 Henry, Kari: **152.12**
 Henry, T.: 246.01
 Henry, Todd: 157.09, **349.17**, 349.18, 434.01
 Henson, Gary: 146.11
 Henze, Martin: **414.03**
 Herbst, Eric: 247.01
 Herczeg, Greg: 414.05D
 Herger, Brendan: 245.14
 Hermanek, Keith: **344.15**
 Hermes, JJ: **132.01**, 145.03, 354.12, 453.04
 Hernandez, Andrew: **348.06**
 Hernandez, Audra: 150.16
 Hernandez, Betsy: **149.26**, **444.14**
 Hernandez, Svea: **413.02D**
 Hernandez Santisteban, Juan: 233.05D
 Hernanz, Margarita: 140.06, 358.11
 Hernquist, Lars: 250.12, 412.02D
 Herpich, Fabio: 436.07
 Herrera, Daniel: 146.13
 Herrera-Camus, Rodrigo: 130.07
 Herrmann, Kimberly: 241.10
 Herrold, Ardis: **444.02**, 444.06
 Herter, Terry: 230.04D
 Hess, Kelley: **210.05**, 441.03
 Hess, Kelley M.: 149.23, 354.04
 Hess, Larry A.: 215.05
 Hess, Logan: **149.01**
 Hess Webber, Shea A.: **315.04**
 Hessels, Jason: **243.19**
 Hessels, Jason W T.: 132.02, 233.02, 233.05D, 243.09, 243.13, 243.16, 243.18, 453.15
 Hewawasam, Kuravi: 246.41
 Hewett, Paul: 222.05D, 250.31
 Hewitt, Ian: **248.04**
 Hewitt, Jacqueline: 153.05, 153.13
 Hewitt, Jennifer: 250.16, 323.04D
 Heyrovsky, David: **438.16**
 Hickish, Jack: 132.02, 231.01
 Hickox, Ryan C.: **105.01**, 216.04, **223.08**, 258.05
 Hicks, Brian C.: 215.01
 Higdon, James: 112.02D
 Higdon, Sarah: 112.02D
 Hildebrandt, Hendrik: 327.02
 Hildebrandt, Sergi: **158.03**
 Hill, Frank: 158.07
 Hill, Joanne E.: 355.55
 Hill, Matthew: 148.14
 Hillenbrand, Lynne: 349.09, 402.01, 439.13, 450.12
 Hillsberry, Daniel: 402.05, 402.06
 Hillwig, Todd: 146.11, 241.04
 Hilton, Gene: 112.02D, 152.19, 215.02D, 314.05D, 322.05, 419.05
 Hilton, James: 362.08
 Hilton, Matt: 327.02
 Hily-Blant, Pierre: 129.06, 147.13
 Himes, Michael D.: 148.08
 Hindman, Lauren: 250.13, **250.37**
 hines, Dean C.: 147.12, 147.19
 Hinkel, Natalie Rose.: **120.01**
 Hinkle, Kenneth: **453.14**
 Hinkley, Sasha: 204.03
 Hinshaw, Gary: 152.19, 314.05D, 419.05
 Hintz, Eric G.: **146.05**, 146.12, 244.21, 348.05, 348.06
 Hintz, Maureen L.: 146.05
 Hinz, Joannah: 142.08
 Hirao, Yuki: **246.17**
 Hirata, Christopher M.: 209.04, 402.01
 Hirata, Mickie: **152.14**
 Hirota, Tomoya: 342.21
 Hirsch, Lea: 211.08, 329.01, 439.13
 Hirschauer, Alec Seth.: **312.02D**
 Hirschi, Raphael: 408.03D
 Hix, William R.: 358.11, 446.02
 Hlavacek-Larrondo, Julie: 306.03D, 342.29, 406.07
 Hlozek, Renée: 245.03
 Ho, Anna: 243.09
 Ho, Kelly: **348.01**
 Ho, Luis: 320.02
 Ho, Shirley: 242.18
 Ho, Wynn: 333.07
 Ho, Wynn CG.: **224.01**, 243.17, 453.11
 Hoadley, Keri: 147.11, **446.17**
 Hoag, Austin: 454.10, 454.12
 Hoag, Ava: 246.16
 Hoang, Bao-Minh: 347.20
 Hoang, Thiem: 414.04
 Hobbs, Lew M.: 331.01
 Hodapp, K.: 152.14, 355.10
 Hodapp, Klaus: 436.04
 Hodge, Jacqueline: 222.03
 Hodges-Kluck, Edmund: 237.17
 Hoekstra, Henk: 327.02
 Hoffman, Jennifer L.: 245.07, **341.02**
 Hoffman, Yehuda: 258.10
 Hoffmann, Samantha: **150.36**, 420.07
 Hofmann, Ryan: **148.25**
 Hogan, Jason: 255.16
 Hogan, Michael: 342.29
 Hogg, David: 349.25
 Hogg, J. Drew: **347.02**
 Holberg, Jay: **157.10**, 354.17, 354.17
 Holbrook, Jarita: **220.04**
 Holden, Bobby: 402.04
 Holland, Anne: 242.12
 Hollenbach, David: 231.05
 Holler, Bryan J.: 144.03, 144.15, 355.17
 Holley-Bockelmann, Kelly: 244.17
 Hollowood, Devon: 252.04
 Holman, Megan: **147.06**
 Holte, Elias Peter.: **246.02**
 Holtzman, Jon: 411.02D, 450.13
 Holwerda, Benne W.: 231.07
 Holwerda, Benne Willemn.: **349.32**, 436.09
 Holz, Daniel: **124.03**, 325.04
 Holz, Daniel E.: 405.07
 Homan, Jeroen: 157.13
 Homeier, Derek: 120.03, 349.20
 Honda, Satoshi: 446.08
 Hong, Jaesub: 421.08
 Hönle, Rainer: 445.12
 Hook, Isobel: 153.21, 327.02
 Hopkins, Philip: 114.03D, 149.54, 257.14, 313.06, 411.03, 449.06
 Hora, Joseph L.: 114.01, 136.01
 Horch, Elliott: 109.02, 349.31
 Hord, Benjamin: **435.06**
 Horesh, Assaf: 124.02, 245.16, 304.07
 Horner, Jonathan: 128.01, **128.04**
 Horner, Scott: 355.10

Hornschemeier, Ann: **223.04**, 227.06, 251.10, 333.01, 347.17, 354.10
 Horst, Sarah M.: 148.39
 Horton, Daniel: 148.13
 Horvat, Martin: 244.09, 244.25
 Hosek, Matthew: **214.05D**
 Hosseinzadeh, Griffin: **209.05D**
 Hostetter, Timothy W.: 362.17
 Hostetter, Carl: 329.03
 Hotokezaka, Kenta: 124.02
 Houck, John C.: 238.01, 238.02, 238.03, 238.04, 238.05, 238.06, 238.07, 238.09, 238.10, 238.11
 Houde, Martin: 130.04, 257.07
 Houghton, Ryan C W.: 306.01D
 Hourihane, Sophie: 350.04
 Houston, Kyle: 246.43
 Hovey, Luke: **446.14**
 Howard, Andrew: 104.04, 104.07, 211.08, 303.06, 329.01, 349.11, 439.13, 439.22
 Howard, Joseph: 354.33
 Howard, SETHANNE: **108.03**
 Howard, Ward S.: 150.23, 231.06, **310.03**, 354.12
 Howe, Glenn A.: 246.41
 Howell, D. Andrew.: 325.06, 325.08
 Howell, D. Andrew: **325.07**
 Howell, Eric: 255.07
 Howell, Steve: 104.04, 109.02, 242.18
 Howk, Chris: 248.09, 302.05, 411.01
 Hrivnak, Bruce: 146.10, **146.11**
 Hsieh, Bau-Ching: 406.03
 Hsueh, Jen-Wei: **415.04D**
 Hu, Esther: 250.11
 Hu, Mengya: **439.05**
 Hu, Renny: 111.03
 Hu, Yue: 247.06
 Huang, Caroline: **420.07**
 Huang, Chelsea Xu.: 201.07
 Huang, Kuang-Han: 454.10, 454.12
 Huang, Shan: 308.01
 Huang, Song: 406.03
 Huang, Xiaosheng: 153.21, **245.14**, 327.02
 Huang, Xinchuan: 247.01
 Huang, Xu: 246.07, 403.05, 439.09
 Huard, Tracy L.: **339.10**
 Hubeny, Ivan: 354.17
 Huber, Daniel: 148.12, 349.40, 450.13
 Huber, Mark: 308.06
 Huber, Robert: 354.11
 Hubmayr, Johannes: 112.02D, 215.02D, 322.05
 Hudec, Rene: 355.35
 Hudson, Hugh: **220.03**
 Huenemoerder, David P.: 237.20, 237.22, 313.03
 Huerta, Eliu: 255.14
 Huff, Cierra: **348.12**, **359.06**
 Huff, Eric: 213.06
 Hughes, A. Meredith.: 147.16, **147.17**, 428.07
 Hughes, A. Meredith: 129.01, 147.09, 147.15, 147.18
 Hughes, Annie: 125.07, 230.01, 322.04
 Hughes, David: 149.59
 Hughes, John P.: 241.11, 446.14
 Hughes, Paul: 360.01
 Hughey, Brennan: 255.07
 Hui, Michelle: 361.14, 453.10
 Huitson, Catherine: 228.07
 Huizenga, Daniel: 326.05D
 Hull, Anthony: 140.09, **140.13**, 140.16, **355.41**
 Hull, Charles: **257.07**
 Hull, Chat: 342.16
 Hull, Samuel: **355.15**, 355.28, 355.35, 355.44, 355.46
 Hummels, Cameron: **203.03**
 Humphreys, Roberta: **335.01**, 341.04, **348.13**, 424.02D
 Hung, Chao-Ling: 149.46, 149.54, 252.06, **328.06**, 342.26
 Hung, Tiara: **405.02D**
 Hunsley, Diana: 256.04
 Hunt, Lucas: **112.05**
 Hunter, Deidre Ann.: 340.03
 Hunter, Todd Russell.: 342.20, **342.21**, 449.01
 Hunting, Emily: 152.08, 246.08
 Huppenkothén, Daniela: **213.03**, **225.03**
 Hurowitz, Jonathan: 241.04
 Hurt, Robert: **360.10**, 360.13
 Husemann, Bernd: 130.01, 227.04
 Hutchens, Zackary: **146.03**
 Hutchinson-Smith, Tenley: **250.12**
 Huterer, Dragan: 327.02
 Hwang, Sungyong: 442.03
 Hyder, Ali: **257.04**
 Hyer, Gregory Edward.: **440.10**
 Hygelund, John: 152.24
 hyman, Scott D.: 215.01, 354.15
 Hynes, Robert I.: 315.07
 Ianna, P. A.: 246.01, 349.17
 Ide, Charles A.: 220.06
 Igarashi, Amy: 150.32, **150.33**, 150.34
 Ignace, Richard: 244.02
 Igoshev, Andrei: **132.03D**
 Ilan, Teva: **438.13**
 Iliadis, Christian: 358.11
 Ilyin, Ilya: 358.10
 Im, Myungshin: 442.03, **446.10**
 Imai, Masataka: 446.08
 Imai-Hong, Amber: 232.03, 360.09
 Imamura, James: 330.01
 Imperato, Sam: 243.06
 Impey, Chris David.: **113.02**, 113.03, 113.05, 113.06, 139.02, **256.02**, 256.07, 360.11
 Indah, Briana: 149.25
 Indebetouw, Remy: 136.11, 214.01, 230.01
 Indriolo, Nick: 150.38, 355.40
 Inneman, Adolf: 355.35
 Intema, Huib: 342.29, 406.07
 Ireland, Jack: 315.04
 Ireland, Michael: 148.12, 152.22
 Irwin, Alexis M.: **344.09**
 Irwin, Jimmy: 309.06D, 347.22, **421.07**, 422.02
 Irwin, Jonathan: 148.18, 334.02, 334.06
 Irwin, Kent: 112.02D, 152.19, 215.02D, 314.05D, 322.05, 419.05
 Irwin, Mike: 436.04
 Irwin, Patrick: 115.04, 133.05, 452.03
 Isaacson, Howard: 104.04, 104.07, 132.02, 211.08, 231.01, 329.01, 349.11, 439.13
 Isbell, Jacob: **316.06**
 Isella, Andrea: 342.15
 Iserlohe, Christof: 445.12
 Ishabashi, Kazunori: 341.04
 Itoh, Ryosuke: 446.03, 446.08
 Ivans, Inese I.: 257.12
 Ivezic, Zeljko: 250.22
 Ivson, Rob: 149.37
 Ivory, KeShawn: **354.06**
 Iwakiri, Wataru: 243.11, 450.09
 Iwasawa, Kazushi: 149.48
 Iyer, Kartheik: 239.02, **239.03**, **426.03**, 426.06
 Izidoro, Andre: 228.08
 Jackiewicz, Jason: 329.06D
 Jacklin, Savannah: 204.02D
 Jacklin, Savannah Renee.: **158.05**
 Jackson, Alan: 115.08
 Jackson, James: 342.03, 342.04
 Jacob, Laurent: 427.02
 Jacobs, Chirstopher S.: 314.01
 Jacobs, Daniel: 228.04
 Jacobson, Shane M.: 152.14, 152.16
 Jacoby, George H.: **241.04**, 241.10
 Jacques, Alice: **136.06**
 Jadhav, Yashashree: **250.15**
 Jaeckel, Felix: 331.06
 Jaehnig, Kurt: 152.08, 246.08
 Jafariyazani, Marziye: **136.16**
 Jaffe, Daniel T.: 241.05
 Jagannathan, Preshanth: 342.28
 Jahoda, Keith: 355.55
 Jain, Sonal: 452.09
 Jakosky, Bruce: 452.09
 Jaliff, Laura: **149.38**
 James, Bethan: 150.38, **210.03**, 355.40
 James, C. Renee: 256.01
 James, David: 446.06
 James, Nicholas John Harris.: **255.11**
 Jameson, Katie: 359.01
 Jamison, Kate: 244.23
 Janesh, William: **340.06**
 Jang-Condell, Hannah: 111.07, 147.19, 148.07, 148.11, 148.27, 148.31, 148.32, 148.35, 148.36, 148.37, 152.25, 246.24, **246.31**
 Jannuzi, Buell: 142.08
 Janowiecki, Steven: 149.21, **309.03**, 340.06
 Jansen, Rolf A.: 258.17, **354.14**
 Jansen, Tiffany: 148.34, **410.06**
 Janusz, Robert: 344.05
 Januszewski, Helen: **434.06**
 Januszewski, William: **355.09**
 Jao, W.-C.: 246.01, 348.03, 349.17, 349.18
 Jaodand, Amruta: 453.15
 Jaodard, Amruta D.: **233.05D**
 Jardine, Moira: 450.03
 Jarka, Kyla L.: 111.07, 148.07, 148.11, 148.27, **148.31**, 148.32, 148.35, 148.36, 148.37
 Jarrett, Tom: 304.06
 Jarugula, Sreevani: 149.41
 Jasiulek, Michael: 421.01
 Jaskot, Anne: **112.06**, 251.09
 Jauzac, Mathilde: 332.04
 Jea, Geonho: 442.04
 Jedrzejewski, Robert I.: 355.01, 355.42
 Jee, Myungkook James.: 153.11, 252.03, 252.09, 252.14, 327.02
 Jeffery, Elizabeth: 146.13
 Jeltema, Tesla: 252.04
 Jenet, Fredrick: 243.13, 442.01, 453.09
 Jenke, Peter: 140.06
 Jenkins, Edward: 237.05
 Jenkins, Matthew: **440.06**
 Jennings, Derrick H.: 216.01
 Jennings, Dr. Donald: 144.17
 Jensen, Hannes: 258.17
 Jensen, Logan: **242.07**
 Jensen, Stanley: 437.03
 Jensen-Clem, Rebecca: **211.05**, 334.01
 Jeong, Donghui: **420.03**, 420.06
 Jester, Sebastian: 257.19
 Jewell, April: 228.04
 Jhabvala, Christine: 152.19, 314.05D, 419.05
 Ji, Tae-Geun: **442.03**
 Ji, Tu: 302.01
 Jia, Hewei: 153.06, 258.15
 Jia, Siyao: 212.01, 237.06
 Jiang, Jian: 153.21
 Jiang, Linhua: 250.04, 440.11
 Jiang, Tianxing: **251.01**
 Jimenez Andrade, Eric
 Faustino: 304.03
 Jimenez- Donaire, Maria Jesus: 322.04
 Jin, Yifei: 210.01
 Jirdeh, Hussein: 232.02
 John, Colin: **257.05**
 John, Hagopian: 246.36
 Johns-Krull, Christopher: 414.05D
 Johnson, Amalya: 149.60, 251.12, **454.15**
 Johnson, Benjamin: 110.05, 149.29
 Johnson, C. I.: 348.07
 Johnson, Calvin: 220.03
 Johnson, Chelen H.: **339.05**
 Johnson, Christian: **344.17**
 Johnson, Elizabeth: **258.12**
 Johnson, Jennifer: 411.02D, 424.03, 450.13
 Johnson, John Asher.: 111.01, 128.01, 204.06, 246.03, 246.13, 314.04, 453.03
 Johnson, Kelsey E.: 360.01
 Johnson, L. Clifton.: **214.06**
 Johnson, Lent Cliff.: 157.06
 Johnson, Lucas Edward.: **309.06D**
 Johnson, Megan: 436.02, 440.20, 440.21

Johnson, Michael: 157.14, 347.21
 Johnson, Payton: **242.02**
 Johnson, Sean: **312.04**
 Johnson, Traci Lin.: 250.41, **415.02D**, 454.10
 Johnson, Tyrel: **132.04**, 233.04
 Johnson, W. Neil: 355.51
 Johnston, Kathryn: 237.09, 258.13, 312.01, 344.03, 362.02, 412.04D
 Johnston, Kyle: **150.18**
 Johnstone, Brittany: 247.11
 Johnstone, Doug: 147.17, 355.10
 Jolly, Antoine: 452.03
 Joncour, Isabelle: **449.04**
 Joner, Michael D.: 146.05, 146.12, 244.21, 348.05, 348.06
 Jones, Alexander: **252.05**
 Jones, Andrea: 242.08, 360.06
 Jones, Ayanna Jayla.: **439.25**
 Jones, Christine: 252.05, 406.05, 406.06, 441.01, 454.10, 454.12
 Jones, Craig R.: 150.05
 Jones, David: 241.04, **308.06**, 420.07
 Jones, Dayton: **115.01**
 Jones, Evan: **438.02**
 Jones, Jeremy: 152.05, **152.26**
 Jones, Kristen: 245.19
 Jones, Kristen M.: **250.49**
 Jones, Liam Dowling.: **148.05**
 Jones, Lynne: 144.08
 Jones, Mackenzie: **105.04D**
 Jones, Megan: **323.06**
 Jones, Michael G.: 149.21, 252.18, 351.08
 Jones, Olivia C.: 214.01
 Jones, Shaela: **338.03**
 Jones, Suzy: 304.06
 Jones, Terry J.: 424.02D
 Jones, Victoria: **250.11**, 354.14
 Jordan, Christopher H.: 247.25, 331.02D
 Jorgenson, Regina A.: 136.10, 237.05, 357.02
 Jose', Jordi: 358.11
 Joseph, Emily: 360.06
 Joshi, Bhavin: **149.19**, 149.39
 Joshi, Manasvita: **205.02**
 Joshi, Ravi: 440.11
 Joslyn, Nick: 150.06
 Jourdain, E.: 438.19
 Jovanovic, Nemanja: 152.10, 303.07, 442.02
 Joyce, Quianah T.: **107.08**
 Joyce, Richard: 453.14
 Juanola-Parramon, Roser: **246.37**
 Juneau, Stephanie: **139.01**, 332.05, **426.08**
 Jung, Intae: **127.03D**, 357.07
 Jørgensen, Jes: 147.10
 Kaastra, Jelle: **106.01**
 Kacprzak, Glenn: 302.04
 Kadler, Matthias: 250.29
 Kafka, Stella: **362.15**
 Kahre, Lauren: **445.02**
 Kaib, Nathan: **228.08**
 Kaiser, Mary Elizabeth: 355.27, **355.34**
 Kaiser, Nick: **135.01**, 308.06
 Kalari, Venu: 157.16
 Kalas, Paul: 329.04D
 Kalirai, Jason: 233.01, **237.10**
 Kallinger, Thomas: 450.13
 Kallman, Timothy: **250.43**, 408.04, 435.05
 Kalmbach, Bryce: 144.08
 Kalogera, Vassiliki: 243.06
 Kaltenegger, Lisa: 355.20
 Kalyaan, Anusha: **147.02**, 428.05
 Kamenetzky, Julia: **247.09**
 Kaminski, Tomasz (Tomek): **125.03**, 408.06
 Kamp, Inga: 147.17
 Kane, Stephen: 128.01
 Kane, Steven: 439.01
 Kannan, Deepti: 148.30
 Kannappan, Sheila: 149.50, 354.28
 Kanodia, Shubham: 152.18, 246.08, 246.45
 Kaplan, David: 243.13, 244.17, 332.06, 361.20
 Kaplan, Kyle: 152.18, 246.08, 246.45
 Kaplinghat, Manoj: 412.05
 Kar, Aman: 111.07, 148.07, **148.11**, 148.27, 148.31, 148.32, 148.35, 148.36, 148.37, 246.24
 Kara, Erin: **205.05**, 250.39
 Karakas, Amanda I.: 241.15
 Karako-Argaman, Chen: 243.13
 Kargaltsev, Oleg: 238.15, 243.03, 243.07, **333.02**, 358.03
 Karim, Alexander: 304.03
 Karim, Md. Tanveer: **237.05**
 Karki, Saket: **438.09**
 Karos, Alexandra D.: 339.05
 Karovska, Margarita: 241.12
 Kartaltepe, Jeyhan: 227.02
 Kasdin, Jeremy: 121.09, 158.02, 246.26, 246.44, 303.04D, 303.07, 355.14, 439.05
 Kasdin, N. Jeremy.: **152.10**, 246.18, 361.15
 Kasen, Daniel: 308.05, 446.06
 Kasevich, Mark: 255.16
 Kashyap, Vinay: 241.14
 Kasliwal, Mansi: 124.02, 124.06, 332.06, 341.07, 361.20, **400.01**
 Kasliwal, Vishal: 250.08
 Kasper, David: **111.07**, 148.07, 148.11, 148.27, 148.31, 148.32, 148.35, 148.36, 148.37, 246.24
 Kaspi, Victoria: 243.13, 243.18, 333.06, 453.11
 Kassim, Namir: 342.30, 354.11
 Kassim, Namir E.: 151.05, **215.01**, 243.14, 354.15
 Kassin, Susan A.: 127.01, 309.02D
 Kastner, Joel: 133.01
 Kastner, Joel H.: **129.06**, 147.13, 147.17, 241.07, 313.03, 349.29
 Kataria, Tiffany: 128.08, **207.09**, **211.01**, 211.06, 334.01, 410.01
 Kato, Takahiro: 153.21
 Katsuda, Satoru: 241.06
 Katynski, Marcus: 358.05
 Katz, Michael: **255.13**
 Katz, Neal: 409.04D
 Kauffmann, Jens: 130.06, **445.07**
 Kaufman, Michael: 237.01, 311.06
 Kavelaars, J.J.: 115.03
 Kaviraj, Sugata: 127.07
 Kawabata, Koji: 446.03, 446.08
 Kawabata, Miho: 446.03, 446.08
 Kawahara, Naoki: **446.03**, 446.08
 Kawai, Hiroki: 450.09
 Kawakita, Hideyo: 144.13
 Kawamura, Akiko: 136.11
 Kawamura, Jonathan: 231.05
 Kawash, Adam: 414.02
 Kay, Laura: 250.06
 Kayitesi, Bridget: 313.05
 Kazanas, Demosthenes: **404.04**, 405.05, 408.04
 Kazlauskas, Algirdas: 344.05
 Keane, Evan: 152.07
 Keane, Jacqueline V.: 102.08
 Kearney, Zoe: **149.59**
 Keek, Laurens: 157.13, 333.03
 Keel, William C.: 110.07, 347.22
 Keenan, Mary: **250.30**, 323.04D
 Keeton, Charles: 255.11, 415.03
 Keil, Shayna: 339.02
 Keith, Celeste: **149.06**
 Keithly, Dean: **246.06**
 Keller, John: 242.08
 Keller, L. D.: 147.06, 348.10
 Kellermann, Kenneth Irwin.: **342.10**
 Kelley, Luke: 250.12, 305.04
 Kelley, Michael SP.: 115.07, 350.06, 452.04
 Kelley, Richard L.: 331.06
 Kelly, Bernard: 255.15, 405.04
 Kelly, Kevin: 255.03
 Kelly, Patrick: **415.05**
 Kelson, Daniel D.: 149.42
 Kempton, Eliza: 148.17, 148.18, 148.29, **310.04**, 410.01, 427.04
 Kendrew, Sarah: 427.04
 Kendrick, Stephen E.: **140.09**, 140.13, 140.16
 Kennea, Jamie: 447.05
 Kennedy, Grant: 342.17
 Kennedy, Mark: 257.02, 358.09, 414.01
 Kennefick, Daniel: 409.03
 Kennefick, Julia: 409.03
 Kenney, Jessica: 150.25
 Kent, Brian R.: **342.14**
 Kentrianakakis, Michael: 220.02
 Kenworthy, Matthew: 152.22, 349.32
 Kenyon, Scott: 144.09
 Keown, Jared: 342.22
 Kopley, Amanda: 248.07, 258.05, **322.04**, 342.11, **342.12**
 Kerber, Florian: 362.13
 Keres, Dusan: 149.10, 411.03
 Kern, Brian: 246.18, 246.35, 361.13
 Kern, Jeffrey: **342.13**
 Kern, Jeffrey S.: 342.14
 Kern, Joshua W.: **146.04**
 Kern, Matthew: 355.15, 355.28, 355.35, 355.44, 355.46
 Kerr, Matthew: **243.14**, 453.05
 Kerr, Matthew T.: 132.04, 157.11, 215.01, 233.04, 255.16, 354.11
 Kerr, Tom: 436.04
 Kerrison, Nicole: 149.60, 251.12, 454.15
 Kessden, Michael: 255.02, 325.04, **415.06**, 421.03
 Keski-Kuha, Ritva: 355.29
 Kessler, Rick: 258.12, 308.06
 Kessler, Sarah: 322.04
 Kevis, Charlotte: 360.11
 Kewley, Lisa: 406.02D
 Khain, Tali: 427.03
 Khakpash, Somayeh: **354.20**
 Khan, Ariba: 444.12
 Khan, Asad: 247.18
 Khan, Rubab: **150.40**, 348.13
 Khandrika, Harish Gautam.: **245.02**
 Khanna, Ramon: **307.05**
 Kharchenko, Vasili: 111.08
 Khatami, David: 446.06
 Khokhlov, Serik: 244.18
 Khostovan, Ali Ahmad: **328.05D**
 Kieda, David: 142.01
 Kielkopf, John: 104.04
 Kiessling, Alina: 140.11, 246.30, 354.08, 355.36, 361.06
 Kihm, Seoneui: **454.07**
 Kikuchihara, Shotaro: 454.10
 Kilbourne, Caroline A.: 331.06
 Kilcrease, David: 452.02
 Kilgard, Roy: 347.10, **354.13**
 Kilpatrick, Brian: **128.08**
 Kim, Alex: 153.21, 327.02
 Kim, Bokyoung: **349.16**
 Kim, Daryl L.: 350.06
 Kim, Dong-Woo: 149.34
 Kim, Doyeon: **153.09**
 Kim, Hwihyun: 445.02
 Kim, Hyunwoo: **448.02**
 Kim, Jeong-Gyu: **449.03**
 Kim, Jin-Ah: **454.06**
 Kim, Juhan: 258.09
 Kim, Keunho: **149.39**
 Kim, Mincheol: **252.03**
 Kim, Seojin Feilx.: **252.14**
 Kim, Wonju: 114.04
 Kim, Woong-Tae: 237.04, **248.01**, 257.14, 449.03
 Kim, Younglo: **209.07**
 Kiman, Rocio: **349.23**
 Kimball, Amy: 342.27, 342.28, 348.09
 Kimball, Mark: 152.19, 314.05D, 419.05
 Kimble, Randy: 355.18, **355.29**, 355.34
 Kimm, Taysun: 110.01, 227.03
 Kinemuchi, Karen: 146.13
 King, Ashley: 347.14
 King, Jeremy: 242.18
 King, Lindsay: 342.29
 Kippen, Marc: 140.05
 Kipping, David: 201.07, 246.19, 310.07, 410.06, 439.20
 Kirby, Annie: 152.24
 Kirk, James: **128.03D**
 Kirk, Jeffrey: 355.29
 Kirkpatrick, Allison: **105.03**, 250.17

Kirkpatrick, J. Davy: 354.29, 354.36, 355.12, 402.01
 Kirshner, Robert: 209.03, 308.06
 Kisielius, Romas: 203.01
 Kiss, Csaba: 361.21
 Kissin, Yevgeni: 115.08
 Kitiashvili, Irina: **334.04**
 Klassner, Frank: 244.07
 Klein, Christopher: 420.07
 Klein, Randolph: **445.12**
 Klessen, Ralf: 136.09, 247.23
 Kleyna, Jan T.: 102.08
 Klimovich, Nikita: 442.02
 Klingler, Noel: 243.03, **243.07**
 Klotz, Alain: 442.07
 Knebe, Alexander: 412.02D
 Kneller, James P.: 408.03D
 Knierman, Karen: **149.15, 256.04, 360.03**, 362.18, 365.01, 365.04
 Knight, J. Scott.: 150.35, 355.29
 Knight, Matthew Manning.: 452.04
 Knotte, Matthew: 150.18
 Knowles, Ben: 329.06D
 Knowles, Kenda: 215.02D, 322.05
 Knudsen, Kirsten Kraiburg.: 222.03
 Knutson, Heather: 111.04, 207.01, 211.05, 211.06, 211.08, 329.01, 349.09, 427.04
 Kober, Gladys V.: 341.08, 348.16, 348.17
 Kobulnicky, Carol: 216.03
 Kobulnicky, Henry: 148.11, 148.27, 148.31, 148.32, 148.35, 148.36, 148.37, 152.25, **216.03**, 246.31, 448.01
 Kobulnicky, Henry A.: 111.07, 148.07
 Kobzar, Oleh: 404.03
 Kocevski, Dan: 361.14
 Koch, Jennifer: 143.03
 Kochanek, Christopher: 440.10
 Kochoska, Angela: **244.09**
 Koda, Jin: 150.17
 Kodama, Tadayuki: 406.03
 Kodra, Dritan: 258.01
 Koekemoer, Anton: **153.03**, 332.04, 354.14, 357.07
 Kogut, Al: 152.19, 314.05D, 419.05, 445.11
 Koh, Justin: 220.03
 Kohl, Steven: 151.02
 Kohler, Jacob P.: **244.06**
 Kohler, Susanna: 444.10
 Kohn, Saul: 150.26, 150.32, 150.33, 150.34
 Kok, Jan: 126.08
 Kolb, Christopher: **244.22**
 Kollmeier, Juna: 257.11, **332.02**
 Kolobow, Craig Pyotr.: **245.05**
 Komossa, S.: 304.01
 Kondratiev, Vlad: 243.13
 Konerding, David: 220.03
 Konopacky, Quinn: 148.20, 148.24, 152.04
 Koo, Bon-Chul: **237.04**, 241.05
 Koo, David C.: 110.03, 258.01
 Kooi, Jason: **338.05**
 Koopmann, Rebecca A.: 252.18, 351.08, 351.13, 354.19
 Koopmans, Leon: 415.04D
 Kopparapu, Ravi: 246.21
 Korcakova, Daniela: 244.18
 Korngut, Phillip: **354.22**
 Kosak, Katie: 440.07
 Kosiarek, Molly: **211.08**, 329.01
 Kosovichev, Alexander: **315.05**
 Kosovichev, Alexander G.: 334.04
 Kospal, Agnes: 147.15, 147.17, 147.18
 Koss, Michael: 140.08, 305.04, **320.01**, 320.02, 320.03, 320.04, 320.05, 320.06, 320.07, 320.08, **343.03**, 405.08
 Kotak, Rubina: 308.06
 Kotulla, Ralf: 150.27
 Kotze, Marissa: 104.01
 Kounkel, Marina: **114.05**
 Kouveliotou, Chryssa: 333.06
 Kovac, Sarah A.: **242.05**
 Kowalski, Adam: 111.05
 Kowalski, Laura: **241.02**
 Kowalski, Marek: 153.21, 327.02
 Kozyreva, Alexandra: 408.03D
 Krabbe, Alfred: 445.12
 Kraemer, Kathleen: 146.08, **348.10**
 Kraemer, Steven B.: 250.48
 Kraft, Ralph: 252.05, **406.05**
 Kramer, Michael: **322.01**, 342.31
 Krasnopolsky, Ruben: 330.03D
 Kratter, Kaitlin M.: 434.06
 Kraus, Adam: 133.06
 Kraus, Adam L.: **148.12**, 148.22, 349.09
 Krause, Oliver: 361.06
 Krauss, Felicia: 250.29
 Krawczyk, Coleman: 340.05
 Krawczynski, Henric: 323.07
 Kreidberg, Laura: 128.08, **207.03**, 228.03, **410.07**, 427.04
 Kremer, Kyle: **232.07**, **423.07**
 Krick, Jessica: 329.01
 Kriek, Mariska: 149.29
 Krimm, Hans Albert.: 343.02
 Krishnarao, Dhanesh: **237.16**, 247.22, 429.03
 Krist, John: 246.15, 246.33, 246.35, 246.44
 Kristensen, Lars: 257.07
 Krizmanic, John: 361.14
 Krochmal, Mark: 242.03
 Krolik, Julian: 124.07
 Kronberger, Matthias: 241.04
 Kroon, John: **132.07**
 Kruczek, Nick: **445.05**
 Kruijssen, Diederik: 237.14
 Kruk, Jeffrey: 355.12, 355.34, **355.39**
 Kruk, Sandor: 110.07
 Krumholz, Mark: 247.19, 355.54
 Kuan, Gary M.: **140.11**
 Kuchar, T A.: 146.08
 Kuchner, Marc: 158.14
 Kuchner, Marc J.: 357.08, **428.01**, 428.03
 Kudritzki, Rolf: 308.06
 Kuehn, Charles: **146.13**
 Kuehne, John W.: 442.03
 Kuehnel, Matthias: 243.11
 Kuettel, Donald H.: 111.02
 Kuhn, Michael A.: **136.08**
 Kulesa, Craig: 231.05, 247.02
 Kulick, John: **438.11**
 Kulier, Andrea: **149.04**
 Kulkarni, Shri: 124.02, 362.04, 405.02D
 Kulkarni, Varsha: 203.01, 203.05, **357.05**
 Kundert, Alisha: 149.47
 Kundu, Arunav: 421.02
 Kunneriath, Devaky: 214.03
 Kuntschner, Harald: 227.04
 Kuntz, Kip D.: 248.03
 Kuo, Cheng-Yu: 123.03D
 Kurczynski, Peter: **208.05**
 Kurtev, Radostin: 136.08
 Kurtz, Michael J.: 362.17
 Kurucz, Robert: 355.27, 355.34
 Kurupparatchi, Dona
 Chathuni P.: 452.08
 Kusmic, Samir: **436.09**
 Kuttyrev, Alexander: 140.09, 355.43
 Kuulkers, E: 438.19
 Kuzio de Naray, Rachel: 425.04, **425.06**, 425.07
 Kuznetsova, Aleksandra: 136.02
 Kwan, Juliana: **420.04**
 Kwon, Ryun Young: 315.04
 Kyne, Gillian: 446.17
 Kyprianou, Mark: 436.12
 La Plante, Paul: 150.30, 150.31
 Lacey, Christina: **340.11**
 Laconte, Keliann: 242.12
 Lacour, Sylvestre: 109.01
 Lacy, Brianna: **148.09**
 Lacy, John: 156.02
 Lacy, Mark: 112.01, 222.01, 250.38, 304.06, **321.02**, **342.27**, 342.28
 Lada, Charlie: 125.07
 Ladd, Edwin: 242.02
 Lagattuta, David: 415.04D
 Laginja, Iva: 152.22, **355.53**
 Laher, Russ: 362.04
 Lai, Shih-Ping: 257.07
 Laine, Seppo: 354.29, **354.36**
 Lainez, Sergio: **258.14**
 Lajoie, Charles-Philippe: 150.35, 355.53
 Lake, Sean: 304.06
 Lam, Daniel: 454.10
 Lam, Michael Timothy.: **132.06**, 150.06, 255.18
 Lam, Raymond: 246.18
 Lamarche, Cody James.: 112.02D, **251.05**
 LaMassa, Stephanie: 238.14, **304.01**
 Lamb, Frederick: 157.13, 243.17
 Lamberts, Astrid: 313.06, 449.06
 Lambros, Scott: 355.29
 Lambros, Zachary Stafford.: **147.16**, 147.18
 Laming, J. Martin.: **241.06**, 341.06
 Lamman, Claire: **349.13**
 Lamperti, Isabella: 320.02, 320.04, 320.08
 Lançon, Ariane: 127.05D
 Lander, Juli: 355.29
 Landry, Luther: 127.02
 Lane, Richard: 257.12, 411.02D
 Lang, Cornelia: 311.06, 445.01
 Lang, Dustin: 149.24, 354.01
 Lange, Jacob: **325.01**
 Langer, William: 231.05
 Lanz, Lauranne: 149.46
 Lanza, A. F.: 349.06
 Lanzuisi, Giorgio: 304.01
 Laporte, Chervin: 237.09
 Laraia, Michael: 362.03
 Larkin, Cormac: **157.16**
 Larsen, Søren: 413.02D
 Larson, Kirsten: **127.06**
 Larson, Lillia: 151.02
 Larson, Rebecca L.: **357.07**
 Larson, Shane: 255.13
 Larson, Steve: 142.08
 Larsson, Stefan: 440.18
 Lascola, Gus: 151.02
 Latham, David: 104.04, 246.07, 246.27, 303.05, 339.08
 Latham, David W.: 334.06, 403.07, 427.03, **431.04**, 439.08, 439.13
 Lau, Marie: **203.02D**, 348.08
 Lau, Ryan: 124.06, 230.04D, **341.07**
 Lauer, Amber: 157.02
 Lauer, Jennifer L.: 238.01, 238.02, 238.03, 238.04, 238.05, 238.06, 238.07, 238.09, 238.10, 238.11
 Laughlin, Greg: 147.14, 452.06
 Laurence, Wendi: 155.06
 Laurens, Andre: 355.13
 Laurent, P.: 438.19
 Laurino, Omar: 238.01, 238.02, 238.03, 238.04, 238.05, 238.06, 238.07, 238.09, 238.10, 238.11
 Lauroesch, James T.: 357.08
 Law, Casey: 132.02, 243.18
 Law, David: 210.01
 Law, Nicholas: 128.05, 150.23, 204.05, 231.06, 310.03, 349.13, **354.12**
 Law-Smith, Jamie: 347.19
 Lawler, James Edward.: **157.03**
 Lawlor, Tim: 209.02D
 Lawrence, Andy: 436.04
 Lawrence, Stephen: 257.04, **365.02**, 414.02
 Lawton, Brandon: 232.02
 Lazarian, Alex: 247.06, 247.24, 247.30, 414.04
 Lazarian, Victor: 247.06
 Lazear, Justin: 152.19
 Lazio, Joseph: 132.06, 250.26, 314.01, 342.31
 Lazio, T. Joseph W.: 255.18, **342.32**
 Lazzati, Davide: 255.09
 Le Fevre, Olivier: 149.14
 Le Gal, Romane: 247.01
 Leahy, Denis: **446.16**
 Learman, Duncan: 339.02
 Leauthaud, Alexie: 406.03
 Lebofsky, Matt: 132.02, 231.01
 Leboulleux, Lucie: 246.36, **246.40**, 355.53
 Lebron, Mayra: 247.31, 252.18
 Lebron Santos, Mayra: **256.06**

Lebrun, F.: 438.19
 Ledvina, Lukas: 438.16
 Lee, Adrian T.: 419.04D
 Lee, Albert: 354.01
 Lee, Cheoljong: 322.04
 Lee, Chin-Fei: 408.06
 Lee, Christoph: 258.13, 356.06
 Lee, Duane M.: 220.06
 Lee, Hye-In: 442.03
 Lee, Hyun-chul: **351.09**
 Lee, Jae-Joon: 241.05
 Lee, Janice: **131.04, 313.05**,
 445.02, 454.04
 Lee, Jinhee: **448.05**
 Lee, Matthias: 225.05
 Lee, Myung Gyoong: 237.04
 Lee, Nicholas P.: 238.01,
 238.02, 238.03, 238.04,
 238.05, 238.06, 238.07,
 238.09, 238.10, 238.11
 Lee, Sang-Yun: 442.03
 Lee, Timothy J.: 247.01
 Lee, Yong-Hyun: **241.05**
 Lee, Young-Wook: 209.07
 Lee-Brown, Donald: **213.05D**
 Lehan, Cory: 155.02, 436.16
 Lehmer, Bret: 149.35, **149.52**,
 223.04, 227.06, 251.10, 333.01,
 347.12
 Lehner, Matthew J.: 115.03
 Lehner, Nicolas: 248.09, 411.01
 Leiendecker, Harrison: **437.03**
 Leigh, Nathan: 325.05, **344.19**,
 349.01
 Leighly, Karen: 250.14
 Leiner, Emily: **109.03D**
 Leisawitz, David: 354.33,
354.35, 355.11
 Leisenring, Jarron: 355.10
 Leising, Mark: 242.18
 Leisman, Lukas: **149.21**
 Leja, Joel: 110.05
 Lemm, Alia D.: **150.12**
 Lemos, Pablo: **327.01**
 Lena, Davide: 250.15
 Lenius, Maria: 148.02
 Leonard, Clare: 303.02
 Leonard, Douglas: 245.07
 Leonard, Liam: 339.02
 Lepine, Sebastien: 244.15,
 348.03, 349.16, 349.20,
349.38
 Lerias, Angela: 150.14
 Leroy, Adam: 125.07, 322.04,
 426.04D
 Lester, Kathryn: **244.04**
 Lestition, Kathleen: 131.03
 Leung, Tsz Kuk: 222.03
 Leung, Tsz Kuk Daisy: **149.37**
 Leuquire, Jacob D.: 246.24
 Levay, Karen: 436.12
 Levesque, Emily: 237.10,
 250.28, 251.03, 341.03, 341.05,
355.25
 Levin, Lina: 243.13
 Levy, Rebecca Chyba.: **130.01**,
 426.04D
 Lewandowska, Natalia: 157.11,
453.05, 453.11
 Lewis, Alexia: 157.06
 Lewis, Ben: 140.13
 Lewis, Briley Lynn.: **144.03**
 Lewis, Hannah: 360.01
 Lewis, Ian J.: 306.01D
 Lewis, James: **302.04**
 Lewis, John Arban.: **453.03**
 Lewis, Nikole K.: 128.08,
 147.19, 148.14, 148.39, 148.43,
 207.04, 246.26, 329.06D,
 410.01, 439.17
 Lewis, Tiffany: **205.03D**
 Lewter, Austin: 360.11
 Li, Aigen: 445.08
 Li, Anna: 444.12
 Li, Gongjie: 347.20
 Li, Haochuan: 429.06
 Li, Hui: 342.15
 Li, Jialu: 322.04
 Li, Jian-Yang: **115.07**, 452.05
 Li, Jiangtao: 237.17
 Li, Jianshu: 153.05, 153.13
 Li, Kunyang: 440.07
 Li, Nan: 258.06
 Li, Qi: 355.54
 Li, Shengtai: 342.15
 Li, Ting: 413.07
 Li, Xiao-dong: 258.09
 Li, Xiaolin: 302.02
 Li, Yiting: **303.01**
 Li, Yuexing: 412.02D
 Li, Yunyang: 237.17, **243.02**,
451.02
 Li, Zhi-Yun: 257.07, 330.03D
 Liang, Ming: 152.08, 246.08
 Lidman, Chris: 153.21, 327.02
 Lieman-Sifry, Jesse: 147.17
 Lien, Amy: 245.09, 320.03,
343.02
 Lieu, Richard: **213.01**
 Lifset, Noah: **354.34**
 Lim, Sungsoon: 252.15, 258.07
 Lim, Tanya: 361.21
 Lin, Andrea: **147.05**
 Lin, Dacheng: 422.02
 Lin, Douglas N. C.: 148.04
 Lin, Kenneth W.: **250.17**
 Lin, Lihwai: 406.03
 Lin, Ming-yi: 320.09
 Lin, Sheng-Chieh: 406.03
 Lin, Yen-Ting: **406.03**
 Lin, Ziyi: **237.03**
 Linahan, Marcella: 339.05
 Lincowski, Andrew: 148.34
 Linden, Sean: 360.01
 Linder, Eric: 153.21, 327.02
 Linder, Tyler: 144.05, 150.25
 Lindor, Bethlee: **246.12**
 Lindstrom, Kyle: 339.12
 Line, Michael: 148.38, 207.04,
 410.01, 410.07, 427.04, 427.07
 Lineberger, Howard: 151.02,
 155.05
 Linford, Justin: 354.15, **414.02**
 Linnartz, H.V.J: **301.02**
 Linsky, Jeffrey L.: 349.06,
424.05
 Lintott, Chris: 110.07, 127.07,
 149.30, 303.06, **307.03**,
 362.03
 Linville, Dylan: **247.20**
 Lipscomb, Charles: 258.05
 Lira, Paulina: 304.01
 Liss, Sandra: 360.01
 Lisse, Carey Michael.: **354.25**,
 449.07
 Lister, Tim: 115.07
 Liszt, Harvey Steven.: **122.01**
 Littenberg, Tyson: **262.01**,
 350.04, 350.04
 Littlefield, Colin: **257.02**,
 358.04, 358.09, 414.01
 Liu, Adrian: 153.09
 Liu, Bin: 230.06, **247.31**
 Liu, Charles: 149.60, 251.12,
 359.03, 454.15
 Liu, Jia: 347.09
 Liu, Mengyao: 360.01
 Liu, Michael C.: 133.07, 137.01,
 349.04, 349.07, 349.09, 349.19,
 349.26
 Liu, Shangfei: **148.04, 342.15**
 Liu, Tingting: **105.02D**, 347.18
 Liu, Weizhe: **149.48**
 Liu, Xin: 250.04, 250.26
 Liu, Xiongwei: 243.02
 Liu, Yiqing: 127.05D
 Liu, Yuanqi: 440.11
 Livermore, Rachael: 149.25,
 153.24, 454.10
 Livingston, John: 211.08,
 303.06, 329.01
 Llama, Joe: 228.04, **450.03**
 Llamas, Jacob: 360.10
 Llop Sayson, Jorge: 442.02
 Lo, K. Y.: 123.03D
 Lockhart, Kelly E.: 362.17
 Lockman, Felix: 152.15, 152.17,
 237.05, **237.07**, 248.09, 331.03
 Lockwood, Alexandra: **232.01**,
 232.02
 Lockwood, Christian A.: 220.06
 Lockwood, Sean: 355.01,
 355.42
 Loewenstein, Michael: **140.03**
 Logsdon, Sarah E.: **152.08**,
 246.08, 349.22
 Loh, Ed: 241.01
 Lokken, Martine Elena.:
354.03
 Lomax, Jamie: 157.06, 355.25
 Lomax, Jamie R.: **341.03**
 Lombardo, Nicholas: **452.03**
 Lomberg, Blaine B D.: 152.22
 Lommen, Andrea: 157.11,
 453.05
 Long, Jeff: 354.11
 Long, Joseph: 355.53
 Long, Knox S.: 248.03, 446.15
 Long, Zachary: 437.02, 449.07,
449.08
 Longobardi, Alessia: 258.07
 Looney, Leslie: 130.04, 445.12
 Lopes, Louise: 419.01
 Lopes de Oliveira, Raimundo:
358.07
 Lopez, Eric: 329.01, 427.03
 Lopez, Laura: 241.09, 247.19
 Lopez, Martin: **435.01**
 Lopez, Sebastian: 357.05
 Lopez Ariste, Arturo: 419.01
 Lopez Rodriguez, Enrique:
123.07
 López-Cámara, Diego: 255.09
 Lopez-Morales, Mercedes:
 128.06, 427.04
 Lopez-Rodriguez, Enrique:
 130.04, 414.04
 Loreda, Thomas: **362.16**
 Lorenz, Brian: **149.42**
 Lorimer, Duncan: 233.02,
 333.05
 Lothringer, Joshua: **329.07**
 Lotz, Jennifer M.: 258.01,
 454.09
 Louie, Dana: **128.06**
 Louie, Tiffany Kaye.: **258.07**
 Lovell, Christopher: **239.02**,
426.02
 Lovell, Mark: 213.07
 Lovellette, Michael: 255.16
 Lovisari, Lorenzo: 347.04,
 454.10
 Lowe, Luke: 152.19, 314.05D,
 419.05
 Lowenthal, James: 216.04
 Lower, Sidney: **149.41**
 Loyd, R.O. Parke: 111.05
 Loyd, Robert: 349.06
 Lozi, Julien: 152.10, 303.07
 Lu, Haiyu: 237.14
 Lu, Honglin: 302.01
 Lu, Hongpeng: 244.14
 Lu, Jessica: 212.01, 214.05D,
 237.06, 237.10, 311.02, 311.07,
 347.06
 Lu, Jianbo: 316.06
 Lu, Muzhou: 220.06
 Lu, Nanyao: 361.21
 Lu, Wenxian: 146.11
 Lu, Xiaoping: 115.07
 Lu, Yu: 110.03
 Lu, Zekun: **247.06**
 Lubber, Nicholas Matthew.:
441.03
 Lubber, Nick: 210.05
 Lucero, Danielle M.: 354.04
 Lucey, Madeline R.: **344.08**
 Lucy, Adrian B.: 358.07
 Ludlam, Renee: 157.13
 Ludwig, Bethany: **241.08**
 Luetzendorf, Nora: 257.09
 Luger, Rodrigo: 403.01,
410.02D
 Luginbuhl, Christian: 122.03,
 142.08
 Luhn, Jacob: **303.03**
 Luisi, Matteo: **230.06**, 247.31
 Lukic, Zarija: 203.04D
 Lumbres, Jennifer: 419.08
 Luna, Gerardo Juan Manuel.:
 358.07, 358.08
 Luna, Omar: **351.08**
 Lund, Michael B.: **204.02D**
 Lundgren, Britt: 302.01,
 440.16, 441.05, 454.08
 Lundquist, Michael: 354.30,
448.01
 Lunnan, Ragnhild: 308.01
 Luo, Bin: 231.03
 Luo, Jing: 442.01, **453.09**
 Luppen, Zachary: 316.06
 Lupu, Roxana: 148.43
 Lurie, John: 246.01
 Lusk, Jeremy Alexander.:
308.04D
 Lusso, Elisabeta: **223.07**
 Lustig-Yaeger, Jacob: 410.02D
 Luther, Kyle: 327.02
 Lutovinov, A.: 438.19
 Lutz, Julie: 157.06
 Ly, Chun: 251.11
 Lykke, Keith R.: 349.05
 Lynch, Ryan: 132.02, 152.17,
 224.06, 233.02, 243.04
 Lynch, Ryan S.: **243.13**, 243.19
 Lyons, Daniel: 216.04
 Lyra, Wladimir: 428.01
 Ma, Jingzhe: 257.15, **302.01**
 Ma, Zhiyuan: 306.04

Maas, Zachary: **349.30**
 Mac Low, Mordecai: 136.09, 247.23, 325.05, 359.03, 444.12, 444.14
 Maccagni, Filippo: 354.04
 Maccarone, T. J.: 223.04, 250.26, 342.33, 421.02
 Maccarone, Thomas J.: 140.06, **140.07**, 227.06, 333.01, 342.32
 MacDougall, Mason: **357.03**
 Mace, Gregory N.: 244.06, 349.04, 349.09
 MacGregor, Meredith Ann.: **125.04**, 136.07, 147.08, 147.15, 147.18, **428.07**
 Machuca, Camilo: 250.45
 Macías, Enrique: 339.09
 MacInnis, Francis: 250.14
 Macintosh, Bruce: 147.19, 148.20, 158.02, 246.10, **246.26**, 339.08, 349.07, 355.14, 361.18
 MacKenty, John W.: 354.17
 Mackey, Dougal: 344.10
 MacLeod, Gordon: 342.21
 MacLeod, Morgan: 244.01
 MacMahon, David: 231.01
 MacMohan, David: 132.02
 Macri, Lucas: 420.07
 Maddau, Piero: 149.51
 Maddalena, Ronald: 149.27, 152.12, **152.15**, 152.17, 247.20
 Maddocks, Sally: 150.12
 Madejski, Grzegorz: 440.18
 Madhusudhan, Nikku: 111.04, 211.03
 Madrid, Alecio: **150.16**
 Madrid, Juan: 344.16
 Madsen, Greg: 340.04
 Maeda, Keiichi: 153.21, 446.03
 Maehara, Hiroyuki: 446.08
 Magalhaes, Antonio Mario Mario.: **436.07**
 Maglieri, Grace: 126.02
 Magnelli, Benjamin: 304.03
 Magness, Camellia: 150.38
 Magnier, Eugene: 349.19, 349.26
 Magnier, Eugene A.: **102.03**, 137.01
 Magno, Macon: **244.02**
 Mahabal, Ashish: **354.31**
 Mahadevan, Suvrath: 152.08, 152.18, 211.02, 244.16, 246.08, 246.45, 303.01
 Mahesh, Nivedita: 116.04
 Mahler, Guillaume: 454.10
 Mahmoodifar, Simin: 157.13, **160.02**, 243.17, 333.03
 Maier, Erin: 316.06
 Maierhofer, Lara: 216.03
 Mainali, Ramesh: 454.10, 454.12
 Majewski, Patrice: **434.05**, 450.08
 Majewski, Steven R.: 211.02, 344.01, 344.13, 421.06
 Maji, Moupiya: **412.02D**
 Majid, Walid: 453.11
 Makai, Zoltan Sandor.: **247.11**, 247.16
 Makarov, Valeri: 436.02
 Makhathini, Sphesihle: 252.08
 Makhija, Krishna: 153.05, 153.13
 Maksym, W. Peter.: 342.28, **347.22**
 Maksym, Walter Peter.: 241.12, 309.06D
 Malan, Sias: 215.03
 Malavolta, Luca: 427.03
 Maldonado, Jessica: 326.05D
 Males, Jared: 303.02
 Males, Jared R.: 419.08
 Maley, Paul D.: 126.08
 Malhotra, Renu: 147.08
 Malhotra, Sangeeta: 149.07, 149.33, 149.39, 251.01, 258.17, 357.07, 402.01
 Maller, Ari: 359.03
 Maloney, Erin: 351.13
 Malz, Alex: 245.03
 Mamajek, Eric: 152.22, **439.13**
 Man, Nicole: **241.09**
 Manara, Carlos: 355.10
 Mandel, Eric: 150.14
 Mandel, Kaisey: 209.03
 Mandel, Shifra: 435.06
 Mandell, Avi: 111.04
 Mandell, Avi M.: 211.03, **329.03**, 355.47
 Mangian, John: **311.07**
 Mann, Andrew: 120.03, **133.06**, 148.06, 148.12, 148.15, 150.19, 344.08
 Mann, Rita: 147.09, 147.17, 355.10
 Mannat, Ken s.: 144.14
 Mannheim, Karl: 250.29
 Manning, Colleen: **131.02**, 131.03
 Manning, Sinclair: **251.06**
 Manos, George: 152.19
 Manset, Nadine: 244.18
 Mansour, Nagi N.: 334.04
 Mantha, Kameswara: 127.02, **258.01**
 Manuel, Joseph: **146.01**
 Marcaide, Jon: 245.09
 Marcello, Dominic: 145.04
 March, Marisa Cristina.: **153.15**
 Marchesi, Stefano: 304.01, 412.01
 Marchesini, Danilo: 149.59
 Marchioni, Lucas: 148.05, **244.11**
 Marchis, Franck: 115.06, 349.07
 Marciniak, Joseph Michael.: **451.03**
 Marcote, Benito: 132.02
 Marengo, Massimo: 146.09, 449.07
 Marganian, Paul: 215.02D, 322.05
 Margheim, Steven: 446.06
 Margolis, Emily A.: **126.05**
 Margutti, Raffaella: 245.13
 Marinacci, Federico: 412.02D, 454.02
 Marinelli, Mariarosa: 149.60, **251.12**, 454.15
 Markwardt, Craig B.: 157.11, 157.13, 320.03, 343.02
 Marley, Mark: **148.43**, 427.05
 Marley, Mark S.: 211.01, 329.06D
 Marlow, Weston: 419.08
 Marois, Christian: 148.20
 Marrone, Dan: 149.51
 Marschall, Laurence: 349.28
 Marscher, Alan: 205.02
 Marshall, Francis: **243.05**
 Marshall, Herman L.: 233.06, 257.19, 440.13
 Marshall, Jameeka: **222.01**
 Marshall, Jennifer L.: 152.01, 413.07, 442.03
 Marshall, Phil: 239.05
 Marsset, Michaël: 115.03
 Martel, Andre: 257.19
 Martel, Jason: 246.41, 355.08, 355.16
 Martellini, Adhara: 258.07
 Marti, Connor J.: 220.06
 Martin, Alec: 349.27
 Martin, Charles Harold.: 237.03
 Martin, Christopher: 149.17, 446.17
 Martin, Emily: 349.22
 Martin, Emily C.: **235.05D**
 Martin, Garreth: 127.07
 Martin, John: **341.04**
 Martin, Pierrick: 243.05
 Martin, Rebecca: 144.12
 Martin, Sergio: 237.14
 Martin, Stefan: 140.11, 355.36, 361.06
 Martin-Carrillo, A.: 438.19
 Martin-Mur, Tomas J.: 314.01
 Martín-Navarro, Ignacio: 227.04
 Martinez, Jose: 243.13
 Martinez, Juan-Carlos: **153.22**
 Martinez, Raquel: **246.25**
 Martinez Oliveros, Juan Carlos: 220.03
 Martínez-Galarza, Juan Rafael.: 149.46, 238.01, 238.02, 238.03, 238.04, 238.05, 238.06, 238.07, 238.10
 Martínez-Galarza, Rafael: 238.09, 238.11, **414.06**
 Martinot, Zachary: **150.26**
 Martins-Filho, Walter: **148.26**
 Martizzi, Davide: 406.02D
 Marton, Gábor: 361.21
 Marx, David: 246.18
 Masci, Frank: 362.04
 Mascoop, Josh L.: 247.11
 Mascoop, Joshua: **247.16**
 Maskoliunas, Marius: 344.05
 Mason, Brian: 342.27, **434.01**
 Mason, Brian Scott.: 215.02D, 248.07, 322.05, **342.11**
 Mason, Charlotte: **226.02D**
 Mason, Nigel J.: 452.07
 Mason, Paul: 358.06, **401.04**
 Massara, Elena: **420.02**
 Massey, Phil: 349.03
 Masson, Jessica: 150.06
 Mast, Damián: 130.01
 Masters, Daniel: 354.08
 Masters, Daniel C.: **153.18**
 Masters, Joseph S.: 342.14
 Masters, Karen: 110.07, 210.01, **340.05**
 Mateo, Mario: 344.17, 434.06
 Mates, John AB.: 215.02D, 322.05
 Mathes, Gavin: 347.09
 Matheson, Thomas: 354.17
 Mathews, Allison M.: 360.01
 Mathieu, Robert: 414.05D
 Mathur, Savita: 450.13
 Matilsky, Loren: **315.03**
 Matra, Luca: 342.17
 Matson, Rachel: **109.02**
 Matsushita, Satoki: 125.07
 Matthee, Jorryt: 328.05D
 Matthews, Brenda: 147.17, **321.04**, **342.16**, 342.17
 Matthews, Keith: 212.01, 237.06, 311.02
 Matthews, Lynn: 146.09
 Mattson, Barbara: **131.07**, **360.05**
 Matuszewski, Matt: 446.17
 Mauldin, Emmalee: 360.11
 Mauro, Francesco: 413.03
 Mawet, Dimitri: 104.02, 147.12, 204.03, 211.05, 246.33, 246.42, 330.02, 334.01, 442.02
 Maxwell, Stephen E.: 349.05
 Mayo, Andrew: **303.05**
 Mayorga, Laura C.: **329.06D**
 Mazoyer, Johan: 147.19, **229.03**, 246.36, 246.40, 355.53, 403.02
 Mazzei, Renato: **252.12**
 Mazzoni, Fernando: **157.04**
 McArthur, Barbara E.: 109.05
 McBreen, Sheila: 361.14
 McCall, Hannah: **434.02**
 McCammon, Dan: 331.06
 McCandliss, Stephan: 140.16, 355.34
 McCarron, Adam: 149.28, **150.08**, 241.10
 McCarthy, Michael: 408.06
 McCarthy, Morgan: **350.05**
 McClain, Bradley: **150.07**
 McClelland, Keri: **242.11**
 McClure-Griffiths, Naomi M.: 237.07, 247.25, 331.02D, 331.03
 McCollough, Michael L.: 238.01, 238.02, **238.03**, 238.04, 238.05, 238.06, 238.07, 238.09, 238.10, 238.11
 McConnachie, Alan: 215.06
 McConnell, Kaela: 351.11
 McCrady, Nate: 111.01, 128.01
 McCrum, Matt: 308.06
 McCully, Curtis: 325.06, 325.07, **325.08**, 446.14
 McCurdy, Ross: 316.06
 McDonald, Michael: 140.06, 427.09
 McDonald, Steven: 362.17
 McDowell, Jonathan: **150.21**
 McDowell, Jonathan C.: 238.01, 238.02, 238.03, 238.04, 238.05, 238.06, 238.07, 238.09, 238.10, 238.11
 McEachern, Maria: 143.03
 McElvey, Raleigh: 360.05
 McElwain, Michael: 148.03, 152.08, 246.08, **355.18**, 355.47
 McElwain, Michael W.: 152.08, 246.08
 McEnery, Julie E.: 361.14
 McFarland, Christina G.: 452.08
 McGilvray, Anna: **340.08**
 McGough, Aylin M.: 111.07, 148.07, 148.27, 148.32, 148.35

McGough, Aylin Marie.: 148.11, 148.31, **148.36**, 148.37
 McGrath, Alex: 143.03
 McGrath, Melissa: 106.03
 McGreer, Ian: 250.07, 304.02D, 440.11
 McGruder, Charles Hosewell.: **143.02**
 McGuffey, Douglas: 355.29
 McGuire, Brett: **342.23**
 McIntosh, Daniel H.: **127.02**, **216.01**, **216.05**, 258.01
 McIntyre, Kathleen: **148.02**
 McIntyre, Travis: 247.31
 McKay, Adam: **144.13**
 McKay, Myles A.: **242.06**
 McKean, John: 415.04D
 McKee, Carolyn: 360.11
 McKernan, Barry: 250.18, 250.34, **325.05**, 359.03, 421.05
 McKinnon, Mark: **321.01**, **342.02**, 342.12
 McKinnon, William B.: 144.03
 McLane, Jacob N.: 152.25, 246.31
 McLaren, Robert: 436.04
 McLaughlin, Brendan M.: 445.06
 McLaughlin, Maura: 132.02, 132.06, 233.03D, 243.13, 244.17
 McLaughlin, Warren: 238.01, 238.02, 238.03, 238.04, 238.05, 238.06, 238.07, 238.09, 238.10, 238.11
 McLean, Ian S.: 349.22
 McLeod, Anna Faye.: 445.03
 McLeod, Brian: 149.36, 152.11
 McMahan, Jeff: 152.19, 215.02D, 314.05D, 322.05, 419.05
 McMann, Natasha: **244.17**
 McMichael, Chelsey: **354.19**
 McMillan, Stephen: 136.09, 244.26, 257.22
 McNair, Shunlante: 360.01
 McNamara, Brian: 342.29
 McNamara, Paul: 361.17
 McNaughton, Andrew: 450.08
 McPartland, Conor: 354.03
 McQuaide, Maria: 355.15, 355.28, 355.35, 355.44, **355.46**
 McQuinn, Kristen: 312.03, 340.08
 McTier, Moiya: **310.07**
 Mead, Lawrence R.: 261.01
 Meadors, Erin N.: 220.06
 Meadows, Victoria: 207.06, 228.04, 427.08
 Medan, Ilija: **247.13**
 Medeiros, Emma M.: 339.05
 Medina, Amber: **204.06**
 Medina, Gustavo: 237.12
 Medlin, Drew: 342.14
 Medling, Anne M.: 149.58
 Meech, Karen J.: **102.08**
 Mehalick, Kimberly: 355.29
 Mehle, Greg: 140.13
 Mehner, Andrea: 341.04
 Mehrle, Nicholas: 402.04
 Mehta, Vihang: **110.04D**
 Mei, Simona: 127.05D
 Meisch, Karen: 242.14
 Meisenheimer, Klaus: 257.19
 Meisner, Aaron: 158.14, 354.01
 Meisner, Aaron Michael.: **144.09**
 Meixner, Margaret: 136.11, 214.01, 354.33, **355.11**, 446.15
 mejia prada, camilo: 246.18, 355.47
 Melchert, Nancy: 149.60, 251.12, 454.15
 Melchior, Peter: **213.02**, **219.03**
 Melendez, Marcio: 149.48
 Melendez, Matthew: 344.13
 Meli, Athina: 404.03
 Mellema, Garrelt: 258.17
 Mello, Melinda: 215.02D, 322.05
 Mellon, Samuel: **152.22**
 Melnick, Gary: 231.05, **354.37**, 355.11
 Melo, Theresa: **136.15**, 247.23
 Melton, Casey: **253.02**
 Mendel, Trevor: 227.01, 306.01D
 Mendes de Oliveira, Claudia: 149.50
 Mendillo, Christopher: **246.41**, 355.08
 Mennesson, Bertrand: 140.11, 148.42, 158.02, 246.30, 246.32, 246.33
 Menou, Kristen: 115.08
 Menten, Karl: 112.02D, 408.06
 Mentzel, Chris: **317.01**
 Mercedes Feliz, Jonathan: **347.15**
 Mereghetti, S.: 438.19
 Merino, Brian Molina.: **149.13**
 Merson, Alex: 354.08
 Meshkat, Tiffany: 147.19, 158.02, **204.03**, 246.46, 330.02, 349.32, 354.29, 354.36, 355.25
 Mesick, Katherine: 140.10
 Messick, Cody: 224.07
 Metcalf, Benton: 415.04D
 Metcalfe, Nigel: 308.06
 Metzger, Brian: **209.08**, 325.05, 422.05, 423.04D
 Mewes, Vassilios: 124.07
 Meyer, Eileen: 250.16, 250.30, **323.02**, 323.04D, 440.17
 Meyer, Jennifer Donovan.: 322.04
 Meyer, Manuel: 355.49
 Meyer, Michael: 355.10
 Meyers, Joshua: 239.05, 327.02
 Mezcuca, Mar: 342.29, 412.01
 Miao, Haixing: 255.05
 Michael, S.: 348.07
 Michail, Joseph M.: **152.21**, 247.24
 Michau, Vincent: 355.53
 Micheli, Marco: 102.08, 115.07
 Michell, Adam: 314.01
 Michelson, Peter: 255.16
 Michilli, Daniele: **243.18**, 243.19
 Mierkiewicz, Edwin J.: 452.08
 Miesch, Mark: 133.03
 Migliore, Christina: **338.04**
 Migliori, Giulia: 123.01
 Mikolajewska, Joanna: 358.05, 453.14
 Mikula, Vilem: 447.01
 Milam, Stefanie N.: **144.15**, 355.11, 355.17, 355.20
 Milam, Stephanie: 354.07
 Milasius, Kristupas: 344.05
 Miles, Drew: **419.03**
 Miles, Korie: 434.01
 Miles, Nathan: **355.33**
 Milingo, Jackie: **349.28**
 Millar-Blanchaer, Max: 148.24, 211.05, 334.01
 Millard, Matthew James.: **241.11**
 Miller, Adam: **245.15**
 Miller, Brendan: 252.17, **349.24**
 Miller, Cole: 243.17
 Miller, Doryan: **348.07**
 Miller, Eric: 309.06D
 Miller, Eric D.: **241.13**, 441.01
 Miller, George: 423.06
 Miller, Jon M.: 157.13, 347.01, 347.05
 Miller, Joseph: 238.01, 238.02, 238.03, 238.04, **238.05**, 238.06, 238.07, 238.09, 238.10, 238.11
 Miller, Matthew: 237.17
 Miller, Michelle: **258.16**
 Miller, Nathan: **430.05**
 Miller, Rossina: 442.01
 Miller, Scott: **256.01**
 Miller, Timothy: 152.19, 314.05D, 419.05
 Miller, Timothy Reid.: 250.51, **250.52**
 Miller-Jones, J. C A.: 342.33
 Miller-Jones, James: 453.15
 milli, Julien: 147.12
 Million, Chase: 158.13
 Mills, Brianna: **350.01**, 357.08
 Mills, Elisabeth: 230.04D, **237.14**, **311.06**, 445.01
 Milne, Peter: 245.07
 Minchin, Robert: **151.06**, 245.19, 247.31
 Mingarelli, Chiara: 224.06
 Mink, Jessica: 150.10, 334.06
 Minor, Quinn: 359.03
 minter, Anthony: 152.17
 Mioduszewski, Amy: 414.02
 Mirel, Paul: 152.19, 314.05D, 361.07, 419.05
 Mirocha, Jordan: 116.01
 Miroshnichenko, Anatoly: **244.18**
 Misawa, Toru: 250.42
 Mishra, Ajay: **445.08**
 Miskiewicz, Chris: 242.11
 Misselt, K.: 355.10
 Mitchell, Daniel A.: 436.13
 Mitchell, Lee: 361.14
 Mitchell, Robert C.: **351.03**
 Mitchell, Sara: 360.05
 Miyazaki, Satoshi: 406.03
 Mizuno, Yosuke: 404.03
 Mo, Wenli: **227.05D**
 Mobasher, Bahram: 136.16, 149.17, 328.05D
 Modjaz, Maryam: 239.01, 308.01
 Moe, Maxwell: 339.11
 Moffett, Amanda J.: **149.45**
 Molnar, Sandor: 404.01
 Momcheva, Ivelina: 149.26
 Momjian, Emmanuel: 210.05, 247.15, 342.14, 441.03
 Moncada, Roberto Jose.: **251.02**
 Monchama, Rachel: 314.01
 Mondrik, Nicholas: 334.02
 Monier, Richard: 157.05
 Monkiewicz, Jacqueline: 149.15, **312.05D**, 362.18, 365.01, **365.04**
 Monnier, John D.: 147.05
 Monroe, TalaWanda R.: 355.01, **355.42**
 Monsalve, Raul A.: 116.02D, **116.04**
 Monson, A. J.: 152.08
 Monson, Andy: 152.18, 246.08, 246.45
 Monson, Erick: 409.03
 Monsue, Teresa: **158.07**
 Montana, Alfredo: 149.59
 Montet, Ben: 234.04, 246.09, 439.07
 Montez, Rodolfo: 157.04, 241.07, 241.12
 Montgomery, Michael Houston.: **443.01**
 Montgomery, Mike: 452.02
 Montgomery, Sharon Lynn.: 147.01
 Montiel, Edward J.: 241.15
 Moody, Dwight: 246.15, 246.18
 Moody, Joseph Ward.: 250.13, 250.37
 Moolekamp, Fred: 213.02
 Mooley, Kunal: **124.02**, 231.02
 Moon, Jun-Sung: **454.14**
 Moon, Nicole Taylor.: **148.28**
 Mooney, Connor: 248.06
 Moor, Attila: 147.15, 147.17, 147.18
 Moore, Amber M.: **247.15**
 Moore, Carolyn: **444.01**
 Moore, Christopher S.: **402.03D**
 Moore, Nathaniel: **149.16**
 Moore, Nicholas: **449.10**
 Moore, Sadie: 316.06
 Morabito, Leah: 342.28
 Moradi, Madeline: 339.05
 Morales, Esteban: 414.06
 Morales, Farisa: 204.03
 Morales, Miguel: 247.27
 Morales-Juberias, Raul: 144.06
 Moran, Edward C.: **238.14**, 250.06, 250.40
 Moran, Sarah E.: **148.39**
 Moraux, Estelle: 109.01, 449.04
 More, Surhud: 406.03
 Moreland, Kimberly D.: **439.06**
 Moreno, Jackeline: **250.08**, 250.32
 Moreno, Jorge: 149.54, 250.12, 257.16
 Moreno Hilario, Elizabeth: **158.17**
 Morgan, Christopher: 440.10, 440.14
 Morgan, Douglas L.: 238.01, 238.02, 238.03, 238.04, 238.05, 238.06, 238.07, 238.09, 238.10, 238.11
 Morgan, Kelsey M.: 331.06
 Morgan, Rhonda: **246.33**

Morganti, Raffaella: 354.04
Mori, Kaya: 435.06, 453.10
Moriarty, Christopher: **150.37**,
246.36
Morihana, Kumiko: 446.08
Moritani, Yuki: 446.03
Morley, Caroline: 234.04,
410.01, 410.07, 427.05, 439.17,
439.24
Morokuma, Tomoki: 153.21,
446.08
Morrell, Nidia: 349.03
Morris, David: 107.08, 361.14
Morris, David C.: **442.07**
Morris, Evan: **349.22**
Morris, Mark: 212.01, 214.05D,
230.04D, 237.06, 247.24,
311.06, 445.01
Morris, Matthew: **355.27**,
355.34
Morris, Melissa Elizabeth.:
149.08, 340.08
Morris, Nathan Ryan.: **148.06**
Morrison, Nancy: 335.01
Morrison, Sarah: 147.08
Morrison, Sean: 203.05
Morrissy, Patrick: **447.02**
Morse, Jon: **201.08**
Morsony, Brian: 252.16,
255.09
Mortazavi Karvani, Seyed
Alireza: **454.09**
Mortier, Annelies: 427.03
Morton, Timothy: 104.04,
303.05
Morzinski, Katie: 303.02
Mosby, Gregory: **149.09**,
355.43
Moscardini, Lauro: 402.01
Moschou, Sofia P.: 148.16
Moseley, Samuel Harvey.:
152.19, 215.05, 314.05D,
354.33, 419.05, 447.01
Moser, Lydia: 237.14
Moses, Julianne: 427.04
Moskal, Jeremiah: 255.09
Moss, Adam: **453.01**
Moss, Vanessa A.: **331.03**
Mosser, Benoit: 450.13
Mossman, Amy E.: 238.01,
238.02, 238.03, 238.04,
238.05, 238.06, 238.07,
238.09, 238.10, 238.11
Motino Flores, Skarleth
Melissa.: **149.11**
Motl, Patrick: 145.04, **255.08**
Motta, Mario: 220.02
Mouette, Jean: 242.11
Moustakas, John: 149.12,
149.24, 149.31, 258.05
Moustakas, Leonidas: 246.32,
304.06, 354.07, 415.03
Mozden, Thomas J.: **116.02D**,
116.04
Mozumdar, Pritom: **446.07**
Mroczkowski, Tony: 215.02D,
322.05
Muders, Dirk: 342.14
Mueller, Guido: 402.05,
402.06, 419.06
Mueller, Jack H.: 145.05
Mueller Sanchez, Francisco:
323.03
Muench, August: **307.08**
Muir, Janet: 142.01
Muirhead, Philip Steven.:
120.03, **120.04**, 427.06
Mukadam, Anjum: 358.09
Mukai, Koji: 358.07, **358.08**,
414.02
Mukherjee, Dipanjan: 342.28
Mukherjee, Oindabi: 257.01
Mukherjee, Reshmi: 440.23,
453.10
Mukherjee, Sunip: 355.08
Mullally, Fergal: 403.06
Mullan, Dermott: 349.10
Mullen, Melissa A.: **146.08**
Mullen, Patrick D.: 253.03,
253.04
Muller-Sanchez, Francisco:
320.05, 440.05
Mullin, Elinor: **140.10**
Muna, Demitri: **213.06**
Munari, Ulisse: 344.05
Mundy, Lee: 331.05D, 339.10,
449.04
Munn, Jeffrey A.: 436.04
Munoz, Ricardo R.: 237.12
Muñoz, Roberto: 127.05D
Munoz Gonzalez, Cesar: **450.11**
Munoz Romero, Carlos
Eduardo: **148.17**
Muñoz-Tuñón, Casiana: 340.02
Munshi, Ferah: 305.01, **340.10**
Murata, Katsuhiro: 446.08
Murgas, Felipe: 104.04
Murph, Susan: 242.15
Murphy, Brian: 146.17
Murphy, Caitlin: 450.06
Murphy, Christopher: **151.08**
Murphy, Edward: 360.01
Murphy, Eric Joseph.: 149.59,
251.07, **321.03**, **342.01**,
342.09, 342.10, 342.11, 342.12,
342.25, 342.26
Murphy, Joseph: **339.08**
Murphy, Nicholas: 338.04,
365.04
Murray, Claire: **247.29**
Murray, James: 442.01
Murray, Norman: 313.06,
449.06
Murray, R. Zachary P.: **158.10**
Mushotzky, Richard: **121.06**,
250.09, 304.05, 320.02,
320.03, 320.04, 405.03,
446.06
Muslimov, Eduard: 419.01
Musoke, Gibwa Rebecca.:
404.01
Mussack, Katie: 315.01
Mutchler, Max J.: 115.07
Mutlu-Pakdil, Burcin: **412.03**
Muzahid, Sowgat: 302.04
Muzerolle, James: **447.12**
Muzzin, Adam: 327.02
Myers, Adam: 250.07, 250.38
Myers, Carey: 150.35
Myers, Joseph L.: **436.16**
Myers, Keenan: 339.05
Myers, Steven T.: 124.02,
231.02, **231.08**
Nagar, Neil: 320.05
Nagaraj, Gautam: **149.05**
Nagasawa, Daniel: **413.07**
Nagayama, Taisukue: 452.02
Nagayama, Takahiro: 446.08
Nagle-McNaughton, Tim:
220.06
Naiman, Jill: 149.54
Nair, Preethi: **309.05**
Najita, Joan: **301.01**, 437.03,
449.09
Najita, Joan R.: 437.03, 449.09
Nakaoka, Tatsuya: 446.03,
446.08
Nakazato, Takeshi: 342.14
Naoz, Smadar: 148.19, 311.02,
347.20
Napier, Kevin: **144.04**, 149.24
Napolitano, Lucas Gabriel.:
146.06
Narayan, Gautham: 145.05,
332.08, **354.17**
Narayan, Ramesh: 311.04
Narayanan, Anand: 250.42
Narayanan, Desika: 257.16,
342.25, 342.26, **355.54**
Nasim, Omar:
Nasim, Syeda N.: 250.18
Nasim, Syeda Sadika.: **250.34**
Nasr, Camella-Rosa: **452.09**
Nataf, David: 354.07
Natalucci, Lorenzo: 438.19
Nave, Gillian: **362.13**, 362.14
Nayak, Michael: **111.02**
Nayak, Omnarayani: 214.01,
313.02D
Nayyeri, Hooshang: 257.15,
328.05D, **355.52**
Nazé, Yaël: 424.04D
Nazli, Kutay: 314.01
Nederlander, Richard: **445.10**
Neff, James E.: 208.05
Neill, Don: 446.17
Neilsen, Joseph: 347.01,
347.05, 347.07
Neilson, Hilding: 146.09
Neiner, Coralie: 419.01
Nelson, Benjamin E.: 104.06D
Nelson, Nicholas: 158.11
Nelson, Olivia: 156.01
Nelson, Robert M.: 144.14
Nelson, Thomas: 358.07,
358.08, 414.02
Nemati, Bijan: 147.19, 246.44,
361.13
Nemec, James: 146.13
Nemiroff, Robert: **143.05**,
150.10, 242.13, **257.01**
Nemmen, Rodrigo: 422.02
Nenkova, Maia: 250.22
Nesvadba, Nicole: **125.08**
Nesvold, Erika: **115.06**, 428.07
Nesvorný, David: 115.03,
201.07
Neufeld, David: 231.05
Neugent, Kathryn: **349.03**
Neureiter, Bianca: 362.13
Neveu, Marc: 439.23
Neveu-VanMalle, Marion:
427.09
Nevin, Rebecca: 323.03, 440.05
Newberg, Heidi: 237.03
Newberg, Heidi Jo.: **212.07**,
451.01
Newman, Andrew B.: 340.09
Newman, Arthur M.: 355.03
Newman, Jeffrey A.: 258.01
Newman, Patrick: **439.01**,
439.19
Newton, Elisabeth: 148.18,
334.02, 334.06
Ng, C.-Y.: 243.07
Ng, Karen: 239.05
Ngo, Henry: **104.02**, 246.42
Nguyen, Chi: **153.07**
Nguyen, Dan T.: 238.01,
238.02, 238.03, 238.04,
238.05, 238.06, 238.07,
238.08, 238.09, 238.10, 238.11
Nguyen, Jayke: **438.10**
Nhan, Bang D.: **152.20**
Ni, Qingling: **323.01**
Nice, David: 243.10, **255.19**
Nichol, Bob: 245.10, 340.05
Nichols, Joy S.: 238.01, 238.02,
238.03, 238.04, 238.05,
238.06, 238.07, 238.09,
238.10, 238.11
Nicola, Andrina: **261.03D**
Nicolás, Medina: 136.08
Nidever, David: **332.05**
Niedner, Malcolm: 355.18
Nielsen, Eric: 246.10, 349.07
Nielsen, Krister E.: **341.08**,
348.16, 348.17
Nielsen, Nikole: 302.04
Niemack, Michael: 112.02D
Niemiec, Jacek: 404.03
Nikola, Thomas: 112.02D,
152.03, 251.05
Nikolov, Nikolay: 211.01
Nikutta, Robert: **250.22**,
332.05
Nikzad, Shouleh: 228.04,
246.33
Nilsson, Ricky: 334.01
Ninan, Joe: 246.08, 246.45
Ninan, Joe Philip.: **152.18**
Ninkov, Zoran: 402.01
Niraula, Prajwal: **104.05**
Nishikawa, Ken-Ichi: **404.03**
Nishimoto, America: 246.13
Nishizawa, Atsushi: 406.03
nissanke, Samaya: 124.02
nissen, joel: 246.33
Nixon, Conor: 452.03
Noble, Scott: **124.07**
Noecker, Martin: **246.35**,
361.13
Noel-Storr, Jacob: **242.19**
Nofi, Larissa: 156.03, 339.12
Nogami, Daisaku: 446.08
Nordgren, Tyler: 220.02
Nordim, Jakob: 153.21, 327.02,
354.09
Nordsieck, Kenneth H.: 341.02
Norman, Dara: 149.50
Norman, Michael L.: 327.05D
Noroozian, Omid: 215.05,
447.01
Norris, Barnaby: 152.10, 303.07
Nota, Antonella: 413.01
Novak, Giles: 130.04, 247.24
Novotny, Steven J.: 152.02
Nowak, Michael A.: 238.01,
238.02, 238.03, 238.04,
238.05, 238.06, 238.07,
238.09, 238.10, 238.11, 440.13
Ntampaka, Michelle: **225.04**
Nugent, Peter: 144.09
Nulsen, Paul: 406.05
Núñez, Alejandro: 158.16
Nunez, Evan Haze.: **339.07**
Nunez, Luis: **148.24**
Nusdeo, Daniel: 157.09
Nusdeo, Daniel A.: **244.13**
Nyland, K. E.: 342.33

Nyland, Kristina: 112.01, 250.26, 323.06, 342.10, 342.27, **342.28**
 Nynka, Melania: **160.03**, 453.11
 N'Diaye, Mamadou: 246.36, 246.39, 355.53, 403.02
 O'Brien, John T.: 250.08, **250.32**
 O'Connell, Julia: 344.13
 O'Connell, Robert: 357.07
 O'Connor, Brendan: 434.07
 O'Dea, Christopher P.: 257.19
 O'Dowd, Matthew: 325.05, 359.03
 O'Meara, John: **103.02**
 O'Mullane, William: **362.10**
 O'Neil, Karen: 152.15, **152.17**
 O'Shaughnessy, Richard: **325.03**, 325.04
 O'Shea, Brian: 149.08, 210.06, 327.05D
 O'Sullivan, Samantha: 243.07
 Oberg, Karin: 129.06, 147.13, 257.08
 Oberst, Thomas: 246.16
 Obrzut, Natalia: **401.01**
 Ocasio, Adrienne: 444.14
 Ochsendorf, Bram: **214.01**
 OConnell, Christine: 216.04
 Odekon, Mary Crone.: **351.13**
 Oelkers, Ryan: 403.04
 Oesch, Pascal: 332.04, 454.10, 454.12
 Oey, Sally: 112.06, 434.06
 Ogaz, Sara: 454.10, 454.12
 Oguri, Masamune: 406.03, 454.10
 Oh, Kyuseok: 320.02, **320.03**, 320.04, 320.08, 405.08
 Ohene, Senyo: 258.05
 Ohira, Yutaka: 241.06
 Ohl, Raymond: 355.29
 Ohshima, Tomohito: 446.08
 Ohstrom, Eva Viktoria: 446.02
 Oishi, Jeffrey: 234.03
 Ojala, Elle: **152.23**
 Ojanen, Winonah: **149.60**, 251.12, 454.15
 Ojha, Roopesh: **250.29**
 Olamaie, Malak: 342.29
 Olatunde, Taiwo Janet.: **361.03**, 402.06, 419.06
 Oldham, Lindsay: 415.04D
 Olinto, Angela V.: **121.07**
 Oliveira, Cristina M.: 150.38, 355.40
 Oliveira, Joana M.: 136.11
 Oliverson, Ronald J.: 452.08
 Olivier, Grace: **247.19**
 Olkin, Catherine: 144.03
 Olling, Robert: 446.06
 Olmedo, Alejandro: 360.11
 Olsen, Knut: **113.08**, 332.05, **362.05**
 Olszewski, Edward: 354.17
 Omelian, Eric: **358.02**
 Omont, Alain: 222.01
 Omoruyi, Osase: **435.04**
 Onishi, Toshikazu: 136.11
 Onken, Christopher A.: 422.08
 Onofrio, Roberto: 226.04
 Onorbe, Jose: 203.04D
 Oosterloo, Tom A.: 354.04
 Orange, N. Brice.: 107.08, 442.07
 Orosz, Jerome: **347.08**
 Orosz, Naomi: **153.01**
 Orr, Laura: 151.02, **155.05**
 Orr, Quinton: 151.02
 Ortega, Carolyn: 308.06
 Orton, Glenn: 115.04
 Osborn, Wayne H.:
 Osburn, Magdalena R.: 401.01
 Osip, David: 427.09
 Oskinova, Lida: 348.02
 Osten, Rachel A.: 158.13, **321.05**, **342.18**
 Ostlin, Göran: 357.07
 Ostorero, Luisa: 123.01
 Ostriker, Eve C.: 449.03
 Ostriker, Jeremiah P.: 423.04D
 Oswalt, T. D.: 157.10
 Oswalt, Terry: 434.05, 450.08
 Otani, Tomomi: 434.05, 450.08
 Otsuka, Masaaki: 446.15
 Ott, Juergen: 342.14, 445.01
 Ouchi, Masami: 454.10, 454.12
 Ousley, Wes: 355.29
 Overduin, James: 242.11, 258.14, 359.09, 359.10
 Owen, Benjamin: **224.05**
 Owen, Caroline Bright.: **150.13**
 Owen, John Michael.: **150.22**
 Owen, Lamar: 242.03
 Owen, William M.: 314.01
 Owocki, Stan: 424.04D
 Ozel, Feryal: 157.13
 Pace, Andrew: 413.07
 Pace, Zach: 149.06
 Pacifici, Camilla: 127.01
 Packer, Benjamin M.: 339.05
 Padgett, Deborah: 204.03
 Padilla, Estefania: **442.09**
 Padilla, Nelson: 149.04
 Paegert, Martin: 403.04
 Paerels, Frits: 445.10
 Pagane, Nicole: **350.04**
 Paglione, Timothy: 158.12, 251.02, **359.03**
 Paillas, Enrique: 149.04
 Pain, Reynald: 153.21, 327.02
 Paine, Scott: 157.14
 Pak, Soojong: 442.03
 Pakey, Donald: 144.05
 Pakmor, Rüdiger: 454.02
 Paladini, Roberta: 354.29, 354.36
 Palencia, Kelby: **429.01**
 Paliya, Vaidehi: 123.04
 Palser, Sage: 150.25
 Palumbo, Daniel: **347.21**
 Palumbo, Michael Louis.: **149.50**
 Pan, Margaret: 147.15, 147.18
 Pan, Yen-Chen: 245.10, 308.06
 Panagia, Nino: 245.09, 247.12
 Pandya, Viraj: 446.14
 Panithanpaisal, Nondh: **153.14**
 Pankow, Chris: 243.06
 Pannuti, Thomas: 340.11
 Pantoja, Carmen: 256.06
 Panurach, Teresa: **349.01**
 Papageorgiou, Andreas: 361.21
 Papovich, Casey: 258.17
 Paredes, Leonardo: **157.09**
 Parisi, Celeste: 344.10
 Park, Changbom: 258.09
 Park, Geumsook: 237.04
 Park, Hyunbae: **258.09**
 Park, Jongwon: **222.04**
 Park, Sangwook: 241.11
 Park, Woojin: 442.03
 Parkash, Vaishali: **425.02D**
 Parmentier, Vivien: 310.04, 427.04
 Parry, Samantha: 402.06, 419.06
 Parshley, Stephen: 112.02D, 152.03
 Parsons, Aaron: 149.22, 153.01, 438.01
 Pasachoff, Jay M.: 220.02, **220.06**
 Pascucci, Illaria: 133.01, 229.01
 Pasetto, Stefano: **257.11**
 Pasha, Imad: **149.29**
 Pasham, Dheeraj: 341.01, 347.05
 Pasham, Dheeraj Ranga Reddy.: 347.01, 347.07, **423.05**
 Pasquali, Anna: 149.39, 357.07, 413.01
 Pasquato, Mario: 448.02
 Past, Matthew: 454.10
 Pastrana, Izabella M.: **152.16**
 Pat, Terrance: 247.21
 Patel, Nimesh A.: **408.06**
 Patel, Rahul: 104.07, 147.19, 246.46, **330.02**
 Paterno-Mahler, Rachel: 454.10, 454.12
 Patil, Pallavi: **112.01**, 342.28
 Patnaude, Daniel J.: 241.11
 Patricelli, Barbara: 255.06
 Patruno, Alessandro: 233.05D, 453.15
 Patterson, G. Wes: 242.08
 Patterson, Keith: 246.18
 Patton, Locke: **251.03**
 Paudel, Rishi R.: **349.10**
 Paudel, Sanjaya: 454.06
 Paul, Nicholas: **150.04**
 Paust, Nathaniel E Q.: 146.06, 348.15
 Pavesi, Riccardo: 149.03
 Pavlov, George G.: 238.15, 243.03, 243.07, 333.02
 Pawlyk, Samuel: 152.19, 314.05D, **419.05**
 Paxson, Charles: 238.01, 238.02, 238.03, 238.04, 238.05, 238.06, 238.07, 238.09, 238.10, 238.11
 Payne, Ifan: 314.03
 Peacock, Mark: 453.06
 Peacock, Sarah: **334.05**
 Pearce, Logan: **148.22**
 Pearson, Chris: 361.21
 Pearson, Kyle: 148.26
 Pearson, Sarah: **212.03D**
 Pecontal, Emmanuel: 152.09
 Peek, Joshua: 247.29, 354.07
 Peek, Joshua E G.: **150.05**
 Peek, Matthew: **454.08**
 Peoples, Molly: 149.08, 150.20, **156.04**, 210.06, **354.02**
 Peille, Philippe: 453.08
 Pellegrin, Kyle: 349.27
 Pellegrino, Andrew: 136.09, **213.04**
 Pellegrino, Craig: **149.57**, 413.07
 Pellerin, Anne: 241.02
 Pena, Ivana: 351.09
 Pena, Melania: **450.06**
 Peñaloza-Murillo, Marcos A.: 220.06
 Penarrubia, Jorge: 412.05
 Peng, Bo: **244.05**
 Peng, Eric: 127.05D, 252.15, 258.07, 344.16
 Penn, Matthew: 220.02, **220.05**, 242.06
 Penny, Matthew: 354.20, **427.01**
 Penny, Sam: 340.05
 Penton, Steven V.: 150.38, 355.40
 Pepper, Joshua: 150.14, 152.23, 204.02D, 246.05, 310.08, 354.20, **403.04**, 403.08
 PeQueen, David J.: 111.07, 148.07, 148.27
 PeQueen, David Jeffrey.: 148.11, 148.31, 148.32, **148.35**, 148.36, 148.37
 Percival, Jeffrey: 152.08, 246.08
 Pereira, Victoria: 360.11
 Pereira, Wellesley: 143.05
 Pereyra, Antonio: 436.07
 Perez, Adrianna: **149.54**
 Perez, Cielo C.: 220.06
 Perez, Karen Isabel.: **452.01**
 Perez, Lucia A.: **351.06**
 Pérez García, Ana María: 361.21
 Perez-Fournon, Ismael: 149.37
 Perez-Gonzalez, Pablo: 112.03
 Perez-Torres, Miguel: 245.09
 Perkins, Jeremy S.: 121.07, **361.14**
 Perley, Daniel: **308.01**, 408.02
 Perley, Richard: 257.19
 Perley, Rick: 252.08
 Perlman, Eric S.: 245.05, 252.02, 257.19, 440.07
 Perlmutter, Saul: 152.09, 153.21, 327.02, 355.34
 Perna, Rosalba: 255.09
 Peroux, Celine: 203.05
 Perrin, Marshall: 147.12, 147.19, **150.35**, 211.05, 229.03, 246.36, 329.04D, 355.53
 Person, Michael J.: 220.06
 Pesce, Dominic: **123.03D**, 351.07
 Pesnell, Dean: 158.07
 Peter, Adrian: 150.18
 Peters, Christina: **245.03**
 Peters, Geraldine: 244.24
 Peters, Matthew L.: **157.06**
 Peters, Thomas: 247.23
 Peters, Wendy: 151.05, 215.01, **342.30**, 354.11, 354.15
 Peters, Wesley: **425.04**
 Peters, William L.: 247.21
 Petersen, Michael: **409.04D**
 Peterson, Avery: 454.10
 Peterson, Bradley: 149.19
 Peterson, J. Matt: 444.02
 Peticolas, Laura: 220.03, 359.04
 Petigura, Erik: 104.07, 211.08, 246.07, 303.06, 329.01, 439.13, 439.22
 Petit, Véronique: 150.18, 362.09, 424.04D
 Petitpas, Glen: **125.07**, 247.32

Petkowski, Janusz: 401.03
 Petric, Andreea: 222.01
 Petro, Noah: 242.08
 Petrone, Peter: 246.36, 355.53
 Petropoulou, Maria: 323.02
 Pettini, Max: 210.03
 Petty, Sara: 304.06
 Petulante, Abigail: 320.03
 Pfeifle, Ryan William.: 123.05, **250.02**
 Pham, Thai: 355.02
 Pharo, John: **149.07**, 149.33
 Phillipps, Steven: 149.45, 344.16
 Phillips, Caprice: **349.04**
 Phillips, Mark: 122.05
 Phillipson, Rebecca: **244.26**
 Phipps, Frederika: **347.04**
 Philips, Alan: **150.03**, 242.17, 362.08
 Philips, Bernard: 140.06, 355.51
 Pierce, Michael J.: **152.25**, 246.31
 Pike, Rosemary E.: 115.03
 Pikhartova, Monika: **437.02**
 Pilachowski, C. A.: 152.25, 246.31, 348.07, 349.30
 Pineda, J. Sebastian: **234.01**
 Pineda, Jaime: 322.02
 Pineda, Jorge: 231.05
 Pingel, Nickolas: **322.06**
 Pinhas, Arazi: 211.03
 Pinsonneault, Marc: **450.13**
 Pintér, Sándor: 361.21
 Piotto, Giampaolo: 414.07
 Piro, Anthony L.: 308.03
 Pirzkal, Nor: 150.24, 227.08, 349.32, 355.19, 357.07
 Pisano, D.J.: 112.05, 322.06, 331.03, 441.03
 Plambeck, Richard: 257.07
 Plavchan, Peter: **121.08**, 128.01, 246.13, 439.01, 439.19
 Plesha, Rachel: 150.38, 355.40
 Plotkin, Richard M.: **423.01**
 Plucinsky, Paul: **241.14**
 Plummer, David A.: 238.01, 238.02, 238.03, 238.04, 238.05, 238.06, 238.07, 238.09, 238.10, 238.11
 Pober, Jonathan: 153.04, 430.01, **430.02**
 Poberezhskiy, Ilya: 246.18, 246.32, 246.35, **361.13**
 Poczos, Barnabas: 225.04
 Pogge, Richard: 314.02D
 Poglitsch, Albrecht: 445.12
 POHL, Martin: 404.03
 Points, Sean D.: 354.17
 Pokhrel, Riway: 147.10, 257.07
 Polidan, Ronald S.: 355.03, 355.08
 Polisenksy, Emil: 151.05, 215.01, 243.14, 354.11, **354.15**
 Polsgrove, Daniel E.: 152.02
 Pomarede, Daniel: 258.10
 Pompea, Stephen: 142.03, **216.02**
 Pompea, Stephen M.,: 142.06, 142.07
 Ponomareva, Anastasia: 354.04
 Pontoppidan, Klaus Martin.: **355.20**, 447.01
 Pooley, Dave: 245.09, 440.05
 Pooley, David: 440.06, 448.03, 449.11
 Pope, Alexandra: 105.03, 149.44, 149.59, 250.17, 328.01, 355.05, 355.11, **355.50**
 Popinchalk, Mark: 360.08
 Poppe, Andrew: 153.07
 Poppenhaeger, Katja: 237.20
 Popping, Gergo: 258.01, 328.01, 342.26
 Poremba, Megan R.: 149.12, 149.24
 Portegies Zwart, Simon: 136.09
 Porter, Frederick S.: 331.06
 Porter, Troy: 330.05
 Posselt, Bettina: 238.15
 Postman, Marc: **354.07**
 Poteet, Charles: 147.19, 229.03
 Pottschmidt, Katja: **243.11**, 333.01
 Poudel, Suraj: **203.05**
 Pound, Marc W.: 339.10
 Pour-Imani, Hamed: **409.03**
 Povich, Matthew Samuel.: **230.03**, 246.10, 339.07
 Powalka, Mathieu: 127.05D
 Powell, Jonas: **147.09**
 Powell, Meredith: 110.06, **320.06**
 Poyneer, Lisa A.: 361.18
 Pradhan, Pragati: **447.05**
 Prager, Brian: 243.09, 360.01
 Prajs, Szymon: 245.10
 Prather, Edward: **113.04**
 Prato, Lisa: 147.07, **156.03**, **339.12**
 Pratt, Jane: **326.04**
 Preibisch, Thomas: 313.03
 Presler-Marshall, Brynn: 247.23
 Prestage, Richard: 150.06, 152.17
 Preston, Lina Levin.: 224.06
 Preston, Robert: 314.01
 Price, Daniel: 132.02, 231.01, 331.03
 Price, Samuel: 157.11
 Price, Sharleen: **440.23**
 Price-Whelan, Adrian: 237.09, 312.01
 Prichard, Laura Jane.: **306.01D**
 Primack, Joel: 127.02, 258.13, 356.06
 Primiani, Rurik: 408.06
 Primini, Francis Anthony.: 238.01, **238.02**, 238.03, 238.04, 238.05, 238.06, 238.07, 238.09, 238.10, 238.11
 Prince, Thomas: **348.18**, 362.04
 Principe, David: 129.06, 133.01, 147.13, **313.03**, 437.01
 Privon, George: 320.05, 323.03
 Prochaska, Jason: 302.01, 302.05
 Prochaska, Travis: 152.01, 442.03
 Proffitt, Charles R.: 355.01, 355.42
 Protopapa, Silvia: 144.03
 Protopapas, Pavlos: 414.06
 Prša, Andrej: 151.03, 244.07, 244.08, 244.09, **244.20**, 244.25
 Pryal, Matthew: 360.01
 Pryor, Carlton: 237.13
 Psaltis, Dimitrios: 157.13
 Ptak, Andrew: 223.04, 227.06, 237.22, **332.01**, 333.01, 347.17, 354.10
 Pucha, Ragadeepika: **340.07**
 Pueyo, Laurent: 147.12, 147.19, 148.14, 229.03, 246.36, 246.39, 246.40, 329.04D, 330.04, **355.37**, 355.53, 403.02, 414.07
 Pulkkinen, Antti: 329.03
 Punzi, Kristina: **133.01**, 349.29
 Purves, Lloyd: 140.09, 140.13, 140.16
 Putko, Joseph: **340.02**
 Puzia, Thomas: 127.05D
 Qi, C.: 129.06, 147.13
 Qi, Yuewen: **257.13**
 Qu, Zhijie: 237.17, **357.06**
 Quataert, Eliot: 308.05
 Queloz, Didier: 427.09
 Querejeta, Miguel: 125.07
 Querrard, Rodney: 355.55
 Quick, Lynnae C.: **439.21**
 Quigley, Rachel: **446.12**
 Quillen, Alice: 350.05
 Quimby, Robert: 308.01, 408.02
 Quinn, Samuel: 246.27, 403.05
 Quinn, Samuel N.: **403.07**, 439.08
 Quinn, Solomon: **438.08**
 Quinones, Juan Manuel.: **144.14**
 Quint, Bruno: 149.50
 Quintana, Elisa: 326.01, 334.07, 349.08, 403.08
 Quiret, Samuel: 203.05
 Qureshi, Ahmed: **148.19**
 Raab, Walfried: 445.12
 Rabago, Ian: **148.23**
 Rabin, Douglas M.: 361.07
 Rachford, Brian: 247.28
 Racusin, Judith: **254.01**, 361.14
 Radice, David: 209.06
 Radigan, Jacqueline: 450.06
 Rafanelli, Gerard L.: **355.03**, 355.08
 Rafelski, Marc: **106.04**, **150.38**, 258.01, 328.03D, 355.40, 357.02, 426.05
 Rages, Kathy: 329.06D
 Raghavan, Deepak: 434.01
 Rahman, Mubdi: 214.01, 250.35
 Rahmani, Christopher: 436.12
 Rahmani, Hadi: 203.05
 Raileanu, Roberta: 355.10
 Rajagopal, Jayadev: 152.08, 246.08
 Rajan, Abhijith: **228.02D**, 349.07
 Rajendran, Surjeet: 255.16
 Ramachandran, Varsha: 348.02
 Ramey, Emily: **150.06**
 Ramirez, Edgar: 436.07
 Ramirez, Solange: 354.29, 354.36
 Ramírez-Ruiz, Enrico: 233.01, 244.01, 347.19, 435.01
 Ramos Padilla, Andres: 149.46, 149.55
 Rampadarath, Hayden: 340.11
 Rampalli, Rayna: **246.27**
 Ramsey, Larry: 246.08, 246.45
 Ramsey, Lawrence: 152.08, 152.18
 Rana, Javed: 124.02
 Ranasinghe, Sujith: 446.16
 Ranc, Clement: **158.04**
 Rand, Richard J.: 248.07
 Randall, Scott: 252.05, **441.01**
 Ranev, Catie: 255.11
 Rangelov, Blagoy: 238.15, 358.03
 Rangwala, Naseem: **247.01**, 247.09
 Rani, Bindu: **205.01**
 Ransom, Scott: 157.11, 224.06, 233.02, 342.31
 Ransom, Scott M.: 132.02, **243.09**, 243.13, 243.15, 243.16, 453.05, 453.09
 Rao, Ramprasad: 257.07
 Rapetti, David: 116.01
 Raposo, Pedro M P.: **143.01**
 Rappaport, Saul: 246.07, 440.06
 Rapson, Valerie: 129.06, 147.13
 Rasio, Frederic: 344.15, 423.07
 Raskin, Cody: 150.22
 Ratzloff, Jeff: 150.23, **204.05**, 231.06, 310.03, 354.12
 Rau, Gioia: 341.08, **348.16**, 348.17
 Raum, Christopher: 419.04D
 Rauscher, Bernard: **152.28**, 355.34, 355.43
 Rauscher, Emily: 148.29, 410.01
 Ravi, Sheth K.: 441.06
 Ravindranath, Swara: 354.07, 355.12
 Rawle, Tim: 112.03
 Ray, Paul S.: **121.03**, 132.04, 140.06, 157.11, 215.01, 233.04, 243.14, **243.17**, 354.11, 453.05, 453.09
 Razzaque, Soebur: **311.05**
 Read, Jocelyn: **224.04**
 Reader, Livia K.: 339.05
 Rebel, Felix: 445.12
 Rebull, Luisa: 136.12, 155.04, **155.06**, **339.01**, 339.02, 339.05, 439.13
 Rector, John: 361.21
 Red, Wesley Alexander.: **247.07**
 Reddy, Francis: 360.05
 Redfield, Seth: 349.06, 428.07
 Redwine, Keith: **112.04D**
 Reed, Brendan: **258.06**
 Reed, Mason: 316.06
 Reed, Michael D.: 146.04, 146.16
 Reed, Phillip A.: **244.19**
 Reedy, Alexander: 445.12
 Rees, Glen: 331.03
 Rees, Richard: **344.12**
 Refregier, Alexandre: 261.03D
 Reginald, Nelson: 220.08
 Regnault, Nicolas: 153.21
 Regos, Eniko: **446.04**
 Reid, Mark: 123.03D
 Reid, Neill: 158.16
 Reiheld, Alison: 155.03
 Reiners, Ansgar: 234.02, 450.07

Reines, Amy: 105.06, 250.26, 440.21
Reines, Amy E.: **305.02**
Reis, Carl: 355.29
Reising, Kiernan: 136.06
Relatores, Nicole C.: **340.09**
Remillard, Ron: 347.05, 347.07
Remillard, Ronald: 140.06, **347.01**
Remington, Tané: 115.09
Remolian, Juan: 258.06
Ren, Bin: 147.12, 147.19, **330.04**
Ren, Yanqiong: 115.07
Replicon, Violet: **354.10**
Ressler, Michael: 402.01
Rest, Armin: 308.06, 354.17, **446.06**
Restaino, Sergio: 152.27, 442.06
Reustle, Alexander: **362.12**
Revalski, Mitchell: 250.45, **250.48**, 404.05
Reyes, Alex: 442.01
Reynolds, Christopher S.: 250.39, 252.16, 347.02, 440.12
Reynolds, Michael: **238.12**
Reynolds, Paul: 355.29
Reynolds, Stephen: 241.03, 244.22
Rhee, Jinsu: **406.01**
Rhoads, James: 149.07, 149.33, 149.39, **258.17**, 355.12, 357.07, 402.01
Rhode, Katherine L.: 340.06, 421.02
Rhodes, Jason: **158.02**, 246.32, 354.08, 402.01
Riabokin, Malanka: 256.07
Ribas, Ignasi: 403.05
Ribaud, Joseph: **316.07**, 354.19, 357.08
Ribeiro, Nadili: 436.07
Ricci, Claudio: 123.05, 250.02, 250.10, 304.07, **320.02**, 320.03, 320.04, 320.05, 320.08
Ricci, Luca: 147.17, 342.15
Ricci, Mariah: **252.17**
Rice, Emily: 158.16, 349.22, 349.33, 349.35, 349.39, 359.03, **360.07**, **360.08**
Rice, Joseph P.: 349.05
Rice, Malena: **147.14**
Rich, Evan: 437.02
Rich, Jeffrey: 252.11
Rich, R. Michael.: 344.17, 348.07, 411.04
Richard, Johan: 112.03, 327.02, 332.04, 426.05
Richards, Emily E.: **151.05**, 342.30, 354.11
Richards, Gordon: 239.04, 250.08, 250.23, 250.24, **250.31**, 250.32, 250.38, 304.01, 304.04D
Richardson, Mark Lawrence Albert.: **110.01**, 454.05
Richardson, Matthew: 155.01, **155.02**, 436.16
Richardson, Whitney: 360.01
Richert, Alex JW.: 428.01
Richey, Christina: **365.03**
Richstein, Hannah: **252.01**
Richter, Matthew J.: 156.02, 241.15, 247.01
Richter, Philipp: 411.01
Riddle, Reed: 128.05
Ridley, Josh: 333.05
Riechers, Dominik A.: 149.02, 149.03, 149.37, 222.03, **321.06**, **342.25**, 342.26
Riedel, A.: 246.01
Riedel, Adric: 334.01, 349.17
Rieke, George: 105.03
Rieke, Marcia: 355.10
Riess, Adam: **117.01**, 308.06, 327.07, 355.34, 420.07, 438.04, 454.10
Rigby, Jane: 250.41, 304.01
Riggs, A J Eldorado: 246.18, 246.36, **246.44**, 402.02, 402.07
Riguccini, Laurie: 440.03
Riley, Alexander: **330.05**
Riley, Allyssa: 355.01, 355.42
Riley, Daniel: 153.05, 153.13
Rinaldo, Alessandro: 213.07
Rines, Josh: 258.05
Ringermacher, Harry I.: **261.01**
Ringwald, Frederick: 358.08
Riquelme, Denise: 237.14
Risaliti, Guido: 223.07
Rivera, Angelica Briana.: **250.24**
Rivera, Daniel I.: 148.07
Rivera, Daniel Ivan.: 111.07, 148.11, 148.27, 148.31, 148.32, 148.35, 148.36, **148.37**
Rivera, Francis: **158.12**
Rivera, Jesse: 442.01
Rizzo, Maxime: 147.19, **148.34**, 152.10, 246.37, 331.05D, 355.47
Rizzo, Monica: **243.06**
Rizzuto, Aaron: 133.06, 148.06, 349.09
Rob, Gontrum: 246.36
Robb, Russell: 244.10
Robberto, Massimo: 402.01, 414.07
Robbins, Dennis: **156.05**, 359.03
Robbins, Lee:
Roberge, Aki: 147.12, 147.17, 147.19, 148.34, 246.21, 246.26, 246.37, 428.07, 439.21
Roberts, Caroline A.: **422.07**
Roberts, Douglas: 214.03
Roberts, Mallory: 243.13
Roberts, Tracy: 155.06
Roberts-Pierel, Justin: **245.04**
Robertson, Brant: 149.51, 354.07
Robertson, Jacob: 145.05
Robertson, Paul: 152.18, 246.08, 246.45
Robertson, Sarena D.: **452.08**
Robinson, Andrew: 250.15
Robinson, Connor: 339.09
Robinson, Jenna: **148.38**
Robinson, Tyler: **148.45**, **207.07**, 246.30, 439.24
Robitaille, Thomas: **307.03**
Robotham, Aaron: 149.45, 306.04
Rocha, Graca: 342.27, **427.07**
Rochford Hayes, Christian: 360.01
Rockcliffe, Keighley E.: 237.03
Rodi, James: **438.19**
Rodney, Steven: 454.10, 454.12
Rodney, Steven A.: 245.04
Rodrigues, Claudia: 436.07
Rodrigues, Myriam: 227.08
Rodriguez, Carl: 423.07
Rodriguez, David: 349.29, 349.33, 428.07
Rodriguez, Jaimee-Ian: **340.13**
Rodriguez, Joseph: **303.08**
Rodriguez, Joseph E.: 204.04, 244.12, 427.01
Rodriguez, Julio: 237.14
Rodriguez, Samelys: 152.19, 314.05D, 419.05
Rodriguez-Gomez, Vicente: 258.01
Rodriguez-Puebla, Aldo: 258.13
Rodruck, Michael: **250.44**
Roederer, Ian: **140.14**, **326.07**
Roediger, Elke: 406.05
Roediger, Joel: 127.05D
Roellig, Thomas: **355.06**, 355.10
Rogers, Alan E. E.: 116.02D, 116.04
Rogers, Leslie Anne.: **246.30**
Rogoszinski, Zeeve: **115.02**
Rojas Ruiz, Sofia: **251.07**
Roman, Michael: 148.29, 220.06
Roman Lopes, Alexandre: 210.01
Roman-Duval, Julia: 150.38, 214.01, 355.40
Romano, Joseph: 224.06
Romanowsky, Aaron: 249.01
Romer, Kathy: 252.04
Romero, Charles: 215.02D, 322.05
Romero, Van D.: 314.03
Romero Matamala, Oscar Fernando.: **362.09**
Romich, Kristine: **359.11**
Roming, Peter: 245.09, **314.06**
Romney, Jonathan D.: 115.01
Roques, J.-P.: 438.19
Rosati, Piero: 327.02
Rosdahl, Karl Joakim.: 110.01
Rose, Benjamin: **245.12**
Rosenberg, Jessica L.: 440.20
Rosenthal, Lee: 149.46
Rosenwasser, Benjamin: 328.02
Rosero, Viviana: **313.04D**
Roshi, Anish: 247.31
Rosolowsky, Erik: 125.07, 322.04, 426.04D
Ross, Nicolas: 250.38
Ross, Timothy W.: **245.19**
Rosseau, Brendan: 220.06
Roth, Katherine: 347.22
Roth, Lorenz: 450.07
Roth, Nathan: 144.13
Roth, Nathaniel: **405.03**
Rothberg, Barry: 123.05, **227.08**, 250.02, 357.07, 440.04
Rots, Arnold H.: 238.01, 238.02, 238.03, 238.04, 238.05, 238.06, 238.07, 238.08, 238.09, 238.10, **238.11**
Rottgering, Huub: 406.06
Rowe, David: 314.07
Rowe, Jamie L.: 155.05
Rowe, Jamie Lynn.: **151.02**
Rowland, Danielle: **340.12**
Roy, Arpita: 152.08, 152.18, 246.08, 246.45
Roy, Namrata: **250.46**, 351.11
Royle, Patricia: 354.14
Royster, Marc: 214.03
Roza, Eduardo: 149.24, 252.04, 258.12, 327.02
Ruan, John: 250.28
Ruane, Garreth: 104.02, 246.42, 246.44, 442.02
Rubenzahl, Ryan: **250.05**
Rubin, Adam: **308.02D**
Rubin, David: 153.20, **153.21**, 327.02
Rubinho, Marcelo: 436.07
Rubinstein, Adam Ezra.: **339.09**
Rud, Mayer: 246.08
Ruda, Jennifer: **144.10**
Rude, Cody: 306.05D
Rudnick, Gregory: 258.05
Rudnick, Lawrence: **217.01**
Rudolph, Alexander L.: **359.02**
Rudzinsky, Ross: 257.06
Ruffio, Jean-Baptiste: 148.20, 246.10, 329.04D, 349.07, 361.18
Rugel, Michael: 408.08
Ruiz, Dary: **437.01**
Ruiz-Lapuente, Pilar: 153.21, 327.02
Rujopakarn, Wiphu: 112.03
Rumsey, Clare: 342.29
Rumstay, Kenneth S.: **143.06**
Runnoe, Jessie: 250.42, 347.09
Rupen, Michael: 414.02
Rura, Christopher: **144.07**
Rusholme, Ben: 362.04
Rusin, Vojtech: 220.06
Russell, Aaron: 339.02
Russell, Christopher: **311.01**
Russell, Helen: 342.29
Russell, Ray W.: 350.06, 449.07
Rustamkulov, Zafar: **439.24**
Rutherford, Thomas: 155.04, 339.02
Ryan, James Lee.: **205.04**
Ryan, PW: 150.10, **150.28**
Ryan, Russell: **150.24**, 349.32, 355.12, 355.19, 357.07, 454.10
Rybarczyk, Daniel R.: **344.11**
Ryder, Stuart D.: 241.05, 245.09
Rykoff, Eli: 149.24, 252.04, 258.12, 327.02
Saar, Steven: 349.28
Sabb, Elena: 354.17, **355.38**, 413.01
Sabiu, Cristiano: 258.09
Sacco, Germano: 129.06, 147.13, 349.29
Sadeghpour, Hossein: **111.08**, 226.04
Sadler, Philip: 444.09
Sadun, Alberto: 250.37
Sage, Leslie John.: **307.04**
Saglia, Roberto P.: 306.01D
Saha, Abhijit: 354.17
Sahnou, David J.: 150.38, 355.34, 355.40
Sahu, Kailash C.: 411.04

Saif, Babak: 255.16
 Saini, Navtej: 314.01
 Sainsbury-Martinez, Felix: **133.03**
 Saito, Tomoki: 446.08
 Saito, Yoshihiko: 446.08
 Sajina, Anna: 105.03
 Sakai, Shoko: 212.01, 311.02
 Sakamoto, Kazushi: 125.07
 Sako, Masao: 153.21
 Sakon, Itsuki: 355.06
 Salazar, Jeffrey David.: **438.01**
 Salim, Samir: **454.04**
 Salinas, Ricardo: 354.30, 453.06
 Salmon, Brett: 454.10, **454.12**
 Salome, Philippe: 241.01
 Salter, Chris: 245.19
 Salvato, Mara: 304.01
 Salvesen, Greg: **423.03**
 Salzer, John J.: 340.06
 Samarasinha, Nalin H.: 115.07
 Sambruna, Rita M.: 257.19
 Samec, Ronald G.: 244.03, **244.10**, 434.03
 Samsing, Johan: 438.13
 Samuels, Shanelle: **148.46**
 Sanchez, Michael Allan.: **449.05**
 Sanchez, Richard: 150.25
 Sánchez, Sebastián F.: 130.01, 426.04D
 Sánchez Almeida, Jorge: 340.02
 Sánchez Portal, Miguel: 361.21
 Sánchez-Conde, Miguel: 355.49
 Sánchez-Janssen, Rubén: 127.05D
 Sanchez-Maes, Sophia Araceli.: **439.16**
 Sand, David: 149.36, **245.11**
 Sand, David J.: 340.07
 Sandell, Goran: **229.05**
 Sanders, David B.: 149.48, 320.05, 354.03
 Sanders, Jeremy: 342.29, 406.07
 Sanders, Nathan: **444.10**
 Sanders, Ryan: **210.04D**
 Sanderson, Kelly Nicole.: **149.23**
 Sanderson, Robyn: 344.03, 362.02
 Sandhu, Jagmit: 314.01
 Sandstrom, Karin: 241.08, 322.04, 355.07, 355.20
 Sanghavi, Suniti: **334.01**
 Sanhueza, Pedro: 122.05, 142.03
 Sankrit, Ravi: 150.38, 355.40, 358.02, 414.04, 446.01
 Sanmartin, David: 354.30, **440.15**
 Santana Da Silva, Luidhy: **440.03**
 Santander-García, Miguel: 241.07
 Santini, Anthony: 354.13
 Santoro, Fernando: 152.08, 246.08
 Santos, Fabio: **130.04**, 152.21
 Santos, Joana: 327.02
 Sarajedini, Ata: 340.01, 344.10, 413.03
 Sarangi, Arkaprabha: 408.04
 Sarantos, Menelaos: 452.08
 Saravia, Claire: 360.05
 Sarazin, Craig L.: 252.12
 Sarbadhicary, Sumit: **326.05D**
 Sargent, Benjamin: **109.07**
 Sargent, Mark: 304.03
 Sarma, Anuj: 247.15
 Sartori, Lia: **250.03**, 320.05, **320.07**
 Sasaki, Ryo: 450.09
 Satyapal, Shobita: **123.05**, 250.02, 250.10, 305.04, 440.04
 Saunders, Clare Myers.: 153.21, **245.18**, 327.02
 Saunders, Nicholas: **403.01**
 Saunders, William: **437.04**
 Saur, Joachim: **450.07**
 Sauvage, Jean-François: 246.40
 Savage, Blair D.: 237.05
 Savchenko, V: 438.19
 Saviane, Ivo: 450.11
 Savransky, Dmitry: 246.04, 246.06, 246.11, 329.04D, 361.18
 Sawczynec, Erica A.: **344.22**
 Saxena, Prabal: 355.47
 Saylor, Dicy Ann: **348.03**
 Scannapieco, Evan: 454.05
 Scargle, Jeffrey D.: 362.16
 Scarlata, Claudia: 110.07, 112.06, **153.17**, 362.03
 Schaefer, Adam: 149.06
 Schaefer, Bradley E.: , **108.01**, **315.07**
 Schaefer, Gail: 147.05, **152.05**, 152.26, 339.12, 450.05
 Schaeuble, Marc: 443.01
 Schaller, Matthieu: 149.04
 Scharwaechter, Julia: 354.30
 Schatz, Dennis: 242.12
 Schawinski, Kevin: **309.01**, 320.02, 320.03, 320.04, 320.05, 320.07, 320.08, 362.11, 405.08
 Schaye, Joop: 149.04
 Schechner, Sara Jane.: , **134.01**
 Schediwy, Sascha: **215.03**
 Schenk, Paul M.: 144.03
 Schilke, Peter: 136.11
 Schiminovich, David: 149.56
 Schindler, Jan-Torge: **304.02D**
 Schindler, Kevin:
 Schinnener, Eva: 304.03, 322.04
 Schinzel, Frank K.: 215.01, 242.04, 342.14
 Schirato, Richard: 140.05
 Schirmer, Mischa: 354.30
 Schlafly, Eddie: 144.09
 Schlafly, Edward: **102.04**, 350.02, **354.01**
 Schlawin, Everett: 427.04
 Schlegel, David: 144.09, 149.24, 354.01
 Schlegel, Eric: 340.11
 Schlichting, Hilke: 147.15, 147.18
 Schlieder, Joshua: 104.07, 303.06, 326.01, 329.01, 403.08, 439.02, 439.13
 Schmelz, Joan T.: **116.06**, 212.08
 Schmidt, Britney: 106.03
 Schmidt, Fabian: 420.03
 Schmidt, Judy: 150.10
 Schmidt, Luke M.: 152.01
 Schmidt, Sarah J.: 158.15, 349.10, 349.23, 349.35, 349.39
 Schmitt, Bernard: 144.03
 Schmitt, Henrique: 157.01, 250.48, 442.06
 Schmitt, Henrique R.: **152.27**
 Schmitz, Denise: 313.06, 449.06
 Schneider, Adam: 158.14
 Schneider, Christian: 111.05, 349.06
 Schneider, Donald: 250.36, 250.38, 302.01
 Schneider, Glenn: 147.12, 428.07
 Schneider, Jeff: 225.04
 Schneider, Michael: **239.05**
 Schneider, Nick: 452.09
 Schnittman, Jeremy: 255.15, **405.04**
 Schödel, Rainer: 237.06, 311.07
 Schoenell, William: 436.07
 Schoenwald, Justin: 112.02D
 Scholz, Paul: 132.02
 Schonhut, Jessica: 349.13
 Schrubba, Andreas: 125.07, 322.04
 Schultheis, Mathias: 424.03
 Schultz, David R.: 253.04
 Schulz, Bernhard: **361.21**
 Schulz, Norbert: 233.06, 237.20, 313.03
 Schulze, Steve: 308.01
 Schwab, Christian: 152.08, 152.18, 246.08, 246.45
 Schwab, Elliana: 421.05
 Schwab, Ellianna: **158.16**, **444.13**
 Schwamb, Megan E.: **115.03**
 Schwarz, Kamber: **229.04D**
 Schwalnic, Daniel: **102.05**, 246.09, 258.12, 308.06, 354.07, **355.45**, 438.04
 Scott, Jennifer: 258.11, 357.04
 Scott, Mekai: 151.02
 Scott, Nicholas J.: **361.16**
 Scoville, Nick: 149.17, 149.44
 Scowcroft, Victoria: 412.04D
 Scowen, Paul: 149.15, 228.04, 312.05D, **355.36**, 361.06
 Seager, Sara: **121.09**, 246.07, 246.30, 401.03, 439.08
 Seaton, Daniel B.: 220.06
 Seay, Christopher: **450.04**, 450.10
 Sebokolodi, Makhuduga Lerato.: **252.08**
 Secrest, Nathan: 123.05, 250.02, 250.10
 Secunda, Amy: **344.03**, **444.12**
 Sefako, Ramotholo: 104.04
 Seidel, Edward: 255.14
 Seifert, Richard: **150.19**, **252.06**
 Seiradakis, John: 220.06
 Seitzer, Patrick: **122.02**, 126.02
 Sekiguchi, Kazuhiro: 446.08
 Selina, Rob: 342.02, 342.03, 342.04, 342.08, 342.09, 342.11, 342.12
 Sell, Paul: 258.05
 Sendra Server, Irene: 454.10
 Sengupta, Sutirtha: **450.02**
 Seo, Byoung-Joon: 246.15, 246.18, 361.13
 Seo, Seongu: 454.07, **454.11**
 Seo, Woo-Young: **257.14**
 Seo, Youngmin: **247.02**, **322.03**
 Sepulveda, Aldo: **148.33**
 serabyn, Eugene: 147.12, 204.03
 Serenelli, Aldo: 450.13
 Seriacopi, Daiane: 436.07
 Serra, Viktoriah: 250.42
 Servin, Juan: **255.02**
 Seth, Anil: 149.36
 Sewilo, Marta: **136.11**
 Seymour, Andrew: 243.18, 243.19
 Shabram, Megan: 403.06
 Shafer, Daniel: **438.04**
 Shah, Ebrahim: 351.13
 Shah, Shivani: **349.11**
 Shaklan, Stuart B.: 140.11, 402.02, 402.07
 Shamir, Lior: 143.05, 150.04, 150.10
 Shanahan, Jesse Carla.: **149.30**
 Shaner, Andrew: 360.06
 Shang, Hsien: 330.03D
 Shangguan, Jinyi: 440.11
 Shankland, Paul: 142.08
 Shao, Michael: 314.01, **332.07**
 Shapley, Alice: 130.02D, 149.51, 328.03D, 402.01
 Shapurian, Golnaz: 362.17
 Sharda, Piyush: 241.14
 Sharon, Chelsea: **222.03**
 Sharon, Keren: 258.06, 454.12
 Sharon, Keren q.: 250.41, 332.04, 415.02D, 454.10
 Sharp, Elmer: 152.19, 314.05D, 419.05
 Sharples, Ray: 306.01D
 Shaulis, Taylor J.: 362.17
 Shawhan, Peter: 361.14
 Shaya, Edward: **258.10**, 446.06
 Shea, Jeanine: 247.25
 Sheardown, Alexander: 406.05
 Sheehan-Klenk, Patrick: 149.43
 Sheets, Holly: **427.02**
 Sheffield, Allyson: 237.09, **312.01**, 359.03
 Sheldon, Keziah: **250.23**
 Shelton, Robin L.: 253.04
 Shelton, Siddhartha: 212.07
 Sheminova, Valya: 157.05
 Shemmer, Ohad: 250.24
 Shen, Yue: 250.04, 250.26, 250.36, 257.18
 Sheppard, Kyle: **211.03**
 Sheth, Kartik: 149.44
 Sheth, Ravi K.: 226.06
 Shetrone, Matthew: 344.13, 411.02D, 450.13
 Shi, Fang: **246.18**
 Shiao, Bernie: 150.01, 158.13, 362.01
 Shields, Douglas William.: 409.03
 Shields, Joel: 246.18
 Shillue, Bill: **342.04**
 Shimizu, Thomas Taro.: **320.09**

Shimoda, Jiro: 241.06
 Shin, Jieun: **126.06**
 Shin, Kaitlyn: **251.11**
 Shinnerer, Eva: 125.07
 Shipp, Nora: **212.05**
 Shiri, Ron: 246.36
 Shirley, Yancy L.: 247.03, 322.03
 Shirron, Peter: 152.19, 314.05D, 419.05
 Shkolnik, Evgenya L.: 148.19, **228.04**, 334.05, 344.07
 Shlosberg, Ariel: 362.13
 Short, Donald: 347.08
 Shortridge, Keith: 150.10
 Shortt, Spencer: 136.06
 Showman, Adam: 410.01
 Shporer, Avi: **104.04**, 334.01
 Shrader, Chris: **257.20**, 404.04, 405.05
 Shrestha, Manisha: **424.06D**
 Shultz, Matt: 424.04D
 Shupe, David: 361.21, **362.04**
 Shuping, Ralph: 448.04
 Shvartzvald, Yossi: 158.05, 310.06
 Siah, Javad: 152.21, 247.24
 Siana, Brian: 328.03D, 426.05
 Sidick, Erkin: 246.18, 246.44
 Siegel, Daniel: **262.04**
 Siegler, Nicholas: **104.03**
 Siellez, Karelle: **107.06**
 Siemens, Xavier: 243.13
 Siemiginowska, Aneta: **123.01**, 205.04, 238.01, 238.02, 238.03, 238.04, 238.05, 238.06, 238.07, 238.09, 238.10, 238.11
 Siemion, Andrew: 132.02, 231.01, 342.24
 Sieth, Matt: 322.04
 Sievers, Jonathon: 215.02D, 322.05
 Sigurdsson, Steinn: 347.22
 Sigut, Aaron: 147.05, 157.06, 434.06
 Silburt, Ari: **115.08**
 Sills, Alison: 136.08
 Silva, Jasmin: 232.03, 360.09
 Silva, Karleyne: 354.30
 Silva Aguirre, Victor: 450.13
 Silverberg, Steven: **428.03**
 Silverman, Jeffrey: 245.01, 360.08
 Silverstein, Michele: 349.18
 Silvia, Devin: 149.53
 Silvis, George: 362.15
 Simmons, Brooke: **127.07**
 Simmons, Brooke D.: 110.07, 258.01, 303.06
 Simmons, Mike: **242.21**
 Simon, Amy: 115.04, **144.01**, 144.06
 Simon, Jacob: 129.01
 Simon, Joseph: **224.03D**, 224.06
 Simon, Joshua D.: 149.36, 257.12, 340.09, 413.07
 Simon, Michal: 339.12
 Simon, Molly: **113.05**
 Simón-Díaz, Sergio: 434.06
 Simone-Gonzalez, Luna: 444.13
 Simons, Raymond C.: 127.01, 127.02, **309.02D**
 Simpson, Christine: **454.02**
 Simpson, Janet P.: **237.01**
 Sims, Peter: **430.01**
 Sinanan-Singh, Jasmine: **258.02**
 Sinclair, James: 115.04
 Sing, David: 211.01, 427.04
 Singal, Jack: 438.02, 440.08
 Singer, Leo Pound.: 124.02, **124.06**
 Singh, Saurabh: **116.03D**
 Sinukoff, Evan: 104.04, 104.07, 211.08, 303.06, 329.01, 439.22
 Sion, E. M.: 157.10
 Sion, Edward Michael.: **358.05**
 Sirbu, Dan: 246.02, **402.02**, 402.07
 Sirsi, Siddhartha: 247.21
 Sitariski, Breann: 237.06
 Sitko, Michael: 437.02, **449.07**
 Sitko, Michael L.: 350.06
 Sivaramakrishnan, Anand: 246.36, 246.39, 246.40, 329.04D, 355.53
 Sivaraman, Bhalamurugan: 452.07
 Siverd, Robert: 104.04, **152.24**
 Skarbinski, Maya: 444.14
 Skelly, Clare: 360.05
 Skiff, Brian: 339.12
 Skillman, Evan: 312.03, 340.08
 Skinner, Jacob: **244.16**
 Skinner, Steve L.: **136.14**
 Skrutskie, Michael: 211.02
 Slane, Patrick O.: 241.11
 Sliski, David: 220.06
 Sliwa, Kazimierz: 125.07
 Sloan, G. C.: 146.08, 348.10
 Slosar, Anze: 420.01
 Slutsky, Jacob: 350.04, **355.23**
 Slyz, Adrienne: 110.01
 Smail, Ian: 251.06, 328.05D
 Smart, Brianna Marie.: **340.04**
 Smartt, Stephen: 308.06
 Smee, Stephen: 402.01
 Smethurst, Rebecca: 127.07, 340.05
 Smidt, Joseph: 153.02, 226.03
 Smirnov, Oleg M.: 252.08
 Smit, Renske: 349.32, **454.03**
 Smith, Aaron: **210.02D**
 Smith, Adam JRW.: **439.17**
 Smith, Arfon M.: **307.06**
 Smith, Beverly J.: 149.49, 440.02
 Smith, Blake: 113.08
 Smith, Britton: 149.08, 210.06
 Smith, Cary: 152.24
 Smith, Chris: 446.06
 Smith, Daniel: 242.18
 Smith, David: 414.08
 Smith, David A.: 243.05
 Smith, Denise: **131.03**, 232.02
 Smith, Erin: 355.18
 Smith, Graeme: 348.01, 348.08
 Smith, Howard A.: 149.46, 149.55, 237.08, 414.06
 Smith, J. Allyn: **242.14**
 Smith, John Allyn.: 145.05
 Smith, John-David: 251.07
 Smith, Karl: 140.05
 Smith, Ken: 308.06
 Smith, Krista Lynne.: 250.09, **304.05**
 Smith, Louis Chad.: 232.02
 Smith, Malcolm: 142.03
 Smith, Mark: 149.07
 Smith, Mathew: 209.07, 245.10
 Smith, Michael: 152.08, 246.08
 Smith, Nathan: 245.01, 245.07
 Smith, Paul: 245.07
 Smith, R. Chris: **122.05**, **142.03**
 Smith, Rachel: 438.14
 Smith, Randall: **237.18**, 237.22, 253.03
 Smith, Robyn: 359.01
 Smith, Rory: 222.04
 Smith, Russell: 306.01D
 Smith, Verne: 211.02
 Smith-Zrull, Lindsay: 143.03
 Smithka, Iliya: 156.01
 Smolčić, Vernesa: 304.03
 Smotherman, Hayden: 144.08
 Smrekar, Suzanne E.: 300.01
 Smullen, Rachel: 434.06
 Sneden, Chris: 156.02, 157.03
 Snow, Theodore: 247.28
 Snyder, Elaine: 149.50
 Snyder, Elaine M.: 150.38, **355.40**
 Snyder, Gregory: 110.07, 127.01, 127.02, 258.01, **426.07**
 Soares-Santos, Marcelle: **219.06**
 Sobeck, Jennifer: **424.03**
 Sobey, Charlotte: 243.18
 Sobolewska, Malgorzata: 123.01, 205.04
 Sobral, David: 149.17, 328.05D
 Soderblom, David: **137.02**
 Sofiatti, Caroline: 327.02
 Sohn, Sangmo Tony.: **237.11**, 355.01, 355.42
 Sokal, Kimberly: 136.14
 Sokal, Kimberly R.: 244.06, 349.04
 Sokoloski, Jennifer: 358.07, 358.08, 414.02
 Soler, Juan: 210.01
 Som, Debopam: 203.05, 357.05
 Somerville, Rachel: 258.01, 342.26, 347.03, 355.36, 361.06
 Song, Inseok: 448.05
 Song, Yiqing: 360.01
 Sonnentrucker, Paule G.: 247.28, **331.01**, 355.01, 355.42
 Sonnett, Gerhard: 444.09
 Soo, Audrey: 444.12
 Soraisam, Monika: 332.08
 Sorber, Rebecca L.: **246.24**
 Sorenson, Benjamin: 339.05
 Sorenson, Christian: **440.14**
 Soria, Roberto: 340.11
 Sorini, Daniele: **203.04D**
 Sorli, Kya: **115.09**
 Sosey, Megan: 355.12
 Soto, Gabriel: **246.11**
 Soummer, Remi: 147.12, 150.37, 246.36, 246.39, 246.40, 355.53
 Sousa-Silva, Clara: **113.09**, **401.03**
 Souto, Diogo: 211.02
 Sowah, Maxine: 444.13
 Spacek, Alexander: **454.05**
 Spadafora, Anthony L.: 153.21, 327.02
 Spagna, Stefano: **342.07**
 Spangler, Steven R.: 130.05D, 338.05
 Sparks, William B.: **106.03**, 257.19
 Sparre, Martin: 136.04
 Speck, Angela: **220.02**
 Speights, Jason C.: 248.05, **248.06**, 248.08
 Spekkens, Kristine: 149.36
 Spencer, John: 106.03
 Spencer, Sean: 157.15
 Spencer, Susan B.: 355.03, 355.08
 Spengler, Chelsea: **127.05D**
 Spicer, Sandy: **347.03**
 Spiegelberg, Josephine: 144.16
 Spiewak, Renee: 224.06, 243.13
 Spitzer, Laura: 132.02, 243.18, 243.19
 Spoon, Henrik: 149.02
 Springel, Volker: 454.02
 Springola, Cristiana: 415.04D
 Squires, Gordon: 131.03, 155.06
 Squires, Gordon K.: **232.04**
 Sramek, Richard A.: 245.09
 Srikanth, Sivasankaran: **342.05**
 St. Laurent, Kathryn: 246.36, **246.39**
 Stacey, Gordon: 112.02D, 152.03, 231.05, 251.05
 Staff, Jan: **145.04**
 Stafford, Jennifer Nicole.: **347.20**
 Staguhn, Johannes G.: 152.19, 314.05D, **354.33**, 355.11, 419.05
 Stahl, H. Philip.: 140.11, 246.33, **246.38**
 Stairs, Ingrid: 233.02, 243.09, 243.13, 243.16
 Stalder, Brian: 109.04
 Stalaker, Olivia: 339.02
 Stalaker, Olivia K.: **155.04**
 Stanchfield, Sara: **215.02D**, **322.05**
 Stancil, Phillip C.: 253.03, 253.04
 Stanford, Spencer: 327.02
 Stansberry, John: 144.03
 Stapelfeldt, Karl: 204.03, 246.30, 246.33, 246.46
 Stark, Antony: 231.05
 Stark, Chris: 147.12, 147.19, 148.34, 150.35, 232.03, 246.39, 439.01
 Stark, Chris S.: 360.09
 Stark, Christopher: **148.42**, 246.30, 439.19
 Stark, Daniel P.: 149.51, 210.03, 426.05, 454.10, 454.12
 Stark, David Vincent.: **210.01**
 Starckenburg, Tjitske: 347.15
 Starrfield, Sumner: 358.10, **358.11**
 Stassun, Keivan G.: 204.02D, 211.02, 244.25, 246.43, 310.08, 314.02D, 403.04
 Staudaher, Shawn: 248.02
 Stauffer, Candice: **245.13**
 Stauffer, John: **136.12**, 339.01, 355.17, 439.13
 Staveley-Smith, Lister: 354.04
 Stawarz, Lukasz: 123.01, 257.19
 Stebler, Shane T.: 111.02
 Steele, Amy: **147.04**, 220.06, **359.01**

Stefanik, Robert: 403.07
Stefansson, Gudmundur: 152.18, 246.08, 246.45, 303.01
Steffen, Jason H.: 104.06D, 148.23
Stefo, James S.: 339.05
Stehlikova, Veronika: 355.35
Steiman-Cameron, Thomas Y.: 211.04D
Steiner, Jack: 347.01, 347.05, 349.12, 440.06
Steiner, James Francis.: **347.07**
Steiner, Ken: 242.03
Steinhardt, Charles: **332.04**
Steinhardt, Paul: 153.14
Steinhauer, Aaron J.: 344.06, 344.09
Steinle, Nathan: **421.03**
Stello, Dennis: 450.13
Stelzer, Beate: 133.01
Stephens, Haynes Forest.: **347.06**
Stephens, Ian: 147.10
Sterling, N. C.: 241.15
Stern, Daniel: 153.18, 223.04, **223.06**, 304.01, 304.06, 304.07, 320.04, 327.02, 343.01, 355.36, **361.06**, 440.05
Stern, S. Alan: 144.03
Stetzler, Steven: **243.12**
Stevens, Abigail: 140.06
Stevens, Daniel J.: **310.02D**
Stevens, Dashiell Naea.: 232.03, 360.09
Stevenson, Kevin: 128.08, **148.14**, **207.08**, 228.07, 355.20, 410.01, 410.07, 427.04
Stevenson, Taylor Shannon.: **446.02**
Stevenson, Thomas R.: 215.05, 447.01
Stewart, Tess: **258.03**
Stiavelli, Massimo: 149.18
Stierwalt, Sabrina: 251.07
Still, Martin: 439.10
Stiller, Robert A.: **358.04**
Stillman, Coley Michael.: **149.12**, 149.24
Stobie, Simon: 215.03
Stockdale, Christopher: **245.09**
Stollberg, Mark: 144.07
Stolovy, Susan: 237.01
Stone, Frances H.: **449.11**
Stone, Nicholas: 415.06, **422.05**, 423.04D
Stone, Robert B.: **304.04D**
Stone-Martinez, Alexander: **450.08**
Storchi-Bergmann, Thaisa: 440.15
Storer, Dara: **153.04**
Storm, Shayee: 331.05D
Storrs, Alex: **158.09**, 258.14, 359.10
Stott, John P.: 306.01D, 328.05D
Stovall, Kevin: 224.06, 243.12, 243.13, 453.09, 453.16
Strader, Jay: 149.36, 453.06
Strait, Victoria: 454.10
Straizys, Vytautas: 344.05
Strampelli, Giovanni Maria: **414.07**, 446.06
Strassmeier, Klaus: 358.10
Stratta, Giulia: 107.08
Straughn, Amber N.: 258.01, 360.05
Strauss, Michael A.: 362.07
Street, Rachel: **158.06**, 228.05
Strelnitski, Vladimir: 136.10
Strickland, Emily: **356.05**
Strid, Grace: 339.05
Striegel, Stephanie: 249.01
Strigari, Louis: 330.05, 413.07
Strobel, D: 450.07
Strohmayr, Tod: 243.17
Strohmayr, Tod E.: 157.13, **333.03**
Strolger, Louis: 245.05, 354.07, 454.10
Stroupe, Darren: **441.05**
Stubbs, Christopher W.: 354.17
Stuik, Remko: 152.22
Su, Kate: **147.08**
Su, Kate YL.: 146.10
Su, Yuanyuan: 252.01, 252.05, 406.05, 441.01
Subasavage, J: 246.01
Subasavage, John: 349.17
Subasavage, John P.: 157.10, 434.01
Subbarao, Mark: 360.13
Subedi, Hari: **303.04D**
Subramonian, Arjun: 348.01
Sudbrink, Don: 242.14
Sugerman, Ben: 257.04
Sugimoto, Kanako: 342.14
Suh, Hyewon: 412.01
Suhaimi, Afiq: 246.24
Sullivan, Dan: 152.19, 314.05D, 419.05
Sullivan, James: **351.01**
Sullivan, Jessica: **241.03**
Sullivan, Kendall: **147.07**, 339.12
Sullivan, Mark: 209.07, 245.10
Sullivan, Woodruff: **108.02**
Sultanova, Madina: **306.05D**
Sumi, Takahiro: 246.17
Summers, Frank: **232.05**
Sumner, Joy: 339.05
Sun, Bangzheng: 247.06
Sun, Bingqing: 311.06
Sun, He: **361.15**
Sun, Meng: 128.07, **421.06**
Sun, Qinghui: **344.06**
Sundeen, Kiera A.: 339.05
Sundheim, Beth A.: 238.01, 238.02, 238.03, 238.04, 238.05, 238.06, 238.07, 238.09, 238.10, 238.11
Sung, Keeyoon: 452.03
Suntzeff, Nicholas: 413.07
Sunyaev, R.: 438.19
Surace, Jason: 362.04
Suri, Veenu: **355.10**
Suriano, Scott: **330.03D**
Sutherland, Dougal: 225.04
Suwannajak, Chutipong: **340.01**
Suzuki, Aritoki: 419.04D
Suzuki, Nao: 153.21, 327.02
Svoboda, Brian: **214.02D**, 247.03
Swade, Daryl: 436.12
Swain, Mark: 228.04, 427.07
Swam, Mike: 436.12
Swar, Prachi: 444.14
Sweckard, Teaghen: **150.25**
Swift, Brandon J.: 247.21
Swiggum, Joe: **157.12**, 224.06, 243.13, 243.15
Switzer, Eric: 116.01, 152.19, 153.09, 314.05D, 419.05
Szkody, Paula: 358.09, **414.01**
Szymkowiak, Andrew E.: 331.06
Tacchella, Sandro: 304.07
Taggart, Kirsty: 308.01
Takagi, Seiko: 446.08
Takahashi, Jun: 446.08
Takaki, Katsutoshi: 446.03
Takakura, Satoru: **261.04D**
Takayama, Masaki: 446.08
Talens, Geert Jan: 152.22
Tallis, Melisa: **361.18**
Tamayo, Daniel: 115.08
Tamburo, Patrick: 211.03
Tamer, A. Joseph.: 256.04
Tamura, Motohide: 152.10, 303.07
Tan, Yan: 148.46
Tanaka, Masaomi: 153.21
Tanaka, Masayuki: 406.03
Tang, Hong: 246.18
Tanner, Angelle: 246.13
Tarantino, Elizabeth: **130.07**
Taraschi, Peter: 152.19, 314.05D, 419.05
Tartaglia, Leonardo: 245.11
Tasker, Nicholas: 436.08
Tauscher, Keith: 116.01
Tayar, Jamie: **326.02D**, 411.02D, 450.13
Taylor, Brook: 152.24
Taylor, Corbin: **440.12**
Taylor, Gregory: 215.01, 250.26, 342.29
Taylor, Joanna M.: 150.38, 355.40
Taylor, John: 155.04, 339.02
Taylor, Malinda Suzanne.: 358.01
Taylor, Meghan: 339.05
Taylor, Morgan: 153.02
Taylor, Rhys: 151.06
Taylor, Stephen: 224.06
Taylor, Stuart F.: **228.06**
Teachey, Alexander: **201.07**, 349.21
Teal, Dillon J.: **246.21**
Team, ALFALFA: 252.17
Team, APPSS: 252.17
Team, Undergraduate ALFALFA: 252.17
Teffs, Jacob: **209.02D**
Teimoorinia, Hossen: 227.01
Telting, John H.: 146.04, 146.16
Templeton, Matthew R.: 362.17
ten Brummelaar, Theo: 152.05, 152.26
Tendulkar, Shriharsh: 132.02
Teng, Stacy: 149.48
Tenn, Joseph S.: **208.01**
Teplitz, Harry: 354.07, 355.12, 426.05
Terheide, Rachel: **244.14**
Terndrup, Donald: 250.14
Terrell, Marie: **339.06**
Terrien, Ryan: 152.18, 244.16, 246.08, 246.45
Terzian, Yervant: 247.31
Teske, Johanna: **120.05**, 211.02, **228.01**, 246.22
Teuben, Peter: 130.01, 150.10, **150.17**, 150.28, 307.10, 331.05D
Thackeray, Beverly: 104.07, **326.01**, 334.07, 349.08
Thakur, Neeharika: 220.08
Thao, Pa Chia: **148.15**
Theissen, Christopher: **133.02**
Theuns, Tom: 149.04
Thierry, Pierre: 442.07
Thilker, David: 313.05, 362.01, 445.02
Thirouin, Audrey: 115.03
Tholen, David J.: 115.07
Thomas, Ben: 245.10
Thomas, Melissa: 360.11
Thomas, Najma: 338.05
Thomas, Peter: 426.02
Thomashow, Eydon: **136.10**
Thompson, Barbara J.: 220.08, 315.04
Thompson, Benjamin: 344.13
Thompson, David J.: **250.20**
Thompson, Donna M.: 362.17
Thompson, Grant: **256.03**
Thompson, Jahreem R.: **355.55**
Thompson, Kristen: **126.07**, **360.02**
Thompson, Mark: 331.04D
Thompson, Samantha: **126.01**
Thompson, Scott E.: 127.02
Thompson, Susan E.: 403.06, **431.05**
Thompson, Todd A.: 209.04
Thorngren, Daniel: **211.07**, 228.01, 410.07
Thornton, Jonathan: 257.22
Thornton, Jonathan Daniel.: **257.21**
Thornton, Stephen: **243.01**
Thorpe, James Ira.: 255.10, 350.04, **361.17**
Thronson, Harley: **355.02**
Thyagarajan, Nithyanandan: **430.06**
Tian, Wenwu: 446.16
Tibbetts, Michael: 238.01, 238.02, 238.03, 238.04, 238.05, 238.06, 238.07, 238.09, 238.10, 238.11
Tielens, Alexander: 231.05
Tilvi, Vithal: 149.33, 258.17, 357.07
Timlin, John: 213.04, **250.38**
Timmerman, Erik: 246.08
Timmons, Nicholas: 257.15
Tinyanont, Samaporn: 334.01
Tiongco, Maria: **413.04D**
Tirrell, Bethany M.: **255.12**
Todorov, Kamen: 207.01, **228.07**
Tofflemire, Benjamin: **414.05D**
Toft, Sune: 454.10
Togi, Aditya: 311.06
Tokuda, Kazuki: 230.01
Tollerud, Erik: 340.12
Tolls, Volker: 114.01, **237.08**
Toloba, Elisa: 127.05D, 149.36, 258.07
Tombesi, Francesco: 149.48, 404.04, 405.05

Tomesh, Teague: **251.08**
Tomic, Matt: 140.13
Tominaga, Nozomu: 153.21
Tomlinson, Joseph: **357.01**
Tomsick, John: 140.06,
223.03
Tong, Hao: 243.02
Tonry, John: 109.04, 308.06
Torres, Guillermo: 104.04,
157.08, 201.07, 339.08, 403.04
Torrey, Paul: 110.07, 257.16,
406.02D
Tóth, Viktor L.: 361.21
Towner, Allison: **449.01**
Townsend, Richard: 424.04D
Townsend, Leisa K.: 339.07
Töyrä, Daniel: 255.05
Trac, Hy: 225.04
Trafton, Laurence M.: 144.03
Trakhtenbrot, Benny: 304.01,
304.07, 320.02, 320.03,
320.04, 320.08
Tran, Debby: **152.04**
Tran, Kim-Vy: 110.02D, 110.05,
406.02D
Trauger, John: 246.32
Trauger, John Terry.: **246.15**,
246.18
Traynor, Liam: **149.34**
Treister, Ezequiel: 304.01,
320.02, 320.04, **320.05**,
320.07, 323.03
Tremblay, P.-E.: 145.05, 233.01
Tremmel, Michael: 305.01
Tremonti, Christy: 149.06,
258.05
Tremou, Evangelina: 453.06
Trenti, Michele: 349.32, 454.10,
454.12
Treuthardt, Patrick: 248.04
Trevor, Max: **250.16**
Triaud, Amaury: 427.09
Trierweiler, Isabella: **452.06**
Tripp, Todd: 302.05
Troland, Thomas: 247.15
Trott, Emery: **438.05**
Trouille, Laura: 158.14, 362.03
Troup, Nicholas: 211.02,
244.16, 246.43, 360.01, 421.06
Troxel, Michael: **219.02**
Troyer, Jon: 453.08
Truebenbach, Alexandra:
430.03D
Trueblood, Mark: 314.02D
Trueblood, Pat: 314.02D
Truitt, Amanda R.: **120.02**,
348.14
Trump, Jonathan: 309.02D
Trung, Vincent: **153.05**, 153.13
Truong, Phuongmai N.: 340.09
Truong, Tuan: 246.18
Tsai, Chao-Wei: 304.06
Tsang, Benny Tsz Ho:
214.04D
Tsuboi, Yohko: 450.09
Tuan, Jin Zong.: 258.07
Tubbs, Drake: 147.06
Tucker, Brad: 446.06
Tucker, Carole: 112.02D,
152.19, 215.02D, 314.05D,
322.05, 419.05
Tucker, Douglas: 145.05
Tucker, Gregory: 128.08
Tufts, Joseph: 152.24
Tully, R. Brent: 258.10, 344.16
Tumlinson, Jason: 149.08,
210.06, 237.10
Turnbull, Margaret: 147.19,
148.34, 158.02, 158.03, 246.26,
355.14
Turner, Jake D.: **310.05D**
Turner, Jeremy: **351.10**
Turp, Dennis: 309.01
Turp, Maximilian Dennis.:
362.11
Turyshhev, Slava: 314.01
Twarog, Bruce A.: 213.05D,
344.06
Twum, Angela: **258.04**
Tychoniec, Lukasz: 257.07
Tyler, Krystal: 227.02
Tyson, Tony: 153.11
Tzanavaris, Panayiotis: 251.10,
333.01
Tzanidakis, Anastasios:
237.09, 312.01
U, Vivian: 149.48, 320.05
U-Yen, Kongpop: 215.05
U-Yen, Konpop: 447.01
Ubertini, Pietro: 438.19
Uchiyama, Yasunobu: 257.19
Udrea, Bogdan: 111.02
Udry, Stephane: 104.04
Ueda, Junko: 125.07, 247.32
Ueda, Yoshihiro: 320.02,
320.04
Uemura, Makoto: 446.03
Ujjainwala, Zakir L.: 339.05
Üllom, Joel: 215.02D, 322.05
Umetsu, Keichi: 454.10, 454.12
Unterborn, Cayman T.: **120.06**
Unwin, Stephen C.: **140.02**
Urbain, Denis: 342.06
Uritsky, Vadim M.: 338.03
Urquhart, James: 114.04,
331.04D
Urrutia Zapata, Fernanda
Cecilia.: **454.01**
Urry, Meg: 110.06, 238.14,
257.19, 304.01, 320.05, 320.06
Ursache, Andrei: 242.06
Usero, Antonio: 125.07, 322.04
Utomo, Dyas: 130.01, 426.04D
Uttley, Phil: 347.01, 347.05,
347.07
Uyama, Taichi: 303.07
Vacca, William: 445.12
Vaillancourt, John: 152.21,
247.24, 414.04
Valdes, Francisco: 354.01
Valdes, Guillermo: **255.17**
Valdez, Laura: 444.13
Vale, Leila R.: 215.02D, 322.05
Valencia, Diana: 115.08
Valencic, Lynne: **237.21**
Valente, Martin: 140.13
Valenti, Jeff: 148.14, 436.12
Valenti, Stefano: 245.11, 245.16,
308.03
Valenzuela, Ana Maria: 246.36
Vallerga, John: 104.01
Valluri, Monica: 422.07, 422.08
Valogiannis, Georgios: **153.12**
Valtchanov, Ivan: 361.21
Van Alfen, Nicholas: **250.13**
van Belle, Gerard: 157.01,
348.15, **349.31**, 442.06
van der Horst, Alexander:
314.06, 354.15, 414.02
van der Hulst, J. M.: 354.04
van der Marel, Nienke: 157.07
van der Marel, Roeland: 237.11,
257.09
Van der meer, Wieb: 143.02
van der Wel, Arjen: 149.17
Van Dyk, Schuyler: 245.09,
361.21
van Eyken, Julian: 152.24
van Gorkom, Jacqueline:
210.05, 441.03
Van Haaften, Lennart: **421.02**
van Haasteren, Rutger: 453.09
Van Hamme, Walter: 434.03
Van Heerden, Elmarie: 115.06
van Leeuwn, Joeri: 243.13
van Loon, Jacco Th.: 136.11
Van Putten, Maurice H.:
327.06
Van Ross, Bryce: **246.22**
Van Sistine, Anglea: 332.06,
361.20
Van Stone, David W.: 238.01,
238.02, 238.03, 238.04,
238.05, 238.06, 238.07,
238.09, 238.10, 238.11
van Velzen, Sjoert: 405.03,
405.06, 415.06, 423.05
van Weeren, Reinout: 252.03,
252.05, 342.29, 406.06
van Zee, Liese: 248.02, 312.03,
340.08
Vanden Bout, Paul: 149.27
Vanderbei, Robert: 246.39,
439.05
Vanderburg, Andrew: 104.04,
204.04, 234.04, 246.07,
246.27, 303.05, 303.08,
349.09, **427.03**, 439.13
Varakian, Matthew: **246.23**
Vardoulaki, Eleni: **304.03**
Varga, Attila: **330.01**
Varga-Verébelyi, Erika: 361.21
Varri, Anna Lisa: 413.04D
Varricatt, Watson: 436.04
Vartanyan, David: **209.06**
Vasei, Kaveh: **328.03D**
Vasiliev, Eugene: 422.05,
422.07
Vasisht, Gautam: 246.13,
439.13
Vasquez, Chelsea: 156.01
Vasquez Soto, Alan: 146.03,
453.04
Vayner, Andrey: 112.03
Vazquez, Gerardo Arturo.:
361.04
Vegetti, Simona: 415.04D
Veillet, Christian: 142.08
Veilleux, Sylvain: 149.48,
247.10, 320.04
Veldhuis, Marten: 362.03
Venters, Tonia: 223.04
Ventura, Jean-Paul: 349.35,
349.39
Verbunt, Frank: 132.03D
Verdugo, Tomas: 258.08
Verheijen, Marc A W.: 354.04
Verma, Aprajita: 251.05
Verschuur, Gerrit: 116.06,
212.08
Verstappen, Joris: 354.04
Vervack, Ronald: 144.13
Vesa, Oana: **349.40**
Vesperini, Enrico: 348.04,
413.04D
Vestrand, Tom: 140.05
Veyette, Mark: **120.03**, 120.04
Viall, Nicholeen: 359.11
Vides, Christina: 144.14,
246.10
Vieira, Joaquin: 354.33
Vieira, Joaquin Daniel.: 149.41,
250.27, 355.11, **355.31**
Vievering, Juliana: **414.08**
Vijayaraghavan, Rukmani:
252.12
Vikhlinin, Alexey: **103.04**
Vila, Maria Begoña.: 355.29
Villadsen, Jackie: 349.08,
360.01
Villadsen, Jacqueline: 326.01,
334.07
Villaescusa-Navarro, Francisco:
351.04
Villanova, Sandro: 344.10,
411.02D, 450.11
Villanueva, Steven: **314.02D**,
403.05
Villar, Ashley: 446.06
Villarroel, Gustavo: 450.08
Villiger, Nathan J.: 146.17
Vink, Jorick: 157.16
Viou, Cedric: 150.06
Visgaitis, Tiffany A.: 255.12
Vishwas, Amit: **112.02D**,
251.05
Vissers, Michael: 215.02D,
322.05
Vivas, Anna Katherina.: 237.12
Vivès, Sébastien: 419.01
Vogel, Stuart N.: 130.01,
359.08, 426.04D
Vogeley, Michael S.: 244.26,
250.08, 250.32, 357.01
Vogelsberger, Mark: 110.07,
406.02D
Volk, Kevin: 146.10
Volkov, Igor: 238.15
Volonteri, Marta: 412.01
von Braun, Kaspar: 349.31,
450.05
Von Hippel, Dr. Ted: 453.01
von Kienlin, A.: 438.19
Voulgaris, Aris: 220.06
Vrba, Fred J.: 436.04, 440.14
Vrinceanu, Daniel: 111.08,
226.04
Vulcani, Benedetta: 454.10
Vulic, Neven: **227.06**, 347.17
Waalkes, William: **148.18**
Wade, Gregg: 424.04D
Wade, Nicholas: **248.08**
Wages, Mitchell: 355.15,
355.28, 355.35, **355.44**, 355.46
Wagg, Jeff: 152.07
Waggoner, Abigail R.: **339.03**
Wagner, R. Mark.: 358.02,
358.11
Wagner, R. Mark: **358.10**
Wagner-Kaiser, Rachel: 344.10
Wagoner, Robert: 250.09
Wahhaj, Zahed: 204.03
Wainscoat, Richard J.: **115.05**,
122.03, **122.04**, **142.02**,
308.06
Waite, Jurij: 351.11
Wakeford, Hannah R.: 211.01,
427.04
Wakker, Bart: 237.05, 302.03D,
355.16, 411.01

Walborn, Nolan R.: 355.01, 355.42
Walder, Madison Victoria.: **237.02**
Waldman, Mark: 355.29
Waldmann, Ingo: 148.26
Waldron, Zach: 354.15
Waldvogel, Kelly: **152.03**
Walker, Ashley L.: **257.08**
Walker, Christopher: 247.02
Walker, Christopher K.: 247.21
Walker, Christopher Kidd.: **231.05**
Walker, Constance E.: 113.08, 139.01, **142.06**, **142.07**, 142.08, 216.02
Walker, Gary: 136.10
Walker, Matthew G.: 344.17
Walker, Stephen: **406.07**
Walkowicz, Lucianne: 332.03
Wall, Joshua Edward.: **136.09**, 257.21
Wallach, Aislynn: 157.06
Wallin, John: 150.10
Walp, Bernie: 246.13
Walsh, Gregory: **243.04**
Walston, Joseph: 151.02
Walter, Donald: **242.18**
Walter, Fabian: 222.03, 342.25, 342.26
Walterbos, Rene: 445.02
Walth, Gregory: **112.03**, 149.13
Walton, Dominic: 341.07
Walts, Alexander: 152.19, 314.05D, 419.05
Wang, Bingquan: 440.11
Wang, Cindy: 302.02
Wang, David: 243.09
Wang, Feige: 440.11
Wang, Jason J.: 361.18
Wang, Jason Jinfei.: 229.03, **329.04D**, 349.07
Wang, Lile: **129.02D**
Wang, Luqian: 244.24
Wang, Ruoyan: 450.04, **450.10**
Wang, Sharon Xuesong: **104.08**, 425.07
Wang, Shiang-Yu: 115.03
Wang, Weichen: **127.01**
Wang, Weiyang: 243.02
Wang, Wenting: 212.04
Wang, Xian: 151.02
Wang, Yuan: 408.08
Wang, Yuankun: **243.16**
Wang, Yun: 354.08, 354.29, 354.36, 355.12, **402.01**
Ward, Jacob L.: 136.11
Ward-Duong, Kimberly: 349.15
Ward-Thompson, Derek: 130.04
Wardle, Mark: 214.03
Wardlow, Julie: 149.37
Ware, Austin: **148.30**
Warfield, Keith R.: 140.11, 246.33
Warmels, Rein: 150.10
warwick, Steve: 246.33
Washington, Dewayne: 360.05
Washington, Immanuel: 150.26
Washington, Robert: 349.18
Wass, Peter: 402.06, 419.06
Wasser, Molly: **242.08**, 360.06
Wasserman, Larry: 213.07
Waters, Chris: 308.06
Watkins, Laura L.: **257.09**, 340.12
Watts, Anna: 140.06
Watts, Duncan: **261.02D**
Watts, Galen: 149.27
Weaver, Harold A.: 144.03
Weaver, Ian: **439.14**
Weaver, John: **227.04**, 362.15
Weaver, Olivia: 251.12
Webb, Natalie A.: **223.02**
Webb, Tracy: 327.02
Webb-Forgus, Rowen: 247.23
Weber, Maria Ann.: **158.11**
Wechsler, Risa: 149.24, 149.51, 327.02
Wegner, Michael: 306.01D
Wehmeyer, Benjamin: **149.32**
Wehrle, Ann: **250.21**
Weigel, Anna K.: **320.08**, 362.11, **404.02D**
Weijmans, Anne-Marie: 210.01
Weinberg, David: 411.02D
Weinberg, Martin: 409.04D
Weinberg, Nevin N.: **128.07**, 421.06
Weinberger, Alycia: 428.07
Weiner, Aaron: 149.55
Weiner, Aaron S.: **149.46**
Weiner, Benjamin: 309.02D
Weinschenk, Sedrick: **146.17**
Weinstein, Alan: **224.07**, 435.04
Weintraub, David: 313.03
Weisberg, Joel: **243.10**
Weiss, Axel: 112.02D, 222.03
Weiss, Jake: 212.07
Weiss, Lauren: 211.08, 329.01
Weisz, Daniel: 214.05D, 340.10
Wells, Mark: 146.15, **244.08**
Wells, Natalie: **358.06**
Welsh, Barry: **104.01**, 147.01
Welsh, William: 347.08
Welty, Daniel: **247.28**, 355.01, 355.42
Welty, Daniel E.: 331.01
Wen, Qi: **140.17**, 140.18
Wenger, Matthew: 113.02, **113.03**, 113.06, 139.02, **256.07**, 360.11
Wenger, Trey: 230.06, 237.04, 247.31, 331.02D
Wenger, Trey V.: 247.07, 247.18, **247.25**, 360.01, 445.04
Wennmacher, Alexandre: 450.07
Werk, Jessica: **106.05**, 302.05
Werne, Thomas: 314.01
Werner, Michael: 247.24, 329.01, **354.26**
Werthimer, Dan: 132.02, 231.01
Weryk, Robert: 115.05
West, Andrew: 133.02
West, Robert: 144.15, 329.06D, 427.07
Westbrook, Benjamin: 419.04D
Wester, William: 145.05
Westerhoff, Thomas: 355.41
Westfall, Kyle: 210.01
Wethers, Clare: **222.05D**
Wetzel, Andrew: 411.03
Wharton, Robert: 243.01, 342.31
Wheatley, Jonathan: 104.01
Wheatley, Peter: 128.03D
Wheeler, Craig: 443.01
Whidden, Peter: **144.08**
Whipple, Parkes: 250.13
Whitaker, Katherine E.: **328.01**
Whitaker, Richard: 215.03
White, Cameron: 250.11, 354.14
White, Ethan: 228.08
White, Jacob: **428.04D**
White, James: 150.38, 355.40
White, Kevin: **428.05**
White, Raymond: 309.06D
White, Russel: 403.07
White, Steven: 152.15, 215.02D, 322.05
White, Tim: 450.05
White, Victor: 246.18
White, Vivian: 220.03
Whitehead, Mark: 150.06, 215.02D, 322.05
Whitelock, Patricia: 420.07
Whiting, Alan: **146.02**
Whitley, Kevin: 250.16
Whitman, Tony: 355.29
Wiebe, Donald: 112.02D
Wiedner, Martina: 355.13
Wiegand, Alexander: 351.01
Wiessinger, Scott: 360.05
Wiggins, Brandon K.: 145.04, 153.02, **226.03**
Wiita, Paul J.: 250.21
Wik, Daniel: 223.04, 227.06, 333.01, 347.17
Wiklund, Tommy: **127.04**, 149.11
Wiktorowicz, Sloane: 211.05
Wilcomb, Kielan: **148.20**
Wilcots, Eric: 149.23
Wilkin, Francis P.: **434.07**
Wilkins, Ashlee: 359.01
Wilkins, Stephen: 349.32, 426.02
Willecke Lindberg, Christina: **151.01**
Willems, Phillip A.: 246.08
Willenbrink, Kathryn A.: **146.10**
Willi, Marco: 362.03
Williams, Ben: 109.06D, 157.06, 227.06, 333.01, 354.07, 362.05
Williams, Benjamin F.: 150.40, 340.08
Williams, Brian J.: **140.04**
Williams, Darius: **152.01**
Williams, George Grant.: **245.07**
Williams, Grant: 142.08
Williams, James K.: **257.06**
Williams, Jonathan: 147.09, 147.17, 157.07, 437.01
Williams, Kurtis A.: 145.01
Williams, Miguel: 144.05
Williams, Peter: **146.07**
Williams, Peter Kelsey George.: **234.03**, 349.10
Williams, Steven: 327.02
Williams, Stewart: 342.14
Williamson, Marc: **239.01**
Williger, Gerard M.: **357.08**
Willis, Jon: 327.02
Willman, Beth: 237.12, 340.07
Willmer, Christopher: 302.05, 354.14
Willner, Steven: 149.46
Wilman, David J.: 306.01D
Wilms, Joern: **237.22**, 243.11, 435.05
Wilner, David: 125.07, 129.01, 129.06, 147.08, 147.13, 147.15, 147.17, 147.18, 247.23, **342.17**, 428.07
Wilson, Christine: 125.07
Wilson, Daniel: 246.18
Wilson, Gillian: 327.02
Wilson, Grant: 149.59
Wilson, Maurice: 111.01, **314.04**
Wilson, Robert C.: **255.20**
Wilson, Robert Forrest.: **211.02**, 360.01
Wilson, Teresa: **143.04**, 150.03, **242.13**, 242.17, **362.08**
Wilson-Hodge, Colleen: 243.17
Wilson-Hodge, Colleen A.: **107.03**, **140.06**, 157.13, 361.14
Windhorst, Rogier: 258.17, 306.04, 354.14, 357.07
Windmiller, Gur: 347.08
Winget, Don: 443.01, 452.02
Winkler, P. Frank.: 248.03
Winston, Elaine: **114.01**
Winter, Henry: 220.02, 338.04
Winter, Lisa M.: **140.05**, 140.10
Winternitz, Luke: 157.11
Winters, J.: 157.09, 246.01, 349.17, 349.18
Winters, Jennifer: **334.06**
Wise, John H.: 327.05D
Wiseman, Jennifer: 136.11
Wisniewski, John: 157.06, 341.03, 428.03, 437.02, 449.07
Wittal, Matthew Michael.: **115.04**
Wittenmyer, Robert: 111.01, **128.01**, 128.04
Wittman, David: 438.10
Witzel, Gunther: 212.01, 237.06, 311.02
Wofford, Alia: 326.01, 334.07, **349.08**
Wojciechowski, Evan: 230.01, **247.08**, 247.26
Wold, Isak: 149.25, 258.17, **328.02**
Wolf, Marsha: 152.08, 246.08
Wolfe, Douglas w.: 355.03, 355.08
Wolff, Michael T.: 157.13, 243.11, 243.17, 333.04
Wolff, Schuyler: 147.12, **330.06D**
Wolfgang, Angie: 148.30, **329.08**
Wolfire, Mark: 231.05
Wolk, Scott: 237.20
Wollack, Edward: 152.19, 215.05, 250.38, 314.05D, 354.33, 419.05, 447.01
Wong, Ivy: 405.08
Wong, Ka-Wah: 309.06D, **422.02**, 444.05
Wong, Kenneth: **226.01**
Wong, Michael: 115.04
Wong, Tony: 130.01, **230.01**, 247.08, 247.26, 426.04D
Wood, Brian: **341.06**
Wood, Charlotte: **450.05**
Wood, Joshua: 250.05

Wood, Kent S.: 132.04, 140.06, 157.11, **233.04**, 243.11, 255.16, 347.07
Wood, Michael: 444.01
Wood, Suzannah R.: **315.01**
Wooden, Diane H.: 350.06
Woodruff, Robert: 140.09, 140.13, **140.15**, 140.16
Woods, T. E.: 408.05
Woods, Tom: 338.01, 402.03D
Woodward, Charles E.: **350.06**, 358.10, 358.11
Woodward, John T.: 349.05
Woolf, Richard: 355.51
Woosley, Stan: 149.51
Wooten, Al: 214.03, 241.01, **342.06**
Workman, Jared: 255.09
Worrall, Diana M.: 257.19
wotta, Christopher: 248.09
Wray, Alan A.: 334.04
Wright, Amy: 242.14
Wright, Darryl: 362.03
Wright, Edward L.: **355.32**, 355.34
Wright, Erika A.: 444.09
Wright, Jason: 128.01, 152.08, 246.08
Wright, Jason T.: 111.01, 152.18, **246.45**, 303.03, 349.11, 349.24
Wright, Shelley: 112.03, 149.13
Wright, Simon: 347.10, 354.13
Wright, Warren: 408.03D
Wrobel, J. M.: 323.06, **342.33**
Wu, Jingwen: 304.06
Wu, Mike: 213.07
Wu, Peter: **356.06**
Wu, Xuebing: 257.18, 440.11
Wu, Ya-Lin: **403.03D**
Wuerker, Wolfgang: 150.25
Wulf, Dallas: **331.06**
Wuyts, Eva: 250.41
Wuyts, Stijn: 258.01
Wyatt, Mark: 342.17
Wyatt, Ryan Jason.: 360.10, **360.12**, **360.13**
Wyatt, Samuel: 245.11
Wyithe, Stuart: 306.04
Wylezalek, Dominika: 440.22
Wyrowski, Friedrich: 114.04
Wysocki, Daniel: **325.04**
Xie, Joan: 354.29, 354.36
Xie, Xiaoyi: **438.12**
Xin, Yeyuan: **442.02**
Xu, Dandan: 415.04D
Xu, Hao: 327.05D
Xu, Kevin: 361.21
Xu, Renxin: 243.02
Xu, Xinfeng: 250.50, **250.51**, 250.52
Xu, Zhilei: **261.05D**
Xu, Zizheng: **247.32**
Xuan, Wenhao: 104.02, **246.42**
Yamaguchi, Hiroya: 140.04
Yamanaka, Masayuki: 446.03, **446.08**
Yamazaki, Ryo: 241.06
Yan, Haojing: 306.04
Yan, Lin: 308.01, 354.29, 354.36, 405.02D, **408.02**
Yan, Wei: 105.01
Yang, Haifeng: **428.02D**
yang, huan: 149.07, 251.01
Yang, Jinyi: 440.11
Yang, Jun: **132.05D**
Yang, Qian: 257.18, **440.11**
Yang, Sheng: 245.11
Yang, Soung-Chul: 344.10
Yang, Yao-Lun: **313.01**
Yao, Su: 440.11
Yao, Xinyu: **246.05**
Yarber, Aara'L: 246.21
Yashiro, Seiji: 220.08
Yasuda, Naoki: 153.21
Ybarra, Jason E.: 344.20, 344.21
Ye, Quan-Zhi: **316.02**
Yen, Mike: 327.02
ygouf, marie: 246.46, 330.02
Yi, Sukyoung ken.: 222.04, 227.03
Yoon, Mijin: **153.11**
Yoon, Suk-jin: 425.03, 448.02, 454.06, 454.07, 454.14
York, Donald G.: 247.28, 331.01
Yorke, Harold: 231.05
Yoshida, Michitoshi: 446.03
Yoshida, Naoki: 153.21
Younes, George: **333.06**
Young, Alexander: 215.02D, 322.05
Young, Andrew: 404.01
Young, C. Alex.: **220.01**
Young, Erick: 231.05
Young, Jason: **425.07**
Young, John S.: 314.03
Young, Karl S.: 140.17, **140.18**
Young, Ken: 342.21, 408.06
Young, Leslie: 144.03
Young, M.: 348.07
Young, Patrick A.: 120.02, 256.04, 348.12, 348.14
Young, Tim: 209.02D
Young, Timothy: **446.13**
Youngblood, Allison: 111.05, 234.01, **338.01**
Yu, Byeonghee: 153.19
Yu, Ka Chun: **448.04**
Yu, Liang: **246.07**
Yu, Lu: 258.01
Yu, Ross: 220.06
Yuan, Tiantian: 406.02D
Yuan, Wenlong: 420.07
Yuan, Xiaoyong: 302.02
Yuen, Ka Ho: 247.06, 247.30
Yukita, Mihoko: 223.04, 227.06, 251.10, **333.01**, 347.17
Yun, Min: 149.44, 149.59, 328.01
Yusef-Zadeh, Farhad: **214.03**
Yusof, Norhasliza: 408.03D
Zackrisson, Erik: 258.17
Zafar, Tayyaba: **445.09**
Zahnle, Kevin: 427.05
Zahorecz, Sarolta: 136.11
Zaidi, Tayeb: 332.08
Zakamska, Nadia: 250.35, 250.38, 440.22
Zamora, Manuel Abelardo.: 136.02
Zamora, Olga: 411.02D
Zane, Silvia: 140.06
Zarka, Philippe: 310.05D
Zasowski, Gail: 344.13, 424.03
Zavala, Jorge: 251.06
Zavala, R. T.: 157.01, 442.06
Zawadzki, Nicole: **339.11**
Zawol, Zoe: 104.02, 246.42
Zbib, Daniela: 444.14
Zdanavicius, Justas: 344.05
Zdanavicius, Kazimieras: 344.05
Zee, Galaxy Woong-bae
Woong-bae.: **425.03**
Zegeye, David Wassie.: **149.20**
Zeidler, Peter: **413.01**
Zeimann, Greg: 149.28
Zellem, Robert: 228.04
Zellem, Robert Thomas.: 148.26, **355.21**
Zemcov, Michael: 153.07, **354.24**
Zenteno, Alfredo: 446.06
Zepf, Stephen E.: 421.02
Zevin, Dan: 220.03
Zezas, Andreas: 149.46, 223.04, 227.06, 251.10, 333.01, 347.17, 421.08
Zhai, Chengxing: **314.01**
Zhang, Ce: 309.01, 362.11
Zhang, Chaoran: **361.20**
Zhang, Dong: **409.05**
Zhang, Haowen: **257.18**
Zhang, Helen: **247.17**
Zhang, Jinsu: 148.04
Zhang, Ke: 339.09
Zhang, Keming: **149.56**
Zhang, Liyun: 244.14
Zhang, Michael: **211.06**
Zhang, Qizhou: 257.07
Zhang, Shangjia: **136.02**
Zhang, Shaohua: 302.01
Zhang, Shawn: 356.06
Zhang, Tianxi: **430.04**
Zhang, Yimiao: **149.10**
Zhang, Yunhao: 252.15
Zhang, Zhoujian: 137.01, **349.26**
Zhao, Feng: 246.32, 361.13
Zhao, Jun-Hui: 237.14
Zhao, Ping: **447.09**
Zhao, Tiffany: 302.02
Zhao, Wei: 123.03D
Zhao, Yinan: 302.01, **302.02**
Zharikov, Sergei: 244.18
Zheng, Xianzhong: 127.02
Zheng, Yong: **309.04D**
Zhou, George: 104.04, 246.07, 303.08, 427.01
Zhou, Hanying: 246.18, 361.13
Zhou, Hongyan: 302.01
Zhu, Chenchong: 115.08
Zhu, Guangtun Ben.: 330.04
Zhu, Qirong: 412.02D
Zhu, Shifu: **123.06**
Zhu, Zhaohuan: 129.05, 144.12
Ziegler, Carl: **128.05**
Zimmerman, Neil: 147.12, 148.03, 148.34, 246.36, 246.37, 246.39, 355.47
Zinn, Joel: 450.13
Zinnecker, Hans: 214.01
Zirm, Andrew: 127.05D
Zittrin, Adi: 306.04, 454.10, 454.12
Zografou, Panagoula: 238.01, 238.02, 238.03, 238.04, 238.05, 238.06, 238.07, 238.09, 238.10, 238.11
Zoo, Galaxy: 149.30
Zou, Xiao-Duan: **452.05**
Zucker, Catherine: 125.07
Zuckerman, Ben: **326.03**, 349.29
Zweibel, Ellen: 251.04, 251.08, 429.04D
Østensen, Roy H.: 146.04, 146.16